

Transactions of the ASME

Air-Preheater Design as Affected by Fuel Characteristics	<i>Hilmer Karlsson and W. E. Hammond</i>	711
Tubular Air-Heater Problems	<i>E. F. Rothemich and G. Parmakian</i>	723
Contamination of Condensate by Heat-Exchanger-Tube Alloys	<i>J. D. Ristroph and E. B. Powell</i>	729
The Motion of a Link Chain Over a Roller	<i>A. E. R. de Jonge</i>	747
Effect of Rotary Regenerator Performance on Gas-Turbine-Plant Performance	<i>D. B. Harper and W. M. Robsenow</i>	759
The Rotary Regenerative Air Preheater for Gas Turbine	<i>A. T. Bowden and W. Hryniskak</i>	767
The Periodic-Flow Regenerator—A Summary of Design Theory	<i>J. E. Coppage and A. L. London</i>	779
A Practical Solution of a Three-Dimensional Flow Problem of Axial-Flow Turbomachinery	<i>L. H. Smith, Jr., S. C. Traugott, and G. F. Wislicenus</i>	789
Some NACA Research on Centrifugal Compressors	<i>I. A. Johnsen and Ambrose Ginsburg</i>	805
Complete Characteristic Circle Diagrams for Turbomachinery	<i>W. M. Swanson</i>	819
Theoretical Consideration of Retarded Control	<i>G. H. Cohen and G. A. Coon</i>	827
A Fast-Response True-Mass-Rate Flowmeter	<i>Yao Tzu Li and Shib-Ying Lee</i>	835
Optimum Three-Mode Controller Settings for Automatic Start-Up	<i>D. W. Pessen</i>	843
Analogies for Hydraulic and Electric Drives in Servomechanisms	<i>Yaoban Chu and L. A. Gould</i>	851
Laminar-Flow Forced Convection in Rectangular Tubes	<i>S. H. Clark and W. M. Kays</i>	859
Effect of Stress Amplitude on Statistical Variability in Fatigue Life of 75S-T6 Aluminum Alloy	<i>G. M. Sinclair and T. J. Dolan</i>	867
Grinding and Lapping Stresses in Manganese Oil-Hardening Tool Steel	<i>H. R. Letner and H. J. Snyder</i>	873
Workpiece and Surface Temperatures in Milling	<i>A. O. Schmidt</i>	883
Creep of Neoprene in Shear Under Static Conditions; Ten Years	<i>W. N. Keen</i>	891
Stress-Crazing of Plastics	<i>J. A. Sauer and C. C. Hsiao</i>	895
Some Design Considerations for Injection-Molding Heating Chambers	<i>G. D. Gilmore and G. B. Thayer</i>	903
Furnace Heat Absorption in a Spreader-Stoker-Fired Steam Generator, Part 1	<i>J. W. Myers and R. C. Corey</i>	909
Furnace Heat Absorption in a Spreader-Stoker-Fired Steam Generator, Part 2	<i>F. G. Feeley, Jr., and E. C. Miller</i>	925
The Venturi as a Meter for Gas-Solids Mixtures	<i>Leonard Farbar</i>	943
Experimental Evaluation of Expansion Factors for Steam	<i>J. W. Murdock and C. J. Foltz</i>	953
Measurement of Pulsating Flow With Propeller and Turbine-Type Meters	<i>R. B. Doudell and A. H. Liddle, Jr.</i>	961
The Pitot-Venturi Flow Element Water Service Report	<i>H. W. Stoll</i>	969

TRANSACTIONS OF THE AMERICAN SOCIETY OF MECHANICAL ENGINEERS

VOLUME 75

JULY 1953

NUMBER 5

Transactions

of The American Society of Mechanical Engineers

Published on the tenth of every month, except March, June, September, and December

OFFICERS OF THE SOCIETY:

FREDERICK S. BLACKALL, JR., *President*

JOSEPH L. KOFF, *Treasurer*
EDGAR J. KATZ, *Asst. Treasurer*

C. E. DAVIS, *Secretary*

COMMITTEE ON PUBLICATIONS:

GEORGE R. RICH, *Chairman*

PAUL T. NORTON, JR.

OTTO DE LORENZI

MORRIS GERR

JOSEPH SCHMERLER } *Junior Advisory Members*

GEORGE A. STETSON, *Editor*

COLIN CARMICHAEL

W. E. RHASER

K. W. CLENDINNING, *Managing Editor*

REGIONAL ADVISORY BOARD OF THE PUBLICATIONS COMMITTEE:

KERR ATKINSON—I

JOHN DE S. COUTINHO—II

WILLIAM N. RICHARDS—III

FRANCIS C. SMITH—IV

HENDLEY BLACKMON—V

CHESTER R. EARLE—VI

RAYMOND G. ROHONG—VII

VENTON L. DOUGHTIE—VIII

Published monthly by The American Society of Mechanical Engineers. Publication office at 20th and Northampton Streets, Easton, Pa. The editorial department is located at the headquarters of the Society, 29 West Thirty-Ninth Street, New York 18, N. Y. Cable address, "Dynamic," New York. Price \$1.50 a copy, \$12.00 a year for Transactions and the *Journal of Applied Mechanics*; to members and affiliates, \$1.00 a copy, \$6.00 a year. Changes of address must be received at Society headquarters four weeks before they are to be effective on the mailing list. Please send old as well as new address. By-Law: The Society shall not be responsible for statements or opinions advanced in papers or ... printed in its publications (B13, Par. 4).... Entered as second-class matter March 2, 1928, at the Post Office at Easton, Pa., under the Act of August 24, 1912.... Copyrighted, 1953, by The American Society of Mechanical Engineers. Reprints from this publication may be made on condition that full credit be given the Transactions of the ASME and the author, and that date of publication be stated.

Air-Preheater Design as Affected by Fuel Characteristics

BY HILMER KARLSSON¹ AND W. E. HAMMOND,² WELLSVILLE, N. Y.

The fuel characteristic that appears to control plugging and corrosion in air preheaters is sulphur content. While other fuel constituents contribute to the degree of the problem, their effectiveness depends upon the sulphur content. The presence of carbon in the fuel gas may aggravate the corrosion problem so that the best combustion conditions must be maintained carefully. In selecting air heaters for new installations, it is not possible to predict with any certainty the type of fuel that will be available during the life of the application; consequently, the air-heater design must provide controls that will maintain the cold-end temperatures within safe limits. The use of Cor-Ten or Mayari-R for the low-temperature surface and the use of cold-end baskets is recommended. Application of effective soot blowers using superheated steam or dry compressed air permits control of deposit formation. In the event that circumstances result in serious deposit formation, provision for water-washing of the heaters will provide an effective remedy. Consistent attention must be given to cold-end temperature under all conditions of operation and in this respect automatic controls should be considered.

TO keep pace with changing economic circumstances, we must strive continually to improve our efficiencies. In this endeavor, in so far as power-generation boilers are concerned, advanced steam temperatures and pressures make it essential that the maximum amount of heat be salvaged from the flue gas. When this heat is reclaimed by preheating the combustion air, we not only improve the heat-balance efficiency but also we generally improve the combustion process. Improvements in the combustion process, not being amenable to ready evaluation, are not always placed in the proper perspective.

If we review the past literature on air preheaters in boiler service, we note that through each time interval the authors mention the necessity of achieving greater efficiencies. To attain this goal each author mentions the desirability of using lower exit-gas temperatures which would require the elimination of plugging and corrosion caused by the presence of sulphur in the fuel among other factors. Some might receive the impression that in each period a new problem has been encountered rather than an extension of the old one. Actually, the penetration into this zone of difficulty has been controlled in each instance by the economic factors of the time, i.e., the relative cost of fuel, equipment, labor, and so on. These factors have been increasing steadily in magnitude so that with time flue-gas temperatures have been lowered steadily, Fig. 1.

¹ Technical Manager, The Air Preheater Corporation. Fellow ASME.

² Chief Engineer, The Air Preheater Corporation. Mem. ASME.

Contributed by the Fuels, Power and Machine Design Divisions, and Low Temperature Flue Gas Corrosion and Deposits Committee and presented at the Annual Meeting, New York, N. Y., November 30-December 5, 1952, of THE AMERICAN SOCIETY OF MECHANICAL ENGINEERS.

NOTE: Statements and opinions advanced in papers are to be understood as individual expressions of their authors and not those of the Society. Manuscript received at ASME Headquarters, September 24, 1952. Paper No. 52-A-125.

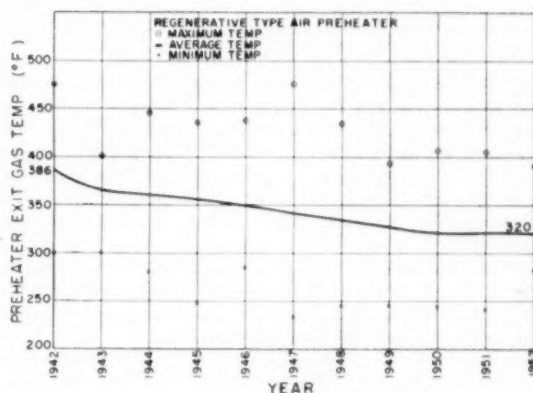


FIG. 1 EXIT-GAS TEMPERATURE TREND IN REGENERATIVE AIR PREHEATERS, 1942 TO 1952

In contemplating operation with low exit-gas temperatures, we must consider the possibility of outage caused by the heat-recovery equipment. Should this occur, the advantages obtained from high efficiencies are offset. Many designers and operators in the face of these circumstances prefer to forego the higher efficiencies and maintain conservative exit-gas temperatures. Others, realizing that the changing economic picture dictates higher efficiencies, are pushing forward into the trouble zone in an effort to achieve acceptable means of obtaining high efficiencies while holding the operating circumstances within acceptable bounds.

Experience with the regenerative preheater indicates that it has been able to meet the demands for low exit-gas temperature and still maintain the requisite availability. The methods adopted to accomplish this are discussed later in the paper.

CORROSION AND PLUGGING

The effect on flue-gas-recovery equipment operating at low exit-gas temperature when burning low-grade fuels is evidenced by the plugging of flue passages and corrosion of heat-transfer surface. The cause of this deposit apparently lies with the formation of sticky films containing sulphur compounds to which fly ash, and the like, may adhere.

There are many theories regarding the mechanisms behind this phenomenon, characterized principally by their disagreement with each other. However, one common factor that appears in all the theories concerns the presence of sulphur in the various fuels. The type of fuel does not appear to be a factor although the method of firing has some influence. Experience indicates that with pulverized-coal firing the phenomenon is of a low order.

When sulphur is burned in the furnace both SO_2 and SO_3 are formed. The relationship indicating the degree to which the sulphur oxidation proceeds in either direction is given by

$$SO_3/SO_2 = \sqrt{O_2/PK}$$

where

O = oxygen
P = total pressure
K = equilibrium constant

and depends as shown upon the oxygen content (excess air), the total pressure, and an equilibrium constant. The equilibrium constant of this reaction as determined by Bodenstein and Pohl can be expressed by

$$\log K = \frac{10,373}{T} - 2.222 \log T - 14.59213$$

where T is in degrees Kelvin. From this it may be seen that high flame temperature and low excess air are desirable in order to keep the formation of SO_3 at a minimum. The situation is complicated by the fact that certain oxides, including iron oxide and vanadium pentoxide, serve as a catalyst in this reaction encouraging the formation of SO_3 .

This equation illustrates what might be expected in burning sulphur in high concentrations and is not necessarily indicative of what happens in a boiler furnace due to the many other elements present. In fact, there is some reason to believe that in the boiler furnace, it would be desirable to increase the oxygen content in order to reduce the effects of sulphur deposits.

SO_2 in the presence of water hydrolyzes to H_2SO_4 , while in the same process SO_2 becomes H_2SO_4 . While both acids are corrosive, the activity of the second makes the first mild by comparison. Further, H_2SO_4 being an active reducing agent will oxidize in the presence of water to H_2SO_5 although the rate of this reaction in flue gases is not established. Consequently the high activity of SO_3 has caused it to be suspected, and most investigators have sought to establish the mechanism of its formation in boiler flue gases. W. F. Harlow (1, 2)³ suggested that SO_3 was not formed in the furnace in any significant quantities since in modern water-tube boilers, the furnace temperature is of the order of 2500 F. He feels rather that SO_2 is converted to SO_3 by surface catalysts on the high-temperature parts of the boiler. In his opinion the catalyst responsible is ferric oxide. He explains the low order of difficulty with pulverized-fuel firing as being due to catalyst poisoning from the fly ash formed by this firing method.

On the other hand, Dr. Wittingham (3) states that SO_3 is formed in the furnace. Other investigators, Johnstone, (4) Rylands and Jenkinson (5) feel that ferric sulphate is responsible for conversion of SO_2 to SO_3 and that this takes place at the deposit zone.

H. F. Johnstone (4) indicates that fly-ash particles may retain unburned pyrites and thus cause the particles to adhere to hot metal surfaces. He states further that it appears the sulphur present in the deposit on economizers and air heaters comes from the sulphur in the fly-ash particles. This sulphur is then oxidized after the fly ash has adhered to the surface.

In his report Johnstone (4) also mentions that he found a slight oxidation of sulphur dioxide taking place at high temperature owing to the catalytic action of flue dust. He also found that the SO_3 concentration did not increase with the decreasing temperatures as the gas proceeds through the boiler and heat-recovery equipment.

Another aspect of the corrosion mechanism appears to have some bearing on the problem concerning the solid matter entrained in the flue gas. There is sufficient material available in the literature to stimulate speculation along this line. Most investigators, Johnstone, Harlow, and Barkley, to mention a few, agree that with pulverized-coal firing the problem is nowhere as acute as with other methods. Barkley, Burdick, and Berk (6)

indicate that the amount of fly ash is a major factor affecting the results. It would appear that the character of solid matter entrained in the gases with pulverized-coal firing interferes with the corrosion mechanism. The nature of this fly ash has been described by Rylands and Jenkinson (5) as consisting of small hollow spheres of fused materials.

On the other hand, there is some limited evidence to indicate that the presence of carbon in the flue gases can increase the severity of the corrosion attack. R. W. Kear (7) states that the presence of carbon accelerates the corrosion rate above the dew point of the clean or filtered gas, Fig. 2. In addition, he found that H_2SO_4 deposits are greatly increased when carbon is present in the flue gas, Fig. 3.

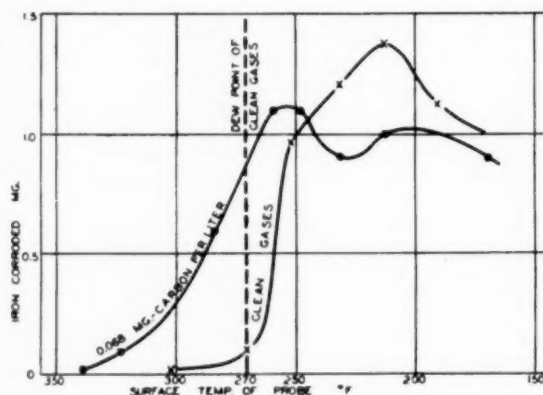


FIG. 2 EFFECT OF CARBON SMOKE ON TEMPERATURE AT WHICH CORROSION OCCURS

[Taken from paper by R. W. Kear, reference (7)]

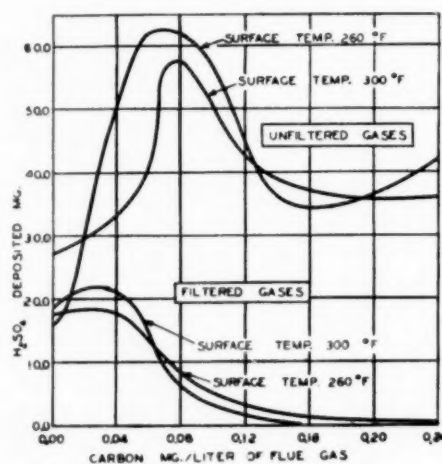


FIG. 3 VARIATION IN AMOUNT OF ACID DEPOSITED FROM FILTERED AND UNFILTERED GASES—DEW POINT 340 F

[Taken from paper by R. W. Kear, reference (7)]

It would appear, therefore, that the presence of carbon in the flue gas can increase the corrosion rate and also raise the dew point of the flue gas over that experienced with clean flue gas.

While there is only limited practical evidence to show that this actually occurs in the heat-recovery equipment, we do have the observation of R. J. Robertson and W. B. Gurney (8), that soot is particularly troublesome in that it contained H_2SO_4 and that it

³ Numbers in parentheses refer to the Bibliography at the end of the paper.

was very sticky. Further, we have the observation of H. F. Johnstone (4), that the dew point of flue gas increased with increased furnace loading. It would not be unreasonable to expect that the unburned carbon content of the flue gas would increase under this condition. We also have the observation of E. F. Tibbetts (9), that improved combustion conditions played a part in avoiding deposit formation. Again, it may be inferred that with poor combustion conditions, unburned carbon will be present in the flue gas.

It is believed the foregoing indicates that carbon present in the flue gas can play a part in the corrosion and plugging of flue-gas-recovery equipment.

It would appear that sulphuric acid is absorbed by the carbon particles and carried to the surface of the economizer and air heater. The nature of the particles in the flue-gas stream resulting from oil and stoker-firing is such that a high absorption rate may be expected.

Carbon may be activated if subjected to temperatures of 1800 F and above. In this condition the carbon particles can absorb SO_2 and SO_3 and water vapor. It is conceivable that the absorption of SO_2 and water vapor by the particle could result in high concentrations of H_2SO_4 . Since H_2SO_4 is an active reducing agent it can oxidize to H_2SO_3 . Kear (7) indicates his belief that the SO_2 is absorbed by the carbon particles and then hydrolyzes to H_2SO_4 . This observation is interesting since it might be of assistance in explaining the small amount of SO_3 measured in the flue gases in the colder zones.

Carbon particles containing a high concentration of sulphuric acid become very sticky and thus provide means for a deposit build-up. This mechanism also would be in keeping with Johnstone's observation that he felt the sulphur present in the deposit was carried there by the fly ash.

Analysis of a number of deposits taken from air heaters indicated that where the fuel burned contained sulphur in significant quantities, those installations that were most troublesome generally contained carbon in the deposit. It further indicated that on other installations, with the same approximate sulphur content which were not troublesome, little or no carbon was found in the deposit. It is appreciated that sufficient situations were not available for analysis to justify any definite conclusion in this regard. It is further appreciated that carbon of itself is not the entire answer and that many other mechanisms exist that will and can cause the difficulty. However, it is felt that careful attention must be given to combustion conditions to avoid aggravating an already serious problem. It is suggested that installations experiencing undue trouble from corrosion and plugging have their air-heater deposit analyzed for the presence of carbon among the other constituents normally reported. If carbon is found in the deposit, improvement in combustion conditions should be adopted to reduce the severity of the attack.

MEANS OF CONTROLLING PLUGGING AND CORROSION

While the problem of plugging and corrosion in air heaters and economizers looms as a large one and one that is not understood completely, it must be mentioned that air heaters are operating successfully. The great majority of installations are basically free of major difficulties; i.e., plugging and corrosion can be controlled so that forced or unscheduled outages are not required. In the case of only a few installations of regenerative air heaters has it been necessary to operate at higher than specified exit-gas temperatures. In each instance the change has been occasioned through a change in the fuel burned after the design had been established.

Minimum Metal Temperatures. While it is interesting to speculate on the nature and mechanism of the corrosion problem, it is probably more to the point to learn how to live with it. While

it is known that the type of fuel-firing equipment and metal temperatures are all factors in the control of corrosion and plugging, it is possible in most cases to deal only with metal temperatures since the other factors are beyond the control of the operator.

The experience of the authors' company regarding acceptable metal temperatures for various fuels is summarized in Fig. 4. These curves indicate the minimum average cold-end temperature at any load for the various fuels and firing methods normally employed.

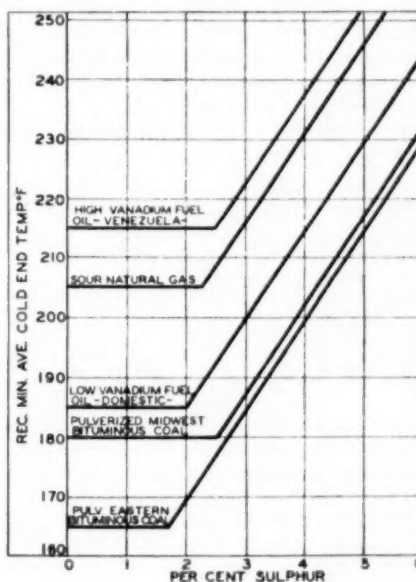


FIG. 4 CURVES SHOWING RECOMMENDED MINIMUM AVERAGE OF COLD-END TEMPERATURES FOR VARIOUS FUELS

If the design condition is such that these minimum temperatures are approached at full-load operation, it will be necessary to provide some means of controlling the metal temperature at reduced loads. Further, in those installations where the ambient temperature can drop appreciably below the designed ambient temperature, it also will be necessary to provide the temperature control at full-load operation. It will be noted that Fig. 4 does not show curves for pulverized-anthracite, sweet natural gas, or stoker firing. The values given in Table I are recommended.

TABLE I RECOMMENDED (MINIMUM AVERAGE COLD END) TEMPERATURES

Anthracite.....	Pulverized	150 F
Gas.....	Natural sweet	160 F
Stoker-firing.....	Bituminous coal	20 deg F over curves
(chain-grate and underfeed	for pulverized bituminous	
stokers)		10 deg F over curves
Stoker spreader.....		for pulverized bituminous

These values are minimal and selection should be made at or above these limits. For design purposes these limits should be compared with the calculated temperature without allowance for leakage. When using these limits as an operating guide, the actual air and gas temperatures may be used.

In discussing cold-end protection, the question naturally arises as to how well these temperatures can be determined. The authors' company, with the assistance and co-operation of the engineers of The Detroit Edison Company, has established through

actual field tests that the measured metal temperatures compare favorably with the average of the cold-end air and gas temperatures in the regenerative heater. Table 2 gives the results of these tests.

TABLE 2 COMPARISON OF MEASURED COLD-END METAL TEMPERATURES WITH AVERAGE COLD-END TEMPERATURES

Evaporator load, lb per hr	Measured metal temperature, deg F	Temperature entering air, deg F	Exit-gas temperature, deg F	Average of air temp and exit-gas temperature, deg F
440000	237.7	119	319	219
370000	230.3	118	299	208.5
230000	219.7	109	280	194.5

The information from which these data were compiled was obtained in 1943 at the Marysville Power Plant of The Detroit Edison Company, Marysville, Mich.

The tests were made on boiler No. 12 having the characteristics given in Table 3.

TABLE 3 CHARACTERISTICS BOILER NO. 12, MARYSVILLE POWER PLANT AP-390, MARYSVILLE DETROIT EDISON COMPANY

General data:				
3 CES boilers type VE-30, 10,080 sq ft; max pressure, 975 psi; boiler-drum pressure 909 psi; total steam temperature 910 F				
Burners: pulverized coal—direct—type T				
Evaporation, lb per hr	440000	370000	300000	
Entering-gas temp, deg F	660	604	545	
Exit-gas temp, deg F	319	299	280	
Air entering temp, deg F	119	118	109	
Air leaving temp, deg F	595	554	511	
Entering gas, lb per hr	522141	433869	352349	
Exit air, lb per hr	388600	312173	231731	

The metal-temperature readings were obtained from iron-constantan thermocouples embedded in the heating elements. Fig. 5 illustrates the manner in which the thermocouples were attached, while Fig. 6 indicates their location in the rotor. A slip-ring arrangement was used to bring the thermocouple leads

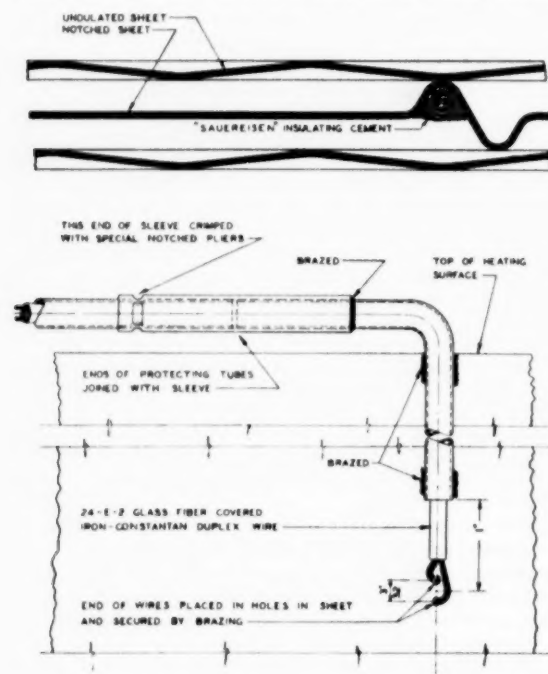


FIG. 5 METHOD OF FASTENING THERMOCOUPLES TO HEATING SURFACE USED IN TEST OF HEATING-SURFACE METAL TEMPERATURE AT MARYSVILLE POWER PLANT OF THE DETROIT EDISON COMPANY

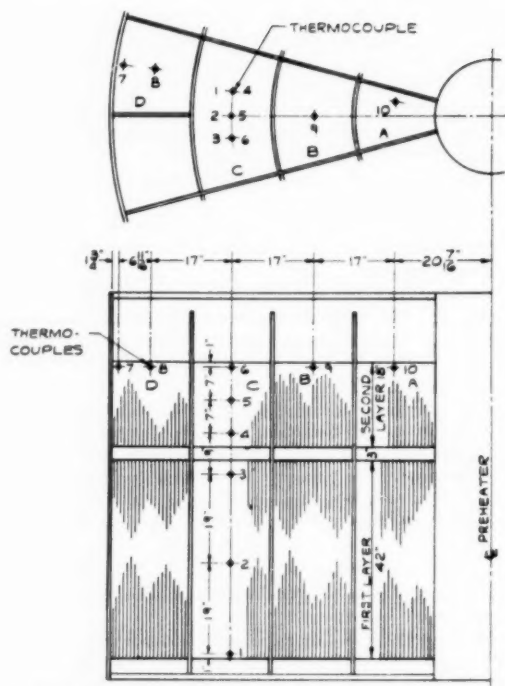


FIG. 6 LOCATION OF THERMOCOUPLES IN HEATING SURFACE USED IN TEST OF HEATING-SURFACE METAL TEMPERATURE AT MARYSVILLE POWER PLANT OF THE DETROIT EDISON COMPANY

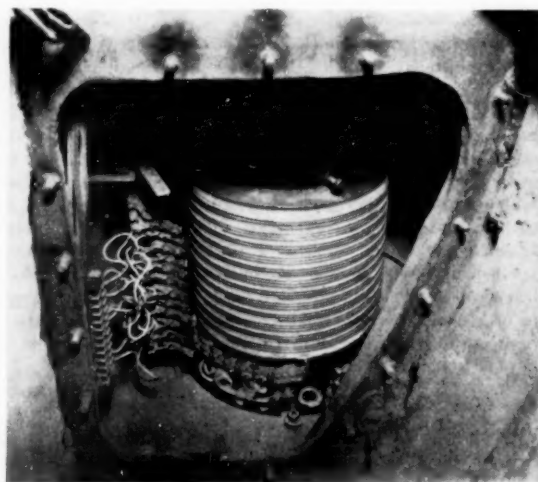


FIG. 7 SLIP-RING ARRANGEMENT USED IN TEST OF HEATING-SURFACE METAL TEMPERATURE AT MARYSVILLE POWER PLANT OF THE DETROIT EDISON COMPANY

out of the heater as illustrated in Fig. 7. Twelve rings were used permitting six simultaneous readings.

Reference to the test results indicated that an acceptable margin is provided by using the average of the cold-end temperatures. In each instance this average is well below the actual minimum metal temperature. It should be noted, however, that these data apply only to the rotary regenerative-type air heater. Owing to

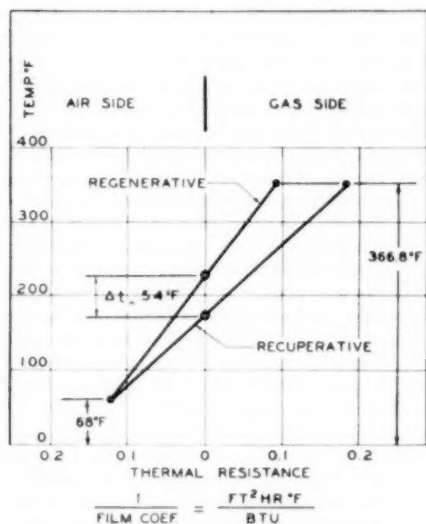


FIG. 8 COMPARISON OF METAL TEMPERATURES IN REGENERATIVE AND RECUPERATIVE AIR HEATERS WHEN OPERATING UNDER SAME TEMPERATURE LIMIT

[Taken from paper by W. Gunz, reference (15).]

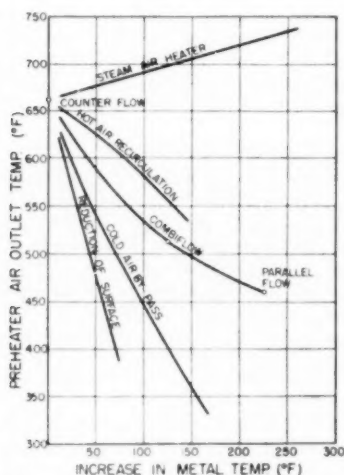


FIG. 9 TEMPERATURE OF COMBUSTION AIR AS A FUNCTION OF METAL TEMPERATURE WITH VARIOUS CONTROL METHODS

[Plotted for condition where flue-gas temperature varied in accordance with

Reduction of temperature of incoming flue gas = 0.3
Reduction of temperature of air to boiler

Taken from paper by T. A. Widell and S. I. Juhasz, reference (10).]

the nature of the heat-transfer process the metal temperature of the regenerative heater is appreciably higher than the recuperative types. This is illustrated in Fig. 8.

Cold-End Protection. The various means for obtaining cold-end temperature protection are well known. For convenience, they are listed as follows:

- 1 Cold-air by-pass.
- 2 Hot-air recirculation.
- 3 Steam-air heaters.
- 4 Combiflow—parallel—counterflow.
- 5 Reduction of surface.

- 6 Economizer by-passing
- 7 Flue-gas recirculation

T. A. Widell and S. I. Juhasz (10) discuss the efficacy of various methods of achieving metal-temperature control. Figs. 9, 10, and 11 present a comparison of the various characteristics of these methods. The original curve did not include steam-air heaters so that this has been added to the plot by the authors.

Combiflow. This may best be explained by reference to Fig. 12. With this method a portion of the air is made to flow in parallel with the flue gas and, by regulating this quantity, a control of metal temperature can be achieved. Dr. S. I. Juhasz is responsible for this proposal, although to the authors' knowledge, no installation has been made as yet.

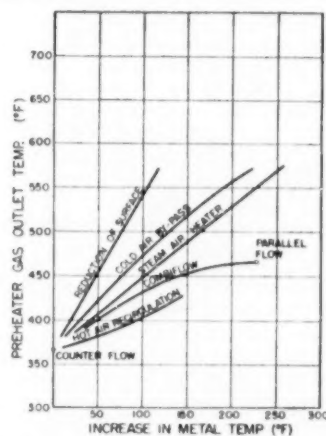


FIG. 10 EXIT-GAS TEMPERATURE AS A FUNCTION OF METAL TEMPERATURE WITH VARIOUS CONTROL METHODS

[Plotted for condition where flue-gas temperature varied in accordance with

Reduction of temperature of incoming flue gas = 0.3
Reduction of temperature of air to boiler

Taken from paper by T. A. Widell and S. I. Juhasz, reference (10).]

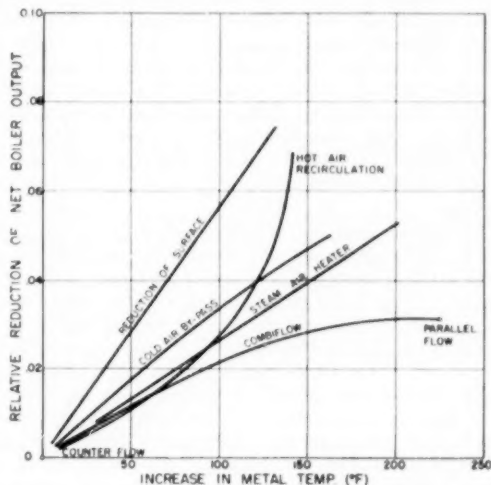


FIG. 11 RELATIVE EFFECT IN BOILER OUTPUT CAUSED BY USE OF VARIOUS CONTROL METHODS

[Plotted for condition where flue-gas temperature varied in accordance with

Reduction of temperature of incoming flue gas = 0.3
Reduction of temperature of air to boiler

From paper by T. A. Widell and S. I. Juhasz, reference (10).]

Cold-Air By-Passing. Cold-air by-passing is probably the cheapest and simplest of the various control methods. However, its effect upon efficiency is detrimental so that where the control may be required for long periods, it may not be justified. It provides a wide-range control so that many times it is combined with more efficient control methods to assure adequate range. To ob-

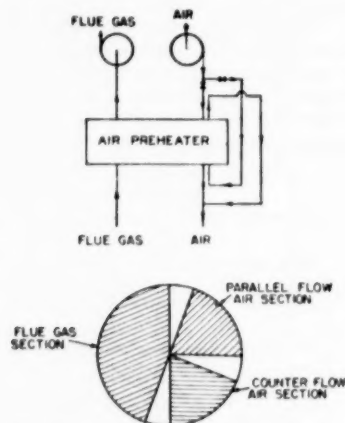


FIG. 12 COMBIFLOW IN LJUNGSTRÖM PREHEATER
[From paper by T. A. Widell and S. I. Juhász, reference (10).]

tain the maximum range, particularly at low loads, dampers should be installed in the air duct to insure sufficient flow through the by-pass duct. This method also provides adequate air temperature for pulverized coals. In evaluating this system we have to consider the lower boiler efficiencies, the reduction in fan power, and the cost of two dampers and by-pass duct.

Hot-Air Recirculation. Hot-air recirculation represents the most efficient method available in so far as the effect of boiler efficiency is concerned. However, its control range is limited by the quantities of recirculated air required for large adjustments in metal temperatures. For this case, it is preferable to combine hot-air recirculation with cold-air by-passing. Thus the efficiency of hot-air recirculation may be realized at all normal conditions, while the occasional demand for increased protection can be obtained through cold-air by-passing. It is sometimes difficult to obtain sufficient mill air temperature for pulverized-coal-firing installations when hot-air recirculation is used. For this condition cold-air by-passing can be combined with the hot-air recirculation so that a suitable air temperature may be obtained.

When hot-air recirculation is arranged to utilize the forced-draft fan for recirculation, the material for the installation is similar to the requirement for cold-air by-passing. A duct is run from the fan suction to the hot-air discharge of the air heater. Two dampers are required, one in the recirculation duct and another in the hot-air duct downstream from the recirculation-duct take-off. This last damper is used to insure adequate flow through the recirculation duct at low loads. It might be mentioned that where the forced-draft fan is used for recirculation, difficulty may be experienced in obtaining adequate control where inlet vanes are used on the forced-draft fan. This can be overcome by arranging the inlet-vane control so that the recirculation duct may connect between the vanes and the fan suction or by using a separate fan for recirculation.

When the separate fan is used better control is achieved, the recirculation system is independent of the forced-draft-fan system, and less power is required.

In evaluating hot-air recirculation, we must consider the change in boiler efficiency, increased fan power, and the cost of the duct, dampers, and fan, if a separate fan is used.

Steam-Air Heaters. The steam-air heater provides an acceptable control method. It provides the highest air temperature, which is desirable, particularly for low-load operation at low ambient temperature. Further, its efficiency is acceptable particularly if bled steam can be used. While it reduces the gas temperature drop in the preheater below that obtained with recirculation, this reduction can be more than offset by the gain in the regenerative feed-cycle efficiency obtained through use of bled steam. The increased air-side system resistance caused by the steam-air heater exists under all operating conditions whether or not the control is used unless special provisions are made. Other methods increase the system resistance only when the control is in operation. In addition to the cost of the steam-air heater, piping, valves, and so on, must be included. Further, suitable credit should be claimed if bled steam is utilized.

Economizer By-Passing. Another method of metal-temperature control that has been used involves by-passing the gases around the economizer in order to raise the gas inlet temperature. While increasing metal temperature this method also increases the air temperature, which is desirable. However, the complications introduced in the boiler through this method have not made it particularly popular.

Flue-Gas Recirculation. On stoker installations a portion of the flue gas leaving the air heater has been mixed with the combustion air as it enters the air heater. Thus the temperature of the air entering the heater is increased with a resultant increase in metal temperature. This method has another advantage for stoker-fired installations since the increase in the CO_2 content of the combustion air causes a reduction in the grate temperatures.

Evaluation of Cold-End Control Methods. The final selection of the most suitable control for a given installation must be based upon economic evaluation of the particular case. Since the factors controlling these evaluations are different for each application, it is not possible to generalize. One study made by Paul Koch (11) indicated that the steam-air heater appeared most economical for the conditions that he assumed if bled steam was used as a source of heat.

The systems studied were evaluated in the following order of decreasing efficiency:

- 1 Steam-air heater using bled steam.
- 2 Hot-air recirculation.
- 3 Steam-air heater using drum steam.
- 4 Cold-air by-passing.

It should be noted, however, that with other evaluation factors the order may change.

The efficacy of these various control methods can be realized only if they are used consistently. In this respect it probably would be desirable in considering new installations to weigh carefully the value of automatic controls.

Forced-Draft-Fan Location. While considering metal temperatures, mention should be made of the importance of taking the combustion air from the hottest part of the boilerhouse. While the advantage achieved is not of prime importance in metal-temperature control, it does provide definite gains. Where it is not possible to do this, such as in outdoor installations, it is necessary to provide protection over a greater range of temperatures. Further, in this connection, importance of protecting the forced-draft-fan inlet from rain and weather, on outdoor installations must be emphasized.

Combustion-Air Temperature. Another factor to be con-

sidered in the design of air heaters for low-temperature operation lies in the selection of the combustion-air temperature. A number of investigations by Gumz, Robertson, Gurney, and others indicate that with high air temperature and low excess air, the combustion of sulphur can be directed principally toward SO_3 . Further, with high air temperature, the combustion should improve and thus reduce the carbonaceous material entering the gas path. These investigators suggest that where circumstances permit, air temperature be considered up to 1000 F.

Design Features. The air-heater designer has endeavored to ease the difficulties accompanying the burning of distress fuels (high sulphur and vanadium) by modifying the equipment design. In this respect an important item concerns the material used. Materials that resist corrosion obviously extend the life of the element and increase the availability. Cor-Ten and Mayari-R have proved superior to other materials that are economically available. Aluminum has not been successful in regenerative heaters.

With the regenerative air heater the corrosion is normally confined to the last few inches at the cold end. It is thus possible to improve element life by making provision to invert the element as the cold end thins. To accomplish this, the cold-end surface is installed in baskets that can be handled readily through the side of the heater.

In addition, the use of side-removal baskets makes it possible to wash the cold-end element outside of the heater should deposit conditions make this necessary.

The importance of heating-element design and the flow length of the passages has led to the design of an improved surface that greatly facilitates cleaning and at the same time reduces appreciably the fluid-flow paths. This surface which is now under test in the field should help reduce the severity of the plugging problem.

Cleaning Methods. Having considered some of the means to reduce deposit formation and corrosion, it is pertinent to discuss what may be done to remove the deposit after it has formed. The soot blower is the commonest device for removing deposits. The effectiveness of the soot blower is dependent to some extent upon the length of the flow passage. While for the average application a soot blower at the cold end is sufficient, special applications may require soot blowers at both hot and cold ends. The use of superheated steam or compressed air has proved superior to saturated steam and is therefore strongly recommended.

Air heaters also can be cleaned by water-washing. In some installations the operators prefer to wash the heaters periodically rather than use soot blowers. In other cases, changes in the contemplated operating conditions, after the installation has been completed, such as low-grade fuels, low load, and low ambient conditions not anticipated, make it necessary to clean the heater by water-washing.

Generally speaking, the need for water-washing of regenerative air preheaters is remote if the heaters are equipped with modern power-operated single or dual-nozzle cleaning devices using superheated steam or compressed air as the cleaning medium. There are installations where load conditions, type of fuels, or inadequate cold-end metal-temperature control results in deposit accumulation beyond the scope of the cleaning devices. Under these conditions, water-washing is used to remove the deposits.

In any given installation, it may or may not be necessary to add some refinements to permit washing. When washing during outages, the preheater rotor often may be run at its normal speed. If, however, it is necessary to restrict the water to one side of the heater, the preheater rotor must be slowed to approximately $1/4$ rpm. This may be done by a portable air motor attached to the back end of the main drive motor. When low rotor speed is used,

it usually will be advisable to control the travel of the washing nozzle to assure that all areas are washed.

Water-washing may be carried out on either air or gas side, whichever is most convenient. Provisions for disposal of the wash water should be included in the duct system. When washing during operation, the air side may be preferred when dust-collecting equipment is located beyond the air preheater.

Many sources of wash water, such as well water, river water, evaporated make-up, blowdown, feedwater, house water, and so on, are used. Hot water (150 to 200 F) is greatly preferred to cold water, and hot alkaline water is better than untreated hot water. In addition, the use of alkaline water will help the operator to determine when the preheater has been thoroughly washed by comparing the pH of the effluent with that of the wash water. In this respect it is recommended that the water be alkalinized to a pH of 11 and that washing continue until the effluent has a pH of at least 9. Soft water should be used where possible.

For vertical and inverted-type preheaters, the pressure required for the wash water is that needed to deliver the desired rate of flow from the nozzle and is normally less than 50 psig. For horizontal preheaters, a higher velocity of the water jet will be required, and normally a water pressure of 100 psig is desirable. The rate of water flow at the higher pressure required for horizontal preheaters can be controlled by the diameter of the washing nozzle or nipple on the cleaning device.

A guide for the quality and quantity of water desirable for washing will be found in Fig. 13.

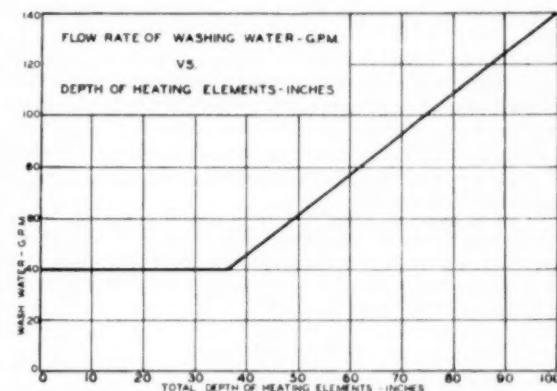


FIG. 13 FLOW RATE OF WASHING WATER IN GALLONS PER MINUTE VERSUS DEPTH OF HEATING ELEMENT IN INCHES

These recommendations are offered since, if water-washing is performed improperly, the water-soluble constituents are leached from the deposit without disturbing the insoluble constituents; thus over a period of time, an insoluble deposit is accumulated.

Where several heaters serve one boiler, it is possible to wash the heater under light load over week ends. In this case, the boiler output is reduced to approximately 50 to 60 per cent of full load and the heater isolated by dampers.

Alkalization of Heating Surface. Alkalization of heating surface has been under consideration for some time. The success of this method will depend upon finding a suitable material which will not react with the sulphur compound to form a more obnoxious compound than that now experienced. Reports of some installations have been received where this method has been used successfully, while others report negative results. In any event, work being done by the authors' company and others is continuing and possibly an acceptable method will be evolved in the near future.

Fuel Additives. The possibility of reducing corrosion and plugging of air heaters by additives to the fuel shows promise according to the recent announcement of one of the boiler companies. This company had developed a process of adding alumina or dolomite to the fuel oil. While the initial objective was to reduce high-temperature deposits, it has been found that the additives appreciably lower the dew point of the gases. If future results continue to show promise, a relatively simple and low-cost solution to the problem will be available for oil fuel.

Owing to the uncertainty of the economic availability of good fuels, the power-plant designer is in a precarious position in his efforts to satisfy the economic demand for lower fuel rates and at the same time provide maximum availability. The authors would like to suggest that under these circumstances the designer consider the following:

- 1 Select the air heater in accordance with the limits suggested in Fig. 4 for the fuel most likely to be used.

- 2 Provide metal-temperature control with sufficient range to permit the proper metal temperature to be obtained when burning the poorest fuel likely to be considered. In addition, the metal-temperature control also should have sufficient range to provide adequate protection for low-load operation at low ambient temperatures.

Should the range of fuels selected make the foregoing impracticable, the other alternative is to select the air heater based upon the best fuel and provide for removal of a layer of the heating element in the event that a poor fuel is selected.

- 3 Select as high a combustion-air temperature as is practicable.

- 4 Provide sufficient range in metal-temperature control to avoid falling below the recommended temperatures for any load or ambient condition. Automatic controls definitely should be considered.

- 5 Soot-blowing should be provided using superheated steam or dry compressed air. Provisions for washing the heater also should be considered.

On the other hand, if the fuel quality is definitely known and not likely to change radically during the life of the plant, it is possible to simplify the installation greatly and disregard many of the protective devices.

CONCLUSION

The authors hope that these comments may be of some assistance to plant designers and operators. They would like to assure them that, in so far as the air-heater design is concerned, every effort is being expended to improve the situation by continued research and design development. In this respect it might be mentioned that the results of a joint project between the authors' company and the United States Bureau of Mines should be available in published form in the near future. This report will deal with low-temperature flue-gas corrosion and deposits. It will include the results of field and laboratory testing on the suitability of a large number of materials. This will summarize investigations that have been in process over a period of nearly 8 years.

ACKNOWLEDGMENT

The authors would like to express their appreciation to the members of the staff who assisted in the preparation of figures, and for their helpful suggestions. Further indebtedness must be acknowledged to the authors of previous papers on this subject. In addition, we are grateful to our customers for their co-operation.

BIBLIOGRAPHY

- 1 "Causes of High Dew Point Temperatures in Boiler Flue Gases," by W. F. Harlow, Proceedings of The Institution of Mechanical Engineers, vol. 151, 1944, pp. 293-298.
- 2 "Causes of Flue Gas Deposits and Corrosion in Modern Boiler Plants," by W. F. Harlow, Proceedings of The Institution of Mechanical Engineers, vol. 160, 1949, pp. 359-368.
- 3 "Formation of Sulphate Deposits and Acid Condensates During Combustion," by Dr. G. Wittingham, 11th International Congress of Pure and Applied Chemistry, London, England, 1947.
- 4 "The Corrosion of Power Plant Equipment by Flue Gases," by H. F. Johnstone, University of Illinois, Bulletin No. 41.
- 5 "Bonded Deposits on Economizer Heating Surfaces," by J. R. Rylands and J. R. Jenkinson, Proceedings of The Institution of Mechanical Engineers, vol. 141, 1944, pp. 291-293.
- 6 "Test Data on Gas-Side Sulphate-Type Deposits on Tubes Beyond Boiler Surface," by J. F. Barkley, L. R. Burdick, and A. A. Berk, Trans. ASME, vol. 70, 1948, pp. 81-87.
- 7 "The Influence of Carbon Smokes on the Corrosion of Metal Surfaces Exposed to Flue Gases Containing Sulphur Trioxide," by R. W. Kear, *Journal of Applied Chemistry*, vol. 1, 1951, pp. 393-399.
- 8 "Steam and Power Plant Economy and Capability at Louisiana Station," by R. J. Robertson and W. B. Gurney, Paper No. 50—Pet-8, ASME, abstract in *Mechanical Engineering*, vol. 72, 1950, p. 1006.
- 9 "Problems Encountered in Burning Heavy Fuel Oil as Related to Attack of Metals at High and Low Temperatures and Fouling of Tube Banks," by E. F. Tibbetts, O. L. Wood, Jr., D. Douglass, and V. F. Estcourt, Paper No. 50—A-136, ASME, abstract in *Mechanical Engineering*, vol. 73, 1951, p. 34.
- 10 "Metal Temperatures in Regenerative and Recuperative Air Preheaters," by T. A. Widell and S. I. Juhász, The Royal Institute of Technology, Stockholm, Sweden, 1952.
- 11 "Tubular Air Heater Performance and Corrosion Problems," by Paul Koch. Presented by Applied Mechanics and Heat Transfer Divisions of ASME Metropolitan Section, March 21, 1951.
- 12 "The Use of Preheated Air in Power Station Boilers," by G. G. Thurlow, The British Coal Utilization Research Association, January, 1951.
- 13 "Heat Transfer and Fluid Resistances in Ljungström Regenerative-Type Air Preheaters," by H. Karlsson and S. Holm, Trans. ASME, vol. 65, 1943, pp. 61-72.
- 14 "Operation and Maintenance of Air Preheaters to Avoid Deposit and Corrosion," by Joseph Waitkus, unpublished ASME paper, 1942 (copy filed in Engineering Societies Library).
- 15 "Korrosionsursachen bei Luft-vorwärmen," by W. Gumz, *Archiv für Warmwirtschaft*, vol. 16, 1935, pp. 149-150.

Discussion

J. F. BARKLEY.⁴ The authors mention co-operative work of The Air Preheater Corporation and the Bureau of Mines, on corrosion and deposits in regenerative air preheaters. The first report of this work is now about complete, but the printing will require some months. Relative corrosion rates of some 65 different types of materials were determined, with some rather surprising results. Studies were made of the different types of deposits accumulating on different materials. From traces to substantial amounts of more than 30 elements were found as constituents of the deposits, including such elements as lithium, gallium, germanium, and thallium. All of the deposits had three predominant characteristics—partial solubility in water, presence of sulphates, and acidity.

In the build-up or accumulation of deposits on an air-preheater plate, both physical and chemical actions were found to be involved. A heterogeneous mass of gases and entrained solids sweeps past the plate, the gases including CO₂, O₂, N₂, H₂O vapor, SO₂, and a little SO₃. The solids, from submicron up to relatively large size, of many shapes, forms, and specific gravities, hard and soft, include a great variety of chemical formations of elements from the fuel and the air. The compounds formed include silicates, oxides, and sulphates; there is often carbon as smoke or

⁴ Chief, Fuels Utilization Branch, Bureau of Mines, U. S. Department of the Interior, Washington, D. C. Fellow ASME.

soot. The ordinary proximate analysis of this dust or "fly ash" will generally show some combustible material. A complete analysis usually will show carbon, hydrogen, nitrogen, silica, aluminum, iron, calcium, magnesium, sodium, potassium, sulphur, and traces or more of a great number of other elements. Analyses of the dust will vary with the fuel used, as well as with the general burning conditions involved in its creation. As the solids sweep past the plate, there is a sandblasting effect by some of the particles, particularly of the harder and larger sizes. This hastens removal of any iron oxide from a new plate, thus exposing the metal. The smallest particles in the gases get enmeshed and are held on the surface of the plate owing to its lack of perfect smoothness. More particles bump, scour, and get trapped, with a varying net result as to thickness of deposit formed. As the air preheater revolves, the plate is then swept with air carrying some water vapor.

Along with these physical happenings, there is continuous and important chemical activity. It is this chemical activity that causes the deposits to be much thicker near the colder areas of the plate than near the hotter. Chemical activity ordinarily is conceived and explained as action that shows immediate or relatively quick results, particularly under optimum conditions. In the case of the chemical activity under consideration, however, optimum conditions, or conditions ordinarily considered to be required, do not necessarily exist. Instead, long-time periods, as weeks and months, and relatively enormous quantities of materials are involved. In the flowing stream of gases and dust the molecules of SO_2 , SO_3 , H_2O , and O_2 gases collide with, adhere to, become enmeshed in, and are bumped away from the solid particles—which include soot, a particularly good absorbent—the heater plate, and themselves. Under optimum temperature conditions, below the boiling point of water, simple chemistry shows that such substances form sulphuric acid, H_2SO_4 , a stable end point of the reactions occurring. If a metal such as iron is added to this system, iron sulphate becomes essentially a stable end point.

Under our present conception of the nature of matter, chemical reactions ending with sulphates are considered to be in process to some extent in the mass of gases and dusts at temperatures well above the "dew point" of the gases. As the temperature drops toward the dew point the extent of the reactions increases. Considerable iron and small amounts of other metals are supplied by coal. The ordinary air-preheater plate not only supplies more iron but also a resting place or trap for a build-up of deposits in the path of great quantities of gases and dusts for long periods of time, really great multiplying factors.

We find, then, a deposit having some dust material, such as silicates, oxides, and soot, and also sulphates of various metals. The water solutions of nearly all of these sulphates are acidic. The over-all net result is an acid attack on the plate that eventually will destroy it, if it will react at all with sulphuric acid.

Choice of plate material ranging from material that readily reacts with acid to one of the nonmetallic type, such as certain ceramic or glasslike materials that are not measurably affected, is an economic problem involving initial and maintenance costs.

WILHELM GUMZ.⁵ This is an extremely interesting and informative paper and the authors are to be congratulated for their many constructive ideas. Particularly, the writer favors the engineering approach that we have to face continuous decrease of fuel quality, and that we should think of methods to live with it.

The statement that the effect of air preheating on combustion has "not always been placed in the proper perspective," should be underlined. That is certainly true for the problem of SO_3 formation. Also, more emphasis should be placed on proper methods of

operation at low rates and of starting cold boilers. Methods of warming up preheaters before starting the furnace would be highly gratifying.

In the discussion of deposits and the formation of these "sticky films," the question arises what comes first, the deposition and bondage of solids to the surface or a deposition of a film of condensing moisture? The writer is inclined to believe that perhaps a very thin layer of solids comes first, a precipitation of moisture next and, if this happens, a more rapid build-up of deposits resulting in clogging and corrosion may occur. The initial stage is similar to the soiling of cold surfaces in ordinary air by thermophilic diffusion, but it is harmless as long as moisture does not come into play.

With respect to the thermodynamics of SO_3 formation, it is perhaps more impressive to show the result in a graph⁶ rather than in an equation, Fig. 14 of this discussion. We are particu-

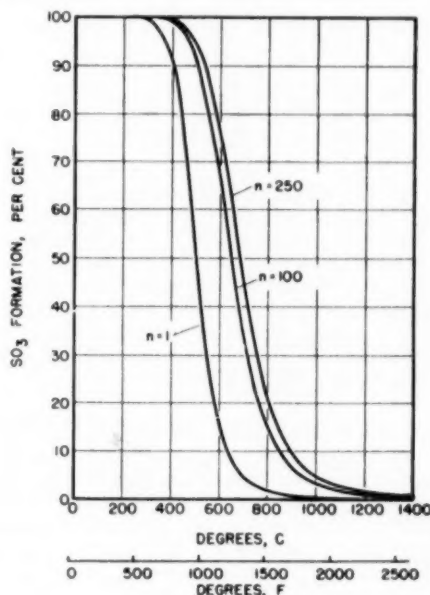


FIG. 14

larly interested in the bottom zone of these curves which indicates that the danger is highest at low temperatures and high excess oxygen, and naturally at high sulphur content of the fuel. In addition, as has been stated, the presence of soot is quite detrimental. All this, however, represents the conditions which we find in starting a cold boiler furnace. The raising of the dew point by soot is little relief because the SO_3 is not taken out of the system but only shifted from one place to another, making the deposits more corrosive.

A variety of possibilities have been shown by the authors how we can operate an air preheater safely even if we approach the danger zone. In connection with stoker-fired boilers, the writer would emphasize the advantage of resorting to flue-gas recirculation. With oil-fired boilers, especially if it comes to the use of low-grade or high-sulphur vanadium-bearing fuel oils, it is believed that the Combiflow is definitely promising.

As an alternative solution a modification of the Combiflow is suggested which may be termed a "two-preheater Combiflow."

⁵ Consultant, Battelle Memorial Institute, Columbus, Ohio. Mem. ASME.

⁶ "Kurztes Handbuch der Brennstoff- und Feuerungstechnik," by W. Gumz, second edition, Berlin-Göttingen-Heidelberg, Springer-Verlag, 1952, p. 283.

Fig. 15 of this discussion shows the principle schematically with gas and air temperatures as a sample of the possible layout. It is essentially an arrangement of one preheater in countercurrent flow and a second one in parallel flow. By rough calculation, it

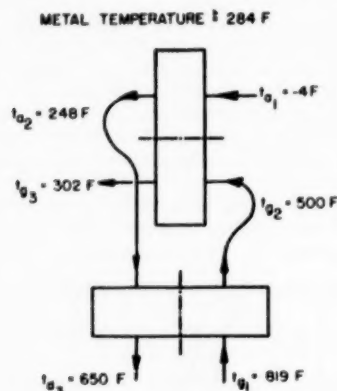


FIG. 15

has been found that with -4 F air-inlet temperature—to select very rough conditions—and 650 F hot-air temperature, an intermediate temperature of about 250 F would be most suitable. With this layout we are able to cool the flue gases to 300 F without falling below a metal temperature of 248 F in any part of the installation. This solution encourages us to investigate the possibilities of pushing the gas exit temperatures even farther down, as has been the general trend throughout recent years. The result is shown in Table 4 of this discussion.

TABLE 4 RESULTS OF LOWERING GAS EXIT TEMPERATURE

Flow pattern	Gas exit temp, deg F	Min metal temp, deg F	Relative surface required ^a	Fuels
Countercurrent	300	149	1	Unsafe for all fuels
Two-preheater Combiflow	300	248	1.123	Fuel oil, 4% S
Two-preheater Combiflow	284	234	1.249	Fuel oil, 3% S
Two-preheater Combiflow	266	217	1.520	Fuel oil, 2% S
Two-preheater Combiflow	248	199	1.707	Fuel oil, 2% S no V_2O_5
Two-preheater Combiflow	230	185	2.017	Midwest pulv coal
Two-preheater Combiflow	212	167	2.482	Eastern pulv coal

^a As compared to countercurrent heat exchange.

With a good fuel oil, for example, one with no more than 2 per cent sulphur and no or little vanadium content, we could go as far down as 250 F gas exit temperature with a lowest metal temperature of about 200 F; and with a fuel oil of lower grade, up to 5 per cent sulphur and with vanadium-bearing ash we still could reach the 300 F mark safely and not fall below 248 F metal temperature. Such temperatures as listed in Table 4 are still justified economically in most cases, depending upon the load factor, if they can be reached without causing operating trouble.

The authors briefly mention a new type of heating-surface design which requires smaller surfaces, lower weights, and hence shorter gas and air passages. With such a heating surface, it should be easy to furnish the required larger surfaces to increase boiler efficiencies with no sacrifice to safe operation and to continuous boiler availability. The writer believes that the power industry is waiting for such improvements at this time where building activity is at a peak.

S. I. JUHASZ.⁷ This paper is a valuable contribution to the literature dealing with flue-gas deposits and corrosion in the low-temperature zone. It treats the problem with emphasis on the metal temperature at the cold end.

As is well known, neither deposit nor corrosion occurs if the following condition prevails in the air preheater

$$\Delta T = T_m - T_d > 0$$

where

T_m = coldest metal temperature at flue-gas exit side

T_d = dew point of flue gas at point where it is in contact with metal surface

ΔT = temperature difference defined by foregoing equation

This equation suggests the importance of a lowered acid dew point or lowered SO_3 content to insure a positive value of ΔT .

According to Harlow, SO_3 is formed from SO_2 on the surface of the superheater and the rate of formation is high if the following conditions exist simultaneously:

- If the flue gas has a high SO_2 concentration.
- If temperature of the surface metal of the superheater is high.
- If the surface has lost its "immunity" because of having changed to Fe_2O_3 , which acts as a catalyst.

As pointed out by the writer at the 1950 International Air Preheater Conference,⁸ the requirement that these three conditions must prevail simultaneously can be used to eliminate SO_3 formation on the superheater. Let us suppose that a steam boiler has to use as basic fuel a high-sulphur residual fuel oil and that the steam temperature is high. In this case the boiler can be designed with two superheaters. The primary superheater is placed in the steam generator and is fired with the high-sulphur residual fuel oil, and the secondary superheating is carried out in a separate superheater which is fired with fuel oil or gas containing little sulphur. As the order of magnitude of heat added to the secondary furnace is less than about 10 per cent, the price of the additional fuel is of minor importance.

The dew point can vary considerably and the laws governing its variation are not exactly known. Because of its critical nature it is the view of the writer that it should be measured in all large boilers. An electric, manual, dew-point meter based upon the principle of H. F. Johnstone⁹ and later improved at the British Coal Utilization Research Association¹⁰ has been found satisfactory for the purpose.

The authors show an excellent way to measure the surface metal temperature in a Ljungström air preheater. It would seem that this method of measurement is at a stage where it could be used not only for pilot plant but also for commercial use.

The authors indicate the various methods that can be used for raising the metal temperature at the flue-gas exit and including the Combiflow method. It might be of interest to describe briefly the evolution of the Combiflow idea.

Let us consider an ordinary air preheater working with counterflow, in which the air and flue-gas entrance temperatures and flow rates are fixed. No restriction is made as to whether the preheater is of the recuperative or Ljungström type.

As is well known, counterflow gives the highest heat recovery or

⁷ Fuels Research Laboratory, Massachusetts Institute of Technology, Cambridge, Mass. Mem ASME.

⁸ "Flue Gas Troubles and Their Remedies," by S. I. Juhasz, International Air Preheater Conference, Stockholm, Sweden, 1950.

⁹ "An Electrical Dew Point Method for the Determination of the Dew Point of Flue Gases," by H. F. Johnstone, University of Illinois Bulletin 27, 1929.

¹⁰ "Developments in the BCURA Dew Point Meter," by P. F. Corbett, D. Flint, and R. F. Littlejohn, *Journal of the Institute of Fuel*, vol. 25, November, 1952, 245-252.

temperature efficiency but it also results in a low metal surface temperature at the cold end. If the flow is changed from counterflow to parallel flow without altering any other conditions, Fig. 16, herewith, the metal surface temperature at the cold end will be increased but also the exit flue-gas temperature, with the result that the efficiency of the steam generator is reduced. If low metal temperature is considered as a cause of "metal consumption" the foregoing conclusion also can be stated in the following way: Counterflow gives low fuel consumption but high metal consumption and parallel flow gives no metal consumption but high fuel consumption. However, parallel flow increases the metal temperature to a value higher than is necessary, for which we have to pay with high fuel consumption.

This led to the idea that a compromise between parallel and counterflow should be adopted. The design of the Ljungström air preheater is favorable from the point of view of such a compromise. For Combiflow the Ljungström is divided into three sections instead of the usual two. Through the first section passes the flue gas, through the second the counterflow air, and through

the third the parallel flow air. The temperature curves derived analytically are shown in Fig. 16. It can be seen that all the temperatures for Combiflow lie between the respective values for parallel and counterflow. A picture of the Combiflow model is shown in Fig. 17 of this discussion.

The metal temperature can be increased in different ways, but irrespective of which method is used the net boiler output is decreased. The paper shows in Fig. 11 the "relative reduction of net boiler output" as a function of increase in metal temperature. In the range of 0-60 F "metal temperature increase" the Combiflow and hot-air recirculation are about equal and give rise to the smallest reduction in net boiler output. Above 60 F Combiflow gives the lowest relative reduction of net boiler output. Owing to this characteristic of Combiflow the latter could be used for insuring that the ΔT remain positive in a case in which it might have been negative either owing to high dew point or low metal temperature.

The writer wishes to congratulate the authors for their interesting paper.

PAUL KOCH.¹¹ The authors have performed a real service to both designers and operators in bringing out and discussing the pertinent points concerning the difficult problems of preheater fouling and corrosion.

The mechanisms behind this corrosion and fouling certainly are complicated and not very conclusive. The discussion on the effect of carbon in the fly ash and flue gases on corrosion and fouling is of interest and we are wondering how important a factor it is. We know that spreader-stoker units have higher percentages of carbon in the fly ash and less trouble with corrosion and fouling than underfeed-stoker units firing the same fuel. However, regardless of the effect on preheater corrosion and fouling, it is always important to have good combustion with a minimum of carbon in the fly ash in order to have the highest efficiency and lowest fuel cost.

Fouling and corrosion have been considerably reduced on several oil-fired units by adding dolomite to the fuel oil in the proportion of approximately one part of dolomite to one part ash. Since the percentage of ash in the fuel oil is small, the cost of the dolomite is relatively low, in the order of $\frac{1}{4}$ of 1 per cent of the fuel cost. Experience with additives, however, is quite limited at this time, but there is every indication that they may be of considerable help in solving our fouling and corrosion problems.

Since corrosion and fouling depend on metal temperatures, the determination of the minimum metal temperature becomes important. On the regenerative heater the metal temperature is determined by averaging the cold-end air and gas temperatures. It is reassuring to note that the test data obtained by The Detroit Edison Company show the actual metal temperature a good 20 deg F higher than the average.

With reference to Fig. 8 of the paper, it is very difficult to compare metal temperatures of a regenerative and recuperative or tubular heater. It is true that many tubular heaters are in operation today having minimum metal temperatures far below the average of the air entering and gas leaving the heater. However, because of the corrosion and fouling problems encountered today, particular attention is given to the design of the tubular heaters to obtain high metal temperatures. This is done by increasing the gas-mass flow, reducing the air-mass flow at the air entrance to the heater and arranging the air ducts to the heater to obtain the desired air distribution entering the heater, adding directional vanes and distributors when necessary. It is preferable, of course, to have the lowest air-mass flow at the cold end of the tubes.

The limiting metal temperatures given in Fig. 4 and Table I

¹¹ The Babcock & Wilcox Company, New York, N. Y.

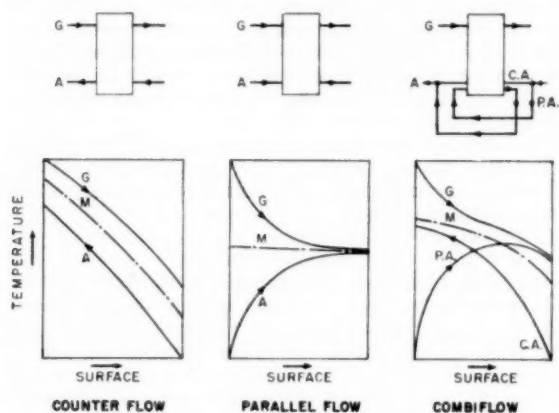


FIG. 16 TEMPERATURE CURVES FOR COUNTERFLOW, PARALLEL FLOW, AND COMBIFLOW

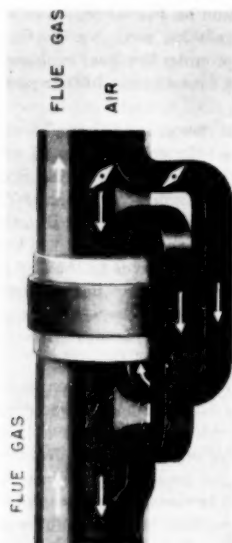


FIG. 17 MODEL OF LJUNGSTRÖM-COMBIFLOW AIR PREHEATER (Swedish Patent.)

TABLE 5 ACTUAL DEW POINTS WHEN FIRING REFINERY GAS AND ACID FUELS—JUNE, 1950

ALL REFINERY GAS ON BOILER							
Grains H_2S per cu ft	Btu per cu ft	Density	Deg F	H_2SO_4 found, Ppm	H_2SO_4 by vol. wet, per cent	Dew point, deg F	Flue gas
4.80	920	0.85	98	220	.00066	185	Clean
2.20	930	0.878		160	.00028	159	Clean
3.56	1090	0.875		130	.00038	164	Clean
4.20	1100	0.86		160	.00048	172	Clean
2.85	1098	0.875	100	150	.00043	169	Clean
		Time 1:30		530		239	Not clean
		1:50		130		164	Clean
		Time 8:50		720		264	Not clean
		9:50		210		183	Clean
ACID SLAG AND NATURAL GAS ON BOILER							
No. burners	Natural gas, per cent	H_2SO_4 found, ppm	Dew point, deg F	Flue gas			
10	37.0	1670	317	Not clean			
10	36.7	640	255	Clean			
10		2900	341	Not clean			
10	52.8	1100	295	Not clean			
10	51.0	570	245	Clean			

of the paper are in fair agreement with our limiting temperatures for tubular air heaters. There is some evidence that the minimum metal temperature should be higher for some of the fuel oils, particularly with high vanadium content.

We are in agreement with the authors' suggestions and recommendations of selecting the air heaters and means of metal temperature control for the expected fuel and load range so as to satisfy the safe minimum metal temperature, providing superheated steam or dry compressed-air soot blowers, considering water washing, and using Cor-Ten when excessive steel corrosion is expected.

R. J. ROBERTSON¹² AND W. B. GURNEY¹³ The authors are to be commended for their thorough presentation of the air preheater, its problems, and solutions to these problems.

Table 5 of this discussion shows the marked increase in "sulphuric-acid dew point" of soot-bearing or unclean flue gases that has been experienced because of improper combustion conditions in the furnace. To eliminate this soot requires more excess air in the furnace; but more excess air increases the SO_2/SO_3 ratio. Higher air temperature to the furnace increases the furnace temperature and thus in turn allows less excess air, better combustion conditions without soot, and lower SO_2/SO_3 ratios.

Higher air temperatures to the furnace are surprisingly effective in protecting air preheaters where high-moisture and/or high-sulphur fuels are burned. We have found no measurable increase in SO_3 over that found at the inlet to the superheater.

Analyses of the ash of the fuel burned is very informative. Our acid fuel contains 8 per cent sulphur and approximately 1 per cent ash of which 80 per cent is iron. Refinery gas, on the other hand, contains less than 0.5 per cent sulphur from hydrogen sulphide and practically no ash. Although the dew point of the acid fuel is considerably higher than that of the refinery gas, its corrosive action on preheater plates is less severe. The ferrous-sulphate film formed on the preheater plate of the acid-fuel-fired boilers acts as a protective film and, although it is hard to scrape off, it is easily washed off, especially if the surface is precoated with lime. On the other hand, the plates of the preheater fired with refinery gas became coated with a form of ferric oxide which is extremely difficult to remove except by sandblasting or with high-pressure high-temperature water jets. Precoating the surfaces with lime practically eliminates this corrosion.

Laboratory studies on iron in 70 per cent sulphuric acid at 250 F disclosed that the rate of corrosion of the iron is enormously reduced (in the order of 100/1) if ferrous sulphate or preheater deposit is present.

¹² Superintendent, Louisiana Station, Gulf States Utilities Company, Baton Rouge, La. Mem. ASME.

¹³ Gulf States Utilities Company.

Washing preheaters under load resulted in rapid corrosion of the plates due to the hot dilute-acid attack of the steel. Minimum corrosion is experienced when the preheater plates are cold and washed with voluminous amounts of cold water followed by coating the metal with dilute lime solution. Lime is preferred because the inert film of calcium sulphate is formed whereas if soda ash or caustic is used, the corrosive film of sodium hydrogen sulphate results.

Not until we were able to determine the sulphuric-acid dew point of the flue gases accurately were we able to get some idea as to what was taking place, what protection was needed, and the effect of firing conditions.

AUTHORS' CLOSURE

Mr. Barkley's comments are pertinent and constitute a valuable addition to the paper. The publication of the report covering the co-operative work of the Air Preheater Corporation and the U. S. Bureau of Mines will furnish additional valuable information on the subject of materials most suitable for low-temperature corrosion applications and the nature and formation of deposits on low-temperature heat-exchanger surface in the power-plant field.

We are indebted to Dr. Gumz for his kind words as well as his simplified presentation on the formation of SO_3 at various temperatures. The suggestion made by Dr. Gumz of combining a parallel flow with a counterflow heat exchanger has considerable merit and should be investigated further as to its practical possibilities.

The importance of dew point as brought out by Dr. Juhasz undoubtedly cannot be fully emphasized and we commend him for his unique solution to the problem of raising the metal temperature at the cold end of a heat exchanger. This suggestion we feel is worthy of further investigation in order to determine its practical adaptability to the power plant of today.

The use of Dolomite additives to the fuel in oil-fired units, as reported by Mr. Koch, is interesting and seems a practical approach to the problem and we hope further experience with this will prove equally encouraging as the results thus far obtained and reported.

The suggestion by Messrs. Robertson and Gurney that high temperature of the combustion air be utilized to reduce air-heater problems is pertinent and the authors are in complete agreement with them on this. The information they have presented concerning the protection obtained by ferrous-sulphate films as compared to ferric-oxide is much appreciated.

The authors appreciate the contributions by all who commented on our paper; these have enhanced its value as a reference in this field.

Tubular Air-Heater Problems

By E. F. ROTHMICH¹ AND G. PARMAKIAN,² WORCESTER, MASS.

This paper discusses the occurrence of air-heater deposits, their effect on performance, maintenance, and design. Actual operating experiences and a survey of a large number of installed tubular air heaters are given to show the extent of the air-heater problems being encountered by steam-generating units fired with pulverized coal, stoker, natural gas, and oil. Suggestions are offered as to methods for minimizing these difficulties by design and operation.

INTRODUCTION

AN investigation of the problems being experienced with tubular air heaters was prompted by an increase in the number of reports of plugging and corrosion of air-heater tubes. High sulphur content in residual fuel oils, as a result of changes in refinery methods and in source of crude oil, was felt to be the main cause for the increase in air-heater difficulties. Introduction of outdoor installations with low ambient-air temperatures also has imposed severe operating conditions which have resulted in increased plugging and corrosion.

A survey of a large number of tubular air-heater installations was made and the data analyzed. The results are discussed in this paper. It is surprising to note that a large percentage of coal-fired installations had experienced difficulty with plugging and corrosion. A maintenance problem on air heaters of steam-generating units fired by natural gas is also worthy of consideration.

OCCURRENCE OF DEPOSITS IN CORROSION

The chemistry of the formation of deposits in the cold end of heaters when burning fuels containing sulphur has been studied and discussed by various investigators.^{3,4} Stated very simply, sulphur dioxide formed in normal combustion of sulphur is oxidized to sulphur trioxide at the proper temperature for the change in the presence of a catalyst such as iron oxide which occurs on boiler and superheater tubes. The presence of sulphur trioxide in the products of combustion elevates the dew point of the gases. Water vapor condenses and forms an acid with the sulphur trioxide and the corrosion of the tube results in iron sulphate. This deposit accelerates the corrosion process by elevating the dew point further. Corrosion and plugging seldom occur during the first year or so of operation, and it often takes 5 to 6 years before corrosion of tubes progresses far enough to require replacements.

Arrangement of heating surfaces of tubular heaters may vary from a single air and gas pass to multiple passes on either or both

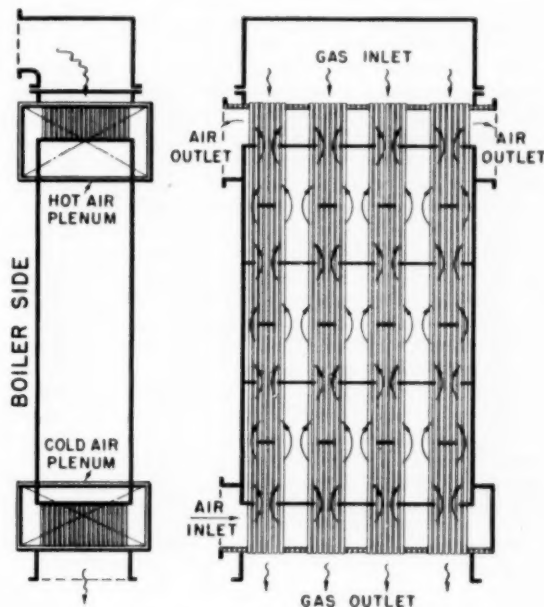


FIG. 1 TYPICAL TUBULAR-AIR-HEATER DESIGN

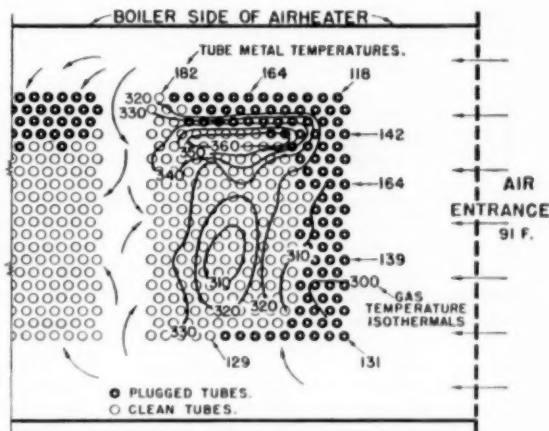


FIG. 2 COLD-END TEMPERATURE CONDITIONS

air and gas sides with either basic counterflow or parallel-flow heat transfer. Fig. 1 shows a conventional heater design arranged for counterflow of gas and air with one gas and one air pass. Uniform air distribution to and from the tube bundles is obtained by the use of large plenum chambers. Air can enter or leave this design of heater from either or both sides.

Fig. 2 shows the location of plugged tubes on one bundle of this heater in an installation where the fuel fired was oil with high sulphur content and where serious plugging and corrosion were encountered. It will be noted that the plugged tubes are at the

¹ Assistant Chief Service Engineer, Riley Stoker Corporation. Mem. ASME.

² Mechanical Engineer, Riley Stoker Corporation. Mem. ASME.
³ "The Corrosion of Power Plant Equipment by Flue Gases," University of Illinois Bulletin No. 228, vol. 28, no. 41, June 9, 1941.

⁴ "Causes of Flue-Gas Deposits and Corrosion in Modern Boiler Plants," by W. F. Harlow, Proceedings of The Institution of Mechanical Engineers, London, England, vol. 160, 1949, pp. 359-368.

Contributed by the Fuels, Power, and Machine Design Divisions and the Research Committee on Low Temperature Flue Gas Corrosion and Deposits and presented at the Annual Meeting, New York, N. Y., November 30-December 5, 1952, of THE AMERICAN SOCIETY OF MECHANICAL ENGINEERS.

NOTE: Statements and opinions advanced in papers are to be understood as individual expressions of their authors and not those of the Society. Manuscript received at ASME Headquarters, October 27, 1952. Paper No. 52-A-124.

periphery of the tube bundle where the impact of lowest-temperature air produces the greatest chilling effect. The plugging is more severe on the boiler side of the heater as a result of uneven gas flow through the tubes.

This pattern of corrosion has been observed on many heater designs, regardless of the type of fuel burned. In general, corrosion and plugging are isolated in the cold end of the heater tubes and seldom extend beyond the region of the cold-air plenum chamber. The results of the survey indicated that the rows of tubes which may plug and corrode may be the first row only but can extend as far back as the eighth row. The average corrosion penetration into the bundle was three rows.

Fig. 2 has been marked to show the location of isothermal lines of gas temperature leaving the heater and metal temperature of individual tubes as measured by thermocouples. The tube-metal temperature is the only true criterion of corrosion and for a particular tube it is determined by the cleanliness of tube wall, temperature levels, and flow intensities on gas and air sides. These combined factors greatly influence the tube-metal temperature of individual tubes in each row shown in Fig. 2. Once a deposit has formed the value of these factors will change, resulting in a lower metal-temperature level and increased corrosion.

Generally, it is considered that the tube-metal temperature is the arithmetic average of the air temperature entering the heater and the gas temperature leaving the heater. This would require a constant cleanliness factor of tubes and equal gas and air-film conductances. These conditions seldom are found in actual practice as indicated by Fig. 3 which compares the actual measured

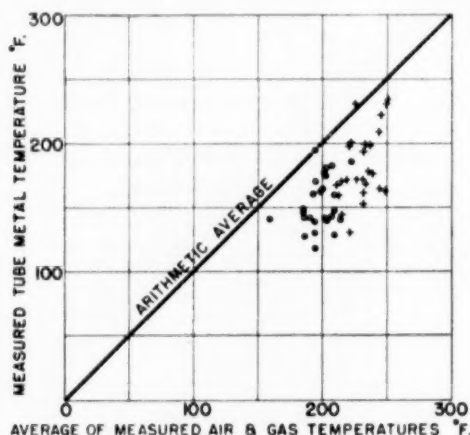


FIG. 3 METAL TEMPERATURE VARIATION AS MEASURED BY THERMOCOUPLES

tube-metal temperature with the average of air temperature entering and gas temperature leaving the heater. In some cases the actual measured tube-metal temperature was 120 F below the mean of the air and gas temperature. The closest that this tube-metal temperature approached the mean temperature was 10 F. Tests conducted with gas-temperature measurement leaving the individual tubes indicated that a difference in mass flow of air and gas could account for an 80 deg F difference in tube-metal temperature where the same mean of gas and air temperature existed.

A number of curves have been plotted by various sources to indicate the safe metal temperature for various concentrations of sulphur in the fuel and for various types of fuels. Other curves include the effect of the percentage of excess air. Some of these curves are based on the theoretical dew-point temperatures, but it

has been shown that very minute quantities of sulphur trioxide can produce wide variations in the dew-point temperatures. It has been reported that a change of 0.001 per cent in the concentration of sulphur trioxide is sufficient to change the dew-point of the flue gas by 40 F.⁵ Because sulphur trioxide is the basic source of the corrosion process and because it is impossible to determine what proportion of sulphur in the fuel eventually will be transformed to sulphur trioxide, it is almost impossible to predict a safe value of tube-metal temperature for a given set of conditions.

A practical method for establishing the safe temperature for any particular installation is to make a survey of the temperature of the surfaces under conditions of light loads and to compare these with the extent of the plugging and corrosion observed. Thermocouples should be attached to tubes which are known to be subject to fouling and corrosion and to other tubes which are known to be clean. The metal temperature of the clean tubes under this light-load condition will indicate a safe temperature level. Somewhere between this temperature and the temperature of the tubes subject to plugging under the same conditions will be the minimum safe tube-metal temperature for this particular installation. This value must be arrived at by trial. It is then possible to take steps to maintain the coldest tubes above this minimum safe tube-metal temperature so that further plugging and corrosion can be either reduced or eliminated. In general, it has been found that very little corrosion occurs at tube-metal temperatures above 200 F, and that corrosion is very rapid when the tube-metal temperature falls below 150 F.

Air-heater deposits vary from soft soot to hard crystalline deposits which completely plug a tube and form stalactites below the air-heater tube sheet. The deposits are very hygroscopic so that once the deposit is formed, absorption of acid is rapid and metal attack pyramids because of the increased insulating effect of the deposit. Table I shows that there is no great disparity in deposit analyses when reduced to iron and sulphur constituents.

TABLE I TYPICAL ANALYSES OF AIR-HEATER DEPOSITS REDUCED TO IRON AND SULPHUR CONSTITUENTS

Fuel type	Percent ^a		
	Fe	S	SO ₃
Tar	27.6	16.1	40.2
Oil	30.6	18.5	46.1
Oil	8.3	12.5	31.2
Coal	28.1	16.0	40.0
Refinery waste fuels	32.1	21.2	53.0
Oil	17.3	17.3	43.1
Oil	18.5	18.5	46.1
Oil	13.6	13.6	33.9
Oil	17.4	17.4	43.5

^a Percentages are on weight basis.

This indicates that the corrosion products formed can be considered independent of the type of fuel fired. Fortunately, the deposits have high water solubilities and can be removed rather easily by hot-water flushing. In a great number of natural-gas-fired installations, corrosion occurs without the presence of deposits. The sulphur content of this fuel is very low and corrosion occurs at metal-temperature levels found to be safe for oil and coal-fired units.

Various methods are available for maintaining a safe tube-metal temperature. These are the use of the cold-air by-pass around the heater, recirculation of hot air to the inlet of the forced-draft fan and steam-air heaters to preheat the air prior to its entrance to the heater. The limitations and advantages of these various arrangements have been discussed elsewhere.⁶

⁵ "Tubular Air-Heater Performance and Corrosion Problems," by P. H. Koch, contributed by the Applied Mechanics and Heat Transfer Divisions and presented at the Metropolitan Section Meeting, March 21, 1951, New York, N. Y., of THE AMERICAN SOCIETY OF MECHANICAL ENGINEERS.

The survey indicated that the use of recirculated air is the most effective method for preventing corrosion and deposits.

EFFECT OF DEPOSITS AND CORROSION ON MAINTENANCE

Air heaters on a large number of oil-fired units were cleaned every 3 months, whereas the maximum period between cleaning of heaters for oil-fired boilers was 1 year, and the average $5\frac{1}{2}$ months. Of the pulverized-coal-fired installations reporting in the survey, 20 per cent indicated that no cleaning of air heaters was necessary, 44 per cent reported that they cleaned once per year, and the average period between cleanings was $7\frac{1}{2}$ months. The natural-gas-fired installations reported that tubes were cleaned yearly or required no cleaning whatsoever.

The time required to clean air heaters varied from 8 man-hours minimum to 160 man-hours maximum, depending upon the type of deposits, method of cleaning, and the size of the heater. Turbine cutters were a very popular method of cleaning, probably because it was a familiar tool to the power-plant operators. However, it appeared that the best method for cleaning crystalline-type deposits was by washing with hot water, and if the tube was plugged completely, to allow it to remain full of water for a period of time to soften the deposits. This washing should be followed as soon as possible by a drying operation, preferably by returning the unit to service so that heat is applied. The arrangement of air heater, hoppers, ducts, and fans will determine whether water-washing is possible.

Some plants have reported cleaning heaters with solid material, while units were in service. One plant operating a 150,000-lb per hr boiler, burning waste refinery fuels, uses 200 lb of No. 3 sand-blast sand, once per week, injected by compressed air into the flue-gas stream at the inlet to the tubes. The sand drops out of the gas stream into an ash hopper at the outlet end of the heater. This method of cleaning practically has eliminated plugging of heater tubes and has reduced the time of semiannual cleaning from 7 man-days to 2 man-days. Another plant operating a 175,000-lb per hr boiler, burning bunker C fuel oil, has found that injection of 200 lb of $\frac{3}{8}$ -in. crushed rock once per week at either side of the gas entrance to the heater practically has eliminated tube fouling. The crushed stone is collected in the dust collector and discarded because of its low price, \$1.38 per ton. By starting with a clean heater and keeping it clean, corrosion and plugging usually can be prevented.

Air-lancing of the air heater with the unit in service also was practiced at one installation fired by coal and appeared to be very effective. The use of intermittent firing by pulverized coal on installations that were designed for both coal and oil-firing was not found generally to be a successful method for cleaning deposits laid down during oil-firing. The most successful user of this method of cleaning operates the pulverizer 1 hr per day every day. Another plant reported that 2 weeks' firing with pulverized coal was required following oil-firing to clean the heater. Naturally, this type of cleaning will be most effective when the fly ash passing through the heater is of a coarse nature.

Coating of air-heater tubes with a lime slurry following the heater washing proved a retardant to corrosion in some installations, but in others no improvement was noticed. Control of humidity of air had been tried, but without effect on the reduction of heater plugging or corrosion. Improvement of gas and air distribution to the heaters resulted in reduced plugging and corrosion, but did not effect complete elimination of the difficulty.

Fig. 4 indicates a method of repair for corroded air-heater tubes which has been very successful for a number of years. This method requires only the replacement of short ends of the tubes in the cold-end section of the heater. This not only has the advantage of requiring a small quantity of tubing, but the short

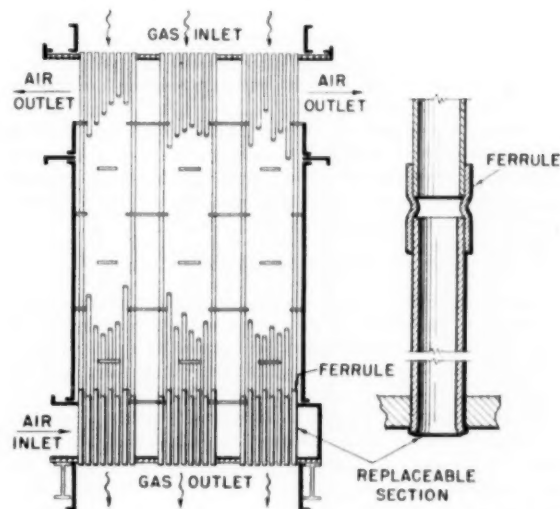


FIG. 4 ARRANGEMENT OF FERRULES AND REPLACED TUBE SECTIONS

pieces used are convenient to handle and are readily installed. Replacement of the entire length of long air-heater tubes not only requires the removal of considerable air-heater casing, but also often requires serious alterations to the building unless suitable access is provided in the building roof or basement level. Since corrosion is concentrated in the cold end of the air heater, it is logical that only the cold end would be replaced. As previously mentioned, plugging and corrosion occur in a few outside rows of tubes in each bundle where the air first enters, making these tubes accessible for this type of repair. It is possible to install heavier-gage tubing using this method of repair and this increases the life of the replacement parts. Of the plants participating in the survey, 66 per cent reported use of this type of repair with no criticism of the method.

Another method of repair consisted of inserting a section of smaller-diameter tube inside the corroded section of tubing and extending it through the corroded section to a section of sound tubing. However, once the deposits have occurred in the original tubes it becomes practically impossible to insert the smaller-diameter tubes. An emergency method used by some plants consists of capping off the corroded tubes to permit a quick repair and early return to service. Some repairs also have been made by replacing the corroded ends of the tube with new sections of tubing welded to the original tube. This method has been used especially where failure of the tube occurred at a considerable distance above the cold-air box. The tube is cut and dropped into the cold-air box to a point where it is convenient to attach a new section by welding. The repaired tube is then set in place and rerolled. Of all these methods, the use of short lengths of tubes and ferrules has proved to be the most effective, quickest, and the most economical.

EFFECT OF DEPOSITS ON PERFORMANCE

The occurrence of deposits on air-heater tubes reduces the heat transfer, resulting in higher exit-gas temperature and lower unit efficiency. Deposits increase the draft loss through the heater and can get to the point where the capacity of the steam-generating unit is limited by the draft loss through this heat-recovery equipment. In one spreader-stoker-fired installation, where the dust collector is installed ahead of the air heater, the plugging of air-heater tubes was so pronounced that it was necessary to steam-

lance the heater tubes daily to obtain satisfactory performance. A large number of oil-fired units have their availability limited by the period between heater cleanings. In some instances the duration of the boiler outage is dependent upon the length of time required to clean the heater.

These effects on performance are naturally variable, depending on load conditions, fuel, and operating procedures. However, their effects can be serious enough to justify substantial changes in equipment, method of operation, or fuel in order to improve performance and reduce maintenance.

FACTORS AFFECTING AIR-HEATER DESIGN

The design of any complex equipment is always a compromise. Although an air heater appears to be a relatively simple piece of heat-transfer equipment, it must be designed to handle the fuels available, cope with low entering-air temperatures, and meet the requirements of high unit efficiency and low auxiliary power. It is virtually impossible to design an air heater to satisfy completely all of these requirements. Hence the design of an air heater must be the joint responsibility of the equipment manufacturer, the consulting engineer, and the ultimate operator. Each must understand the problems involved, and arrive at a compromise which results in the best arrangement possible.

During the design stages, consideration should be given to the following methods for maintaining metal temperatures at the cold end of the air heater above minimum values which are known to cause corrosion: (a) Air by-passing; (b) air recirculation; (c) steam-air heater; (d) gas by-passing; (e) two-section air heater with short cold-end tubes; (f) air-heater ferrules; (g) parallel-flow air heater; (h) counterflow/parallel-flow air heater; (i) using highest air temperature possible; (j) selecting corrosion-resistant materials.

When the air by-passing method is used, a portion of the air from the forced-draft fan is diverted around the heater and discharged into the hot-air duct. This reduces the air-side film conductance by reducing the mass flow entering the cold end of the heater. Since a portion of the air is by-passed, the gas temperature is raised as a result of reduction of heat recovery, and this along with the reduced film conductance on the air side results in higher tube-metal temperature.

When air recirculation is used a portion of the hot air from the outlet of the air heater or the hot-air duct to the burners is returned to the inlet of the forced-draft fan to raise the temperature of the air entering the heater. The increase in metal temperature is obtained by the arbitrary increase in air temperature entering the heater. In general, this method of raising the tube-metal temperature will obtain the same effect as air by-passing with less loss in efficiency. Recirculation is very effective at light loads where there is sufficient fan capacity available for recirculation of considerable amounts of air. However, this method has limitations when it is necessary to recirculate at full load as may be the case for outdoor installations. The added fan capacity required can increase the size of the fan and its drive appreciably above that required for normal capacity operation of the boiler. The use of steam-air heaters ahead of the tubular heater overcomes this objection. A steam heater can result in a unit efficiency comparable with that obtained by air recirculation, depending on the source of steam supply. Some designs of steam heaters have a comparatively low draft loss so that they do not increase the required fan power appreciably. This type of protection to air heaters appears to be most ideally suited to the outdoor installation in cold climates where air temperatures entering the air heater fall to low values in winter.

Gas by-passing of heaters is usually resorted to only in the case of adverse fuels and where reduction in unit efficiency does not

result in any appreciable economic loss. It is necessary to isolate an air heater completely from gas flow with the by-pass in use; otherwise the stagnant gas in the heater tubes will be cooled by air passing over the heater and will result in rapid corrosion. Since it is difficult to isolate the gas side of an air heater completely from some gas flow this type of by-pass is not a preferred method for control of corrosion.

Although a two-section air heater is a more costly arrangement and requires more space and fan power, it is a popular method. This arrangement permits easy repair of corroded tubes which by design are consigned only to the short cold-end section of the heater. In like manner, the initial installation of short sections of tubes using air-heater ferrules is another method permitting easy maintenance of the heater.

Although a parallel-flow heater requires more heating surface for a given heat-transfer duty as compared to a counterflow heater, this compromise results in a higher tube-metal temperature and hence less corrosion and plugging. Often the seriousness of the corrosion and space considerations may justify the use of the less efficient parallel-flow heater. It is possible to provide a heater, combining counterflow and parallel-flow sections with proper ducts and dampers to obtain full counterflow at high loads and partial parallel flow at low loads to obtain the advantages of parallel flow at the cold end of an air heater. Such an arrangement, however, is rarely possible and is quite costly.

Use of hot air from the top of the boiler room, air from air-cooled walls, air from ducts adjacent to boiler settings or flue-gas ducts are other methods for raising tube-metal temperatures by increasing the air temperature entering the cold end of a heater.

Air heaters normally are constructed of low-carbon-steel tubing. Other materials have been tested in an attempt to find a material that will better withstand the corrosion action in air-heater tubing. Table 2 shows the results of a comparison of seven different materials tried in one heater that was experiencing severe corrosion difficulties. This was an oil-fired unit burning oil with $4\frac{1}{2}$ to $5\frac{1}{2}$ per cent sulphur. It was disappointing to find that none of the so-called corrosion-resistant materials was any better, or, in fact, as resistant as the normal low-carbon-steel tubing now used. Some resinous coatings have been tested with no apparent increase in corrosion resistance over bare tubes.

Fig. 5 shows an ordinary steel tube and an aluminum tube which had been placed in the breeching of a boiler for a period of 4 years. The metal temperatures averaged 150 F. Eastern bituminous coal with 1 per cent or less sulphur was burned on a single-retort underfeed stoker. As can be seen, the aluminum tube is a complete failure, whereas the ordinary low-carbon-steel tube has lost only half of its wall thickness. Experience with aluminum tubes on a pulverized-coal-fired installation burning low-volatile eastern bituminous coal with 2 to $2\frac{1}{2}$ per cent sulphur was similar and this installation returned to the use of steel tubes. The use of aluminum tubes was a complete failure in a refinery plant burning waste fuels.

A research program has been under way for over a year using glass tubing. Special designs have been worked out for sealing the ends of the glass tubes in normal steel air-heater tube sheets. No corrosion has occurred and the glass tubes have successfully withstood the abuses of vibration, expansion, and handling. Corrosion-resistant glass tubes can be located strategically in the critical outer rows of tube bundles and at the air entrance to heaters to prevent corrosion in these areas. Tests of this material and other metals and coatings are continuing.

Air-heater arrangements should be given careful consideration in regard to uniform air and gas distribution. Practical space limitations make this a most difficult problem and may require the use of spreader, turning, and deflecting vanes. Wherever

TABLE 2 TUBE MATERIALS INSTALLED AT COLD END NEAREST AIR INLET OF BOILER FIRED WITH 4.5 TO 5.5 PER CENT SULPHUR OIL FUEL

Item no.	Material	Date installed	Date inspected	50 per cent of full load		80 per cent of full load		Reported condition	
				Metal temp, deg F	Gas temp, deg F	Metal temp, deg F	Gas temp, deg F		
A	18-8 stainless steel	8/5/48	11/3/48	120	300	130	380	Corroded at rolled end	21 1/2 x 11 BWG
B	Brass	8/5/48	2/28/49	130	320	170	380	Complete failure	21 1/2 x 11 BWG
1	B&W Croloy no. 1 1/4	12/3/48	2/28/49	120	300	130	380	Very little corrosion*	21 1/2 x 13 BWG
2	B&W Croloy no. 5	12/3/48	2/28/49	125	310	145	370	Badly plugged—still in service	21 1/2 x 13 BWG
3	Alcoa 38-H14	12/3/48	2/28/49	170	315	170	375	No corrosion*	21 1/2 x 13 BWG
4	Alcoa 618-T6	12/3/48	2/28/49	130	320	160	380	Tubes plugged	21 1/2 x 13 BWG
5	Alcoa Alclad inside 38-H14	12/3/48	2/28/49	125	310	150	380	Slight corrosion*	21 1/2 x 13 BWG
								Partially plugged	

	18-8 Stainless	ANALYSIS OF MATERIAL			
		Croloy 1 1/4	Croloy 5	Alcoa 38-H14	Alcoa 618-T6
Zinc	0.08 max	0.15 max	0.15-0.20 max	0.10	0.20
Iron	2.0 max	0.30-0.60 max	0.50 max	0.70	0.70
Carbon	0.03 max	0.03 max	0.03 max		
Manganese	0.03 max	0.03 max	0.03 max	1.1-5.0	0.15
Sulphur	0.03 max	0.03 max	0.03 max		
Phosphorus	0.03 max	0.03 max	0.03 max		
Silicon	0.75 max	0.5-1.00	0.50 max	0.60	0.4-0.80
Chromium	18-20	1.1-3.0	4-6.0		0.15-0.35
Nickel	8-11				
Molybdenum		0.45-0.65	0.45-0.65		
Copper				0.20	0.15-0.40
Magnesium					0.8-1.2
Titanium					0.15
Aluminum				Remainder	Remainder

* Later inspection revealed excessive corrosion and materials were considered unsatisfactory for air-heater service.



FIG. 5 COMPARATIVE CORROSION RATE OF LOW-CARBON-STEEL AND ALUMINUM TUBES

possible, the unit should be arranged so that the heater can be washed conveniently and the wash water drained away if a corrosion problem is anticipated. Since the use of solid cleaning material has proved very effective for heaters in service, means should be provided for introducing this material into the entrance of the heater and removing it from the exit ahead of the induced-draft fan. Wherever possible, dust collectors ahead of heaters on coal-fired units should be avoided to prevent serious plugging of air heaters. If a choice is available the flue gas should leave an air heater in a downward direction to prevent condensate formed at the cold end from flowing the entire length of the tube.

This arrangement also permits water-soaking of tubes plugged at the cold end to soften and free the deposits.

CONCLUSION

Plugging and corrosion of tubular air heaters is widespread in every section of the country with all types of fuels and air-heater arrangements. To minimize corrosion the initial design of the unit should include some method for raising tube-metal temperature such as air by-passing, air recirculation, or other means. The operator should determine the safe tube-metal temperature for his particular installation by attaching thermocouples on the air-heater tubes and collecting temperature data during the normal operation. Once this minimum safe tube-metal temperature has been established for his particular unit the operator can maintain the coldest tube above this temperature by the method provided by the designer.

It is possible to clean air heaters in service, and more attention should be given to this phase of operation and design to maintain clean air-heater tubes. Once plugging has occurred it is possible to remove the deposits by the use of hot water, since these deposits are mostly water-soluble. When high-sulphur fuels are to be fired the designer should attempt to provide for water-washing of the air heater in the initial design.

In like manner, provisions should be made in design for the repair of corroded sections of the air-heater tubes, either by the use of short tube lengths and ferrules or by the use of a two-section air heater, if appreciable corrosion is anticipated.

If proper consideration is given to the design and operation of tubular air heaters the result would be a relatively low-cost heat-recovery apparatus which is effective, economical, and has excellent availability.

Discussion

H. KARLSSON.⁶ The authors' presentation of tubular-air-heater problems is very interesting and it is noted that the problems and remedies used are the same as those involved in the case

⁶ Technical Manager, Air Preheater Corporation, Wellsville, N. Y. Fellow ASME.

of regenerative-type air preheaters with the exception that the mechanics of maintenance are different.

The facts brought out by the authors with reference to experiments with different materials in the tubes of the low-temperature zone agree very well with the experience obtained in experimental work on regenerative-type air preheaters.

The use of glass for the cold-end portion of the tubular unit apparently shows promise not only from a corrosion viewpoint, which would be anticipated, but also from a mechanical viewpoint. It is hoped that this method will provide an economical means for overcoming some of the difficulties mentioned by the authors.

It is noted from Fig. 3 that measured tube-metal temperatures fall below the arithmetic average of air entering and gas leaving the unit. The information is not in accord with that obtained in the case of regenerative-type units.

The writer agrees with the authors' conclusion that by giving proper consideration to the design and operation, difficulties from low-temperature operation of air preheaters of units burning difficult fuels can be reduced, and believes that this applies not only to the tubular type of unit but also the regenerative.

The authors are to be congratulated for the thorough manner in which they have presented their subject.

P. KOCH.² The problems in design, operation, and maintenance of tubular air heaters caused by corrosion and fouling, so well presented by the authors, are generally about the same as those encountered in our tubular air heaters.

While most of our heaters last a good many years and have no particular fouling trouble, the writer's company experienced severe plugging and corrosion within as short a time as 6 months on some high-sulphur-oil and refinery-oil-fired units.

The determination of the minimum allowable metal temperature by installing thermocouples and observing the metal temperatures of the clean and fouled tubes at light loads is not entirely clear to the writer since in some cases the fouling also may occur at high loads. However, installing thermocouples in the coldest portion of the tubes and establishing the minimum metal temperature from observation and inspection are recommended. These metal temperatures then are used as a guide in the operation of any metal temperature-control equipment installed on the unit. If fouling and corrosion difficulties are experienced, metal temperatures also will indicate the amount of improvement obtained by changes or additions of control equipment.

The experience of the writer and his associates indicates that the minimum allowable metal temperature varies considerably, 160 to 280 F, depending on the type of fuel, amount of sulphur, method of firing, composition of ash, and other factors. For instance, no corrosion is expected at metal temperature of 160 F when firing anthracite or sweet natural gas, while excessive corrosion may occur up to as high as 280 F when firing high-sulphur and vanadium oils. Several marine economizer sections recently taken from a unit firing Persian Gulf oil and operating with about 245 F water entering and 300 F leaving were examined. After about 3 years' service, the tubes failed from corrosion and thinning of the tube wall. Corrosion was most severe at the cold end of the economizer but extended to

within a short distance of the hot end, where the water temperature was about 290 F.

It is interesting to note that oil-fired units had to be cleaned on an average of every 5½ months and pulverized-coal-fired units every 7½ months. Presumably, these units had to be shut down to be cleaned. This brings out the importance of considering means of increasing or controlling the metal temperatures and providing cleaning or washing in service, particularly in those cases where high availability is desirable. Heaters designed in two parallel sections and arranged with dampers are being water-washed successfully at night or over week ends when the units are operating below two-thirds load by shutting off and washing one side of the heater at a time.

The various methods that should be considered when designing a new unit or improving an existing one are covered thoroughly. The importance of good air distribution at the entrance to the heater should be stressed. This is particularly true of heaters designed with relatively low air velocities across the tubes at the air entrance. In a number of units excessive fouling and corrosion were reduced considerably by installing directional vanes and distributors in the air duct at or near the entrance of the heater. Therefore it is important that consideration be given to the relative position of the forced-draft fan and the air heater and to the shape and size of the duct connection in the design stage of the unit.

The writer agrees with the authors that finding corrosion-resistant material and coatings is very disappointing. The writer's company has been, and is, continuing to test materials and coatings in its research laboratory and in the field. Aluminum has given good results in some cases and poor results in others. Cor-Ten looks relatively good to date. Pyrex-glass tubes and enamel-coated tubes look promising and are being investigated.

With the proper consideration given to the design and operation, it is agreed that tubular heaters will give entirely satisfactory service.

AUTHORS' CLOSURE

The authors wish to thank the discussers for their contributions to this paper. In general, they confirm our experiences with corrosion of different materials at the cold end of tubular air heaters.

Mr. Koch indicated that good results had been obtained in some cases using aluminum tubes and poor results in others. Our experience with aluminum tubes has been consistently poor. Testing of various types of ceramic, plastic, and metallic coatings is continuing.

It has been suggested that the corrosion problem might be approached by lowering the dew point of the gases through the introduction of additives to the fuel oil, rather than by preventing corrosion after the moisture has been formed. This may be the effect of the Dolomite additive that is reported to have decreased air-heater plugging and corrosion. This approach to the problem is worthy of considerable study and testing.

The results of the research in corrosion-resistant materials and investigations in lowering the dew point of the gas when coupled with proper control of tube-metal temperature should result in information that will assist in reducing the maintenance of tubular air heaters.

² The Babcock & Wilcox Company, New York, N. Y.

Contamination of Condensate by Heat-Exchanger-Tube Alloys

By J. D. RISTROPH¹ AND E. B. POWELL²

Results are presented from condensate contamination studies conducted at two steam power stations to evaluate the influence of temperature of condensate, of differing dissolved gas content, and of cumulative service time upon the degree of metallic contamination to be expected in steam condensate of the general character described from flowing contact with tubing of twelve alloys commercially used in power-plant heat exchangers. The influence of cyclohexylamine on the rates of contamination is also indicated. The testing procedures are briefly described.

THE accumulation of foreign metal and metallic oxides on the internal heating surfaces of high-pressure boilers has become a source of growing concern to the steam power industry in the United States. Especially over the past ten years with the advent of the 2000-psi and higher-pressure steam generators, such deposits have been found serious hazards (1, 2, 3, 4, 5, 6, 7, 8).³ These deposits all retard heat transfer and so tend to high temperature in the tube walls, tending in turn to overheating or corrosion or both. Deposits of copper origin seem to have the further objectionable property of masking the evolution of hydrogen from the affected surface, which might otherwise give advance warning of the impending failure (4). Operating experience has pointed to corrosion and solution of metals of the steam-condensate-feedwater part of the system, external to the boiler proper, as normally the major source of the boiler-heating-surface metallic deposits in the so-called 100 per cent condensate-feedwater-type plant to which the present paper directly refers (2, 4).

Contemplating addition of three 750,000-lb-steam per hour, 1555-psi-gage controlled-circulation boilers, initial and reheat steam temperature 1000 F, to meet the rapidly growing load of its system and desirous of minimizing all interference with continuity of operation from the higher-pressure equipment, Virginia Electric and Power Company decided upon investigation of heat-exchanger-tube alloys as potential sources of metallic contamination of condensate flowing in contact with them. The test equipment would employ steam condensate actually as produced in the power plant and otherwise follow conditions of normal operation and would, in addition, be used to investigate the influence of such special chemicals as might promise reduction in corrosion and solution of piping and other parts of the steam-condensate system.

LOCATION OF TEST EQUIPMENT

With the objectives just outlined in view, studies were in-

¹ Chief Chemist, Virginia Electric and Power Company, Richmond, Va.

² Consulting Engineer, Stone & Webster Engineering Corporation, Boston, Mass. Fellow ASME.

³ Numbers in parentheses refer to Bibliography at end of paper.

Contributed by the Joint Research Committee on Boiler Feedwater Studies and presented at the Annual Meeting, New York, N. Y., November 30-December 5, 1952, of THE AMERICAN SOCIETY OF MECHANICAL ENGINEERS.

NOTE: Statements and opinions advanced in papers are to be understood as individual expressions of their authors and not those of the Society. Manuscript received at ASME Headquarters, September 29, 1952. Paper No. 52-A-63.

stituted at the Virginia Electric Bremo and Chesterfield power stations. The Bremo unit selected includes a steam generator of 625,000 lb per hr rated capacity, 1385 psi-gage drum pressure, 950 F steam temperature, and turbine of 66,000 kw rated capability with five stage heaters, the highest receiving steam from the 10th stage of the turbine, designed pressure at rated capability 306 psi gage, corresponding temperature in drips of 424 F. The unit selected for the investigation at Chesterfield Power Station included a steam generator of 650,000 lb per hr rated capacity, 925 psi gage drum pressure, 875 F steam temperature, and turbine of 66,000 kw rated capability with four stage heaters. The highest-temperature heater of the Chesterfield unit takes steam from the 8th stage of the turbine, designed pressure at rated capability 150 psi gage, corresponding drip temperature 365 F. At rated capability the designed steam pressure for the 15th stage heater of this latter unit is 15 psi gage, corresponding drip temperature 250 F. These three stage heaters at the two power stations were considered to afford the maximum reasonably feasible range in available temperature of drips and were accordingly adopted for the condensate-contamination study.

At Bremo Power Station the chemicals normally used for water conditioning at the time of the tests were sodium hydroxide, sodium metaphosphate, and sodium sulphite. Sodium sulphite was introduced continuously at the deaerator outlet giving concentrations of 5-10 ppm SO_2 in the boiler water. Sodium hydroxide was introduced continuously immediately ahead of the economizer to raise the alkalinity of the feedwater to pH 8.0-8.5. Sodium metaphosphate was fed, in automatically controlled slugs, directly to the boiler drum to maintain in the boiler water concentration of 2-5 ppm PO_4 . Silica and chloride concentrations in the boiler water averaged each approximately 1 ppm and total solids about 100 ppm. Blowdown was about $\frac{1}{2}$ per cent of boiler feed. At Chesterfield Power Station the water conditioning chemicals in use at the time of the tests were merely sodium hydroxide and sodium metaphosphate both being fed directly to the boiler drum, intermittently under automatic control. Sodium sulphite was not used. The phosphate concentration in the boiler water was maintained about 10 ppm PO_4 and silica, chlorides, and total solids about the same concentration as at Bremo Power Station. The rate of blowdown was approximately $\frac{3}{10}$ per cent of the boiler feed. The alkalinity of the feedwater, maintained naturally without chemical treatment, ranged from pH 7.7 to pH 8.3 approximately.

ARRANGEMENT OF TEST EQUIPMENT

The twelve alloys identified in Table I were decided upon as affording reasonable coverage of commercial materials appropriate for feedwater heat-exchanger tubing. Fifty feet of small tube seemed likely to offer adequate simulation of the power-plant heat-exchanger condition, although the corroding liquid would be flowing within the tube instead of on the outside. The higher rate of contamination per unit of flow made available by such attenuation of the condensate path would, of course, be of very distinct advantage in the higher concentrations attained in the condensate and in hastening desired test results. Three-eighths-inch-OD tubing of 0.035-0.040 in. wall thickness was found commercially available in all alloys to be tested, and was adopted for

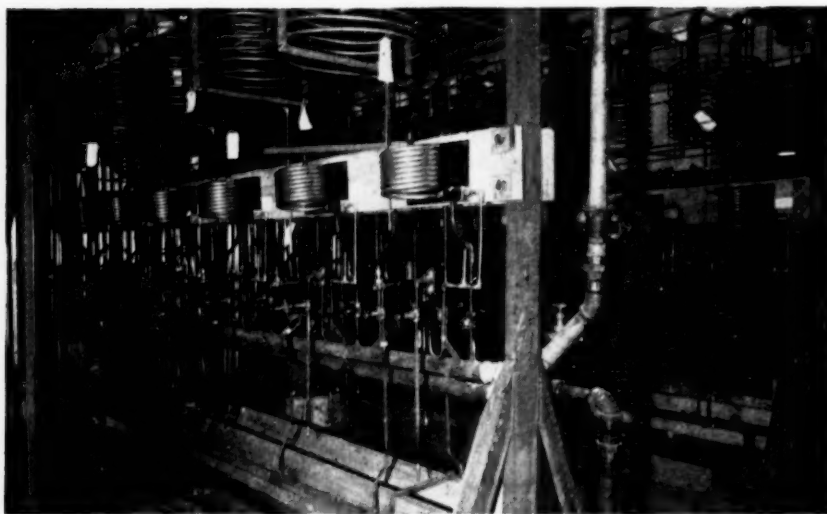


FIG. 1 ALLOY TEST COILS IN PROCESS OF INSTALLATION AT CHESTERFIELD POWER STATION

TABLE 1 CONTAMINATION TEST ALLOYS

Alloy	Approximate composition
Phosphorized copper	Copper 99.9% phosphorus 0.03%
88-10-2 Cu-Zn-Sn	Copper 88% zinc 10% tin 2%
Antimonial admiralty	Copper 71% zinc 28% tin 1% antimony 0.03%
Arsenical admiralty	Copper 71.5% zinc 27.5% tin 1% arsenic 0.04%
Phosphorized admiralty	Copper 71% zinc 28% tin 1% phosphorus 0.05%
Aluminum bronze	Copper 94.1% aluminum 5.5% arsenic 0.03%
Arsenical aluminum brass	Copper 77.2% zinc 20.6% aluminum 2.1% arsenic 0.05%
90-10 Cu-Ni 0.8 Fe	Copper 88.8% nickel 10% iron 0.75% manganese 0.45%
70-30 Cu-Ni 0.4 Fe	Copper 69% nickel 30.2% iron 0.4% manganese 0.1% zinc 0.1%
70-30 Cu-Ni 0.6 Fe	Copper 68.3% nickel 30.2% iron 0.6% manganese 0.6% zinc 0.1%
Monel	Copper 30.0% nickel 67% iron 1.4% manganese 1.0%
316 Stainless steel	Iron 68% chromium 17% nickel 10% molybdenum 2.5% manganese 2%

the individual specimens accordingly. The general arrangement of alloy test coils as photographed during installation at Chesterfield Power Station is shown in Fig. 1. To prevent any appreciable loss in condensate temperature the test coils were insulated heavily, in groups of six.

After review of available methods of measuring metallic contamination in water, the use of ion-exchange resin for recovery and concentration of the metals and their oxides, a process tried briefly by B. J. Cross on his studies of the 2000-psi boiler at Somerset Power Station of Montaup Electric Company, with spectrophotometric determination of concentration in the leaching liquid, was adopted as offering the greatest promise of appropriate precision within reasonable limits of technical manpower. In the interval, development in resin exchangers had advanced markedly and two types, a carboxylic cation exchanger and a combination of sulphonic cation exchanger and strongly basic anion exchanger in a monobed, seemed to offer sufficient promise to warrant practical trial. While as indicated in Fig. 3 the single resin cation exchanger of carboxylic type was found more efficient in requirement of leaching liquid, the monobed was the more effective in recovery of traces of metals and metal oxides and other contaminating substances from the condensate. The adsorption of suspended material by the carboxylic resin was very doubtful. Preliminary studies also demonstrated that tightly packed glass wool was much more effective than glass beads as filter material

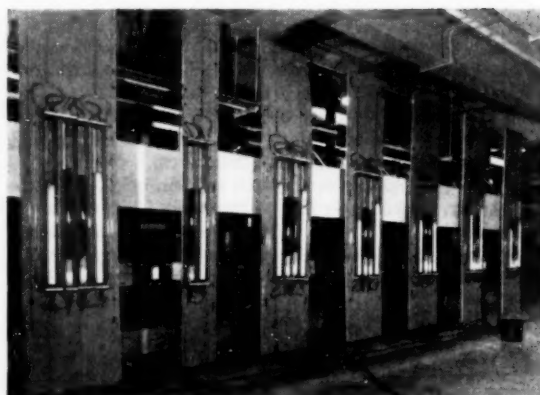


FIG. 2 METALLIC RECOVERY EQUIPMENT INSTALLED AT BREMONO POWER STATION

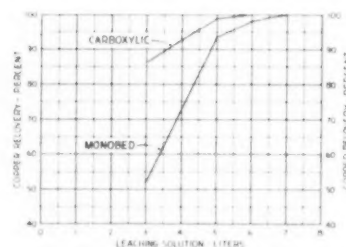


FIG. 3 LEACHING EFFICIENCIES OF EXCHANGE RESINS AS RELATED TO VOLUME OF LEACHING SOLUTION

for collection of suspended solids ahead of the exchanger. The monobed-resin combination and glass-wool filter were adopted. The arrangement of metallic recovery equipment is shown in the photograph of the installation at Bremono Power Station, Fig. 2. Separate 48-in. lengths of 2-in. Pyrex glass tubing were used for filter and ion exchanger on each test coil. The test equipments

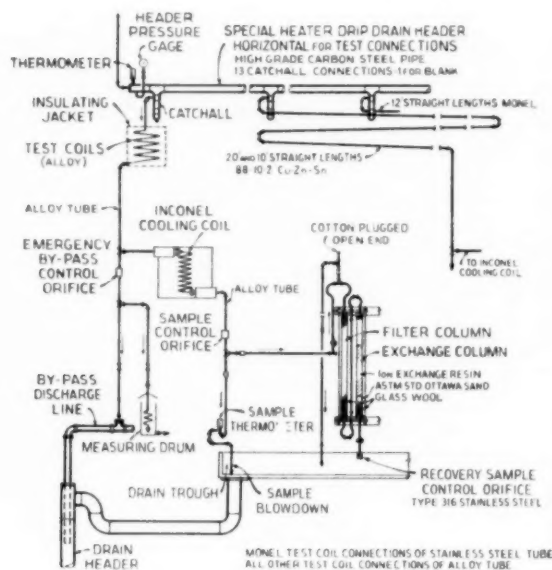


FIG. 4 DIAGRAMMATIC ARRANGEMENT OF ALLOY TEST COILS AND METALLIC RECOVERY EQUIPMENT

at the two stations were essentially identical in all respects. The drip, or condensate, flow path through the alloy test coils and the recovery equipment is shown diagrammatically in Fig. 4.

Control of flow through the test coils is provided on the 10th stage installation at Bremono and the 8th stage at Chesterfield by stainless-steel orifices discharging to overflow at constant positive static head and, on the 15th stage at Chesterfield, merely by constant positive static head at overflow. The fixed positive head on the test coil overflow permits assured diversion of part of the condensate flow to the recovery equipment, the glass-wool filter, and monobed exchanger. Inconel cooling coils are provided ahead of the recovery equipment. Control of flow through the recovery equipment is by stainless-steel orifices at the point of final discharge for return to the station condensate system. A 13th connection is provided on the individual stage-heater drip distributing header which, omitting the alloy specimen, is in all respects identically equipped for establishment of a blank.

OPERATION OF TEST EQUIPMENT

Analytical runs on the condensate test equipment were of 100 hr duration. After the first three such runs on drips from each of the three stage heaters, all subsequent analytical runs were immediately preceded by nonanalytical runs of 100 hr or more duration, except for run No. 4 on the Bremono 10th stage equipment where a 4-day delay intervened for repair of piping on the main unit. For this discussion, the period either of an isolated analytical run, or of a nonanalytical run and an immediately following analytical run combined, will be referred to as a test period.

Aside from one or two unavoidable interruptions from shutdown of the generating unit or for test piping repair, condensate flow in the test coils on the higher-pressure stage heaters was maintained continuously during test periods. On the Chesterfield 15th stage heater tests, in addition to an interruption from shutdown of the unit, it was necessary to interrupt the test period when including week ends to avoid subjecting the test equipment to subatmospheric pressures under the lower unit loading. At all times of interrupted flow the test coils were kept submerged.

In the higher-temperature equipment of the 10th stage installation at Bremono and the 8th stage installation at Chesterfield the condensate flow rate in the test coils was controlled at about 4.5 fps. In the 15th stage heater installation at Chesterfield the flow rate, limited by the low pressure of steam in the stage heater, was about 2.2 fps.

Except for a delay of about 4 days following run No. 3 on the Bremono 10th stage equipment caused by nonavailability of condensate during outage of the generating unit, all analytical runs were followed immediately by leaching-regenerating of the recovery equipment. During this process, which for one heater group occupied about 10 days or more, to avoid risk of too serious contamination of feedwater the condensate flow was discontinued, the test coils standing submerged. Where no nonanalytical test run intervened between analytical runs, the individual alloy condensate path was then flushed continuously 10–20 min before cutting in the metallic recovery equipment, with the intent of removing any accumulation of abnormal concentration of metallic contamination. Where immediately preceded by a nonanalytical run, the analytical run was of course merely a continuance of the nonanalytical. Throughout all test periods, tests for dissolved gases, pH, and electrical conductivity were made about twice daily on condensate as delivered to the test assembly and as discharged from each test coil after filtration and deionization.

RESULTS OF TESTS—NORMAL PLANT FEEDWATER TREATMENT

The associated observations and general results of the condensate-contamination tests secured on the equipment on the 8th stage and 15th stage heaters at Chesterfield Power Station are summarized in Table 2 and Table 3, respectively, and the corresponding data on the 10th stage heater tests at Bremono Power Station are given in Table 4. The rates of copper contamination of the condensate found on the analytical runs for the different alloys on the tests are shown graphically for the three stage heaters in the same sequence in Fig. 5, Fig. 6, and Fig. 7. As the graphs of these three charts are of value chiefly for indication of progressive trends and to follow the individual alloy contamination on them is somewhat difficult, the relative magnitudes of copper contamination picked up by the drips on selected runs are shown graphically in Fig. 8 and Fig. 9. Copper contamination derived from the different alloys on the Chesterfield 15th stage heater on the 1400–1500 hr run, on the Bremono 10th stage and Chesterfield 8th stage heaters on the respective 1600–1700 hr runs, and on the Bremono 10th stage heater on the 2550–2650 hr run is in Fig. 8. Fig. 9 gives a comparison of copper contamination picked up by the Bremono 10th stage heater drips on the 1600–1700 hr, on the 2350–2450 hr, and on the 2550–2650 hr runs. Relative rates of iron contamination as derived from contact with type 316 stainless steel are shown in Fig. 10. Attention is called to the earlier statement that all analytical runs were of 100 hr duration. The two numbers used in identifying the different runs in Fig. 8 and Fig. 9 give the cumulative hours elapsed at the beginning and closing of the particular run.

Data on the condensate as delivered to the test specimens are given immediately below the heading in each table. Condensate leaving the exchangers was almost exactly neutral and the conductivity generally rather close to 0.10 mmho per cm cube at 25°C, quite often less.

It will be noted that the first three analytical runs on all three installations show, in general, relatively high values of contamination. In the Bremono 10th stage installation, maximum contamination rates are recorded for several alloys on the fourth analytical run. Copper from antimonial admiralty, arsenical aluminum brass, 70–30 copper-nickel 0.4 iron and 0.6 iron, and 90–10 copper-nickel 0.8 iron and iron from type 316 stainless steel are at substantially the maximum rates on this run. In

TABLE 2 ANALYSIS OF DRIPS TO TEST COILS AND RESULTING METALLIC CONTAMINATION 8TH STAGE HEATER—CHESTERFIELD POWER STATION

Test no.	1	2	3	4
Conductivity, mmho	1.23	1.19	1.17	0.65
pH	8.2	7.8	7.7	7.6
CO ₂	0.22	0.12	0.05	0.09
NH ₃	0.03	0.02	0.02	0.01
O ₂ , ml/liter	0.002	0.003	0.002	0
Temperature, F	369	367	367	368
Pressure, psi gage	163	159	160	161
Cumulative hours	100	200	300	1700

Copper pickup—ppb per sq ft alloy surface

Phosphorized copper	0.43	6.03	4.98	1.48
88-10-2 Cu-Zn-Sn	11.90	54.53	13.08	0.96
Antimonial admiralty	9.00	52.22	14.07	3.83
Arsenical admiralty	13.15	5.94	10.24	0.69
Phosphorized admiralty	3.18	12.20	12.17	0.78
Aluminum bronze	14.88	41.86	12.97	3.22
Arsenical Al brass	2.68	4.35	11.61	1.01
90-10 Cu-Ni 0.8 Fe	5.12	4.74	1.23	1.23
70-30 Cu-Ni 0.4 Fe	0.36	1.93	0.67	0.90
70-30 Cu-Ni 0.6 Fe	0.27	0.91	0.47	0.71
Monel	0.71	0.40	2.60	0.69

Iron pickup—ppb per sq ft alloy surface

316 Stainless steel	8.15	5.19	2.74	2.86
Conductivity—mmho per cm cube at 25 C.				

TABLE 3 ANALYSIS OF DRIPS TO TEST COILS AND RESULTING METALLIC CONTAMINATION 15TH STAGE HEATER—CHESTERFIELD POWER STATION

Test no.	1	2	3	4
Conductivity, mmho	1.45	1.14	1.17	0.68
pH	8.3	8.2	8.0	7.8
CO ₂	0.08	0.08	0.09	0.04
NH ₃	0.04	0.03	0.03	0.01
O ₂ , ml/liter	0	0	0.008	0.002
Temperature, F	243	245	244	245
Pressure, psi gage	15.8	14.8	13.9	14.8
Cumulative hours	100	200	300	1500

Copper pickup—ppb per sq ft alloy surface

Phosphorized copper	0.66	3.87	a	1.91
88-10-2 Cu-Zn-Sn	2.37	2.63	1.89	2.77
Antimonial admiralty	1.63	4.23	1.92	1.42
Arsenical admiralty	0.49	2.15	a	0.98
Phosphorized admiralty	2.36	4.08	1.89	2.01
Aluminum bronze	2.50	4.62	a	3.94
Arsenical Al brass	0.85	4.65	a	3.70
90-10 Cu-Ni 0.8 Fe	0.46	4.17	1.07	4.27
70-30 Cu-Ni 0.4 Fe	0.24	2.00	0.31	1.41
70-30 Cu-Ni 0.6 Fe	0.15	1.41	0.22	1.19
Monel	0.09	0.05	2.29	1.06

Iron pickup—ppb per sq ft alloy surface

316 Stainless steel	7.32	2.08	a	5.43
Conductivity—mmho per cm cube at 25 C.				

^a Unfortunately, the final samples of five test coils on run No. 3 were unavoidably lost, and it was impossible to secure the analytical results.

the Chesterfield 8th stage installation, although 90-10 copper-nickel 0.8 iron, the two 70-30 copper-nickel alloys, and type 316 stainless steel show no significant change between the third and fourth analytical runs, the general contamination trend indicated in the fourth analytical run is downward. Unfortunate loss of many drip samples from the third analytical run on the Chesterfield 15th stage heater installation prevents a similar comparison of the two final runs on that heater. However, comparison with the earlier analytical runs on drips from the same heater suggests either maximum contamination rates in the fourth analytical run or a downward trend beginning in the third or fourth analytical run.

In general, determination of iron contamination was limited to condensate from the type 316 stainless-steel test coil, and from one or two of the nonferrous-alloy test coils used for evaluation of the iron blank. On the initial analytical run on the Brema 10th stage heater test equipment, exploratory determinations were made for iron contamination from every alloy specimen. The results indicated almost as high an initial rate of iron contamination from the 70-30 copper-nickel alloys and Monel as from the type 316 stainless steel:

70-30 Cu-Ni 0.4 Fe—0.022 ppm—5.00 ppb per sq ft contact surface
70-30 Cu-Ni 0.6 Fe—0.013 ppm—3.16 ppb per sq ft contact surface
Monel 1.4 Fe—0.025 ppm—5.74 ppb per sq ft contact surface
316 SS 68.0 Fe—0.029 ppm—6.54 ppb per sq ft contact surface

The measured iron contamination from Monel approximates so

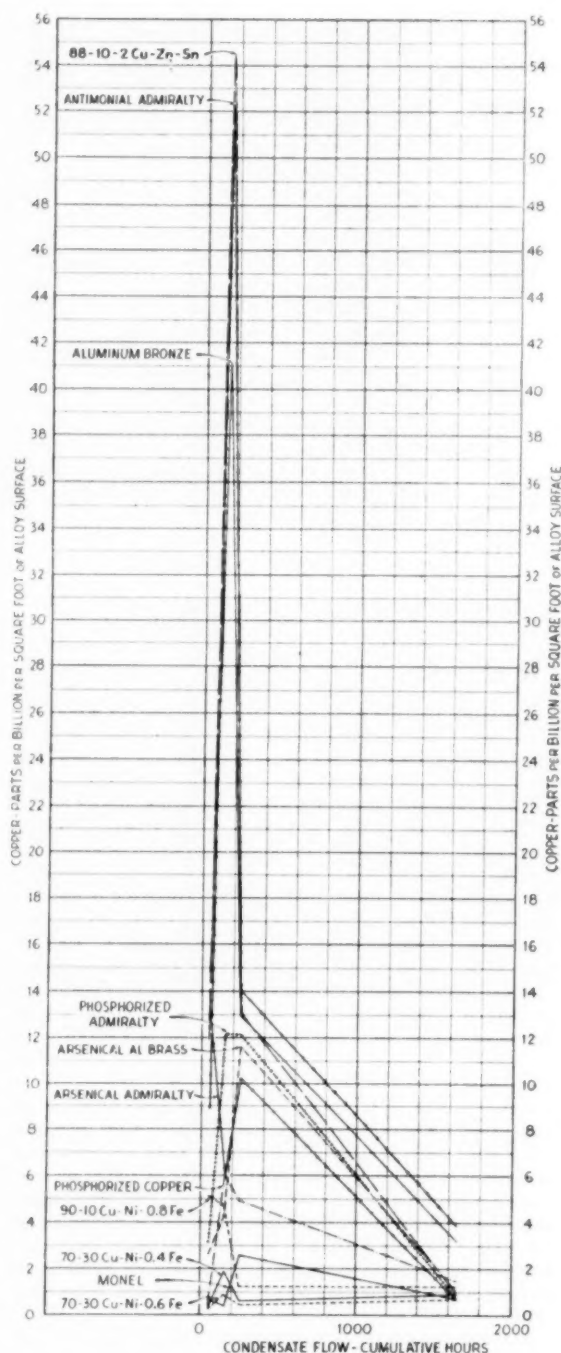


FIG. 5 CONDENSATE CONTAMINATION FROM COPPER IN TEST ALLOYS CHESTERFIELD POWER STATION 8TH STAGE HEATER—DRIP TEMPERATURE 368 F

(Contamination rate expressed in parts per billion per sq ft of alloy contact-surface area.)

nearly that from type 316 stainless steel that use of the stainless steel in making connections to the Monel test coil can hardly have

TABLE 4 ANALYSIS OF DRIPS TO TEST COILS AND RESULTING METALLIC CONTAMINATION 10TH STAGE HEATER—BREMO POWER STATION

Test no.	1	2	3	4	5	6 ^a	7
Conductivity, mmho	0.46	0.42	0.41	0.50	1.33	1.85	0.60
pH	6.4	6.3	6.5	6.7	6.7	8.5	6.4
CO ₂ , ppm	0.27	0.30	0.10	0.03	0.13	0	0.10
NH ₃ , ppm	0	0	0	0	0	0.05	0
O ₂ , ml/liter	0	0	0	0	0	0	0
Temperature, F	417	426	412	418	417	408	404
Pressure, psi gage	292	321	274	304	303	278	257
Cumulative hours	100	200	300	1100	1700	2450	2650
Copper pickup—ppb per sq ft alloy surface							
Phosphorized copper	11.08	2.20	8.12	7.80	2.80	0.34	0.87
88-10-2 Cu-Zn-Sn	14.99	3.58	12.01	5.66	4.46	0.67	2.93
Antimonial admiralty	14.17	10.45	11.79	12.46	4.49	0.81	1.23
Arsenical admiralty	8.35	3.54	7.19	3.49	1.93	0.64	0.26
Phosphorized admiralty	3.23	4.22	6.04	4.45	4.15	0.81	1.55
Aluminum bronze	5.82	19.26	12.12	10.02	6.09	0.23	1.48
Arsenical Al brass	0.50	1.36	6.33	7.00	4.73	0.64	1.29
90-10 Cu-Ni-0.8 Fe	3.48	4.13	11.21	11.81	5.12	1.61	0.46
70-30 Cu-Ni-0.4 Fe	2.00	2.27	2.77	4.35	2.43	1.25	0.39
70-30 Cu-Ni-0.6 Fe	1.70	1.49	1.99	5.13	2.38	0.66	0.34
Monel	1.93	0.44	0	0.83	0.96	0.83	1.88
Iron pickup—ppb per sq ft alloy surface							
316 Stainless steel	6.54	5.63	1.80	7.10	4.26	0	2.70
Conductivity—mmho per cm cube at 25 C.							

^a Cyclohexylamine added to feedwater with pH controlled at 8.5.

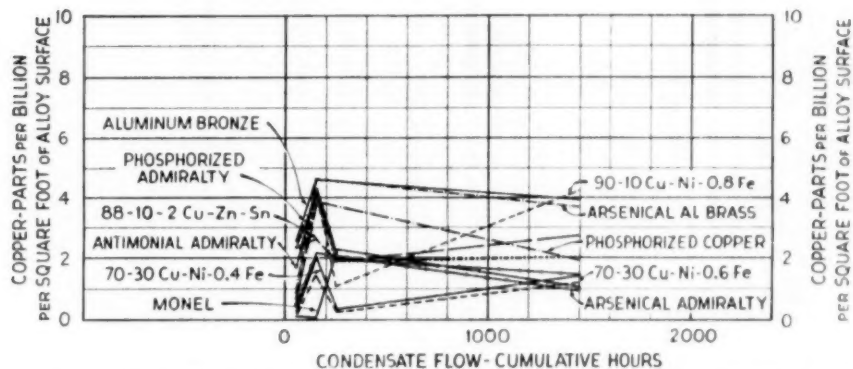


FIG. 6 CONDENSATE CONTAMINATION FROM COPPER IN TEST ALLOYS, CHESTERFIELD POWER STATION 15TH STAGE HEATER—DRIP TEMPERATURE 245 F

(Contamination rate expressed in parts per billion per sq ft of alloy contact-surface area.)

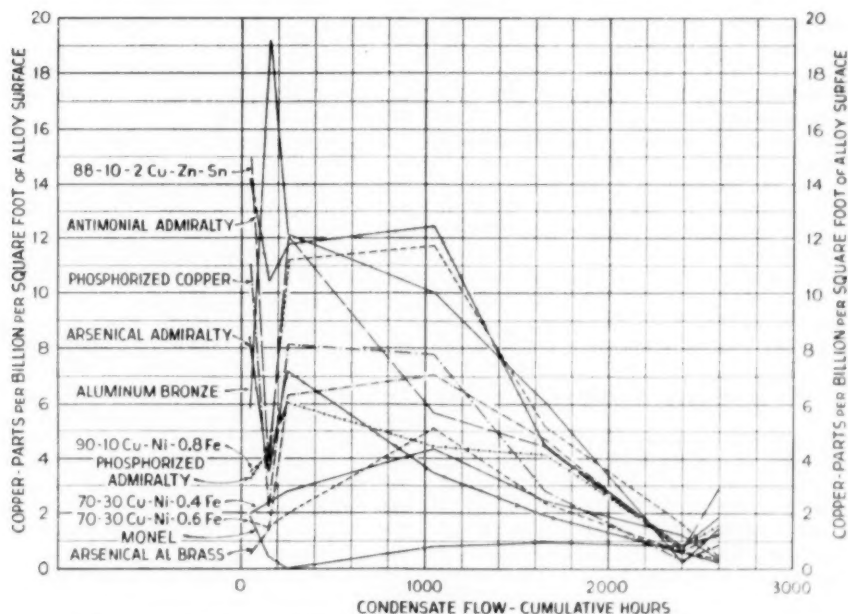


FIG. 7 CONDENSATE CONTAMINATION FROM COPPER IN TEST ALLOYS, BREMO POWER STATION 10TH STAGE HEATER—DRIP TEMPERATURE 404-426 F

(Contamination rate expressed in parts per billion per sq ft of alloy contact-surface area.)

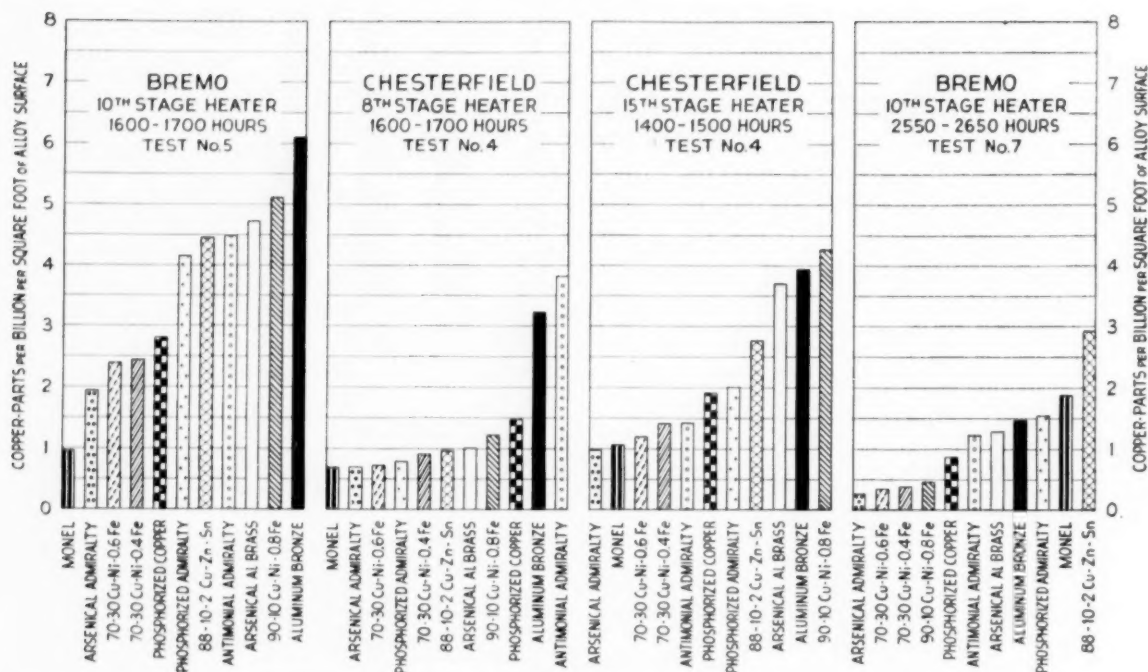


FIG. 8 Comparison of Contamination Rates From Copper in Test Alloys Under Different Stage Heater Drip Compositions and Temperatures on Selected Test Runs—Normal Feedwater Treatment Used

been a significant factor in the result. Nickel interference, however, may have been a major factor in these four iron determinations, especially in the contamination from Monel (10). Service experience has sometimes indicated a high rate of initial attack of condensed steam on copper-nickel alloy. Probably further tests would show quite appreciable decrease in actual iron and nickel interference, if the latter has been a factor in the indicated result.

Some of the recorded variations in contamination rates seem incompatible with the associated data of the tabulations. There seem three possible sources of irregularity, (a) differences in effectiveness of purging from the 10-20 min flushing before diverting condensate flow to the recovery equipment on analytical runs not immediately preceded by nonanalytical runs, (b) differences in stage of protective film development attained by the different metals, (c) differences in dissolved-gas content of the condensate more significant than the spot-test averages of the tabulations would indicate.

Corrosion products settling in the test coils during idle periods may have been of varying tenacity of adherence, influenced by length of idle period and by character of the deposit peculiar to the metal specimen and the corrosive constituents in the condensate.

The arsenical admiralty coil specimens on all three installations had been used for a 50-hr preliminary run at BreMo station on condensate of about 440 F. For simplification of presentation, this initial 50-hr service has been disregarded in tables and charts. The phosphORIZED admiralty test coil which had been used on the preliminary run for comparison of resins was accidentally damaged and was replaced in its entirety before beginning the main tests. The 100-hr shorter nonanalytical run preceding the analytical run of test No. 4 on the Chesterfield 15th stage heater installation will, of course, have afforded less time for protective film development than available to the alloy

specimens of the Chesterfield 8th stage installation on the same numbered test or to the specimens of the BreMo 10th stage installation on test No. 5. Much more important differences in stage of protective film development, however, would be expected from difference in susceptibility of the different alloys to such developments under the changing environmental conditions of the tests. The record of copper contamination in BreMo 10th stage heater drips from 90-10 copper-nickel 0.8 iron would seem to afford a striking illustration of peculiarity in protective film development.

All analytical figures, except those for metallic contamination, were from infrequent spot tests and cannot be expected to cover the full range encountered. In the Chesterfield tests, the spot samplings of drips indicated rather wide variations in oxygen content. There may have been significant variations in concentration of oxygen and other dissolved gases in the heater drips of both stations. Traces of oxygen were probably present at times during all test periods.

The metallic contamination found in the heater drips during the analytical runs at the two stations is given in terms of parts per million of condensate weight in Table 5. The tubes of the BreMo 10th stage and Chesterfield 8th stage heaters are 70-30 copper-nickel and those of the Chesterfield 15th stage heater are admiralty. The evidence of the blank copper contamination values, which are checked by the determination on condensate discharge from the type 316 stainless-steel specimens, would seem that corrosion or solution of copper had been unusually high in the Chesterfield 8th and 15th stage heaters on run No. 2 and in the BreMo 10th stage heater on run No. 3. The influence of heightened corrosive activities seems to have extended to some of the nonferrous alloys in each of the test groups. For some of the other specimens the higher concentration of copper in the drips reaching the test assembly may have been sufficient to cause measurable decrease in avidity of the condensate for copper, or the

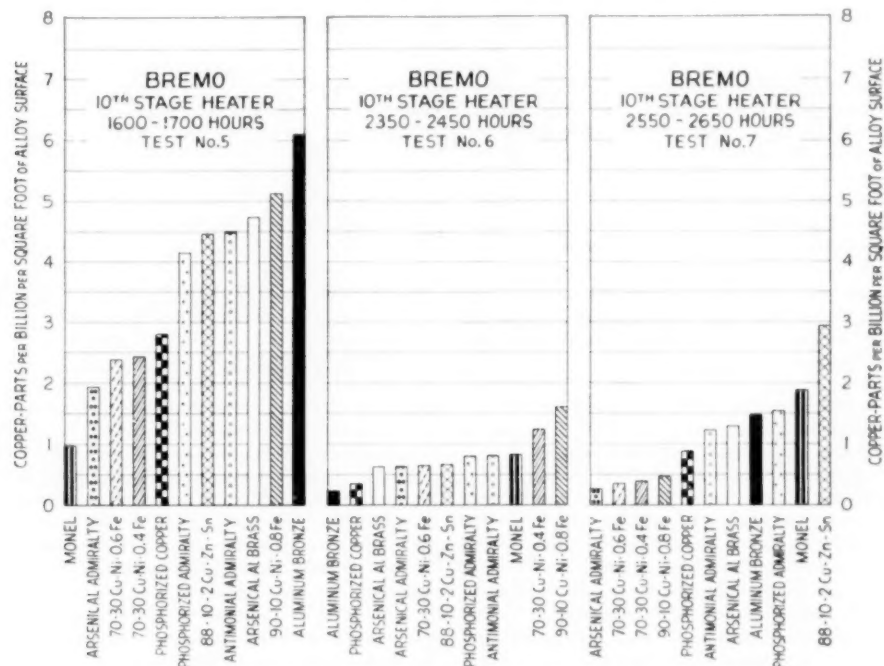


FIG. 9 COMPARISON OF CONTAMINATION RATES FROM COPPER IN TEST ALLOYS IN BREMO 10TH STAGE HEATER DRIPS ON SELECTED TEST RUNS OVER DIFFERENT CUMULATIVE HOURS—NORMAL FEEDWATER TREATMENT AND CYCLOHEXYLAMINE FEEDWATER TREATMENT USED SUCCESSIVELY

TABLE 5 INITIAL CONTAMINATION OF DRIPS

BreMO Power Station Test no.	Copper		Iron	
	8th Stage	15th Stage	8th Stage	15th Stage
1	0.0117	0.0107	0.050	0.043
2	0.0270	0.0111	0.042	0.051
3	0.0073	0.0073	0.045	0.044
4	0.0050	0.0106	0.044	0.033
5				
6				
7				

Chesterfield Power Station Test no.	Copper		Iron	
	8th Stage	15th Stage	8th Stage	15th Stage
1	0.0024	0.0031	0.028	0.034
2	0.0214	0.0128	0.025	0.034
3	0.0092	0.0077	0.028	
4	0.0020	0.0080	0.031	0.033

TABLE 6 EFFECT OF FLOW VELOCITY ON CONTAMINATION OF CONDENSATE AT 440 F FROM ARSENICAL ADMIRALTY 10TH STAGE HEATER—BREMO POWER STATION

Test coils	A	B	C
Flow velocity, fps	3.15	6.63	10.85
Copper picked up, ppm	0.0073	0.0029	0.0023
Copper picked up, ppb per sq ft	1.72	0.68	0.54
Copper picked up, per hr, lb $\times 10^{-4}$	2.4	2.0	2.6

alloys were highly resistant to the particular corrosive agent.

Flow rates through the Chesterfield 15th stage heater test coils were about 2.2 fps, approximately one half those in the coils on drips at the higher temperatures. The preliminary test run earlier mentioned, run on 440 F drips from the BreMO 10th stage heater for determining upon the required velocity of condensate flow, indicated that, for the specimen arrangement and environment of the test, for flow rates within the range of approximately 3 fps to 11 fps, the copper pickup in terms of condensate contamination, parts per billion per sq ft of alloy contact-surface area, varied in inverse proportion to the flow velocity sufficiently to make the weight of copper picked up per unit of time almost in-

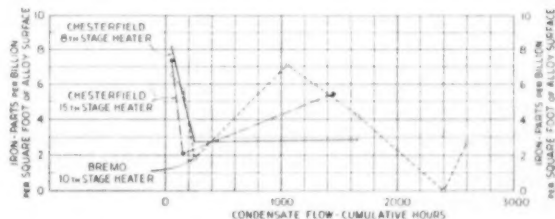


FIG. 10 APPARENT CONDENSATE CONTAMINATION FROM IRON IN TYPE 316 STAINLESS STEEL

dependent of the velocity of flow. The copper-contamination values from this preliminary run are given in Table 6. The maximum contamination rate recorded in lb per hr was for the highest velocity but only one third higher than the minimum, which was for the intermediate velocity. The test was made on arsenical admiralty not previously used. Consequently, variations from undetermined causes may be too great for definite conclusions. The indication is strong, nevertheless, that, because of the lower velocity of condensate flow, arsenical admiralty in the Chesterfield 15th stage coils should have caused higher contamination in parts per billion per sq ft contact-surface area than in the Chesterfield 8th stage or BreMO 10th stage coils for the same temperature and quality of condensate. Influence of shorter time for protective-film development in the Chesterfield 15th stage coil on test No. 4 would have been in the same direction. The higher contaminations reported for the higher-pressure stage tests of the alloy must be attributed to much more severe activity of condensate.

An interesting feature of the results from all three of the stage heater tests is the apparently large influence which, under the conditions of these tests, may be exerted by minor constituents

TABLE 7 EFFECT OF CYCLOHEXYLAMINE ON BOILER FEED-PUMP POWER REQUIREMENT—BREM0 POWER STATION

Test no.	1	2	3	4
Date	9/7/51	9/17/51	10/22/51	5/28/52
Feedwater pH control	Caustic soda	Caustic soda	Caustic soda	Cyclohexylamine
Feed pump condition	Accumulating deposit	Manually cleaned	Accumulating deposit	Self-cleaning
Turbine load, kw	77000	77000	78000	76500
Drum pressure, psi	1357	1355	1375	1370
Steam flow, lb/hr	678000	679000	682000	684000
FW pressure, psi	1455	1480	1505	1490
FW temperature, °F	435	432	433	435
Pump no.	A C	A C	A C	B C
Suction pressure, psi	473 472	452 458	449 452	475 475
Discharge pressure, psi	1490 1500	1480 1500	1505 1515	1490 1490
Motor, amperes	240 240	174 174	197 200	180 180

in certain of the alloys. Arsenical admiralty alloy showed less susceptibility to corrosion than antimonial admiralty. Also, the 70-30 Cu-Ni 0.6 iron imparted distinctly less contamination than the corresponding alloy of 0.4 iron content.

TRIAL OF CYCLOHEXYLAMINE AT BREMO POWER STATION

Iron contamination in the feedwater had been a source of considerable annoyance and expense on the high-pressure unit at Brema Power Station. Iron oxide accumulated on boiler feed-pump casings and impellers, on flowmeter orifices, attenuator spray nozzles, and other objects imposing interference with feedwater flow. The effects of the accumulation on boiler feed-pump performance may be judged roughly from comparison of tests numbered 1 and 2 in Table 7, where test No. 2 shows the effect of pump cleaning on the motor ampere input, which had increased by more than one third above normal. Test No. 3, made about five weeks after the cleaning operation, shows a quite appreciable increase in power requirement. Differences in net effective pump outputs on the different tests prevent the motor amperes from affording precise measure of fouling, but they are believed adequate for the purposes of the tabulation. The net output appears, for test No. 2, to have been a little higher than for test No. 1, and for test No. 3, somewhat higher than for test No. 2.

W. W. Cerna, in describing German wartime developments and practice in steam-boiler feedwater treatment, referred to the use of ammonia and ammonium salts for neutralization of carbon dioxide and control of alkalinity (9). Prof. F. G. Straub also reported instances, in his American practice, of marked benefit in reduction of metallic contamination effected by small concentrations of ammonia in feedwater (7). As pointed out earlier in the present paper, metallic contamination is a problem affecting many high-pressure power plants. The reports of corrosion of nonferrous metals from ammonia made it seem inadvisable to recommend any large-scale use of ammonia, or chemicals liable to have ammonia as a breakdown product, without definite investigation of effects on all alloys likely to be encountered in the feedwater-steam-condensate system. Advantage was accordingly taken of the corrosion-test equipment at Brema Power Station to make a preliminary trial of one of the recommended ammonium compounds, cyclohexylamine. Addition of this material to the feedwater of the high-pressure unit at Brema Power Station was begun on November 7, 1951, maintaining the alkalinity of the feedwater about pH 8.5, at the same time discontinuing introduction of caustic soda ahead of the economizer. Caustic soda, at decreased rate, was fed with the phosphate directly to the boiler drum. The cyclohexylamine requirement was approximately 75 ml per day on a steam-generating rate of 12,600,000 lb per day, equivalent to less than $1/100$ ppm in terms of weight of steam generation. By November 29, about three weeks after beginning use of cyclohexylamine, the motor input at corresponding boiler load had dropped to 190 amp. The motor ampere input observed May 28, 1952, without resort to mechanical cleaning since introduction of the cyclohexylamine, is shown by the results reported under test No. 4 of Table 7. Significant

TABLE 8 EFFECT OF CYCLOHEXYLAMINE ON IRON CONTAMINATION OF BOILER FEEDWATER—BREM0 POWER STATION

Date	7/13/51	12/20/51
Condensate at hot well, Fe	0.22 ppm	0.07 ppm
Feedwater to economizer, Fe	0.16 ppm	0.08 ppm

improvements were also shown by flowmeter indications and attenuator performance. The effect as indicated by iron concentration in the feedwater is shown in Table 8.

Effects of the cyclohexylamine treatment reflected in observations of Brema 10th stage heater drip contamination from the different test alloys are shown in test No. 6, Table 4. Effects of that treatment are reflected also to some extent in the iron contamination shown by test No. 7, the same table, which followed complete clearing of cyclohexylamine from the plant system. Test No. 6 shows not only complete avoidance of iron contamination from type 316 stainless steel but marked decrease in contamination from all nonferrous alloys except Monel. All copper-nickel alloy specimens show less marked decrease in contaminating effect than the other nonferrous alloys on the average. Condensate contaminations by copper from the different alloys on test runs during and immediately before and after the use of cyclohexylamine are compared graphically in Fig. 9. Complete avoidance of iron contamination from type 316 stainless steel is shown by the Brema 10th stage graph in Fig. 10. The behavior of Monel is so surprising that effort will be made on further tests to confirm or correct the present indications.

GENERAL

Some figures are given in Table 9 as illustrations of divergence from the test values which may occur in the actual power-plant equipment. The figures show, in the same terms of parts per billion per sq ft area of exposed contact surface of the specific

TABLE 9 METALLIC CONTAMINATION IN HEATER DRIPS

	Copper		Iron	
	Ppm	Ppb per sq ft	Ppm	Ppb per sq ft
Chesterfield P.S.				
8th Stage Heater				
Tests 1-4, inc.	0.0087	0.0049	0.028	0.13
15th Stage Heater				
Tests 1-4, inc.	0.0079	0.0058	0.034	0.20
Brema P.S.				
10th Stage Heater				
Tests 1-5, inc.	0.0136	0.0066	0.048	0.22
Test No. 6	0.0050	0.0024	0.044	0.20
Test No. 7	0.0106	0.0051	0.033	0.15

metal, the average condensate contamination found during the four analytical runs on drips from each of the Chesterfield 8th stage and 15th stage heaters and during the first five, normal feedwater treatment, analytical test runs on drips from the Brema Power Station 10th stage heater, also on the individual sixth and seventh analytical runs on drips from the Brema 10th stage heater. The contamination carried by the heater drips on reaching the test equipment may conceivably include small traces of both copper and iron carried by the steam. Expectably, however, such metals or their oxides would have been largely sepa-

rated from the steam in passage through the turbine stages ahead of the heater.

As mentioned earlier in the paper, the tubes in the Chesterfield 8th stage heater and the Brema 10th stage heater are of 70-30 copper-nickel and in the Chesterfield 15th stage heater admiralty. It will be noted that the copper contamination in parts per billion per sq ft of alloy surface apparently acquired within the periods of test in the 8th and 15th stage heaters at Chesterfield were, in each case, about 0.5 per cent of the corresponding average test values. The relationship will have been influenced by the states of protective-film development in the respective test coils, which expectably will have been different, and doubtless by less obvious offsetting factors. For the Brema 10th stage heater the copper contamination acquired within the heater was about 0.2 per cent of the corresponding average test value for the first five tests and for the sixth test. For test No. 7, however, the copper contamination from the heater was about 1.3 per cent of the corresponding test figure.

Comparison of iron contamination from carbon steel of plant equipment and from test specimens of stainless steel seems far-fetched. The corrosion resistance of the stainless steel, however, permitted a nearer relation between iron contamination acquired external to the test coils and iron picked up from the type 316 stainless-steel test coils than correspondingly reported for the copper comparison. For the Chesterfield 8th stage and 15th stage installations, the average iron contributions from the respective heaters and connecting piping were 2.7 and 4 per cent of the type 316 stainless-steel test coil values. Again, influence of time for protective film development should be considered in comparing the two percentages. For the Brema 10th stage installation, the average iron contributions from the heater and connecting piping on the first five tests with normal treatment of the feedwater and for test No. 7 were respectively 4.3 and 5.5 per cent of the simultaneous values from the type 316 stainless-steel test coil. On test No. 6 the type 316 stainless-steel coil contributed no iron contamination.

The three stage heaters are set with tubes vertical and steam baffles horizontal making 10-12 steam passes across the heating surface. The respective paths of exposure for contamination of condensate in the heaters are of course very complex. Dimensionally, in relation to the flow of drips in the test coils, the heater flow paths for copper contamination are short and wide and the paths for iron contamination considerably shorter in effective average length and very considerably wider. In the steel piping by which the condensate is conveyed from the heater shell to the alloy test specimens, velocities approximated those in the test coils but the piping represented only 8 to 16 per cent of the exposed iron surface in the flow path.

CONCLUSIONS

Under conditions average for the tests, all alloys tested develop protective films which tend to decrease their contaminating effects.

Under conditions of environment and nature and concentration of prior contamination of drips used in the present tests made under conditions of feedwater treatment normal for the respective power plants, most of the twelve alloys tested would initially give relatively high rates of condensate contamination. Within a few hundred operating hours the condensate contamination from any specific one of the alloys would attain a maximum rate, and then progressively decrease to a relatively minor rate peculiar to the individual alloy and the chemical and physical environment.

Under conditions of normal feedwater and boiler-water treatment and of dissolved-gas content normal to the drips from the stage heaters used on the tests, temperature range approximately

245 F to 425 F, and within the exposure time limits of the tests, Monel, 70-30 copper-nickel, and arsenical admiralty should be grouped as heat-exchanger alloys of nonferrous or copper-bearing type showing least tendency to contribute copper contamination to condensate and aluminum bronze and aluminum brass as tending to contribute most highly to contamination by that metal. Also, under conditions of feedwater treatment normal for the plants on which the tests were made, type 316 stainless steel apparently contributed iron contamination at rates not very far from the averages for copper contamination shown by the nonferrous alloys on the corresponding test runs.

Increase of condensate temperature causes increase in contamination from all alloys. For many of the alloys tested, however, the influence of differences in gas concentrations, occurring merely as features of ordinary operation of the power plants, greatly outweighed the effects of 45-60 F difference in temperature between the Chesterfield 8th stage and Brema 10th stage heaters.

For several alloys, apparently a higher corrosive activity of dissolved gases caused much higher contamination rates on test No. 2 of the Chesterfield 8th stage heater installation than recorded for the same alloys on the Brema 10th stage heater test No. 2 at about 60 F higher temperature. The effect of lower gas content combined with 120-125 F further lowering of temperature in the drips from the Chesterfield 15th stage heater test No. 2 is quite marked, notwithstanding the shorter time for protective film development in the 15th stage test coils. On the other hand, comparison of Chesterfield test No. 4 will show that, under some conditions of contamination, drips from the 15th stage heater may be more corrosive of some alloys than simultaneously produced drips from the 8th stage heater at the higher temperature. This is evident even allowing for inverse variation of contamination with effective velocity of condensate flow, unless it should be that the shorter protective-film development period has been a very important factor.

Treatment of feedwater with cyclohexylamine effected marked decrease in rates of contamination imparted by all nonferrous alloys tested and prevented entirely iron contamination from type 316 stainless steel. The response of the nickel-bearing nonferrous alloys to the cyclohexylamine treatment was less marked than the response of the other nonferrous alloys, sufficiently so that the copper-nickel alloys were displaced by aluminum bronze, aluminum brass, phosphorized copper, and arsenical admiralty at the most favorable end of the scale.

The rate of condensate contamination to be expected from contact with any alloy, nonferrous or ferrous, at any time is strongly influenced by the nature and extent of prior nonmetallic contamination of the condensate, possibly also by its prior metallic contamination, and by the arrangement and dimensions of the metal surfaces giving contact exposure to the condensate path. Continuance and intimacy of contact are of major importance. Effects of these several factors should be more definitely explored before attempting direct application of the present reported test results as criteria for contamination to be expected under any other set of conditions.

ACKNOWLEDGMENTS

The authors desire to record their appreciation of the courtesies shown them on the test work and preparation of the paper by many members of the staffs of Virginia Electric and Power Company, Rohm & Haas Company, Hall Laboratories Incorporated, and Stone & Webster Engineering Corporation, especially by the following:

Mr. J. G. Holtzelaw of Virginia Electric and Power Company, in giving his permission for publication of the paper.

Mr. T. E. Crossan of Virginia Electric and Power Company,

in his often much-needed encouragement during the conduct of the tests.

Mr. F. P. Crowell, superintendent of Bremo Power Station, and Mr. F. H. Spies, superintendent of Chesterfield Power Station, in making personnel available for assistance in conduct of the tests at the respective stations and in adjusting load distribution to meet the test requirements.

Mr. Ralph Palmer, superintendent of Twelfth Street Power Station, in making available laboratory personnel and facilities for carrying out the analytical work on the metallic recovery process.

Mr. E. J. Breton, formerly of Rohm & Haas Company, in his helpful suggestions on preparation and operation of the ion-exchange resins, and his former principals, in furnishing resins for exploratory tests and in promptness in meeting all requests.

Mr. A. W. Davenport, superintendent of construction of Stone & Webster Engineering Corporation, and his chief mechanical supervisor, Mr. R. J. Jeffers, in affording priority in both attention and expedition to the installation of the test equipments.

Mr. R. A. Grammer and Mr. H. O. Ames, Jr., of Stone & Webster Engineering Corporation, in their skillful preparation of all charts of the paper.

BIBLIOGRAPHY

- 1 "Operating History and Performance of 2000-Psi Forced-Circulation Boiler at Somerset Station of Montaup Electric Company," by G. U. Parks, W. S. Patterson, and W. F. Ryan, Trans. ASME, vol. 68, 1946, pp. 411-427.
- 2 "Special Studies of the Feedwater-Steam System of the 2000-Psi Boiler at Somerset Station of Montaup Electric Company," by W. D. Bissell, B. J. Cross, and H. E. White, Trans. ASME, vol. 68, 1946, pp. 429-442.
- 3 "Water Conditioning for the 2000-Psi Boiler at the Somerset Station of Montaup Electric Company," by W. W. Cerna and R. K. Scott, Trans. ASME, vol. 68, 1946, pp. 443-451.
- 4 "Experience With Instruments and Control Equipment for 2000-Psi Boiler at Somerset Station of Montaup Electric Company," by W. D. Bissell and E. B. Powell, Trans. ASME, vol. 68, 1946, pp. 453-466.
- 5 "Steel, Heat, and Water: Localized Formation of Magnetic Iron Oxide in Power Boilers," by H. M. Rivers and W. M. Sonnett, Proceedings of the Midwest Power Conference, 1950, pp. 114-121.
- 6 "Experimental Studies of Iron Oxide Deposits in Boilers," by C. Jacklin and W. H. Thompson, Proceedings of the Midwest Power Conference, 1950, pp. 108-113.
- 7 "Recent Developments of Boiler Water Research," by F. G. Straub, Proceedings of the Midwest Power Conference, 1948, pp. 295-297.
- 8 "Prevention of Corrosion and Metal Attack in the Steam Water Cycle of the Steam Power Plant," by F. G. Straub and H. D. Ongman, *Corrosion*, vol. 7, 1951, pp. 312-315.
- 9 "German Power Plant Steam Generators and Water Conditioning Systems," by W. W. Cerna, Proceedings of the Seventh Annual Water Conference, 1947, pp. 1-23.
- 10 "Colorimetric Determinations of Traces of Metals," by E. B. Sandell, Interscience Publishers, New York, N. Y., vol. 3, 1950, p. 376.

Discussion

C. L. BULOW.⁴ This paper contains much interesting information regarding the corrosion resistance of a representative group of copper-base alloys. The data for 70-30 cupro nickel containing 0.4 per cent iron, aluminum brass and arsenical admiralty indicated that the copper pickup by the condensate depends upon the alloy, composition of the solution, initial film on the tube surface, the time to remove this initial film, the time to build up a new film, and temperature.

The composition of the solution varied appreciably as regards

⁴Corrosion Metallurgist, Bridgeport Brass Company, Bridgeport, Conn.

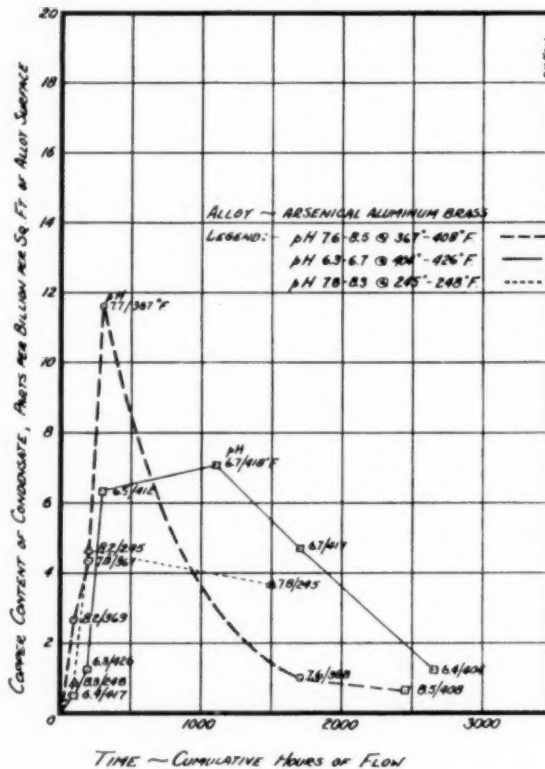


Fig. 11

the concentration of carbon dioxide and ammonia, and the pH reflected the various ratios of these two gases. It was found that the solutions could be grouped into two major groups, the first group showing a pH ranging from 6.3 up to 6.7 and the second group showing a pH ranging from 7.6 up to 8.5. Plotting of all of the data presented in Tables 2, 3, and 4 resulted in some interesting curves. The copper pickup was plotted against time, using values found in the two pH groups. This resulted in two curves covering the two pH ranges for each of the three alloys mentioned.

In Fig. 11 of this discussion the curves obtained for arsenical aluminum brass showed that the film initially present on this alloy hindered copper pickup by the condensate. In the high pH range this film was more rapidly removed than in the low pH range and resulted in a maximum copper pickup after approximately 300 hr. Thereafter a new film began to form on the metal surface which gradually became more resistant to corrosion by the condensate, and after 2400 hr was evidently still in the process of forming a stable film on the aluminum-brass surface.

The aluminum brass in the lower pH range took a somewhat longer period of time to remove the initial film and even after 2650 hr had not formed a stable film. Evidently another 700 hr would have been needed to see this alloy perform at its best in the lower pH range. This behavior of the aluminum brass appears to be consistent with what is known about this alloy where its corrosion resistance is controlled to a considerable extent by the stability of the aluminum-oxide film which forms on the surface. Based on the solubility characteristics of this film, it is expected that it would be more stable in the lower pH range than in the higher pH range. Therefore it would be very interesting to see what the copper pickup would be after another 1000 hr exposure.

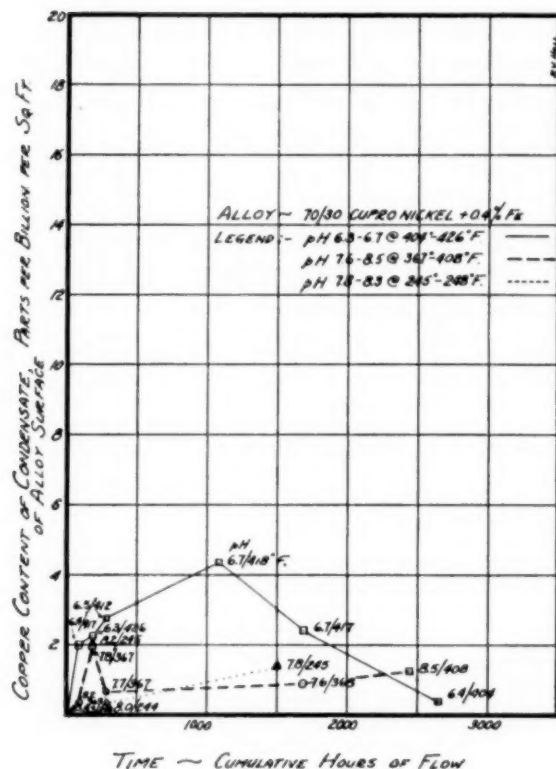


FIG. 12

The data for the 70-30 cupro nickel, Fig. 12, herewith, containing 0.4 per cent iron resulted in somewhat similarly shaped curves for the two pH ranges. In the high pH range the maximum copper pickup occurred after 200 hr, whereas in the lower pH range the maximum copper pickup occurred after 1100 hr. The data obtained in this investigation appear to be consistent with those obtained from other investigations regarding the behavior of 70-30 cupro nickel. Generally, in the absence of carbon dioxide and chlorides, we would expect the corrosion resistance of this alloy to be greater in the higher pH range than in the lower pH range. In this instance the behavior of the 70-30 cupro nickel was better at the higher pH values, with the exception that the curves obtained for the two pH ranges crossed one another at approximately 2150 hr. A longer time of exposure would be required to determine where the curves really level off.

The curves for arsenical admiralty, Fig. 13, showed considerable scatter during the first 200 or 300 hr. Evidently this is due to the condition of the initial film existing on the admiralty tube surfaces. In the low pH range a very smooth curve was obtained with the exception of one point at 200 hr. This curve showed that with the passage of time a much more stable film was building up on the arsenical admiralty tube surface, which in turn reduced the copper pickup by the steam condensate. The slope of the curve indicated that the film may not have yet obtained its maximum stability even after 2650 hr. The scatter of the points for the high pH range suggested rapid removal of the initial film from the admiralty surface, followed by very rapid building up of a protective film on its surface.

It is anticipated that similar treatment of the data compiled for the other alloys would result in curves characteristic of these materials in this environment.

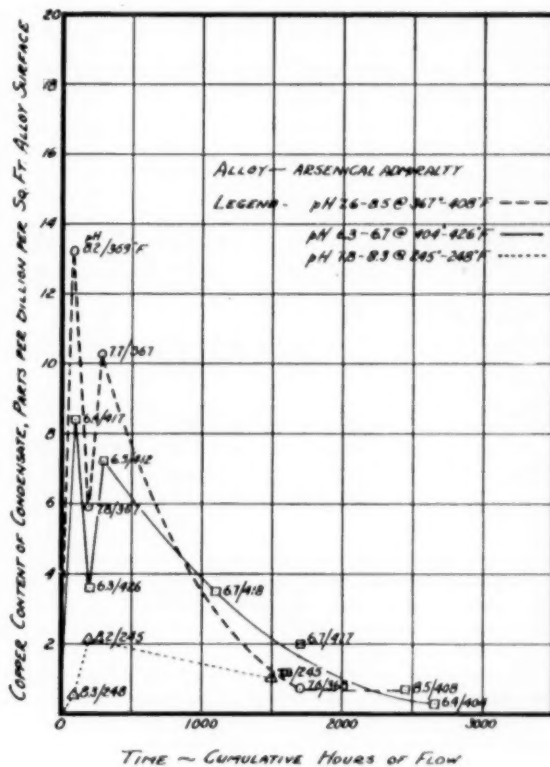


FIG. 13

The shape of the curves obtained is representative of what should be expected where film-covered copper alloys are exposed to weakly corrosive solutions. Generally, this initial film effect can be reduced considerably by dissolving the films in a suitable acid immediately preceding initiation of the test. Careful degreasing of the tubes prior to the acid treatment also may be necessary, since oil films may interfere with acid-cleaning.

W. V. DRAKE⁵ AND W. L. THOMPSON.⁶ In an industry that is expanding as rapidly as the power industry the paper should prove most interesting and informative. The authors are to be congratulated on a timely and valuable contribution to the power industry.

As pointed out in the opening paragraph, the accumulation of foreign metal and metallic oxides on the internal heating surfaces of high-pressure boilers has become a source of growing concern to the steam power industry in the United States. We at West Penn Power Company have been no exception.

In order to minimize and control this condition a test program was set up March 26, 1951, at Mitchell Power Station, a 170,000-kw steam station in the West Penn Power System. The test program involved the following equipment and procedures:

- 1 Three boilers, 500,000 lb steam per hr, 1400 psig drum pressure, 925 F steam temperature.
- 2 Two turbogenerators, two-cylinder, tandem-compound, double-flow, impulse-reaction type, 65,000 kw, full-load rating 81,250 kw, 3600 rpm, condensing-steam turbines.

⁵ Manager of Power Production, West Penn Power Company, Pittsburgh, Pa. Mem. ASME.

⁶ West Penn Power Company.

3 Three extraction heaters:

- (a) High-pressure heater—349 psia—426 F—Monel tubes
 (b) Intermediate-pressure heater—137 psia—346 F—Monel tubes
 (c) Low-pressure heater—130 psia—194 F—admiralty tubes

4 Addition of cyclohexylamine to feedwater system to increase pH to 8.6.

5 Study effect on feedwater flowmeter readings.

6 Chemical tests on boiler feedwater and condensate.

The chemicals normally used are potassium hydroxide, potassium metaphosphate, and potassium sulphite. The chemicals are added continuously to maintain in the boiler water a concentration of 2–5 ppm PO_4 , 3–5 ppm SO_3 . The total solids in the boiler are maintained below 500 ppm.

The data in Table 10 of this discussion show the effect of the addition of cyclohexylamine to the feedwater system.

TABLE 10 EFFECT OF ADDING CYCLOHEXYLAMINE TO FEEDWATER SYSTEM

Date Sample	Before 3/26/51		After 7/19/51	
	Feedwater	Condensate	Feedwater	Condensate
Fe, ppm.....	0.08	0.12	0.03	0.03
Cu, ppm.....	0.01	0.01	0.01	0.01

The percentage reduction of iron (Fe) in the feedwater during the period of treatment was approximately 52 per cent. The results corroborate the test data shown in Table 8 of the paper. The amount of copper present in the feedwater system remained substantially the same.

The effect of the addition of the cyclohexylamine on the boiler feedwater flow nozzles is shown in Table 11 of this discussion.

TABLE 11 EFFECT OF ADDING CYCLOHEXYLAMINE ON FEEDWATER FLOW NOZZLES

	—Errors in feedwater flowmeter readings, per cent—	
	March 26, 1951	October, 1951
No. 1 boiler.....	6.9	3.5
No. 2 boiler.....	5.0	3.5
No. 3 boiler.....	10.1	8.5

The errors as determined by calibration tests on the feedwater flowmeters were at times reduced by as much as 50 per cent. However, after 3 or 4 months the readings became stable and did not vary greatly from the readings given for October, 1951.

The increase of condensate temperature causing an increase in contamination from the alloys tested, as brought out in the paper, confirms the results of a metal test conducted at the Springdale Power Station of the West Penn Power Company in 1948 and 1949, under the direction of Mr. M. D. Baker. Feedwater at 100 F, 250 F, and 430 F was passed over a weighted stainless-steel test specimen (18–8 type) for 210 days with the results given in Table 12, herewith.

TABLE 12 RESULTS ON STAINLESS-STEEL SPECIMEN OF FEEDWATER FLOW

Temperature, F	Loss of metal mg./dm ² /day
100	0.042
250	0.114
430	0.127

Under Conclusions it is stated that, while the initial corrosion rate would be high after placing equipment in service, it could be expected to decrease progressively to a relatively minor rate. Does this mean that, after the period of high attack, the corrosion can be ignored? If this is what is meant, we cannot agree as attack on the metal in the feedwater system at Mitchell is still a problem.

What conclusions have been reached regarding the use of cyclohexylamine? Is it beneficial? If so, can it be recommended in systems having nickel alloys?

C. E. KAUFMAN⁷ AND E. A. YORKGITSIS.⁷ Gradual loss of metal in the extensive preboiler system of the modern power plant is important because of the possibility that failures will be produced not only in the equipment attacked, but in the boiler too. Because little quantitative information has heretofore been available, the factual data in the paper are most welcome.

Since metal is always dissolved to a greater or lesser extent, we are constantly faced with the question of what can be done to minimize the damage.

Of particular interest is the effectiveness of cyclohexylamine in reducing iron pickup and deposition in the Brema Station condensate-feedwater cycle and in reducing corrosion rates of the nonferrous alloys which were tested. We have data and experience confirming this information.

As at Brema, cyclohexylamine is ordinarily added in other plants to minimize condensate corrosion of ferrous metals through increase of pH. At the same time, however, cyclohexylamine gives protection to nonferrous metals.

In some places where we have recommended cyclohexylamine, 2-in. \times 1-in. low-carbon, cold-rolled steel test strips and a few soft copper strips have been installed in the condensate systems. Results of tests which ran for about 30 days at two plants are listed in Table 13 of this discussion.

TABLE 13 COMPARATIVE CORROSION-RATE DATA OBTAINED WITH TEST STRIPS IN RETURN SYSTEMS BEFORE AND DURING TREATMENT WITH CYCLOHEXYLAMINE

Type of plant	Metal tested	Corrosion rate, mg./dm ² /day Before treatment	Corrosion rate, mg./dm ² /day During treatment	Per cent corrosion reduction
Manufacturer of electrical supplies	Steel	43	2.2	95
	Copper	1.0	0.1	90
Producer of grain products	Steel	103	4.4	96
	Steel	28	3.7	87
	Copper	6.7	1.9	72

Cyclohexylamine has been especially effective at small cost in utility stations such as the Brema Plant. Plant men and our engineers collected data in one station operating at a boiler-drum pressure of 1350 psi and a superheated-steam temperature of 925 F. The iron in the feedwater during the first 3 months of treatment was reduced in one turbine system from 0.16 to 0.06 ppm and in the other turbine system from 0.09 to 0.04 ppm. During this same period the ammonia in the steam-condensate-feedwater cycle increased from 0.04 to 0.05 ppm before treatment to 0.06 to 0.07 ppm after a stable state was obtained with treatment. This ammonia increase represented 10 to 15 per cent decomposition of cyclohexylamine at the 1350-psi pressure.

E. H. KRIEG.⁸ There has been much concern in the past over the effect of copper deposits in boilers and there is much reason to believe that such deposits have been the cause of a great deal of trouble. Therefore any means to reduce copper deposits is a step toward increasing boiler availability and reducing maintenance costs. This much-needed paper represents a painstaking effort to obtain quantitative results and is of such wide scope that the challenge of obtaining additional data and even more definitive results could well be taken up by others in the utility industry as well as by the manufacturers.

Almost every one seems to have a pet corrosion inhibitor, and the engineer is beset by the problem of whether to select anti-monial, arsenical, or phosphorized admiralty. There have not been available too many data on which to be really sure of the selection. In this paper are presented data that will assist in selecting heater tubing and this is another forward step in the efforts to increase the availability and decrease the cost of maintenance of power-plant equipment.

⁷ Hall Laboratories, Inc., Pittsburgh, Pa.

⁸ Consulting Engineer, Stone & Webster Engineering Corporation, Boston, Mass. Fellow ASME.

F. L. LAQUE.⁹ At the outset we must recognize the prodigious amount of work and expense that was required to design, assemble, and operate the apparatus used in this investigation—we can also assume that an equal amount of patience was needed in coping with the many experimental difficulties that are bound to arise in a study such as this. We must then be grateful to the authors for their efforts in throwing light on this important subject.

The factors that determine the rates of corrosion of metals by steam condensate are very complex and no doubt vary from day to day during normal operations. This is especially true of the amounts of dissolved gases present, as noted by the authors. Presumably, after sufficient exposure has occurred to permit the development of films on the metal surfaces, the amount of metal that is acquired by the condensate is determined by the state of dynamic balance between the forces tending to remove protective films mechanically or chemically and those tending to keep such films in good repair. It is not surprising, therefore, that trends of metal pickup were not consistent and that all the metals did not follow the same pattern in this respect. If it were practical to do so with the apparatus as set up (or some modification of it), to catch the corrosion products for analysis, it would be of considerable interest to determine how much of the corrosion products existed in an ionized state and how much was present as insoluble compounds in suspension in the condensate. Subsequent effects on the surfaces with which the condensate would come into contact might be quite different, depending on the nature and extent of these effects and thus an additional basis for rating the alloys might be established.

In spite of these natural complexities of the basic problem and of the experimental methods used, the data provided appear to be adequate to support the conclusions reached by the authors and to indicate which alloys will contribute least contamination to the water.

The demonstrated advantage of the presence of iron in the cupro-nickel alloys is in line with similar effects in salt water and is probably due to an improvement in the characteristics of their protective films. A comparison with alloys of still lower iron content, e.g., under 0.10 per cent, might have established this point even more definitely.

The basis for the fairly consistent superiority of the arsenical admiralty brass over the other brasses is not clear—especially in view of the fact that the presence of arsenic in the aluminum brass evidently did not exert a similar effect in improving the protective qualities of the films that developed on this alloy.

The extent of iron pickup from the Type 316 stainless-steel coils was indeed surprising in view of the expectation that this alloy would be much more resistant to corrosion by the hot condensate than any of the copper alloys. The return to substantial iron pickup after termination of the sixth run with cyclohexylamine treatment at the Bremo Station indicates that the alloy itself was attacked and the iron pickup was not due to some initial contamination of the surface of the stainless steel.

The extent of initial iron pickup from the cupro-nickel and Monel coils in the Bremo 10th stage tests is difficult to understand. The iron in these alloys is in solid solution. It is unlikely that it would suffer preferential leaching by the condensate. Therefore it should have been accompanied by a much higher copper pickup than shown by the data presumably for the same run in column 1 of Table 4 of the paper. This supports the action of the authors in questioning the reliability of their figures for iron pickup from the cupro-nickel alloys.

It is evident that corrosion of iron may be reduced by the use of

cyclohexylamine with a simultaneous reduction in corrosion of the copper-base alloys in the system—in fact, from the data in Table 5 on the analysis of the drips from the 10th stage heater at Bremo, it seems that this treatment was more effective in reducing copper pickup from the 70-30 cupro-nickel tubes than in reducing iron pickup from the steel in this system.

From the area exposed in a 50-ft-long test coil, it can be calculated that for a rate of flow of 4.5 fps the rate of solution of copper required to give a copper pickup of 1 ppb per sq ft in 100 hr is about 0.6 mg per sq dm per day. For pure copper this would be equivalent to wasting of the metal at a rate of only 0.0001 in. per year—for lower-copper-content alloys, the wastage would be increased proportionately. Perhaps these figures could be checked by assuming, for example, that the 70-30 cupro-nickel tubes in the 10th stage heater at Bremo are corroding at the highest rates indicated, e.g., about 3 mg Cu per sq dm per day (equivalent to 5 ppb Cu per sq ft surface in Table 4) and then calculating what the copper content of the drips should be in parts per million. This could be compared with the amount usually found as indicated by the various analyses reported in Table 5. While a close check need not be expected, any substantial differences in the order of magnitude should be significant.

S. T. POWELL.¹⁰ The authors should be complimented on the new approach they have found to a difficult problem. It is our opinion that the method described in this paper may prove to be a new and useful tool for the study of minute concentrations carried in the feedwater supply of high-pressure steam power plants.

The ingenious use of ion-exchange units to accumulate copper and iron from feedwater samples makes it possible to determine the source of these contaminants with an accuracy which has never been possible in spot-sampling surveys. It has been our experience that even composite samples taken over several hours show conflicting results, and that many confirming tests must be made to establish trends and the response of the feedwater cycle to variations in treatment. On the other hand, in the ion-exchange procedure, the quantities dealt with are sufficiently large to give convincing data, and if pickup of metals varies from time to time there is no danger of missing the incidence of high contamination that spot-sampling might fail to detect.

The authors discuss the following possible sources of irregularity in their results:

Differences in effectiveness of purging resulting from the 10 to 20-min flushing before diverting condensate flow to recovery equipment on analytical runs not immediately preceded by non-analytical runs. It has been our observation that it takes from several hours to more than a day to purge a system completely and reach stable conditions.

Differences in dissolved-gas content of the condensate more significant than the spot-test averages of the tabulations would indicate. It is just as difficult to obtain accurate analyses of dissolved gas as it is to obtain accurate analysis of the metals recovered by the ingenious system herein described. The results could be broadened by the use of recording instruments, for instance, oxygen recorders, hydrogen recorders, and conductivity and pH recorders. In the modern steam-power plant, quality of the condensate has improved so greatly and the contained solids are so low that flowing samples with a continuous record or cumulative samples over a long time period seem to be necessary to obtain consistent results.

The authors described, also, how iron-oxide accumulations on the boiler feed-pump casings and impellers and other objects have caused interference with feedwater flow. We are presently concerned with several other plants throughout the country in which similar observations have been made. It appears to be rather

¹⁰ Consulting Chemical Engineer, Baltimore, Md. Fellow ASME.

⁹ In charge, Corrosion Engineering Section, Development and Research Division, The International Nickel Company, Inc., New York, N. Y.

definitely indicated that a survey and study of such difficulties should be undertaken. Meanwhile, it is believed the authors may have pointed the way in which some of these studies should be directed.

With regard to the use of cyclohexylamine, we do believe that a word of caution is necessary when it is contemplated to use either this or related amines for feedwater treatment. The author is familiar with two cases of the use of cyclohexylamine with conflicting results. At one plant in which extremely careful control has been maintained at all times, it is used to raise the pH of the feedwater to about 8.5 to protect the preboiler system, beginning with the hot-well, and the treatment has effected marked improvement. The concentrations used have been of the order of magnitude of less than 0.01 ppm. In the other case, the amine was used indiscriminately and without suitable control, resulting in attack on copper alloys. Frequent or continuous measurement of pH should accompany the use of any of the amine series of compounds.

One of our group who has just returned from a European assignment, learned that ammonia was used in German power-station practice when the operators were unable to obtain hydrazine which previously had been used for chemical deaeration. Elevation of the pH with ammonia retarded corrosion of boiler steel and had no adverse effect on copper alloys in the feed system as long as oxygen and carbon dioxide were entirely absent. Its application as a panacea is not considered safe, and it should be limited to plants subject to thorough chemical control.

AUTHORS' CLOSURE

Limitations on available time made it necessary to interrupt the condensate contamination tests prior to securing the full extent of specific information desired on certain aspects of the metallic contamination problem. However, soon after preparing the paper it proved feasible to make another run on the 10th stage heater test equipment at Bremo Power Station. During the interval and throughout the new test run, designated Bremo 10th stage heater test No. 8, completed on October 31, 1952, cyclohexylamine was continuously present in the plant system on all periods of operation, the rate of treatment with this chemical being approximately the same as reported for the earlier Bremo 10th stage heater test run No. 6 recorded in the paper. In accord with practice adopted at the beginning of the series, until test work was actually resumed the test coils had remained idle, merely flooded with condensate. Rates of condensate flow and

TABLE 14 ANALYSIS OF DRIPS TO TEST COILS AND RESULTING METALLIC CONTAMINATION 10TH STAGE HEATER—BREM0 POWER STATION

Test no.	5	6 ^a	7	8 ^a
Conductivity, mmho/cm	1.33	1.85	0.60	2.05
pH	6.7	8.5	6.4	8.6
CO ₂ , ppm	0.13	0	0.10	0
NH ₃ , ppm	0	0.05	0	0.06
O ₂ , ml/liter	0	0	0	0
Temperature, F	417	408	404	410
Pressure, psi gage	303	278	257	284
Cumulative hours	1700	2450	2650	4000

Copper pickup—ppb per sq ft alloy surface

Phosphorized copper	2.80	0.34	0.87	0.23
88-10-2 Cu-Zn-Sn	4.46	0.67	2.93	1.29
Antimonial admiralty	4.49	0.81	1.23	0.46
Arsenical admiralty	1.93	0.64	0.26	0.19
Phosphorized admiralty	4.15	0.81	1.55	2.28
Aluminum bronze	6.09	0.23	1.48	0.34
Arsenical brass	4.73	0.64	1.29	0.21
90-10 Cu-Ni 0.8 Fe	5.12	1.61	0.46	4.22
70-30 Cu-Ni 0.4 Fe	2.43	1.25	0.39	3.60
70-30 Cu-Ni 0.6 Fe	2.38	0.66	0.34	2.92
Monel	0.96	0.83	1.88	1.24

Iron pickup—ppb per sq ft alloy surface

316 Stainless steel	4.26	0	2.70	0
---------------------	------	---	------	---

^a Cyclohexylamine added to feedwater with pH controlled at 8.5 approximately.

other general procedures of the analytical run were essentially the same for test run No. 8 as on the preceding seven runs on the same test equipment. The data secured on the new test run are entered in Table 14 as an extension of Table 4, with corresponding data of test Nos. 5, 6, and 7 made on the same equipment repeated for convenience of reference. The rates of copper contamination from the different alloy specimens found on the four tests are shown graphically in chronological sequence in Fig. 14 and arranged with respect to character of chemical treatment in Fig. 15. Iron contamination from type 316 stainless steel was again zero.

Fig. 14 is drawn in two sections, distinctly separating the graphs for contamination rates from the nonferrous specimens of copper-nickel and of nickel-free types to present more clearly the apparent difference in influence upon the specimens of each type from the change from the previous normal feedwater treatment with drips of pH 6.3-6.7 to cyclohexylamine treatment with more alkaline drips, pH 8.5 approximately. It will be noted that the response of the alloy specimens of each type on resumption of cyclohexylamine treatment of the feedwater results in seemingly characteristic trends in reference lines, downward toward decrease in contamination rates from nickel-free alloys and upward from copper-nickel alloys. Also, among the specimens

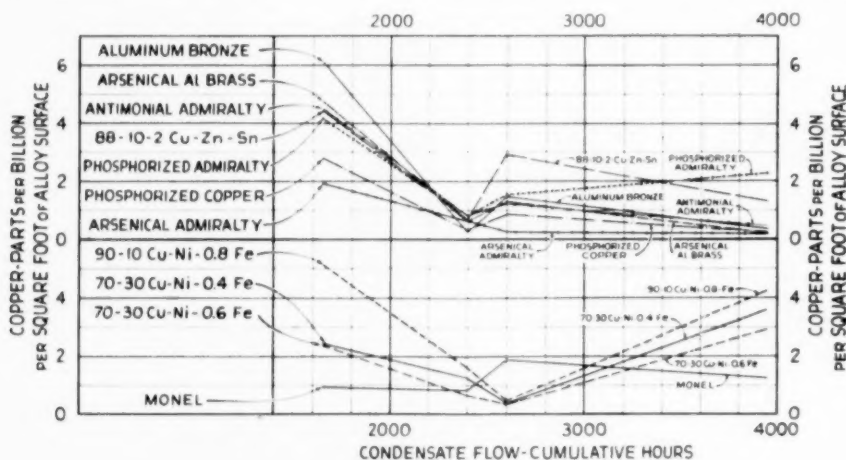


Fig. 14

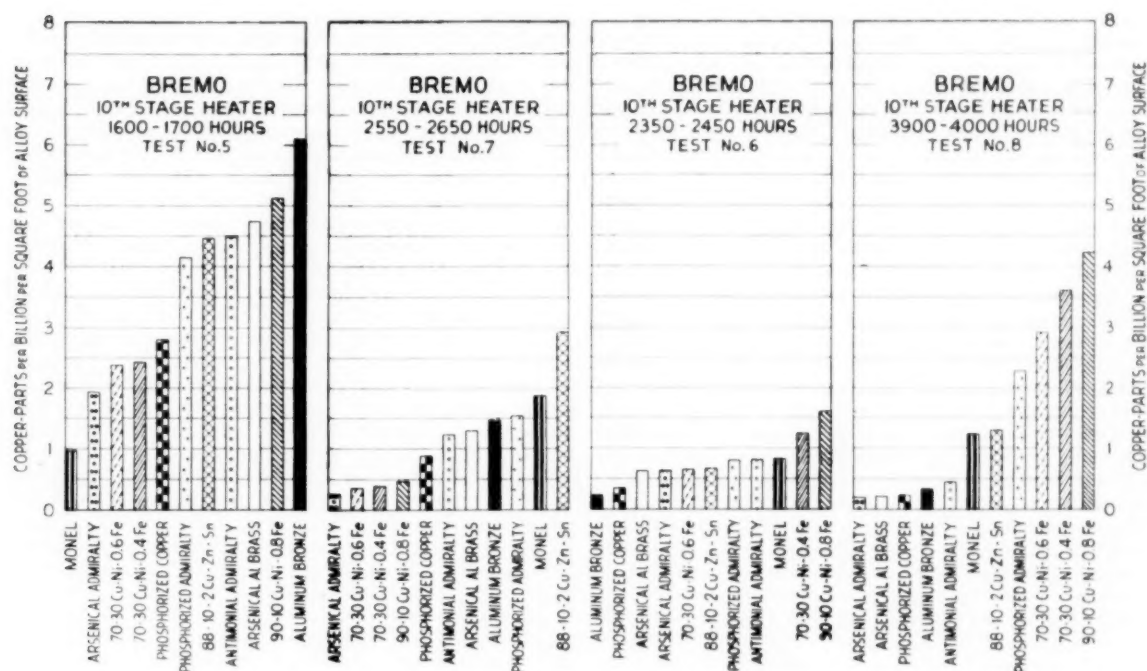


Fig. 15

of each alloy type there is an exception, phosphorized admiralty showing an increase in contamination rate and Monel a decrease in contamination rate.

In the paper, attention is called to the very minor decrease in rate of copper contamination from Monel following initiation of the cyclohexylamine treatment shown by BreMo test No. 6 and to the marked increase in rate of copper contamination from this alloy which appears in the results of BreMo test No. 7 after the temporary return to the previous normal treatment of feedwater. On referring back to Table 4, the record of copper contamination from Monel suggests that protective-film development on the alloy under the conditions of test might be highly sensitive to small changes in chemistry of the heater drips. It would also appear that the Monel specimen practically devoid of protective-film development imparted contamination at only relatively moderate rate. BreMo test No. 7 seems about on a par with test No. 1 in protective-film development. Whether test No. 8 records a transient or stable state of film development is of course uncertain from a single test. Further study seems needed for confident understanding of the Monel behavior. For the other copper-nickel alloy specimens, the records of BreMo test Nos. 6, 7, and 8 seem to give striking evidence of the temporary persistence of protective-film effects imparted by film development under particular chemical conditions or combination of chemical conditions followed by impairment in protective effectiveness when one of the factors in the original film development has been withdrawn. Copper-contamination rates from the nickel-free nonferrous alloy specimens show apparently permanently persistent beneficial effects from use of cyclohexylamine treatment in all except phosphorized admiralty and possibly 88-10-2 Cu-Zn-Sn. The higher contamination rate shown for aluminum bronze on BreMo test No. 8 as compared with test No. 6 seems too slight to be of real significance. The authors are without satisfactory explanation of the behavior of 88-10-2 Cu-Zn-Sn and phosphorized admiralty.

The paper called attention also to the high iron contamination from copper-nickel alloy specimens indicated on the initial run on BreMo 10th stage heater test equipment and suggested the probability of nickel interference in the iron determinations. Tests for nickel contamination from the several nickel-bearing specimens on test No. 8 showed only traces too minute to influence the iron determination at this time, the largest nickel contamination being from Monel, approximately 0.2 ppb per sq ft of contact surface. At the same time, in contrast with "iron" contamination rates ranging roughly from 3 ppb per sq ft of contact surface from the 70-30 Cu-Ni-0.6 Fe specimen to 6 ppb per sq ft of contact surface from the Monel specimen reported for the initial BreMo test run, on test No. 8 on the same equipment "iron" contamination of condensate from these essentially copper-nickel alloys was found to be nil, within the limits of error, except for the 70-30 Cu-Ni-0.6 Fe specimen from which the iron pickup found was a little below 2 ppb per sq ft of contact surface. It is thought that in the case of this 70-30 Cu-Ni-0.6 Fe specimen on test No. 8 some small particles of iron oxide must have washed through from the heater shell or connecting piping, which seems especially likely as the iron contamination shown concurrently from phosphorized copper was a little over 2 ppb per sq ft of contact surface, from 88-10-2 Cu-Zn-Sn about 1 ppb per sq ft of contact surface, and from arsenical admiralty a little below 4 ppb per sq ft of contact surface. While the evidence is rather indirect, the authors conclude the "iron" contamination from all relatively high nickel alloys found on the initial 10th stage heater test run at BreMo Power Station was chiefly a nickel interference phenomenon.

The analyses of drips supplied to the test coils on BreMo test run No. 8, including the respective "blank" concentrations for copper and iron, reflect the influence of the continuous presence of cyclohexylamine in the system throughout the more than 9 month interval between completion of test No. 7 and completion of test No. 8, aside from an approximately 3 week period for

routine overhaul of the main turbine. The prior copper contamination of the stage heater drips as supplied to the test coils on the latter run was about 0.0029 ppb per sq ft of contact surface, equivalent to less than 0.1 per cent of the corresponding contamination rate from the 70-30 Cu-Ni 0.4 Fe test coil. In actual magnitude of contamination, this is slightly higher than the value for the drips on test No. 6 but appreciably lower than for any of the other previous runs on the Brema 10th stage heater test equipment. Prior iron contamination of the stage heater drips was apparently 0.047 ppm, a value close to the average for Brema tests 1 to 5, inclusive, and for test No. 6 but considerably higher than found for test No. 7. These values for prior metallic contamination of the 10th stage heater drips, considered in relation to the contamination rates reported from the 70-30 Cu-Ni 0.4 Fe test specimen on the same heater, seem to indicate (1) that significant difference exists between solubility relations of ammonia, cyclohexylamine, and carbon dioxide in the insulated coils of the test specimen and corresponding solubility relations in the condensed film continually forming on and flowing from the cooler heat-absorbing surface of the heater tubes and (2) that, as solubility relations for these important gases in the heater shell and drip piping are probably about the same as in the test coils, the actual magnitude of iron contamination picked up in the 10th stage heater under the previous normal condition of feedwater treatment had not made as significant contribution to the total iron contamination accumulated in the condensate-feedwater system as that from the lower temperature parts of the system in which the solubility of carbon dioxide was higher.

In oral discussion, A. A. Berk called attention to the possibility of trouble from breakdown of cyclohexylamine and from formation of an insoluble bicarbonate of that chemical. The authors have considered these warning comments rather important in the interest of the prospective user of cyclohexylamine in boiler-feedwater treatment. Largely from Mr. Berk's Bureau of Mines Technical Paper 714 on the properties of such amines, also from the courtesy of other users, the authors have been clearly aware of possibilities of adverse results from casual or inadvised handling of the cyclohexylamine treatment. From the authors' viewpoint, adverse results are possible in the use of the majority of boiler-water and boiler-feedwater chemicals in high-pressure service unless genuine care is maintained. To date, no trouble has been experienced in the use of cyclohexylamine at the stations of Virginia Electric and Power Company. In one instance slight breakdown of cyclohexylamine to ammonia was found when maintaining pH 9.0 in the feedwater. By lowering the control point to pH 8.8 the breakdown was decreased from 0.20 ppm NH_3 a negligible value, in the order of 0.05 ppm NH_3 . However, no increase in copper content of the feedwater was noted during the brief period of the higher ammonia concentration. The authors have not attempted use of cyclohexylamine in combating high dissolved carbon-dioxide content of the feedwater. It would seem probable that, under such conditions, deposition of cyclohexylamine bicarbonate might occur, but to date this has not been encountered at the power stations of Virginia Electric and Power Company.

The authors are grateful to Mr. Bulow for adding so constructively to the technical interpretation of the test data. They do not have the benefit of a subsequent run of 1000 hr on arsenical aluminum brass in contact with condensate of the lower pH range regarding which Mr. Bulow expresses interest but, after 1300 hr additional exposure to solution flow of pH 8.6 and temperature of 410 F approximately, the copper pickup found for the arsenical aluminum brass coil was 0.21 parts per billion per sq ft of alloy surface which, while possibly not yet the equilibrium value, is somewhat closer to the leveling-off stage. In the same connection, Mr. Bulow's Fig. 11 points up rather interestingly

the greater effectiveness of the pH 8.5 condensate of 408 F, in bringing the protective-film development on the specimen previously subjected to pH 6.3-6.7 condensate of 412-426 F to about the same stage in 750 hr of exposure which would have been had by initial and continual exposure to flow of the pH 7.6-7.8 condensate of 367-369 F. It would appear that, in the pH 6.3-6.7 condensate of 404-426 F, still an additional 700 hr or more would have been required to attain equivalent protective development. The rapid loss of protective film in contact with the pH 6.4 condensate on changing to the conditions of test No. 7 suggests that a difference in film chemistry is required to meet the greater severity of the latter conditions.

From the data of test run No. 8 which have been quoted earlier in the closure, the curve for 70-30 Cu-Ni 0.4 Fe exposed to condensate flow at 410 F and pH 8.5 may level off at a higher contamination rate than expectable for the pH 6.4-6.7 condensate. Protective-film development on the arsenical admiralty specimens would seem rather sensitive to change in pH value of the condensate, which is another feature on which the authors are glad to see Mr. Bulow bring such clear light. The third curve on each of Mr. Bulow's charts, presenting data for condensate conditions of pH 7.8-8.3 at 244-248 F, tends to give more prominence to the influence of temperature than the charts of the original paper. It will, however, be apparent from Mr. Bulow's discussion of the other two curves that difference in pH value may contribute very importantly in determining relative position and shape of the contamination rate curves.

Experience at one of the other power stations of the West Penn system generally similar to that reported by Mr. Drake and Mr. Thompson in combating iron-oxide accumulation in the feedwater system at Mitchell Power Station was a very important factor in encouraging use of cyclohexylamine by Virginia Electric and Power Company, and the authors are glad to see publication of these valuable data. The inclusion of the data of Table 12 on the effect of feedwater flow in contact with 18-8 type stainless steel is also a very appropriate contribution, especially as the authors are advised in subsequent personal communication that the test was made with flowing deaerated feedwater of pH 7.5-8.5 under conditions which prevented atmospheric contact.

Mr. Drake and Mr. Thompson raise questions on features of the paper some of which had not been made very definite. The first seven test runs did not cover a sufficient period of flowing contact of condensate with alloy specimens to show positive leveling off of the contamination rates. Test No. 8 has recorded effects of further opportunity for protective-film development under cyclohexylamine treatment in the boiler-feedwater system and the results indicate a much closer approach to leveling off in contamination rates from certain of the alloys and actual increase in contamination from others. The authors' observations indicate that cyclohexylamine treatment proves distinctly beneficial in decreasing contamination from iron and also from some of the nonferrous tube materials. The authors are far from satisfied that this chemical furnishes a complete answer to the condensate contamination problem, especially with respect to copper-nickel alloys other than Monel. They are currently of the opinion that complete disposal of dissolved oxygen at normal hot well temperature is the most urgent of the remaining unsolved problems of high-pressure-boiler feedwater treatment.

The records furnished by Mr. Kaufman and Mr. Yorkgitis from results secured in different plants using cyclohexylamine treatment of boiler feedwater are also very welcome additions to the discussion. The data quoted by these discussers are in good agreement with results secured by Virginia Electric and Power Company at Brema and Possum Point Power Stations.

Mr. LaQue refers to the desirability of distinguishing between the corrosion products ionized and those in the suspended state in

the condensate flowing from the test coils. The information so obtainable would undoubtedly be of considerable interest and value. To secure the information, however, would have involved considerably more work and time than could reasonably be arranged. Effort was made to separate the dissolved and suspended materials, and this was the function of the glass-wool filters, but the prime purpose in view was to effect complete recovery of all contained metals. As actually employed, the glass-wool filters were found to retain a widely ranging proportion, 44 per cent to 95 per cent, of the recovered metallic contamination, and the proportion retained was not consistent for any particular coil or set of coils. The variations were believed due in large measure to variations in air content of the filters after the leaching process and in density attained in packing the glass wool.

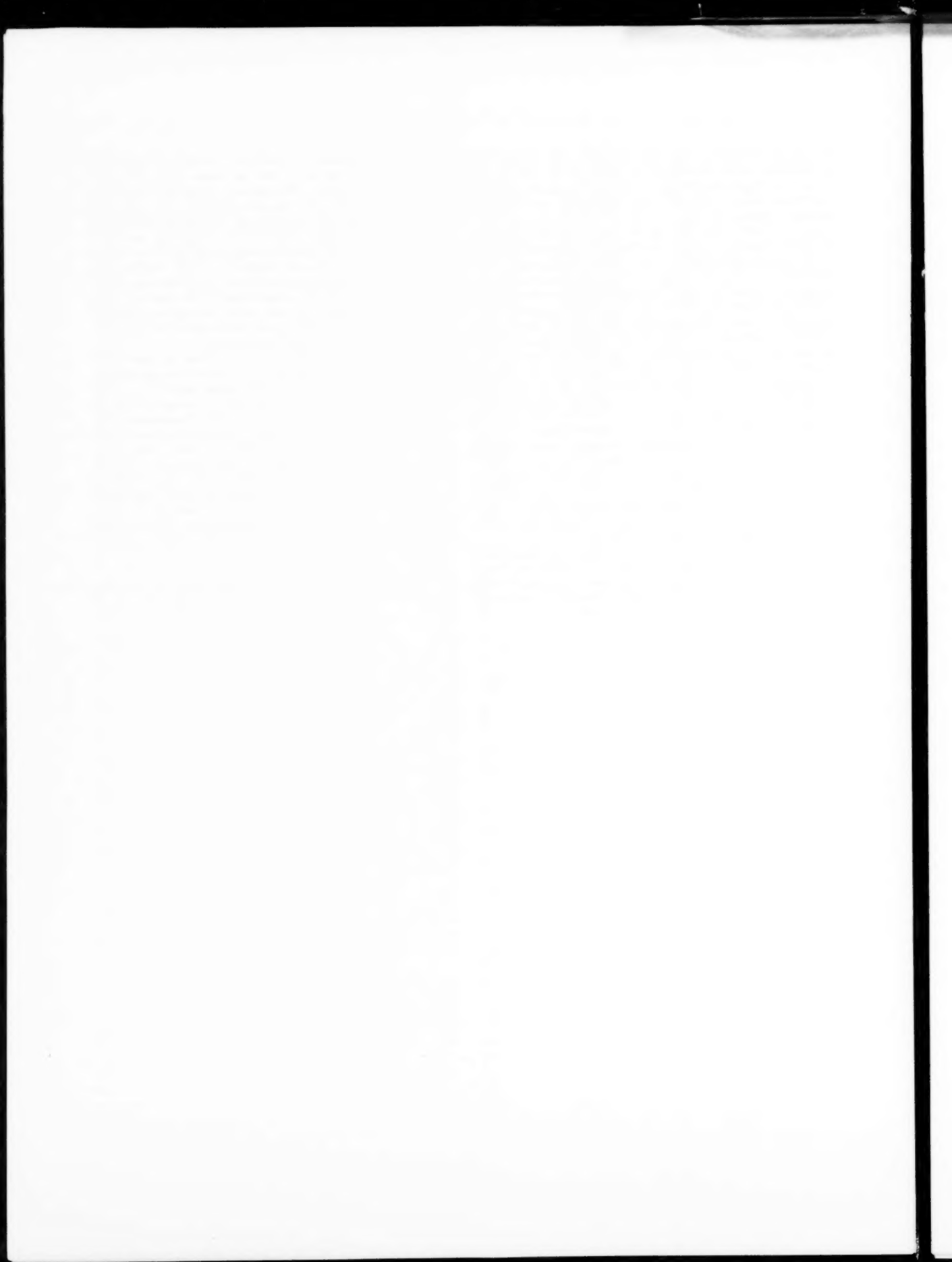
Nickel interference in the photometric determinations for iron contamination in the condensate from the test coils was suggested in the paper as a probable major source of "iron" picked up from the Monel and 70-30 Cu-Ni coils on the initial test run. As mentioned earlier in the closure, the determinations made for test run No. 8 would considerably strengthen the probability that nickel interference had been a major factor in the "iron" values questioned, in fact rather indicate that nickel interference had been the entire source of the iron. Also, from test No. 8 the anticipation of the original paper, that the source of "iron" contamination from these alloys would be substantially depleted in time, would seem quite reasonably fulfilled.

The 70-30 copper-nickel of the Chesterfield 8th stage heater tubes included 0.03 per cent iron and, in the case of the Brems 10th stage heater tubes, the alloy included approximately 0.4 per cent iron. The admiralty of the Chesterfield 15th stage heat-exchanger tubes was of the arsenical inhibited type. However,

continuity and intimacy of condensate contact with the metal surface differ indeterminately and, as pointed out in the paper, the relative dimensions of the paths of condensate flow in the heaters as compared with the path through a test coil are so markedly different that quantitatively the contamination rates under the test-coil and power-plant conditions are necessarily widely different. The research program set up, as closely as seemed practicable, identical conditions for the several alloys to ascertain comparative contamination rates under these identical conditions. Numerical conversion of specific test-coil results to contamination rates expectable in the power plant of different design will call for somewhat more research than has been so far undertaken to the knowledge of the authors.

The potential value of data from more frequent samplings of condensate for dissolved gas content for correlation and interpretation of the changing contamination rates reported for the different alloys, to which S. T. Powell refers, is recognized by the authors and, in fact, they believe, can hardly be overemphasized. In the Virginia Electric and Power Company more recent high-pressure plant installations the several recording instruments, for dissolved oxygen and hydrogen, conductivity, and pH, mentioned by Mr. Powell, are all included. Also, as will doubtless have been inferred from their response to Mr. Berk's oral discussion, the authors are in full sympathy with warnings of caution in application of chemicals to boiler-water or boiler-feedwater treatment. This, however, is a matter which seems in need of more general emphasis.

The recognition which Mr. Krieg, Mr. LaQue, and Mr. S. T. Powell generously accord the effort involved in work of the nature and scope which the paper reports is much appreciated by the authors.



The Motion of a Link Chain Over a Roller

By A. E. RICHARD de JONGE,¹ NEW YORK, N. Y.

A coal-cutting excavator is described in which trouble was encountered with link chains carrying excavating buckets. The chains were moved by an upper hexagon tumbler driven by an electric motor. The trouble was traced to the link chains passing over too small a deflecting roller. An investigation into the geometry of the problem is presented and it is shown that the mechanical three or multibody problem can be reduced to a problem in kinematic geometry by eliminating the forces, but retaining their lines of action. A solution for this problem is given. The principal object, namely, the derivation of the correct dimension for the deflecting roller to prevent the troublesome condition that existed, has been solved.

INTRODUCTION

IF a link chain, like that of a bucket conveyor, is to be deflected from its path, rollers are commonly used. The questions arising immediately are: "Is the size of such roller immaterial?" and "what should its diameter be?"

To understand why these questions are being asked, a case may be described which the author was called upon to solve a long time ago. A somewhat similar case was referred to the author recently, indicating that this problem is by no means thoroughly understood as yet. It will here be considered with respect to the former and rather more spectacular case.

A European firm of excavator and dredger builders was also building open-pit coal-mining excavators. For a number of years there had been no trouble with these latter. At that time the firm had received an order for six such large machines, the rough outline of the operating mechanisms of which is shown in Fig. 1.

Item 1 is the car carrying and partly housing the operating mechanisms, 2 are its wheels and axles with which it travels on rails 3 laid, on sleepers 4, parallel to the mountainside or coal ledge, from which the coal is to be cut. M is an electric motor which through shafts, couplings, and gears drives an upper hexagon tumbler 5, over which link chains 6 run to a lower octagon tumbler 7, and from there over a deflecting roller 8 back to the upper hexagon tumbler 5. The two link chains 6 carry buckets 9 at every fourth link pair, these buckets being open at the back and part of the bottom to allow the coal to be discharged from them as they pass over the upper tumbler 5.

On the shaft of the lower octagon tumbler, there is also fixed a sprocket wheel 10 which, by means of a link chain 11 drives another sprocket 12 and by it a shaft 13 located in boom 14 which is

suspended by blocks and tackles from a fixed boom 15. On shaft 13, an octagon tumbler 16 is fixed which drives two link chains 17 that pass over a second octagon tumbler 18 at the top of boom 14. Every fourth pair of links of these chains carries a number of cutters 19 in a frame, the cutters in successive frames being offset with respect to those of the preceding frame to cover the whole width between the link chains. The chains are guided in channels so that the cutters can be forced to cut the coal, in strips, from the mountainside coal seam, or ledge, 20, whence the lumps of coal tumble down the mountainside to form a heap 21, from where they are scooped up by the buckets 9, which lift them up and discharge them over a chute 22 onto a belt conveyer 23. The latter discharges the coal by means of scrapers 24, into a discharge hopper 25, traveling on a girder 26 suspended from the main structure by framework 27. The traveling hopper discharges the coal into railway coal cars 28 which are waiting on tracks laid parallel to that of the machine.

The driving motor of the operating mechanism and that driving the machine along the mountainside were electric motors, the former with automatic electromagnetic cutout for preventing overloads that might wreck the apparatus.

As will be seen from Fig. 2(a), the tumbler teeth for the link chains 6 were formed so as to have plane faces forming an extension of the sides of the hexagon tumbler, having no teeth.

When the first machine was erected in the field and was tried

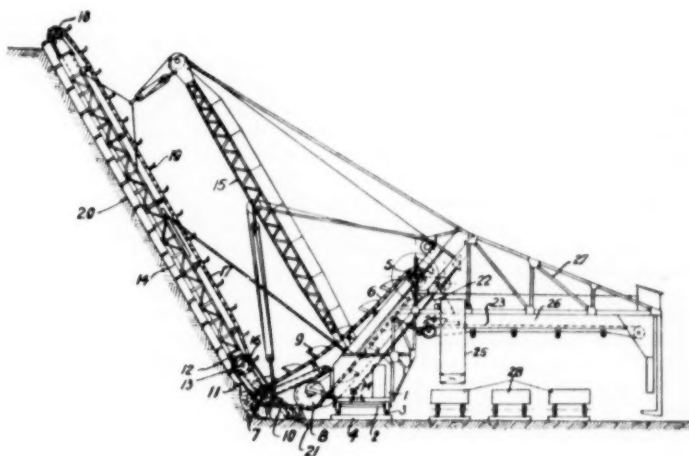


FIG. 1 GENERAL ARRANGEMENT OF COAL-CUTTING EXCAVATOR

out by the erector, his report came back stating that it was not working properly, and that, in particular, the chain links lifted up on the straight tooth faces from the hexagon tumbler sides, as shown in dotted lines in Fig. 2(a), and then dropped back under the many tons of weight of chains and buckets with a terrific crash. The impact thus produced would have destroyed both chains and tumblers in a short time.

It was at this point that the author was called in for consultation. Not being able to get any further facts, he suggested the obvious, namely, to form the teeth of the tumbler so that the chain links would drop onto them properly but could no longer slip up on flat surfaces, see Figs. 2(b) and (c). It cured this trouble

¹ Mechanical Engineer, Consultant, Reeves Instrument Corporation. Mem. ASME.

Contributed by the Machine Design Division and presented at the Annual Meeting, New York, N. Y., November 30-December 5, 1952, of THE AMERICAN SOCIETY OF MECHANICAL ENGINEERS.

NOTE: Statements and opinions advanced in papers are to be understood as individual expressions of their authors and not those of the Society. Manuscript received at ASME Headquarters, August 15, 1952. Paper No. 52-A-55.

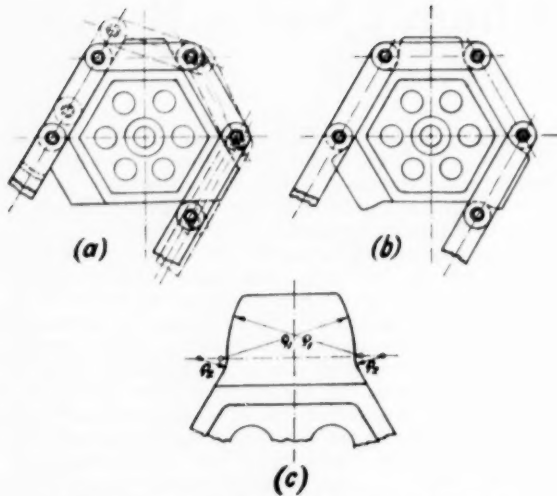


FIG. 2 ARRANGEMENT OF UPPER HEXAGON TUMBLERS
(a, Hexagon tumbler with straight-face teeth. b, Hexagon tumbler with curved teeth. c, Curves of modified tumbler teeth.)

as the chain links did no longer lift up from the tumbler, but the report from the erector then stated: "Now the machine does not work at all." He explained that the automatic cutout was working continually, throwing out the switch, so that a man had to hold it down all the time in order to let the machine work.

There was obviously something wrong for which he could not account. The chief design engineer, in whose department the machine had been designed, was despatched to the site, and returned scratching his head, but offering no explanation for this strange behavior. Next the "General Director" and the "Engineer-in-Chief" of the firm went to the site, but returned, likewise completely baffled. Then the situation was revealed to the author and he was asked to inspect the machine and try to find a remedy.

When the author arrived near the site at one end of a horse-shoelike valley, on the other end of which the machine was located and working, he could hear, across the miles of valley, the tremendous bangs of the chain riding up on the teeth of the tumbler with flat-face teeth, which had been reinstalled in the machine, and then dropping back under the heavy weight. It sounded like continuous heavy machine-gun fire. Certainly, if allowed to continue, this would have destroyed chains and tumbler and even the motor and driving gears in a very short time.

After installing the hexagon tumbler with the correctly formed teeth in the machine in place of that with straight-face teeth, there was no more noise and banging at the hexagon tumbler. In fact, the chain worked very smoothly on it, although the entire driving mechanism seemed to labor heavily. However, the automatic cutout had to be held down by the erector to let the machine work.

These observations suggested to the author that the source of trouble must lie elsewhere. The next and most obvious assumption was to investigate the lower octagon tumbler and the chain passing over it, for this tumbler still had straight-face teeth. This was not possible directly, because of the large lumps of coal which were falling down from the mountainside as they were cut by the cutters of the cutter chains. They would have killed any one daring to go even near that end. Hence the author had a "roof," or shield, on posts built of heavy boards, which was carried by four husky men in the nature of protecting

roofs when storming a walled city in ancient times. After it was completed, it was carried to the outer end with the author under it for making observations. Although there was the terrific clatter of the chunks of coal falling on to the roof, the author was able to observe conditions very well, and after a short time came to the conclusion that there was nothing wrong either with the lower octagon tumbler and the bucket chains passing over it, or with the intermediate chain drive, or even with the cutter chains and the octagon tumblers over which they passed.

This left but one place where something might be wrong, namely, the point where the heavy bucket chains passed over the deflecting roller 8. An inspection there revealed some strange noises which could not be recognized and explained immediately. Unfortunately, the position of the roller was such that the movement of the chain over it could not be observed. This was all the evidence the author had to base his investigation on.

For a full day, this phenomenon baffled him too, but then suddenly he perceived what was happening.

MOVEMENT OF A SINGLE BAR OVER A ROLLER

In order to understand what was taking place, let us consider first the movement of a bar, or chain link, over a roller, with forces acting on the bar near its ends. This problem involves three bodies, the frame containing the bearings for the roller shaft, the roller, and the bar rolling on the roller. The motions of the bar with respect to the roller and to the fixed frame are of interest and have to be investigated.

It is best to idealize the problem by using the skeleton method of representation. When the bar is moving over the roller, its center line through the pin centers touches a circle, the radius of which is larger than that of the roller by one half the width of the bar, see Fig. 3. Let us designate the radius of this ideal circle

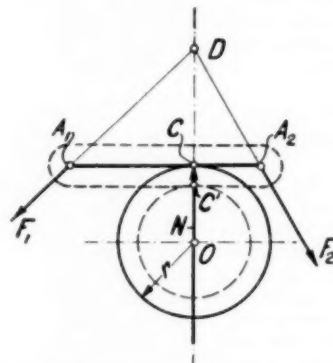


FIG. 3 EQUILIBRIUM POSITION OF A SINGLE LINK PASSING OVER A ROLLER—ROLLER AND LINK ROTATING

with r and the length of the bar between pin centers $A_1A_2 = l$, with the force F_1 acting at A_1 and the force F_2 acting at A_2 in the directions indicated. The reaction of the roller onto the bar is N and is acting radially from the center O of the roller in the contact normal n . As the bar is a *restrained*, but not a *constrained* system, it is subject to forces for the determination of its instantaneous position. In order that the bar be in equilibrium under the influence of these forces, it is necessary that the forces F_1 , F_2 , and N must meet in one point D . If they do not meet in one point, motion will take place and, if the friction at the contact point C between bar and actual roller is great enough to prevent slipping of the bar on the roller, the roller will start turning and the bar rolling on it until it arrives in a position where the three

forces F_1 , F_2 , and N meet in one point D . This will then be the position of equilibrium for that instant.

As the bar moves over the roller, its end points A_1 and A_2 describe involutes relative to the ideal roller circle, see Fig. 4. When the directions of the forces are not changing, but are only shifted parallel to themselves, it is easy to obtain a curve c for the intersections D' of the two force directions f_1 and f_2 of F_1 and F_2 , and also curves c_1 and c_2 for the intersections of the lines of

parallel displacements, lie on a straight line c parallel to A_1A_2 . This line intersects the fixed normal n at a point D which determines the equilibrium position of A_1A_2 by parallels DA_1 and DA_2 drawn to the forces F_1 and F_2 respectively.

The same would hold true even when the directions of the forces were changing. In that case, a curve c would be obtained instead of the straight line, but otherwise the solution remains similar.

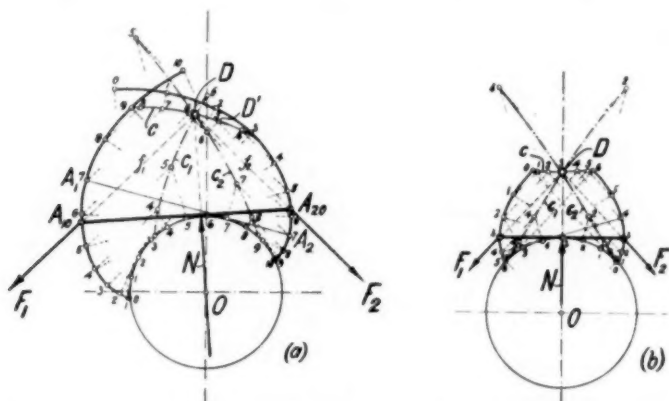


FIG. 4 DETERMINATION OF EQUILIBRIUM POSITION OF A SINGLE LINK PASSING OVER A ROLLER

(a, With random direction of forces. b, With direction of forces touching ideal roller circle in extreme positions of link.)

action of the forces F_1 with N and F_2 with N respectively. All three curves must intersect in a common point D which determines the equilibrium position of the bar. Since two of the curves suffice for the determination of the equilibrium point D , the third curve may be used as a check on the accuracy of the drawing work. The instantaneous position of equilibrium of the bar is obtained by drawing through D parallels to the given directions of the forces F_1 and F_2 , the parallels meeting the respective involutes in the end points A_{10} and A_{20} of the bar in its equilibrium position.

In Fig. 4(a) the directions f_1 and f_2 of the two forces F_1 and F_2 were chosen at random. It is clear that in the case of a chain link, in which the forces are transmitted by the adjoining links, the minimum angle between the force directions will be that when the forces, in the extreme positions, pass through the points of origin of the respective involutes, tangential to the ideal roller circle. In that case the equilibrium position, due to the symmetry, must be that in which the center of the link is in contact with the ideal roller circle, see Fig. 4(b).

In the cases just described, both bar and roller were turning about the center O of the roller and, in addition, the bar had a rolling motion relative to the ideal roller circle. On the other hand, it may be desirable to obtain the equilibrium position for a definite direction of the link, or bar, relative to the frame, or, in other words, when the bar and roller move so that the bar is translated in its direction only. In this case, the contact normal n to the bar has a fixed position relative to the frame, see Fig. 5, and the position of the bar has to be found where the given directions of the forces F_1 and F_2 both intersect this normal in a common point. This is easily obtained as follows:

Assume, for the same direction of bar A_1A_2 , a number of positions $A_{10}A_{20}$, $A_{11}A_{21}$, $A_{12}A_{22}$, . . . , see Fig. 5. Draw through these end points the respective parallels to the force directions of F_1 and F_2 , the parallels meeting in points D_0 , D_1 , D_2 , . . . which, when the directions of the forces F_1 and F_2 are not changing except for

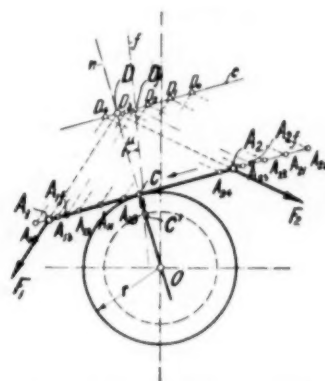


FIG. 5 DETERMINATION OF EQUILIBRIUM POSITION OF A LINK PASSING IN ITS OWN DIRECTION OVER A ROLLER

Friction between roller and bar can also be considered easily by drawing through the contact point C' between actual roller and bar a straight line $C'f$ at an angle μ (friction angle) to the normal OC' inclined in the direction opposite to the motion of the bar. It should be noted that the point C' lies on the actual roller and not on the ideal roller circle. The point of intersection D_f of c with $C'f$ determines the equilibrium position $A_{1f}A_{2f}$ of the link in this case, see dash-dotted lines in Fig. 5.

The directions of the forces F_1 and F_2 , although slightly varying in practice, may, in first approximation, be considered constant or nonvarying except for a small parallel displacement.

Since, in the machine described in the introduction, the velocities of the bucket chains as well as of the cutter chains were relatively low, no important dynamic forces were set up during the motion so that the static investigation will give approximately correct results.

MOVEMENT OF TWO BARS, OR LINKS, OVER A ROLLER

We come now to the case of two links, joined together by a pin, moving over a roller. This problem can be handled geometrically (graphically) with relative ease, but is difficult to solve analytically, except for the case where the directions of the forces at the outer ends of the two links are parallel.

Before making a detailed analysis of the geometry of a pair of links moving over a roller under the influence of a pair of forces F_1 and F_2 of any direction, it is best to get first a general idea of what takes place in the simplest case, when both forces F_1 and F_2 are parallel. Although this is a special case, it will serve to illustrate the type of motion encountered even in the more general case where the forces may have any feasible directions.

Using again the skeleton method of representation, explained previously, with the links represented by segments of straight lines and the roller by an ideal circle of a radius larger than that of the actual roller by one half the width of the links, we will consider now the various important phases of the motion under

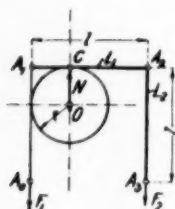


FIG. 6 PHASE 1

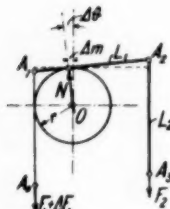


FIG. 7 PHASE 2



FIG. 8 PHASE 3

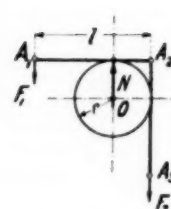


FIG. 9 PHASE 4

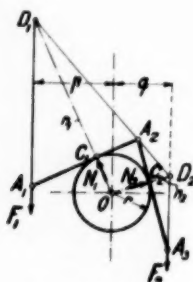


FIG. 10 PHASE 5

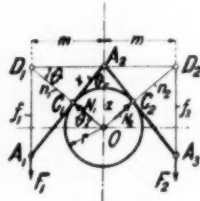


FIG. 11 PHASE 6

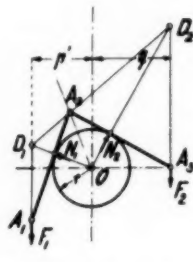


FIG. 12 PHASE 7

FIGS. 6 TO 12 PHASES OF MOTION OF A PAIR OF CHAIN LINKS PASSING OVER A ROLLER; FORCES ACTING PARALLEL TO ONE ANOTHER

the assumption that F_1 is the pulling force and F_2 the resistance to be overcome. The links A_1A_2 and A_2A_3 may be considered as part of a chain.

First Phase. Under the influence of the pull F_1 , the link A_0A_1 of the chain has just pulled the link $L_1 = A_1A_2$ into the horizontal position (or perpendicular to pull and resistance), as shown in Fig. 6, while the link $L_2 = A_2A_3$ hangs down vertically under the influence of the resistance F_2 . In this case, we have for the condition of equilibrium, with the designations given in the figure

$$F_1 = F_2 \frac{l - r}{r} \quad [1]$$

l being the length of all the links of the chain and r the radius of the ideal roller circle.

Second Phase. Link A_0A_1 pulls, under the influence of a slightly increased force $F_1 + \Delta F_1$, link $L_1 = A_1A_2$ through a small angle $\Delta\theta$. The equation of equilibrium becomes now, see Fig. 7,

$$(F_1 + \Delta F_1)(r - \Delta m) = F_2(l - (r - \Delta m))$$

or, since $\Delta m = r\Delta\theta$

$$F_1 + \Delta F_1 = F_2 \frac{l - r(1 - \Delta\theta)}{r(1 - \Delta\theta)} \quad [2]$$

which, for $\Delta F_1 = 0$ and $\Delta\theta = 0$, passes into Equation [1]. We get also from Equations [1] and [2]

$$\Delta F_1 = F_2 \frac{l}{r} \frac{\Delta\theta}{1 - \Delta\theta} \quad [3]$$

which equation shows that ΔF_1 increases rapidly when $\Delta\theta$ increases.

Third Phase. When the inclination $\Delta\theta$ of link L_1 becomes large enough to overcome the friction the bearings of the roller and the rolling friction of link L_1 on the roller, the latter will start turning and link L_1 rolling on the roller toward the

left until an equilibrium condition is reached. In that case we have, see Fig. 8,

$$\left. \begin{aligned} F_1 x &= F_2 x' \\ F_1 &= F_2 \frac{x'}{x} \end{aligned} \right\} \dots \dots \dots [4]$$

and when $x' = x = l/2$, then

$$F_1 = F_2 \dots \dots \dots [5]$$

Fourth Phase. As the angle $\Delta\theta$ increases still further, link L_1 rolls further toward the left until link L_2 touches the ideal roller circle. Then we have, see Fig. 9,

$$F_1(l - r) = F_2 r$$

or

$$F_1 = F_2 \frac{r}{l - r} \dots \dots \dots [6]$$

Fifth Phase. So far, only one link has been rolling on the roller. From now on two links are moving over the roller. Link L_1 pulls link L_2 up on the roller and both move together with the roller until a position of equilibrium is obtained. In that case, the verticals through A_1 and A_3 have from the vertical through O the distances p and q respectively, so that we get, see Fig. 10,

$$F_1 p = F_2 q$$

or

$$F_1 = F_2 \frac{q}{p} \dots \dots \dots [7]$$

There is, however, a further condition that has to be observed, namely, that when F_1 and n_1 (the contact normal of link L_1) intersect in D_1 , and when F_2 and n_2 (the contact normal of link L_2) intersect in D_2 , then the three points D_1 , A_2 , and D_2 must be col-

linear, otherwise equilibrium of the links on the roller would not exist. This condition must always obtain when more than one link is touching the roller at the same time.

Sixth Phase. Joint A_2 arrives in the vertical through O , so that A_1 and A_2 have equal distances m from the vertical through O . In that case, see Fig. 11,

$$F_1 m = F_2 m$$

or

$$F_1 = F_2 \dots \dots \dots [8]$$

However, the second condition stated under Fifth Phase must again obtain, namely, that the horizontal through A_2 must intersect the force lines f_1 and f_2 in D_1 and D_2 , and these points must also lie on the contact normals n_1 and n_2 of the respective links. How this condition can be satisfied in the general case will be shown later. For this special case, a simple calculation will show how the correct location of the links L_1 and L_2 can be obtained.

In Fig. 11 the correct configuration of the ideal roller circle and of the links L_1 and L_2 is shown. The length of the links is l and the radius of the ideal roller circle r , while θ is the angle made by the normals n_1 and n_2 with the horizontal through O , the center of the ideal roller circle. Due to complete symmetry of the figure with respect to the vertical through O , the horizontal through A_2 must meet the force lines f_1 and f_2 in D_1 and D_2 respectively, and n_1 and n_2 , respectively, pass through these two points. Let $A_2 D_1 = A_2 D_2 = m$, $A_2 O = z$, $A_2 C_1 = A_2 C_2 = x$. Then

$$r = x \tan \theta$$

$$\frac{r}{x} = \frac{\sin \theta}{\sqrt{1 - \sin^2 \theta}}$$

$$\frac{r^2}{x^2} = \frac{\sin^2 \theta}{1 - \sin^2 \theta} \dots \dots \dots [9]$$

Further

$$x = m \sin \theta$$

or

$$m = l \sin \theta$$

$$x = l \sin^2 \theta \dots \dots \dots [10]$$

Substituting Equation [10] into [9], we get

$$\frac{r^2}{x^2} = \frac{x}{l - x}$$

whence

$$x^3 + r^2 x = r^2 l \dots \dots \dots [11]$$

This is a cubic equation for $A_2 C_1$. Having thus obtained x , $O A_2 = z$ is found from

$$z^2 = x^2 + r^2 \dots \dots \dots [12]$$

so that the configuration of links and roller is determined. It can also be obtained by determining the angle θ . From $r = x \tan \theta$ and $x = l \sin^2 \theta$, we find

$$\sin^2 \theta + \frac{r^2}{l^2} \sin^4 \theta = \frac{r^2}{l^2} \dots \dots \dots [13]$$

Equations [12] and [13] indicate that the resultant configuration can be obtained only from an equation of the sixth degree.

Seventh Phase. F_1 increases further pulling link $L_2 = A_2 A_3$ beyond the position where A_2 is located on the vertical through O . A_2 now lies to the left of this vertical, and the distances of the lines of action of forces F_1 and F_2 are, respectively, p' and q' , whence, see Fig. 12,

$$F_1 p' = F_2 q'$$

$$F_1 = F_2 \frac{q'}{p'} \dots \dots \dots [14]$$

If F_1 increases further, link L_1 will finally get into the vertical position and link L_2 into the horizontal position, but so that link L_1 touches the ideal roller. This phase is the same as the first phase. The cycle of motion then repeats itself for every new link that mates with the roller.

If the forces F_1 are now compared with the constant resistance F_2 , we get the results given in Table 1.

TABLE 1 COMPARISON OF FORCES F_1 WITH CONSTANT RESISTANCE F_2

Phase	Pull Resistance = F_2	$l = 3r$	$l = 4r$
1	$\frac{l-r}{r} = \frac{l}{r} - 1$	2	3
2	$\approx \frac{l-r}{r} = \frac{l}{r} - 1$	≈ 2	≈ 3
3	$\frac{x'}{x}$	$\frac{x'}{x}$	$\frac{x'}{x}$
4	$\frac{r}{l-r}$	1/2	1/3
5	q/p	q/p	q/p
6	1	1	1
	$\frac{q'}{p'}$	q'/p'	q'/p'
8 = 1	$\frac{l-r}{r} = \frac{l}{r} - 1$	2	3

In phase co-ordinates, the curve of variation of the pulling force F_1 during the passage of one link looks like that shown in Fig. 13. On the other hand, if the irregular motion due to the movement of the chain over the roller and over a hexagon tumbler is taken into consideration, the curve of variation, in time co-ordinates for the passage of one link over the roller, looks like that shown in Fig. 14. In both cases, two curves are given, for $l = 3r$ and $l = 4r$.

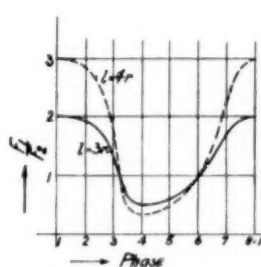


FIG. 13 PHASE DIAGRAM

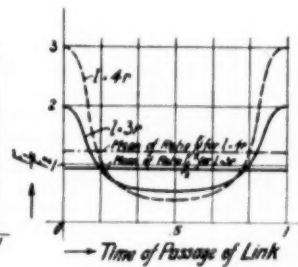


FIG. 14 TIME DIAGRAM OF PASSAGE OF ONE LINK OVER A ROLLER

The latter figures show that the average pulling force, for which, for example, the machine described in the introduction was constructed, is indicated by the full line, or the dash-dotted line, which are well below the maximum force encountered during the passage of each link. This explains why the automatic electromagnetic cutout was tripping the switch continually during each passage of a link over the roller.

After having thus, in the simplest case, investigated qualita-

tively the events that occur during the passage of each link over a roller, the quantitative values have to be determined. In the simplest case, in which pulling force and resistance are parallel, this offers no great difficulty. The general case, however, is not tractable analytically as will be shown. Since the special case can be derived easily from the general case, the latter shall now be considered.

TWO LINKS PASSING OVER A ROLLER

Analysis of the General Case

Let, in Fig. 15, O be the center of the ideal roller circle of radius r , A_1A_2 the link system in a random position, moving over the roller, being pulled by the force F_1 acting at A_1 , and being resisted by the force F_2 acting at A_2 . A is the joint common to both links. Let C_1 and C_2 be the respective points of contact of the links $L_1 = A_1A$ and $L_2 = AA_2$ with the ideal roller circle, and OC_1 and OC_2 the respective contact normals n_1 and n_2 .

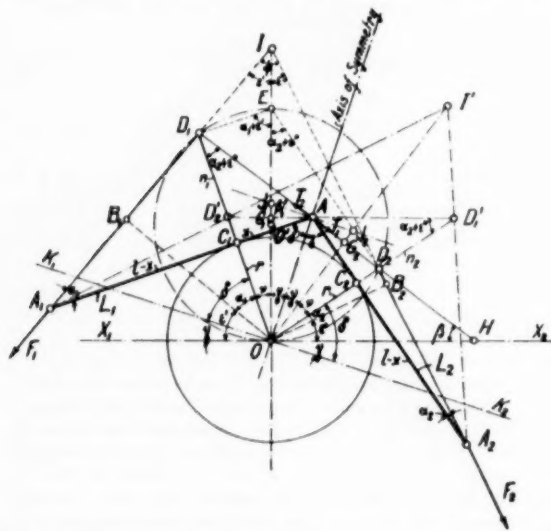


FIG. 15 DIAGRAM FOR ANALYSIS OF EQUILIBRIUM POSITION OF A PAIR OF LINKS PASSING OVER A ROLLER

In order that the link system, that is, a four-body system, be in equilibrium, the forces acting on each link must meet in a single point. Hence, if T_1 be the force exerted at A by link L_2 on to link L_1 , and T_2 the force exerted at A by link L_1 on to link L_2 , and if the contact forces exerted by the roller on the two links are, respectively, N_1 and N_2 acting along the contact normals $OC_1 = n_1$ and $OC_2 = n_2$, then the forces F_1 , N_1 , T_1 acting on link L_1 must intersect at D_1 on n_1 , and the forces F_2 , N_2 , T_2 acting on link L_2 must intersect at D_2 on n_2 . Since the two forces T_1 and T_2 must balance one another, they must be equal in magnitude = T , and must act along the same line D_1AD_2 , but in opposite senses.

This latter condition that the three points D_1 , A , D_2 must be collinear transforms the problem from a purely mechanical one into a geometrical one, for in this necessary and sufficient condition, the forces F_1 and F_2 do no longer appear, but solely their directions. Thus the position of equilibrium must be obtainable by purely geometrical means, i.e., by kinematic geometry.

It is obvious that the resultant of F_1 and F_2 must pass through the point of intersection I of their lines of action, and since the two roller reactions N_1 and N_2 , which balance these forces, pass through O , the resultant R of F_1 and F_2 must also pass through O and be directed along IO . Let the perpendicular to IO at O be

X_1OX_2 , and let us drop perpendiculars from O on to the directions of the forces F_1 and F_2 , namely, OB_1 and OB_2 respectively. Further, let the angles $D_1OB_1 = \alpha_1$, $D_2OB_2 = \alpha_2$, $B_1OX_1 = \epsilon'$, and $B_2OX_2 = \epsilon''$. The angles made by the lines of action of F_1 and F_2 with links L_1 and L_2 , respectively, are α_1 and α_2 , because their arms are perpendicular to those of α_1 and α_2 respectively. Let angle $AOI = \gamma$.

Next, it becomes necessary to determine the direction of the line D_1AD_2 . In order to do this, we consider the line OA as axis of symmetry, because the triangles AOC_1 and AOC_2 are congruent. Thus, if the entire figure be turned out of its plane through an angle of 180° about the axis of symmetry OA , the points D_1 and D_2 will fall to D_1' and D_2' respectively, while OI will fall to OI' . Thus the line symmetrical to D_1AD_2 will be $D_1'AD_2'$, and the angle $AOI' = \text{angle } AOI = \gamma$. Due to the symmetry, D_1' must lie on OC_2 produced, and D_2' on OD_1 . If now perpendiculars be drawn to OD_1 at D_1 and to OD_2 at D_2 , they will meet OI in E_1 and E_2 respectively. Angle $D_1E_1O = \alpha_1 + \epsilon'$ and angle $D_2E_2O = \alpha_2 + \epsilon''$. Since the angle $D_1OD_2 = 180 - (\alpha_1 + \epsilon') - (\alpha_2 + \epsilon'')$, and since the sum of angles D_1E_1O and D_2E_2O is $(\alpha_1 + \epsilon') + (\alpha_2 + \epsilon'')$, it follows that the two points E_1 and E_2 must coincide in E on OI , and a circle may then be passed through the points O , D_1 , E , D_2 , having its center O' on OI . Angles OD_1E and OD_2E are right angles and angles D_1OD_2 and D_1ED_2 are supplementary angles. Consequently angle $OD_1A = \alpha_2 + \epsilon''$, and this must also be the angle $AD_1'O$ of the symmetrical figure. Since angle $D_1'OX_2 = \alpha_2 + \epsilon''$, AD_1' must be parallel to OX_2 ; that is, it must make a right angle with OI' at G_1 . The symmetrical point to G_1 , namely, G_2 , must lie on OI' , and the line D_1AD_2 must also make a right angle with OI' . It is now clear that the perpendicular to OA at A will be the bisectrix J_1AJ_2 of the angle $D_1AG_1 = \beta$, and since the triangles J_1AG_1 and AOG_1 are right-angled triangles, angle $J_1AG_1 = \frac{1}{2} \text{ angle } D_1AG_1 = \frac{1}{2} \beta = \gamma$, or $\beta = 2\gamma$.

It is now easy to determine the equal angles D_1OG_1 and D_2OG_2 which, since angle $OD_2'A = \alpha_1 + \epsilon'$, are $\nu = 90 - (\alpha_1 + \epsilon')$. The angles $A_1AO = A_2AO = \delta$ and $AOG_1 = AOG_2 = \gamma$ are also found readily. For, if K_1OK_2 be perpendicular to OA at O , angle $C_1OK_1 = \delta$ and angle $K_1OX_1 = \gamma$, likewise angle $C_2OK_2 = \delta$ and angle $K_2OX_2 = \gamma$. Since angle $X_1OK_1 = X_2OK_2 = \gamma$, it follows that $\delta + \gamma = \alpha_1 + \epsilon'$ and $\delta - \gamma = \alpha_2 + \epsilon''$, from which we get

$$\delta = \frac{\alpha_1 + \epsilon'}{2} + \frac{\alpha_2 + \epsilon''}{2} = \frac{\alpha_1 + \alpha_2 + \phi}{2}$$

where angle $\epsilon' + \epsilon'' = \phi$, and

$$\gamma = \frac{\alpha_1 + \epsilon'}{2} - \frac{\alpha_2 + \epsilon''}{2}$$

Since angle $A_1IO = \epsilon'$ and $A_2IO = \epsilon''$, it is clear that the angle made by the directions of the two forces F_1 and F_2 is $A_1IA_2 = \epsilon' + \epsilon'' = \phi$.

It is, therefore, easy to find the position of the line D_1AD_2 when α_1 , α_2 , ϵ' , and ϵ'' are known. In general, they will not be known, however. What is known, generally, are the directions of the forces F_1 and F_2 which may be assumed to be acting always parallel to themselves, neglecting the slight angularity variation introduced by the varying distances of O from their lines of action due to the movement of the chain links over the roller as well as over the pulling and resisting tumblers. The position of OA may then be chosen arbitrarily, but the position of A on OA has still to be determined, as has also the direction of OI .

To elucidate the difficulties, an analytical treatment shall be given first which will show why an analytical solution cannot

be obtained and why a geometrical solution must be resorted to.

ANALYTICAL INVESTIGATION

Let l be the length of the chain links between pin centers, and x the distance of their common point A from the points of contact with the ideal roller circle of radius r . The angle δ , or x , or $OA = z$ are to be determined, as any one of them will establish the position of A on OA .

The equilibrium conditions for AA_1 and AA_2 require that the sum of the moments of the forces acting on the links, as well as the sum of their components in the direction of and perpendicular to the links be zero. If $AC_1 = AC_2 = x$, and $A_1C_1 = A_2C_2 = x'$ then, since $T_1 = T_2 = T$,

$$F_1 x' \sin \alpha_1 = T x \cos (\alpha_2 + \epsilon'') \quad [15]$$

$$F_2 x' \sin \alpha_2 = T x \cos (\alpha_1 + \epsilon') \quad [16]$$

$$F_1 \sin \alpha_1 + T \cos (\alpha_2 + \epsilon'') = N_1 \quad [17]$$

$$F_2 \sin \alpha_2 + T \cos (\alpha_1 + \epsilon') = N_2 \quad [18]$$

$$F_1 \cos \alpha_1 = T \sin (\alpha_2 + \epsilon'') \quad [19]$$

$$F_2 \cos \alpha_2 = T \sin (\alpha_1 + \epsilon') \quad [20]$$

also

$$x + x' = l \quad [21]$$

$$\delta = \frac{\alpha_1 + \alpha_2 + \phi}{2} \quad [22]$$

$$\epsilon' + \epsilon'' = \phi \quad [23]$$

$$\gamma = \frac{\alpha_1 + \epsilon'}{2} - \frac{\alpha_2 + \epsilon''}{2} \quad [24]$$

$$\beta = (\alpha_1 + \epsilon') - (\alpha_2 + \epsilon'') = 2\gamma \quad [25]$$

$$\frac{r}{x} = tg \delta \quad [26]$$

From Equations [15] and [19] we get

$$x' tg \alpha_1 = x \cot (\alpha_2 + \epsilon'')$$

$$x' = l - x = x \frac{1}{tg \alpha_1 tg (\alpha_2 + \epsilon'')}$$

or

$$l = x \left(1 + \frac{1}{tg \alpha_1 tg (\alpha_2 + \epsilon'')} \right) = x \frac{1 + tg \alpha_1 tg (\alpha_2 + \epsilon'')}{tg \alpha_1 tg (\alpha_2 + \epsilon'')}$$

whence

$$\frac{x}{l} = \frac{tg \alpha_1 tg (\alpha_2 + \epsilon'')}{1 + tg \alpha_1 tg (\alpha_2 + \epsilon'')} \quad [27]$$

Furthermore

$$\frac{r}{x} = tg \delta = tg \frac{\alpha_1 + \alpha_2 + \phi}{2} \quad [28]$$

From Equations [27] and [28] we get

$$\frac{r}{l} = e = tg \delta \frac{tg \alpha_1 tg (\alpha_2 + \epsilon'')}{1 + tg \alpha_1 tg (\alpha_2 + \epsilon'')} \quad [29]$$

However, we had found from symmetry considerations that

$$\delta + \gamma = \alpha_1 + \epsilon' \quad [30]$$

$$\delta - \gamma = \alpha_2 + \epsilon'' \quad [31]$$

whence

$$\alpha_1 = \delta + \gamma - \epsilon' \quad [32]$$

$$\alpha_2 = \delta - \gamma - \epsilon''$$

or, according to Equation [31]

$$\alpha_2 + \epsilon'' = \delta - \gamma \quad [33]$$

If we now put

$$\left. \begin{aligned} tg \delta &= w \\ tg \gamma &= v \\ tg \epsilon' &= t \end{aligned} \right\} \quad [34]$$

and, temporarily,

$$tg(\delta + \gamma) = \psi$$

we get, from Equations [29], [32], [33], and [34]

$$e = w \frac{tg(\delta + \gamma - \epsilon') tg(\delta - \gamma)}{1 + tg(\delta + \gamma - \epsilon') tg(\delta - \gamma)} \quad [35]$$

Since

$$tg(\delta - \gamma) = \frac{tg \delta - tg \gamma}{1 + tg \delta tg \gamma} = \frac{w - v}{1 + wv} \quad [36]$$

and

$$tg(\delta + \gamma - \epsilon') = \frac{tg(\delta + \gamma) - tg \epsilon'}{1 + tg(\delta + \gamma) tg \epsilon'} = \frac{\psi - t}{1 + \psi t} \quad [37]$$

we get, with

$$tg(\delta + \gamma) = \frac{tg \delta + tg \gamma}{1 + tg \delta tg \gamma} = \frac{w + v}{1 + wv} = \psi \quad [38]$$

from Equation [35]

$$e = w \frac{\frac{\psi - t}{1 + \psi t} \frac{w - v}{1 + wv}}{1 + \frac{\psi - t}{1 + \psi t} \frac{w - v}{1 + wv}}$$

which, after some transformations gives

$$e = \frac{\psi(w^2 - wv) - w^2 t + w t}{\psi \{ (1 + wv)t + w - v \} + 1 + wv - t(w - v)}$$

Substituting herein Equation [38]

$$e = \frac{\frac{w + v}{1 + wv} (w^2 - wv) - w^2 t + w t}{\frac{w + v}{1 + wv} \{ (1 + wv)t + w - v \} + 1 + wv - t(w - v)}$$

which, after some transformations, yields

$$e = \frac{w^3(1 + vt) - w^3(v^2 + 1)t + w(vt - v^2)}{w^3[2vt + 1 - v^2] + [2vt + 1 - v^2]}$$

This, resolved for w , gives

$$w^3(1 + vt) - w^3 \{ (v^2 + 1)t + e(2vt + 1 - v^2) \} + w(vt - v^2) - e(2vt + 1 - v^2) = 0 \quad [39]$$

This cubic could be solved if t were known or could be found. Unfortunately, this is not the case as t varies with v and w , that is, with γ and δ ; γ itself varies with the relative magnitude of the forces F_1 and F_2 . Hence an analytical solution does not seem feasible.

For one special case, however, the foregoing cubic equation can be solved, namely, when $t = tg\epsilon' = 0$, or $\epsilon' = \epsilon'' = 0$ and $\phi = 0$. In this case, the directions of the forces F_1 and F_2 become parallel and γ is known or can be assumed; thus v is known and constant for the position chosen. Consequently, we get

$$w^3 - w^2 e(1 - v^2) - wv^2 - e(1 - v^2) = 0 \quad [40]$$

where $e = r/l$ and $v = tg\gamma$ are known and $w = tg\delta$ can be found.

If it were possible to determine $w = tg\delta$ for the general case, it would be easy to determine also x and the distance $OA = z$. Since $w = tg\delta = r/x$, we get, by substituting this value into Equation [39], after some simple transformations

$$x^3 - x^2 \frac{r(vt - v^2)}{e(2vt + 1 - v^2)} + x \frac{r^2 \{ (v^2 + 1)t + e(2vt + 1 - v^2) \}}{e(2vt + 1 - v^2)} - r^3 \frac{1 + vt}{e(2vt + 1 - v^2)} = 0 \quad [41]$$

This is again a cubic equation which could be solved were $v = tg\gamma$ and $t = tg\epsilon'$ known beforehand. Since both depend on x , however, a solution is not feasible. Only when $t = 0$, and γ becomes definitely known, can a solution be obtained, for we get then

$$x^3 + x^2 \frac{lv^2}{1 - v^2} + xv^2 - \frac{r^2 l}{1 - v^2} = 0 \quad [42]$$

which cubic can be solved readily.

Finally, if $OA = z$, then $z = \sqrt{r^2 + x^2}$, or $x = \sqrt{z^2 - r^2}$. If the latter value be substituted for x in Equation [41], we obtain a very complex equation of the sixth degree, but since neither t nor v is known, it would be of no value.

If, in the simplified case, x were substituted in Equation [42], an equation of the sixth degree, which is solvable however, would be obtained, for we get then

$$(z^3 - r^3) \sqrt{z^2 - r^2} + \frac{(z^2 - r^2)lv^2}{1 - v^2} + r^2 \sqrt{z^2 - r^2} - \frac{r^2 l}{1 - v^2} = 0$$

or

$$z^3 \sqrt{z^2 - r^2} = \frac{l}{1 - v^2} \{ r^2 + r^2 v^2 - z^2 v^2 \}$$

and when we put

$$\frac{l}{1 - v^2} = \lambda$$

we get

$$z^3 \sqrt{z^2 - r^2} = \lambda r^2 (1 + v^2) - \lambda z^2 v^2$$

whence

$$z^6 - z^4 \{ r^2 + \lambda^2 v^4 \} + z^2 \{ 2\lambda^2 r^2 v^2 (1 + v^2) \} - \lambda^2 r^4 (1 + v^2)^2 = 0 \quad [43]$$

This equation of the sixth degree can be solved readily if one puts $z^2 = y$. This yields

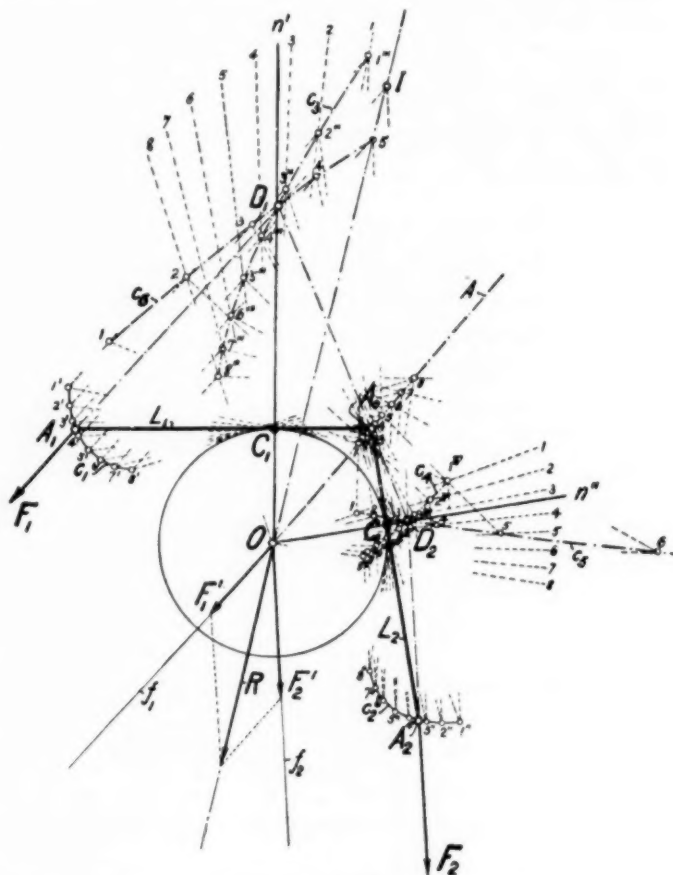


FIG. 16 GRAPHICAL DETERMINATION OF THE EQUILIBRIUM POSITION OF A PAIR OF LINKS PASSING OVER A ROLLER

$$y^3 - y^2 \left\{ r^2 + \frac{v^4 l^2}{(1 - v^2)^2} \right\} + y 2r^2 r^2 l^2 \frac{1 + v^2}{(1 - v^2)^2} + r^4 l^2 \left(\frac{1 + v^2}{1 - v^2} \right)^2 = 0 \quad [44]$$

which cubic determines y and thus z^2 , from which z follows directly.

As will be evident from this investigation, an analytical solution in the general case is not feasible. Thus one is forced to resort to a graphical solution, which can be obtained rather easily.

GRAPHICAL SOLUTION

In Fig. 16 let O be the center of the ideal roller circle, r its radius, l the lengths of the chain links between pin centers. Let f_1 and f_2 be the directions of the two external forces F_1 and F_2 , indicated at center O , F_1 being the pulling force and F_2 the resistance which is assumed to be constant. It will thus be seen that if F_2' be a vector of constant length on f_2 from center O , corresponding to the resistance F_2 , and if f_1 be the direction of the vector F_1' , corresponding to the pulling force F_1 , then the re-

sultant vector R will not have a constant direction, but its direction will vary with the magnitude of vector F_1' . Thus the angles ϵ' and ϵ'' will not be known beforehand, as was previously stated, nor will the angle γ be known beforehand, because the direction OI of the resultant R varies. Only one of its arms, OA , will have a given position with respect to forces F_1 and F_2 . For a graphical solution, this latter statement is a sufficient requirement.

Choose the position of OA . In order to find the correct position A_0 of A on OA , mark out a number of points on OA beyond the ideal roller circle, say 1, 2, 3, . . . From these points, draw tangents to the ideal roller circle and make their lengths $AA_1 = AA_2 = l$. The end points of these tangents are $1', 2', 3', \dots$ and $1'', 2'', 3'', \dots$ which lie, respectively, on the two curves c_1 and c_2 , c_1 for the end points A_1 of link L_1 and c_2 for the end points A_2 of link L_2 . Next draw the respective contact normals n_1', n_2', n_3', \dots for the various positions of link L_1 , and $n_1'', n_2'', n_3'', \dots$ for the positions of link L_2 . Now, draw through the end points $1', 2', 3', \dots$ parallels to the direction of F_1 and through the end points $1'', 2'', 3'', \dots$ parallels to the direction of F_2 . These parallels intersect their respective contact normals in points $1''', 2''', 3''', \dots$ and $1''', 2''', 3''', \dots$ of two curves c_3 and c_4 , respectively. Join the points of intersection $1''', 2''', 3''', \dots$ of one of these curves, say c_3 , with the respective co-ordinated points 1, 2, 3, . . . on OA and let these lines intersect the respective co-ordinated contact normals n_1', n_2', n_3', \dots for the link L_2 . The points of intersection will lie on a curve c_5 , which meets curve c_2 in a point D_2 . From D_2 draw a parallel to the direction of force F_2 , which intersects curve c_2 in A_2 . The tangent from A_2 to the circle determines the desired position A_0 of A on OA .

The proof for the accuracy of the position of point A_0 can be given in several ways:

1 Join D_2 with A_0 and let D_2A_0 produced intersect curve c_4 , yielding D_1 . The parallel to the direction of F_1 through D_1 and the tangent A_0A_1 to the circle from A_0 must meet in the point A_1 which, if the construction were accurate, must lie on curve c_1 .

2 Or, draw from A_0 the tangent to the circle, which meets curve c_1 at A_1 . A parallel to F_1 through A_1 meets the line D_2A_0 produced in D_1 , which point must lie on curve c_4 if the construction is accurate.

Instead of determining curve c_5 , a curve c_6 may be obtained by reversing the procedure, thus yielding point D_1 . In two further ways analogous to the foregoing, the point A_2 may be found or the point D_2 . Thus sufficient checks are available for the correct position of A_0 .

When the entire construction is repeated for a number of different positions of line OA , a locus for the points A_0 during the passage of one link pair of a chain over the roller is obtained, from which the forces F_1 may be found readily. These may then be plotted in a time diagram for the passage of one link, giving the curve of the pull F_1 and its variations with respect to the constant resistance F_2 .

The correct time diagram for the variation of the pulling force F_1 can be determined only when the complete layout of the drive is known, for it depends on the (more or less) uniform rotation of the upper hexagon tumbler driven by the electric motor, and has to take into consideration the variation of the motion of the link chain due to its passage over this tumbler (polygonal deviation). It will also be seen that allowance—even if only approximately—can be made for the slight variations of the directions of the chain pull F_1 and of the resistance F_2 due to passage of the chain over the upper and lower tumblers and over the roller. Inasmuch as the position of the chain links and of the locus of A_0 is not known beforehand, this allowance can only be approximate, but will yield the locus of A_0 with excellent approximation. The locus shows there exists an oscillation of point A_0 with respect to the roller during the passage of the link system.

There is another way in which to determine the locus of A_0 , namely, by giving the direction of one of the links, say, of $L_2 = l = A_2A$ as a tangent to the ideal roller circle, and the directions f_1 and f_2 of the forces F_1 and F_2 instead of assuming the position

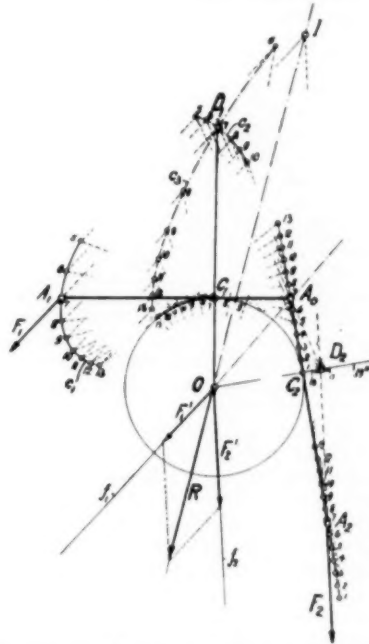


FIG. 17. ALTERNATIVE METHOD OF GRAPHICAL DETERMINATION OF THE EQUILIBRIUM POSITION OF A PAIR OF LINKS MOVING OVER A ROLLER, ONE LINK BEING DISPLACED IN ITS OWN DIRECTION

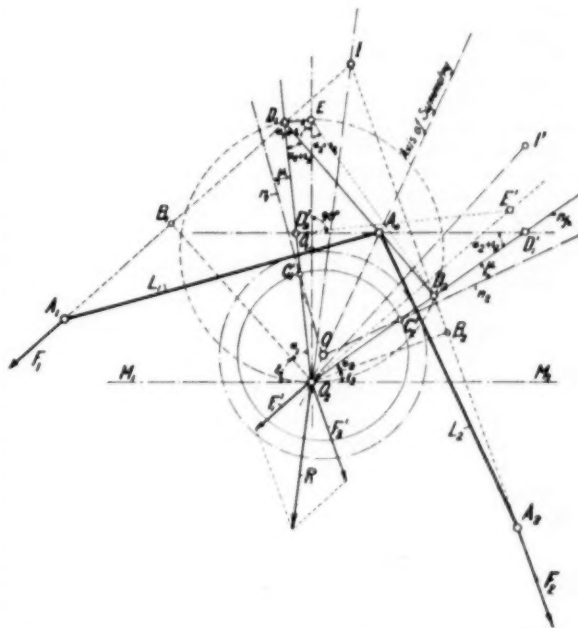


FIG. 18. DIAGRAM FOR ANALYSIS OF THE EQUILIBRIUM POSITION OF A PAIR OF LINKS MOVING OVER A ROLLER, TAKING FRICTION OF THE LINKS ON THE ROLLER INTO CONSIDERATION

of the line OA . In this case, Fig. 17, the link is moved along in its own direction thus determining on its directional line two sets of points, A_2 : 1, 2, 3, . . . , and A_6 : 1, 2, 3, The normal n^* , in this case, is fixed. From the A_6 points 1, 2, 3, . . . , the respective co-ordinated tangents A_6A_1 to the ideal roller circle are then drawn, yielding for the end points A_1 points 1, 2, 3, . . . which lie on a curve c_1 , and to these tangents the contact normals n' : 1, 2, 3, . . . are drawn. Through the end points of A_2 : 1, 2, 3, . . . of link L_2 , parallels are then drawn to the direction of the force F_2 , which intersect the fixed normal n^* in D_1 points 1, 2, 3, Through these points and the corresponding A_6 -points, straight lines are next drawn which intersect the various parallels to F_1 through the A_1 points 1, 2, 3, . . . in points of a curve c_2 . These same parallels to the direction of force F_1 through the A_1 -points intersect the corresponding normals n' in points of a curve c_3 . This curve meets curve c_2 in D_1 . A parallel to the direction of force F_1 from D_1 intersects curve c_1 in the correct point A_1 , from which the tangent to the ideal roller circle determines the correct point A_6 on the line of link L_2 and thus the correct point A_2 .

If the drawing is accurate, the length of link A_1A_6 , thus obtained, must be equal to that of the given link L_3 , and the straight line from the correct D_2 -point through A_6 must pass through the point D_1 .

This second way is sometimes the easier method of determining the locus for A_6 . Allowance for slight variations in the directions of the forces F_1 and F_2 again may be made, at least approximately.

The methods described may be used also in the case when it is desired to consider the friction between the links and the roller. The "friction lines" deviate by an angle μ from the contact normals n_1 and n_2 and are always inclined in the direction opposite to the motion of the links on the roller. Thus, if the point A_6 moves closer to the center O of the roller, the friction lines are inclined toward A_6 , but if A_6 moves away from the center O they are inclined away from A_6 . In the case of the friction lines being used, the position of the resultant R of F_1 and F_2 changes its direction, as it passes no longer through the center O of the roller, but through the point O_2 in which the two friction lines meet, see Fig. 18, which shows also the geometry existing in this case.

Since the points D_1 and D_2 now lie on the friction lines, and since the line $D_1A_6D_2$ remains a straight line (neglecting the slight friction at the pivot pin A_6) it is still possible to use the methods described and shown in Figs. 16 and 17 for obtaining the correct position of the point A_6 , and thus the locus for A_6 , provided the friction lines are substituted for the contact normals.

CURE OF THE TROUBLE CAUSED BY VARIATION OF FORCE F_1

The principal question in the problem described at the begin-

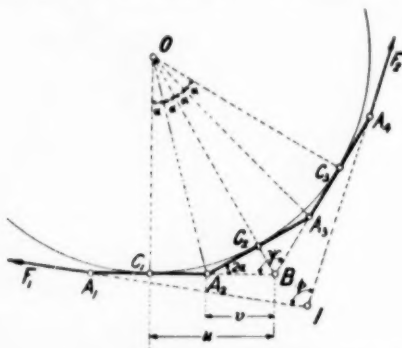


FIG. 19 DIAGRAM FOR THE DETERMINATION OF THE MINIMUM DIAMETER FOR A TROUBLE-FREE ROLLER

ning was not to make a mathematical analysis, but to find quickly a remedy for the troublesome condition that existed.

From the explanations given here, it is obvious that the variation in the pulling force comes about by the movement of the chain links relative to the roller over which they are supposed to be guided like a rope or belt over a sheave. When the roller is smaller than it should be, this motion is a rather complex motion consisting of several separate motions which pass into one another, namely:

1 When two links are in contact with the roller, the motion is that shown in Fig. 15 for two links.

2 When, then, suddenly only one link remains in contact with the roller, the conditions presented in Figs. 4 or 5 prevail.

Thus there is a constant change from one condition to the other with an accompanying change in the distances of the pulling force F_1 and the resistance F_2 from the center O of the roller. When the distance of F_2 is the larger, the force F_1 has to overcome a greater moment; hence F_1 increases. As the distance of F_2 from O becomes smaller until the direction of F_2 touches the roller, F_1 becomes smaller and the more so as its distance from O increases. This is the condition that existed in the machine described at the beginning.

In order to prevent this variation in the pulling force F_1 or, at least, reduce it to a very small and tolerable amount, one has to adopt only the following simple rule:

Rule. To prevent variations in the pulling force, it is necessary and sufficient that at least three links, instead of one or two links, be in contact with the roller at all times.

(By thus eliminating the motions of the links relative to the roller, wear is also reduced to a minimum.)

It becomes, now, necessary to establish a relationship for the radius of the ideal roller circle so that always three links will be in contact with the roller and will be in equilibrium.

Let, in Fig. 19, r be the radius of the ideal roller circle with which three links A_1A_2 , A_2A_3 , and A_3A_1 are in contact. Let the angle made by A_1A_2B with A_1A_3B be ψ and the angle made by the directions of the lines of the forces F_1 and F_2 be ϕ . Then, there must be

$$\psi \geq \phi$$

Also, angle $C_2A_2B = 2\alpha$, when the angles $C_1OA_2 = A_2OC_2 = C_2OA_3 = A_3OC_2 = \alpha$. Let, further, $C_1B = u$ and $A_2B = v$. Then

$$v = \frac{l}{2 \cos 2\alpha} \quad [45]$$

Furthermore:

$$\frac{u}{r} = \tan 2\alpha = \frac{2 \tan \alpha}{1 - \tan^2 \alpha} \quad [46]$$

and

$$\frac{l}{2r} = \tan \alpha = \xi \quad [47]$$

Thus

$$\frac{u}{r} = \frac{2\xi}{1 - \xi^2}$$

However

$$u = \frac{1}{2}l + v = \frac{1}{2}l \left(\frac{1 + \cos 2\alpha}{\cos 2\alpha} \right) \quad [48]$$

whence

$$\frac{u}{r} = \frac{l}{2r} \frac{1 + \cos 2\alpha}{\cos 2\alpha} = \frac{2\xi}{1 - \xi^2}$$

or, with Equation [47]

$$\frac{u}{r} = \xi \frac{1 + \cos 2\alpha}{\cos 2\alpha} = \frac{2\xi}{1 - \xi^2}$$

from which

$$(1 - \xi^2)(1 + \cos 2\alpha) - 2 \cos 2\alpha = 0$$

or

$$1 - \xi^2 - (1 + \xi^2) \cos 2\alpha = 0$$

whence

$$\cos 2\alpha = \frac{1 - \xi^2}{1 + \xi^2} \dots \dots \dots [49]$$

Since $\psi \geq \phi$

$$\frac{\psi}{2} = 90^\circ - 2\alpha \geq \frac{\phi}{2}$$

and

$$\sin \frac{\psi}{2} = \cos 2\alpha \geq \sin \frac{\phi}{2}$$

or

$$\sin \frac{\phi}{2} \leq \frac{1 - \xi^2}{1 + \xi^2}$$

whence

$$\xi^2 \leq \frac{1 - \sin \frac{\phi}{2}}{1 + \sin \frac{\phi}{2}}$$

With Equation [47], this gives

$$\frac{l^2}{4r^2} \leq \frac{1 - \sin \frac{\phi}{2}}{1 + \sin \frac{\phi}{2}}$$

whence

$$r \geq \frac{l}{2} \sqrt{\frac{1 + \sin \frac{\phi}{2}}{1 - \sin \frac{\phi}{2}}}$$

which gives

$$r \geq \frac{l}{2} \frac{1 + \sin \frac{\phi}{2}}{\cos \frac{\phi}{2}} \dots \dots \dots [50]$$

or

$$r \geq \frac{l}{2} \frac{\cos \frac{\phi}{2}}{1 - \sin \frac{\phi}{2}} \dots \dots \dots [51]$$

It thus becomes apparent that the radius of a trouble-free ideal roller circle depends on the angle ϕ made by the directions of the forces F_1 and F_2 and, therefore, can be determined only when the exact layout of the chain drive is known. In the case described

at the beginning, the angle ϕ was 130° , and $\phi/2 = 65^\circ$; hence $2r/l = 4.52$, or the diameter must be 4.52 times the length of the link. This was larger than the diameter of the roller that was originally installed. After a new roller of that diameter-link ratio was installed in accordance with the author's request, no further trouble was encountered.

SUMMARY

It has been shown that when a link chain is passed over too small a deflecting roller, great variations in the chain pull and thus in the forces of the driving mechanisms result. The three or multibody mechanical problem has been reduced to a kinematic problem by omitting the forces, but retaining their directions. A study of the geometry of the problem has been carried out which shows that an analytical solution is not feasible, but that a geometrical solution can be obtained easily. Finally, a derivation is presented for obtaining the correct minimum roller diameter for trouble-free operation.

Discussion

ALLAN H. CANDEE.² In addition to the ingenious solution of a puzzling problem and the successful cure of a serious mechanical difficulty, the author's comparison of the geometrical method and the analytical method is particularly interesting. It may be well to consider what the two methods are, when applied to a problem like that of the paper. Perhaps not everyone will agree, but the analytical method may be said to mean the following:

A general equation is set up stating the relations of the variables.

A diagram may be used on which to base the equation, but for the most part, the reasoning is by algebraic thinking.

The operations of algebra and calculus are applied, and the solution is obtained by manipulating and transforming the equation.

The geometrical method is based wholly on diagrams and geometrical constructions.

Determinations may be made by drawing to scale, or exact values may be calculated by triangulation.

The thinking is about geometrical relations, and as in the present case, may involve kinematic geometry.

Conceivably, analytical calculations following the procedure illustrated by the successive configurations of points, lines, and curves shown in the diagrams of the paper, could be carried out; but it looks as if the number of man-hours spent in such a process would be prohibitive. If one arrived at an answer in that way, it would still be by means of geometrical thinking.

The writer agrees with the author that when the principles of advanced kinematic geometry are known and are applicable to a problem, they provide a valuable short cut over analytical methods.

AUTHOR'S CLOSURE

The author would like to thank Mr. Candee for his kind evaluation of this work and for the general comments he made concerning the value of geometrical versus analytical methods. It might be admitted readily that, had the author approached the problem analytically, he would probably never have found a solution for it.

In a previous paper,³ the author has drawn attention to the fact that machine-design problems should be attacked preferably

² Mechanical Engineer, Gleason Works, Rochester, N. Y. Fellow ASME.

³ "What is Wrong With 'Kinematics' and 'Mechanisms'?" by A. E. Richard de Jonge, *Mechanical Engineering*, vol. 64, 1942, pp. 273-278.

bly from a geometrical point of view, because, as stated there, "design on the drawing board requires geometrical methods as a logical means of approach."

It should not be lost sight of, however, that there exist also problems, mostly in dynamics of machinery, which may profitably be solved analytically. Yet, even in that field, there are now powerful geometrical methods available which yield solutions readily and with little effort.

Consequently, a clear survey should always be made first to determine which method of attack, the geometrical or the analytical, is likely to offer the greater possibility of success in any particular case.

Although it is often a matter of personal training, and thus of preference, which method of attack for the solution of a problem is chosen, it still is the author's considered opinion that no modern engineer can afford to study only one of these methods and thus become very one-sided, but that every good engineer should become proficient in both kinds of methods, geometrical as well as analytical, so as to be able to choose, in every case, that kind which will lead quickest and with most certainty to a successful solution of any particular problem under consideration.

It is a sad fact that in the United States the education of engineers is still predominantly analytical and ignores the simple and straightforward methods of geometrical analysis developed in Europe, particularly in Germany and Russia, which are as yet little known and very little studied here. The blame for this has been laid on the colleges, but they do not seem to have realized as yet their responsibility, nor to have taken steps to remedy this situation. We are living in times where it is essential to use the simplest and most effective methods, which frequently are the geometrical ones, to obtain quickly easily visualizable results, thus releasing the brain power of our engineers, and especially of the younger ones, for more important tasks.

However, it is gratifying to know that the author's continued efforts during the past decade of advocating the study of geometrical methods are beginning to bear some fruit if it is permissible to judge from the many letters from individuals and firms which he has received, asking for further guidance, information, references to the literature, and for actual help in solving some of their pressing problems. He feels thereby richly rewarded for his attempt to draw attention to a field of engineering science which has been very neglected in this country.

Effect of Rotary Regenerator Performance on Gas-Turbine-Plant Performance

By D. B. HARPER¹ AND W. M. ROHSENOW,² CAMBRIDGE, MASS.

A comparison of typical solutions for determining rotary-regenerator performance is presented. Curves showing the effect of leakage on regenerator effectiveness and plant performance are presented. Specific examples are investigated showing the effect on plant performance of variations in regenerator rotational speed, matrix length, and mass velocity of the gas passing through the matrix.

NOMENCLATURE

The following nomenclature is used in the paper:

- A = total matrix surface area, per side, sq ft
- A' = matrix surface area per unit volume, sq ft/cu ft
- c = specific heat of matrix, Btu/lb deg F
- C_p = specific heat (const press) of gas, Btu/lb deg F
- d = wire diameter, ft
- f = matrix fraction voids to solid
- G = mass flow per unit matrix frontal area, lb/hr sq ft
- $G' = G/f$
- h = heat-transfer coefficient, Btu/hr sq ft deg F
- k = thermal conductivity, Btu/hr ft deg F
- l = matrix length, ft
- m = total matrix mass, per side, lb
- m' = matrix mass per unit volume, lb/cu ft
- n = regenerator rpm
- p = pressure, psf
- r = compression ratio
- S = matrix frontal area, sq ft
- w = mass rate of flow, lb/hr
- W = cycle work output Btu/lb
- θ = time period, hr

$$\Lambda = \text{reduced length} = \frac{Ah}{wc_p} = \frac{A'h_l}{G'c_p}$$

$$\pi = \text{reduced period} = \frac{Ah\theta}{mc} = \frac{A'h\theta}{m'c}$$

$$\eta_R = \text{regenerator effectiveness} = (t_{a2} - t_{a1}) / (t_{g1} - t_{a1})$$

$$\eta_{\max} = \text{maximum plant efficiency at } \partial\eta/\partial r = 0$$

$$\eta_c = \text{compressor efficiency}$$

$$\eta_t = \text{turbine efficiency}$$

$$\Delta p/p = \Sigma \frac{\Delta p}{p} \text{ for pressure-drop in piping, combustion chamber, and regenerator matrix}$$

$$\Delta\omega = \text{regenerator leakage rate, lb/hr}$$

$$t = \text{gas or air temperature (see Fig. 4)}$$

INTRODUCTION

The efficiency of a simple gas-turbine plant can be increased

¹ Research Assistant, Department of Mechanical Engineering, Massachusetts Institute of Technology.

² Associate Professor, Department of Mechanical Engineering, Massachusetts Institute of Technology. Jun. ASME.

Contributed by the Gas Turbine Power Division and presented at the Annual Meeting, New York, N. Y., November 30-December 5, 1952, of THE AMERICAN SOCIETY OF MECHANICAL ENGINEERS.

NOTE: Statements and opinions advanced in papers are to be understood as individual expressions of their authors and not those of the Society. Manuscript received at ASME Headquarters, October 10, 1952. Paper No. 52-A-149.

by using a regenerative cycle in which a heat exchanger is used to transfer heat from the hot turbine-exhaust gas to the cooler compressor-discharge air, Fig. 1. Generally the type of heat exchanger considered for gas-turbine applications has embodied a stationary wall separating the hot and cold fluids. These have commonly taken the shell-and-tube geometry, arranged for either counterflow or crossflow passes.

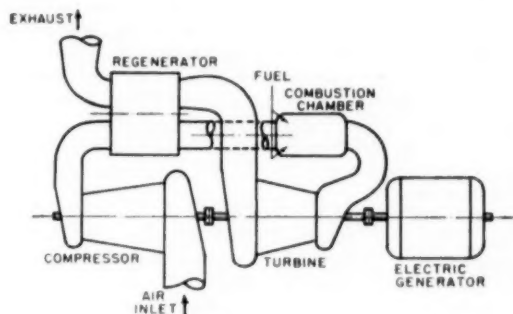


FIG. 1 REGENERATIVE GAS-TURBINE CYCLE

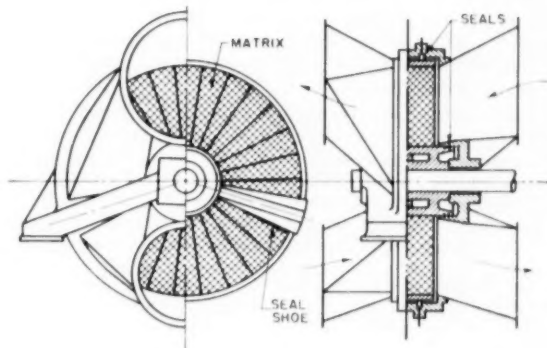


FIG. 2 ROTARY REGENERATOR

The suggestion that a rotary-type regenerator, similar to the Ljungström air preheater, be used as a gas-turbine-plant regenerator is generally attributed to Rudolf Ritz (1).³ Fig. 2 shows a possible arrangement. In this particular illustration the regenerator consists of a compartmented rotor disk to carry the energy-storage material (or matrix), a system of sealing shoes bearing against the rotor faces, and the necessary ducting to conduct the flow of gases. The rotor compartments together with the sealing shoes prevent the direct flow of the high-pressure air into the low-pressure gas stream, but allow the free flow of air and gas in their respective paths. The matrix elements, which are carried in the rotor compartments, have thus been separated from the pressure-retaining components of the regenerator and

³ Numbers in parentheses refer to the Bibliography at the end of the paper.

can take on any form which gives the required heat-storage characteristics in combination with a sufficiently small pressure drop. The matrix elements may consist of packings of wire mesh or expanded metal of various arrangements of corrugated sheet metal. As the rotor rotates, heat is transferred to the matrix while in the exhaust-gas stream and heat is transferred from the matrix while in the cooler compressed-air stream.

The principal advantage of the rotary regenerator is the possibility of designing a more compact unit than is possible with the conventional shell-and-tube or plate-fin stationary surface type. Calculations, such as those of Cox and Stevens (2), show that as passage diameter is reduced to very fine dimensions, heat-exchanger volume, for a given effectiveness and pressure drop, can be reduced appreciably. The matrix of the rotary regenerator can be finely divided, without structural difficulty, and the resulting matrix volume may be one tenth or less than the corresponding tube-bundle volume of a conventional heat exchanger. The sealing and ducting arrangements, and so on, especially for multidisk regenerators of larger capacities, would occupy a considerable volume but indications are that a regenerator could be built to occupy perhaps $1/3$ or $1/4$ of the volume of a conventional heat exchanger.

Inherent in the operation of a rotary regenerator is a leakage of some of the high-pressure air into the lower-pressure turbine-exhaust-gas side.

Leakage will occur at the seals owing to constructional difficulties and thermal distortion. As these seals are present on each side of the rotor, cold air will leak into the cooled gas stream and will not pass through the matrix; and heated air will leak into the hot gas stream and return through the exhaust side of the regenerator. In addition to seal leakage there is the positive-displacement or "let-down" loss of compressed air trapped in the matrix compartments as they pass the seals into the gas side. The let-down loss will be proportional to matrix rpm, and to the pressure ratio across the regenerator. The seal leakage may be considered essentially independent of rotational speed but will depend on pressure ratio.

The purpose of this paper is to investigate the effect of leakage and pressure drop in a rotary regenerator on gas-turbine-plant performance, and to illustrate the effect of the regenerator dimensions: length, cross-sectional area, and rotative speed on the regenerator and plant performance.

PARAMETERS AFFECTING REGENERATOR PERFORMANCE

The theoretical analysis of heat-storage regenerators has been carried out in many forms. Because of the continuous reversal of flow and the number of possible parameters to be included, complete solutions of the problem are very complex. Four of the simplest solutions for regenerator effectiveness are listed here to indicate the type of result obtained.

The principal parameters obtained are the reduced length (or surface) Λ and the reduced time period π . There is a value of Λ and π for both the air and gas passes. The following approximate solutions neglect the effects of longitudinal conduction and leakage. The simplest of the solutions assumes $\pi/\Lambda \approx 0$, i.e., when the heat capacity of the gas passed per period is much less than the heat-storage capacity of the matrix. By defining an over-all transmittance for the regenerator and using mean temperatures of matrix and fluids, the effectiveness for this limiting case is found to be

$$\eta_R = \frac{1}{1 + 1/\Lambda_g + 1/\Lambda_a} \quad [1]$$

A further approximate solution, generally attributed to Rummel (3), which uses an over-all transmittance but makes allow-

ance for transverse conduction can be obtained, for $(wc_p \theta)_a = (wc_p \theta)_g$, in the form

$$\frac{1}{\eta_R} - 1 = \frac{1}{\Lambda_g} + \frac{1}{\Lambda_a} + \frac{1}{2.5} + \frac{(wc_p \theta)_m}{2.5 K \rho A^2 (\theta_g + \theta_a)} \quad [2]$$

A solution of Tipler (4) assumes linear temperature gradients and takes the form

$$\eta_R = \frac{2 \Lambda_a / \pi_a}{\coth \left(\frac{\pi_a}{2 + \Lambda_a} \right) + \coth \left(\frac{\pi_g}{2 + \Lambda_g} \right)} \quad [3]$$

An iterative solution of the general differential equations, assuming perfect conductivity in the matrix perpendicular to the flow, has been made by Saunders and Smoleniec (5) for the case $\Lambda_a = \Lambda_g$ and $\pi_a = \pi_g$. Their result for a range of Λ and π is reproduced in Fig. 3(a). The results of Equations [1], [2], and [3] for $\Lambda = 5, 10$, and 20 have been compared with this solution in Fig. 3(b), the last term of Equation [2] being neglected as is valid for large Λ/m .

From inspection of Fig. 3(a) it can be seen that for high values of regenerator effectiveness, Λ must be large and π small. This

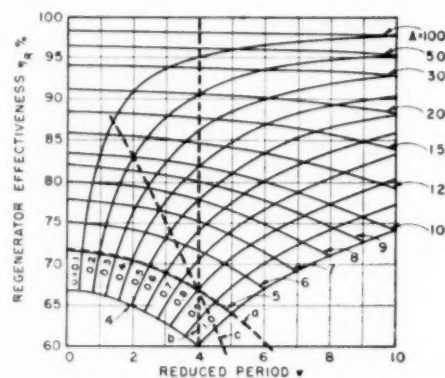


Fig. 3(a) THERMAL RECOVERY FOR REGENERATOR OF GIVEN REDUCED TIMES, REDUCED LENGTHS, AND UTILIZATION FACTORS

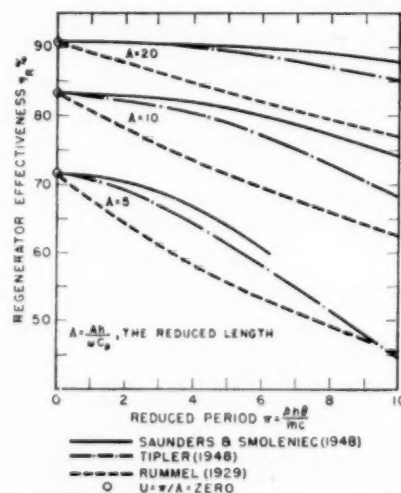


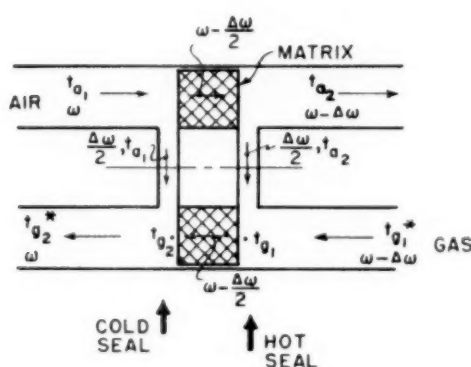
Fig. 3(b) COMPARISON OF REGENERATOR THEORIES $\Lambda_a = \Lambda_g$, $\pi_a = \pi_g$

suggests the use of a short period θ (i.e., high rpm); however, the let-down loss of compressed air carried in the matrix cells increases with rpm. This let-down loss together with the seal leakage will reduce the efficiency and specific work output of the gas-turbine plant. The leakage of air is thus a parameter in the design of the regenerator and of the complete gas-turbine plant.

EFFECT OF LEAKAGE ON REGENERATOR EFFECTIVENESS

The calculated values of regenerator effectiveness illustrated in Fig. 3 have been obtained assuming no leakage of air into the hot-gas stream. For analysis of the leakage effect, half the let-down loss may be added to the leakage at each seal, and be assumed to have the same temperature as the air at the seal faces of the rotor. This assumption will not introduce much error as the let-down air temperature will range from the air temperature at the cold-seal face to that at the hot-seal face.

(a) ASSUMED LEAKAGE PATHS



(b) GAS SIDE OF HOT SEAL

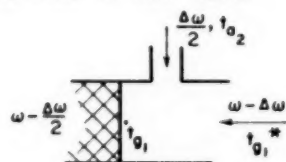


FIG. 4 LEAKAGE ASSUMPTIONS

Fig. 4(a) shows schematically the manner in which leakage has been assumed to occur. The effectiveness of the regenerator has been defined as

$$\eta_R = \frac{t_{a2} - t_{a1}}{t_{g1} - t_{a1}} \quad [4]$$

With reference to Fig. 4(a), the regenerator effectiveness with leakage accounted for must be defined as

$$\eta_R^* = \frac{t_{a2} - t_{a1}}{t_{g1}^* - t_{a1}} \quad [5]$$

Equating enthalpies on the gas side of the hot seal, Fig. 4(b), with the assumption of constant specific heat gives

$$t_{g1}^* = \frac{\left(1 - \frac{1}{2} \frac{\Delta\omega}{\omega}\right) t_{g1} - \frac{1}{2} \frac{\Delta\omega}{\omega} t_{a2}}{1 - \frac{\Delta\omega}{\omega}} \quad [6]$$

From Equations [4] and [5]

$$\eta_R^* / \eta_R = (t_{g1} - t_{a1}) / (t_{g1}^* - t_{a1}) \quad [7]$$

Using Equations [4] and [6] in [7] gives

$$\frac{\eta_R^*}{\eta_R} = \frac{2(1 - \Delta\omega/\omega)}{2(1 - \Delta\omega/\omega) + (\Delta\omega/\omega)(1 - \eta_R)} \quad [8]$$

Thus the correction to calculated regenerator effectiveness for the effect of leakage is given by

$$\eta_R - \eta_R^* = \frac{\eta_R (\Delta\omega/\omega)(1 - \eta_R)}{2 - (\Delta\omega/\omega)(1 + \eta_R)} \quad [9]$$

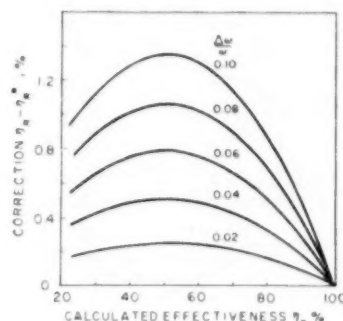


FIG. 5 EFFECT OF LEAKAGE ON REGENERATOR EFFECTIVENESS

Fig. 5 is a plot of Equation [9] for various values of η_R and $\Delta\omega/\omega$ and shows the magnitude of the correction to be small. Thus the effect of leakage on the effectiveness of the regenerator is not serious. This results from the definition of regenerator effectiveness being based upon temperature only. For this reason rotary-regenerator performance must be defined to include both temperature effectiveness and a leakage-loss parameter.

EFFECT OF LEAKAGE AND PRESSURE DROP ON PLANT PERFORMANCE

Calculations were performed employing perfect-gas relations and constant values of specific heat to illustrate the effect of leakage and pressure drops on gas-turbine-plant performance. For these calculations a turbine plant with 60 F inlet air, 1500 F turbine-inlet gas, compressor efficiency 85 per cent, and turbine efficiency of 88 per cent has been assumed.

For a regenerative gas-turbine cycle to be considered, thermal efficiency must be one of the most important factors. Thus the cycle will be designed to operate at or near the point of maximum efficiency. The compression ratio for maximum cycle efficiency is dependent upon regenerator effectiveness, pressure-drop loss, and leakage loss. Figs. 6, 7, 8, and 9 show the effect of these parameters on the gas-turbine cycle of Fig. 1 at the maximum thermal-efficiency point. For interpretation of the curves the pressure-drop parameter $\Delta p/p$ must be interpreted as $\Sigma(\Delta p/p)$ of the ducting, combustion chamber, and the drop through the air and gas sides of the regenerator.

Figs. 6 and 7 show maximum cycle efficiency versus regenerator effectiveness for a range of pressure and leakage loss. Curves of the corresponding compression ratio for maximum efficiency have been superimposed. Figs. 8 and 9 show cycle work output at maximum efficiency versus regenerator effectiveness for the same range of parameters. Curves of maximum efficiency and the corresponding compression ratio have been superimposed. Thus for a given regenerator effectiveness, parasitic pressure loss, and leakage loss, the cycle work output at maximum efficiency,

the maximum efficiency, and the required compression ratio for maximum efficiency can be found immediately. For regenerators of high effectiveness the point of maximum efficiency occurs at a low compression ratio which is advantageous for reducing the leakage loss in the regenerator. However, the specific work out-

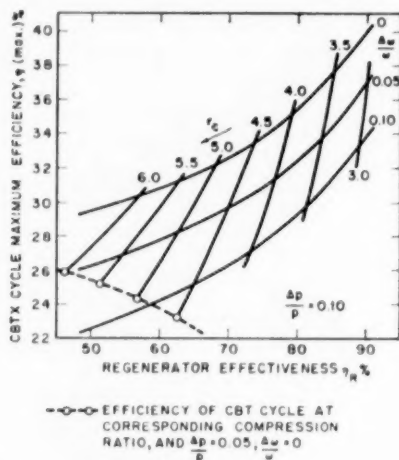


FIG. 6 MAXIMUM CYCLE EFFICIENCY; $\Delta p/p = 0.10$

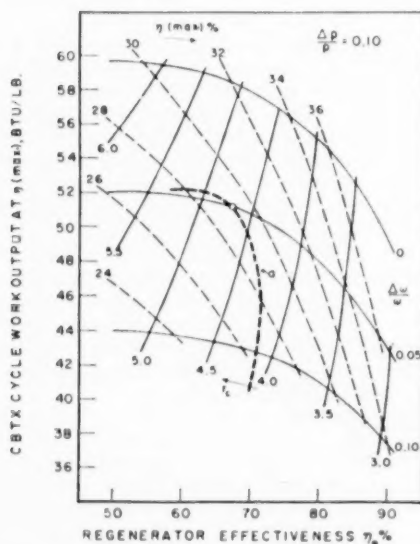


FIG. 8 WORK OUTPUT AT MAXIMUM CYCLE EFFICIENCY; $\Delta p/p = 0.10$

put of the cycle is seen to be low. Reheat and/or intercooled compression could be used to increase the work output, while maintaining the required thermal efficiency and the desired low compression ratio to reduce the leakage effects in the regenerator.

Reference to these curves shows that leakage loss has a greater effect on plant efficiency and work output than either pressure loss or regenerator effectiveness. Thus the degree to which leakage can be reduced in the rotary regenerator will be a measure of how successful this type of heat exchanger will be when applied to the gas-turbine plant.

EFFECT OF REGENERATOR DIMENSIONS ON PLANT PERFORMANCE

The previously calculated curves may be used to investigate the effect of the quantities l , G , and n on plant performance. These quantities might be interpreted as regenerator dimensions since l is the matrix length, G the mass velocity which is a measure of matrix cross-sectional area, and n the rotor rpm is a measure of the period θ , a time dimension associated with regenerator operation.

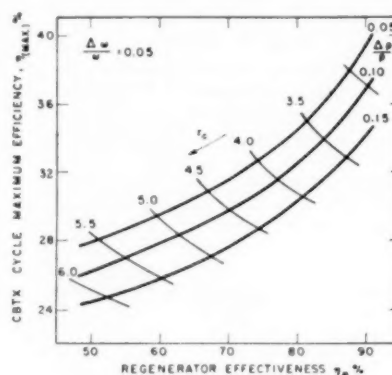


FIG. 7 MAXIMUM CYCLE EFFICIENCY; $\Delta \omega/\omega = 0.05$

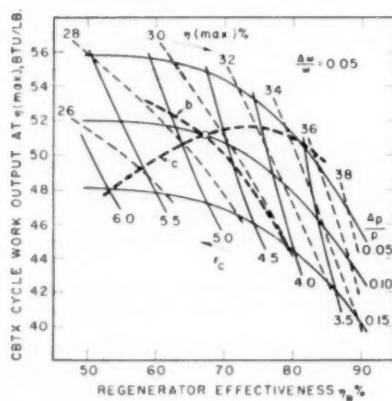


FIG. 9 WORK OUTPUT AT MAXIMUM CYCLE EFFICIENCY; $\Delta \omega/\omega = 0.05$

To illustrate the effect of these quantities on plant performance a calculation was made holding all of these quantities constant except one which is allowed to vary from its magnitude at some arbitrarily selected operating point. In each of these calculations the same type of matrix is assumed, and a constant plant power output maintained. Then A'/C_p and $A'/m'c$ are constant in magnitude.

In order to relate the calculation showing the effect of the quantities l , n , and G , each calculation was made arbitrarily to pass through the conditions at $A = 5$, $\pi = 4$, $\Delta p/p = 0.10$, and

$\Delta\omega/\omega = 0.05$. At these conditions with $t_1 = 60^\circ\text{F}$, $t_3 = 1500^\circ\text{F}$, $\eta_c = 0.85$, $\eta_r = 0.88$, the following results are read from Figs. 3(a) and 9: $\eta_R = 0.67$, $\eta_{\max} = 29.1$ per cent, $r = 4.7$ at η_{\max} , and work output is 51.2 Btu per lb at η_{\max} .

Effect of n . To investigate the effect of changing the rotational speed of the matrix on the design point performance l , G , and $\Delta p/p$ were held constant. If $\Delta p/p$ is taken as 0.10 then Fig. 8 may be used along with Fig. 3(a) to make the calculations.

The heat-transfer data for matrices are correlated (6) by

$$\frac{hd}{k} = 0.5 \left(\frac{G'd}{\mu} \right)^{0.5} \quad [10]$$

Then for this case h is constant; so Λ is also a constant. For this

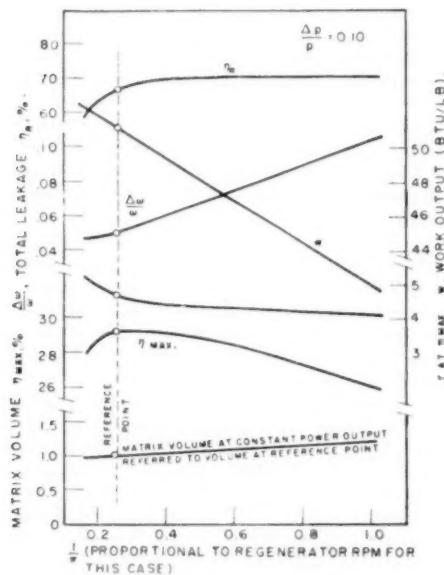


FIG. 10 EFFECT OF ROTOR SPEED ON PLANT PERFORMANCE AT DESIGN-POINT CONDITIONS

study select $\Lambda = 5$, and take $\Delta\omega/\omega$ for the seal leakage = $\Delta\omega/\omega$ for the let-down leakage = 0.025, that is, a total $\Delta\omega/\omega = 0.05$, when $\pi = 4$. Let seal leakage be unaffected by n and proportional to $(r-1)$ but let let-down leakage be proportional to n and $(r-1)$. The curves in Fig. 10 then may be drawn by matching points in Fig. 3(a) along the $\Lambda = 5$ line with points at corresponding values of η_R and $\Delta\omega/\omega$ in Fig. 8 (curve a). The results in Fig. 10 are plotted against $(1/\pi)$, which is proportional to n since (Ah/mc) is constant in this calculation.

Inspection of Fig. 10 shows plant efficiency going through a maximum value because as n increases the let-down leakage increases continuously and the regenerator effectiveness η_R approaches a maximum value. Note also that as n increases the specific work output (Btu/lb) decreases owing to the leakage effects. Then for the same power output a larger rate of flow is required and hence a larger compressor and turbine. A curve showing how the matrix volume increases with n is shown in the form of the ratio of matrix volume at a particular value of π to the value at $\pi = 4$. This matrix volume is corrected to a constant power output at the reference point at $\pi = 4$.

Effect of l . With G and n (or θ) constant the magnitude of π is constant and Λ is proportional to l since all other quantities involved are constant. The increased matrix length has been

assumed not to increase the let-down leakage. This assumes the actual matrix length is being varied within a rotor compartment of fixed length. Thus for constant n , the leakage doesn't change if the effect of slight changes in pressure ratio on leakage are neglected. The curves in Fig. 11 may be drawn by matching points on a vertical $\pi = 4$ line in Fig. 3(a) with points at corresponding values of η_R and $\Delta p/p$ in Fig. 9 (curve b) assuming $\Delta\omega/\omega$ is constant at 0.05. As l changes, $\Delta p/p$ changes in direct proportion to l . Allowing 0.03 as $\Delta p/p$ for all piping and combustion chamber and 0.07 for the regenerator at the reference point; then the total $\Delta p/p = 0.03 + 0.07 (\Lambda/5)$.

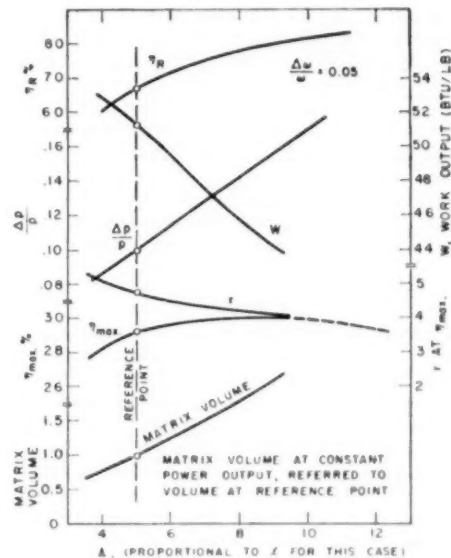


FIG. 11 EFFECT OF MATRIX LENGTH ON PLANT PERFORMANCE AT DESIGN-POINT CONDITIONS

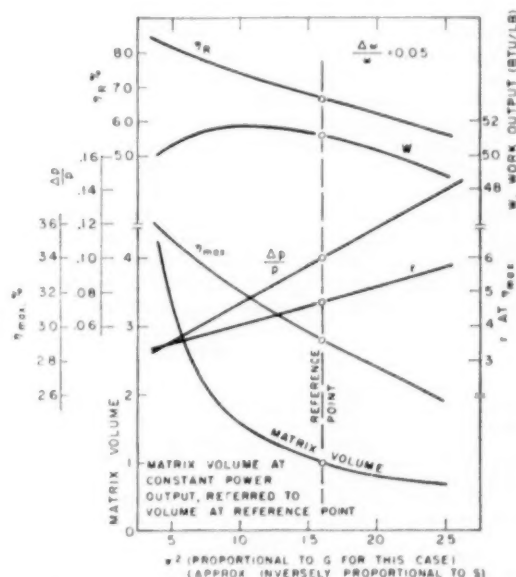


FIG. 12 EFFECT OF MATRIX MASS VELOCITY ON PLANT PERFORMANCE AT DESIGN-POINT CONDITIONS

The curves in Fig. 11 show the matrix volume increasing almost linearly with l . The departure from linearity results because the volume was corrected to constant work output at the reference point. Design-point cycle efficiency increases because η_R increases with l . As l continues to increase, cycle efficiency levels off and will finally decrease because of the effect of the increasing $\Delta p/p$.

Effect of G . With l and n (or θ) constant, neither Λ nor π is constant, but since from Equation [10] $h \sim G^{1/2}$, $\Lambda \sim G^{-1/2}$ and $\pi \sim G^{1/2}$. Hence as G changes from its magnitude at the reference point, Λ and π follow curve (c) as shown in Fig. 3(a). In this case $\Delta p/p$ for the matrix is assumed to be proportional to G (reference 7); hence since $\Delta p/p = 0.10$ at the reference point and the $\Delta p/p = 0.03$ for piping and combustion chamber the total $\Delta p/p = 0.03 + 0.07(\pi/4)^2$. Proceeding as before with Figs. 3(a) and 9, the results shown in Fig. 12 may be obtained and plotted against π^2 since $\pi^2 \sim G$ for this case. Also, with constant l and nearly constant work output per pound of fluid, π^2 is approximately inversely proportional to the cross-sectional area.

The design-point cycle efficiency decreases as G increases because regenerator effectiveness decreases and $\Delta p/p$ increases. Also, the matrix volume is approximately inversely proportional to G .

CONCLUSIONS

This analysis of the effects of the performance of a rotary regenerator on gas-turbine-plant performance indicates design conditions that the regenerator must fulfill in this application.

The effect of leakage on the temperature-based regenerator effectiveness has been shown to be small. Even if the leakage distribution were more unfavorable than that assumed in the analysis, the effect could not exceed twice that indicated by Fig. 5.

The direct effects of leakage, pressure drop, and regenerator effectiveness on plant performance at the maximum efficiency point as shown by Figs. 6, 7, 8, and 9, illustrate the importance of the leakage.

The effect of the regenerator n , l , and S has been shown by Figs. 10, 11, and 12. An optimum regenerator rpm at which plant efficiency will be a maximum has been shown to exist. There is also an optimum regenerator length, for a given matrix design, beyond which the regenerator size increases rapidly and plant efficiency increases very slightly.

The curves resulting from the present analysis are representative of the family of curves which would cover all reasonable design conditions. In the analysis, heat-transfer and flow-friction characteristics for matrices had to be assumed as did the range of pressure drop and leakage loss. However, the arbitrary reference point used in preparing the curves in Figs. 10, 11, and 12 is within the range of practical interest. Trends similar to those shown in these figures would be observed for specific matrix characteristics and for other ranges of the variables.

BIBLIOGRAPHY

- 1 "Summary of the Theory and Construction of a Rational Gas Turbine," by L. Ritz, Institute for Thermodynamics, Aerodynamical Research Laboratory, Göttingen, Germany.
- 2 "The Regenerative Heat Exchanger for Gas Turbine Power Plant," by M. Cox and E. K. P. Stevens, W.E.P. No. 60, The Institution of Mechanical Engineers, vol. 163, 1950, pp. 193-205.
- 3 "Die Berechnung der Wärmespeichern auf Grund der Wärmedurchgangszahl," by K. Rummel, *Stahl und Eisen*, vol. 48, 1928, pp. 1712-1715.
- 4 "A Simple Theory of Heat Regenerators," by W. Tipler, Technical Report I.C.T./14, Shell Petroleum Company, Ltd.

5 "Heat Regenerators," by O. A. Saunders and S. Smoleniec, Proceedings 7, International Congress for Applied Mechanics, vol. 3, 1948, pp. 91-105.

6 "Heat Transfer in Regenerators," by O. A. Saunders and S. Smoleniec, The Institution of Mechanical Engineers, General Discussions on Heat Transfer, Section 5, 1951.

7 "Heat Transmission," by W. H. McAdams, McGraw-Hill Book Company, Inc., New York, N.Y., 1942, p. 124.

Discussion

DAVID ARONSON.⁴ This paper is an exceptionally clear and simple presentation of a complex topic. Criticism of some of the details of the paper is given from the standpoint of industrial gas-turbine applications where a regenerator must have at least 80 per cent effectiveness and preferably 85 to 90 per cent to compete with a more conventional recuperator of tubular or extended-surface design.

From that standpoint, the choice of a combined leakage (let-down plus seal leakage) of 5 per cent limits the applicability of the paper. Likewise, the choice of a pressure-drop ratio of 10 per cent is beyond the optimum for gas turbines using regenerators of 85 or 90 per cent effectiveness. The usefulness of the paper would be extended if the authors were to indicate curves for zero leakage and zero pressure-drop ratio so that interpolation could be made readily.

Curves in Figs. 6, 7, 8, and 9 show the effects of leakage and pressure drop on plant efficiency and work output. In the range of high regenerator effectiveness, the effect of a 1 per cent pressure drop is about equivalent to 1 per cent leakage as regards plant efficiency, although the authors' comment is that the effect of leakage is much more serious. This conclusion is, however, applicable to work output.

The writer also disagrees with the remarks about the curves in Fig. 3(a) of the paper. For high effectiveness high values of Λ are required, but there is considerable latitude in the selection of the value of π , reduced period. For example, at 85 per cent regenerator effectiveness one could choose a value of Λ equal to 15 which means a reduced period of 9, or a value of Λ equal to 12 which means a reduced period of 3. Hence a threefold change in the value of π corresponds to only a 25 per cent change in Λ . Of course if one were to use the equation of Rummel, shown as a dashed line in Fig. 3(b), the effect would be more pronounced. However, the conditions used by Rummel are not applicable to the type of regenerators considered in present design studies for industrial application. They might cover porous sheet metal of high conductivity.

The conclusion that leakage has a negligible effect on the temperature effectiveness of the regenerator simplifies the analysis. If the authors could now show us how to combine the effect of pressure-drop ratio with leakage ratio for a given cycle, the comparison of regenerator with recuperator design would be simplified greatly.

The indications that high plant efficiency is associated with low compression ratio arises from the selection of a cycle without intercooling. The authors might be able to show that the compression ratio is applicable to an intercooled cycle, but that the ratio is that between stages of intercooling. Of course work-output figures would no longer be applicable.

The present paper is undoubtedly entirely adequate for the present stage of development of the rotary regenerator. As design improvements are made, particularly in the matter of sealing, then further refinements in the study may be justified.

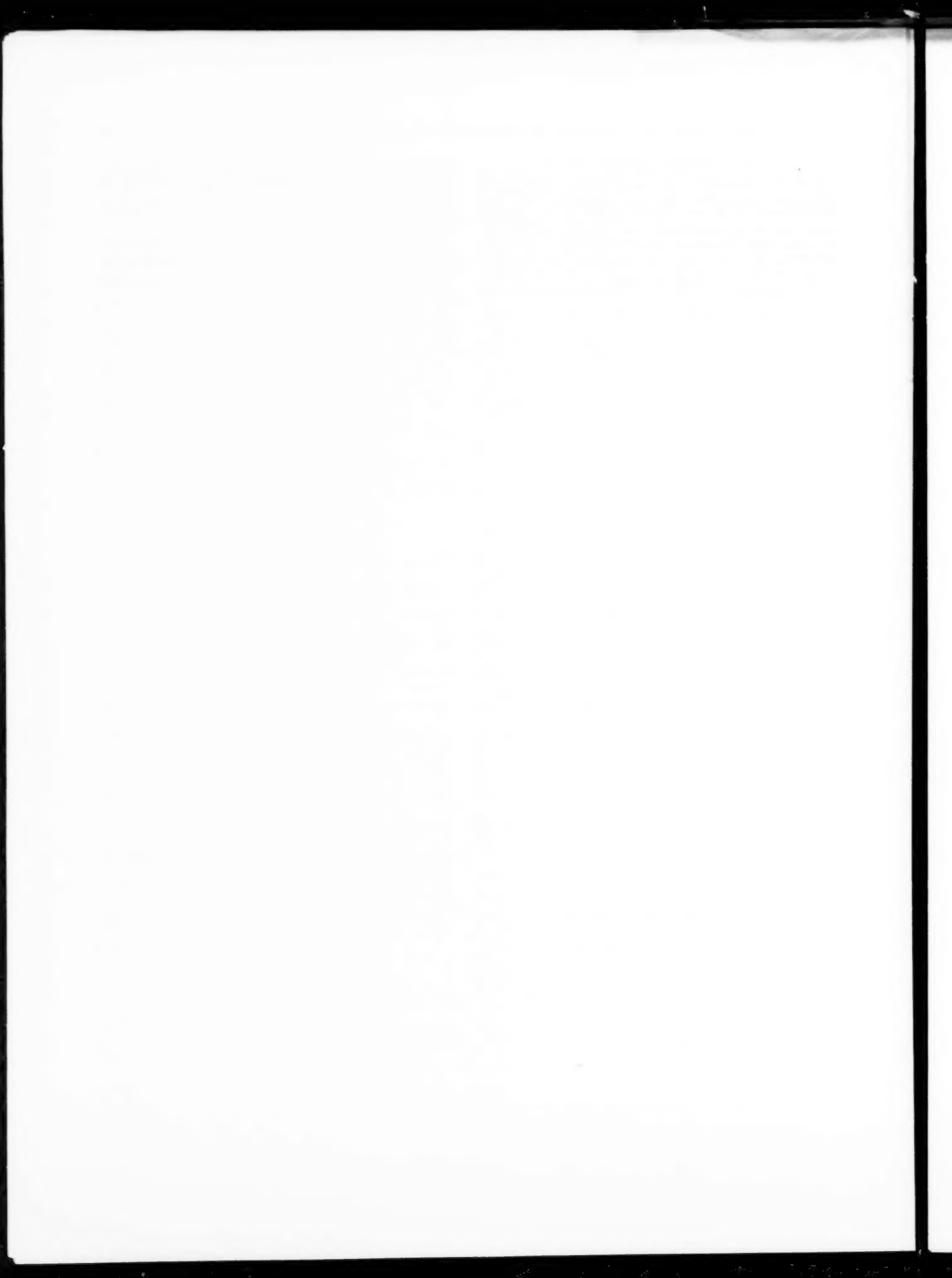
⁴ Engineering Specialist, Worthington Corporation, Harrison, N. J. Mem. ASME.

AUTHORS' CLOSURE

In this paper the assigned magnitude and range of regeneration effectiveness, pressure-loss ratio and leakage-loss ratio were chosen to illustrate the effect of these quantities rather than as a design study for a particular case. Mr. Aronson, however, suggests using higher regeneration effectiveness values. In certain applications where severe space limitations exist, such as the gas-turbine locomotive, a regenerator with 70 per cent effectiveness would be acceptable if the size and installation requirement could

be met. The two existing Brown Boveri gas-turbine locomotives with conventional crossflow tubular exchangers have been reported to have a regenerator effectiveness of the order of 40 per cent. In any event our purpose is to show trends, not to present a design study.

The suggested possibility of a combined pressure-drop and leakage-loss parameter for comparison of rotary regenerator and recuperator design should be given consideration in future investigations.



The Rotary Regenerative Air Preheater for Gas Turbines

By A. T. BOWDEN¹ AND W. HRYNISZAK,¹ NEWCASTLE-UPON-TYNE, ENGLAND

After some brief definitions, the paper deals with the influence of a regenerative air preheater on the performance of a simple open-cycle gas turbine, and formulas are given to show this influence, as well as the connection between the regenerator dimensions and the condition of minimum fuel consumption.

NOMENCLATURE

The following nomenclature is used in the paper:

Subscripts:

- 1 = inlet position (of matrix)
- 2 = outlet position (of matrix)
- g = gas
- a = air
- gs = gas side
- as = air side
- M = matrix

Properties of Gas and Air:

- T = temperature (degree temperature)
- ΔT = $(T_2 - T_1)$ temperature rise of air
- ΔT_1 = $(T_g - T_a)_1$ difference between inlet temperatures
- P = pressure (weight/length²)
- W_{ac} = mass-flow per second (weight/time)
- A = area (length²)
- μ = viscosity (weight, time/length²)
- g = acceleration due to gravity (length/time²)
- R = gas constant (length/degree temperature)
- c = specific heat (heat/weight, degree temperature)

Dimensionless Groups:

- Nu = Nusselt number
- Re = Reynolds number
- Pr = Prandtl number
- $C_{R,S}$ = resistance coefficient, referred to surface
- η_h = degree of conversion
- $\eta_{h,c}$ = influence of contact time
- $\eta_{h,k}$ = influence of heat conductivity
- $\eta_{h,i}$ = influence of inlet conditions
- η_T = temperature efficiency
- η_P = pressure efficiency
- η_W = mass flow efficiency
- η_O = power output efficiency
- η_H = heat input efficiency

Properties of Matrix:

- A_M = area of matrix (length²)

$$a_m = \frac{(A_{as} + A_{gs})_M \text{ initial}}{(W_a + W_g)_{ac}} \begin{matrix} \text{(Total) specific (initial)} \\ \text{area of matrix} \\ \text{(length}^2, \text{ time/weight)} \end{matrix}$$

- H_M = height of matrix (length)
- D_M = hydraulic diameter of matrix (length)
- ρ_M = specific weight of matrix (weight/length³)
- Φ = permeability (transflux/initial area)
- Φ = gas-side area/air-side area
- N = number of gas (or air) sides
- n = rotor speed, rpm
- V = volume (length³)

Functions:

$$f_1(\Phi) \cong \frac{1 + \Phi}{2} \left[\left(\frac{1}{g\mu_a} \right) + \left(\frac{1}{g\mu_g} \right) \frac{1}{\Phi} \right]$$

$$f_2(\Phi) \cong \frac{1 + \Phi}{2} \left[\left(\frac{\mu RT}{P^2} \right)_a + \left(\frac{\mu RT}{P^2} \right)_g \frac{1}{\Phi} \right]$$

$$f_3(\Phi) = \left(\frac{1 + \Phi}{2} \right)^{-0.5} \text{ (where pressure in space between rotor and stator is low, like gas pressure)}$$

$$\left(\frac{1 + \Phi}{2\Phi} \right)^{-0.5} \text{ (where pressure in space between rotor and stator is high, like air pressure)}$$

Remarks:

The following are main assumptions regarding the formulas given:

- (a) Specific weight (mass) flow and specific heat of gas and air about the same.
- (b) Laminar flow in the matrix, Equations [4] to [7].
- (c) Seal with "rough" surface (or labyrinth seal), Equation [11].

The mathematics have been kept as simple as possible so as to show various influences involved.

The constants in Equations [4], [5], [11], and [12] depend on the system of units for weight, length, and time introduced.

Const₂ is additionally governed by shape of (laminar flow) channels of matrix.

Const₃ is additionally affected by kind and effective tightness of seals.

Const₄ is in addition to be computed from reference (8)² (see Bibliography).

DEFINITIONS

To prevent any misunderstanding in the interpretation of certain terms, a few brief definitions may be appropriate.

As regards the actual heat exchangers, the term "recuperative" is given to the heat-conducting, continuous-flow type, and "regenerative" to the heat-accumulating periodic-flow type.

To keep within a reasonable compass, discussion is confined to the rotary type of regenerative heat exchanger (Ljungström type) (1),² although several of the problems discussed could apply

² Numbers in parentheses refer to the Bibliography at the end of the paper.

¹ C. A. Parsons & Company, Limited.
Contributed by the Gas Turbine Power Division and presented at the Annual Meeting, New York, N. Y., November 30-December 5, 1952, of THE AMERICAN SOCIETY OF MECHANICAL ENGINEERS.

NOTE: Statements and opinions advanced in papers are to be understood as individual expressions of their authors and not those of the Society. Manuscript received at ASME Headquarters, September 26, 1952. Paper No. 52-A-74.

equally well to other types. To narrow down the field still further, this paper will be concerned with a regenerator used as the air preheater in a simple open-cycle gas turbine. However, the conditions relating to working temperature, temperature and pressure gradients, and other factors are so severe that they may cover several other applications beyond the gas turbine.

The part involved in the exchange of heat is termed the "matrix," and this definition is fairly straightforward in so far as the recuperator is concerned. With the regenerator, however, the parts impinged upon periodically by the two heat-exchanging gases share in the exchange of heat, which means not only the matrix designed for the purpose, but other parts of the rotor as well. The effect of these latter parts, however, is usually negligible compared with the former.

By "initial area" of the matrix is meant its maximum area measured perpendicular to the direction of flow (just before the gases enter and after they leave the matrix), and by "height" its dimension in the direction of flow. The "transflux area" is the minimum area of flow between the bodies forming the matrix, and its "permeability" is the ratio transflux/initial area. When reference is made to the "specific area" the (initial) area referred to the unit mass-flow per second of the impinging gas, is indicated. The sum of the initial areas on the air and gas sides referred to the sum of the mass-flow per second of the air and gas, is one of the most important characteristics of the regenerator.

Use is made of the nondimensional method of representing the thermodynamical relations governing the heat transfer and the resistance in the air preheater and linking these properties with the thermodynamical properties of the other components of the gas turbine. For this purpose a distinction is made between the "internal" and "external" efficiencies of the air preheater.

The internal efficiencies are defined as follows

$$(a) \text{ Temperature efficiency} = \eta_T = \frac{\Delta T}{\Delta T_i} \dots \dots [1]$$

as a measure of the temperature gain (loss) occurring in the rotor (matrix).

$$(b) \text{ Pressure efficiency} = \eta_P = \frac{P_2}{P_1} \dots \dots \dots [2]$$

as a measure of the pressure loss caused by both the rotor and the stator.

$$(c) \text{ Mass-flow efficiency} = \eta_W = \left(\frac{W_2}{W_1} \right)_{acc} \dots \dots [3]$$

as a measure of the mass-flow losses caused by the clearance between the rotor and stator, as well as by the carry-over of gases from one side to the other, due to the cavities of the rotor and its movement.

The power output of the gas turbine is influenced mainly by the pressure and mass-flow efficiencies, and the heat input mainly by the temperature efficiency.

The external efficiencies of the air preheater are related to the performance of the gas turbine, viz, its power output and its heat input (both per unit mass-flow).

$$\eta_o = \frac{\text{Power output with actual air preheater (including power loss)}}{\text{Power output with ideal air preheater (excluding power loss)}}$$

$$\eta_H = \frac{\text{Heat input with actual air preheater (including heat loss)}}{\text{Heat input with ideal air preheater (excluding heat loss)}}$$

The product of these two efficiencies gives the over-all (external) efficiency of the air preheater referring to the specific fuel consumption of the gas turbine.

The acceptable values of these efficiencies depend very largely on the whole thermodynamical layout of the gas turbine, being affected mainly by the turbine and compressor inlet temperatures and the changes in the gas and air properties in these components. The pressure efficiency (roughly between 92 and 94 per cent) and the mass-flow efficiency (roughly between 97 and 99 per cent), are influenced in different ways by the specific area of the matrix. This area, in turn, affects the temperature efficiency (roughly between 80 and 90 per cent), so that general optimum considerations lead to the best pressure ratio of the turbomachines, the best specific area of the matrix, the best dimensions for rotor and stator, and the best speed for the rotor.

From the foregoing it is clear that there is no close specific limit to the acceptable efficiencies of the regenerator. The main dimension which may be limited is the specific area of the matrix, depending on the design and arrangement of the air preheater as influenced by the design and arrangement of the other components of the gas turbine.

DIFFERENCES IN WORKING CONDITIONS OF REGENERATIVE AIR PREHEATERS IN GAS AND STEAM TURBINES

The rotary regenerative air preheater has been used for many years in steam-turbine practice. Hitherto, it has been used mainly for unsupercharged boilers, although attempts have been made to apply it to supercharged boilers, i.e., those in which the pressure of the air supply is considerably higher than that of the exhaust gases. The function of an air preheater in a gas turbine (2) is very similar, except that the conditions as regards the temperatures and pressures of the heat-exchanging gases are even more severe. Hence any success achieved in the development of the rotary regenerative air preheater for gas turbines may improve its chances of being used for other similar purposes as well.

GENERAL DEVELOPMENT TREND OF GAS-TURBINE AIR PREHEATERS

There are at present two main trends in gas-turbine development (3):

(a) The simple open-cycle gas turbine of comparatively low efficiency and low cost, for purposes where fuel consumption is not important.

(b) The high-efficiency gas turbine, competing (in certain power ranges) with the steam turbine and the reciprocating combustion engine.

High efficiencies can be realized by (a) raising the turbine-inlet temperature (and inlet pressure) and (b) recovering waste heat by, say, air preheating. In the latter case the best turbine-inlet pressure is reduced and hence the turbine-outlet temperature is increased. This temperature has its effect on the mean working temperature of the air preheater, which is limited at present to between 300 and 400 C for reasons such as the safe working of seals, cost of materials and manufacture, and so on. Thus it seems that, at any rate for the present, either of the two methods (a) or (b) is practicable, but not both together.

A very efficient air preheater is necessary to enable the gas turbine to compete successfully with these other prime movers as regards specific fuel consumption. A high-temperature efficiency can be achieved only by a high resistance in the matrix because of the relation between this resistance and the heat transfer. To keep the pressure efficiency high as well, large specific areas are required so as to reduce the velocities of the gas and air when passing through the matrix

$$a_M^2 = \left(\frac{\text{const}_1}{1 - \eta_P^2} \right) \left(\frac{2}{\eta_{H-actual}} \right) \left(\frac{\eta_T}{1 - \eta_T} \right) f_1(\Phi) f_2(\Phi) \dots [4]$$

To reduce the bulk of the preheater, the development trend is

to reduce the hydraulic diameter of the matrix so as to decrease its height

$$H_M = \text{const}_2 \left(\frac{2}{\eta_{h, \text{actual}}} \right) \left(\frac{\eta_T}{1 - \eta_T} \right) \left(\frac{D_M^2}{a_M} \right) f_1(\Phi) \quad [5]$$

This reduction in matrix height is accompanied by a similar reduction in weight and hence cost of materials

$$\frac{(W_{as} + W_{gs})_M}{(W_a + W_g)_{rec}} = (1 - \phi_M) H_M a_M \rho_M \quad [6]$$

together with reduction in its cavities

$$\frac{(V_{as} + V_{gs})_{M, \text{carry-over}}}{(W_a + W_g)_{rec}} = \phi_M H_M a_M \quad [7]$$

thus reducing the carry-over losses and so increasing the mass-flow efficiency when a regenerator is used.

INFLUENCE OF REGENERATIVE AIR PREHEATER ON PROPERTIES OF GAS TURBINE

The difference in the method of heat transfer in a regenerative and in a recuperative air preheater affects the mechanical design and thermodynamical properties of each.

As regards the thermodynamical properties, it is necessary to consider the influence of the mass-flow losses resulting from the seals and from the carry-over of air caused by the movement of the rotor, and the effect of this movement on the temperature gain of the air.

The regenerator and recuperator are thermodynamically equivalent provided their external efficiencies are the same. Referred, for instance, to the specific fuel consumption of the gas turbine, this means that the additional mass-flow loss of the regenerator must be balanced (as regards its effect on specific fuel

consumption), by a reduced pressure loss and/or an increased temperature gain, Fig. 1.

The optimum layout conditions of the gas turbine in terms of, say, its specific fuel consumption are affected by all three internal efficiencies in the general form

$$\frac{\eta_T}{1 - \eta_T} = f[\eta_P, \eta_M \text{ and } (P_1 T_1 W_{acc}) \text{ other components}] \quad [8]$$

Equation [8] links the properties of the air preheater with those of the other components of the gas turbine so as to obtain the optimum pressure ratio of the turbomachines for a maximum efficiency.

Adequate means must be provided for maintaining the internal efficiencies, that is, means for preventing a drop in temperature gain and a rise in pressure and mass-flow losses at the different loads of the gas turbine throughout its service life.

As regards the mechanical design, the regenerator requires (additionally to the recuperator)

- A subdivision of the casing into a rotor and a stator.
- An effective seal between these two parts.
- Means for supporting the rotor in the stator.
- A drive for the rotor.

These additional features affect the cost of manufacture, testing, and maintenance of the air preheater.

A comparison, say, of production costs, gives the following:

	Recuperator	Regenerator
Matrix.....	Expensive	Inexpensive
Fixing of matrix.....	Expensive	Inexpensive
Casing		
Stator.....	Inexpensive	Expensive
Rotor.....	None	Expensive
Sealing between rotor and stator.....	None	Expensive
Support of rotor in stator.....	None	Expensive
Rotor drive.....	None	Expensive

For the same performance, the higher costs of the regenerator owing to its seals, bearings, and drive have to be offset by the cheaper matrix and its fixing. It is therefore proposed to deal with these items in the following sections.

TYPES OF MATRIX AND THEIR PERFORMANCE

An advantage of the regenerator is that it can use several types of matrix. There are two main types at present, viz., the plate (corrugated) type, and the wire (gauze) type (4). In the channels of the corrugations the flow is laminar; the characteristics governing heat transfer and resistance depend on the shape of these channels. In the range of Reynolds numbers usually applicable to gas-turbine air preheaters, the flow in the wire gauzes is partly viscous and partly turbulent.

Several suggestions have been made as to the appropriate tests to be applied to matrices of the type mentioned, but it is considered that the best tests are those which reproduce as far as possible the actual conditions in the air preheater.

Where rig tests are carried out at low temperature and pressure gradients, it seems useful to express their results (derived from one and the same test) in the form of an "ideal degree of conversion"

$$\frac{\eta_{h, \text{ideal}}}{2} = \frac{Nu}{C_{f, h} Pr Re} \quad [9]$$

dividing the total resistance into a "useful" part required for the transfer of heat (based on the Osborne Reynolds law), and a "parasitic" part.

When this degree of conversion in the plate and wire matrices is being compared it must be referred in both cases to one and the

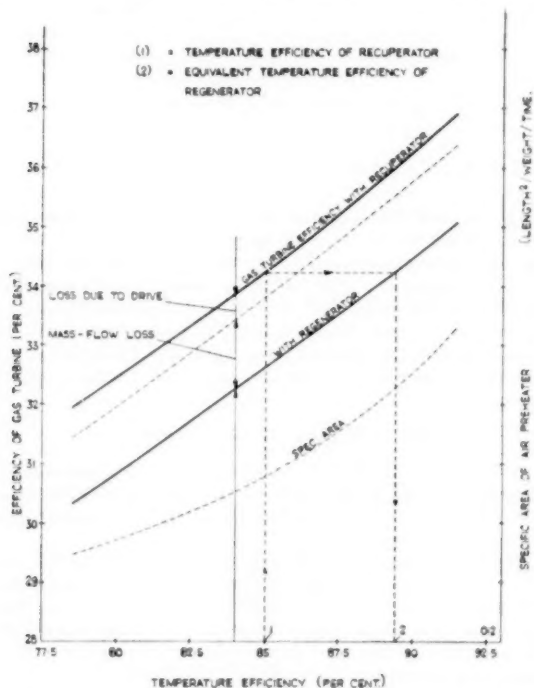


FIG. 1 INFLUENCE OF POWER LOSS DUE TO REGENERATOR ON EFFICIENCY OF GAS TURBINE

same area. The test results for the wire matrix are usually referred to the initial area and the wire diameter. The arrangement of the wires also affects the "ideal" degree of conversion in such a way that wide-meshed gauges give figures similar to those obtained with the corrugations, Fig. 2.

With the plate type, its permeability must be allowed for, since the test results are usually referred to the transflux area. Permea-

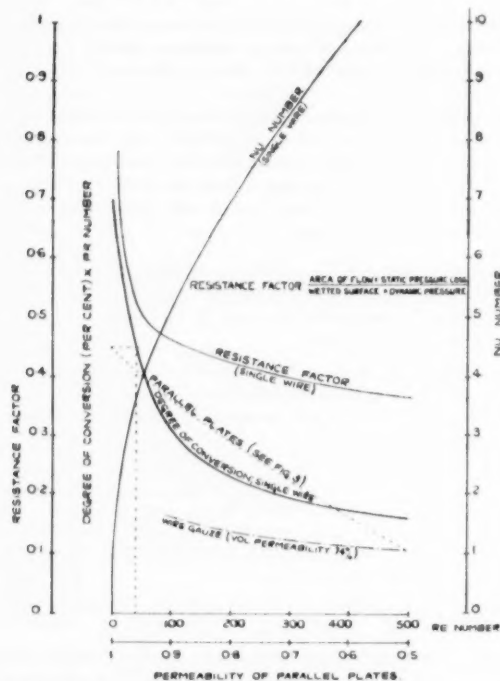


FIG. 2 IDEAL DEGREE OF CONVERSION OF WIRE AND WIRE GAUZE

bility is governed by the shape of the channels of the corrugations and their wall thickness. With this type of matrix the permeability unfortunately is linked with the hydraulic diameter in such a way as to reduce the former when the latter is reduced, Fig. 3.

The "actual" degree of conversion differs considerably from the ideal figure

$$\eta_{h, \text{ actual}} = (\eta_s \eta_h \eta_r \eta_{\text{ideal}})_h = (0.95 \text{ to } 0.97) \eta_{h, \text{ ideal}} \quad [10]$$

There are several reasons for this, such as the following:

- Flow conditions at inlet and outlet of matrix (5).
- Heat conduction in matrix parallel and perpendicular to flow (6).
- Influence of contact time between matrix and gases (7).
- Influence of seals (flow of carry-over gases).

It is difficult to separate the foregoing effects and to ascertain the size of the effective thermal and dynamical surfaces of the matrix in terms of the kind and arrangement of the seals and the rest of the rotor assembly. For different types of rotor (including the matrix), the heat-transfer and resistance data leading to the actual degrees of conversion have to be obtained more or less under actual operating conditions in order to get a true picture of the regenerator performance.

An advantage of the wire matrix is the smaller influence of heat conduction as compared with the plate type. It has been

found in some cases, however, that the wires have a tendency to flatten out during the operation time when they contact each other, and this increases both the resistance and the heat conduction.

The size of the bodies forming the matrix is limited by the danger of burning-out, when for instance, unburned fuel is left in the exhaust gases, say, due to the failure of a combustor, or the like. The limit of plate thickness and wire diameter may be in the order of 0.008 to 0.010 in.

Generally speaking, gauges allow of smaller hydraulic diameters than do corrugations. The speed of the rotor is governed by the necessary contact time between matrix and gases. Small hydraulic diameters give a low-weight matrix and high rotor speeds which often make sliding seals impossible; whereas large hydraulic diameters give higher weights accompanied by low speeds and

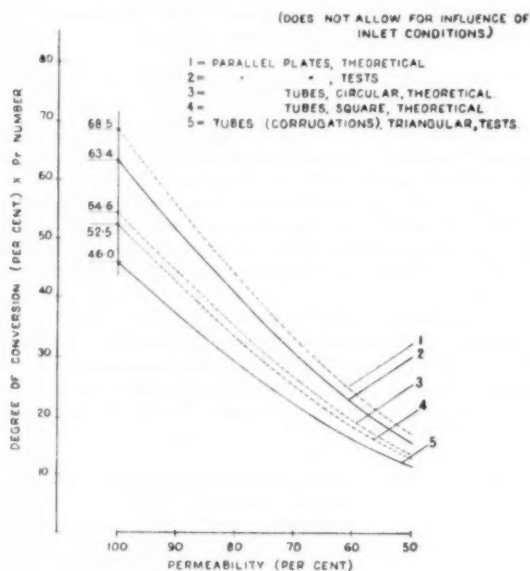


FIG. 3 IDEAL DEGREE OF CONVERSION OF PLATE-TYPE MATRIX

hence the possibility of using efficient sliding seals. These facts are important for the choice of the proper type of matrix to suit the regenerator of a gas turbine used for a particular purpose.

In this respect it is also worth mentioning that the part-load behavior of the wire matrix is different from that of the plate matrix. The increase in temperature efficiency is faster with the latter than with the former. This is important where the specific fuel consumption of the gas turbine in the part-load region matters.

SEALS BETWEEN ROTOR AND STATOR

While it may be possible to design a metal-to-metal contact seal bearing over the whole width of the rotating element, it is probably better to restrict the bearing area and to run the rest of the seal with a fine clearance.

Tests have been carried out with shoes made from bronze and other materials running on stainless-steel faces operating under temperatures of up to 550 C and without a lubricant other than the oxide film which forms under the operating conditions. Such an arrangement has given quite a fair service over a reasonable period.

The success of such a seal depends upon building up a thin stable oxide layer, and to obtain such a film the composition of the

materials used can be varied to suit the operating temperature of a given heat exchanger. If the oxide film becomes too thick, it is apt to spall. It is probably desirable, however, in all kinds of contact seals, and certainly those operating in the hot-gas region, to introduce some form of lubricant such as MoS_2 , or graphite. While in time such materials become oxidized at high operating temperatures, they are stable for quite a long period and by quite straightforward methods can be applied to the rotating surfaces at regular intervals of, say, hourly duration.

For the seals on the cold-gas side, and for the ends of a drum-type generator, carbon seals are probably as good as any other, although some synthetic materials such as bakelized asbestos have given very good service.

Porous materials impregnated with indium, lead, or other pressure-lubricating materials, are also suitable for the cooler conditions.

It is, of course, possible to arrange for nonsliding seals which will maintain a fine clearance under operating conditions, and a number of devices already have been produced to accomplish this.

Much of the success expected from a given type of seal depends on the freedom from distortion obtained under running conditions. Unless good mating surfaces and a very small effective clearance between them are maintained, the mass-flow loss due to clearance will be correspondingly high, but even with properly selected materials and with lubrication between the two rubbing surfaces of the sliding seals, the length of the seal necessarily must be short. It is almost axiomatic that the sliding surfaces should be as small as possible so as to reduce the rubbing to a minimum, and all design tendencies for modern regenerative air preheaters have been in this direction.

The size of the matrix governs the size of the rotor in which it is embedded and hence the size of the stator surrounding the rotor. Thus the length of seals depends on the size of the matrix and is considerable for a high-efficiency regenerator. In addition, this length depends on the kind of rotor used, and the division into seals with a high-pressure and low-pressure difference depends, in addition, on the method of sealing adopted.

The more conventional rotors are the disk and the drum types. Both have their advantages and disadvantages. If, for instance, only a single disk is used, the initial area of the matrix is usually restricted, but the space occupied by the regenerator is a minimum. The drum, on the other hand, is not restricted as regards initial area, but the bulk of the regenerator is larger owing to the unused space at its center.

The inside seals are located between a gas side and an air side; they are short, but fairly complicated in shape and hence rather unsuitable for effective sealing. The total length depends on the number of sides in the regenerator.

The outside seals are long (total length independent of number of sides), and circular in shape and therefore suitable for effective sealing. With the usual method of sealing they are located between the inlets and outlets of both sides and the space between rotor and stator. This space can be either closed from or open to the atmosphere.

At the present stage of development the outside seals can be made almost tight (about 0.01 lb/sec/ft), but the inside seals are still a problem in this respect. Hence the main development in the future will be concentrated upon improving the effectiveness of the inside seals by reducing the effective clearance and the length.

Because of the difference in shape and hence the effectiveness of the two kinds of seals, the optimum (diameter/length) ratio of the drum is fairly large.

Besides affecting the mass-flow loss due to clearance

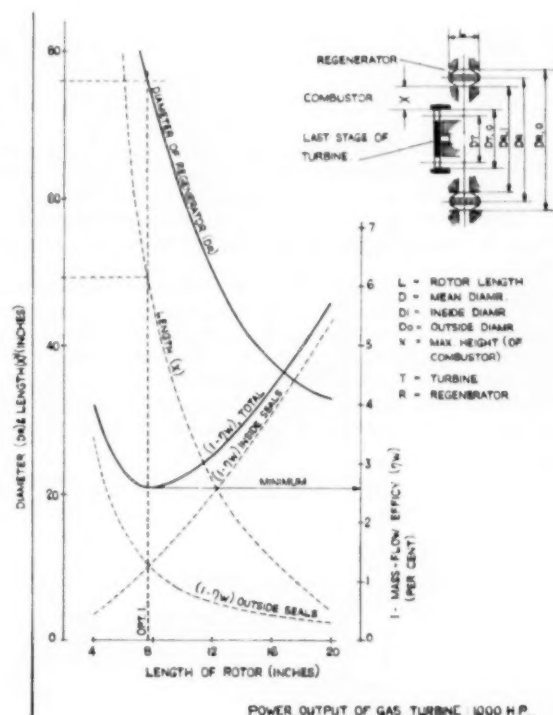


FIG. 4(a) INFLUENCE OF ROTOR DIMENSIONS ON MASS-FLOW EFFICIENCY DUE TO CLEARANCE

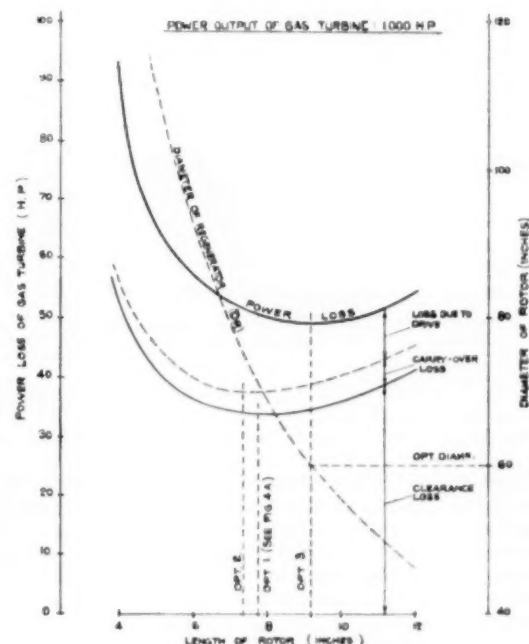


FIG. 4(b) INFLUENCE OF ROTOR DIMENSIONS ON POWER LOSS OF GAS TURBINES

$$\eta_{WP, \text{ clearance, max}} = 1 - \text{const}_3 a_M^{0.25} \left[\frac{N}{(W_a + W_g)_{\text{sec}}} \right]^{0.75}$$

$$f \left(\frac{A_{\text{rotor 1-2}}}{A_{\text{matrix}}} \right) f_2(\Phi) \dots [11]$$

the dimensions of the drum also affect the mass-flow loss due to carry-over, and the pressure loss. For this reason the optimum (diameter/length) ratio is usually smaller than that mentioned, if the different effects of mass-flow and pressure losses on the power output of the gas turbine are taken into account, Fig. 4.

The length of the inside seals can be curtailed by reducing the inlet and outlet areas of the rotor, this reduction decreasing the mass-flow loss (due to clearance) and increasing the pressure loss. Similar considerations referring to the power-output of the gas turbine lead to an optimum (inlet or outlet area/initial area) ratio. The reduction of the inlet and outlet areas results in higher gas velocities, so that everything must be done to make the re-

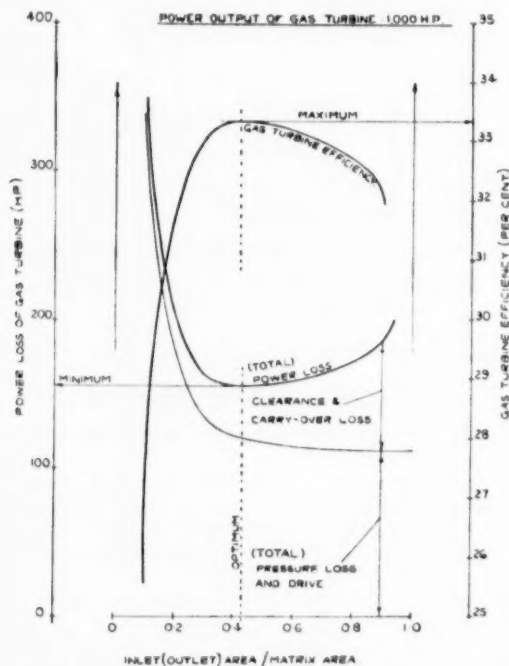


FIG. 5 OPTIMUM INLET (OUTLET)-AREA/MATRIX-AREA RATIO OF REGENERATOR

distance of the rotor near these areas as low as possible in order to reduce the pressure loss, Fig. 5.

When such a reduction in inlet and outlet areas is made, the rotor has to be divided into an inlet portion, a middle portion (accommodating the matrix) and an outlet portion. In this case meridional walls have to be provided, so as to get the necessary tightness in the circumferential direction. Such a division is always necessary when a wire matrix is used. The optimum number of walls depends on the extent to which the inlet and outlet areas of the rotors are obstructed in the circumferential direction by the thickness of the walls as well as by the inside seals.

It will be appreciated that during the movement of the rotor, the pressure on these seals varies according to the variation of gas pressure in the chambers (formed between the walls) which are

wholly or partly covered over by the shoes of the inside seals. It therefore becomes necessary to press these shoes against the rotor by springs, or by pneumatic or hydraulic devices, with a pressure that varies according to the opposite pressure exerted by the gas, so as to keep the wear of the sliding seals within reasonable limits.

The inlet portion of the rotor should take the form of an efficient diffuser (depending on the resistance of the matrix) and the outlet portion the form of an efficient nozzle.

Any such increase in rotor cavities, however, results in increased carry-over losses, and this affects the reduction in mass-flow loss and hence the optimum considerations just outlined.

Depending on the method of sealing adopted, this mass-flow loss is also affected by the distribution of the whole initial area of the matrix on its gas and air sides. A study of the effect of this distribution on the internal and external efficiencies of the regenerator as influencing the performance of the gas turbine leads to an optimum (gas side/air side) ratio, Fig. 6, which is also

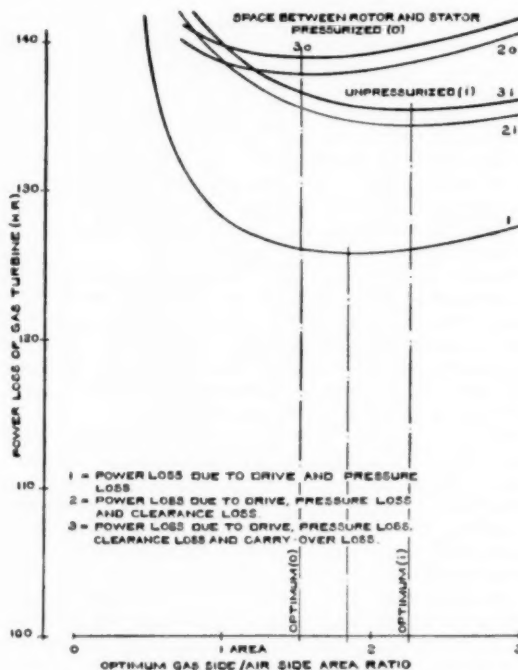


FIG. 6 OPTIMUM GAS-SIDE-AREA/AIR-SIDE-AREA RATIO OF REGENERATOR

governed by the kind and state of the gas in the (closed or open) space between rotor and stator. The optimum value of this ratio changes with the gas-turbine load, mainly because of the change in the pressure of air and gas. This point must be remembered when designing an air preheater for a gas turbine, say, one working mainly at low loads.

SUPPORTING AND DRIVING THE ROTOR

In certain designs of regenerator the supporting and driving of the rotor could be combined with the sealing. The commoner method, however, is that in which all three functions are separated.

Supporting. Any known method of supporting a low-speed rotor in a stator can be adopted provided that a low friction loss

and high precision (for the seals) are achieved. Other points to be kept in mind are the following:

- (a) Separating the bearing from the high-temperature part.
- (b) Balancing the gas forces by selecting at least two air and gas sides equally distributed over the rotor.
- (c) Insuring safe working of the bearing (lubrication) in the case where the closed space between rotor and stator is filled, say, with high-pressure air.

The best rotor speed can be found only by tests, which means that elaborate calculations are usually unnecessary. Its approximate value (8) can be obtained from

$$\frac{n}{60} \cong \frac{\text{const. } c}{N} \frac{(W_{as} + W_{gs})_{\text{acc}}}{c_M (W_{as} + W_{gs})_M} \left(\frac{1}{1 - \eta_{a,c}} \right)^{0.5} \left(\frac{\eta_T^3}{1 - \eta_T^3} \right)^{0.5} \quad [12]$$

provided that the reduction of the degree of conversion due to the influence of contact time is not more than 10 per cent. As regards the choice of rotor speed, it should be noted that it affects not only the temperature gain (degree of conversion), but also the mass-flow losses resulting from carry-over, and the like.

It also affects the power required for driving the rotor. Opti-

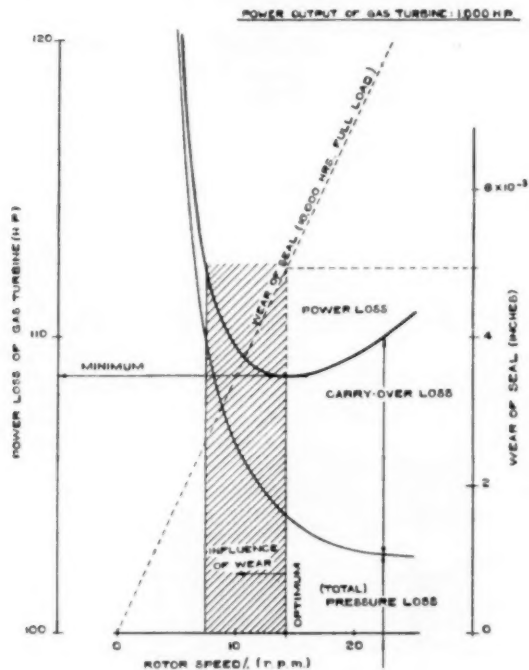


FIG. 7 CHOICE OF ROTOR SPEED

mum considerations show that the best speed is low and is further decreased when sliding seals are adopted, due to its effect on wear, Fig. 7.

Driving. There are several possible methods of driving the rotor. It can either be directly driven by the heat-exchanging gases themselves, or indirectly driven by the turbine of the gas turbine. With a mechanical transmission a high-reduction gear is necessary. Similar gears also are needed if an electric or hydraulic transmission is interposed between the turbine rotor and regenerator rotor. Because of the small power input of the

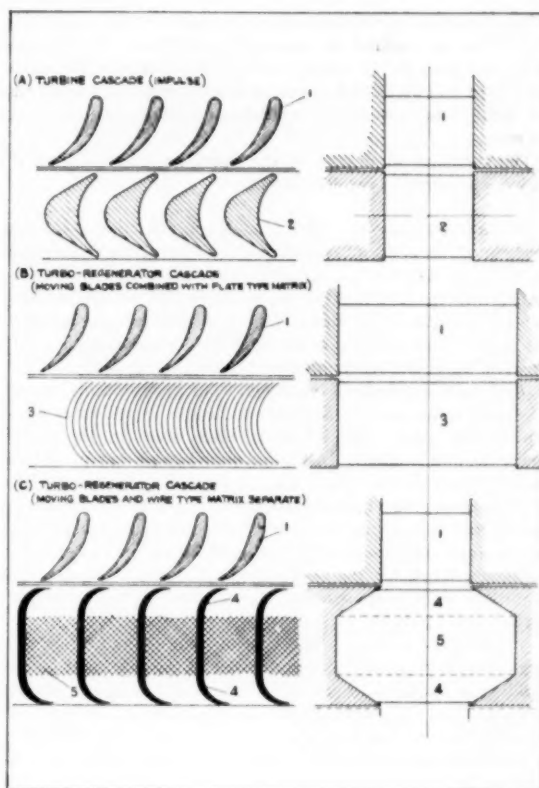


FIG. 8 TURBINE CASCADE COMBINED WITH REGENERATOR MATRIX TURBOREGENERATOR

regenerator, such a transmission has a fairly low efficiency

When the rotor is driven by the heat-exchanging gases themselves, the preheater works as a turboregenerator (9) combining the functions of a regenerative heat exchanger and a turbine. The meridional walls of the rotor are then shaped as moving blades, with fixed blades arranged in the stator. Small resistances due to mechanical and aerodynamical friction are necessary in this case, Fig. 8.

GENERAL DESIGN FEATURES OF REGENERATIVE AIR PREHEATER

The air preheater can be designed satisfactorily only by considering its effect on the gas turbine as a whole. As the simple open-cycle gas turbine with air preheating works on a low-pressure cycle, the parasitic pressure losses play a decisive part in its performance, mainly because of the influence of the preheater.

In the simple jet-type gas turbine the gas velocities in its compressor, combustor, and turbine are high and of roughly the same magnitude. When an air preheater is introduced into this type of gas turbine, the high air and gas velocities at the compressor and turbine outlets must be reduced to a very low figure before they can enter the preheater matrix. An effective conversion of velocity into pressure is therefore of vital importance. The influence of, say, pressure and mass-flow losses due to the regenerator can be reduced considerably by providing efficient diffusers between the outlets of the turbomachines and the inlets of the regenerator. Effective diffusers mean large spaces which may be affected by the resistance of the matrix.

The type of air preheater adopted depends on the general layout of the gas turbine, its size, and its purpose. For the time being, anyhow, highly efficient rotary regenerators of the single-rotor type will be limited to gas turbines of relatively small output until more experience is available, especially with regard to the seals.

The influence of design on the operating conditions of the seals is illustrated in Fig. 9 (a to c).

(a) *Axial-Flow Drum.* This type of rotor is suitable for relatively small areas both in the inlet and outlet of the rotor and in the matrix. The inside and outside seals are located in the same plane, while the high and low-temperature seals are separated on two parallel planes, the distance between which is the height of the rotor. This distance under temperature gradients has little effect on the operating conditions of the seals, Fig. 9(a).

(b) *Axial-Flow/Radial-Flow Drum.* This type of rotor demands relatively small areas in the inlet and outlet of the rotor where the flow is axial, and relatively large areas in the matrix where the flow is radial. Inside and outside seals, as well as high- and low-temperature seals, are on one and the same plane. Hence a more or less uniform average temperature (about 300 C), can be achieved for all seals, especially where additional heat-conducting media are provided such, for instance, as a sodium or potassium filling for the hollow sealing plates. The operating conditions of the seals are not, of course, affected by the expansion of the rotor, Fig. 9(b).

(c) *Radial-Flow Drum.* This type of rotor allows for relatively large areas both in the inlet and outlet of the rotor and matrix. Inside and outside seals can be on different planes perpendicular to each other. The high- and low-temperature planes are again separated by the height of the rotor. The operating conditions of the inside seals are greatly influenced by the expansion of the rotor under temperature gradients, as the dimension which matters is the diameter of the rotor, and this usually is rather large, Fig. 9(c).

There are, of course, several other possible drum constructions,

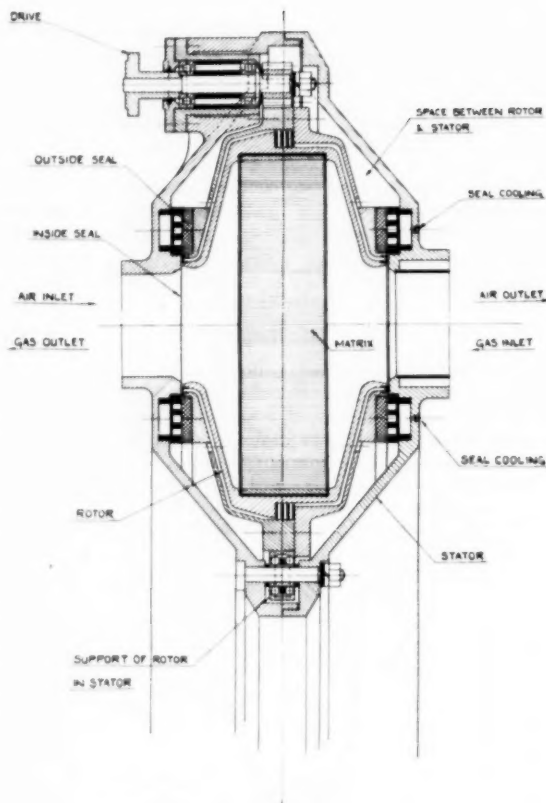


FIG. 9(a) AXIAL-FLOW DRUM REGENERATOR

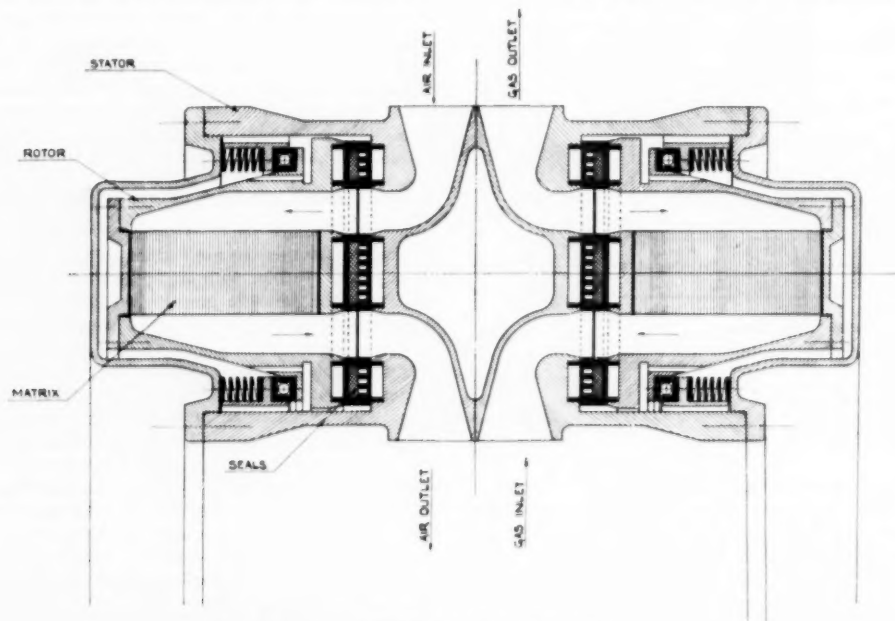


FIG. 9(b) AXIAL-FLOW/RADIAL-FLOW-DRUM REGENERATOR

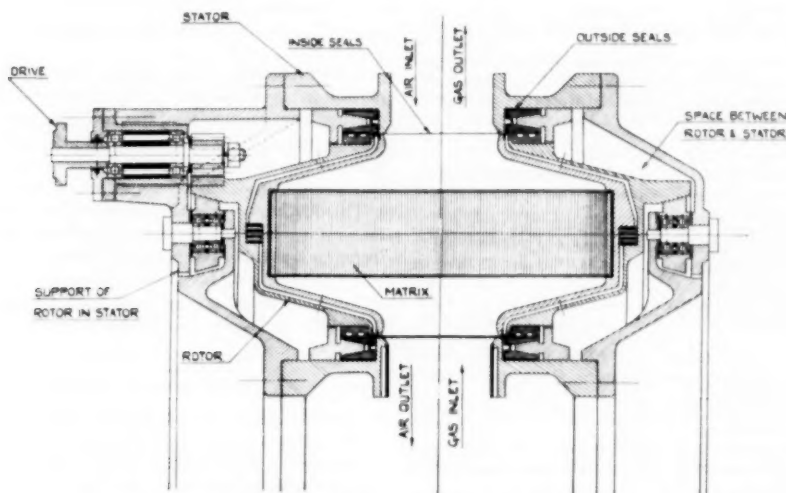


FIG. 9(c) RADIAL-FLOW DRUM REGENERATOR

but as far as can be seen, there is no "best" construction. The choice of design is very largely determined by the working together of the regenerator and the other components of the gas turbine, with due regard to the minimum possible effect on the power loss resulting from the regenerator, and the maximum possible recovery of exhaust heat.

With a single-drum rotor the space at its center can be used for other parts of the gas turbine such as the diffusers mentioned, or even other components such as the turbine and the combustors. If such use can be made, a further advantage of the drum is the fact that it allows for a layout of the gas turbine where the components acted on by the high-velocity gases can be located in the middle (small areas) of the gas turbine, and those acted on by the low-velocity gases can be arranged around the circumference (large areas).

The possibility of connecting the air preheater with the other components of the gas turbine through short and efficient ducts also has its bearing on the design. The outlets from the turbomachines have either an annular shape or are in any case arranged in the form of a uniformly interrupted annulus. In view of what has been said about the pressure losses, the tendency will be to use some kind of annular combustor so as to reduce its pressure loss as far as possible. Regenerators with a single rotor are rather difficult to connect with these annular inlets and outlets. This problem is solved more easily with a large number of air and gas sides. Such an increase means extending the length of the inside seals, but on the other hand, a more equal distribution of pressure and temperature over the rotor and stator is possible, resulting in less distortion and hence a more effective seal. Another advantage is the reduced speed.

In connection with the points raised in the preceding paragraph, it may be advisable to build up the air preheater from several small and separate elements, say, with a single-disk rotor. This arrangement would have the following advantages:

(a) The effective gap caused by the rubbing surfaces would be reduced because of the smaller dimensions, always assuming that the reduction in the effective gap would be greater than the increased length of the outside seals.

(b) It would be easier to manufacture smaller seals so as to achieve the necessary tightness. Production methods such as sintering, and the like, can be used.

(c) The preheater would be cheaper as the small elements could be mass-produced.

(d) There could be more latitude in the location of the preheater (elements) at the best place.

(e) This arrangement would give greater independence as regards the design of the other components of the gas turbine.

(f) Any practical efficiency for nearly any size of gas turbine can be achieved by selecting the number of elements to suit.

CONCLUSIONS

The advantages of the regenerative-type heat exchanger are that small hydraulic diameters can be attained readily, and that when the normal counterflow arrangement is used the matrix is self-cleaning to some extent, particularly during that part of the operating cycle when high velocities and pressure differences are experienced. Against this must be considered the problem of providing an efficient seal between the air and gas flows.

In comparison, if flame-trap matrices are employed in both, the recuperator can be designed to have hydraulic diameters of the same order as those in the regenerator (10). The matrix, however, is not self-cleaning, and thus continuous outside provision must be made to keep it in working order. This necessarily involves an equivalent power loss, but one which can justifiably be compared with the auxiliary power losses of the regenerator, Fig. 1. The separation of the gas and air flows, however, must be made in the matrix itself, which complicates the problem of cheap and simple manufacture.

The interrelation of these advantages and disadvantages, especially that concerning the problem of sealing the regenerator and the effective cost of its solution, will be the main criterion in the assessment of the relative merits of the two types of heat exchangers.

BIBLIOGRAPHY

- 1 "Development of the Ljungström Steam Turbine and Air Preheater," by F. Ljungström, *Proceedings of The Institution of Mechanical Engineers*, vol. 160, 1949, pp. 211-223.
- 2 "Heat Transfer and Fluid Resistance in Ljungström Regenerative-Type Air Preheaters," by H. Karlson and S. Holm, *Trans. ASME*, vol. 56, 1934, pp. 61-72.
- 3 "The Regenerative Heat Exchanger for Gas Turbine Power Plant," by M. Cox and R. K. P. Stevens, *Proceedings of The Institution of Mechanical Engineers*, vol. 163, 1950, pp. 193-205.
- 4 "The Prospects of Land and Marine Gas Turbines," by H. Con-

stant, Proceedings of The Institution of Mechanical Engineers, vol. 159, 1948, pp. 191-197.

3 "Materials and Performance—Symposium on High Temperature Steels and Alloys for Gas Turbines," by A. T. Bowden and W. Hrynyszak, The Iron and Steel Institute Special Report No. 43, 1951.

4 "Heat Transfer and Pressure Drop Characteristics of Four Regenerative Heat Exchanger Matrices," by A. Ambrosio, C. D. Coulbert, and F. E. Romie, ASME Paper No. 51-SA-34.

"Heat Transfer in Regenerator," by A. O. Saunders and S. Smolenskie, The Institution of Mechanical Engineers, General Discussion of Heat Transfer, 1931, Sect. 5.

"Heat Transfer and Pressure Drop in Heat Exchangers With Laminar Flow," by H. Glaser, M.A.P. Volkenrode, M.A.P.-VG 96, 1947.

5 "Heat Transfer in Regenerators," by H. Glaser, *Zeitschrift VDI*, vol. 4, 1938, pp. 112-115.

6 "On Influence of Heat Conduction in Flow Direction on Efficiency of Heat Exchangers," by P. Hentrich, M.A.P. Volkenrode, M.A.P.-VG 195, 1947.

"Regenerators With Longitudinal Heat Conduction," by B. H. Schulz, The Institution of Mechanical Engineers, General Discussion on Heat Transfer, 1951, Sect. 5.

7 "On the Theory of Heat Exchange in Regenerators," by H. Hausen, *ZAMM*, vol. 9, 1929, pp. 173-300.

"Thermal Analysis of the Contra-Flow Regenerative Heat Exchanger," by C. E. Hiffe, Proceedings of The Institution of Mechanical Engineers, vol. 159, 1948, pp. 363-372.

"Wärmeübertragung in Gegenstrom, Gleichstrom und Kreuzstrom," by H. Hausen, Julius Springer, Berlin, Germany, 1950.

8 "Calculation of Perfected Heat Exchange in Regenerators," by H. Hausen, *VDI, Verfahrenstechnik*, 1952, no. 2.

"A Simple Theory of the Heat Regenerator," by W. Tipler, Shell Petroleum Company, Ltd., Technical Report No. ICT/14.

9 "The Turbo-Regenerator As Applied to Gas Turbines," by W. Hrynyszak, The Institution of Mechanical Engineers, General Discussion on Heat Transfer, 1951, Sect. 5.

10 "Gas-Turbine-Plant Heat Exchangers," by W. M. Kays, A. E. London, and D. W. Johnson, ASME Research Report, 1951.

Discussion

DAVID ARONSON.³ The authors have given a well-stated comparison between the two types of heat exchangers, the heat-conduction, continuous-flow type, and the heat-accumulating periodic-flow type. It might be well if we could come to some agreement in this country as to the best names to apply to these two types so that the confusion now prevalent would be ended.

The development of the concepts of internal and external efficiencies is extremely helpful in cycle analysis. These are all referred to a possible 100 per cent efficiency, and are directly applicable to cycle heat and power balances.

Some of the terms appear somewhat unfamiliar to the writer. The term "resistance factor" defined as

$$\frac{\text{Area of flow} \times \text{static pressure loss}}{\text{Wetted surface} \times \text{dynamic pressure}}$$

is evidently what we call "friction factor," f .

The authors state: "A high-temperature efficiency can only be achieved by a high resistance in the matrix because of the relation between this resistance and the heat transfer." High resistance is assumed to mean high heat-transfer factor, which we designate by j , the Colburn factor.

Equation [9] of the paper considers an "ideal degree of conversion"

$$\frac{\eta_{h,ideal}}{2} = \frac{Nu}{C_{R,S} Pr Re} = \frac{j (Pr)^{-1/2}}{C_{R,S}}$$

³ Consulting Engineer, Worthington Corporation, Harrison, N. J. Mem. ASME.

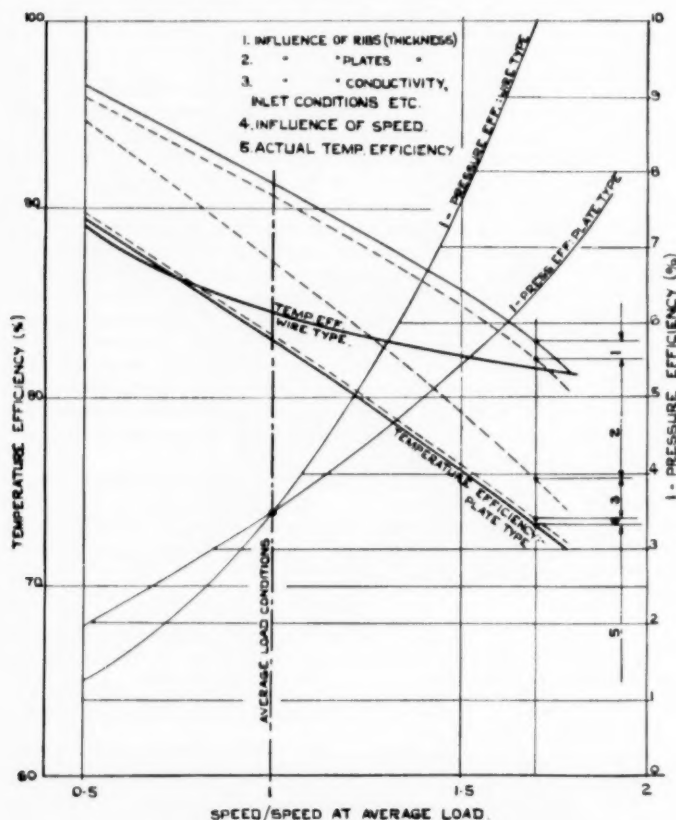


FIG. 10 CHANGE OF TEMPERATURE AND PRESSURE EFFICIENCY FOR WIRE END-PLATE-TYPE MATRIX

If this ratio is based on the Reynolds number calculated from the mass-flow rate at the entrance to the matrix, then it serves as a criterion of the geometry of the regenerator for a given service. A high value of this degree of conversion means a smaller frontal area than does a low value. On the other hand, a high value generally will be associated with a longer flow path so that the volume of actual matrix might be larger for a high value of this degree of conversion.

The statement is made: "the part-load behavior of the wire matrix is different from that of the plate matrix. The increase in temperature efficiency is faster with the latter than with the former." The writer believes this is applicable if the flow is in the laminar region. The distinction is in the opposite direction in the turbulent region. Since there is a good possibility that operation will be in the intermediate region, any generalization is likely to have exceptions to the rule.

AUTHORS' CLOSURE

Mr. Aronson is right in his interpretation of what we term the "resistance factor" and which is also called "friction factor."

The definition Mr. Aronson gives for the "ideal degree of conversion" is correct. Instead of the Colburn factor, the Stanton number could have been introduced as well. Unfortunately, all these factors and numbers, useful as they are for heat-transfer calculations, are not yet generally known and appreciated, so that we kept to the more conventional terms like Nusselt number, Reynolds number, and Prandtl number, bearing in mind that we were compelled to introduce several terms such, for instance, as "degree of conversion," etc.

As Mr. Aronson points out, a high degree of conversion results in a small frontal area, but also makes for a large height of matrix for a given hydraulic diameter, and vice versa. However, it should be pointed out that the frontal area is usually by far the biggest problem in the design of regenerative air preheaters of high

temperature, pressure, and mass-flow efficiencies. The height can be reduced—in certain limits of course—by reducing the hydraulic diameter of the matrix.

Because of these small hydraulic diameters, mentioned in our paper, the flow in the matrix is characterized by Reynolds numbers of between roughly 50 and 250 under full-load conditions. This means that flow in plate-type matrices is always laminar, apart from the influence of inlet conditions, which admittedly may have an appreciable effect on the flow characteristics. However, this effect has not yet been properly elucidated. Flow in the wire matrices has the characteristics of a mixed viscous and turbulent flow, which can be fairly well assessed by an extended Stokes law. Our statements as to the behavior of these two types of matrix referred only to the comparison between the *laminar-flow* plate matrix and the wire matrix in the range of small Reynolds numbers mentioned.

To illustrate this, Fig. 10 shows the change of temperature and pressure efficiencies of a plate-type and a wire-type matrix. The regenerator concerned has, for both types, the same over-all area, that is to say, the initial area of matrix plus the additional areas needed for ribs, walls, etc. The change of pressure and temperature efficiencies is plotted against the speed of the gas turbine concerned, referred to the speed at its average load. As the gas turbine is of the vehicle type, a very small average load was considered as the most suitable layout load. The diagram also shows, for the plate matrix, the influence of the reduction in area due to the thickness of the ribs and plates, as well as the influence of conduction in these plates, the flow conditions at their inlets and outlets, and the influence of rotor speed. The temperature efficiency of the wire matrix is about the same as that of the plate matrix at average load, but the temperature efficiency of the wire matrix changes less than that of the plate matrix when the load is changed.

The Periodic-Flow Regenerator—A Summary of Design Theory

By J. E. COPPAGE¹ AND A. L. LONDON,² STANFORD, CALIF.

A description is given of the periodic-flow rotary regenerator, and it is contrasted to the other types of heat-exchanger systems which may be employed to "regenerate" or "recuperate" the exhaust-gas thermal energy in a gas-turbine plant. The advantages in principle of the periodic-flow type are considered briefly, and the mathematical complexities of analysis of the more exact theory of its performance are indicated. Available special solutions, obtained by numerical-graphical methods, provided by Hausen, Nusselt, Boestad, Iliffe, and Saunders and Smoleniec are reviewed and their limitations pointed out. An algebraic equation solution corresponding to the special case of high rotative speeds is shown to be exactly the same as the well-known equation for a direct-transfer-type counterflow exchanger. These results are supplemented with an "approximate theory" solution which has the advantage of being in closed form, and the limitations on accuracy of this solution are considered. Recommended design curves are presented using a set of simple nondimensional parameters, of the same nature as those employed for direct-transfer-type exchangers, and which are readily usable for the gas-turbine regenerator-design problem. The curves result from a rational extrapolation of the special case solutions of Hausen, employing the approximate theory as well as the results of Iliffe, to other situations of interest to the gas-turbine designer. An illustrative problem is included.

NOMENCLATURE

The following nomenclature is used in the paper:

- A = with subscript c or h denotes cold- or hot-fluid-side heat-transfer area, sq ft
- A_f = flow cross section area at section x , sq ft
- B = factor used in Equation [12] and defined there, deg F hr/Btu
- c = specific heat capacity—of fluid with subscript c or h , of rotor with subscript r , Btu/lb deg F
- C = capacity rate, Wc —of fluid with subscripts c or h , of rotor solid phase with subscript r , Btu/hr deg F
- h = unit conductance for thermal convection, Btu/(hr sq ft deg F)
- L = flow length of matrix, ft
- M_r = mass of matrix, lb
- q = heat-transfer rate, Btu/hr
- t = temperature—of fluid with subscript c or h , of rotor with subscript r , deg F
- U = over-all unit conductance for a direct-type exchanger surface, Btu/(hr sq ft deg F)

¹ Graduate Student, Stanford University. Jun. ASME.

² Professor of Mechanical Engineering, Stanford University. Mem. ASME.

Contributed by the Gas Turbine Power Division and presented at the Annual Meeting, New York, N. Y., November 30–December 5, 1952, of THE AMERICAN SOCIETY OF MECHANICAL ENGINEERS.

NOTE: Statements and opinions advanced in papers are to be understood as individual expressions of their authors and not those of the Society. Manuscript received at ASME Headquarters, September 9, 1952. Paper No. 52-A-93.

- W = flow rate—of fluid with subscript c or h , of rotor solid phase with subscript r (rev per hr \times rotor mass), lb/hr
- x = location of matrix section measured from hot flow inlet face, ft
- ϵ = regenerator effectiveness, actual heat-transfer rate to thermodynamically limited maximum possible transfer, Equation [6a], nondimensional
- ρ = density of fluid, either hot or cold as specified by subscript, h or c , lb/ft³
- θ = time, hr
- θ_c, θ_h = duration of matrix element in cold and hot flow stream, respectively, hr
- ϕ = denotes functional relationship

Nondimensional Parameters:

- ϵ = regenerator effectiveness, see foregoing ($\epsilon_{rc}, \epsilon_{rh}$ defined under Equation [12]).
- $NTU_c = \left(\frac{hA}{C} \right)_c$ cold-side number of heat-transfer units
- NTU_o = over-all number of heat-transfer units, defined by Equation [7a]
- C_c/C_h = capacity rate ratio of flow streams
- C_r/C_c = capacity-rate ratio rotor matrix to cold stream
- $(hA)^* = (hA)_c/(hA)_h$ symmetry factor relating to thermal resistance (or conductance) "balance" of regenerator design

INTRODUCTION

The simple gas-turbine plant, consisting only of compressor, combustion chamber, and turbine components, has the advantages of light weight and compactness. However, it suffers from a poor specific fuel consumption relative to the modern steam-power and reciprocating internal-combustion-engine systems. Cycle modifications which can compensate for this deficiency are (a) intercooling during compression, (b) reheating during turbine expansion, (c) exhaust-gas thermal-energy regeneration, and (d) combinations of the foregoing. The greatest improvement is brought about by regeneration, especially when it is employed in conjunction with intercooling. Moreover, the addition of a regenerator results in a flat fuel economy versus load characteristic, which is highly desirable for the transportation-type prime mover—the gas-turbine locomotive, the marine gas-turbine plant, or the aircraft turboprop.

Although the addition of a regenerator is highly attractive from a thermodynamic point of view, its bulk, shape, mass, or cost may be such as to nullify the thermodynamic advantages. Optimum design therefore will call for a careful consideration of different types of regenerators. The three types of heat-exchanger systems which have been proposed for this service are described schematically in Fig. 1. These are (a) the direct-transfer type, (b) the liquid-coupled indirect-transfer type, and (c) the periodic-flow type.

The theory of the direct-transfer type is conventional and is covered in reference (1).³ The liquid-coupled indirect-transfer

³ Numbers in parentheses refer to the Bibliography at the end of the paper.

system, Fig. 1(b), is considered in references (2) and (3). While the theory in this case is more complex than for the direct-transfer type, nevertheless it is quite straightforward and complete solutions are available. In contrast, the theory of the periodic-flow-type regenerator is much more difficult and only a limited number of solutions are available from several different sources. Moreover, these solutions were obtained principally by approximate numerical methods. Since this type of exchanger possesses several very important advantages over the other types, it is of importance to the gas-turbine designer that these solutions be collected and evaluated. It is the purpose of this paper to present such a summary, to make specific recommendations for design based on available solutions, and to indicate the area where additional solutions are needed.

DESCRIPTION OF THE PERIODIC-FLOW TYPE

The periodic-flow type and the liquid-coupled indirect-transfer type, Figs. 1(b and c), are similar in some measure. The rotating matrix provides a "flow" of solid-phase metal, from the hot gas to the compressed-air stream, for the purpose of transporting the otherwise wasted thermal energy from the turbine exhaust to the compressed air prior to combustion.

In this manner, the fuel requirement in the combustion chamber is reduced and the plant specific fuel consumption improved. Thus thermodynamically the exhaust-gas thermal energy is in part recuperated or regenerated, and this same thermodynamic function is served regardless of the type of heat-exchanger system used. For this reason, in spite of fairly common terminology to the contrary, the terms recuperator and regenerator will not be restricted to the direct-transfer type and the periodic-flow type, respectively, but rather the term regenerator will be used in its thermodynamic sense for all three types of heat-exchanger systems described in Fig. 1.

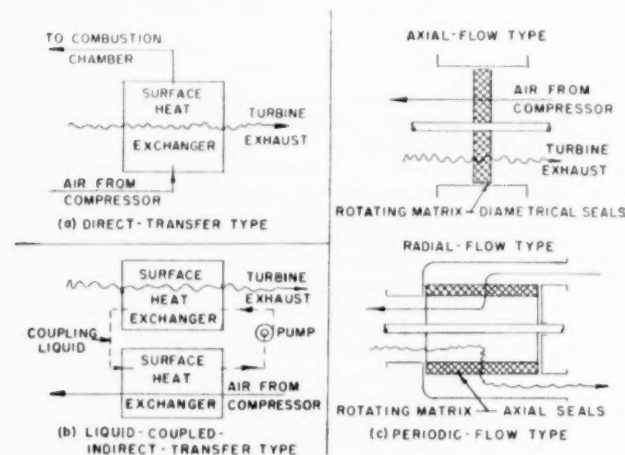


FIG. 1 TYPES OF GAS-TURBINE REGENERATORS

The qualification "periodic-flow" type was selected since each part of the matrix, because of its continuous rotation, is exposed to a regular periodic flow of hot and cold gas streams.

The principal advantages of the periodic-flow type relative to the others described in Fig. 1 are as follows:

- 1 A matrix-type surface provides on the order of 700 to 2000 sq ft of transfer area per cubic foot of matrix volume (20-mesh to 50-mesh stacked screens) as compared to a maximum of 400 to 600 sq ft per cu ft of cold-side plus hot-side area obtainable from

the most compact extended surfaces usable in the direct-transfer-type system.⁴ This advantage allows higher regenerator effectiveness for the same weight and space limitations.

- 2 The matrix-type surface is relatively inexpensive and can be fabricated readily out of high-temperature materials (including ceramics).

- 3 The periodic reversal of flow prevents any permanent flow-stagnation regions in the matrix, and as a consequence a continuous self-cleaning action is afforded. This behavior has been demonstrated convincingly in long service experience with Ljungström air preheaters, employed extensively in central-station boilers with the dirtiest of fuels.

In contrast, there are several major disadvantages of the periodic-flow type which should be frankly recognized. These are as follows:

- 1 Seals suitable for pressure differentials of 4 to 7 atm (between the compressed air and low-pressure-turbine exhaust) represent a major developmental problem.

- 2 Many changes of flow direction are required, as compared to the liquid-coupled indirect-transfer system, Fig. 1(b), resulting not only in flow losses, but also expensive ducting.

- 3 Restrictions in pressure drop make necessary a large flow area with the usual matrix surface. As a consequence, the advantage of small matrix volume is somewhat nullified by the requirement of bulky approach ducting, see Fig. 1(c).

The constant parameters relating to the heat-transfer performance of the periodic-flow regenerator are as follows:

h_c, h_h = convective conductances, for cold and hot sides, respectively

A_c, A_h = matrix-transfer areas, cold and hot side, respectively, at any instant

C_c, C_h = flow-stream capacity rates (Wc_p); for cold and hot gas flows, respectively

C_r = capacity rate of rotor ($W_r c_r$)

$t_{h(in)}, t_{h(out, avg)}$ = hot-fluid terminal temperatures

$t_{c(in)}, t_{c(out, avg)}$ = cold-fluid terminal temperatures

Here are 11 parameters. In the direct-type exchanger only eight parameters are involved since C_r does not exist, and the A 's and h 's reduce to a single over-all conductance-area product. Investigation shows that five nondimensional parameters are the minimum requirement for complete expression for the periodic-flow-type-exchanger performance, as contrasted to only three for the direct type, reference (1).

PERIODIC-FLOW REGENERATOR THEORY

The differential equations for the heat-transfer behavior of a flow tube in the matrix, Fig. 2, will now be presented together with the associated idealizations:

- 1 The thermal conductivity of the matrix is zero in the gas and air-flow directions, and infinite in the normal direction to the flow.
- 2 The specific heats of the two fluids and the matrix material are constant with temperature.
- 3 No mixing of the fluids occurs during the switch from hot to cold flows.
- 4 The convective conductances between the fluids and the matrix are constant with flow length, x .
- 5 The fluids pass in counterflow directions.
- 6 Entering-fluid temperatures are uniform over the flow cross section and constant with time.

⁴ Reference 1, Table 6.

7 Regular periodic conditions are established for all matrix elements.

The first of these idealizations is shown by Hausen (4) to be satisfied for most cases of practical importance. Rough estimates show that for a reversal time of $1/4$ sec (two complete cps) which is near the maximum permissible frequency without undue "carry-over loss," the effect on the exchanger effectiveness of finite thermal conductivity normal to the flow, is less than 0.5 per cent for steel walls up to 0.2 in. thick, and for ceramic walls up to 0.05 in. thick. Iliffe (5) summarizes additional work on this matter. Thermal conduction in the direction of flow may be prevented almost entirely, but even continuous matrices of reasonable wall thickness have negligible longitudinal heat transfer (5).

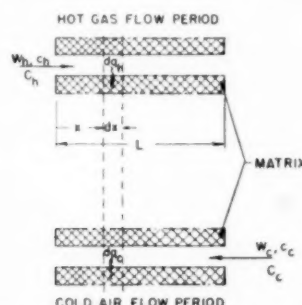


FIG. 2 ELEMENTAL FLOW PASSAGE AND ASSOCIATED FLOW MATRIX (For Equations [1] and [2].)

Saunders and Smolenec (6) investigated the second idealization for a typical case and found that the variation in fluid and matrix specific heats resulted in less than a 1 per cent error in the effectiveness. The idealization of no flow mixing is closely met when the flow-passage length is short, and such shortness of length appears to be good design procedure for the most suitable types of surfaces.

The fourth, fifth, and sixth idealizations parallel those usually made in conventional heat-exchanger-design theory. The seventh idealization of regular periodicity corresponds to the usual assumption of steady-state flow conditions.

On the basis of these idealizations the following differential equations and boundary conditions may be expressed. For the hot-gas flow, energy balances on the element dx , Fig. 2, yield

$$\frac{dq_h}{dx} = \frac{M_r c_r}{L} \frac{\partial t_r}{\partial \theta} \quad [1]$$

$$\frac{dq_h}{dx} = - \left(W_h c_h \frac{\partial t_h}{\partial x} + \rho_h A_f c_h \frac{\partial t_h}{\partial \theta} \right) \quad [2]$$

The convective-heat-transfer-rate equation is

$$dq_h = h_h \frac{A_h}{L} (t_h - t_r) dx \quad [3]$$

Elimination of dq_h yields the two equations

$$\left. \begin{aligned} W_h c_h \frac{\partial t_h}{\partial x} + \rho_h A_f c_h \frac{\partial t_h}{\partial \theta} &= - \frac{M_r c_r}{L} \frac{\partial t_r}{\partial \theta} \\ &= - \frac{h_h A_h}{L} (t_h - t_r) \end{aligned} \right\} \dots [4a]$$

For the cold-gas flow a similar pair of equations results

$$\left. \begin{aligned} W_c c_c \frac{\partial t_c}{\partial x} + \rho_c A_f c_c \frac{\partial t_c}{\partial \theta} &= \frac{M_r c_r}{L} \frac{\partial t_r}{\partial \theta} \\ &= \frac{h_c A_c}{L} (t_c - t_r) \end{aligned} \right\} \dots [4b]$$

The boundary conditions are as follows

$$\left. \begin{aligned} \text{For interval of hot flow} \\ t_{h(in)} &= \text{const at } x = 0 \\ \text{For interval of cold flow} \\ t_{c(in)} &= \text{const at } x = L \end{aligned} \right\} \dots [5]$$

In cycle studies as well as in design work, the over-all heat-transfer performance of the regenerator is most conveniently expressed as the heat-transfer "effectiveness" ϵ which compares the actual heat-transfer rate to the thermodynamically limited maximum possible heat-transfer rate (1). This definition (for $C_c < C_h$ as is the case for the regenerator) results in

$$\epsilon = \frac{1}{\theta_c} \int_0^{\theta_c} \left(\frac{t_c - t_{c(in)}}{t_{h(in)} - t_{c(in)}} \right) d\theta \quad [6a]$$

where θ_c is the cold-fluid time interval. Alternatively, Equation [6a] becomes

$$\epsilon = \frac{t_{c(out, avg)} - t_{c(in)}}{t_{h(in)} - t_{c(in)}} \quad [6b]$$

where $t_{c(out, avg)}$ is a bulk average temperature of the cold air stream after passage through the regenerator.

The immediate problem is to obtain solutions of Equations [4a] and [4b] in agreement with the boundary conditions, Equations [5], and then express the result as the regenerator effectiveness, ϵ , in terms of certain nondimensional parameters suitable for design work. After a consideration of the various possibilities in this respect the following nondimensional parameters were selected

$$\epsilon = \phi \left[\frac{C_c}{C_h}, \frac{C_r}{C_c}, (hA)^*, NTU_o \right] \quad [7]$$

with NTU_o defined by

$$NTU_o = NTU_c \left[\frac{1}{1 + (hA)^*} \right] \quad [7a]$$

Effectively ϵ is a function of four nondimensional parameters with either NTU_o or, alternatively, NTU_c as the last one in Equation [7]. Because of the parallels that can be drawn with the direct-type regenerator, however, NTU_o is preferred in this presentation. Reference to the nomenclature will demonstrate the readily grasped physical significance of these groupings. To provide a sense of magnitudes for these parameters, the following tabulation was prepared to indicate extreme ranges of values to be expected in gas-turbine-design work:

$$\begin{aligned} \epsilon &= 50 \text{ to } 90 \text{ per cent} \\ C_c/C_h &= 0.90 \text{ to } 1.00 \\ C_r/C_c &= 1 \text{ to } 10 \\ (hA)^* &= (hA)_c/(hA)_h = 0.2 \text{ to } 1 \\ NTU_c &= 2 \text{ to } 20 (\sim \text{twice } NTU_o) \\ NTU_o &= 1 \text{ to } 10 \end{aligned}$$

There is no complete analytical solution available for Equations [4] and the boundary conditions [5]. The particular solutions contained in the literature, with one exception, are obtained by approximate graphical-analytical methods. The one rigorous analytical solution available is for the special case of $C_r/C_c = \infty$.

Then the behavior becomes identical in form to that of a counterflow direct-type exchanger (1) and is given by

$$\epsilon = \frac{1 - e^{-NTU_o(1 - C_r/C_h)}}{1 - \frac{C_r}{C_h} e^{-NTU_o(1 - C_r/C_h)}} \quad [8]$$

where it can be shown from the definition of NTU_o , Equation [7a], that

$$NTU_o = \frac{1}{C_c} \left[\frac{1}{(hA)_c} + \frac{1}{(hA)_h} \right] \quad [9]$$

This last expression for NTU parallels that for the direct type of exchanger

$$NTU = \frac{AU}{C_c}$$

where, for this case, for negligible wall thermal resistance

$$\frac{1}{AU} = \left[\frac{1}{(hA)_c} + \frac{1}{(hA)_h} \right]$$

Thus, in this limiting case, the periodic-flow-type regenerator would have the same performance as a counterflow direct-type unit possessing the same hot-side and cold-side transfer areas and the same convection coefficients, providing only that the thermal resistance offered by the wall structure was negligible, as is the usual case. Another point of interest is the particularly simple form assumed by Equation [8] for the case of $C_r/C_h = \text{unity}$

$$\epsilon = \frac{NTU_o}{1 + NTU_o} \quad [8a]$$

which, of course, is again of the same form as the solution for a counterflow direct-type exchanger (1).

Equation [8] is graphed, Figs. 4 and 5, for the special cases of $C_h/C_c = 1.00$ and 0.90 , of interest in gas-turbine-regenerator design. Note from Fig. 4 that the solution for $C_r/C_c = 10$, to be considered later, is quite close to the limiting solution of $C_r/C_c = \infty$, which demonstrates that Equation [8] is useful for design purposes for large magnitudes of C_r/C_c .

The several special solutions obtained by numerical methods will now be presented.

Hausen's Analysis. Hausen (4) obtained solutions for the

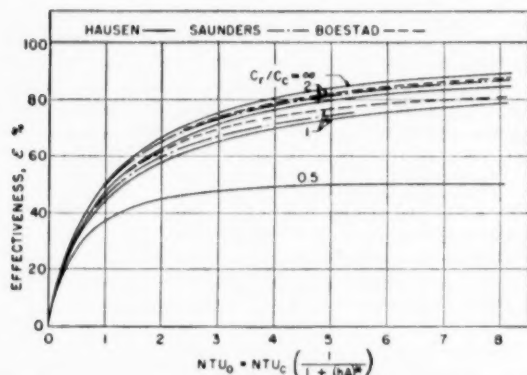


FIG. 3 COMPARISON OF SOLUTIONS ϵ VERSUS NTU_o FOR $C_h/C_c = 1$, $(hA)^* = 1$
(Hausen reference 4, Saunders and Smolenice reference 6, Boestad reference 8.
 $C_r/C_c = \infty$ curve is same as for direct-type counterflow exchanger.)

special case of $C_r/C_h = \text{unity}$ and $(hA)^* = \text{unity}$. He employed two methods. The first was based on the characteristic solution of Equation [4] and involved the evaluation of a large number of integrals. The second method, known as the "heat-pole" method, was founded on the solution of Equation [4] for the case where the initial temperature of a matrix tube at the start of the cold cycle, Fig. 2, is uniformly at $t_{h(0)}$. The final solution was

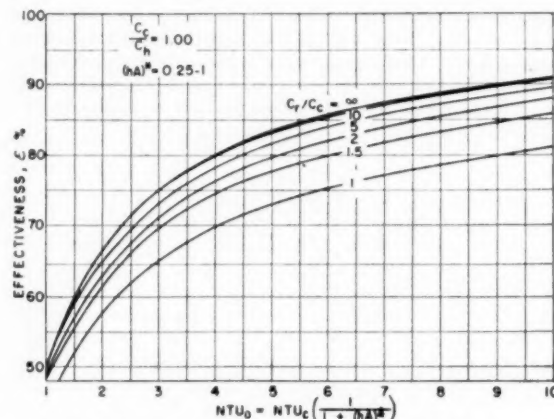


FIG. 4 DESIGN CURVES ϵ VERSUS NTU_o FOR $C_h/C_c = 1$
(See Table 1.)

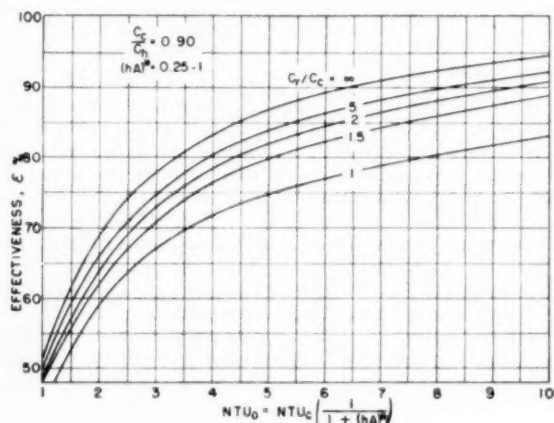


FIG. 5 DESIGN CURVES ϵ VERSUS NTU_o FOR $C_h/C_c = 0.90$
(See Table 2.)

built up from this special case by a graphical and analytical procedure. These methods are described more completely by Iliffe (5). Results were computed for magnitudes of C_r/C_c ranging from about 0.2 to ∞ . However, only the curves for $C_r/C_c \geq \text{unity}$ are of interest in the regenerator application. Hausen's results for $C_r/C_c = 0.5, 1, 2$, and ∞ are presented graphically in Fig. 3.

Nusselt's Analysis. Nusselt (7), starting with the same differential equations as Hausen, also obtained a symbolic solution for the special case of $(hA)^* = \text{unity}$ and $C_h/C_c = \text{unity}$. Apparently computations from his equation are sufficiently laborious so that no performance curves have been presented.

Iliffe's Analysis. Iliffe, starting with Nusselt's result succeeded in reducing the complexity of the calculations. Moreover, he extended the solution so it was not limited to $(hA)^* = \text{unity}$ and he calculated performance curves for $(hA)^*$ of 1, 0.5,

and 0.333, with the remaining limitation still of $C_c/C_h = \text{unity}$. These results will be employed later in arriving at the recommended design curves in Figs. 4 and 5.

Analysis of Saunders and Smoleniec (6). These authors employed a numerical relaxation technique in the solution of the differential equations and obtained performance curves for a range of C_r/C_c but still limited to both C_c/C_h and $(hA)^* = \text{unity}$. The performance curves for $C_r/C_c = 1$ and 2, and ∞ are plotted, Fig. 3, for comparison with the similar results of Hausen. It is to be noted that Hausen's results for $C_r/C_c = 1$ and 2 are about 2 points lower on ϵ than the corresponding Saunders and Smoleniec results.

Boestad's Analysis (8). The original article was not available at the time of writing this paper, but from reference (9) the results of Boestad's analysis were obtained. This solution is semi-empirical, based on a number of approximations. For the case of $C_c/C_h = \text{unity}$

$$\epsilon = \epsilon_{(C_r = \infty)} - \Delta\epsilon \dots \dots \dots [10]$$

where $\epsilon_{(C_r = \infty)}$ is the effectiveness for $C_r/C_c = \infty$, obtained from Equation [8a] and the correction factor

$$\Delta\epsilon = \frac{1}{10} (\epsilon_{(C_r = \infty)})^2 \left(\frac{C_c}{C_r} \right)^2 \dots \dots \dots [11]$$

is to adjust for the finite rotational speed of the matrix.

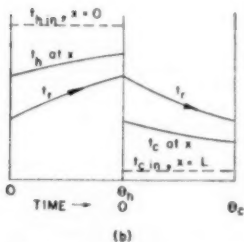
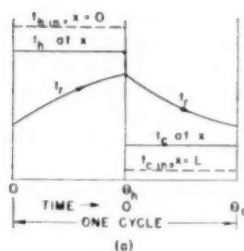


FIG. 6 TEMPERATURE CONDITIONS AT A CROSS SECTION
(a) For approximate theory.
(b) For actual situation.)

Each fluid phase is completely mixed at any cross section so that one temperature characterizes the state of the hot fluid and one temperature characterizes the state of the cold fluid at the section in question for all times.

This specification results in the type of temperature distribution described in Fig. 6(a). Obviously, such conditions are exactly correct only at the hot-gas inlet section, $x = 0$, for time 0 to θ_h and at the cold-gas inlet section, $x = L$, for time 0 to θ_c , where the time intervals are as shown. At all other sections, and even for the cold flow at section $x = 0$ and the hot flow at section $x = L$, one would anticipate the behavior described qualitatively in Fig. 6(b). Nevertheless, for higher rotational speeds, i.e., C_r/C_c large, the

idealization of uniformity of t_h and t_c becomes more correct and in the limit for $C_r = \infty$ it is exact.

The results of the approximate analysis may be expressed (for $C_c < C_h$)

$$\epsilon = \frac{1 - e^{-BC_r}}{1 - \frac{C_c}{C_h} e^{-BC_r}} \dots \dots \dots [12]$$

with

$$BC_r = \frac{C_r}{C_c} \left(1 - \frac{C_c}{C_h} \right) \left(\frac{1}{\epsilon_{xc}} + \frac{1}{\epsilon_{xh}} - 1 \right)$$

$$\epsilon_{xc} = 1 - e^{-\frac{NTU_c}{C_r/C_c} [1 + (hA)^*]}$$

$$\epsilon_{xh} = 1 - e^{-\frac{NTU_h}{C_r/C_c} [1 + (hA)^*]/(hA)^*}$$

Note that ϵ from Equation [12] is expressible in terms of the four nondimensional parameters

$$\left[\frac{C_c}{C_h}, \frac{C_r}{C_c}, NTU_c, (hA)^* \right]$$

specified in Equation [7]. It can be demonstrated for $C_r/C_c = \infty$ that the approximate Equation [12] is correct in this limiting case and reduces to Equation [8] (using L'Hospital's rule for indeterminate forms of equations). This is in accord with the view previously reached that the idealization of t_h and t_c functions of x only, Fig. 6(a), is exactly valid for $C_r = \infty$.

For the case of $C_c/C_h = \text{unity}$ (again using L'Hospital's rule), Equation [12] reduces to

$$\epsilon = \frac{1}{1 + \frac{C_r}{C_c} \left(\frac{1}{\epsilon_{xc}} + \frac{1}{\epsilon_{xh}} - 1 \right)} \dots \dots \dots [12a]$$

and with the additional restriction of $C_r/C_c = \infty$ it will, as it should, reduce to the previous Equation [8a].

It can be anticipated that Equation [12] will yield magnitudes of ϵ which are low. The reason for this is that the idealization on which Equation [12] is founded postulates complete mixing at a section, Fig. 6(a). This mixing is a thermodynamically irreversible process and, as such, invariably will result in a lower ϵ . This point can be demonstrated more forcibly by a further consideration of Equation [12a] for the limiting case of an infinite area matrix exchanger. Then $(hA)_h, (hA)_c = \infty$, $\epsilon_{xc}, \epsilon_{xh} = 1$, and Equation [12a] reduces to

$$\epsilon = \frac{1}{1 + \frac{C_r}{C_c}} \dots \dots \dots [12b]$$

Thus for all finite C_r/C_c ratios ϵ is less than unity for the infinite exchanger. In contradiction to this, however, the more correct theory demonstrates that for $C_r/C_c \geq 1$, ϵ should be identically unity.

This discrepancy imposes a limit on the usefulness of the approximate theory Equations [12] and [12a]. Nevertheless, for $C_r/C_c \geq 10$ and $\epsilon < 80$ per cent, Equation [12a] does provide good agreement with the more exact solutions. This results from the fact that in this region C_r/C_c has but a minor influence. As a consequence, the following important conclusion which will be of later use is suggested, namely:

The approximate theory, Equation [12], can be used to provide information on the relative effect of the C_c/C_h

ratio so that the firm design curves known for $C_c/C_h = 1$ can be extrapolated to $C_c/C_h < 1$ for which no adequate design curves are now available.

This conclusion is, admittedly, somewhat speculative and is presented here as an expedient to use until more exact solutions are available.

RECOMMENDATIONS FOR DESIGN

A review of the results of the available analyses suggests the following conclusions:

1 Firm design curves of ϵ versus NTU_o are available for the restrictive conditions $C_c/C_h = \text{unity}$ and $(hA)^* = \text{unity}$.

2 For the special case of $C_c/C_e = \infty$ a complete solution in closed form (same as for the direct-type counterflow exchanger) is available for any C_c/C_h and $(hA)^*$.

3 Iliffe's results can be employed to determine the influence of $(hA)^*$. The approximate theory also can be employed in this connection.

4 The approximate theory, in lieu of a better method, can be used to provide a reasonable basis for extrapolating the firm design curves of item 1 to conditions of $C_c/C_h < \text{unity}$.

This approach was used to arrive at the recommended design curves in Figs. 4 and 5. Note that the graphical representation is for ϵ a function of C_c/C_h , C_r/C_e , NTU_o —only three nondimensional parameters instead of four as suggested in Equation [7]. The reasons for this considerable simplification follow:

Influence of $(hA)^$.* Hausen, Saunders and Smoleniec, and Johnson (11) all recommend the application of the $(hA)^* = \text{unity}$ curves, for the case of $(hA)^*$ other than unity, by the expedient of using an average (hA) in the NTU_o expression of Equation [7a], namely

$$NTU_o = \frac{(hA)_{\text{avg}}}{C_c} \left(\frac{1}{1 + 1} \right) = \frac{(hA)_{\text{avg}}}{2C_c} \quad [13]$$

However, they differ in their recommendations as to the type of average to be employed. Hausen recommends a harmonic average

$$\frac{1}{(hA)_{\text{avg}}} = \frac{1}{2} \left[\frac{1}{(hA)_h} + \frac{1}{(hA)_c} \right] \quad [14]$$

Saunders and Johnson both recommend an arithmetic average

$$(hA)_{\text{avg}} = \frac{1}{2} [(hA)_h + (hA)_c]$$

Of course, for $(hA)^*$ close to unity both averages yield essentially the same result. But for an $(hA)^* = 0.25$, for instance, which may be an extreme case encountered in regenerator design, the Hausen average yields $(hA)_{\text{avg}}/(hA)_h = 0.400$, while the arithmetic average yields 0.625. The corresponding influence on the predicted area requirement, for a given effectiveness, would amount to 56 per cent.

The results of Iliffe for $(hA)^* = 0.500$ and 0.333 resolve this question in favor of the Hausen average. Moreover, calculations based on the approximate theory support this conclusion down to $(hA)^* = 0.250$, not only for $C_c/C_h = \text{unity}$ but also for $C_c/C_h < \text{unity}$. Also for the limiting case of $C_r/C_e = \infty$, the exact solution Equation [8] gives precisely this type of average.

As a conclusion to this consideration the Hausen average Equation [14] is recommended for substitution into Equation [13] to obtain NTU_o and thence ϵ from Figs. 3 and 4. This is the basis for the representation employing only three instead of the four nondimensional parameters specified in Equation [7].

Influence of C_c/C_h . In the usual gas-turbine regenerator $C_c/C_h \cong 0.96$, reference (12), Table 3. However, under special circumstances C_c/C_h may be reduced further below unity. For

this reason the design curves, Fig. 5, were prepared for $C_c/C_h = 0.90$. Thus by interpolation between this set and Fig. 4 the range $0.90 \leq C_c/C_h \leq 1$ can be covered.

Fig. 4 for $C_c/C_h = \text{unity}$ was obtained directly from Hausen's curves. These were used in place of Saunders' results because they are moderately more conservative (see Fig. 3) especially for values of C_r/C_e of the order of unity.

Fig. 5 was prepared by the following method: The approximate theory, Equations [12] and [12a], was used to get $\epsilon = \phi(NTU_o, C_r/C_e)$ for both $C_c/C_h = 1.00$ and 0.90. The ratio of these effectivenesses, at common magnitudes of $(NTU_o, C_r/C_e)$, was then applied, point by point, to the ϵ -curves in Fig. 4 (for $C_c/C_h = 1$) to obtain the curves for $C_c/C_h = 0.90$ in Fig. 5.

Illustrative Problem. The following numerical example is presented to demonstrate that in spite of the large number of variables involved in this type of problem, the curves in Figs. 4 and 5 provide the designer with a ready means either to specify the matrix-area requirement for a desired effectiveness, or alternatively to determine the ϵ to be anticipated from a given matrix core.

Suppose the following parameters are given for an open cycle, 9:1 pressure ratio plant (see cycle A, Table 3 of reference 12):

- Specific flow rate of compressor air, 38.6 lb/shp-hr plant rating.
- Flow streams capacity-rate ratio, $C_c/C_h = 0.97$.
- Matrix to compressed-air capacity-rate ratio, $C_r/C_e = 5.00$.
- Specific heat of compressed air, $c_p = 0.248$ Btu/(lb deg F).
- Convective-conductance ratio, $h_c/h_h = 1.25$.
- Cold side conductance, $h_e = 20$ Btu/(hr sq ft deg F).
- Matrix-area ratio $A_e/A_h = 0.500$ (e.g., 110-deg air-flow angle, 220-deg gas-flow angle, 30-deg angle for seals).
- Cold-side heat-transfer area at any instant, $A_e = 4.00$ sq ft/shp of plant rating.

On this basis the independent nondimensional parameters for Equation [7] become

$$C_c/C_h = 0.97, C_r/C_e = 5.00, (hA)^* = 0.625$$

Number of transfer units on cold side

$$\left(\frac{hA}{C} \right)_c = \frac{4 \times 20}{38.6 \times 0.248} = 8.36$$

The over-all number of transfer units from Equation [7a]

$$NTU_o = 8.36 \frac{1}{(1 + 0.625)} = 5.14$$

Then from Fig. 4, for $C_c/C_h = \text{unity}$, $\epsilon = 82.0$ per cent; and from Fig. 5, for $C_c/C_h = 0.90$, $\epsilon = 84.2$ per cent. A linear interpolation for $C_c/C_h = 0.97$ yields $\epsilon = 82.7$ per cent as the final result.

Neglect of the C_c/C_h effect means that the predicted ϵ would be low by 0.7 points in this example. This "conservatism" represents the performance of 5 to 6 per cent of the transfer area because of the asymptotic character of the ϵ - NTU_o relation. Or alternatively, for interpreting test results, a 5 to 6 per cent error would result in the calculated convection coefficient.

SUMMARY AND CONCLUSIONS

1 Previous solutions for the periodic flow regenerator are limited in scope and, moreover, some disagreement exists between the design curves proposed by different workers.

2 These previous solutions have been evaluated, an appropriate set of nondimensional parameters specified, and a supplementary approximate theory presented. This approximate

TABLE 1 PERIODIC-FLOW REGENERATOR PERFORMANCE
(For $C_c/C_h = 1$ —Fig. 4)

NTU _c	1	1.5	2	5	∞
0	0	0	0	0	0
1.0	0.445	0.477	0.488	0.498	0.500
1.5	0.520	0.556	0.571	0.589	0.600
2.0	0.579	0.616	0.630	0.650	0.667
2.5	0.618	0.662	0.674	0.694	0.714
3.0	0.650	0.696	0.710	0.730	0.750
3.5	0.676	0.723	0.740	0.759	0.778
4.0	0.698	0.744	0.762	0.781	0.800
4.5	0.715	0.762	0.781	0.800	0.818
5.0	0.729	0.776	0.796	0.816	0.833
5.5	0.741	0.788	0.809	0.828	0.846
6.0	0.752	0.800	0.820	0.839	0.857
6.5	0.761	0.808	0.830	0.848	0.868
7.0	0.771	0.817	0.838	0.857	0.875
7.5	0.779	0.825	0.846	0.864	0.883
8.0	0.786	0.832	0.854	0.871	0.889
8.5	0.793	0.839	0.860	0.877	0.895
9.0	0.800	0.845	0.867	0.883	0.900
9.5	0.805	0.851	0.873	0.889	0.905
10.0	0.810	0.857	0.879	0.895	0.910

theory has the advantage of providing a closed-form solution, although admittedly it is of limited direct applicability.

3 The approximate theory provides a reasonable basis for extrapolating the known solutions for $C_c/C_h = \text{unity}$ and $(hA)^* = \text{unity}$ to other conditions of interest in the regenerator-design problem.

4 Figs. 4 and 5 (and Tables 1 and 2) are the recommended design curves resulting from this study. An illustrative problem demonstrates their ready applicability.

5 Additional solutions, obtainable by analog-computer methods, are highly desirable to support and to extend Figs. 4 and 5, or possibly supplant them. In such calculations it would be desirable to obtain at least three and preferably four significant figures in the results.

ACKNOWLEDGMENTS

The Office of Naval Research, the USN Bureau of Ships, and the Bureau of Aeronautics are jointly sponsoring a heat-transfer research project at Stanford University on compact surfaces. This paper was prepared on this project as a preliminary to design studies of applications of some recently tested matrix surfaces (13).

The authors express their appreciation to the sponsoring agencies and also to the AEC for the fellowship support which made this investigation possible for the senior author.

BIBLIOGRAPHY

- "Gas Turbine Plant Heat Exchangers—Basic Heat Transfer and Flow Friction Design Data," by W. M. Kays, A. L. London, and D. W. Johnson, ASME Monograph, April, 1951.
- "The Liquid-Coupled Indirect-Transfer Regenerator for Gas-Turbine Plants," by A. L. London and W. M. Kays, Trans. ASME, vol. 73, 1951, pp. 529–542.
- "Liquid-Coupled Regenerators for Turboprops," by A. L. London and W. M. Kays, *Aeronautical Engineering Review*, October, 1952, p. 42.
- "On the Theory of Heat Exchange in Regenerators," by H. Hausen, ZAMM, vol. 9, 1929, pp. 193–200; and "Accomplished Calculations of Heat Exchange in Regenerators," by H. Hausen, VDI *Beihft Verfahrenstechnik*, No. 2, 1942, MAP Reports and Translations No. 312, November 1, 1946.
- "Thermal Analysis of the Contra-Flow Regenerative Heat Exchanger," by C. E. Iliffe, Proceedings of The Institution of Mechanical Engineers, vol. 159, 1948, p. 363.
- "Heat Transfer in Regenerators," by O. A. Saunders and S. Smolenski, IME-ASME General Discussion on Heat Transfer, London, England, September, 1951, Section 5, Sixth Paper, p. 443.
- "Der Beharrungszustand im Winderhitzer," by W. Nusselt, *Zeitschrift des Vereines deutscher Ingenieure*, vol. 72, 1928, p. 1052.
- "Die Wärmeübertragung im Ljungström Luftwärmer," by G. Boestad, *Feuerungstechnik*, Stockholm, Sweden, vol. 26, 1938, pp. 282–286.
- Personal communication by Sven Holm, Air Preheater Corp., Wellsville, N. Y.

TABLE 2 PERIODIC-FLOW REGENERATOR PERFORMANCE
(For $C_c/C_h = 0.90$ —Fig. 5)

NTU _c	1	1.5	2	5	∞
0	0	0	0	0	0
1.0	0.445	0.478	0.489	0.500	0.513
1.5	0.528	0.558	0.572	0.594	0.615
2.0	0.591	0.620	0.639	0.661	0.689
2.5	0.635	0.670	0.690	0.708	0.741
3.0	0.670	0.708	0.728	0.746	0.778
3.5	0.697	0.739	0.758	0.778	0.807
4.0	0.716	0.763	0.783	0.803	0.831
4.5	0.733	0.782	0.802	0.822	0.851
5.0	0.747	0.798	0.818	0.838	0.867
5.5	0.759	0.811	0.832	0.852	0.881
6.0	0.769	0.822	0.844	0.863	0.892
6.5	0.778	0.833	0.854	0.873	0.901
7.0	0.787	0.842	0.863	0.882	0.909
7.5	0.795	0.851	0.872	0.890	0.917
8.0	0.803	0.859	0.880	0.897	0.923
8.5	0.810	0.866	0.888	0.904	0.929
9.0	0.817	0.873	0.895	0.910	0.934
9.5	0.823	0.880	0.902	0.916	0.940
10.0	0.830	0.887	0.909	0.922	0.945

10 "The Counterflow Rotating Regenerator," by A. L. London, unpublished Lecture Notes, Stanford University.

11 "Regenerator Heat Exchangers for Gas Turbines," by J. E. Johnson, Royal Aircraft Establishment Report No. Aero, 2266, 1948.

12 "The Gas-Turbine Regenerator—the Use of Compact Heat-Transfer Surfaces," by A. L. London and W. M. Kays, Trans. ASME, vol. 72, 1950, pp. 611–621.

13 "The Heat Transfer and Flow Friction Characteristics of Porous Media," by J. E. Coppage, PhD thesis, Stanford University.

Discussion

G. M. DUBINERRE.⁵ Any small element of a rotary regenerator, under the usual assumptions, can be regarded as a cross-flow exchanger with a gas stream and a metal "stream." A simple method of calculating crossflow exchangers is given elsewhere,⁶ and this analysis can be extended, to the rotary regenerator. The large number of subdivisions, necessary for accuracy, can be handled by automatic computing equipment. This is a project which the writer proposes to carry out.

A preliminary study shows that the authors' wish for verification of existing data is well founded. For example, if we take the case $C_c = C_h = C_r = 1$, $h_c A_c = h_h A_h = 2$, so that $\text{NTU}_c = 2$ and $\text{NTU}_h = 1$, consider each heat-transfer surface as a unit, and assume that arithmetic-mean temperature differences are valid, then a simple arithmetic calculation gives $E = 0.500$. Of course this is too crude. If we subdivide each stream in half, a similar calculation gives $E = 0.474$. One third gives $E = 0.470$, and one fourth, $E = 0.468$. If these results are plotted, it will be seen that they approach a limiting value, $E = 0.465$. This is quite different from the value $E = 0.445$ shown in the authors' Table 1.

The writer has found that errors of this sort tend to arise when the procedure is to carry calculus as far as it will go, then resorting to a numerical procedure. If the numerical procedure is applied directly to the physical problem, there is less chance of propagating errors of computation and of curve-plotting.

Some additional references are furnished herewith.^{7,8}

D. B. HARPER.⁹ The relationship for ϵ when $C_r/C_c = \infty$ and

⁵ Department of Mechanical Engineering, The Pennsylvania State College, State College, Pa. Mem. ASME.

⁶ IME-ASME General Discussion on Heat Transfer, 1951, pp. 304, 305.

⁷ "Heat Transfer and Fluid Resistances in Ljungström Regenerative-Type Air Preheaters," by H. Karlson and S. Holm, Trans. ASME, vol. 65, 1943, p. 61.

⁸ "Metal Temperature in Regenerative and Recuperative Air Preheaters," by T. A. Widell and S. Z. Juhasz, Trans. Royal Institute of Technology, No. 54, Stockholm, Sweden, 1952.

⁹ Research Assistant, Massachusetts Institute of Technology, Cambridge, Mass.

TABLE 3 EXCESS OF EQUATION [16] OVER VALUES IN TABLE 1 OF PAPER; $C_c/C_h = 1$

NTU _s	1	1.5	2	5	∞
1	0.010	-0.014	-0.016	-0.008	0
2	0.013	0.001	0	0.002	0
3	0.016	-0.001	-0.001	0.003	0
4	0.011	-0.003	-0.006	0.001	0
5	0.011	0.005	-0.008	-0.001	0
6	0.009	-0.006	-0.009	0	0
7	0.006	-0.007	-0.011	0.001	0
8	0.002	-0.010	-0.014	-0.003	0
9	-0.001	-0.012	-0.016	-0.003	0
10	-0.004	-0.017	-0.021	-0.006	0

TABLE 4 EXCESS OF EQUATION [16] OVER VALUES IN TABLE 2 OF PAPER; $C_c/C_h = 0.90$

NTU _s	1	1.5	2	5	∞
1	0.005	-0.006	-0.008	0	0
2	0.005	0.013	-0.008	0.011	0.001
3	0.011	0.007	0.002	0.014	0.001
4	0.014	0.002	-0.002	0.009	0.002
5	0.013	-0.001	-0.003	0.009	0.002
6	0.016	-0.004	0.010	0.004	0
7	0.014	-0.003	-0.005	0.010	0.004
8	0.011	-0.006	-0.008	0.003	0.007
9	0.008	-0.008	-0.012	0.008	0.008
10	0.004	-0.013	-0.016	0.006	0.007

$C_c/C_h = 1$ (Equation [8a] of the paper) may be extended in an equally simple form for variations of C_c/C_h in the range 0.9 to 1.0. For this range of the capacity rate ratio of the flow streams the logarithmic-mean temperature difference may be replaced by $1/2 [(t_{h \text{ out}} - t_{e \text{ in}}) + (t_{h \text{ in}} - t_{e \text{ out}})]$. In this case Equation [8] will be

$$\epsilon = \frac{NTU_s}{2 \left(1 + \frac{C_c}{C_h} \right) NTU_s + 1} \quad [15]$$

For $NTU_s = 10$, $C_c/C_h = 0.9$, Equation [15], herewith, gives $\epsilon = 0.952$ or 0.007 higher than the value tabulated in Table 2 of the paper. For lower values of NTU_s and/or higher C_c/C_h the agreement becomes almost exact.

Equation [15] of this discussion may be corrected for finite C_r/C_c in an empirical manner. Corbitts¹⁰ correction factor

$$\left[1 - \frac{(C_r/C_c)^2}{9} \right]$$

fits Saunderson's solution well but to fit Hausen's solution in the $(NTU)_s$, C_r/C_c range of this paper the exponent on (C_r/C_c) should be somewhat greater than 1. Since this correction factor will certainly be approximate

$$\left[1 - \frac{(C_r/C_c)}{9} \right]$$

is adequate and has the advantage of being simple. Thus the final relationship may be written

$$\epsilon = \left[\frac{NTU_s}{2 \left(1 + \frac{C_c}{C_h} \right) NTU_s + 1} \right] \left[1 - \frac{1}{9 \left(\frac{C_c}{C_h} \right) \left(\frac{C_r}{C_c} \right)} \right] \dots [16]$$

The amount which Equation [16] exceeds typical values in Tables 1 and 2 of the paper is given in Tables 3 and 4 of this discussion. As the error is large only near $NTU_s = 1$ and $NTU_s = 10$, Equation [16] is a very acceptable design guide for regenerator performance as it accounts for varying $(hA)^*$ and C_c/C_h , and gives a result generally within 1 per cent of that obtained from the curves of Figs. 4 and 5 of the paper. It has the added advantage of not requiring interpolation for values of C_c/C_h not graphed. Equation [16] gives the same value $\epsilon = 82.7$ per cent for the illustrative problem in this paper.

¹⁰ Referred to in discussion of authors' reference (5).

AUTHORS' CLOSURE

It is worth while at this point to compare the nondimensional parameters proposed for use in this paper to those previously employed in the literature. This comparison is given in Table 5. The advantage of the proposed groupings is evident when Equation [7] is compared to

$$\epsilon = \phi(\Lambda_c, \Lambda_h, \pi_c, \pi_h) \quad [17]$$

as proposed by Hausen and Saunders. It is evident from Table 5 that either the hot side or cold side heat-transfer area appears in all of the independent parameters of Equation [17]. In contrast, for the parameters in Equation [7], the heat transfer areas appear only in NTU_s and $(hA)^*$. Moreover, it is demonstrated in the text that $(hA)^*$ can be eliminated as a separate parameter and included only in NTU_s as defined by Equation [7a]. Thus the transfer areas appear explicitly in one and only one independent parameter.

TABLE 5 COMPARISON OF TERMINOLOGY

Term	Symbol		Equivalent in
	Saunders (6)	Hausen (4)	present terminology
Reduced surface	l_{rc}	A_c	$= NTU_c$
	l_{rh}	A_h	$= NTU_h$
Reduced period	τ_{rc}	π_c	$= \frac{NTU_c}{C_r/C_c}$
	τ_{rh}	π_h	$= \frac{NTU_h}{(C_c/C_h)(C_r/C_c)}$
Ratio of reduced surfaces	$\frac{l_{rc}}{l_{rh}}$	A_c/A_h	$= NTU_c/NTU_h = \frac{(hA)^*}{C_c/C_h}$
Ratio of reduced periods	$\frac{\tau_{rc}}{\tau_{rh}}$	π_c/π_h	$= \frac{NTU_c}{NTU_h} \frac{C_c}{C_h} = \frac{(hA)_c}{(hA)_h} = (hA)^*$
Utilization factor	U_c		$= \frac{1}{C_r/C_c}$
	U_h		$= \frac{1}{C_r/C_h} = \frac{1}{(C_c/C_h)(C_r/C_c)}$

TABLE 6 CORRECTIONS TO TABLE 1 AS DETERMINED FROM JOHNSON'S RESULTS¹¹

NTU _s	$\Delta\epsilon$ for $C_c/C_h = 1$ and the indicated capacity rate ratios			
	1	1.5	2	5
	C_c/C_r			
0	0	0	0	0
1.0				
1.5				
2.0				
2.5	.018			.011
3.0	.016	.011	.013	
3.5				
4.0	.012		.009	
4.5	.009	.009		
5.0	.007		.008	.010
5.5				
6.0		.011	.008	
6.5				
7.0			.009	
7.5		.012		.012
8.0			.008	
8.5				
9.0			.006	
9.5				
10.0			.004	.008

$\Delta\epsilon = (\epsilon, \text{Johnson}^{11} - \epsilon, \text{Table 1}).$

After reading Professor Dusinberre's comments, the work of Johnson¹¹ was brought to the attention of the authors. The careful calculations of Johnson reported in tabular form support the Saunders and Smoleniec graphical results in preference to those of Hausen's; see Fig. 3. For this reason the authors are changing their recommendation to the use of the results reported by Johnson. The corrections to be added to the entries of Tables

¹¹ "Regenerator Heat Exchangers of Gas Turbines," by J. E. Johnson, ARC Technical Report No. 2630, Her Majesty's Stationery Office, London, England, 1952.

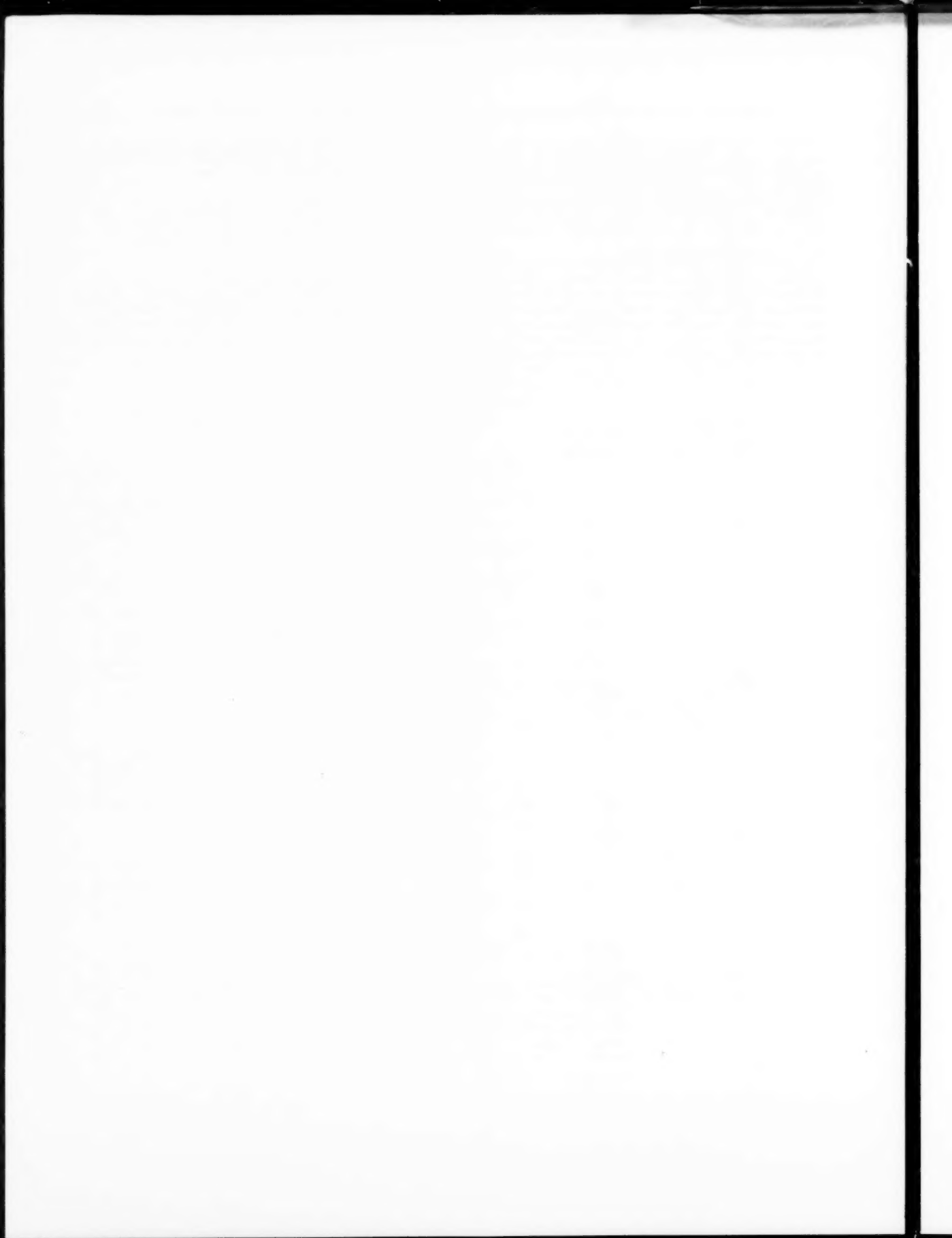
1 and 2 may be established from Table 6. As can be seen, these corrections, though small, are significant. Moreover, they are a maximum in the area where Professor Dusenberre made his check calculation and they support his correction of 0.02 to be applied to the ϵ for $NTU_o = 1$, $C_c/C_r = 1$. It is hoped that Professor Dusenberre will report his additional calculations in the near future, particularly for magnitudes of $C_c/C_h < \text{unity}$, as these cases are not considered by Johnson.

Mr. Harper makes the point that a relatively simple algebraic expression such as Equation [16] may be used to determine the effectiveness. This expression is based on the relation for $\epsilon = \phi(NTU_o)$ for true counter flow with $C_c/C_h = 1$ and $C_r/C_o = \infty$. Then, empirically determined modifying terms are introduced to account for $C_c/C_h < 1$ and $C_r/C_o < \infty$. This is an interesting and useful result. However, it is noted that Equation [16]

can be improved by using the original Corbitts' correction factor involving $(C_r/C_o)^2$ instead of to the first power, and omitting the (C_c/C_h) quantity in the second bracket. Thus

$$\epsilon = \left[\frac{NTU_o}{\frac{1}{2} \left(1 + \frac{C_r}{C_h} \right) NTU_o + 1} \right] \left[1 - \frac{1}{9 \left(\frac{C_r}{C_o} \right)^2} \right] \dots [18]$$

This equally simple equation will be found to be in better agreement with Johnson's results¹¹ as incorporated in Table 6. Equation [16], as it stands, yields ϵ on the low side by a maximum of about 2.5 per cent at $C_r/C_o = 2$. For the limiting cases of $C_r/C_o = 1$ and ∞ , the two Equations [16] and [18] are in essential agreement.



A Practical Solution of a Three-Dimensional Flow Problem of Axial-Flow Turbomachinery

By L. H. SMITH, JR.,¹ S. C. TRAUGOTT,² AND G. F. WISLICENUS,³ BALTIMORE, MD.

During the past decade three-dimensional flow problems of turbomachinery have been solved for frictionless fluids under the assumption of an infinite number of vanes. However, the practical application of this advancement to the design of turbomachinery has not yet reached a state of acceptance commensurate with the practical importance of this theoretical development. The present paper endeavors to contribute toward such application by presenting the principles of the theory in a physically simple manner, and by illustrating its application by two examples, solving the general problem by two successive approximations. The first approximation disregards the departures of the meridional streamlines from their straight and parallel potential-flow pattern; the second approximation takes account of these departures on the basis of the first. The vorticity of the flow is assumed to be strong. The time and means required for working out each of the examples were found to fall within the practical limits of a competently staffed engineering department.

NOMENCLATURE

The following nomenclature is used in the paper.

- c_p = specific heat at constant pressure, ft-lb/lb-deg R
- g = acceleration of gravity, ft/sec²
- h = static enthalpy per unit weight, ft-lb/lb
- H = total energy ($V^2/2g + h$), ft-lb/lb
- I = relative total energy ($H - UV_\theta/g$), ft-lb/lb
- m = meridional co-ordinate, ft
- n = normal (to stream surfaces) co-ordinate, ft
- N = number of blades, dimensionless
- p = static pressure, lb/ft²
- R = principal radius of curvature of streamline, ft
- r = radial co-ordinate, ft
- r_m = radius of curvature in meridional plane, ft
- T = absolute temperature, deg R
- U = velocity of runner ($\vec{\omega} \times \vec{r}$), ft/sec
- \vec{V} = absolute fluid velocity, ft/sec
- W = fluid velocity, relative to runner, ft/sec
- z = axial co-ordinate, ft
- Γ = circulation around axis of rotation, ft²/sec
- Γ_v = circulation around vane element, ft²/sec

¹ Research Staff Assistant, Department of Mechanical Engineering, Johns Hopkins University. Jun. ASME.

² Research Assistant, Department of Mechanical Engineering, Johns Hopkins University. Jun. ASME.

³ Chairman, Department of Mechanical Engineering, Johns Hopkins University. Mem. ASME.

Contributed by the Hydraulic and Gas Turbine Power Divisions and presented at the Annual Meeting, New York, N. Y., November 30-December 5, 1952, of THE AMERICAN SOCIETY OF MECHANICAL ENGINEERS.

NOTE: Statements and opinions advanced in papers are to be understood as individual expressions of their authors and not those of the Society. Manuscript received at ASME Headquarters, September 22, 1952. Paper No. 52-A-168.

- $\vec{\zeta}$ = vorticity of absolute flow ($\vec{\zeta} \equiv \nabla \times \vec{V}$), 1/sec
- θ = absolute peripheral angular co-ordinate, deg or radians
- ρ = mass density, lb-sec²/ft⁴
- φ = angle defined in Fig. 4, deg, radians
- ω = angular velocity of rotor, 1/sec

Subscripts:

- i = inside (hub) position
- m = meridional component
- n = normal (to meridional stream surface) component
- o = outside (tip) position
- r = radial component
- z = axial component
- θ = peripheral component
- 1, 2, 3, . . . stations along axis (see Fig. 17 or 29)

INTRODUCTION

The classical, one-dimensional theory of turbomachinery is well known to be insufficient for the description of the flow distribution whenever the cross-sectional dimensions of the fluid passages are of the same general magnitude as a significant length of the same passage. The resulting three-dimensional flow problem usually has been broken up into 2 two-dimensional flow problems, focusing attention either on the flow distribution in meridional ($\theta = \text{const}$) planes while assuming uniformity of flow in the peripheral direction ("axial symmetry," "infinite number of vanes"), or on the flow distribution between the vanes along coaxial stream surfaces, considering the form of these surfaces, i.e., the meridional flow picture, as given.

The present paper is concerned with the former of these two problems. This problem was first attacked in detail by Lorenz in 1906 (1).⁴ Its solution was obtained at that time by assuming the meridional velocity to have a potential. This assumption demands that the peripheral fluid velocity is also described by a (multivalued) potential; i.e., it forms a vortex of uniform angular momentum (free vortex). All fluid velocities for this case are irrotational. Furthermore, the vane forces must not have a component normal to the meridional stream surfaces.

With the development of axial-flow compressors and turbines for maximum head and through-flow it became desirable to depart from the "free-vortex" pattern of the peripheral fluid motion to enable Mach-number limitations to be met more uniformly along the blade span. From energy considerations it is immediately clear that in this case the meridional flow also must depart from a potential flow pattern.

The problem of departures from the potential flow pattern of the peripheral and meridional flow components and of their corresponding interaction has been the subject of several recent contributions to the theory of turbomachinery, for example, see Bibliography (2-5). The present paper will attempt to sum up the results of this theoretical development in a manner permitting its practical application to the design of turbomachinery. This application demands the consideration of strong departures from potential flow patterns, thus precluding the possibility of an

⁴ Numbers in parentheses refer to the Bibliography at the end of the paper.

analytically closed solution using the familiar method of "small perturbation," such as given by Marble (2) and others. The solution suggested here shares with that of Wu and Wolfenstein (3) the advantage of being, within the limits of its basic assumptions, quite general, and is in all its details capable of very straightforward physical interpretations.

PHYSICAL CHARACTERISTICS OF THE FLOW PROBLEM

In the preceding section the present problem was described as one connected with departures from a free-vortex flow which is characterized by a uniform value of its "circulation" ($\Gamma_o = \Gamma = \Gamma_i$ in Fig. 1) or a uniform value of its angular momentum.

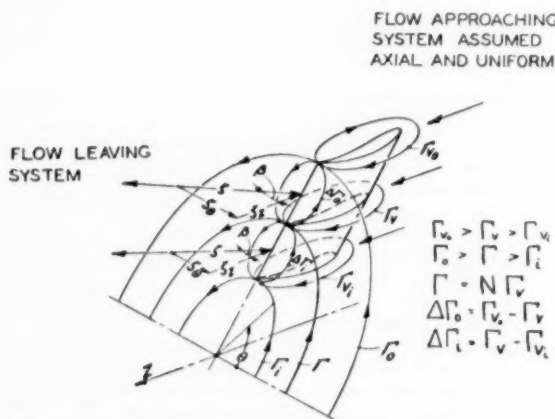


Fig. 1 VORTEX SYSTEM OF A VANE IN AN AXIAL-FLOW VANE SYSTEM WITH NONUNIFORM VANE CIRCULATION

For three-dimensional considerations it is advisable to use the more basic concept of vorticity because of its clear vectorial character. For present purposes vorticity may be characterized roughly as a velocity gradient describing a departure from the potential flow pattern. The present flow problem thus is seen to involve the concepts of radial gradients in angular momentum (or equivalently radial gradients in the circulation about the axis of rotation, Γ) and the "trailing vorticity" which is, in general, shed from the vanes when the vane circulation Γ_v is not constant over the span (radial extent) of the vanes.

Fig. 1 is an attempt to show graphically the interrelation between these concepts. For simplicity of representation the flow is shown entering the vane with uniform axial velocity and without rotation about the axis. The angular momentum of the flow leaving the system is described by its circulation which, in the case considered, is equal to N times the circulation Γ_v of each vane, where N is the number of vanes (6). Assuming nonuniform vane circulation so that $\Gamma_o > \Gamma_v > \Gamma_i$ (where Γ_v applies to the mid-section of the vane) and consequently $\Gamma_o > \Gamma > \Gamma_i$, we see by this relation a simple expression of the well-known physical fact that a vane circulation increasing toward the outside (for example) produces a flow of increasing angular momentum toward the outside. The difference in angular momentum or circulation in the discharging stream between, say, the mid-radius and the outer radius is

$$\Gamma_o - \Gamma = N(\Gamma_o - \Gamma_v) = N \Delta \Gamma_o$$

where $\Delta \Gamma_o \equiv \Gamma_o - \Gamma_v$ is in this case the circulation of the trailing vorticity between the two vane sections considered which, according to either Helmholtz' vortex law or Prandtl's wing theory, must be just equal to the difference in the "bound vorticity" or

vane circulation between the two stations considered. The analogous relation exists obviously between the innermost and the mid-vane sections. The circulations of the complete trailing vortex pattern of a system with 12 vanes are shown in end view in Fig. 2.

In the preceding example the presentation was made physically clear by discussing the flow around a finite number of vanes. It was shown that vortex sheets (sheets across which there is a discontinuity in velocity) are shed from the vanes and it follows that the trailing vorticity is concentrated in these sheets. With the assumption of axial symmetry, which will be made presently

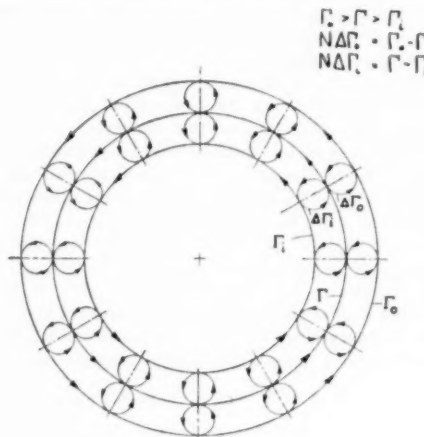


Fig. 2 END VIEW OF A TRAILING VORTEX PATTERN FOR AN AXIAL-FLOW SYSTEM OF $N = 12$ VANES

to enable a simpler mathematical solution, it is necessary to think of an infinite number of vanes each shedding an infinitely weak vortex sheet. This concept then corresponds to that of distributed vorticity, ξ . According to the vortex law of Helmholtz, the trailing vorticity must follow the direction of the flow leaving the vane system. For axial approach to the system, as assumed here, the flow leaving the system cannot be axial, forming with the axial direction the angle β (measured in a tangential plane). The axial component of the vorticity (ξ_a) accounts for the departure from constant angular momentum, i.e., from the potential pattern of the peripheral fluid motion, whereas the peripheral component of the trailing vorticity (ξ_o) represents a departure of the meridional flow (flow in planes normal to the peripheral direction) from a potential flow pattern. This is the kinematic expression of the fact that a vane system of nonuniform circulation produces, together with departures from the free-vortex or potential pattern of the peripheral component of the discharging flow, also a corresponding effect on the meridional component of this flow as previously suggested on the basis of energy considerations. Specifically, for axial-flow machines the axial velocity is under such conditions no longer constant. The fact that in the case considered here the vorticity vectors have the directly opposite direction to the corresponding velocities, Fig. 1, results from the directional definition of vorticity and therefore has no deeper physical significance.

In closing the present consideration on the physical characteristics of the flow problem, attention should be focused on the fact that the trailing vortex sheets as shown in Figs. 1 and 2, obviously induce not only peripheral and axial fluid motions but also radial motions which are seen in Fig. 2 to vary periodically along the peripheral direction of the system. It can be shown

that these periodic radial motions tend to zero as the vane spacing is made smaller and smaller for the same total circulations and vorticity in the discharging flow. For the present considerations this is the principal reason why this theory will assume complete axial symmetry in the sense of going to the limit of an infinite number of (frictionless) vanes, thereby eliminating all variations of the flow conditions in the peripheral direction.

The theoretical simplifications resulting from this elimination of the peripheral co-ordinate θ , and with it the unsteadiness connected with the rotation of one vane system relative to another fully justify this step for the purpose of arriving at a tractable problem. It should be recognized, however, that there is no known physical reason why this assumption should be considered as sufficiently accurate to describe the flow through actual vane systems of finite vane spacing. The chief justification for the assumption of axial symmetry lies in the fact that under this assumption theoretical results can be obtained which may then be compared with careful test results in order to obtain a check on the validity of this and other assumptions made.

DERIVATION OF THE BASIC EQUATIONS

In the following, equations will be derived that describe analytically the flow conditions discussed previously.

The assumptions necessary to arrive at practically useful and reasonably simple relations are the following:

(a) Isentropic flow, specifically the absence of fluid friction and of heat transfer; ideal gas law.

(b) Axial symmetry of flow, defined to mean complete uniformity of flow in the peripheral direction.

(c) Steady flow.

(d) No fluid body forces. This assumption limits considerations primarily to flow in the space outside of the vane systems, since the latter are replaced with assumption (b) by fields of continuously distributed forces.

The most direct way of deriving the equations describing this problem probably would result from the application of the vortex laws of a frictionless fluid to the boundary conditions of turbomachinery under the assumptions made. However, this method would not be as likely to reveal the physical mechanism described by the equations as the use of some simple considerations of flow energy and "radial equilibrium."

The total energy of a flowing gas is expressed (in foot-pounds per pound of fluid) by

$$H = \frac{V^2}{2g} + h \quad [1]$$

where V is the absolute velocity ft/sec, g the gravitational acceleration, and h the enthalpy of the moving gas as measured by instruments moving with the gas, ft-lb per lb.

Under assumption (a) this energy H will be constant along the streamlines as long as one does not pass through the influence of a moving-vane system. Considering two neighboring streamlines not passing through a moving-vane system, Fig. 3, it is evident that the difference in total energy dH between these two streamlines will remain constant along the flow. Consequently, the relation between two stations 1 and 2 not separated by a moving-vane system is, with reference to Fig. 3 (n is a co-ordinate everywhere normal to the meridional stream surface)

$$dH = \left(\frac{\partial H}{\partial n} \right)_1 dn_1 = \left(\frac{\partial H}{\partial n} \right)_2 dn_2 = \text{const} \quad [2]$$

$$\left(\frac{\partial H}{\partial n} \right)_2 = \left(\frac{\partial H}{\partial n} \right)_1 \frac{dn_1}{dn_2} \quad [3]$$

expressing the simple fact that the gradient of total energy

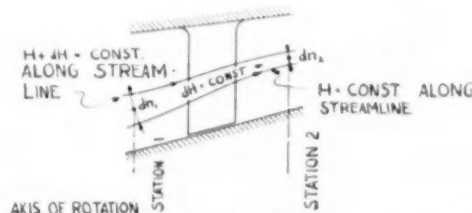


FIG. 3 FLOW THROUGH A STATIONARY VANE SYSTEM OR VANE-FREE SPACE

normal to the meridional streamlines (or surfaces) is inversely proportional to the normal distance between these streamlines. The distance dn or Δn between the streamlines may not be accurately obtainable by scaling, but the significant ratio dn_1/dn_2 can be calculated from the meridional velocities and the densities by the continuity relation

$$\frac{dn_1}{dn_2} = \frac{\rho_2 V_{m2} r_2}{\rho_1 V_{m1} r_1} \quad [4]$$

Differentiating Equation [1] with respect to n

$$g \frac{\partial H}{\partial n} = \frac{1}{2} \frac{\partial}{\partial n} (V^2) + g \frac{\partial h}{\partial n} \quad [5]$$

Putting

$$\frac{\partial h}{\partial n} = c_p \frac{\partial T}{\partial n}$$

and using the equation of state of an ideal gas and the relation between the pressure p and the mass per unit volume ρ for isentropic changes, it can be shown that

$$g \frac{\partial h}{\partial n} = \frac{1}{\rho} \frac{\partial p}{\partial n} \quad [6]$$

For any curved flow the pressure gradient normal to the flow is related to the velocity V of the flow and the radius of curvature R of the streamlines by the condition of radial equilibrium

$$\frac{1}{\rho} \frac{\partial p}{\partial n} = \frac{V^2}{R} \quad [7]$$

For a flow with a peripheral component V_θ and a meridional component V_m it seems simplest to consider the peripheral flow in the development of a conical section O, A , Fig. 4, normal to the local direction of the meridional streamlines, with the apex O of the cone on the axis of the machine. In the development of this conical section the radius of curvature of the peripheral flow is obviously $r/\cos \varphi$, where r is the shortest distance from the axis of rotation as shown in Fig. 4 and φ the local inclination of the meridional streamline against the axial direction. Counting the increment along the normal to the meridional stream surface as positive when increasing the distance from the axis of rotation, the foregoing relation becomes, for the pressure gradient normal to the meridional streamlines (surfaces)

$$\frac{1}{\rho} \frac{\partial p}{\partial n} = \frac{V_\theta^2}{r/\cos \varphi} \pm \frac{V_m^2}{r_m} \quad [8]$$

where r_m is the radius of curvature of the meridional streamlines. The plus sign applies to the case shown in Fig. 5, the minus sign to that shown in Fig. 4, referring to the direction of curvature of the meridional streamlines.

Considering that the total velocity V can be expressed by its

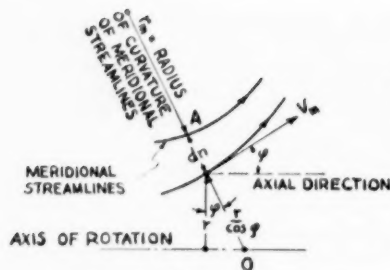


FIG. 4

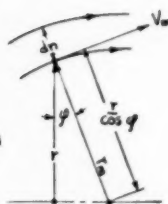


FIG. 5

peripheral and meridional components ($V^2 = V_\theta^2 + V_m^2$), the first term on the right-hand side of Equation [5] may be written in the form

$$\frac{1}{2} \frac{\partial}{\partial n} (V^2) = V_\theta \frac{\partial V_\theta}{\partial n} + V_m \frac{\partial V_m}{\partial n} \quad [9]$$

Substituting from Equations [6], [8], and [9] into Equation [5] the following relation is obtained

$$g \frac{\partial H}{\partial n} = V_\theta \left(\frac{\partial V_\theta}{\partial n} + \frac{V_\theta}{r \cos \varphi} \right) + V_m \left(\frac{\partial V_m}{\partial n} \pm \frac{V_m}{r_m} \right) \quad [10]$$

According to the usual definition of vorticity the expressions within the parentheses can be written as the components of the vorticity parallel to V_m (ζ_m), and parallel to V_θ (ζ_θ), respectively

$$\zeta_m = \frac{\partial V_\theta}{\partial n} + \frac{V_\theta}{r \cos \varphi} \quad [11a]$$

$$\zeta_\theta = - \left(\frac{\partial V_m}{\partial n} \pm \frac{V_m}{r_m} \right) \quad [11b]$$

Equation [10] may thus be written in the form

$$g \frac{\partial H}{\partial n} = V_\theta \zeta_m - V_m \zeta_\theta \quad [12]$$

Considering that the velocity and vorticity components normal to the meridional flow surfaces are zero, Equation [12] also may be given the vector form

$$g \frac{\partial H}{\partial n} = [\vec{V} \times \vec{\zeta}] \quad [13]$$

It will be understood that the last equation could have been derived more directly from the laws of vortex flow of an ideal fluid. However, the physical background of this equation, involving the energy relations [1] and [2], and the condition of radial equilibrium, Equation [8], might have been obscured by presenting Equation [13] directly.

In order to derive a corresponding relation to Equations [10], [12], and [13] for the flow through rotating-vane systems it is customary to introduce the concept "relative energy" I , by the definition

$$I = H - \frac{U V_\theta}{g} = \frac{V^2}{2g} + h - \frac{U V_\theta}{g} \quad [14]$$

Since the term, by which the relative energy I differs from the energy of the absolute flow H , was chosen to be the familiar term in Euler's momentum equation of turbomachinery, applying to a station in front of or behind a rotating-vane system, it is easy to see that I is constant along (meridional) streamlines through rotating-vane systems, Fig. 6. All relations previously derived

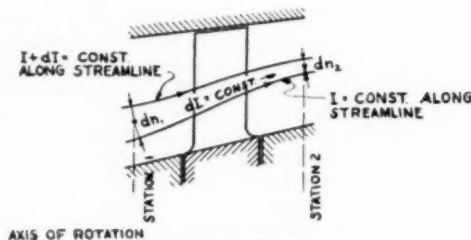


FIG. 6 FLOW THROUGH A ROTATING VANE SYSTEM

for H apply then to I if one simply introduces the additional term $U V_\theta/g$ into all relations concerned. Particularly

$$\frac{\partial}{\partial n} \left(\frac{U V_\theta}{g} \right) = \frac{1}{g} \left(U \frac{\partial V_\theta}{\partial n} + V_\theta \frac{\partial U}{\partial n} \right)$$

However

$$\frac{\partial U}{\partial n} = \omega \frac{\partial r}{\partial n} = \frac{U}{r} \cos \varphi$$

and hence

$$\frac{\partial}{\partial n} \left(\frac{U V_\theta}{g} \right) = \frac{U}{g} \left(\frac{\partial V_\theta}{\partial n} + \frac{V_\theta}{r \cos \varphi} \right) \quad [15]$$

Subtracting the last expression from Equation [10] as demanded by the definition of the relative energy, Equation [14], the following relation is obtained

$$g \frac{\partial I}{\partial n} = (V_\theta - U) \left(\frac{\partial V_\theta}{\partial n} + \frac{V_\theta}{r \cos \varphi} \right) + V_m \left(\frac{\partial V_m}{\partial n} \pm \frac{V_m}{r_m} \right) \quad [16]$$

Defining $\vec{W} = \vec{V} - \vec{U}$ we have $(V_\theta - U) = W_\theta$ and $V_m = W_m$. It is therefore physically clearer if the foregoing relation is written in terms of the relative flow

$$g \frac{\partial I}{\partial n} = W_\theta \left(\frac{\partial V_\theta}{\partial n} + \frac{V_\theta}{r \cos \varphi} \right) + W_m \left(\frac{\partial V_m}{\partial n} \pm \frac{V_m}{r_m} \right) \quad [17]$$

and, analogous to Equations [12] and [13]

$$g \frac{\partial I}{\partial n} = W_\theta \zeta_m - W_m \zeta_\theta \quad [18]$$

or

$$g \frac{\partial I}{\partial n} = [\vec{W} \times \vec{\zeta}] \quad [19]$$

The last equation together with the corresponding Equation [13] permit us to formulate the present result in the following manner:

The gradient of the total flow energy and of the relative energy normal to the meridional flow is given by the vector product of the flow velocity relative to the system and the vorticity of the absolute flow.

It follows from the assumption of frictionless flow and axial symmetry that the gradient of the energies as defined cannot have a component parallel to the meridional stream surface; i.e., this gradient is normal to the meridional stream surface. On the other hand the vector products $\vec{V} \times \vec{\zeta}$ and $\vec{W} \times \vec{\zeta}$ are also normal to the meridional stream surface since for a frictionless flow (outside of the vane systems) not only the velocity but also the vorticity $\vec{\zeta}$ cannot have a component normal to the meridional

stream surface. Hence in Equations [13] and [19] the gradients $\partial H/\partial n$ and $\partial I/\partial n$ can be interpreted vectorially. These equations then express the equality of two vectors in direction as well as magnitude, both directed normal to the meridional stream surface. This result directly reflects the original assumption of frictionless flow.

For the practical application of the foregoing relations not the energy gradients as such but the law governing the behavior of this energy gradient, as expressed by Equation [3], is decisive. The corresponding law for the relative energy is, by the foregoing definition and Fig. 6, the same, i.e.,

$$\left(\frac{\partial I}{\partial n}\right)_2 = \left(\frac{\partial I}{\partial n}\right)_1 \frac{dn_1}{dn_2} \dots \dots \dots [20]$$

Equation [4] also may be used with Equation [20] as well as with Equation [3].

Combining Equations [3], [20], and [4] with Equations [10], [13], [17], and [19] one obtains for the relation between two stations 1 and 2 on the same meridional streamline before and behind a stationary and rotating-vane system, respectively:

For stationary-vane systems or vane-free space

$$\left[V_{\theta 1} \left(\frac{\partial V_{\theta}}{\partial n} + \frac{V_{\theta}}{r/\cos \varphi} \right)_1 + V_{m1} \left(\frac{\partial V_m}{\partial n} \pm \frac{V_m}{r_m} \right)_1 \right] \frac{1}{\rho_1 r_1 V_{m1}} = \left[V_{\theta 2} \left(\frac{\partial V_{\theta}}{\partial n} + \frac{V_{\theta}}{r/\cos \varphi} \right)_2 + V_{m2} \left(\frac{\partial V_m}{\partial n} \pm \frac{V_m}{r_m} \right)_2 \right] \frac{1}{\rho_2 r_2 V_{m2}} \dots [21]$$

Vectorially

$$\frac{|\vec{V}_1 \times \vec{\xi}_1|}{\rho_1 r_1 V_{m1}} = \frac{|\vec{V}_2 \times \vec{\xi}_2|}{\rho_2 r_2 V_{m2}} \dots \dots \dots [22a]$$

or

$$\frac{V_{\theta 1} \xi_{m1} - V_{m1} \xi_{\theta 1}}{\rho_1 r_1 V_{m1}} = \frac{V_{\theta 2} \xi_{m2} - V_{m2} \xi_{\theta 2}}{\rho_2 r_2 V_{m2}} \dots \dots \dots [22b]$$

For rotating-vane systems

$$\left[W_{\theta 1} \left(\frac{\partial V_{\theta}}{\partial n} + \frac{V_{\theta}}{r/\cos \varphi} \right)_1 + W_{m1} \left(\frac{\partial V_m}{\partial n} \pm \frac{V_m}{r_m} \right)_1 \right] \frac{1}{\rho_1 r_1 V_{m1}} = \left[W_{\theta 2} \left(\frac{\partial V_{\theta}}{\partial n} + \frac{V_{\theta}}{r/\cos \varphi} \right)_2 + W_{m2} \left(\frac{\partial V_m}{\partial n} \pm \frac{V_m}{r_m} \right)_2 \right] \frac{1}{\rho_2 r_2 V_{m2}} \dots [23]$$

Vectorially

$$\frac{|\vec{W}_1 \times \vec{\xi}_1|}{\rho_1 r_1 V_{m1}} = \frac{|\vec{W}_2 \times \vec{\xi}_2|}{\rho_2 r_2 V_{m2}} \dots \dots \dots [24a]$$

or

$$\frac{W_{\theta 1} \xi_{m1} - W_{m1} \xi_{\theta 1}}{\rho_1 r_1 V_{m1}} = \frac{W_{\theta 2} \xi_{m2} - W_{m2} \xi_{\theta 2}}{\rho_2 r_2 V_{m2}} \dots \dots \dots [24b]$$

It should not be too surprising that completely analogous expressions are obtained for stationary and rotating vane systems. In both cases the vorticity added by the particular vane system has, as trailing vorticity, the direction of the flow leaving the system relative to that system, whether stationary or rotating. This means the vorticity shed from a system does not add to or subtract from the vector product of the vorticity and the flow relative to that system; i.e., it leaves that product unchanged as expressed in essence by Equations [22] and [24]. Thus these equations express principally the facts shown in Fig. 1 and discussed in connection therewith, considering that Fig. 1 could be applied also to rotating systems simply by replacing the absolute velocity V and its components by the relative velocity W and its components.

METHODS OF SOLUTION

Equations [21] through [24b] may be used in the following manner to predict flow with vorticity through a stage or blade row of a turbomachine:

The flow may be assumed as given at station 1 or 2, e.g., at one side of the blade row considered. This determines completely one side of the equation with which we are concerned, although the determination of the velocity gradients $\partial V_{\theta}/\partial n$ and $\partial V_m/\partial n$ from an arbitrarily given velocity distribution involves, in the general case, the familiar difficulty of differentiating a numerically or graphically given function.

For the other side of the same equation one may now choose one of the two components of the flow and then numerically or graphically calculate the other. To carry out this (as well as the foregoing) operation it is necessary to approximate in advance the local inclination φ , as well as the local radius of curvature r_m of the meridional streamlines at the two stations considered. The required approximation must be derived from a lower-order approximation of the entire flow. The potential pattern of the meridional flow may be used as first approximation for φ and r_m . With such an assumption the before-mentioned numerical or graphical calculation of the missing flow component can be completed except for a constant of integration. If the missing velocity component is the meridional one (which is usually the case) then the constant of integration is to be determined from the condition of continuity. For incompressible fluids the average meridional velocity may be calculated immediately from the given rate of volume flow. If one estimates at which point of the cross section the local velocity may be expected to agree with the average velocity (usually near its center), the numerical process of integration may be started at that point with a given V_m and the corresponding slope of the V_m -curve, $\partial V_m/\partial n$, calculated. With this slope the V_m -values at neighboring points may be estimated and the process repeated. The convergence of the resulting sequence of iterations is usually very fast.

For compressible fluids it is usually possible to estimate the average density of the gas in the cross section considered, and thus calculate the rate of volume flow and average meridional velocity from the given rate of mass flow. This is difficult only when the meridional velocities are near the acoustic. The subsequent procedure is the same as before.

If the peripheral component of the flow is to be determined the constant of integration, i.e., the initial value for a step-by-step process of integration as described before, is usually given by certain requirements regarding the angular momentum of the flow in the cross section considered, which follow from the prescribed performance of the machine and the distribution of its load over its stages.

The easiest and practically most significant case of application is (at present) that of axial-flow machines. There the potential flow pattern which is to be used as "first approximation" has straight meridional streamlines parallel to the axis of the machine. Consequently, everywhere the inclination φ of these streamlines is zero and their radius of curvature r_m is infinite. If we also add the assumption that $\rho_2 r_2 V_{m2} = \rho_1 r_1 V_{m1}$ (or $dn_2 = dn_1 = dn = dr$), Equations [21] through [24b] assume the form

For stationary systems

$$V_{\theta 1} \left(\frac{\partial V_{\theta 1}}{\partial r} + \frac{V_{\theta 1}}{r} \right) + V_{m1} \frac{\partial V_{m1}}{\partial r} = V_{\theta 2} \left(\frac{\partial V_{\theta 2}}{\partial r} + \frac{V_{\theta 2}}{r} \right) + V_{m2} \frac{\partial V_{m2}}{\partial r} \dots [25]$$

Vectorially

$$|\vec{V}_1 \times \vec{\xi}_1| = |\vec{V}_2 \times \vec{\xi}_2| \dots [26a]$$

or

$$V_{\theta 1} \zeta_{m1} - V_{m1} \zeta_{\theta 1} = V_{\theta 2} \zeta_{m2} - V_{m2} \zeta_{\theta 2} \quad [26b]$$

For rotating systems*

$$W_{\theta 1} \left(\frac{\partial V_{\theta 1}}{\partial r} + \frac{V_{\theta 1}}{r} \right) + W_{m1} \frac{\partial V_{m1}}{\partial r} =$$

$$W_{\theta 2} \left(\frac{\partial V_{\theta 2}}{\partial r} + \frac{V_{\theta 2}}{r} \right) + W_{m2} \frac{\partial V_{m2}}{\partial r} \quad [27]$$

Vectorially

$$|\vec{W}_1 \times \vec{\zeta}_1| = |\vec{W}_2 \times \vec{\zeta}_2| \quad [28a]$$

or

$$W_{\theta 1} \zeta_{m1} - W_{m1} \zeta_{\theta 1} = W_{\theta 2} \zeta_{m2} - W_{m2} \zeta_{\theta 2} \quad [28b]$$

The foregoing equations were presented (6) where they were derived by applying the condition of radial equilibrium in its simplest form, Equation [7], to the flow at the inlet and discharge sides of stationary and rotating axial-flow vane systems.

After solving the simplified Equations [25] through [28b] one can plot the approximate meridional streamlines by using the condition of continuity at successive stations. The local radius of curvature r_m may be obtained graphically or numerically from these streamlines and may be used in the basic Equations [21] through [24b] for a second approximation. After some experience it is possible to anticipate approximately the effect of the r_m -term in these equations on the meridional velocity distribution, and thereby improve the accuracy of r_m as introduced by this step of approximation.

In most practical cases of axial-flow machinery the inclination of the streamlines φ will be so small that departures of $\cos \varphi$ from unity can be disregarded, although its consideration would not be difficult.

The foregoing procedure is in principle that by which the following examples were worked out. It will be seen that the higher approximation just mentioned differs but slightly from that obtained by disregarding the curvature of the meridional streamlines, i.e., by using Equations [25] through [28b], although the vorticity, i.e., the originally postulated departures from a potential flow pattern were about the strongest that may reasonably be expected for axial-flow machines. The first introduction of the curvature of the meridional streamlines (resulting from the vorticity of flow in axial-flow machines) may therefore safely be regarded as the final step in this process of successive approximation (again excluding the case of near acoustic meridional velocities in the cross sections considered).

In closing this discussion on methods of solutions it seems advisable to focus attention briefly on the special case when the flow approaching a stationary-vane system is irrotational. Under this condition the simplified Equations [25] and [26b] permit an extremely simple graphical solution which is not only practically useful but, beyond that, illustrates vividly the simplicity of the physical facts expressed by this theory.

The equation governing the flow at the discharge side of the system is obviously

$$\vec{V} \times \vec{\zeta} = 0 \quad [29]$$

or, explicitly

$$V_{\theta} \left(\frac{\partial V_{\theta}}{\partial r} + \frac{V_{\theta}}{r} \right) + V_m \frac{\partial V_m}{\partial r} = 0 \quad [30]$$

Equation [29] expresses clearly the fact that in this case the entire

vorticity is shed as trailing vorticity from the vanes as illustrated in Fig. 1. Therefore the velocities by which this flow differs from a potential flow must be normal to the velocity leaving the vanes. On this simple basis one may derive graphically from a given velocity diagram at radius r_A the velocity diagram at a nearby radius r_B as shown in Fig. 7. If the flow were irrotational, the velocity at r_B would be given by the velocity V_B^* whose end point B^* is derived from A by the law of constant angular momentum. The departure ΔV from this potential flow pattern, leading from B^* to the final point B , must then be normal to V_B to satisfy Equation [29]. The point B may then be fixed if V_{mB} or $V_{\theta B}$ is specified.

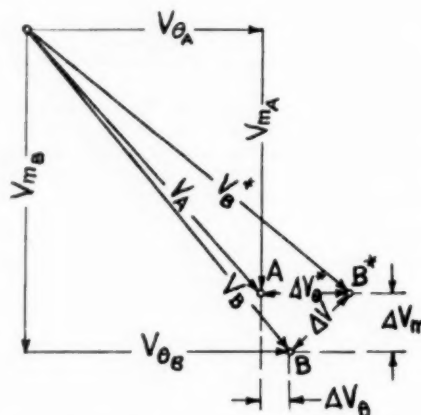


FIG. 7 VELOCITY DIAGRAM FOR NONUNIFORM VANE CIRCULATION

It can also be shown that the geometric relation between ΔV_{θ} , ΔV_m , ΔV_{θ^*} , as shown in Fig. 7, and the (small) radial step Δr satisfies Equation [30] in terms of finite differences. Most illuminating appears to be the fact that the step from B^* to B , based on the vector Equation [29] leaves the magnitude of the velocity V_B^* or V_B substantially unchanged, thus also satisfying the energy requirement mentioned earlier in this paper.

The method of solution illustrated in Fig. 7 applies on the basis of Equation [28a] also to rotating-vane systems if the absolute velocity V is replaced by the relative velocity W . The step from A to B^* must in this case obey the free-vortex law of the absolute, not of the relative flow.

The graphical solution indicated was used by one of the authors for several years in work on aircraft gas turbines. A similar procedure was also suggested by Pinnes (5).

APPLICATION TO MULTISTAGE AXIAL COMPRESSORS

Two independent examples were worked out in order to establish by actual application whether the principles and methods outlined in the preceding sections could be used for design purposes. This question was affirmatively answered by deriving the velocity distributions for two compressors of strong vorticity (nonuniform circulation) within approximately 500 man-hours for each example, including a rather lengthy procedure of trial and error to arrive at some degree of optimization for the given design conditions.

For both examples it was decided to use at the inlet to the first rotating blade row a "prerotation" of the entering gas varying approximately along a straight line from a maximum value at the tip to zero at the hub. The hub-to-tip diameter ratio was chosen to be 0.50.

The inlet condition therefore differed from the potential flow

pattern more drastically than the familiar "solid-body" type of prerotation, so that the vorticity was quite strong and certainly precluded the application of small perturbation solutions. However, this choice of prerotation also corresponded, in the opinion of the authors, to the practical requirements of axial compressors for maximum pressure rise per stage with given limitations in the Mach number of the flow relative to the blade rows. The peripheral component of the fluid velocity at the blade tips, entering the runner blades, was of the order of one third of the peripheral velocity of the blades.

It was found that with the degree and form of prerotation chosen for the first runner inlet, the first runner could not be designed for uniform energy input or circulation over the radial extent of its vanes. This will be demonstrated by referring to Equation [28b] applied to the first rotating blade row.

It is easy to show⁸ that for uniform circulation of the runner blades $\zeta_{m1} = \zeta_{m2} = \zeta_m$. Furthermore, for the same volume flow and cross section before and after the runner there is some radius where $W_{m2} = W_{m1} = W_m$. With this understanding Equation [28b] appears in the form

$$\zeta_m (W_{\theta 2} - W_{\theta 1}) = W_m (\zeta_{\theta 2} - \zeta_{\theta 1}) \quad [31]$$

Since the peripheral component W_{θ} of the relative velocity changes in the direction of the runner motion, i.e., in the positive direction, it follows that $W_{\theta 2} - W_{\theta 1} > 0$. Hence, since all other terms are positive, $\zeta_{\theta 2} > \zeta_{\theta 1}$, i.e., the vorticity of the meridional flow increases through a pump runner of constant circulation.

For the prerotation chosen it follows from Equation [30] that the vorticity of the meridional flow between the stationary guide vanes and the first-stage runner

$$-\frac{\partial V_m}{\partial r} = \zeta_{\theta} > 0 \text{ or } \frac{\partial V_m}{\partial r} < 0 \quad [32]$$

Thus the meridional velocity decreases toward the outside, and it then follows from the preceding considerations that after the first-stage runner the meridional velocity would decrease still faster toward the outside. Under the actual conditions chosen the meridional velocity would indeed drop to imaginary values at the tip after the first-stage runner, which indicates that it is impossible to balance the flow. This behavior can be avoided by increasing the first-stage runner-blade circulation toward the blade tip, a necessity for the inlet conditions chosen in the examples. This nonuniform energy input to the gas of course must be partly eliminated in the following stages. The two examples chosen differ principally by the fact that in the first case this equalization of the energy input is distributed over several stages, while in the second case it is completed in the second stage.

Since the prerotation selected for these examples has as its primary purpose the limitation of the Mach number of the flow relative to the initial blade rows, it was natural to make a consistent choice of the velocities at the inlets to the various blade rows, meaning that these velocities should be uniformly high in relation to the acoustic. Furthermore, it was stipulated that not simply the head per stage but the power, i.e., the head times the rate of flow, should be a maximum for given limitation in Mach number. The totality of the conditions prescribed was intended to give a realistic picture of the applicability of the theory under the practical requirements of compressor design. These conditions were, of course, not met by an automatic method of mechanical calculations. With a procedure of trial and error, requiring considerable judgment with respect to the over-all significance of every step taken, and reasonable competence, the method suggested here was found to be entirely practical.

It is impossible to give within the limits of this paper a com-

plete account of the details of procedure. For this the reader is referred to the complete reports of this work given under references (7) and (8). In the following only a brief summary of this work is given. The design of a compressor with more than two stages will be presented first.

COMPRESSOR DESIGNS

Figs. 8 through 11 show some possible velocity distributions at the inlet (subscript 2) and the discharge (subscript 3) of the first-stage runner. It will be noted that here as well as in the following diagrams the radii are made dimensionless by dividing by the tip-radius r_o , and the velocities by dividing by the runner-tip velocity U_o . The inlet to the stationary guide-vane system ahead of station 2 is uniform and purely axial and is therefore not shown. Subscripts o apply to the tip, subscripts i to the hub sections.

The significant variable in these various trials is the ratio of the limiting inlet velocity V_L into the rotor or following stator row to the tip velocity of the runner U_o . For each of the chosen configurations the power (head times rate of flow) was determined. It was found to be a maximum at $V_L/U_o = 0.75$, Fig. 9. However, $V_L/U_o = 0.80$, Fig. 10, was selected since the power was only 5 per cent less than the maximum whereas the velocity diagrams for $V_L/U_o = 0.80$ were found to be more favorable than at the exact maximum. In particular, the axial velocity at the outside of the (first) runner discharge was at $V_L/U_o = 0.80$ not so dangerously low as at $V_L/U_o = 0.75$. Furthermore, the power distribution over the cross section was at $V_L/U_o = 0.80$ somewhat more uniform than at other values.

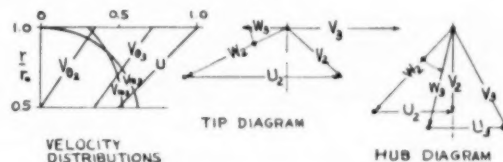


FIG. 8 VELOCITY DISTRIBUTION AND DIAGRAMS FOR $V_L/U_o = 0.72$



FIG. 9 VELOCITY DISTRIBUTION AND DIAGRAMS FOR $V_L/U_o = 0.75$

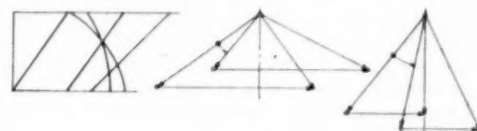


FIG. 10 VELOCITY DISTRIBUTION AND DIAGRAMS FOR $V_L/U_o = 0.80$

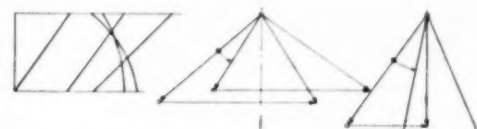


FIG. 11 VELOCITY DISTRIBUTION AND DIAGRAMS FOR $V_L/U_o = 0.86$

⁸ Reference 6, chapter 11.

The velocity distributions and diagrams from station 3 (discharge of first runner system) through station 6 (discharge of the second-stage diffuser) are shown in Figs. 12, 13, and 14, respectively. The resulting angles of deflection are (as before) indicated by curved arrows. The angles are seen to be quite high which is to be expected for a design of maximum power input, but has here the added significance of testing the application of the theory to systems with large deflections.

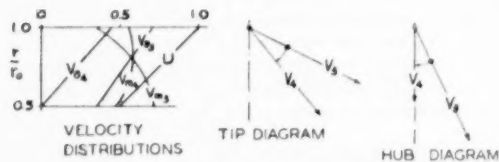


FIG. 12 VELOCITIES OF FIRST DIFFUSER

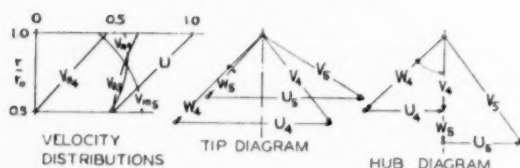


FIG. 13 VELOCITIES OF SECOND RUNNER

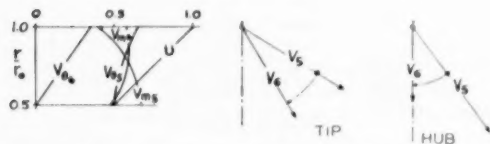


FIG. 14 VELOCITIES OF SECOND DIFFUSER

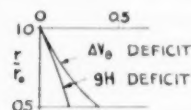


FIG. 15 DEFICITS AFTER FIRST STAGE

For the design of the stages following the first it is, of course, essential to compensate for the fact that in the first stage more energy (head) was added near the tip than near the hub. Fig. 15 shows the "deficit" in head H and peripheral deflection ΔV_θ , after the first-stage runner as a (dimensionless) function of the (dimensionless) radius. It was assumed that this deficit would be eliminated within four stages, so that the second stage was designed to compensate for one fourth of the deficit shown in Fig. 15.

Since the velocity diagrams in Figs. 12, 13, and 14 continue to maintain reasonable form, the design proposed appears to be capable of being continued through the higher stages. The procedure was thus terminated at the discharge of the second stage.

The solution obtained so far represents but the first approximation of the flow with vorticity since the changes in radial spacing and the curvature of the meridional streamlines were so far disregarded. These effects were then determined on the basis of the first approximation in the following manner:

The radial distribution of the rate of through-flow was determined for the various cross sections investigated and plotted in terms of r times V_m , as shown in Fig. 16. Equal parts of the areas under these curves would give the radial locations of

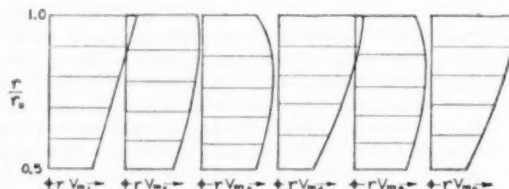


FIG. 16 CONTINUITY DIAGRAMS FOR INCOMPRESSIBLE FLOW

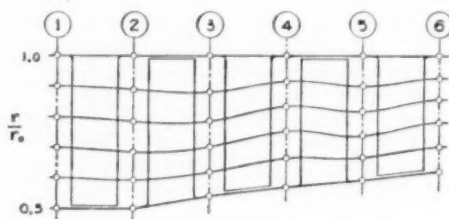


FIG. 17 STREAMLINES, RADIAL SHIFT BASED ON FIRST APPROXIMATION

the meridional streamlines in the sections considered under the assumption of an incompressible fluid and uniform hub and tip diameters throughout the machine. These radial locations were then corrected outwardly to account for the volume changes of the gas, solving for a compressor with constant outside diameter and increasing hub diameter in such a manner that the meridional (axial) velocities are, in the radially displaced positions, the same as according to the first approximation of the vortex flow for an incompressible fluid and constant hub diameter. The result of this procedure is given in Fig. 17, showing for the first time the radial displacements and curvatures of the meridional streamlines resulting from the vorticity of the flow as previously calculated.

From Fig. 17 one may now determine the local radii of curvature of the streamlines. This permits the solution of the more accurate Equations [21] through [24b]. A formula proposed by Wu and Wolfenstein (3) was used in order to anticipate the effect of the meridional curvature term on the meridional curvature itself. The results of the second approximation are shown in Figs. 18, 19, and 20 in solid lines in comparison with the previously determined approximations for these velocity distributions which are given in broken lines. From the velocity distributions as shown it is, of course, easy to derive velocity diagrams conforming to this higher approximation. However, the comparison between the solid and the broken curves shows that the corrections from the first to the second approximation are rather small in spite of the high vorticity of flow considered. In general, the higher approximation tends to reduce the velocity variations from one station to the next.

In the example just described the integration of the equations of flow for the first approximation was carried out analytically by prescribing for the peripheral velocity distributions V_θ , simple forms (straight lines and hyperbolas) permitting easy analytic expression of these curves as well as of the necessary integrals. However, the general procedure described does not depend on the choice of this particular method of integration. In working out the second approximation and the next example, the method of integration chosen was predominantly graphical, but the general principles of the procedure were essentially the same.

As mentioned before, the second example deals with a two-stage compressor, with the purpose of investigating whether a nonuniform energy input in the first stage of such a machine can

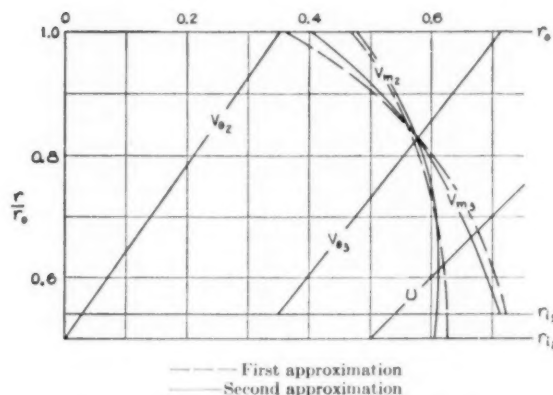


FIG. 18 VELOCITY DISTRIBUTION OF FIRST RUNNER

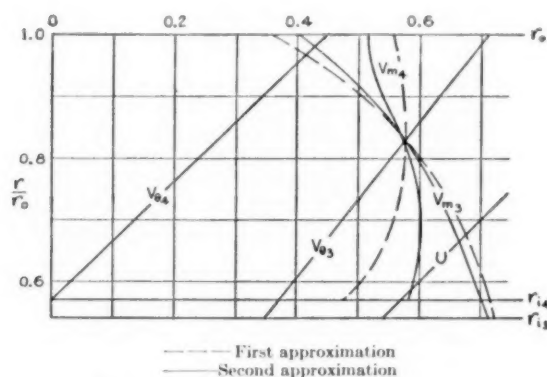


FIG. 19 VELOCITY DISTRIBUTION OF FIRST DIFFUSER

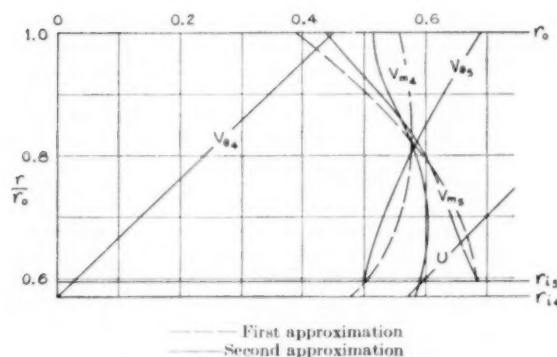


FIG. 20 VELOCITY DISTRIBUTION OF SECOND RUNNER

be balanced to a practically sufficient degree in the second stage alone.

Whereas in the first example the velocities entering the various blade rows were limited with respect to the acoustic velocity directly only at the root and tip sections, it was decided to determine in this example the distribution of the peripheral fluid velocity ahead of the first-stage runner for all radii from the condition of uniform relative inlet velocity to the runner ($W_2 = V_L = \text{const.}$). The resulting set of curves of $V_{\theta 2}$ as a function of

r/r_0 is shown in Fig. 21 (subscript 2 applies to the station between the first stator and the first runner system, and so on, see Fig. 29).

For a given choice of the ratio of the limiting relative inlet velocity $W_2 = V_L = 0.751 U_o$, Fig. 22 shows the axial velocities corresponding to three curves A, B, C, in Fig. 21.

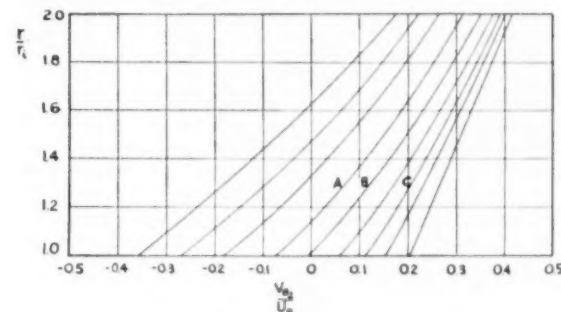


FIG. 21 INLET PERIPHERAL VELOCITY

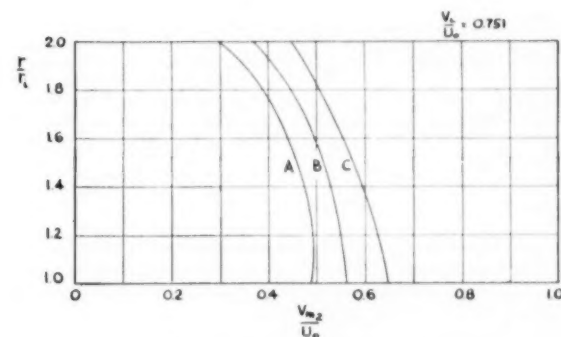


FIG. 22 INLET AXIAL VELOCITY

Solutions of the velocity distributions at the remaining stations 3 to 5 (see Fig. 29) are shown in Figs. 23 and 24 selected to obtain a uniform limiting velocity V_L in the second stator as well as in the first rotor, and, of course, aiming at a reasonably uniform energy distribution at the last station.

Owing to the detailed requirements placed upon the initial velocity distribution it did not seem advisable to approximate the curves by simple expressions that could be integrated analytically. Instead, Equations [25] and [27] were integrated graphically by solving these equations for the derivatives of the velocities in question and then drawing the desired curve from its given directions. An example is shown in Fig. 25 for the axial-velocity distribution at station 3. The selection of the proper curve from the family obtained in this manner is made on the basis of the condition of continuity.

From the peripheral velocities shown in Fig. 23 it is seen that the solution obtained does not appear to be entirely satisfactory. Considering that the changes in peripheral velocity across a runner are proportional to the runner head (here $V_{\theta 3} - V_{\theta 2}$ and $V_{\theta 5} - V_{\theta 4}$) it is seen that the head-input distribution is extremely nonuniform. Negative values of $V_{\theta 4}$ indicate very large turning angles in the second stator. It thus seemed desirable to investigate other design possibilities.

The principal parameter that could be varied was, as in the previous example, the peripheral velocity of the runner, expressed by the ratio V_L/U_o . Subsequently it was decided to drop the requirement that the inlet velocity to the second stator row should be subjected to the same limitation V_L as the first runner

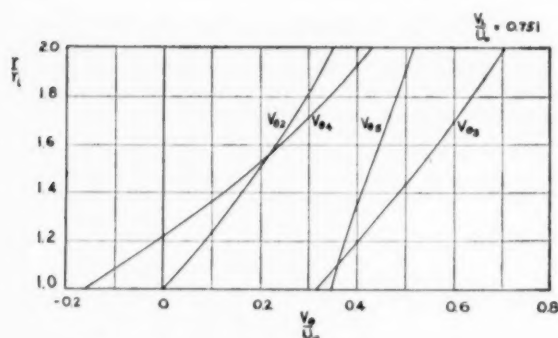


FIG. 23 PERIPHERAL VELOCITIES AT STATIONS 2 TO 5

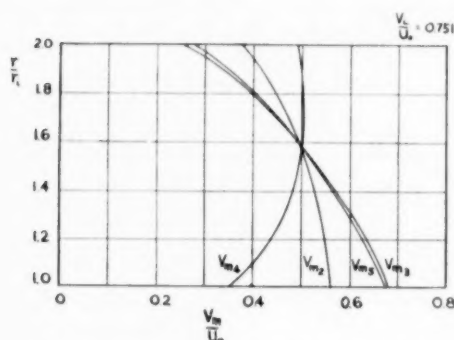


FIG. 24 AXIAL VELOCITIES AT STATIONS 2 TO 5

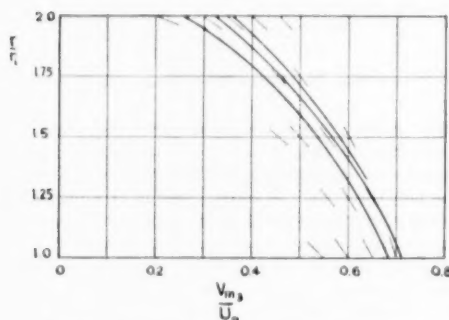


FIG. 25 EXAMPLE OF GRAPHICAL INTEGRATION

system. Of the six combinations investigated we present in Figs. 26 and 27 one that appears quite promising, although no definite statement can be made as to the optimum solution of this design problem. The velocity diagrams that result from the distribution curves in Figs. 26 and 27 are shown in Fig. 28 for the root and tip sections. The diagrams for other radii of course may be drawn readily and the vane profiles corresponding to these vector diagrams may be derived according to standard procedures.

As in the preceding example, the solutions presented so far were obtained from the simplified Equations [25] and [27], disregarding the curvature of the meridional streamlines and variations in their spacing. Only after a rather definite flow configuration has been chosen does it seem advisable to examine closer approximations. For the exploration of various design possibilities, as described before, it would be unwise to use anything but the first approximation for vortex flow.

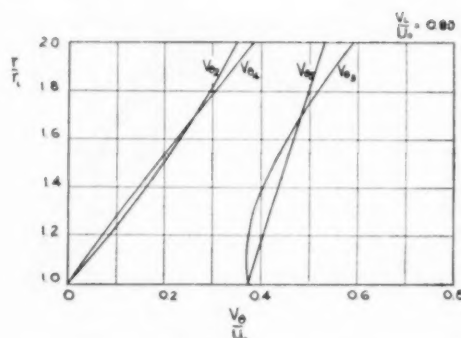


FIG. 26 PERIPHERAL VELOCITIES, FINAL SELECTION

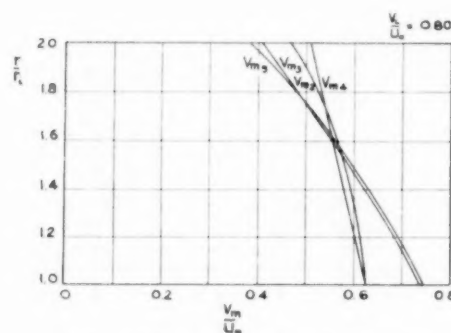
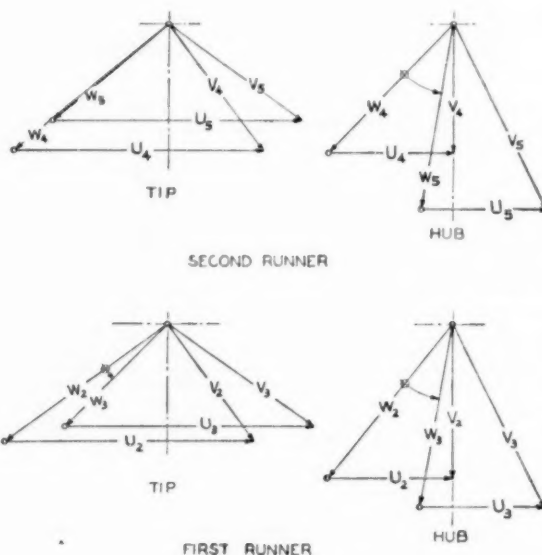


FIG. 27 AXIAL VELOCITIES, FINAL SELECTION

FIG. 28 VELOCITY DIAGRAMS, $V_L/U_0 = 0.80$

The meridional streamlines corresponding to the axial-velocity distributions given in Fig. 27 are shown in Fig. 29. In this case the new velocity distributions resulting from this form of the streamlines were not calculated in detail. Instead, the greatest

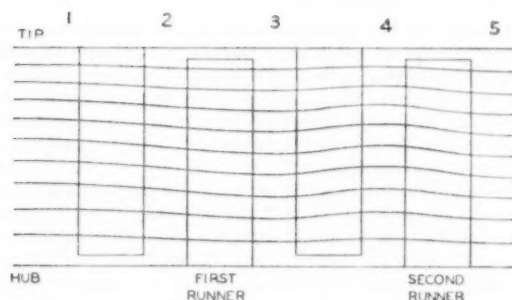


FIG. 29 STREAMLINES, FROM AXIAL VELOCITIES OF FIG. 27

variation in velocities resulting from the curvature of the meridional streamlines was calculated for two ratios of the stage length L (one rotor plus one stator row) to the hub radius r_h . It was found that for L/r_h approximately equal to 1.8 the variation of the peripheral or the axial-velocity components from their first vortex-flow approximation was 2 per cent, for L/r_h about 1.5 this variation was 5 per cent.

It may be of interest to note that for the velocity distributions shown in dimensionless form in Figs. 26, 27, and 28, with $V_L/U_o = 0.80$, a Mach number of V_L of 0.835, and an acoustic velocity of 1080 fps, one obtains with a tip velocity of 1125 fps for each stage an average polytropic head of 14,950 ft, giving with a polytropic efficiency of 85 per cent a pressure ratio of 1.55 in two stages. Since the hub-to-tip diameter ratio was assumed to be 0.5, such a compressor would compare favorably in size and weight with modern practice in the aeronautical and wind-tunnel fields.

In this example the compressibility of the gas was not taken into account explicitly, but there is no reason why this could not be done, for instance, in the same manner as outlined in connection with the first design example.

CONCLUSIONS

It has been shown that on the basis of Equations [25] through [28b] as first approximation, and Equations [21] through [24b] as second approximation, it is possible to determine the velocity distributions and vector diagrams of axial-flow machines with strong departures from a free-vortex (constant-circulation) flow pattern. The differences between the first and second approximation of the vortex flow are small so that the first approximation, Equations [25] through [28b], is sufficient for the exploration of design variations. On the other hand, the differences between the conventional free-vortex flow and the first approximation of the flow with vorticity are of first order of magnitude and cannot be neglected whenever departures from the free-vortex pattern are essential for the flow problem on hand. Fortunately, the first approximation of the vortex flow is often extremely simple to obtain, so that there is no reason to neglect completely the effects of vorticity even in exploratory investigations.

The methods of solution presented here are not limited to axial-flow machines. In the more general case the potential pattern of a curved meridional flow can be used to obtain the required first approximation for curvature and spacing of the meridional streamlines.

Not taken into account is the effect of the finite spacing of the vanes in the peripheral direction. This departure from axial symmetry may be the more serious the greater the vorticity as well as the general loading of the machine.

Investigations such as the present one, which are not limited to small vorticity and/or small deflections of the flow therefore tend

to emphasize the urgency of a serious attack on the truly three-dimensional flow problem of turbomachinery.

BIBLIOGRAPHY

- 1 "Neue Theorie und Berechnung der Kreiselräder," by H. Lorenz, R. Oldenbourg, 1906.
- 2 "The Flow of a Perfect Fluid Through an Axial-Flow Turbomachine With Prescribed Blade Loading," by F. E. Marble, *Journal of the Aeronautical Sciences*, vol. 15, 1948, pp. 473-485.
- 3 "Application of Radial-Equilibrium Conditions to Axial-Flow Compressor and Turbine Design," by C. H. Wu and L. Wolfenstein, NACA Technical Note No. 1795, January, 1949.
- 4 "Theoretical and Experimental Investigations of Axial Flow Compressors (Summary Report)," by J. T. Bowen, R. H. Sabersky, and W. D. Rannie, Mechanical Engineering Laboratory, California Institute of Technology, Pasadena, Calif., January, 1949.
- 5 "The Theoretical Possibilities for Balanced Flow in Compressor and Turbine Design," by R. W. Pinnes, ASME Paper No. 50-A-66, November, 1950.
- 6 "Fluid Mechanics of Turbomachinery," by G. F. Wislicenus, McGraw-Hill Book Company, Inc., New York, N. Y., 1947, pp. 175-177.
- 7 "The Design of a Subsonic Multistage Axial-Flow Compressor for Maximum Power Per Stage," by L. H. Smith, Jr., MS thesis, Mechanical Engineering Department, The Johns Hopkins University, Baltimore, Md., May, 1951.
- 8 "A Two-Stage Axial-Flow Compressor With Non-Uniform Energy Addition Per Stage," by S. C. Traugott, MS thesis, Mechanical Engineering Department, The Johns Hopkins University, Baltimore, Md., May, 1951.
- 9 "Die Konstruktion der Francis-Schaukel nach der Lorenzen Turbinentheorie," by Bauersfeld, *Zeitschrift des Vereines deutscher Ingenieure*, vol. 56, 1912, pp. 2045-2051.

Discussion

C. C. ALSWORTH.⁶ The authors present the problem of finding the velocity distribution in an axial-flow turbomachine in a straightforward and readily understandable manner. Use has been made of the fact that knowledge of the vorticity distribution coupled with the continuity relation leads to a solution of the velocity distribution. The manner of deriving the basic equations is simple and should be easily understood. However, as pointed out in the paper, the equations can be solved more directly using the methods of vector analysis. By taking account of the curvature of streamlines in the meridional plane, the solution becomes a quasi-three-dimensional one (it is three dimensional in so far as the assumption of axial symmetry is valid) and should yield a fairly accurate solution for the streamline shape.

Of course, one must understand that the solution will be a reasonably close approximation of the actual flow pattern only if the assumptions of axial symmetry and inviscid flow actually are satisfied. Numerous investigations have disclosed that these are often reasonable assumptions. However, if the deviation is large, some account should be taken of these effects. Such deviations must be expected in modern high-pressure designs using special flow profiles and operating close to the stall.

It would seem that the method presented is rather time consuming for the applications presented. These examples could be handled in a satisfactory manner by other methods, such as Marble's (2). The method proposed by the authors should find successful application in such problems as those involving mixed-flow machinery where radial forces are of greater significance.

R. O. BULLOCK.⁷ One of the greatest problems in the design of compact and efficient turbomachines is that of accounting for

⁶ Aerodynamicist, Propulsion Research Corporation, Inglewood, Calif. Jun. ASME.

⁷ Lewis Flight Propulsion Laboratory, National Advisory Committee for Aeronautics, Cleveland, Ohio.

the three-dimensional character of the flow without spending a prohibitive amount of time for analyzing each design. Any paper dealing with this problem is, therefore, a welcome contribution to the literature. The present paper is doubly welcome at this time because of the insight one obtains from the authors' excellent discussion of the relations existing between the gradients of vorticity and velocity.

The working equation and method of solution presented in this paper are similar to those outlined by Stodola, and attributed to Flugel and Lorenz for determining the axial-symmetric flow in a rotor or stator. The technique is consequently also similar to that described by Hamrick, Ginsburg, and Osborn.⁸ A rigorous derivation of the fundamental equation is presented by Wu.⁹ In this paper Wu suggests solving the equations by an alternate method which is more amenable to high-speed computing techniques. Again, however, the principal value of the present paper arises from the excellent description of the problem rather than in the development of radically new techniques.

The one adverse comment to be made on the paper is the fact that it has neglected the problem within the boundaries of a rotor or stator; it is in these very regions that radial-flow distributions can give the most unexpected trouble and produce effects that will alter completely the conclusions based on an analysis of the flow beyond the blade boundaries. This fact is evident from the previously cited work of Hamrick, Ginsburg, and Osborn⁸ in which it was shown that at low flow conditions air could not flow through a particular impeller without the formation of eddies or flow separation. That the exact three-dimensional flow field does not differ markedly from that indicated by combining such a two-dimensional axial-symmetric solution with the corresponding two-dimensional blade-to-blade solution has been shown by Stanitz.¹⁰ One important indication from his work is that the distribution of losses, or entropy gradients, has a greater effect on the actual flow field than the assumption that the three-dimensional flow field is accurately depicted by combining 2 two-dimensional solutions.

Inasmuch as the labor involved for obtaining the solutions presented in the subject paper is by no means negligible, a compressor designer may very well wonder whether or not this work is worth doing. Even greater skepticism may be expressed about extending the analysis to include the flow within the blade passages. In some instances, this question can be answered by comparing the solution obtained by neglecting completely radial equilibrium with that obtained by the technique used for getting the first approximation in the subject paper. The difference between the flow angle, velocity, and Mach number at a given radius obtained from the two solutions will indicate whether or not additional refinements are necessary. When the vorticity is high, when the Mach number of the flow is at a high subsonic level, or when the curvature of the passage boundaries is large, however, the previously discussed approaches to the three-dimensional problem must be carried out in detail if high-performance turbomachinery is to be designed. If such analysis is not done, disappointing performance in the final design may be erroneously attributed to an unsympathetic boundary layer or unknown Reynolds-number effects.

⁸ "Method of Analysis for Compressible Flow Through Mixed-Flow Centrifugal Impellers of Arbitrary Design," by J. T. Hamrick, A. Ginsburg, and W. M. Osborn, NACA Technical Note No. 2165, August, 1950.

⁹ "General Through-Flow Theory of Fluid Flow With Subsonic or Supersonic-Velocity in Turbomachines of Arbitrary Hub and Casing Shapes," by C. H. Wu, NACA Technical Note 2302, March, 1951.

¹⁰ "Comparison of Two- and Three-Dimensional Potential Flow Solutions in a Rotating Impeller Passage," by John D. Stanitz, NACA Technical Note 2806, 1952.

WALTER DOLL,¹¹ In the design of axial compressors for use in aircraft gas-turbine power plants it is always desirable to obtain a maximum amount of performance for a minimum amount of size and weight. To do this properly requires an intimate knowledge of blading operating limitations and a reasonably accurate flow-pattern design procedure to optimize performance and size within these limitations.

To be of practical value to the designing engineer, a flow-pattern system, such as presented in the paper, should satisfy several requirements. (a) It should account for the fluid motion in a reasonably accurate manner. (b) The equations and solutions should be expressed in such a form that the designer can see readily the relative significance of variables at his disposal. (c) It must be possible to solve the relations quickly, since many solutions are necessary for the study and design of a single basic compressor. Many compressors may be studied for a single power-plant design.

The present paper appears to be an improvement over the available literature, at least relative to the last two requirements. Experience indicates that the first-approximation procedure presented in the paper should be sufficiently accurate for most stage mapping and optimizing studies. If the radial distributions of work and tangential velocity are prescribed in some systematic manner which permits integration of the equations, then the system can be put on digital computing machines and a large number of designs computed in a very short time. Evaluation of the results in terms of available blading-limit data will then produce an optimized design system of ready use for the designer. It should be possible to handle a majority of the cases of interest by this procedure.

There is a need for a second-approximation system. The actual flow patterns in low hub/tip ratio stages of strong nonvortex design differ from the first-approximation solutions in the direction of the second-approximation corrections presented in the paper. While this difference does not greatly affect the estimated flow and pressure-ratio values of the stage design point, it may be of concern in the optimum assignment and use of blading limits, particularly relative to off-design and multistage operation. A corrective system probably will be of use only in the first two or three stages. In the higher hub/tip ratio stages, the flow will be more influenced by the "real" flow effects of blade end clearances, casing-wall boundary layers, and cumulative deviations from initial design assumptions.

It would be desirable to have an analytical procedure for applying the second approximation. Graphical methods are slow and not always very consistent. Also, it would seem that the correction system should recognize the blade aspect ratio, or ratio of blade length to chord. It is logical to believe that the stream curvature between blade rows can be different for large differences in aspect ratio, depending upon how well the flow is stabilized within each blade row, how large the axial clearances may be, and how much succeeding rows may overlap due to radial chordal taper.

The authors should be encouraged to try their skill next on extension of the present work to the problem of optimizing stage design for off-design operation. This might be stated as asking for a design flow-pattern distribution which will not change shape appreciably when operated at lower or higher velocity ratios. Or the question might be how to minimize blade-incidence changes in the critical loading regions of rotor tip and stator root. Final accounting for off-design characteristics will require the ability to handle radial variations in entropy (as related to losses) and work (as related to blade turning-angle variations with incidence, particularly when stalled).

¹¹ Technical and Research Engineer, Pratt & Whitney Aircraft, East Hartford, Conn.

K. E. FRANSSON.¹² This paper is an important contribution to the technical literature in the field of axial-flow turbomachines. The authors have spared no effort to explain their mathematical work in terms of the physics involved; their illustrative diagrams are particularly good.

For the design of most axial-flow machinery, the use of simplified equations such as Equations [25] and [27] of the paper will result in sufficient accuracy. In the solution of these equations, the writer has found it convenient to resort, with good accuracy, to a substitution function of the form

$$R' = K - \frac{b_2 r}{b_1 + b_2 r}$$

in which b_1 , b_2 , and K are constants used to set the tangential velocity and its rate of variation radially. This permits rapid analytical consideration of several velocity distributions.

In addition to the moderate radial displacement of streamlines in an axial-flow machine under the influence of a centrifugal field, there is of course the gross displacement of those streamlines due to local leakage and changes in circulation, particularly at blade ends. The over-all effects of these shifts on performance are known in a general way. Experimental engineers have noticed the rapid changes in load which occur on single-stage turbine and compressor test rigs when the flow breaks away and then re-establishes itself at the root of the rotating blades. cursory analytical treatment of these local shifts indicates that the curvature of the streamlines around local disturbances is several times that which one would calculate from the influence of the centrifugal field alone. Until our knowledge of these end effects is more complete than is indicated by the technical literature at the present time, it is questionable whether the second approximation indicated by the solution of Equations [21] and [23] of the paper is worth while.

The object of the calculation of these nonvortex patterns at design is the minimization in compressors of Mach-number losses at rotor tips and stator roots. However, it must be recognized that, except in special cases, undesirable rotational components are thereby introduced into the flow. In turbines designed for solid rotation, these losses account for 2 to 3 per cent of stage losses, by calculation. The methods outlined in the paper provide an analytical tool for the evaluation of such losses.

J. W. MCBRIDE.¹³ This paper should be a substantial contribution to a better appreciation of the importance of radial-flow considerations in the practical performance design of axial-flow turbomachinery. The authors' approach of developing the analysis from a simplified, yet basically accurate, flow-pattern model through illustrative design examples is of particular interest and value. It is unfortunate that this approach was not rounded out by inclusion of comparisons between measured flow distributions and those predicted by their method.

Except as it contributes to improved understanding of the problem, the practical value of improving the simple linearized radial-equilibrium solution by inclusion of the radial displacement of the flow appears questionable. The writer's experience indicates that the real fluid effects, especially those at the walls, those of clearances, and so on, are more important than the usual second-order corrections in establishing the flow-distribution patterns. It was found that the velocity distributions predicted by the simple radial-equilibrium solution are in better agreement with test than those predicted by the improved approximations.

However, these tests showed that the effect of radial displacements of the streamlines was not negligible, but rather, that effects could not be reliably accounted for by analytical methods. It was found that the chordwise load distribution of the blading and the casing boundary-layer growth were important factors in establishing this radial displacement which was, accordingly, dependent upon the compressor operating condition. In addition, the assumption of axisymmetry, although correct on the average, required local consideration as W_φ was found to vary by as much as ± 20 per cent from its mean value across a pitch spacing. Consequently, this phenomenon also played an important role in establishing the blading flow pattern.

These findings were based on comparison between a set of carefully controlled tests with the predicted velocity distributions from progressively improved solutions of the equation

$$W_r \frac{\partial W_r}{\partial r} + \frac{W_\varphi}{r} \frac{\partial W_r}{\partial \varphi} + W_z \frac{\partial W_r}{\partial z} - \frac{(\omega r + W_\varphi)^2}{r} + \frac{1}{\rho} \frac{\partial p}{\partial r} = L_r$$

where L_r and $\partial p/\partial r$ express the radial distribution of loss. This equation for the relative velocities in rotating cylindrical polar co-ordinates is identical with the authors' Equations [25] and [27] for their assumptions of isentropic steady flow with no body forces.

The findings lead to the development of a system which takes simple radial-equilibrium solution for its starting point and adds empirical corrections to consider the blading-type, profile characteristics, aspect ratio, aerodynamic operating conditions, losses, and so on. It should be pointed out, however, that the improved radial-equilibrium solutions are invaluable, even though quantitatively questionable, in establishing the form to be adopted for the empirical corrections and to guide test programs.

The computation time required by the authors' approach is considered somewhat excessive for many industrial-design problems. Other solutions using hand calculation machines now require approximately 4 man-hours to establish the blading at the design point, with approximately 12 additional man-hours for each "off-design" operating point. These solutions are carried out by non-professional computers using tabular forms and require only minimum supervision from the engineers. Efforts are now under way to improve these required times through use of commercially available computing equipment. In this way we believe that it will be possible to reduce the cost and time of such calculations to the point where they can become a matter of routine design practice.

Adaptation of machine computation reduces the desirability of expressing the radial-equilibrium solutions in a normal co-ordinate system, as has been done by the authors, apparently to facilitate graphical solutions. Further, machine calculation, by virtually eliminating the disadvantages of heavy calculation programs, permits increasingly refined procedures.

We should like to point out that perhaps the principal design advantage of equilibrium flow-type axial turbomachinery blading appears to us to lie in the possibility of using it to establish optimum stage designs on sound aerodynamic bases, which may include such specific conditions as are desirable from performance, operating range, work capacity, and other similar requirements.

We have found, however, that these conditions at the "design" point can be established only after careful consideration of their influence on "off-design" operation since these latter usually establish whether or not a machine is satisfactory.

R. W. PINNES.¹⁴ The current analysis is limited to the open spaces between the blade rows. It is believed that, to obtain optimum performance, the analysis will eventually have to be

¹² Chief Design Analysis, Pratt & Whitney Aircraft, East Hartford, Conn. Mem. ASME.

¹³ Chief, Aero-Thermodynamic Research, Carrier Corporation, Syracuse, N. Y.

¹⁴ Head, Power Plant Research and Analysis Section, Bureau of Aeronautics, Washington, D. C. Mem. ASME.

carried through the blade rows, with proper consideration of blade effects. One of the difficulties with the current method is believed to be in establishing the radii of curvature of the streamlines accurately. Having attempted to work with radius of curvature, the writer is convinced that it is extremely difficult to get accurate and consistent values, even with more complete streamline data. It has been proposed that a sinusoidal curve be assumed between the radial points established between the blade rows. Although this is a reasonable assumption in the absence of any more accurate data, any such assumption introduces an element of uncertainty in the analysis. It also should be noted, in this regard, that different chordwise distributions of blade loading, and different radial blade forces (i.e., the degree of non-radiality of the blade elements) would change radius-of-curvature values, and consequently, in an ultimate analysis, would have to be given consideration.

It would appear that the authors have tended to understate the importance of these curvature effects. In several places in the paper it is stressed that these effects are "small." Although this is generally true, there are places where these effects are quite significant. In the first example presented in the paper, the meridional velocity at the hub, at station 4, is changed by about 20 per cent, as shown in Fig. 19. As would be expected, these effects tend to be greatest where the peripheral-velocity components are smallest, i.e., at the rotor hub for the velocity distribution assumed in the example.

Also, in the second example presented in the paper, it is again stated that these effects are small. A figure of 2 per cent difference is quoted for a ratio of stage length to hub radius (L/r_h) of 1.8, and 5 per cent for a ratio of 1.5. It should be noted that these L/r_h ratios are not representative of current practice. Values of L/r_h of 1.0, and smaller, are believed to be more representative, even for inlet stages of low hub-tip ratios. Extrapolating the data given, differences of 10 per cent, and greater, can be expected for more realistic values of L/r_h . In any event, the significance of the parameter L/r_h is not understood. It would appear that an aspect-ratio factor, $L/(r_o - r_h)$, would be the significant parameter.

It is believed that the authors have made an important contribution in further demonstrating the importance of balanced flows other than free-vortex flow, and in presenting a practical method of analyzing such flows. The additional flexibility which these flows make available to the designer of turbomachinery to help obtain a specific design objective is demonstrated clearly. It is hoped that the authors will continue their work toward a rigorous attack on the truly three-dimensional flow problem in turbomachinery."

C. H. Wu.¹⁵ The authors are to be congratulated on this interesting paper. The solutions are obtained in a realistic manner taking into account large flow deflection and large departures from free-vortex flow. The writer would like to make a few comments on this general problem of three-dimensional flow in turbomachines.

The first comment concerns the names H and I , which are of general interest in the field of turbomachinery. As regards H , since it is the sum of sensible internal energy u , the product of pressure and volume pv , and the kinetic energy $V^2/2g$; and since the product pv is not an energy contained in a moving substance, and is merely a product of two properties in a stationary substance, it is not quite appropriate to call H total energy. As regards I , although the combination of $(h + W^2/2g - \omega^2 r^2/2g)$ or its equivalent $(H - UV_\theta/g)$ appeared often in literature of turbomachines, no short name for it has been given. From the

first combination it is seen that not only the relative flow but also the idea of change of radial position of a fluid particle in a rotating passage is involved. Since I has the same basic importance in the description of flow in a rotating blade row as H in a stationary blade row, turbomachine engineers should give it an appropriate short name. For instance, we may call $(h - \omega^2 r^2/2g)$ "rothalpy" and its combination with $W^2/2g$ "total rothalpy."

It seems rather difficult to draw streamlines passing through points determined only in the gaps between blade rows, and to obtain the radius of curvature from them; also to draw a line normal to these streamlines and to obtain the variation of several quantities along this line. In the case of a multistage machine having a variable hub or casing radius, the normal line starting in the gap may even extend into the blades, in which region a few more equations would be required to solve the problem. For a single-stage compressor of a type similar to the authors', detailed computations¹⁶ made for incompressible and compressible flows show that the meridional streamlines in the blade regions follow closely simple sine curves. In these and similar cases, then, it seems that it would be more convenient to calculate the effect of the radial flow analytically by assuming simple sine equations for the streamline shape and to proceed the computation along a radial line in the gap, see Bibliography (3) of the paper. In another case of an axial-flow gas turbine, detailed computations¹⁷ show that the streamlines have quite complicated shapes, and that the compressibility of gas and radial twist of the blades have equally important and opposite effects on the shape of the streamlines. In these and similar cases, a check of the simple solution is very desirable.

It should be noted that when solution is obtained by the method of successive approximations, it is necessary, at least in a typical case, to proceed sufficiently far enough to ascertain the convergence of the solution. For example, even if the difference between the first and second approximation may be small (Figs. 19 and 20 of the paper seem to indicate that the difference is not quite small) the second approximation could still be not close to the exact value. The first approximate solution of the authors' is the same as the usual method based on "simple radial equilibrium." Results obtained in Bibliography (3) of the paper and in references 16 and 17, cited in this discussion, show that the radial displacements across the blade so determined are many times greater than the actual value. In Bibliography (3) of the paper, an approximate equation for the radial displacement of the streamline across the blade is obtained to speed up the successive corrections.

Because of the difficulty in solving the three-dimensional problem, Lorenz simplifies the problem to the flow along a given surface by considering extremely thin buckets arranged extremely close together. This idea of flow along a surface is often overlooked when one interprets Lorenz's equations by a strictly mathematical axial-symmetric approximation. Stodola¹⁸ tries to avoid the misunderstanding about the Lorenz equations by a new derivation of the equations and points out that "the derivatives of the pressure refer really to the change in the direction of the jet surface." This is also why, in the inverse or design prob-

¹⁵ "A General Theory of Three-Dimensional Flow With Subsonic and Supersonic Velocity in Turbomachines Having Arbitrary Hub and Casing Shapes," by C. H. Wu, ASME Paper No. 50-A-79, Part II, or "Subsonic Flow of Air Through a Single-Stage and a Seven-Stage Compressor," by C. H. Wu, to be published as a Technical Note by NACA.

¹⁷ "Matrix and Relaxation Solutions That Determine Subsonic Through Flow in an Axial-Flow Gas Turbine," by C. H. Wu, NACA TN, 2750, July, 1952.

¹⁸ "Steam and Gas Turbines With a Supplement on the Prospects of the Thermal Prime Mover," by A. Stodola, McGraw-Hill Book Company, vol. 2, 1927, pp. 990-991.

¹⁶ Professor of Mechanical Engineering, Polytechnic Institute of Brooklyn, Brooklyn, N. Y.

lem, the integrability condition for the stream surface (as first pointed out by Bauersfeld) is necessary.

When the blades are not close together, one can still follow a mean stream surface which divides the mass flow in the channel formed by two adjacent blades. The form of the mathematical equations thus obtained is the same as that with the assumption of the axial symmetry, but all the derivatives now refer to the changes of fluid properties on the mean stream surface. In the direct problem, the shape of the mean stream surface, as a first approximation, may be assumed to be that of the mean camber surface of the blade. In the design problem, the shape of the mean stream surface is computed after all the velocity components are obtained.¹⁸

This approach not only permits a more realistic physical interpretation of the solution, but also avoids many difficulties involved in the assumption of axial symmetry. For instance, in the case of widely spaced blades, what are the meanings of the blade-force term and of the values obtained from the axially symmetric solution? Further serious difficulties are encountered on the vorticity components. With the assumption of axial symmetry, the radial and axial components of the absolute vorticity become $-\partial V_\theta/\partial z$ and $r^{-1} \partial(V_\theta r)/\partial r$, respectively. The first component is now not equal to zero even in free-vortex blading; whereas in the actual three-dimensional flow $-\partial V_\theta/\partial V_z$ is canceled by $r^{-1} \partial V_z/\partial \theta$. Similarly, both vorticity components under this assumption would not equal zero in the blade regions of inlet guide vanes designed for variable circulation, although the flow is everywhere irrotational up to the trailing edge of the blades.

AUTHORS' CLOSURE

The authors wish to thank all discussers sincerely for their constructive contributions. It is indeed heartening to find so many interesting comments on the subject paper. Taken as a whole, the discussions represent a cross section of contemporary thinking on the subject and, therefore, are distinct contributions in themselves.

No attempt will be made here to answer the discussions individually or in full detail since it is believed that there is general agreement on the basic concepts involved. Concerning the question of methods to be used and number of approximations to be made, it is noted that some of the discussions answer each other. However, some final comments will be made.

It is interesting that some of the discussers think the second approximation should be made more rigorous by including flow details inside the blade rows and more accurate curvature measurements, while others think the second approximation is unnecessary. The authors feel that the first approximation is accurate enough for the selection of over-all characteristics for the machine, but that the detailed flow analysis which must be made when designing blade shapes should include the second approximation, and indeed, the effects of secondary flow as well.

The practical difficulty of finding the radius of curvature of the meridional streamlines, and, more generally, of differentiating any graphically or numerically given function, is of course well recognized by the authors. To overcome this difficulty it seems essential to make use in some form or other of the continuity of the functions involved, in the present case of the continuity of first and (perhaps) second derivatives of the streamlines along as well as across the meridional flow picture. This consideration emphasizes the question of the effect of the vanes raised by several discussers. It is indeed an unanswered question whether the first and second derivatives of the meridional streamlines in this

axially symmetrical solution should be continuous across the vane edges. For axial compressors the authors feel that the blade effects will be small with blades of high-aspect ratio, because in this case the "bound" vane-vortex-lines are very nearly radial so that the vane vorticity has little or no effect on the meridional flow.

Also well recognized are the advantages of numerical methods using modern calculating machines. By comparison, graphical methods may appear outdated. This is believed to be entirely true only in relatively well-established fields of analysis. In other cases where the nature of the results and, indeed, the existence of a solution is not known from previous experience, it is felt that graphical methods offer greater safety against the possibility of mistakes. With graphical procedures that are close to the physical phenomena analyzed one sees the mistakes when made. Furthermore, it is possible that the convergence of the solutions sought here can be assured in marginal cases better by drawing the solutions with careful consideration of all facts known about the flow to be investigated.

Apparently there has been some misunderstanding about the time required to use the design method suggested in the paper. The 500 man-hours mentioned should not be interpreted as being only the time necessary for finding the flow distributions shown, but rather the over-all amount of time spent on the problems, including time spent on the evolution of the method itself. Since the writing of the paper, one of the authors has used the method to design a stage consisting of three blade rows. After the general design characteristics were specified, it took only 24 man-hours to find the velocity distributions for all three rows, including both approximations. The work was done graphically with six radial points being taken for each row.

Perhaps the most serious objection to the design method outlined in this paper is centered around the simplifying assumption of axial symmetry. The justification for this assumption is based on the reasoning that as the number of blades in a row is increased in such a way as to keep the total circulation constant, the flow picture obtained approaches the axisymmetric solution in the same sense that any function broken up into a discrete number of steps approaches a smooth curve as the number of steps is increased. Hence, the terms "axisymmetric solution" and "infinite number of blades solution" are often used interchangeably. Carrying the analogy of the stepped function further, we see that, when taking a derivative of a stepped function, we get zero for the trends and infinity for the risers regardless of how many steps we have, so long as we have a finite number. The derivative of the curve which the stepped function approaches is finite, however. So it is with the flow through inlet-guide vanes. The vorticity (which is analogous to a derivative) is zero in between the vanes and infinite on the vanes and on the vortex sheets that trail from the vanes. When we go to the limit of an infinite number of vanes (from the stepped function to the smooth curve), the vorticity becomes finite and continuous. The physical justification for this is the fact that we are primarily interested in the velocity and not the vorticity, i.e., in the function and not the derivative. If the number of vanes is small, then the assumption of axial symmetry is indeed questionable and should certainly be checked experimentally. The elucidation of a different method of approach more adaptable to widely spaced vanes, such as that suggested by Dr. Wu, would indeed be welcome. The authors believe that the investigation of three-dimensional effects should be given priority over further refinements of axially symmetrical solutions and, indeed, over such interesting subjects as off-design conditions.

THE [illegible]

[illegible]

[illegible]

[illegible]

[illegible]

[illegible]

[illegible]

[illegible]

[illegible]

[illegible]

[illegible]

[illegible]

[illegible]

[illegible]

[illegible]

[illegible]

[illegible]

[illegible]

[illegible]

[illegible]

[illegible]

[illegible]

[illegible]

[illegible]

[illegible]

[illegible]

[illegible]

[illegible]

[illegible]

[illegible]

[illegible]

[illegible]

[illegible]

[illegible]

[illegible]

[illegible]

[illegible]

[illegible]

[illegible]

[illegible]

[illegible]

[illegible]

[illegible]

[illegible]

[illegible]

[illegible]

[illegible]

[illegible]

[illegible]

[illegible]

[illegible]

[illegible]

[illegible]

[illegible]

[illegible]

[illegible]

[illegible]

[illegible]

[illegible]

[illegible]

Some NACA Research on Centrifugal Compressors

By I. A. JOHNSEN¹ AND AMBROSE GINSBURG,² CLEVELAND, OHIO

This paper presents a summary of some of the results obtained in the NACA program of aerodynamic research on centrifugal compressors, including both theoretical and experimental aspects. The material presented is not intended to give specific design rules, but rather is intended to give some insight into the flow processes in centrifugal turbomachinery, to establish general trends of good design practice, and to indicate portions of the field that remain to be explored. The paper is arranged in three sections; (a) impeller research, (b) diffuser research, and (c) general aspects of application of centrifugal compressor to aircraft gas-turbine engines.

INTRODUCTION

THE basic aerodynamic requirements of compressors for aircraft power plants include high efficiency, high pressure ratio, large mass flow for a given frontal area, and a large useful operating range. In addition, it is desirable that the compressor be mechanically simple, rugged, and inexpensive to manufacture. Since the centrifugal type of compressor possesses these mechanical attributes, it is apparent that if good aerodynamic characteristics can be obtained, it will have wide application in gas-turbine power plants.

For many years the design of centrifugal compressors has been largely an art, and most of the research on this compressor type has been conducted on a rather empirical basis. With the advent of jet propulsion and gas-turbine engines, however, it became apparent that the improvement of aerodynamic characteristics of centrifugal compressors was extremely important and necessary. At that time the NACA, which had been conducting experimental research on radial and mixed-flow centrifugal compressors, became acutely aware of the lack of understanding of the flow processes in centrifugal turbomachinery. This lack of theoretical background resulted primarily from the geometric complexity of the flow passage and the inability to apply simple airfoil analogies as was the case in the axial-flow compressor. It was apparent that considerable theoretical work was required and that this work must be co-ordinated closely with experimental researches. Of necessity, the initial analyses were based on simplifying assumptions; as the program progressed, successive refinements were incorporated in the attempt to approach a complete and rigorous analysis of flow.

As a supplement to the theoretical approach, the experimental research also was accelerated. For example, since it was apparent that the key to the problem was in the rotating impeller, an experimental facility was constructed wherein actual flow measure-

ments could be made within the passages of the rotating impeller to determine flow conditions therein. This technique provided data that previously had not been available.

This paper has been prepared to point out some of the pertinent information acquired in the NACA program of experimental and theoretical research. The material presented is not expected to give specific design rules, but rather is intended to give some insight into the flow processes in centrifugal compressors, to establish general trends of good design practice, and to indicate portions of the field that remain to be explored.

IMPELLER RESEARCH

Compression in a centrifugal compressor is accomplished by increasing the moment of momentum of the air by means of (a) an increase in angular velocity of the air about the impeller axis, and (b) an increase in radius of rotation of the air as it flows through the impeller. The increase in angular velocity of the air is sometimes called the inducer function, and the increase in radius of rotation is called the impeller function. These two actions in a centrifugal impeller may occur separately, but, in general, are partly or completely overlapping. However, as a matter of convenience, the two functions will be discussed separately in this paper.

Inducer Function

Efficiency Consideration. The inducer function of imparting angular velocity to the entering air may cause large direct losses; and disturbances of flow in the inducer may affect the functioning of all other compressor components, thereby creating indirect losses. The inducer is generally regarded as the most critical component of centrifugal compressors; this is a result of the following unfavorable conditions that generally exist in inducers:

- 1 High turning. The inducer is required to turn the air (relative to the impeller) through a large angle in a short distance.
- 2 High loading. The number of blades used to accomplish this high turning is limited by aerodynamic and mechanical considerations; as a result, individual blade loadings are high.
- 3 High Mach numbers. The relative Mach numbers are high near the inlet tip of the inducer blades.

A one-dimensional analysis of losses in inducers (1)³ has indicated that large losses can occur when the inducer operates at off-design angles of attack. The analysis further indicated that the losses for negative angles of attack (high weight flow) can be expected to be considerably more serious than for positive angles of attack (low weight flow).

These general trends were verified in tests of a 48-in-diam radial-flow impeller, Fig. 1, that was instrumented to provide internal measurements of static and total pressure (2, 3). This study showed that the condition existing across the impeller inlet is a predominant factor in the over-all performance of the compressor. For example, at maximum flow, Fig. 2, the measured total pressure along the driving face of the impeller drops off very rapidly in this entrance region; this lost energy is never wholly

³ Numbers in parentheses refer to the Bibliography at the end of the paper.

¹ Chief, Compressor Research Branch, Lewis Flight Propulsion Laboratory, National Advisory Committee for Aeronautics.

² Chief, Turbine Aerodynamics Branch, Lewis Flight Propulsion Laboratory, National Advisory Committee for Aeronautics.

Contributed by the Hydraulic and Gas Turbine Power Divisions and presented at the Annual Meeting, New York, N. Y., November 30—December 5, 1952, of THE AMERICAN SOCIETY OF MECHANICAL ENGINEERS.

NOTE: Statements and opinions advanced in papers are to be understood as individual expressions of their authors and not those of the Society. Manuscript received at ASME Headquarters, October 31, 1952. Paper No. 52-A-131.



FIG. 1 48-IN-DIAM RADIAL-FLOW IMPELLER

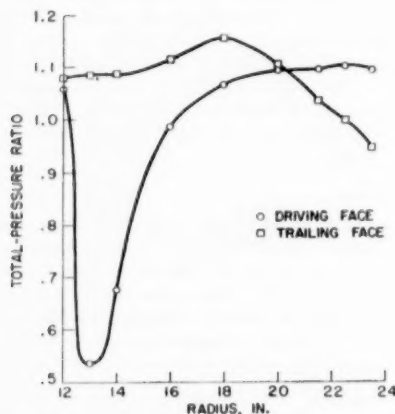


FIG. 2 TOTAL-PRESSURE DISTRIBUTION ALONG BLADE FACES OF 48-IN. IMPELLER AT MAXIMUM FLOW

recovered and results in low over-all efficiency. This condition is the result of the fact that the large negative angle of attack has caused a separation on the driving face of the blade at entrance. This effect is reduced as the mass flow is reduced. At low flows the losses were again in evidence, this time on the trailing face, and as predicted, were considerably less than those at high flows. Peak efficiency operation was found to occur at 0 deg angle of attack (considering available flow area as equal to that of the annulus minus area taken up by the blades). These general results indicate that improved operation could be realized if blade leading edges could be designed for more efficient accommodation of the inlet-flow variation.

Mass Flow Considerations. In addition to reducing efficiency, this entrance condition also provides a possible limitation on the mass flow that a compressor can pass. The theoretical analysis of flow in inducers (1) indicated that a minimum "effective" flow area exists in the inlet as a result of the separation that occurs when the angle of attack becomes negative; that is, a throat is formed as a result of the separation. This throat moves down-

stream if the flow is increased further. The maximum weight flow depends on the area and efficiency of flow at the critical radius in the impeller; both area and efficiency are adversely affected by the leading-edge separation.

This inlet-choking phenomenon has been shown experimentally for a mixed-flow compressor (4). In this study, the outside diameter of the impeller was successively cut down from 12.0 in. to 10.76 and 9.52 in. and the impeller was operated at higher rotational speeds to maintain the same impeller tip speeds. Fig. 3 shows these impeller-diameter revisions on an axial-plane section of the impeller. Fig. 4, a plot of maximum volume flow against impeller angular velocity, shows that the maximum flow varies

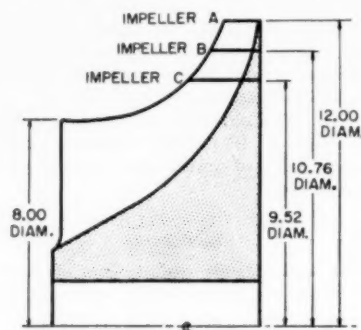


FIG. 3 IMPELLER DIAMETER REVISIONS

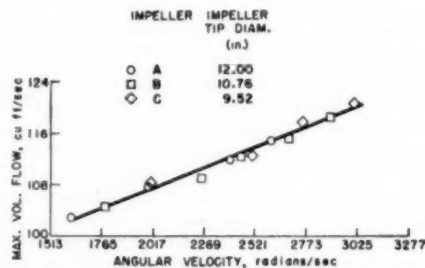


FIG. 4 CORRELATION OF MAXIMUM VOLUME FLOW OF IMPELLERS WITH IMPELLER ANGULAR VELOCITY

linearly with impeller angular velocity. This indicates that the conditions of sonic velocity in the compressor system occurred in the inducer section.

In Fig. 5 the blade-inlet angle of attack is plotted against Mach number relative to the blade inlet at a root-mean-square blade diameter. For the three impellers, A, B, and C, values of static-pressure-ratio index are plotted as contours. This index is a ratio of the minimum static pressure measured along the stationary impeller shroud to the static pressure at the impeller-blade inlet; in all cases this critical pressure drop occurred in the inducer section. The heavy solid line represents the maximum-volume-flow line for the range of impeller speeds tested; it is seen to present a linear relation between the maximum negative blade-inlet angle of attack and blade-inlet relative Mach number. A critical value of static-pressure-ratio index of approximately 0.50 existed for each of the impellers. Again, these data indicate that the compressor-flow restriction resulted from a critical pressure drop in the inducer section of the impeller.

Separate Component Investigation. On the basis that inducer performance is extremely important, inasmuch as it affects efficiency, pressure ratio, and mass flow of the compressor, the NACA

conducted a program of study of inducers. A family of inducers was designed and constructed and tested as separate components (5, 6). These inducers were designed for lower blade loading and more gradual angular acceleration than the "bent-bucket" entrances of the conventional centrifugal impellers that were in ex-

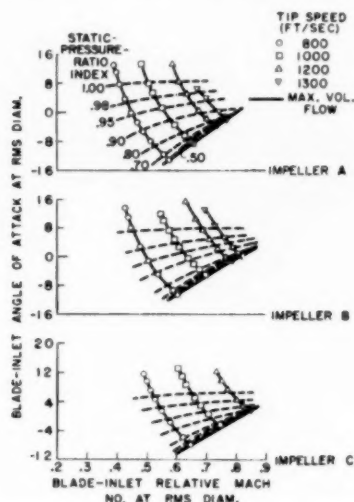


FIG. 5 RELATION OF MAXIMUM VOLUME FLOW OF IMPELLERS WITH INLET ANGLE OF ATTACK, INLET RELATIVE MACH NUMBER, AND STATIC-PRESSURE DROP ALONG STATIONARY SHROUD

istence at that time. It was felt that short-radius circular-arc bending imposed air loadings that were beyond expected possibilities for efficient flow and also prevented the blades from being set at the optimum angle to the air stream along the entire leading edge. Therefore single-stage deep inducers were designed for constant angular acceleration over the axial depth. This design basis gives a profile which, developed on a plane, is a parabola. The inducers had the same design entrance conditions but with axial depths of 4, 3, and 2 in.; the 4-in. inducer was tested with 24 and 12 blades.

A typical inducer of this series is shown in Fig. 6. This study effectively provided an evaluation of the effect of blade loading on inducer performance for the constant-acceleration case. In the absence of an adequate theory of inducer functioning, separate component ratings were made on the basis of temperature-rise efficiency and approach to solid-body rotation of the discharge air. The inducers had separate component efficiencies of the order of 80 per cent, with the inducer with minimum loading (4 in., 24 blades) the best from the point of view of approach to wheel rotation and adiabatic efficiency. The results also showed that the entrance loss was the major determinant of inducer efficiency; as in the case of the radial inlet impeller, large losses resulted from off angles of attack. The desirability of efficient accommodation of inlet-flow variations was verified by the fact that rounding the entrance edges of the blades (from an as-machined condition) resulted in a 7-point increase in efficiency.

In order to establish the relative performance level of bent-bucket inducers, the inducer section from a conventional impeller also was studied as a separate component. The efficiency of this inducer section was found to be very low in the operating range of the impeller of which it was a part, indicating that the application of the parabolic-inducer idea would result in significant improvements in centrifugal-compressor performance. Parabolic inducers were applied throughout the aircraft-engine

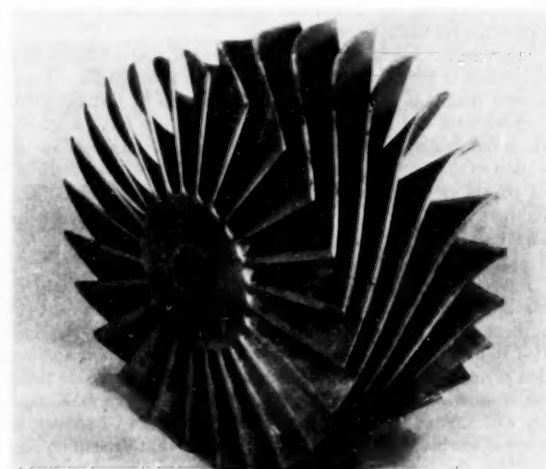


FIG. 6 INDUCER OF CONSTANT ANGULAR ACCELERATION FAMILY

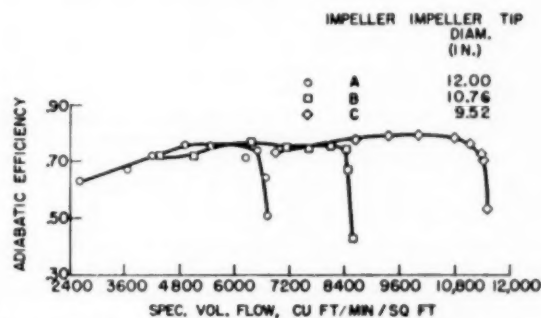


FIG. 7 PERFORMANCE OF IMPELLERS A, B, AND C AT IMPELLER TIP SPEED OF 1200 FT PER SEC

industry with good results. As an example, the change from a bent-bucket circular-arc inducer to a parabolic (constant-acceleration) inducer in a large centrifugal compressor investigated at the NACA resulted in a 7-point increase in peak impeller efficiency at all speeds, and an increase of 13.6 per cent in peak impeller-total-pressure ratio at design speed.

Investigation of Division of Work. The success of inducers in which the tangential acceleration was distributed over large path length raised a question as to how far the inducer function should be carried in an impeller. It was to study the effects of changing the proportion of total energy addition between the inducer function and the impeller function, that the impeller previously referred to (Fig. 3 and reference 4), was cut down progressively in diameter and operated at faster rotative speeds in order to maintain the same tip speed. The inducer was a constant-acceleration design similar to those previously described. In the 12.00-in-diam impeller, 22 per cent of the total energy ideally would be due to the angular acceleration; for the 10.76-in-diam impeller, 27 per cent of the work; and for the 9.52-in-diam impeller, 35 per cent of the work. The remainder, in each case, resulted from the increase in radius of rotation.

Fig. 7 shows the adiabatic efficiency of the compressor at a tip speed of 1200 ft per sec. As would be expected from the point of view that the impeller inlet operates over a fixed range of angles of attack, the maximum specific volume flow increased with the increase in rotative speed while the volume flow range remained

essentially constant. Maximum efficiency increased from 0.75 to 0.79 as the tip diameter was reduced.

The results of this investigation indicated that adding a large proportion of the total energy in the inducer is beneficial. It also showed that high relative Mach numbers can be utilized at the inlet without any serious consequences; in this case, a relative Mach number at the inducer tip of 1.03 was reached. With operation in the transonic range at the impeller inlet, any detrimental effects on impeller performance resulting from high Mach numbers appear small as compared to the desirable effects that are obtained by increasing the proportion of the total energy that is added in the inducer.

Investigation of Blade Curvature. Up to this point only the parabolic type of inducer had been investigated. As a next step in the inducer program, an experimental investigation was initiated to investigate the effect of various rates of angular acceleration (7). Three impellers were used which had the same design characteristics except for the curvature of the inducer blades. In line with the results of the "division of work" study, however, the scope of the investigation was not limited to that type of impeller in which the angular velocity of the air is accelerated to the angular velocity of the impeller before any appreciable compression by centrifugal force is allowed. In this type of impeller the blade loading is suddenly reduced at the end of the inducer section, which may cause irretrievable pressure losses and flow separation. (The discontinuity in blade force that theoretically exists at the junction of inducer and impeller blade elements is treated, in reference 8.) Therefore, in these research impellers, the blade curvature was distributed throughout the entire depth of the impeller; at each point in the impeller, angular and Coriolis accelerations were imparted simultaneously to the air.

The three impellers tested, which had blade shape as the only variable, had the following blade curvatures, Fig. 8:

1 Impeller D—Parabolic blade curvature. As in the inducers discussed previously, this design provided that a particle following the blade with constant axial component of velocity would have a constant acceleration.

2 Impeller E—Elliptical blade curvature. This impeller added rotation at a higher rate at the entrance than impeller D, with a constantly decreasing rate through the impeller.

3 Impeller F—Circular blade curvature. This impeller added rotation at the entrance at a higher rate than either impellers D or E.

Results of this investigation indicated that, in general, the impeller with parabolic curvature (impeller D) was most desirable,

particularly for high-pressure-ratio application. Fig. 9 shows the comparative performance of these three impellers at a constant pressure ratio of 2.60.

The maximum rate of angular acceleration of the air increased in the order D, E, F. From the point of view of efficiency, impellers D and E were superior, indicating that high acceleration rates are to be avoided. The range at constant pressure ratio increased with decreasing rate of curvature at the inlet, with impeller D being the best. The maximum specific volume flow (choked flow), however, increased with increasing severity of curvature, Fig. 10. Analysis of the phenomenon showed that in impeller D, which had the lowest maximum flow, the limitation was a choking in the inducer (9). It was found in this analysis that a more rapid rate of curvature at the inlet, such as existed in impeller E, reduces the relative velocities and thereby delays choking. The selection of blade curvature from the mass-flow point of view, therefore, depends on whether large range or large maximum flow is desired.

An alteration to the elliptically bladed impeller E was made to

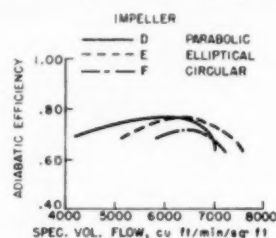


FIG. 9 COMPARISON OF THREE IMPELLERS AT CONSTANT PRESSURE RATIO OF 2.60

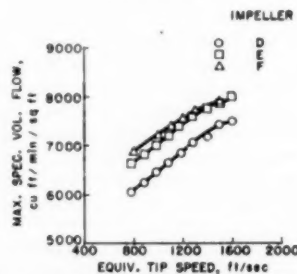


FIG. 10 COMPARISON OF MAXIMUM SPECIFIC VOLUME FLOW OF THREE IMPELLERS

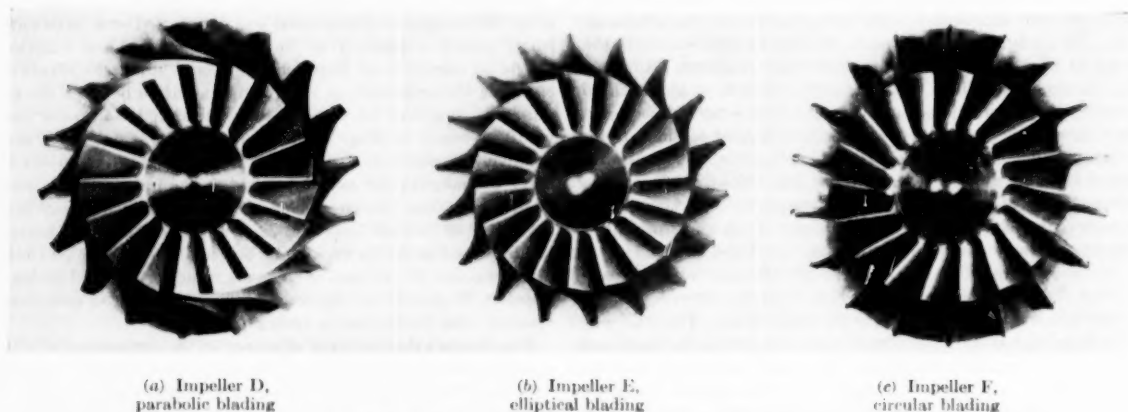


FIG. 8 IMPELLERS FOR BLADE-CURVATURE INVESTIGATION

increase still further the mass-flow capacity. Alternate blades were cut back for one fourth the axial depth of the impeller, Fig. 11, thus increasing the entrance area and also the blade loading in the entrance region. Fig. 12 shows the effect of this alteration on range and maximum volume flow capacity. The alteration more than tripled the range and the maximum flow was increased from 8000 to 9100 cfm per sq ft. With fewer blades and increased entrance area, the inducer not only was able to accommodate more flow, but also was able to operate over a greater range of inlet angles of attack.

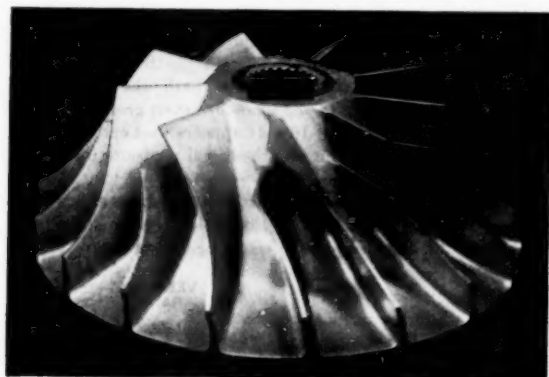


FIG. 11 ALTERATION TO ELLIPTICALLY BLADED IMPELLER E

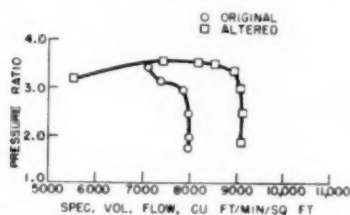


FIG. 12 IMPROVEMENT IN IMPELLER FLOW CAPACITY OF IMPELLER E

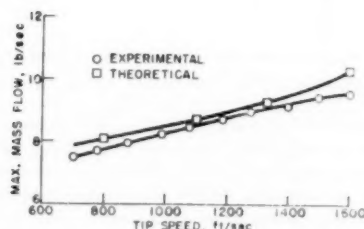


FIG. 13 COMPARISON OF PREDICTED AND ACTUAL MAXIMUM MASS FLOWS OF IMPELLER D

Analysis of Inducer Flow Conditions. Of significance to the designer is the fact that these values of maximum flow can be predicted by theoretical methods developed for analyzing compressible flow between hub and shroud of arbitrarily designed mixed-flow impellers (9). Application of this analysis method to impeller D, Fig. 8, showed that the choking flow in the inducer can be predicted with a reasonable degree of accuracy. The agreement between the predicted and actual maximum mass flow, as a function of tip speed, is shown for this impeller in Fig. 13. Viscosity effects, which are not considered in these analyses, may be the cause for the predicted flow values to be slightly higher than those actually obtained.

This analysis method is also useful in that it provides an indication of the variation of angle of attack that will exist across the leading edge of the inducer blade. For example, this analysis of impeller D showed that a nonuniform axial velocity existed at the impeller inlet, due primarily to the curvature within the impeller in the hub-to-shroud plane. Since the impeller was designed for a constant axial velocity at the inlet, this resulted in a variation in angle of attack across the leading edge. The hub-shroud contour of the passage upstream of the inlet may cause similar variations. It is obviously desirable to maintain an optimum angle of attack across the entire leading edge; design variables which may be utilized to achieve this condition include upstream channel curvatures, impeller hub and shroud curvatures, leading-edge sweep, deviation from radial blade elements, and radial variation in blade thickness. By proper design control of these variables, it is likely that desired inlet conditions can be attained.

Impeller Function

As previously pointed out, in most impeller configurations the impeller function cannot be separated from the inducer function. Therefore, this section may deal occasionally with portions of the passage in which the angular velocity of the air is being increased. In general, however, this section will consider the radial flow of the fluid after it is inside the passage, as differentiated from the discussion of the entrance condition in the previous section.

The losses in the flow channels of impellers for centrifugal compressors result from viscosity of the fluid. Simple friction losses are significant because of high relative velocities and the large amount of wetted flow surface. Boundary-layer effects may be appreciable since adverse velocity gradients of considerable magnitude usually exist along the channel walls. If these velocity gradients in the direction of flow are negative and sufficiently large, the boundary layer may separate, with attendant losses and disrupting of the potential flow. The pressure differences that exist within centrifugal-impeller channels also may create "secondary" flows. That is, when the boundary-layer flow is not in equilibrium with the pressure gradient across the channel, a flow normal to the through-flow may arise; this type of flow has been designated a secondary flow. These secondary flows alter the desired potential flow pattern and cause direct losses as a result of the partial dissipation of the energy absorbed from the through-flow to create the secondary motions.

It is apparent, therefore, that thick boundary layers should be avoided and in particular, that gradients within the channel should be controlled.

Theoretical investigations of the potential flow in centrifugal impellers will be of value in this respect if adverse velocity and pressure gradients in the direction of flow can be controlled, thereby eliminating the basic source of separation. With the present state of the art, viscosity effects cannot be considered in these theoretical flow solutions. However, theoretical techniques have been developed which consider other essential features, namely, (a) compressibility, (b) three-dimensional geometry of the channel, and (c) rotation of the channel. Using techniques of this type, impellers can be designed in which velocities do not decelerate excessively along the blade surfaces. This section will discuss some of the theoretical and experimental work that has been done along these lines.

Three-Dimensional Flow Analysis. Complete three-dimensional solutions for incompressible flow in centrifugal-impeller passages have been made, using relaxation techniques (10). This process, however, is extremely tedious and results are difficult to interpret. The significant result of this study is that, in general, the complete three-dimensional solution can be reduced validly to 2 two-dimensional solutions. It is believed that the compressible-flow problem can be handled in a similar manner; that is,

considerably simpler two-dimensional solutions can be made in (a) the meridional or hub-to-shroud plane, Fig. 14 (a), and (b) the blade-to-blade plane, Fig. 14 (b). These two-dimensional solutions describe the flow in the impeller passages. As was shown by Ruden (11), meridional-plane solutions give a good approximation of the mean flow between blades if the spacing is not too great. Blade-to-blade solutions then can be obtained for every flow surface of revolution generated by rotating a streamline in the meridional plane. The combination of these two types of two-dimensional solutions give a quasi-three-dimensional solution which is essentially the same as a complete three-dimensional solution. For convenience, therefore, this paper will consider the flow in the impeller passage in these two principal planes.

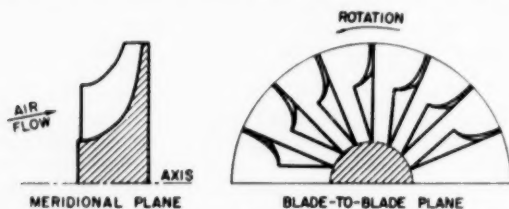


FIG. 14 PRINCIPAL PLANES CONSIDERED IN TWO-DIMENSIONAL ANALYSES

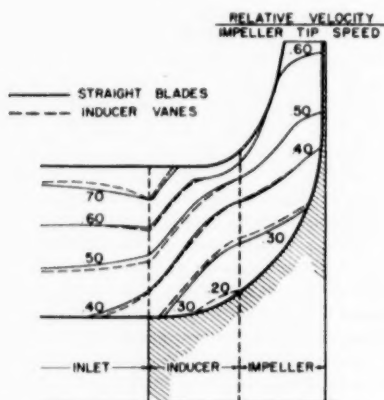


FIG. 15 RELATIVE VELOCITIES IN IMPELLER WITH AND WITHOUT CURVED INDUCER VANES

Analysis of Flow in Meridional Plane. The starting point for impeller design is felt to be the meridional contour; this feeling is dictated by the following considerations: As shown in reference (8), the velocities in this meridional plane are essentially independent of blade shape (for thin blades), and are primarily determined by the hub-to-shroud contour. Fig. 15 shows lines of constant relative velocity for (a) an impeller with blades that are curved in the inducer region, and (b) an impeller in which the curved vanes were removed and straight impeller blades extended indefinitely upstream. The good agreement between the two indicates that, in this case, the velocities in the hub-to-shroud plane are determined primarily by hub-shroud contours and are little affected by blade curvatures. Also, as previously discussed, choking velocities in mixed-flow impeller types have been predicted with a reasonable degree of accuracy from a consideration of flow in this plane (9). Therefore the hub-shroud contour appears to be a reasonable starting point for design.

This hub-to-shroud analysis method has been shown to be valuable in establishing radial variations in angle of attack at the impeller inlet. Another result of this method of analysis which

is of interest is the variation of relative velocity within the impeller. Fig. 16 shows the relative velocity variation for impeller D, Fig. 8(a), in the form of contours of ratio of relative velocity to inlet stagnation speed of sound, shown in the hub-to-shroud plane. Large variations in velocity exist from hub to shroud. Along the shroud, the velocity is near sonic at the inlet, with deceleration along the entire path length to the impeller outlet. A similar condition exists along the impeller hub from A to B. These decelerations, of course, are highly conducive to boundary-layer build-up and flow separation. Since the results are typical of impellers of this type, they probably furnish a partial explanation of low efficiencies that exist. The relative velocity distribution as obtained in this solution represents the mean condition from blade to blade. Since the velocity along the suction surface is larger than that along the mean flow path, the decelerations along the suction surface of the blade are even greater than the average value shown in Fig. 16. It appears that careful consideration should be given the hub-to-shroud contours in order to minimize these decelerations.

Analysis of Flow in Blade-to-Blade Plane. Analyses of flow in the blade-to-blade plane (12, 13, 14, 15, 16) have given still further insight into the flow processes in centrifugal impellers. A repre-

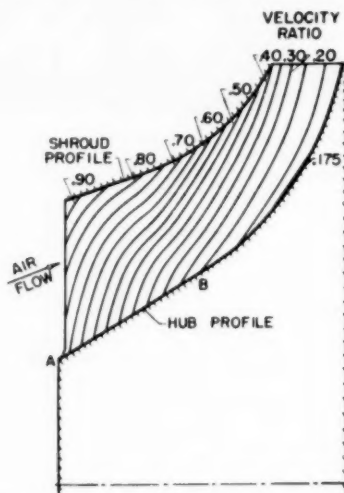


FIG. 16 RELATIVE VELOCITY CONTOURS IN IMPELLER D

sentative velocity variation along the blade surfaces in the blade-to-blade plane at design flow is shown in Fig. 17(a). Along the driving face at inlet, the velocity decelerates; this, however, is probably not too serious a condition since the boundary-layer conditions at this point are likely to be good. The flow then accelerates to the impeller tip, which is a favorable condition. In general, then, the driving-face conditions can be expected to be good.

On the trailing face of the impeller, Fig. 17(a), acceleration takes place near the inlet, followed by a deceleration to the impeller tip. This deceleration is believed to be one of the major sources of loss in centrifugal impellers. Examination of conventional designs indicates that this gradient can be expected to be extreme and it is likely that a separation of the boundary layer results. For example, results of the analysis on the parabolic-bladed impeller, Fig. 8 and reference (9), indicated an extreme gradient, which may very well account for the large losses encountered. Considerable research is required to establish "limits" for this deceleration; the application of criteria similar to those proposed in reference (17) is indicated.

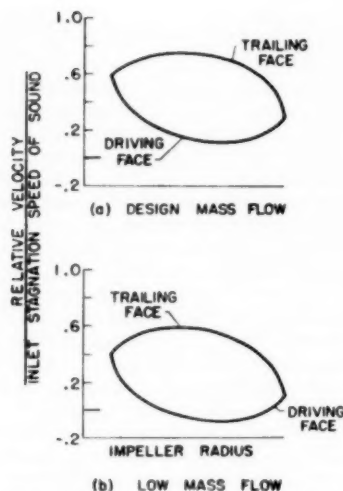


FIG. 17 Velocity Variation Along Blade Surfaces in Blade-to-Blade Plane

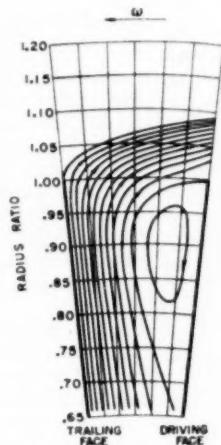


FIG. 18 Relative Streamlines in Blade-to-Blade Plane for "Eddy" Condition

At low flow conditions, another phenomenon arises which is of interest; velocities on the driving face at inlet decrease to the point where they become negative, Fig. 17(b). That is, an "eddy" forms in the passage as illustrated by a plot of the streamlines in the blade-to-blade plane, Fig. 18. As pointed out in reference (13), this tendency to eddy becomes greater with increased rotational speeds, lower flows, and fewer blades. Correlation of theoretical and experimental results have shown that this eddy formation may provide an exciting force for surge.

Experimental Study of Flow in Blade-to-Blade Plane. An insight into the behavior of a viscous fluid in the blade-to-blade plane was obtained in the internally instrumented 48-in. impeller, Fig. 1 and reference (2). A comparison of the theoretically predicted static-pressure distribution along the blade surfaces (obtained using the method of reference 16) and the corresponding experimentally determined pressures at design flow are shown in Fig. 19. Good agreement exists over most of the passage; i.e., distributions of ideal and experimental torque are approximately the same. A comparison of theoretical and experimental velocities, Fig. 20, shows larger variations, however, primarily due to the existence of losses in total pressure (which were not considered in the theoretical analysis). The eddy which was predicted along the driving face (negative velocity between $r = 18$ in. and $r = 20$ in.) was not found experimentally. The absence of the eddy may be attributed to a reduction in flow area due to boundary layer and to an increase in specific volume resulting from losses. The gradient of velocity along the trailing face is essentially as predicted.

A further indication of the nature of flow in the passage at design conditions can be obtained by examination of relative efficiency contours in the passage, Fig. 21. The greatest inefficiencies are seen to exist in the region of the trailing-face tip. On the other hand, the efficiency along the driving face remained at 100 per cent for most of the passage length. It is believed that because of the pressure gradient from the driving to the trailing face, the boundary layer is removed from the driving face and transferred to the trailing face by a secondary flow process. The deceleration along the trailing face and the shifting of low-energy air to the trailing face, therefore, provide an explanation for the low efficiency in this region.

The variation in efficiency from driving to trailing face shows up further as a variation in total pressure across the passage at

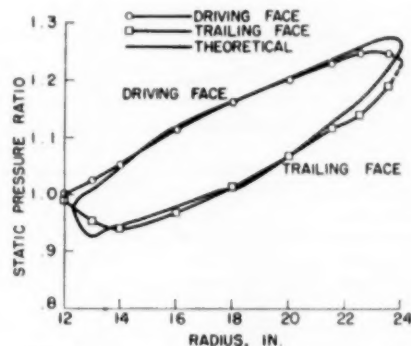


FIG. 19 Static-Pressure Distribution Along Blade Faces of 48-In. Impeller at Design Flow

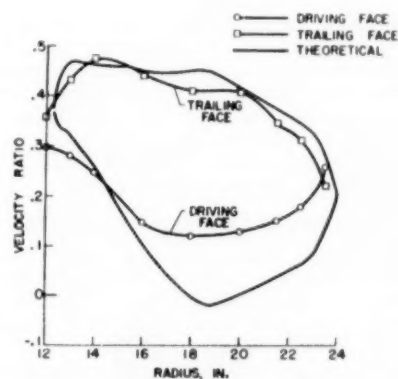


FIG. 20 Velocity Distribution Along Blade Faces of 48-In. Impeller at Design Flow

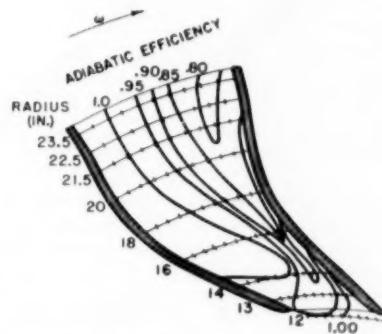


FIG. 21 Efficiency Distribution Throughout Passage of 48-In. Impeller at Design Flow

the impeller tip, Fig. 22. Since static pressures must be equal on the driving and trailing faces, the velocity at the driving face is therefore higher than that on the trailing face, Fig. 20. This condition undoubtedly results in mixing losses upon diffusion and, thereby, contributes to poor diffuser performance.

The general conclusion drawn from this research was that the internal impeller efficiency could be improved by reducing the velocity deceleration along the trailing face. Therefore the passage area was revised to provide a prescribed (and improved) velocity distribution. Physically, this was accomplished by

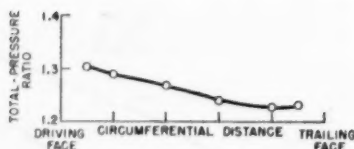


FIG. 22 TOTAL PRESSURE DISTRIBUTION ACROSS PASSAGE AT IMPELLER TIP OF 48-IN. IMPELLER AT DESIGN FLOW

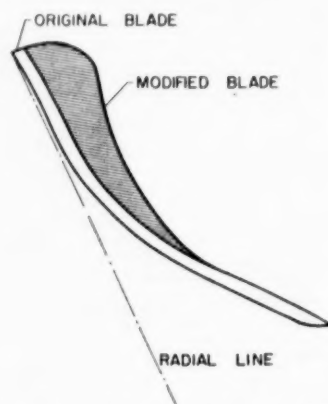


FIG. 23 COMPARISON OF ORIGINAL AND MODIFIED BLADE SHAPES OF 48-IN. IMPELLER

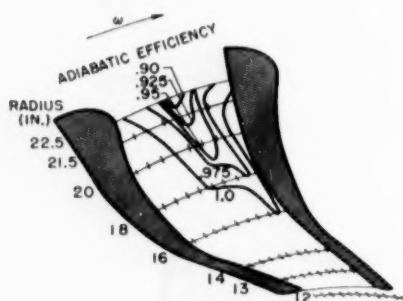


FIG. 24 EFFICIENCY DISTRIBUTION THROUGHOUT PASSAGE OF MODIFIED 48-IN. IMPELLER AT DESIGN FLOW

gluing balsa wood to the driving face of the impeller blade, leaving the trailing face and the blade height unchanged (18). A comparison of original and modified blade shapes is shown in Fig. 23. Internal flow efficiency existing at design in this passage is shown in Fig. 24; a substantial improvement over Fig. 21 is evident. An efficiency of 1.0 exists over a major portion of the passage, with small "islands" of reduced efficiency existing midway between blades. The previous reduction in efficiency along the trailing face has been virtually eliminated. Efficiency contours are not shown beyond the 22.5-in. radius, since the velocities in this region obviously are not controlled.

The significance of this investigation is that it has shown that the internal efficiency of centrifugal impellers can be improved by proper control of flow-surface velocities. This general result gives credence to the NACA philosophy of seeking theoretical potential-flow design methods in which various "real-flow" limits of this type may be imposed.

Indicated Trends of Design. As a result of these researches, possible sources of losses have been indicated. The question then arises, what can be done to optimize the channels and thereby

improve performance? Certain general trends have been noted and can be summarized as follows:

1 Passages should be designed to minimize adverse gradients. Potential flow techniques (9, 15, 16) have been developed to the point where they provide rapid and sufficiently accurate methods for design and analysis. By careful manipulation of curvatures in the meridional and blade-to-blade planes, it is believed that adverse gradients can be minimized. As pointed out previously, however, the exact values of the allowable gradient have not been established. Criteria for boundary-layer separation such as those given in reference (17) may be applicable.

2 The use of backward-curved blades may reduce the possibility of boundary-layer separation. As pointed out in reference (14), the undesirable deceleration along the trailing face becomes less as the blades become more backwardly curved. This reduction in velocity gradient is accomplished even though the tip speed must be increased to maintain the same work input.

3 A mixed-flow impeller has lower velocity gradients than an equivalent radial-flow impeller (12). Therefore it appears that a mixed-flow configuration is desirable from the point of view of boundary-layer separation.

4 The kinetic energy of the fluid at the impeller outlet becomes a smaller percentage of the total energy as blades become more backwardly curved (14). Therefore a compressor with backwardly curved impeller blades is probably desirable in that a larger portion of the static-pressure recovery takes place in the impeller, and the diffuser problem becomes less critical.

5 The tendency to form undesirable eddy flows on the driving face of the blade becomes less if the blades are curved, either forward or backward (14).

DIFFUSER RESEARCH

Experimental data taken at the discharge of centrifugal impellers have shown large gradients in average total pressure and angle across the passage from front to rear shrouds. Analysis of the leaving conditions from the 48-in. impeller, as noted earlier, showed blade-to-blade variations. Hot-wire-anemometer studies have verified the existence of large variations in velocity from blade to blade and from hub to shroud, as well as substantial blade wakes (19). These discharge conditions make large mixing losses inevitable, and these losses are normally charged to the diffuser. It is quite apparent, however, that this problem must be attacked initially in the impeller. Before high diffuser efficiencies can be obtained, impellers must be developed which deliver the air with reasonable uniformity. The problems of obtaining these uniform conditions at the impeller discharge have been discussed in the preceding section. This portion of the paper will cover some of the NACA research efforts to recover the energy from the nonuniform and turbulent stream which usually enters the diffuser.

Vaneless Diffuser

General Considerations. The simplest concept of centrifugal-compressor diffusion is one where the rotational-velocity component is removed by an increase in radius (conservation of moment of momentum) and the radial velocity component is controlled by wall divergence. In general, the major portion of the kinetic energy leaving an impeller is in the form of rotation. On the other hand, the radial component controls choking and is the predominant factor in controlling separation. From these facts, certain advantages result. Since choking is determined by the radial component of velocity, limiting relative velocities usually occur in the impeller first. Therefore compressor operating range is usually wide with a vaneless diffuser, making it a desirable configuration for applications where frontal area

is not important. Another advantage is that a supersonic tangential velocity can be diffused without shock losses; this is significant in high-pressure-ratio, high-tip-speed applications.

One-Dimensional Analysis of Flow. A one-dimensional analysis of flow in a vaneless diffuser was made, considering compressibility, friction, and area change (20). As a result of this study, it was found that even with conservative friction coefficients (and neglecting mixing losses at the impeller tip) the friction losses in vaneless diffusers are considerable. Computed diffuser efficiencies are in the low 80's, and result basically from the large ratio of friction area to flow area. This then constitutes a major disadvantage of the vaneless diffuser; the diameter is large and the efficiency is low.

This analysis also considered the effect of diffuser wall spacing on diffuser performance. It was found that in a parallel-walled diffuser (with a constant friction coefficient and a constant mass flow), efficiency increased with an increase in diffuser wall spacing. However, the variation in efficiency was small. Hence it appears that the diffuser design should be based on other considerations, including the stabilizing of the nonuniform flow leaving the impeller, variation in actual friction coefficient through the diffuser, the optimum diffusion rate for the radial component of flow, and the like. These design considerations must be evaluated experimentally.

Experimental Investigation of Various Design Parameters. The first requirement of a vaneless diffuser is to convert the nonuniform flow at the impeller outlet into a steady flow with a uniform velocity profile. A transition profile or "throat" design must be established. The second requirement is that the diffuser convert the kinetic energy to pressure as rapidly as possible without incurring separation.

The problem therefore was to establish the optimum transition profile and then to determine the optimum area expansion in the diffuser proper. The design criteria selected for the experimental investigation were (a) the contraction (throat-to-inlet) ratio for the throat section, and (b) the "equivalent cone" divergence as measured along the flow path. Diffusers were studied with equivalent cone divergence angles of 4, 6, and 8 deg, and contraction ratios of 0.62, 0.72, and 0.93 (21). As a result of these studies, it was found that the optimum contraction ratio was 0.72, and the optimum divergence was the 6-deg equivalent cone. This finding is consistent with results of conical diffuser tests.

A further investigation was conducted wherein the effect of reduction in diffuser diameter was studied, and the location and magnitude of losses in the diffuser were determined (22). These tests conducted, using a high-efficiency-type mixed-flow impeller, established the following loss pattern: Diffuser entrance losses were approximately constant (6 per cent of impeller-outlet efficiency) for all diffuser diameters. Losses in the interior of the diffuser were small compared to the entrance loss. As expected, the exit loss was large and was essentially a "dump" loss.

This general trend for internal losses was verified by studies of the friction coefficient through the diffuser (23). Measured friction coefficients were compared with those for turbulent flow in a smooth pipe. These studies showed large losses at the diffuser entrance (3 times pipe values) and minimum losses in the interior of the diffuser (equal to pipe values). As a result, average values of friction coefficient were about 50 per cent higher than those found for smooth pipes. From the results of the one-dimensional analysis and these friction-coefficient studies, it is apparent that the vaneless diffusion process has inherently large frictional losses. Some improvement in performance may be realized by increasing the impeller flow and the diffuser wall spacing to the extent that the ratio of friction area to flow area, and the flow-path length are both decreased.

Vaneless-Vaned Diffuser. Consideration of the diffuser problem indicates that a vaned diffuser which utilizes a vaneless transition section to stabilize the flow and reduce the Mach number to a subsonic level has the potential of combining some of the better features of the vaneless and vaned diffuser. Blades are then utilized to remove the rotation at a higher rate than by a simple increase in radius; the diameter and flow-path length are thereby reduced. However, the flow range may be less than that of a vaneless diffuser because of the angle-of-attack problem at the entrance to the vaned section. For example, the range of one compressor investigated was increased 35 per cent when a vaneless diffuser was substituted for a vaned diffuser. The general design problem also becomes more critical in a vaned diffuser; the vanes must be carefully matched to the impeller and must be located at the proper radius in the diffuser. An example of the critical nature of the design problem is shown by the experience with a large centrifugal compressor from a turbojet engine (24) where the flow capacity of the compressor was limited by choking in the vaned collector. Revision of the vanes resulted in improved matching of the impeller and diffuser, increased efficiency, and increased air-flow capacity.

The vaneless-vaned design approach warrants considerable research effort; the use of high-solidity channel theory similar to that used in impeller research is indicated. However, it is felt that successful diffuser development requires that efficient impellers (which will deliver reasonably uniform air at the diffuser inlet) be available for conducting the experimental phase of this research.

Scrolls. As pointed out previously, large losses occur at the exit of vaneless diffusers, particularly if diameter is limited. A possibility for maintaining efficiency as well as a reduced diameter is to use a short vaneless section in conjunction with a scroll to recover the energy that is normally "dumped" into a collector.

The NACA conducted a program of research on a family of diffusing scrolls in combination with a small-diameter (20-in.) vaneless diffuser (25). The effect of variations in certain form parameters on compressor performance were examined. Several scroll cross sections, Fig. 25, were investigated. The angle between diverging walls was varied from 24 to 80 deg; one asymmetrical cross section was studied; the surface finish was varied. As a result of this investigation, it was found that the changes in scroll geometry and surface condition resulted in negligible differences in compressor performance. However, the substitution

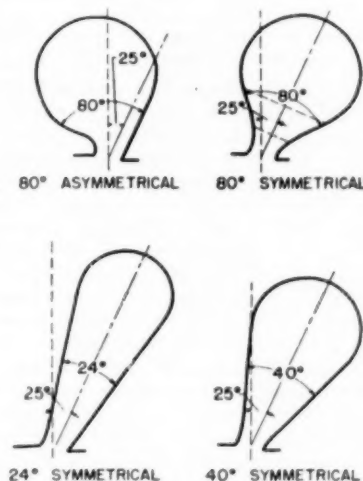


FIG. 25 CROSS SECTIONS OF SCROLLS

of the scroll for a conventional collector ring, both with the 20-in. diffuser, gave increases of 3 to 12 points in compressor efficiency, substantial increases in pressure ratio, and extended the operating range. Fig. 26 shows the comparison of performance of two configurations, namely, 20-in. vaneless, and 34-in. vaneless (both with a collector ring) with the performance for the compressor with the scroll. The performance with the scroll is essentially equal to that with the 34-in. vaneless diffuser and substantially better than the 20-in. vaneless diffuser. The use of scrolls of this type may be advantageous in certain applications.

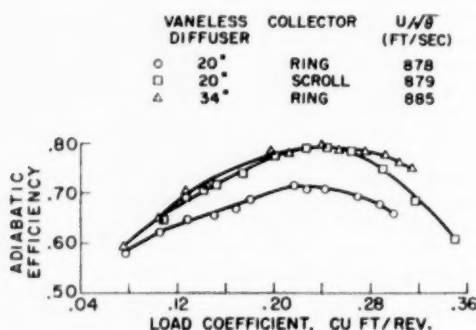


FIG. 26 ADIABATIC EFFICIENCY OF MIXED-FLOW IMPELLER WITH VARIOUS DIFFUSERS AND COLLECTORS AT ACTUAL TIP SPEED OF 900 FT PER SEC

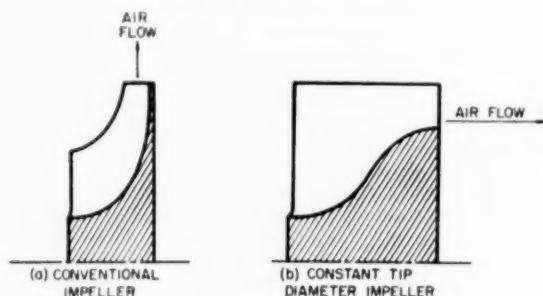


FIG. 27 IMPELLER CONFIGURATIONS

GENERAL ASPECTS OF APPLICATION OF CENTRIFUGAL COMPRESSORS TO GAS-TURBINE ENGINES

In order for the inherent structural and economical advantages of the centrifugal compressor to be utilized in the highly competitive aircraft gas-turbine-compressor field, the prime requirement of extremely high air-flow capacities per unit of compressor frontal area first must be achieved. This must of course be accompanied by an efficient compression process. The conventional-type centrifugal compressor is basically handicapped, air-flow capacity wise, by having the impeller exit diameter considerably larger than the impeller inlet diameter, Fig. 27(a). This geometry also further prohibits large air-handling capacities on a frontal area basis since the diffuser is of necessity larger in diameter than the impeller. It is necessary therefore to alter the basic geometry of both the impeller and the diffuser. General trends that have been established in the previously discussed NACA research provide a basis for future design thinking.

The obvious change would be to make the impeller tip diameter constant from inlet to exit. This type of impeller may be described as a very high solidity axial-flow rotor. However, it must be noted that some of the compression is still obtained by an

increasing radius of rotation. Fig. 27(b) shows an impeller passage of this type. Typical characteristics may be noted as follows:

- 1 Impeller tip diameter is constant from inlet to exit.
- 2 Inlet-eye areas are very large to allow increased air-flow capacities.
- 3 Rapid changes in hub-shroud curvature are used to reduce the channel-passage area. These rapid curvatures result from aerodynamic considerations and the desire to maintain a minimum axial rotor depth.
- 4 Air discharges from the impeller in basically two directions, axial and circumferential.

Impeller-design problems that require considerable research become apparent. The high inlet relative velocities that result from the high inlet-blade speeds must be considered. These high inlet relative velocities will have considerable effect on the inlet losses and choking characteristics of the impeller. Experimental and theoretical investigations of blade and hub-shroud shapes to insure optimum pressure and velocity gradients for an efficient process are required. Flow conditions must be established at the impeller exit which will reduce the critical nature of the diffuser. It is apparent that the diffuser performance will be more critical for this type of configuration, Fig. 27(b), than for a radial-flow impeller. Because of the constant tip diameter, a change in radius cannot be used to reduce the velocity ahead of the diffuser vanes. Therefore the velocities entering the diffuser blading may be very high, probably in the supersonic range for high-pressure-ratio units. Diffuser blading and passage shapes must be evolved to diffuse this supersonic stream efficiently.

Centrifugal compressors of this type are being investigated. The background of experimental and theoretical knowledge on centrifugal compressors built in the past has proved highly effective in these new designs. It has been found that the potential flow theories together with the experimental data on impeller choking and pressure and velocity-gradient control studies in the two-dimensional radial-flow compressor are directly applicable. Recent results have indicated that the competitive future of the centrifugal compressor in the aircraft gas-turbine field is promising.

BIBLIOGRAPHY

- 1 "Theoretical and Experimental Analysis of One-Dimensional Compressible Flow in Rotating Radial-Inlet Impeller Channel," by Seymour Lieblein, NACA TN 2691, 1952.
- 2 "Experimental Investigation of Flow in the Rotating Passages of a 48-Inch Impeller at Low Tip Speeds," by D. J. Michel, A. Ginsburg, and John Mizisin, NACA RM E51D20, 1951.
- 3 "An Analysis of Flow in Rotating Passage of Large Radial-Inlet Centrifugal Compressor at Tip Speed of 700 Feet Per Second," by V. D. Prian and D. J. Michel, NACA TN 2584, 1951.
- 4 "Effects on Performance of Changing the Division of Work Between Increase of Angular Velocity and Increase of Radius of Rotation in an Impeller," by Ambrose Ginsburg, W. K. Ritter, and John Palasies, NACA TN 1216, 1947.
- 5 "Preliminary Investigation of Deep Inducers as Separate Supercharger Components," by W. K. Ritter and I. A. Johnsen, NACA ARR E5128, 1945.
- 6 "Performance Comparison of Two Deep Inducers as Separate Components and in Combination With an Impeller," by W. K. Ritter, Ambrose Ginsburg, and W. L. Beede, NACA ARR E5J03, 1945.
- 7 "An Investigation of the Effect of Blade Curvature on Centrifugal-Impeller Performance," by R. J. Anderson, W. K. Ritter, and D. M. Dildine, NACA TN 1313, 1947.
- 8 "Two Axial-Symmetry Solutions for Incompressible Flow Through a Centrifugal Compressor With and Without Inducer Vanes," by G. O. Ellis, J. D. Stanitz, and L. J. Sheldrake, NACA TN 2464, 1951.
- 9 "Method of Analysis for Compressible Flow Through Mixed-Flow Centrifugal Impellers of Arbitrary Design," by J. T. Hamrick, Ambrose Ginsburg, and W. M. Osborn, NACA Rep. 1082, 1952. (Supersedes NACA TN 2165.)

- 10 "Comparison of Two- and Three-Dimensional Potential-Flow Solutions in a Rotating Impeller Passage," by G. O. Ellis and J. D. Stanitz, NACA TN 2806, 1952.
- 11 "Investigation of Single Stage Axial Flow Fans," by P. Ruden, NACA TM 1062, 1944.
- 12 "Two-Dimensional Compressible Flow in Turbomachines With Conic Flow Surfaces," by J. D. Stanitz, NACA Rep. 935, 1949. (Supersedes NACA TN 1744.)
- 13 "Two-Dimensional Compressible Flow in Centrifugal Compressors With Straight Blades," by J. D. Stanitz and G. O. Ellis, NACA Rep. 954, 1950. (Supersedes NACA TN 1932.)
- 14 "Two-Dimensional Compressible Flow in Centrifugal Compressors With Logarithmic-Spiral Blades," by G. O. Ellis and J. D. Stanitz, NACA TN 2255, 1951.
- 15 "Approximate Design Method for High-Solidity Blade Elements in Compressors and Turbines," by J. D. Stanitz, NACA TN 2408, 1951.
- 16 "A Rapid Approximate Method for Determining Velocity Distribution on Impeller Blades of Centrifugal Compressors," by J. D. Stanitz and V. D. Prian, NACA TN 2421, 1951.
- 17 "Attainable Circulation About Airfoils in Cascade," by A. W. Goldstein and Artur Mager, NACA Rep. 953, 1950. (Supersedes NACA TN 1941.)
- 18 "Effect of Changing Passage Configuration on Internal-Flow Characteristics of a 48-Inch Centrifugal Compressor. I—Change in Blade Shape," by D. J. Michel, John Mizisin, and V. D. Prian, NACA TN 2706, 1952.
- 19 "Investigation of Flow Fluctuations at the Exit of a Radial-Flow Centrifugal Impeller," by J. T. Hamrick and John Mizisin, NACA RM E52H11, 1952.
- 20 "One-Dimensional Compressible Flow in Vaneless Diffusers of Radial- and Mixed-Flow Centrifugal Compressors, Including Effects of Friction, Heat Transfer and Area Change," by J. D. Stanitz, NACA TN 2610, 1952.
- 21 "Method of Designing Vaneless Diffusers and Experimental Investigation of Certain Undetermined Parameters," by W. B. Brown and G. R. Bradshaw, NACA TN 1426, 1947.
- 22 "Experimental Study of Effect of Vaneless-Diffuser Diameter on Diffuser Performance," by G. R. Bradshaw, and E. B. Laskin, NACA TN 1713, 1948.
- 23 "Friction Coefficients in a Vaneless Diffuser," by W. B. Brown, NACA TN 1311, 1947.
- 24 "Performance Investigations of a Large Centrifugal Compressor From an Experimental Turbojet Engine," by Ambrose Ginsburg, J. W. R. Creagh, and W. K. Ritter, NACA RM ESH13, 1948.
- 25 "Design and Performance of Family of Diffusing Scrolls With Mixed-Flow Impeller and Vaneless Diffuser," by W. B. Brown and G. R. Bradshaw, NACA Rep. 936, 1949. (Supersedes NACA TN 1568.)

Discussion

E. M. KNOERNSCHILD.⁴ The authors are to be congratulated for a comprehensive summary report which covers almost all phases of compressor design. The writer would like to present a few additional problems.

In Fig. 6 of the paper the authors show an inducer with very close spacing of blades. It appears to the writer that if the layout of such an inducer had been chosen according to current axial-compressor theory, the solidity of the blading could have been decreased, thereby resulting in a lower blade number and smaller friction losses in the inducer.

In an attempt to obtain a relation for the permissible deceleration of the flow within the impeller as a function of the blade-outlet angle, the writer submits the following question: Which part of the velocity distribution around the blade (see Fig. 17 of the paper) should be used as a characteristic value? There are three distinct regions of deceleration to be considered: (a) at the inducer, (b) along the driving face, (c) along the trailing face.

It appears that quite a large deceleration can be tolerated at the inducer without adverse effects owing to the small boundary layer at the leading edge (assuming a correct inducer design). The average deceleration along the trailing face is smaller than

that along the driving face, with the exception of a small segment near the blade trailing edge where any separation does not affect the flow too severely. The largest range of continuous strong deceleration apparently is along the driving face. The slope of this range might be considered a criterion for a comparison of different blade configurations and may be used as a separation parameter.

This would differ from axial-blading-design practice where the continuous deceleration along the trailing face generally is used as a criterion for determining a separation parameter.

In the survey on radial-impeller research, the writer misses some studies on the influence of blade force on the meridional flow, as brought forward by Meyer⁵ and Wislicenus.⁶ The writer thinks the use of the three-dimensional blade effects for changing the meridional-flow pattern might be another step to improve compressor performance.

The authors propose an improvement in compressor performance by using axial outflow and constant-tip diameter (see Fig. 27 of the paper). The writer thinks the authors lose one of the advantages of centrifugal compressors namely, the thinning out of the boundary layer by centrifugal action. In other words, they now have to cope with smaller permissible blade loading at the blade tip with an axial turbomachine as compared with a centrifugal machine.

In a compressor of the design shown in Fig. 1 of the paper, the leading edges of the impeller should theoretically be laid out according to the velocity distribution of the flow coming around the bend from axial to radial direction. Have the authors any conception why the free-vortex distribution around this bend usually degenerates to such an extent that a blade-inlet design based on constant-velocity distribution (one-dimensional theory) yields, in most cases, better results than one based on the free-vortex (two-dimensional) distribution?

C. F. KOENIG.⁷ The authors make the statement: "For many years, the design of centrifugal compressors has been largely an art. . . ." This statement is only too true, as any student of the "art" will admit readily. The authors are to be commended for the very worth-while experimental and analytical investigations described in this paper, which should contribute much toward eliminating some of the artistic aspects of centrifugal-compressor design.

The authors intentionally have avoided setting down specific design rules derived from their experiments. This in no way affects the intrinsic value of the data presented, but inspection of these data indicates that, possibly with some minor rearranging, some very respectable design rules might appear quickly.

A very important variable, from the compressor designer's point of view, is the rotative or shaft speed of the compressor. It may be held that aerodynamic performance properly is referred to blade speed, and that, in so far as aerodynamics is concerned, the shaft speed is immaterial. Actually, the compressor aerodynamicist almost never has a free hand in choosing the shaft speed, and his ultimate design is a compromise with the requirements of the driving turbine or motor, limiting outside dimensions, bearings, shaft seals, and similar factors. It develops, therefore, that the aerodynamic problem is not to design the most efficient compressor possible, but, rather, to design the most efficient compressor possible within the permissible

⁵ "Beitrag zur Theorie fest stehender Schaufelgitter," by Richard Meyer, *Mitteilungen aus dem Institut für Aerodynamik der Technische Hochschule*, Zurich, Switzerland, No. 11, 1946.

⁶ "Fluid Mechanics of Turbomachinery," by George Wislicenus, McGraw-Hill Book Company, Inc., New York, N. Y., 1947, chapter 58.

⁷ Assistant Chief Engineer, Compressor Department, De Laval Steam Turbine Company, Trenton, N. J.

⁴ Research Department, Carrier Corporation, Syracuse, N. Y.

speed range. Under these circumstances, it is convenient to have basic performance data arranged to include shaft speed as one of the variables.

For aerodynamic-design purposes, the shaft speed N usually is combined with the volume flow through the compressor Q and head H (work done per pound of fluid) to form a parameter which defines the general proportions of the compressor rotor. One widely used parameter of this nature is the specific speed N_s , where

$$N_s = \frac{N \sqrt{Q}}{H^{0.75}}$$

A low-specific-speed rotor, for example, would run at a low shaft speed, pass a small flow, and develop a high pressure ratio (i.e., a high head). Conversely, a high-specific-speed rotor would run at a high speed, pass a large flow, and develop a low pressure ratio. Typical rotors for low- and high-specific-speed compressors are illustrated schematically by this writer in Fig. 28.

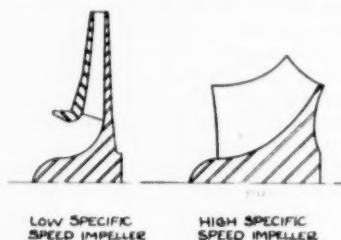


FIG. 28 TYPICAL COMPRESSOR ROTORS

The authors cover several items in their paper that have particular significance when the specific speed of the compressor is considered. For example, it is shown in the authors' discussion on division of work in the rotor that too much energy addition in the "impeller function," as compared to the "inducer function," will be detrimental to performance. It is also stated that a high ratio of friction area to flow area and a long flow-path length in the diffuser will result in excessive losses. All of these characteristics are inherent in a low-specific-speed compressor. On the other hand, in a rotor where the inducer function is predominant and there is little increase in the radius of rotation of the fluid, it is stated that high relative velocities at the inlet become a problem. It also is stated that it becomes difficult to achieve efficient deceleration in a diffuser without a large increase in radius. These characteristics are synonymous with high speed, high flow, and relatively low work—in other words, high specific speed.

It seems reasonable to conclude from the authors' discussion that very low and very high specific speeds should be avoided where maximum performance is desired from a compressor, and that there is some range of specific speeds within which best results will be obtained. Experience has shown that such indeed is the case. Very good results have been obtained from compressors of medium specific speeds in which mixed-flow impellers with backwardly curved blades (as suggested by the authors) were used. Published data to date are insufficient to establish a reliable correlation between specific speed and performance, but it appears that the authors' data cover a broad enough range to make notable contributions toward this end.

The writer wishes to congratulate the authors and their colleagues at NACA for their valuable work with centrifugal compressors, and hopes that reports on more of the same will be forthcoming in the future.

G. F. WISLICIENUS.⁸ The paper and the NACA reports listed in its Bibliography constitute an important contribution to the science and art of centrifugal-pump and compressor design. Although many of the reports quoted have been used extensively, a summary such as the authors' is essential for putting the available data to best use. Besides the application of this information to aircraft compressors, it is to be hoped that its publication will accelerate the adoption of aircraft-design principles in other fields of compressor application.

The volume of information presented in abstract form is so great that the space allowed can hardly do justice to it. For example, the description of the vane shapes of impellers D, E, and F as "parabolic," "elliptical," and "circular" is insufficient to identify what may be the really deciding differences between these impellers. Fig. 8 of the paper shows that circumferential extent ("wrap") of the impeller vanes decreases progressively from D to F, indicating that the geometric characteristics of the vanes change in more than one respect.

In connection with Fig. 15 of the paper, the authors conclude that the action of the impeller vanes has but a minor effect on the velocity distribution of the meridional flow. The writer feels that this conclusion is too general and may not apply in certain cases of practical importance.

Based on the work of Lorenz,⁹ Bauersfeld¹⁰ developed a general criterion of conditions under which the vanes of turbomachinery should not have any effect on the meridional-flow picture. This criterion, which, of course, is based on a theory of frictionless flow, states that the meridional flow may be described by a velocity potential only if the "bound vortex lines," representing the deflecting effect of the vanes, lie in the meridional planes. This is obvious as, under this simple condition, the bound vorticity representing the ideal vane action does not have a peripheral component, i.e., a component normal to the meridional planes, thus leaving the meridional flow irrotational. Bauersfeld presented this criterion as a principle of good vane design for hydraulic turbines. Today we would not agree with this conclusion. Nevertheless, the classical work by Lorenz and Bauersfeld does present the theoretical mechanism for describing the effect of the vanes on the meridional flow of turbomachinery in terms of the peripheral components of the bound vorticity of the vanes.

This principle¹¹ was used to describe the effect of radial or mixed-flow impeller vanes on the meridional-flow distribution, using, as example, the same type of vanes commonly used for aircraft applications, i.e., vanes forming a straight helical surface with axially varying pitch.¹² In the axial part of the impeller, the curvature of vanes of this general form, as considered in connection with Fig. 15 of the paper, may well be expected to have only a minor effect on the meridional flow, because, in this part of the runner, the bound vortex lines (approximately lines of constant total head) more or less run at right angles to the axis of rotation, thus agreeing generally with the direction of radial sections through vanes of this type, and are, therefore, themselves approximately radial. On the other hand, in the radial part of the impeller, the bound vortex lines swing progressively toward a direction parallel to the axis of rotation. Only in the case of plane radial vanes, considered in the paper for this part of the runner, will such vortex lines lie in meridional planes.

⁸ Chairman, Department of Mechanical Engineering, Johns Hopkins University, Baltimore, Md. Mem. ASME.

⁹ "Neue Theorie zur Berechnung der Kreisrädler," by H. Lorenz, R. Oldenbourg, 1905.

¹⁰ "Die Konstruktion der Francis-Schaukel nach der Lorenzschen Turbinentheorie," by Bauersfeld. *Zeitschrift des Vereins deutscher Ingenieure*, vol. 56, 1912, pp. 2045-2051.

¹¹ "Fluid Mechanics of Turbomachinery," by G. F. Wislicenus, McGraw-Hill Book Company, New York, N. Y., 1947, chapter 11.

¹² *Ibid.*, Chapter 23.

In the general case of helical vanes (with their radial-generating lines normal to the axis of rotation), the position of the vortex lines in the radial part of the impeller, makes it impossible for these vortex lines to lie in meridional planes. This introduces into the meridional flow a vorticity of the same order of magnitude as the vane vorticity representing the peripheral deflection of the absolute flow by the impeller. Unfortunately, for helical vanes with radial elements, the resulting velocity differences in the meridional flow are additive to those produced by the general curvature of the meridional flow. Therefore the total nonuniformities of meridional velocities may be quite serious. Fig. 135 of footnote⁶ indicates that the order of magnitude of the effect to be expected appears to be far from negligible. On the other hand, it also shows that this effect is not difficult to approximate by numerical or graphical procedures, although this vane effect on the meridional flow may well be so strong as to require a series of successive approximations for its adequate determination.

It is hoped that the work of the NACA in the field of the radial- and mixed-flow runner will continue and will include an experimental check of the vane effects described which may prove to be essential for the development of impellers as shown in Fig. 27 of the paper.

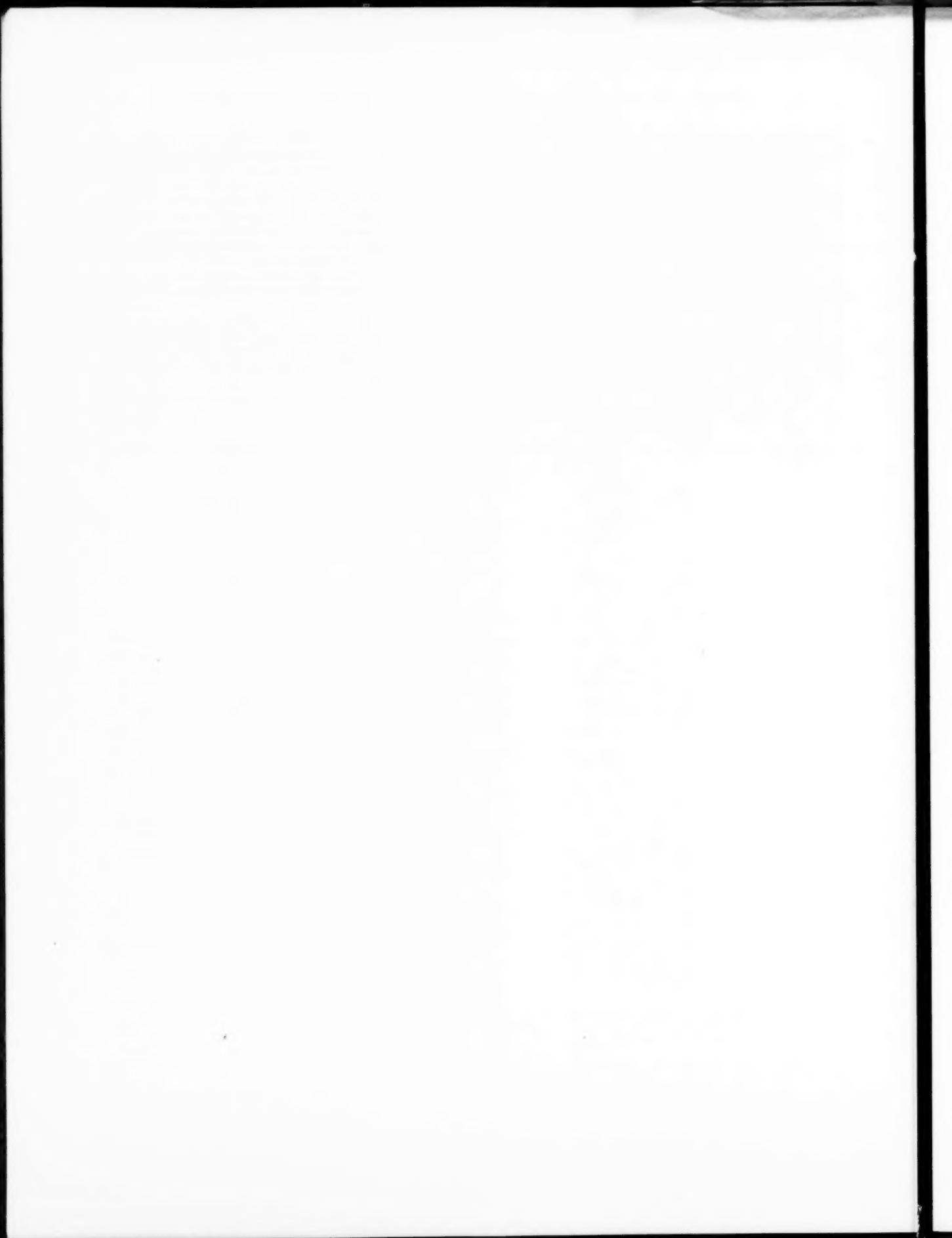
AUTHORS' CLOSURE

The authors wish to express appreciation to Messrs. Knoernschild, Koenig, and Wislicenus for their pertinent comments and suggestions.

In answer to Mr. Knoernschild's query regarding that part of the velocity distribution which should be considered as characteristic, it is the authors' feeling that the critical region exists along the trailing face. Experimental investigations of radial and mixed-flow centrifugal compressors, including the 48-in. impeller reported in this paper, appear to substantiate this premise. The problem in centrifugal impellers is therefore analogous to that in axial-flow blade rows.

The authors agree with Prof. Wislicenus and Mr. Knoernschild's views that vane action may have a significant effect on the meridional flow; it was not the authors' intent to ignore this vane action or to conclude generally that the vane action would have a minor effect.

The authors do believe, however, that impeller design should start with analysis of flow in the meridional plane, considering vane action. The method presented in reference (9), which includes the blade force term, is suggested for this meridional-plane analysis.



Complete Characteristic Circle Diagrams for Turbomachinery

By W. M. SWANSON,¹ CLEVELAND, OHIO

The experimental test results for operating a hydraulic turbomachine in every possible manner (noncavitating) are presented for a representative single-stage axial-flow and mixed-flow pump. A comparison is made among the three basic types of machine, axial, radial, and mixed flow. A new method for representing, on a single diagram, the efficiencies in all types of operation is proposed and demonstrated for the case of these three pumps. A method for predicting the complete characteristics from ideal flow considerations is given.

NOMENCLATURE

The following nomenclature is used in the paper:

- A = impeller discharge area
- b = width of impeller outflow passage
- C_H = experimental head-speed coefficient based on mean outlet diameter = $H / \frac{u_m^2}{g}$
- C_Q = experimental capacity coefficient based on mean outlet diameter = $\frac{Q}{Au_m}$
- C_T = experimental torque-speed coefficient based on mean outlet diameter = $\frac{T}{\rho Au_m^3 D_m^2}$
- c = absolute flow velocity
- D_i = inner diameter at outlet (hub diameter)
- D_m = mean diameter at outlet
- D_o = outer diameter at outlet (OD)
- g = gravitational acceleration
- H = head
- n = rotational speed, rpm
- n_s = specific speed, gpm, ft, rpm units
- Q = flow rate (capacity)
- T = torque
- u_m = peripheral velocity at impeller mean diameter
- u_o = peripheral velocity at impeller OD
- β = angle between relative and peripheral velocity (outlet flow angle)
- η = power ratio; η_p pump efficiency; η_t turbine efficiency
- ρ = fluid density
- τ = dimensionless torque coefficient
- ϕ = ideal flow coefficient = $\frac{C_{m2}}{u_{m2}}$
- ψ = ideal head coefficient = $\frac{C_{H2}}{u_{m2}^2}$
- 2 = subscript referring to outlet

¹ Instructor, Case Institute of Technology. Jun. ASME. Contributed by the Hydraulic Division and presented at the Annual Meeting, Atlantic City, N. J., November 25-30, 1951, of THE AMERICAN SOCIETY OF MECHANICAL ENGINEERS.

NOTE: Statements and opinions advanced in papers are to be understood as individual expressions of their authors and not those of the Society. Manuscript received at ASME Headquarters, February 24, 1953.

INTRODUCTION

The idea of determining operating characteristics at conditions other than those for which a machine (pump) was primarily designed was presented originally by Kittredge and Thoma (1, 2)² in 1931. The normal pump characteristics at constant speed were determined and additional head and torque data were obtained beyond the zero head and torque points (capacity axis) in a region where the torque and mechanical power became output, and a turbine operation resulted. Data also were obtained for the case of reversed flow direction giving rise to a power-dissipation type of operation. The data were presented on a percentage basis, +100 per cent being the head, flow rate, torque, and revolutions at the best efficiency point of the normal pump operation. A similar set of characteristics was obtained for constant negative speeds. In order to complete the operating picture, constant-capacity characteristics were obtained, percentage head and torque being plotted against speed.

In 1937 the complete characteristics of a centrifugal pump were presented on a single diagram by R. T. Knapp (3) at the suggestion of Dr. von Kármán. This convenient representation gave contours of constant head and torque plotted on capacity versus speed co-ordinates (all percentage values) leading to the eight sectors of operation shown in Fig. 1. Since the complete operat-

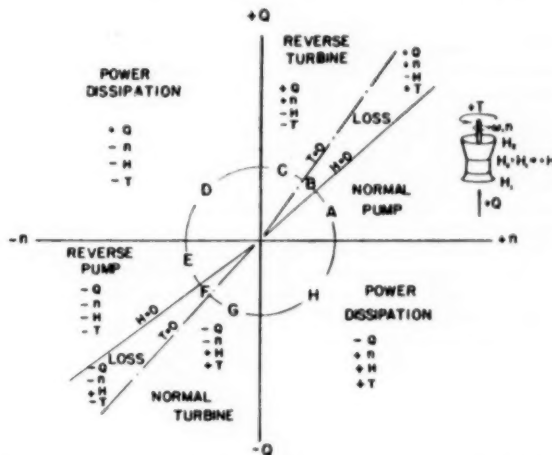


FIG. 1 SIGN CONVENTIONS; ALL QUANTITIES DESIGNATED POSITIVE WHEN UNIT OPERATED AS NORMAL OR BEST EFFICIENCY PUMP

ing characteristics for every possible type and condition of operation were given, this diagram was referred to as a complete characteristic or the Kármán-Knapp circle diagram.

The various applications of such methods of characteristic representation are well covered in references (1, 2, 3, 4, 5, 6) and will not be repeated here. It has been noticed that for most single-suction single-stage pump units, the maximum efficiencies

² Numbers in parentheses refer to the Bibliography at the end of this paper.

are about the same for normal pump or normal turbine operation. This might indicate the possibility of designing one unit for a dual purpose where possible. A possible practical dual-operation application would be a pump storage system in a multiple-unit hydroelectric installation. Water would be pumped into a reservoir during low-load periods and run back through the unit during peak-load periods.

The complete characteristics are useful for designing driving components and other parts of complete pump or turbine installations. The installation can be designed taking into account loads and stresses at any abnormal operating condition. Also, the available characteristics supply a comparison of the basic types where one unit may be designed for a dual purpose, such as a pump and turbine.

Published complete characteristic diagrams have been available previously for radial-flow pumps only. However, in noticing some of the basic differences in the characteristics of axial-flow, mixed flow, and radial-flow machines, it was of interest to obtain and compare the complete characteristics for the three types.

DEVELOPMENT OF IDEAL COMPLETE CHARACTERISTIC

If Newton's laws of motion relating to torque and momentum are applied to the flow through the vane geometry of a pump impeller, and the exit-flow direction is that of the blade-chord line at the exit (i.e., according to the Euler infinite vane theory), a relation between the torque T , capacity Q , and rotational speed n , may be obtained. It will be assumed also that the inlet flow is meridional (i.e., it has no rotational component), uniform, and irrotational, and the fluid is incompressible, i.e., ideal. The dimension constants of the impeller geometry and the density of the fluid will enter as parameters. The result is

$$T = \rho Q \left(u_{m2} + \frac{Q}{A} \cot \beta_2 \right) \frac{D_m}{2} \quad [1]$$

where β_2 is measured from the direction of the rotational-velocity vector. (It should be noted that $\cot \beta_2$ is usually a negative quantity.)

Multiplying this expression by the rotational speed ω in radians per sec gives the energy input. If no losses are considered, the mechanical input equals the hydraulic output

$$T\omega = \rho g Q H \quad [2]$$

and an expression is obtained for the head, H .

Consider a specific machine with a fixed geometry (exit area A , impeller outside diameter D_m , and exit blade angle β_2) so that these factors may be lumped into constants of proportionality. Using the foregoing relations

$$Tn = \rho Q n \left[n \left(\frac{\pi D_m}{60} \right) - Q \frac{\cot \beta_2}{A} \right] \frac{D_m}{2} \quad [3]$$

or

$$T = K_1 Q (n - K_2 Q) \quad [4]$$

where

$$K_1 = \frac{\rho \pi D_m^2}{120} \quad \text{and} \quad K_2 = \frac{60 \cot \beta_2}{\pi D_m A}$$

and

$$H = \left(\frac{\pi D_m}{60g} \right) n \left[n \left(\frac{\pi D_m}{60} \right) - Q \frac{\cot \beta_2}{A} \right] \quad [5]$$

or

$$H = K_3 n (n - K_2 Q) \quad [6]$$

where

$$K_3 = \left(\frac{\pi D_m}{60} \right)^2 \frac{1}{g}$$

These are the ideal relations desired. In particular, consider that this machine was designed as a pump. Then in the design region of pump operation, all of the characteristic variables arbitrarily will be designated as positive quantities and this design or best efficiency pump type of operation will be referred to as the normal pump type of operation. Having adopted this sign convention, any other type of operation will follow in normal sequence as shown in Fig. 1. This diagram shows all the zones of operation for a real pump.

If Equation [6] is plotted in the usual manner as an H - Q characteristic at constant speed, the result is the usual Euler straight-line characteristic with negative slope. It was assumed that the rotor had an infinite number of vanes; however, it is possible to derive an ideal characteristic for a finite number of blades of given chord length, spacing, and stagger angle. A number of cascade or lattice theories have been derived which give a constant correction factor to the Euler infinite-vane head (7, 8, 9, 10, 11, and others). The ideal torque-capacity relation at constant speed is seen from Equation [4] to be parabolic and concave downward. Since the speed is constant, this is also the ideal shaft or input-power curve.

Usually turbomachine characteristics are given only in the first quadrant (normal pump zone of operation in the case of a pump); however, considering an ideal system, there is nothing to prevent these characteristics from being extended in both directions beyond the zero head (or torque) and capacity axes, similar to the experimental procedure described in the introduction. The characteristics for a hypothetical axial-flow impeller (described in a later section) are presented in Figs. 2 and 3. The co-ordinate values in these figures are fractions of design-point values, all characteristic quantities being given the value of +1 (or +100 per cent) at the design point.

If all of the original assumptions are held valid, a set of impeller characteristics may be obtained in a similar manner for the negative direction of rotation ($-n$).

The equations of the characteristics as derived from the Euler and energy equation, Equations [1] and [2], would give smooth continuous curves. However, a cusp is shown at the beginning of the regions of no useful output in Figs. 2 and 3 (zones D and H). This is because the equations have assumed a fixed leading edge for the entire flow variation such that, for negative flows, the leading edge is the same as for the positive flow direction. However, assuming that the leading and trailing edges are reversed in relation to the blade, when the flow is reversed, the equations still can apply by giving the magnitudes of the characteristic quantities. Since the foregoing equations were derived only for the ideal case, there is no way this behavior can be determined from them, nor is any method possible whereby they may be altered to predict such a behavior. Graphs of the characteristic quantities obeying square-law relationships then will have cusps at the origin, Figs. 2 and 3. The input and output power still can be considered numerically equal, but opposite in sign. This opposition of sign gives a ratio of input to output of -1 which may be thought of as a dissipation operation. This is a definite departure from the assumptions of ideal flow in that no mechanism has been predicted or defined for the power dissipation which now consists of both mechanical and hydraulic power which are being fed into the machine and, consequently, into the fluid.

To get the stalled torque (at $n = 0$) and other points hard to

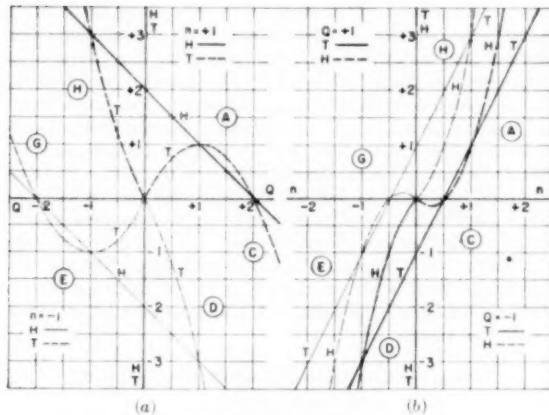


FIG. 2 HYPOTHETICAL PERCENTAGE CHARACTERISTICS FOR AN AXIAL-FLOW IMPELLER

(a, Heavy solid line, head-capacity characteristic at positive design speed; heavy dashed line, torque-capacity characteristic at positive design speed; light lines are for negative design speed. b, Heavy solid line, torque-speed characteristic at positive design capacity; heavy dashed line, head-speed characteristic at positive design capacity; light lines for negative design capacity.)

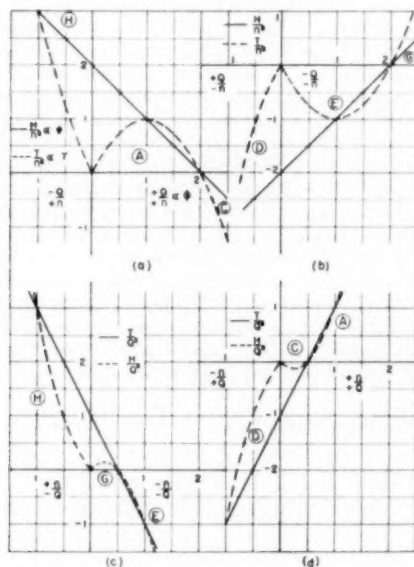


FIG. 3 HYPOTHETICAL PROPORTIONAL PERCENTAGE CHARACTERISTICS FOR AN AXIAL-FLOW IMPELLER

(a, b, Solid lines, proportional head-capacity characteristics; dashed lines, proportional torque-capacity characteristics. c, d, Solid lines, proportional head-speed characteristics; dashed lines, proportional torque-speed characteristics.)

reach, another set of characteristics may be constructed for $Q = \text{constant}$ with abscissa n and ordinates T and H which give straight line $T-n$ and parabolic $H-n$ functions (i.e., $Q = \text{constant}$ in Equations [4] and [6]), but with cusps on the H lines at the origin where the dissipation zones begin. In this case, as the direction of rotation is reversed while maintaining a constant-flow magnitude and direction, the leading and trailing edges of the blades are assumed interchanged, a condition which is not predicted by Equation [6]. Assuming this switch between leading and trailing edge makes the ideal one step closer to the real operation, and makes the four characteristic plots compatible.

These two sets of constant $+n$ and $-n$ head and torque versus capacity characteristics may be presented for various speeds as families of characteristics, or, preferably, the two families may be reduced to two dimensionless characteristics with the aid of the similarity or affinity relationships among the geometric and fluid parameters and the characteristic variables. These constant $+n$ and $-n$ dimensionless characteristics then will be proportional to H/n^2 and T/n^2 versus Q/n , e.g., Equation [6] when divided by n^2 gives $\frac{H}{n^2} \propto 1 - K_2 \frac{Q}{n}$, and Equation [4] gives $\frac{T}{n^2} \propto \frac{Q}{n} - K_2 \frac{Q^2}{n^2}$.

These two sets of characteristics include every type of operation possible for a turbomachine and correspond to Figs. 2(a) and 3(a) for $+n$ and Figs. 2(a) and 3(b) for $-n$. The H and T versus n characteristics at constant $+Q$ and $-Q$ may be obtained from Equations [4] and [6]. These also may be made dimensionless, the relationships being proportional to $T/Q^2 \propto n/Q - K_2$ (Equation [4]), and $H/Q^2 \propto \frac{n^2}{Q^2} - K_2 \frac{n}{Q}$ (Equation [6]). Notice that the head-speed characteristic is parabolic and the torque-speed characteristic is a straight line, the latter being the usual turbine characteristic. This turbine characteristic will appear in the first quadrant when the flow and speed are negative, i.e., $-n$ and $-Q$, the ratio being positive. These relationships are shown in Fig. 3.

Every possible condition and type of operation has been indicated analytically for the ideal case. For a graphical representation, two graphs are required as in Fig. 2, or four as in Fig. 3, one each for constant $+n$, $-n$, $+Q$, and $-Q$. Or the four plots in Fig. 3 may be combined to give two if the abscissa values of $+Q$ and $-Q$, both being positive, are plotted on the positive axis $+n$ and $-n$, both being positive, are plotted on the positive axis of one graph.

Now consider a method to present all the information on a single diagram. Still assuming a pump impeller, a design point of operation is chosen. All of the characteristic quantities are given the value of $+100$ per cent at this condition of operation. All of the characteristic values then are divided by the design-point values so that the characteristics all are presented as percentages of design values. This will give relationships of per cent H/n^2 versus Q/n , and so on, Fig. 3. To conclude this development, it is necessary to choose a specific type of machine, since some basic differences exist in certain types of operation, mainly in the reverse pumping zone. However, there is no loss of generality in the application of the method to any type of turbomachine. In the region of reverse pump operation, the characteristics shown in Figs. 2 and 3 are necessarily those for an axial-flow machine.

IDEAL CHARACTERISTIC FOR AXIAL-FLOW IMPELLER

The following is an example of the derivation of the single complete characteristic diagram for a simple, hypothetical, axial-flow pump impeller.

For clarity of representation, assume that (a) the design head is one half the head at shutoff, (b) the unit has no flow guidance at inlet or outlet, and (c) the vanes are symmetrical and have no camber. If these assumptions are applied to the foregoing development and in particular to Equation [1], the following simplified equations relating the characteristics are obtained

$$H = n(2n - Q) \dots \dots \dots [7]$$

$$T = Q(2n - Q) \dots \dots \dots [8]$$

or

$$K_1 = K_2 = 2 \text{ and } K_3 = 1/2$$

(where all values are percentages of design-point values).

To represent these equations graphically, choose per cent Q as the ordinate and per cent n as the abscissa. With these co-

ordinate axes, lines of constant per cent H and per cent T can be plotted. These constant per cent H and per cent T lines are seen to be hyperbolas with $Q = 0$, $n = 0$ and $Q = 2n$ as asymptotes. The $+100$ per cent and -100 per cent T and H contours are shown in Fig. 4. Families of such curves for different percentage values of H and T would present the entire story for the flow for this one simple case. It also is possible to find any flow condition from the 100 per cent curves with the aid of the proportionality laws.

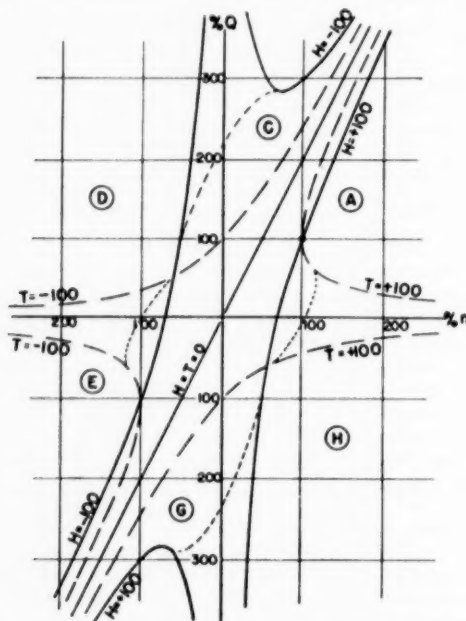


FIG. 4 IDEAL COMPLETE CIRCLE CHARACTERISTIC FOR STRAIGHT, NONCAMBERED BLADE AXIAL-FLOW IMPELLER
(Solid lines are $+100$ and -100 per cent constant head; dashed lines are $+100$ and -100 per cent constant torque; dotted lines are a first approximation to a real fluid.)

An alternative method consists of beginning with the four constant-speed and constant-capacity plots in dimensionless form (ψ and τ versus ϕ , etc.) reducing these to proportional form as in Fig. 3, determining the equations of the characteristics from only the four straight-line characteristics and then making the co-ordinate transformation to the Q - n axes. In doing this, the dimensionless characteristics are determined; then the percentage characteristics are obtained, Fig. 3, and from these the co-ordinate-axis transformation is made to the Q - n axes. This method is mentioned because it more nearly parallels the experimental procedure described later.

The foregoing method, although applied to a specific simplified machine, is perfectly general and may be applied to any type of pump to obtain the ideal complete characteristics.

REAL FLOW CONSIDERATIONS

In the ideal diagram, Fig. 4, there are two conditions that vary greatly from those expected in operation with a real fluid. These are the infinite Q indicated to obtain a finite head at zero speed (locked rotor), and the infinite n indicated to obtain a finite T at zero Q (shutoff). These are the $n = 0$ (for H) and $Q = 0$ (for T) asymptotes, respectively. Both are based upon assumptions of an ideal (frictionless) fluid, and state that, since no resistance to the flow exists, (a) at the locked-rotor condition, a very small H will give an infinite Q (and a finite T), and (b) at shutoff a very small T will produce an infinite speed (and a finite H). For a real fluid,

a finite applied head will produce only a finite flow due to fluid-friction losses, so that as a first approximation to a real fluid, the constant-head curve may be connected across the Q -axis in a manner similar to that indicated by the dotted lines in Fig. 4. For the shutoff condition, a finite torque will give only a finite speed, or the actual torque curves might resemble more closely the dotted lines. Also, since the operation is not 100 per cent efficient because of internal friction, the $H = 0$ and $T = 0$ values would not be coincident, but would include the missing loss sectors, B and F in Fig. 1. Considering that normal pump operation is from zero Q to zero H , the line of zero T would be expected to be at a greater Q/n ratio than the zero-head line. Also, as the operating conditions vary more and more from the design or best efficiency condition, the separation and internal friction losses will become greater.

EXPERIMENTAL DETERMINATION OF COMPLETE CHARACTERISTIC

The procedure for the determination of the experimental characteristic diagram was similar to the foregoing description of the development of the ideal diagram. The steps were as follows: (a) Dimensionless constant-speed and constant-capacity characteristics were determined experimentally; (b) the efficiency was calculated and the best-efficiency point at normal pump operation was determined; (c) the percentage characteristics were calculated (corresponding to Fig. 3); and (d) the complete characteristic diagram was determined. The procedure was a point-by-point calculation, since no analytical expression could be determined for the experimental data. The constant n runs were made by setting the speed, varying the capacity, and recording the resulting values of head and torque. For every possible type of operation, the speed was varied from zero to the limits allowed by the apparatus. Three or four constant-speed runs were made over a range bracketing the design speed and varying by a factor of about three. The constant-capacity runs were carried out in similar fashion. The dimensionless plots then gave a check of experimental accuracy and the validity of the proportionality laws. The accuracy was quite satisfactory (e.g., the data spread was less than one per cent in the neighborhood of the best-efficiency points) and the proportionality laws were found to hold in every case. The dimensionless coefficients were defined as follows:

Capacity-speed coefficient, $C_Q = \frac{Q/A}{u_m^2}$ (experimental equivalent of ϕ)

Head-speed coefficient, $C_H = \frac{H}{u_m^2/g}$ (experimental equivalent of ψ)

Torque-speed coefficient, $C_T = \frac{T}{\rho A u_m^2 \frac{D_m}{2}}$ (experimental equivalent of τ)

Following Stepanoff (4) the mean peripheral velocity (u_m) is based on the mean diameter D_m , which is defined for free-vortex blading by the outer and inner diameters at the flow outlet (D_o and D_i) as $D_m = \sqrt{(D_o^2 + D_i^2)/2}$. The constant-capacity coefficients are defined as $K_s = \frac{1}{C_Q}$, $K_H = \frac{C_H}{C_Q^2}$, and $K_T = \frac{C_T}{C_Q^2}$.

It then follows that the pumping efficiency is $\eta_P = \frac{C_Q C_H}{C_T}$, and the turbine efficiency is $\eta_T = K_T/(K_s K_H)$.

It is necessary to establish a convention for the signs of the characteristic quantities. All four quantities, Q , n , H , and T are

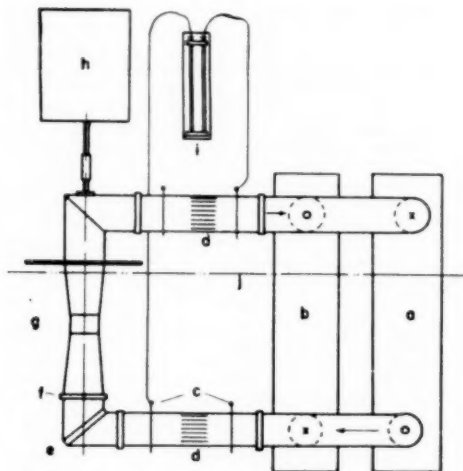


FIG. 5 SCHEMATIC DIAGRAM OF UNIT INSTALLATION SHOWING NORMAL FLOW CIRCUIT

- | | |
|---------------------------------|-------------------------|
| (a) Inlet header | (f) Victaulic couplings |
| (b) Outlet header | (g) Bowl unit |
| (c) Piezometer rings | (h) Dynamometer |
| (d) Straightening vane sections | (i) Manometer |
| (e) Vaned elbow | (j) Floor level |

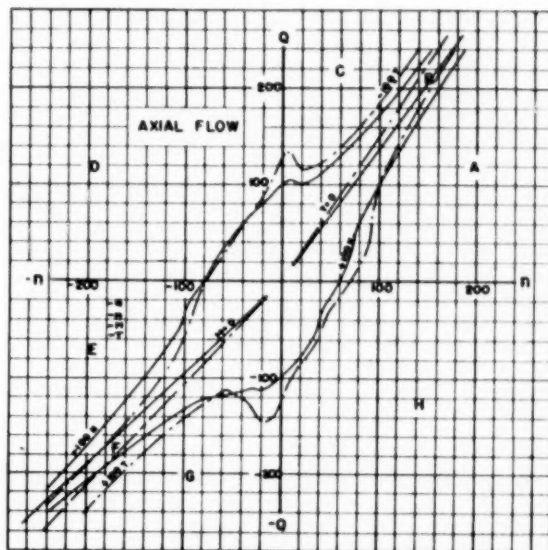


FIG. 6 COMPLETE CIRCLE CHARACTERISTIC DIAGRAM FOR A 10-IN. AXIAL-FLOW PUMP OF $n_s = 13,500$

(Solid lines are + and -100 per cent constant head; dot-dashed lines are + and -100 per cent constant torque.)

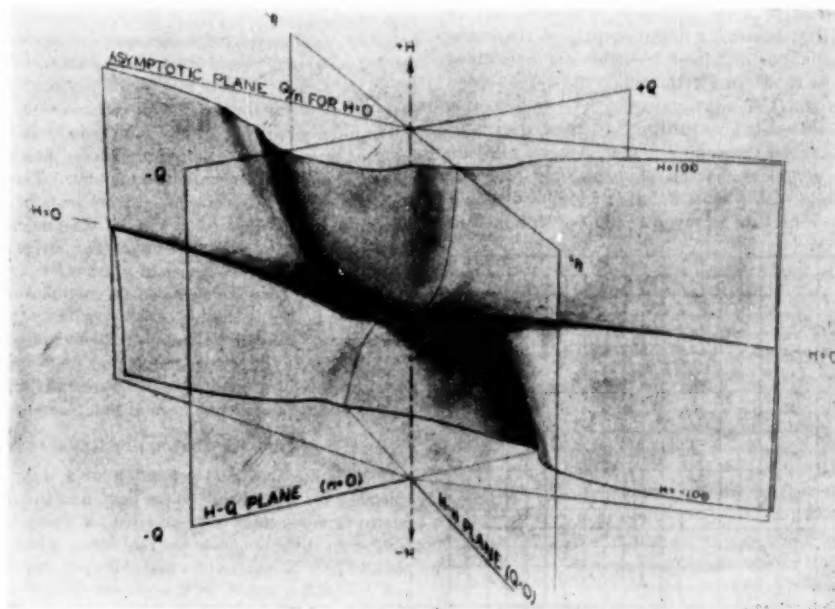


FIG. 7 THREE-DIMENSIONAL H - Q - n SURFACE REPRESENTATION OF FIG. 6

designated positive in the zone of normal or best-efficiency pump operation. Positive hydraulic power HQ is then output and positive mechanical power Tn is input. On a basis of arbitrarily defined Q - n axes, the signs are determined in a logical sequence as shown in Fig. 1 for an axial-flow unit. The boundaries of each of the useful zones are the normal limits of operation. For example, the region of normal pump operation (zone A) is bounded by $Q = 0$ (shutoff) and $H = 0$.

For the determination of a complete axial-flow characteristic,

a 10-in. pump of standard commercial practice was tested in the Hydraulic Machinery Laboratory of the California Institute of Technology in a special circuit providing for close regulation and determination of any desired type of flow (13). A schematic sketch of the circuit layout is shown in Fig. 5.

COMPLETE CHARACTERISTIC OF AXIAL-FLOW UNIT

The complete characteristic of an axial-flow unit was determined by the method described and is shown in Fig. 6. The

essential differences between this and an ideal diagram, as noted under the section on real flow considerations, are seen here. Small loss zones (B and F) are seen between each pump and turbine zone, with large dissipation zones (D and H) going from turbine to pump (counterclockwise). The finite shutoff torque and locked-rotor head values are shown. A comparison of the analytical and experimental diagrams for this particular unit showed a good correspondence in the normal pump region for capacities above 50 per cent. The reverse pump zone E would not show very good agreement between ideal and real flow conditions because of the blades operating with reverse camber, interchanged leading and trailing edges, and poor guide-vane conditions.

The complete characteristic representation covering all possible operating conditions would be represented best by 2 three-dimensional surface plots; one $T-Q-n$ and one $H-Q-n$ surface. A schematic sketch of the $H-Q-n$ surface, as it would appear for this unit, is shown in Fig. 7.

COMPARISON OF AXIAL, MIXED, AND RADIAL-FLOW MACHINES

The procedure for determining the ideal characteristics of a centrifugal or radial-flow machine would be difficult. Reverse rotation of the axial-flow unit logically produced reverse flow. The operation of a radial-flow unit in reverse rotation resembles the operation of a radial-flow fan with forward-curved vanes so that the flow is still in the same (+ Q) direction as for operation as a normal pump. In this case the reverse pump zone of operation is seen to be in the second quadrant (+ Q , $-n$). The efficiency remains positive since the ratio of (+ Q)($-H$) to (T)($-n$) is still positive, denoting a useful output. A characteristic diagram for a radial-flow unit (double suction), as determined by R. T. Knapp (3), is shown in Fig. 8. While the specific speed shown is figured from the Q , H , and n -values of the double-suction pump so that each half would give 1270 specific speed, the single-suction pump built later for the same Q , H , and n -values had substantially the same complete characteristics making these and later comparisons valid with respect to either a double or single-suction pump. The difference in reverse pump operation from

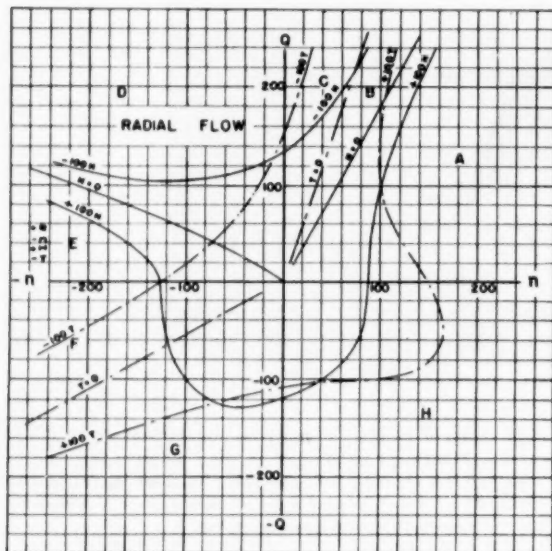


FIG. 8 COMPLETE CIRCLE CHARACTERISTIC DIAGRAM FOR A DOUBLE-SUCTION RADIAL-FLOW UNIT OF $n_s = 1800$
(Solid lines are + and -100 per cent constant head; dot-dashed lines are + and -100 per cent constant torque.)

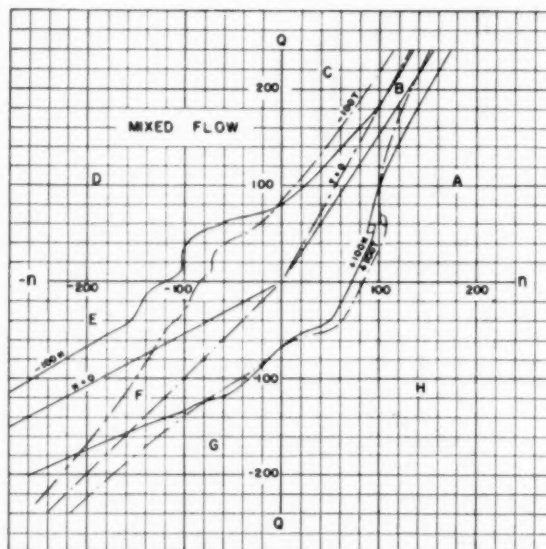


FIG. 9 COMPLETE CIRCLE CHARACTERISTIC DIAGRAM FOR A 10-IN. MIXED-FLOW UNIT OF $n_s = 7550$
(Solid lines are + and -100 per cent constant head; dot-dashed lines are + and -100 per cent constant torque.)

that of the axial-flow unit is noticed readily. Other variations noted are (a) larger friction-loss zones, B and F, which might be attributed to larger surfaces in moving contact with the fluid, and (b) a less effective zone of energy dissipation H, which is perhaps mainly due to the inward flow direction.

The difference in operating characteristics in the reverse pumping zone posed the interesting problem of how a mixed-flow unit would behave as a reverse rotation pump. The complete characteristic diagram was determined from tests of a commercial 10-in. unit, and is presented in Fig. 9. The behavior is essentially the same as for the axial-flow unit. The size of the reverse pump zone is smaller at the expense of a larger loss zone F. Bumps in the dissipation zone D also indicate a combination of effects. This particular unit was in the higher-specific-speed range with the mean through-flow direction being at an angle of only 35 deg from the axis so that the reverse pump zone might have been expected to fall in the third quadrant. A notable feature of this unit was the instability loop in the normal pump zone.

METHOD OF EFFICIENCY REPRESENTATION

Considering the ideal operation of a unit, by definition its efficiency is everywhere 100 per cent, and the power ratio of output to input is unity and positive for every type of operation. Neither of these holds for the real case. The power ratio will be positive only in regions of a useful output and negative in the loss and dissipation zones, as is apparent from Fig. 2, or any of the circle diagrams.

A satisfactory method of representing efficiency, or power ratio, on a single diagram at first appears difficult.³ Consider an attempt to extend the pump efficiency (η_p). The ratio of HQ to Tn can be extended beyond the zero value obtained for zero head (as shown in Fig. 10) but, as the torque approaches zero, this ratio can be seen to approach minus infinity. In the negative Q -direction, HQ and T get very large with n remaining constant, so that this ratio again approaches minus infinity. The inverse ratio,

³ It is possible to show iso-efficiency contours on the circle diagram, Fig. 2; however, some difficulty is encountered in the loss and dissipation regions and the diagram becomes complicated.

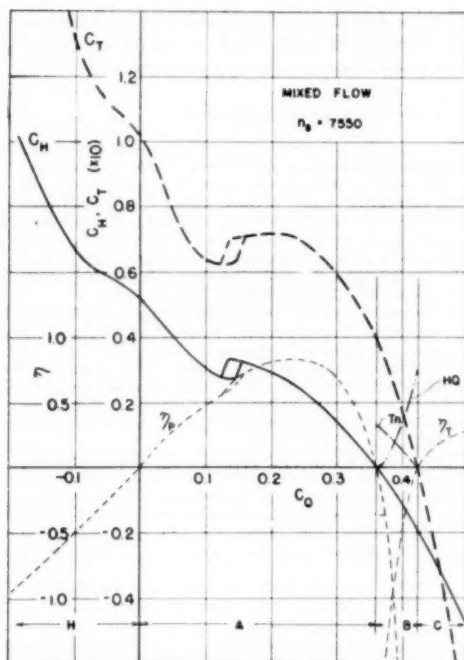


FIG. 10 HEAD AND TORQUE-CAPACITY CHARACTERISTICS FOR POSITIVE ROTATION SHOWING POWER AND EFFICIENCY REPRESENTATION IN A ZONE OF NO USEFUL OUTPUT (Solid line, dimensional head-capacity characteristic; dashed line, torque-capacity characteristic; dotted line, efficiency versus dimensionless capacity; dot-dot-dashed lines, hydraulic HQ , and mechanical power Tn .)

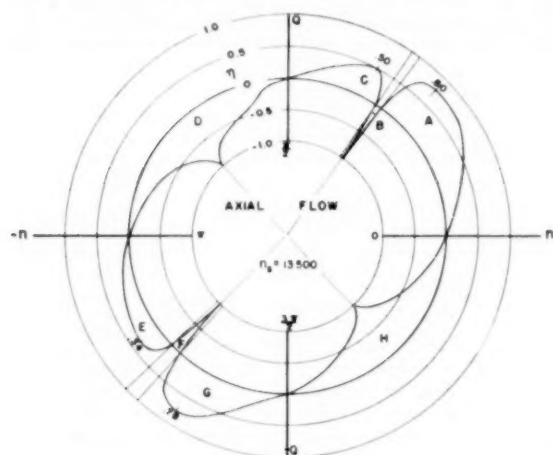


FIG. 11 POWER-RATIO CIRCLE CHARACTERISTIC FOR AN AXIAL-FLOW PUMP

or turbine efficiency (η_T) also will show similar difficulties. However, considering the hydraulic and shaft power between the pump and turbine zones (zone B), each is seen to be zero or finite with a point of intersection where their ratio will be -1 . Between each pump and turbine zone such a condition will exist. Therefore the assumptions are made that any operation, where HQ exceeds Tn in absolute value, will be a pump-type operation and that an operation where Tn is greater in absolute value will be a turbine-type operation. On this basis, a scheme for representing the entire

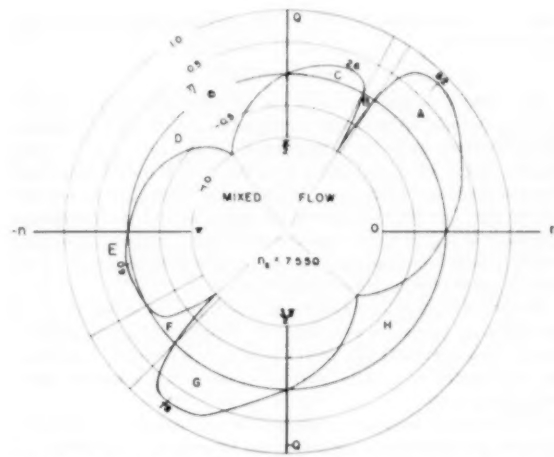


FIG. 12 POWER-RATIO CIRCLE CHARACTERISTIC FOR A MIXED-FLOW PUMP

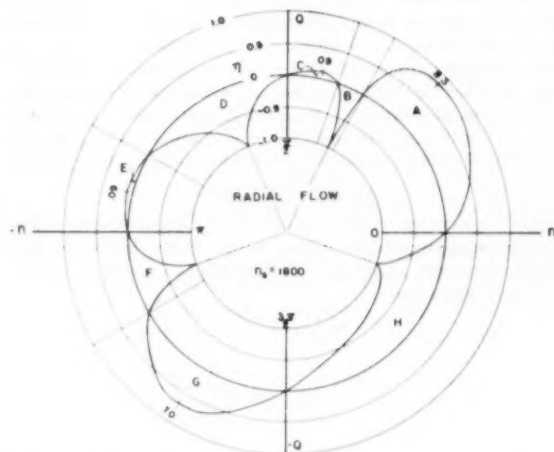


FIG. 13 POWER-RATIO CIRCLE CHARACTERISTIC FOR A RADIAL-FLOW PUMP

power ratio or efficiency history on a single diagram was determined by Prof. A. Hollander of the California Institute of Technology.

With the foregoing assumptions, values of power ratio are plotted radially between the limits of $+1$ and -1 on Q - and n -coordinates. The resulting diagrams are shown in Figs. 11, 12, and 13. The cusps are of some interest in that they indicate the angles of zero lift and maximum stall. The axial-flow unit shows lines connecting these cusps to be nearly perpendicular, indicating a low solidity and a small camber. For the axial-flow unit, the magnitudes of the efficiencies in the abnormal zones can be attributed to conditions described in the section, Complete Characteristics of an Axial-Flow Unit. For the radial-flow pump, the maximum efficiency in the normal turbine zone is usually equal to, or a little greater than the maximum normal pump efficiency for a simple single-stage unit. That this is not the case here may be attributed primarily to the adverse flow conditions obtained when operating a double-suction unit with the flow reversed. The reverse pump efficiency would be expected to be low as would the reverse (outflow) turbine efficiency. The mixed-flow unit

shows a combination of effects but, predominantly, axial-flow characteristics.

CONCLUSIONS

The complete characteristics for an axial-flow pump (with a specific speed of 13,500) and a mixed-flow pump (with a specific speed of 7550) have been presented for the first time. These characteristics when compared with those for a radial-flow pump (equivalent single-suction specific speed = 1270) give a comparison for the three basic types over a wide range of specific speeds. The manner in which the axial and radial-flow tendencies combine for the mixed-flow performance can be seen with reference to the experimental characteristics obtained.

A new method of a complete representation of efficiency at all conditions of operation is presented. Pump and turbine efficiencies (or power ratios) and power ratios for power-loss conditions are represented as a radial parameter on capacity versus speed-co-ordinate axes.

A theoretical complete characteristic is possible to determine, but is of a limited value because of the adverse flow conditions encountered at conditions of abnormal operation. A comparison of ideal and experimental characteristics for the axial-flow unit tested ($n_s = 13,500$) showed good agreement between capacities of from 50 per cent to the zero-head capacity. There is little basis for any comparison at any other operating condition as indicated by the low efficiencies in all zones of operation except those of normal pump and normal turbine. However, such an ideal diagram is desirable if a unit is to be designed for more than one specific type of operation. By considering the deviations noted here and with the experimental circle diagrams available, the total actual circle characteristics may be estimated fairly closely.

ACKNOWLEDGMENT

The experimental work was carried out under the very able and appreciated guidance of Prof. Aladar Hollander, whose suggestions, interest, knowledge, and experience have been a great help and inspiration.

The author also wishes to acknowledge the Peerless Pump Division of the Food Machinery Corporation for supplying the pumps on which these experiments were conducted.

BIBLIOGRAPHY

- 1 "Vorgänge beim Ausfallen des Antriebes von Kreisel pumpen," by D. Thoma, *Mitteilungen des Hydraulischen Institute der Technischen Hochschule, Munich, Germany*, vol. 4, 1931, pp. 102-104.
- 2 "Centrifugal Pumps Operated Under Abnormal Conditions," by C. P. Kittredge, vol. 73, 1931, pp. 881-884. (English translation of 1.)
- 3 "Complete Characteristics of Centrifugal Pumps and Their Use in the Prediction of Transient Behavior," by R. T. Knapp, *Trans. ASME*, vol. 59, 1937, pp. 683-689 (for 8-in. pumps).
- 4 "Some Characteristics of Centrifugal Pumps," by R. T. Knapp, preprints of ASME University of California and Stanford Summer Meeting, June, 1934 (for 4-in. pumps).
- 5 "Centrifugal and Axial Flow Pumps," by A. J. Stepanoff, John Wiley & Sons, Inc., New York, N. Y., 1948, chapters 5 and 8.
- 6 "Special Operating Conditions of Centrifugal Pumps," by A. J. Stepanoff, *Hydraulic Institute Fourth Annual Contest Engineering Papers*, 1944.
- 7 "Centrifugal-Pump Performance as Affected by Design Features," by R. T. Knapp, *Trans. ASME*, vol. 63, 1941, pp. 251-260.
- 8 "Die Strömung um die Schaufeln von Turbomaschinen," by F. Weig, J. A. Barth, Leipzig, Germany, 1935.
- 9 "Fluid Mechanics of Turbomachinery," by G. F. Wislicenus, McGraw-Hill Book Company, Inc., New York, N. Y., 1947, p. 451, chapters 7 and 9.
- 10 "A Study of the Theory of Axial-Flow Pumps," by G. F. Wislicenus, *Trans. ASME*, vol. 67, 1945, pp. 451-463.
- 11 "Das Förderhöhenverhältnis radialer Kreiselpumpen mit logarithmischspiraligen Schaufeln," by A. Busemann, *Zeitschrift für Angewandte Mathematik und Mechanik*, vol. 8, 1928, pp. 372-384.
- 12 "Konforme Abbildung in Hydraulische Probleme," by W. Spannhake, VDI Verlag, Berlin, Germany, 1926.
- 13 "Complete Circle Characteristic Diagrams for Turbomachinery," by W. M. Swanson, thesis, California Institute of Technology, 1951.
- 14 "Laboratory Development for Study of Flow in Rotating Channels," by R. T. Knapp, A. Hollander, A. J. Acosta, and W. C. Osborne, paper presented at the Annual Meeting, New York, N. Y., 1948, of THE AMERICAN SOCIETY OF MECHANICAL ENGINEERS.

Theoretical Consideration of Retarded Control

BY G. H. COHEN¹ AND G. A. COON,² ROCHESTER, N. Y.

This paper is concerned with a theoretical study of the control of a single-capacity process with dead-period lag. Characteristic equations corresponding to the application of proportional, proportional-plus-derivative, proportional-plus-reset, and proportional-plus-reset-plus-derivative responses are used to graph the controller parameters necessary to obtain a desired degree of stability. The degree of stability is taken to be associated with the amplitude ratio of the lowest-frequency harmonic mode. Effects of the various controller parameters are shown and a method is suggested to determine the adjustable parameters for a desired degree of stability.

EVER since the publication by Callender, Hartree, and Porter (1)³ considerable attention has been directed to the study of the dynamics of control of retarded systems. Some interest has been shown in the "optimum adjustment" of the control parameters for particular types of control functions and process characteristics (2-7). It is the purpose of this paper to study the control of a single-capacity process with dead-period lag. The controller will be assumed to be conventional; i.e., it will have available proportional, integral or reset, and derivative responses.

The two principal components of the control loop are the process and the controller. The process is considered to include all parts of the installation exclusive of the controller. For this discussion the final control element or valve will be included with the process.

The process can be characterized by its reaction curve which is the chart record obtained when the valve is given a sudden sustained disturbance with the controller disconnected. Such a record is shown in Fig. 1(a) for a unit change in pressure. There appears to be a period of time during which the pen moves but little and this dead time or lag L may be of some magnitude in comparison with the transfer lag (the lag due to the lumped capacity of the process). The dead time is due to the fact that the process is really a continuum where the parameters which describe the process are distributed. The lag due to the finite time of transport of the signal (for example, a long tube which carries a compressible fluid) is called a distance-velocity lag. If the continuum contains no inertia, it may be represented by a number of cascaded lumped resistance-capacity networks. Increasing the number of the cascaded elements gives a better approximation to the continuum since the order of contact with the time axis increases with the number of elements in the lumped circuit approximation. However, the complexity of the problem increases with the number of elements.

¹ Research Engineer, Engineering Research Department, Taylor Instrument Companies, Jun. ASME.

² Mathematician, Engineering Research Department, Taylor Instrument Companies.

³ Numbers in parentheses refer to Bibliography at end of paper. Contributed by the Industrial Instruments and Regulators Division and presented at the Fall Meeting, Chicago, Ill., September 7-11, 1952, of THE AMERICAN SOCIETY OF MECHANICAL ENGINEERS.

NOTE: Statements and opinions advanced in papers are to be understood as individual expressions of their authors and not those of the Society. Manuscript received at ASME Headquarters, September 12, 1951.

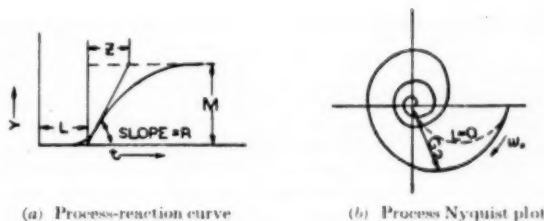


FIG. 1

A good approximation which has the advantage of simplicity may be obtained by introducing a certain amount of dead time along with one or two resistance-capacity elements. In this paper we approximate the reaction curve by using dead time and a single-capacity lag.

The following differential equation can be used as the first approximation to the process

$$\frac{dY}{dt} + \frac{R}{M} Y = R \Delta F(t - L) \quad [1]$$

where Y = pen deviation from set point, in.

R = unit reaction rate, in/psi min

t = time, min

M = process sensitivity, in/psi

L = dead-period lag, min

ΔF = controller output change, psi

Z = process time constant, min

The frequency response G_2 is

$$G_2 = \frac{Y(i\omega_0)}{\Delta F(i\omega_0)} = \frac{R e^{-i\omega_0 L}}{R + i\omega_0 M}, \quad i = \sqrt{-1}$$

as shown in Fig. 1(b) where ω_0 is the applied angular frequency.

We will consider a controller to regulate the process which has proportional, integral and derivative response functions. This controller may be represented by the following differential equation

$$-\Delta F(t) = S \left[U \int_0^t Y(\sigma) d\sigma + Y(t) + T \frac{dY(t)}{dt} \right] \quad [2]$$

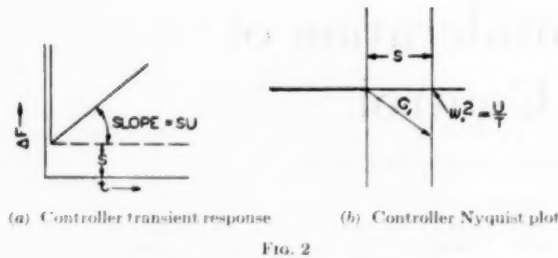
where S = proportional sensitivity, psi/in

U = reset rate, min⁻¹

T = derivative time, min

The controller response to a unit step in pen deviation and frequency response G_1 are shown in Figs. 2(a) and 2(b). It is more interesting to make a phase-magnitude plot for a sinusoidal variation in $Y(t)$ as shown in Fig. 3. This shows that the conventional controller can be considered as a band-rejection filter and amplifier, the low-frequency corner being determined by the reset rate and the high-frequency corner by the derivative time. Proportional sensitivity sets the amount of gain in the rejection band.

Since we are concerned with "regulators" we will consider



only those disturbances which can be represented by a change in load and not by a change in set point. One can easily go from one to the other. In this investigation the load change occurs at the valve end of the process at zero time and produces the same reaction curve as a step change in pressure at the valve. For the approximation to a single-capacity process with dead-period lag we can write

$$\frac{dY(t)}{dt} + \frac{R}{M} Y(t) = R \Delta F(t - L) + R \Delta D(t - L) \dots [3]$$

where ΔD is the load change, psi. In order to get the control-loop equation in nondimensional form, we introduce the following notation:

$$\mu = \frac{RL}{M} = \text{self-regulation index of process} \\ (\mu \rightarrow 0 \text{ when } M \rightarrow \infty)$$

$$\tau = \frac{t}{L} = \text{dimensionless "time"}$$

$$\theta(\tau) = \frac{Y(L\tau)}{RL\Delta D_0} = \text{dimensionless "pen deviation"}$$

$SRL =$ dimensionless proportional sensitivity setting

$UL =$ dimensionless reset "rate" setting

$T =$ dimensionless derivative time setting

$L =$

$v_1 = SRL(UL) =$ integral parameter

$v_2 = SRL =$ sensitivity parameter

$v_3 = SRL \left(\frac{T}{L} \right) =$ derivative parameter

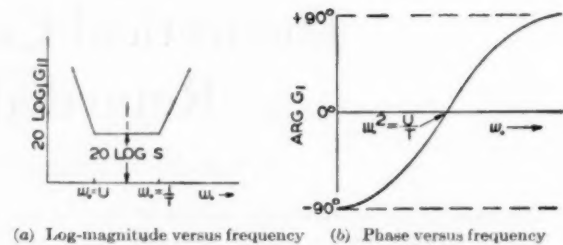
For a constant disturbance ΔD_0 the control loop may be represented by the differential equation

$$\frac{d\theta}{d\tau} + \mu\theta(\tau) = -v_1 \int_0^{\tau-1} \theta(\sigma) d\sigma - v_2 \theta(\tau-1) \\ - v_3 \frac{d\theta(\tau-1)}{d\tau} + 1 \dots [4]$$

The ultimate aim in the adjustment of controllers is to obtain a response curve which will satisfy the user's requirement for good control. The quality of control is therefore relative to the application. The user usually wants minimum area under the response curve, minimum deviation, and minimum cycling. Ziegler and Nichols (2) suggest that the amplitude ratio of the response curve be about 0.25, and this is a commonly accepted rule of thumb in the process industry.

Since retarded action implies that the response curve consists of an infinite number of harmonic modes, it would be fruitless to prescribe the amplitude ratio for each mode. We shall, therefore, designate the "degree of stability" to be associated with the amplitude ratio of the fundamental (lowest-frequency) harmonic mode.

Adjustment of the controller will be based on information ob-



tained from the control region. We define the control region to be the graphic relationship between the adjustable control parameters necessary to obtain a prescribed degree of stability of the response curve. The characteristic equation of the control loop is used to plot the control region.

The control region may also be obtained by means of the well-known methods of frequency analysis. Instead of using the amplitude ratio of the fundamental harmonic mode as a measure of degree of stability, the loci of "constant magnitude" are commonly used. Since this method has received considerable attention in the past years, we will not consider it as a basis of analysis. Moreover, there is at times serious error in estimating stability and response from these diagrams (8).

We will now consider the special cases of proportional control, proportional-plus-derivative control, proportional-plus-reset control, and proportional-plus-reset-plus-derivative control.

PROPORTIONAL CONTROL ($v_1 = v_2 = 0$)

The control relationships are obtained from the characteristic equation which for this case becomes

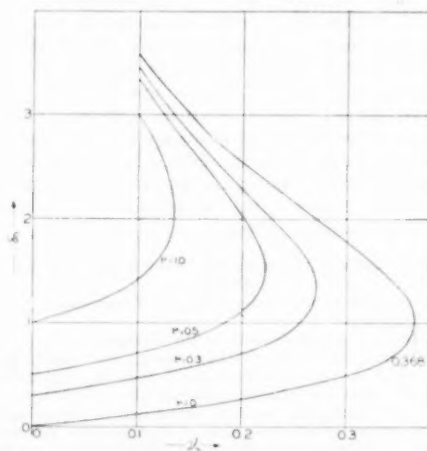
$$p + \mu + v_2 e^{-p} = 0 \dots [5]$$

There is an infinite number of roots corresponding to Equation [5], the real roots ($p = -\delta_n$) being shown in Fig. 4. We are interested primarily in the pair of complex roots with the lowest-frequency component which we denote by

$$p = \omega(-\tau \pm i) \dots [6]$$

where $a =$ amplitude ratio of fundamental mode

$$\tau = -\frac{1}{2\pi} \ln a$$



$\omega = 2\pi \frac{L}{P}$ dimensionless angular frequency of fundamental mode

$P =$ period, min

Substitution of Equation [6] into [5] and separation of the real and imaginary parts yields

$$\frac{\tan \omega}{\omega} = \frac{1}{\omega r - \mu}$$

and

$$\nu_2 = \frac{\omega}{\sin \omega} e^{-r\omega}$$

The foregoing equations define the control region for proportional control as shown in Fig. 5. The sensitivity parameter is plotted against the self-regulation index μ . The solid lines are contours of constant amplitude ratio a of the fundamental while the broken lines are loci of constant dimensionless period P/L .

If the disturbance is a Heaviside step of height ΔD_0

$$\theta(\tau) = \frac{1}{\nu_2 + \mu} + \sum_{n=0}^{\infty} A_n e^{-\omega_n \tau} \cos(\omega_n \tau - \phi_n) + \sum_n B_n e^{-\delta_n \tau} \dots [\tau]$$

provided there are no repeated roots of the characteristic equation and where

$A_n =$ harmonic amplitudes

$\omega_n =$ harmonic frequencies

$\phi_n =$ associated phase angles

$r_n \omega_n =$ damping constants for each harmonic mode

$\delta_n =$ damping constants corresponding to real roots

The amplitudes of the first three harmonics are shown in Table 1.

TABLE 1 APPROXIMATE AMPLITUDES OF HARMONICS, PROPORTIONAL CONTROL

(Amplitude ratio of fundamental = 0.25)			
μ	A_0	A_1	A_2
0	0.858	0.0332	0.010
0.1	0.836	0.0332	0.010
0.3	0.696	0.0332	0.010
0.5	0.588	0.0332	0.010
0.7	0.502	0.0332	0.010
1.0	0.406	0.0332	0.010

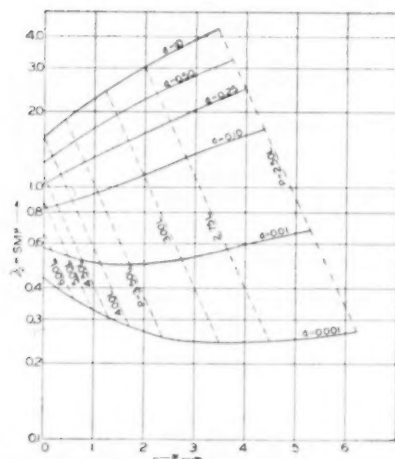


FIG. 5 CONTROL REGION FOR PROPORTIONAL CONTROL

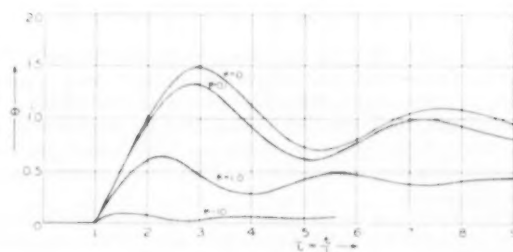


FIG. 6 RESPONSE CURVES FOR PROPORTIONAL CONTROL, $a = 0.25$

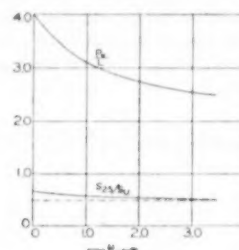


FIG. 7 COMPARISON OF ULTIMATE AND 0.25 AMPLITUDE RATIO SENSITIVITIES

TABLE 2 OFFSET, INITIAL DEVIATION, AND PERIOD, PROPORTIONAL CONTROL

(Amplitude ratio of fundamental = 0.25)					
μ	SRL	θ_i	P/L	ν_1	$\theta(\tau_1)$
0	1.03	0.970	4.7	2.97	1.49
0.10	1.05	0.870	4.4	2.86	1.33
1.0	1.30	0.435	3.4	2.28	0.68
10.0	5.19	0.066	2.2	2.00	0.10

It is evident that for $0 \leq \mu \leq 1$ all of the higher harmonics in Equation [7] are negligible in comparison with the fundamental. Thus, if one chooses the amplitude ratio of the fundamental to be 0.25, the response curve will have approximately this degree of stability.

The offset $1/(\nu_2 + \mu)$ and the time and magnitude of the initial deviation (height of the first peak) of the response curve are shown in Table 2 for various values of self-regulation and an amplitude ratio of 0.25. It is seen that the initial deviation is about one and one-half times the offset.

A few representative response curves are shown in Fig. 6 for the case of proportional control. These curves are easily sketched by obtaining from Fig. 5 the sensitivity setting ν_2 and period for the process characteristic and desired degree of stability. For an amplitude ratio of 0.25, the time and amount of initial deviation as well as the offset may be determined from Table 2.

Fig. 7 shows the ratio of the sensitivity settings S_{25} necessary to obtain an amplitude ratio of 0.25 to the settings necessary to obtain an amplitude ratio of unity (the ultimate sensitivity S_u) as well as the period corresponding to this ultimate sensitivity.

PROPORTIONAL-PLUS-DERIVATIVE CONTROL ($\nu_1 = 0$)

The characteristic equation corresponding to this case is

$$p + \mu + e^{-P}(v_2 + v_3 p) = 0$$

As before, we obtain the equations for the control region

$$\nu_3 = (r \sin \omega - \cos \omega) e^{-\omega r} - \mu e^{-\omega r} \frac{\sin \omega}{\omega}$$

$$v_2 = (1 + r^2)e^{-r\omega} \omega \sin \omega - \mu e^{-r\omega} (r \sin \omega + \cos \omega)$$

Figs. 8 and 9 show the μ -contours in the control region for amplitude ratios of 0.25 and 1.0 (the stability-limit case). As one chooses settings along a 0.25-amplitude contour for a fixed μ , it is found that the controlled response changes considerably in character. Table 3 shows what happens to the offset, the time of initial deviation, the magnitude of the initial deviation, and period for $\mu = 0$.

It is evident that for the offset to be a minimum v_2 should be between 0.3 and 0.4. For larger values of v_2 the offset increases at a rapid rate. The corresponding values are shown in Table 4 for a self-regulation index μ of 0.3.

If 0.25-amplitude ratio is desirable and if minimum offset is required, then the controller can be adjusted according to Table 5. The period, initial deviation, magnitude of initial deviation, offset, and linear approximations for the settings also are shown for various values of μ .

TABLE 3 CHARACTERISTICS OF RESPONSE CURVES, PROPORTIONAL-PLUS-DERIVATIVE CONTROL

$\mu = 0$		$a = 0.25$			
v_1	v_2	θ_f	P/L	r_f	$\theta(r_f)$
0.1	1.120	0.89	1.21	2.80	1.36
0.2	1.195	0.81	3.84	2.67	1.27
0.3	1.235	0.81	3.49	2.57	1.20
0.4	1.225	0.82	3.13	2.49	1.15
0.5	1.081	0.93	2.74	2.45	1.12

TABLE 4 CHARACTERISTICS OF RESPONSE CURVES, PROPORTIONAL-PLUS-DERIVATIVE CONTROL

$\mu = 0.3$		$a = 0.25$			
v_1	v_2	θ_f	P/L	r_f	$\theta(r_f)$
0.1	1.182	0.68	3.76	2.55	1.02
0.2	1.245	0.65	3.48	2.45	0.98
0.3	1.267	0.64	3.17	2.38	0.94
0.4	1.228	0.65	2.86	2.31	0.91

TABLE 5 CHARACTERISTICS FOR PROPORTIONAL-PLUS-DERIVATIVE CONTROL WITH MINIMUM OFFSET AND 0.25 AMPLITUDE RATIO

$v_2 \approx 0.161 \mu + 1.240$					
$v_1 \approx -0.111 \mu + 0.335$					
μ	θ_f	P/L	r_f	$\theta(r_f)$	
0	0.81	3.40	2.55	1.17	
0.1	0.75	3.31	2.48	1.09	
0.3	0.64	3.16	2.38	0.94	
0.5	0.55	3.05	2.28	0.83	
0.7	0.49	2.96	2.20	0.74	
1.0	0.42	2.88	2.12	0.64	

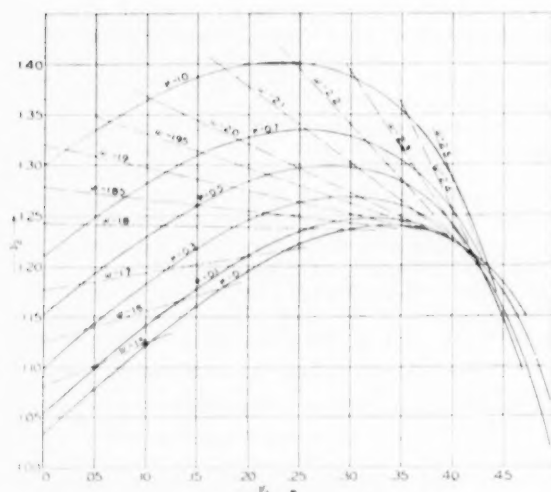


FIG. 8 CONTROL REGION FOR PROPORTIONAL-PLUS-DERIVATIVE CONTROL, $a = 0.25$

The response curves for $\mu = 0$ and $\mu = 0.3$ are shown in Fig. 10.

PROPORTIONAL-PLUS-RESET CONTROL ($v_2 = 0$)

The addition of reset response removes offset, but tends to make the system more unstable. The characteristic equation for this case may be written

$$p^2 + p\mu + e^{-r} (v_1 + v_2 p) = 0$$

and the control region is defined by

$$\begin{aligned} v_2 &= \omega e^{-r\omega} [2r \cos \omega + (1 - r^2) \sin \omega] \\ &\quad + \mu e^{-r\omega} [r \sin \omega - \cos \omega] \\ v_1 &= v_2 r \omega + \omega^2 e^{-r\omega} [(1 - r^2) \cos \omega - 2r \sin \omega] \\ &\quad + \mu \omega e^{-r\omega} [r \cos \omega + \sin \omega] \end{aligned}$$

These equations allow one to plot the control region shown in Fig. 11. The control parameter v_2 is plotted against v_1 for various μ and for an amplitude ratio of 0.25. The contours for the stability-limit case and for critical damping are shown in Figs. 12 and 13, respectively.

It is also known that the control area is

$$\int_0^\infty \theta(\sigma) d\sigma = \frac{1}{v_1}$$

As one progresses along a particular contour of 0.25 amplitude ratio, it is found that the control area does not change very much in the neighborhood of maximum v_1 but the frequency does. It is desirable to keep the frequency as large as possible and retain minimum control area.

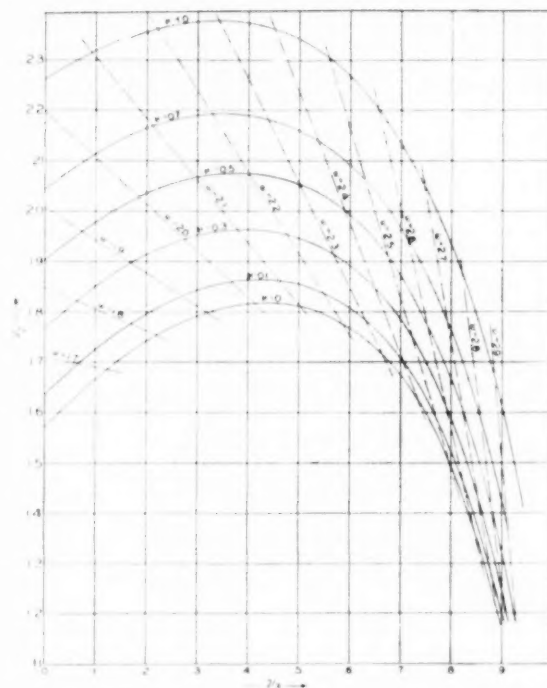


FIG. 9 STABILITY LIMITS FOR PROPORTIONAL-PLUS-DERIVATIVE CONTROL

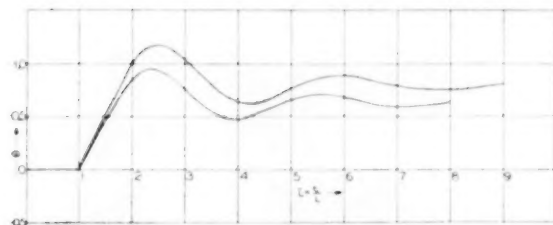


FIG. 10 RESPONSE CURVES FOR PROPORTIONAL-PLUS-DERIVATIVE CONTROL, $a = 0.25$, MINIMUM OFFSET (Upper curve $\mu = 0$, lower curve $\mu = 0.3$)

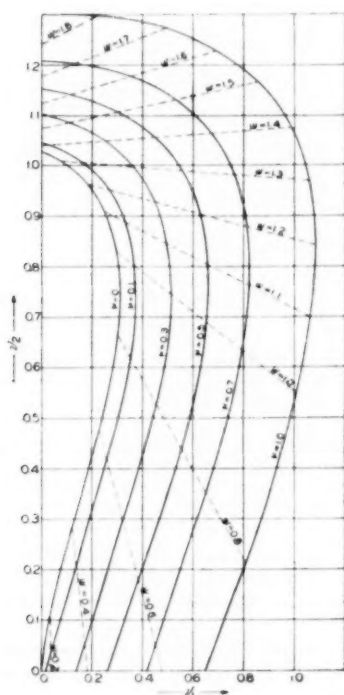


FIG. 11 CONTROL REGION FOR PROPORTIONAL-PLUS-RESET CONTROL, $a = 0.25$

Fig. 14 shows response curves for settings chosen along the 0.25 amplitude contour in the control region.

If it is desirable that the response curve be critically damped so that most of the area of the curve is above the control point, then Fig. 13 is used. For this case the criterion of minimum control area is the selection of the maximum value of v_1 on the contour of critical damping.

PROPORTIONAL-PLUS-RESET-PLUS-DERIVATIVE CONTROL

If derivative action is added to a proportional-plus-reset controller, the characteristic equation is

$$p^2 + p\mu + e^{-\rho}(v_1 + v_2 p + v_3 p^2) = 0$$

Again we find

$$v_2 = e^{-\omega} [(2r\omega - \mu) \cos \omega + [\mu r + \omega(1 - r^2)] \times \sin \omega] + 2r\omega v_3$$

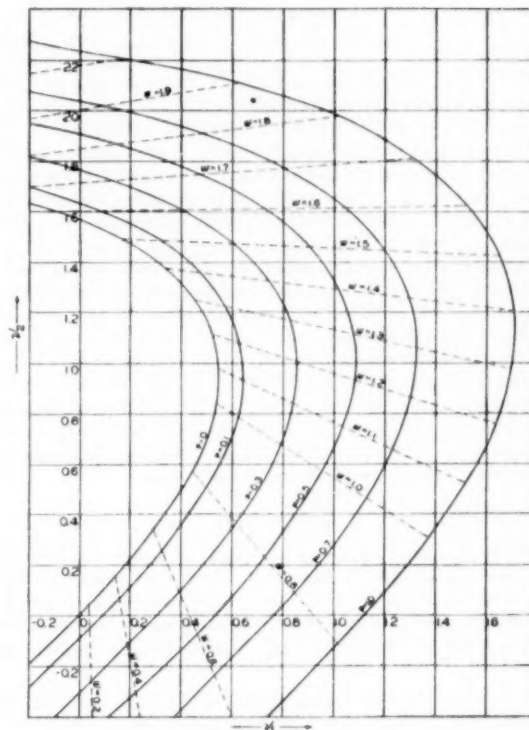


FIG. 12 STABILITY LIMITS FOR PROPORTIONAL-PLUS-RESET CONTROL

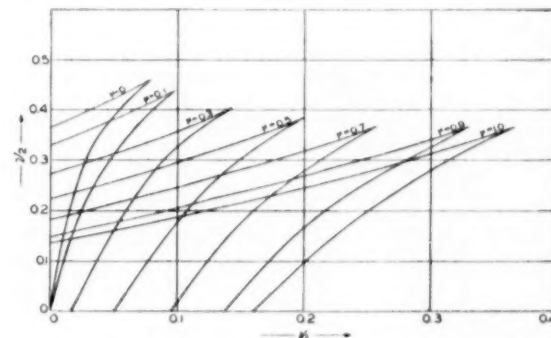


FIG. 13 CRITICAL DAMPING CONTOURS FOR PROPORTIONAL-PLUS-RESET CONTROL

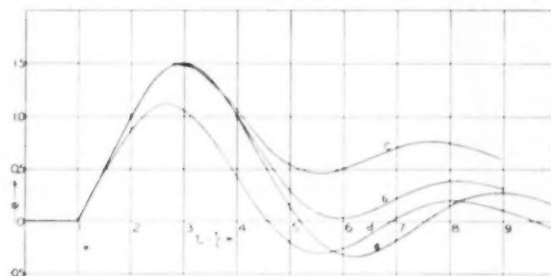


FIG. 14 RESPONSE CURVES FOR PROPORTIONAL-PLUS-RESET CONTROL

(a) $\mu = 0$, $v_1 = 0.27$, $v_2 = 0.90$; (b) $\mu = 0$, $v_1 = 0.18$, $v_2 = 0.96$; (c) $\mu = 0$, $v_1 = 0.073$, $v_2 = 1.01$; (d) $\mu = 0.3$, $v_1 = 0.45$, $v_2 = 0.93$

$$v_1 = \omega r v_2 + \omega e^{-\omega t} \{ [\mu r + \omega(1 - r^2)] \cos \omega t + (\mu - 2r\omega) \times \sin \omega t \} + \omega^2(1 - r^2)v_2$$

The control regions obtained from the foregoing equations are shown in Figs. 15 and 16 when the fundamental harmonic component of the response curve has an amplitude ratio of 0.25.

There is an infinite number of modes which add up to the actual response. The introduction of derivative makes it possible to have a set of values of v_3 , v_2 , and v_1 yield not only a mode having 0.25 amplitude ratio but also a critically damped mode. The contours for the stability limit are shown in Figs. 17 and 18.

Representative response curves for parameters chosen on a 0.25 amplitude ratio contour for $\mu = 0$ and $\mu = 0.3$ are shown in Figs. 19 and 20. The values of the parameters in Fig. 20 were taken so as to make the control area a minimum when $v_3 = 0.5$ (curve a), to make the parameter v_2 a maximum when $v_3 = 0.5$ (curve b), and to satisfy both 0.25 amplitude ratio and critical damping when $v_3 = 0.5$ (curve c). The parameter $v_3 = 0.5$ gives approximately the largest possible value of v_2 satisfying simultaneously the condition of the critical damping and 0.25 amplitude ratio. Curve c may be considered optimum.

CONCLUSIONS

We have shown how the control regions are used to determine the control-parameter settings for a prescribed degree of stability of the response curve. One must be able to obtain the process constants μ , R , and L from the process-reaction curve and to write the linearized approximate equations for the controller.

Since there is a degree of latitude in the actual controller settings, this method suffices for most practical cases. This is evi-

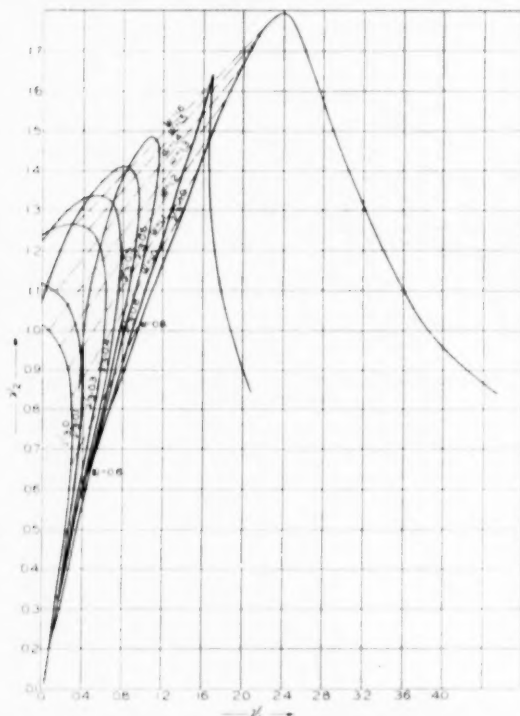


FIG. 15 CONTROL REGION FOR PROPORTIONAL-PLUS-RESET-PLUS-DERIVATIVE CONTROL, $\mu = 0$, $a = 0.25$

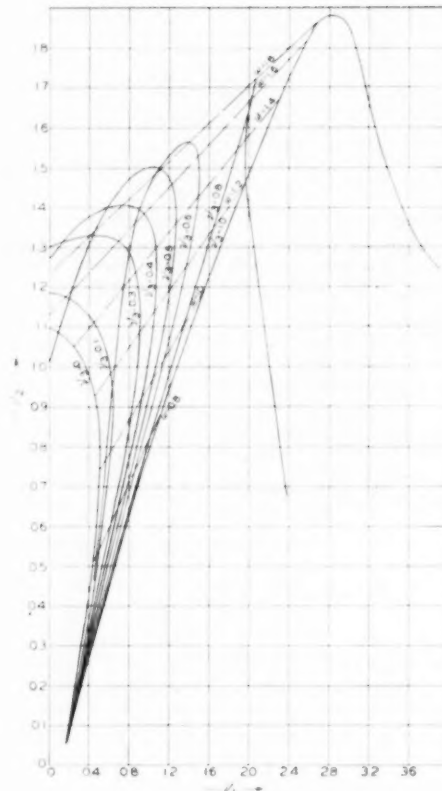


FIG. 16 CONTROL REGION FOR PROPORTIONAL-PLUS-RESET-PLUS-DERIVATIVE CONTROL, $\mu = 0.3$, $a = 0.25$

dent by the fact that the settings prescribed by Ziegler and Nichols have been commonly accepted. However, the Ziegler-Nichols settings do not take into consideration the self-regulation of the process.

We therefore suggest the following settings, if the degree of stability specified by 0.25 amplitude ratio for the fundamental mode is desirable:

Proportional control (criterion, 0.25 amplitude ratio)

$$v_2 = 1.03 + 0.35 \mu \dots \dots \dots [8]$$

Proportional-plus-derivative (criteria, 0.25 amplitude ratio and minimum offset)

$$\left. \begin{aligned} v_2 &= 1.24 + 0.16 \mu \\ v_1 &= 0.34 - 0.11 \mu \end{aligned} \right\} \dots \dots \dots [9]$$

Proportional-plus-reset (criteria, 0.25 amplitude ratio and compromise between minimum area and period)

$$v_2 = 0.9 + 0.083 \mu \quad v_1 = 0.27 + 0.6 \mu \dots \dots [10]$$

Proportional-plus-reset-plus-derivative (criteria, 0.25 amplitude ratio and critical damping modes dominant, maximum v_2)

$$v_2 = 1.35 + 0.25 \mu \quad v_1 = 0.54 + 0.33 \mu \quad v_3 = 0.5 \dots [11]$$

If there is no interaction between controller adjustments then one can obtain the actual controller adjustments as follows

$$S = \frac{v_2}{RL} = \text{sensitivity, adjustment knob setting}$$

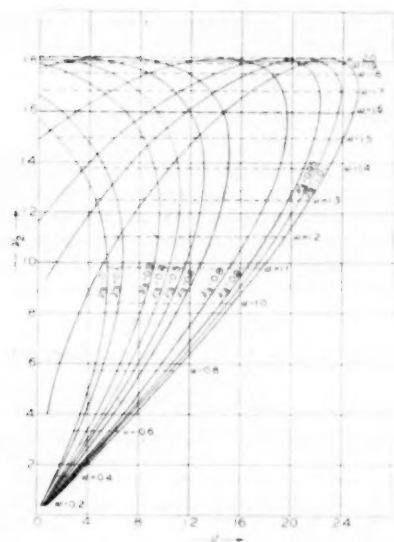


FIG. 17 STABILITY LIMITS FOR PROPORTIONAL-PLUS-RESET-PLUS-DERIVATIVE CONTROL, $\mu = 0$

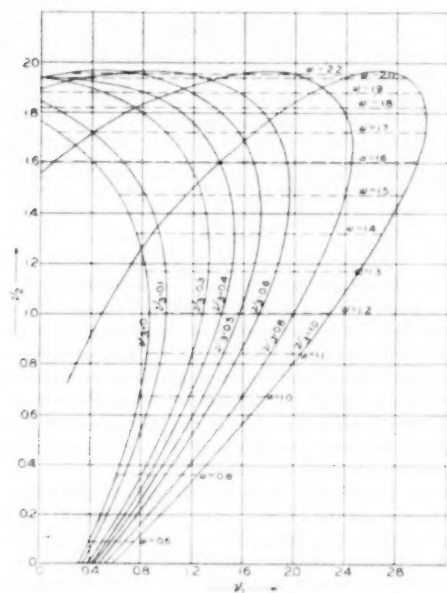


FIG. 18 STABILITY LIMITS FOR PROPORTIONAL-PLUS-RESET-PLUS-DERIVATIVE CONTROL, $\mu = 0.3$

$$U = \frac{v_1}{v_2 L} = \text{reset rate, adjustment knob setting}$$

$$T = \frac{v_2}{v_3} L = \text{derivative time, adjustment knob setting}$$

If there is interaction between controller settings, then the parameters v_1 , v_2 , and v_3 are first obtained from the linearized controller equation. For example, a cascade controller (9) has the following relation between adjustable parameters and the control constants

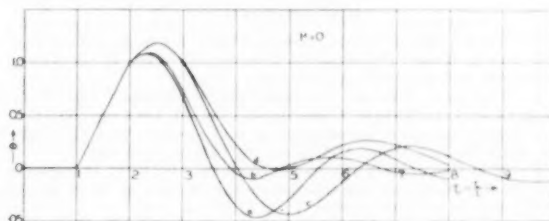


FIG. 19 RESPONSE CURVES FOR PROPORTIONAL-PLUS-RESET-PLUS-DERIVATIVE CONTROL

(a) $v_1 = 0.8$, $v_2 = 1.41$, $v_3 = 0.5$; (b) $v_1 = 0.54$, $v_2 = 1.35$, $v_3 = 0.5$; (c) $v_1 = 0.57$, $v_2 = 1.21$, $v_3 = 0.3$; (d) $v_1 = 0.34$, $v_2 = 1.27$, $v_3 = 0.3$

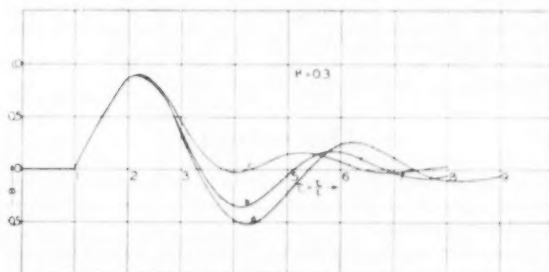


FIG. 20 RESPONSE CURVES FOR PROPORTIONAL-PLUS-RESET-PLUS-DERIVATIVE CONTROL

(a) $v_1 = 1.24$, $v_2 = 1.45$, $v_3 = 0.5$
(b) $v_1 = 1.02$, $v_2 = 1.5$, $v_3 = 0.5$
(c) $v_1 = 0.64$, $v_2 = 1.43$, $v_3 = 0.5$

$$v_2 = S'(1 + U'T')RL \quad v_1 = S'U'RL^2 \quad v_3 = S'T'R \quad [12]$$

where S' = adjustable knob labeled "Sensitivity"

U' = adjustable knob labeled "Reset Rate"

T' = adjustable knob labeled "Derivative Time"

Relationships [11] yield v_1 , v_2 , and v_3 , and then Equations [12] are used to obtain S' , U' , T' , the actual knob settings of the cascade controller.

The control regions show that increasing the self-regulation index μ makes the loop gain SM smaller so that for a fixed process sensitivity, M , the controller sensitivity S decreases. Also, the control area and period decrease as μ increases.

The use of reset to remove offset makes the control less stable since a smaller value of sensitivity must be used in comparison with proportional alone. Moreover, the control-region graphs show that the period increases with the addition of reset to proportional control.

The addition of derivative action allows one to use increased sensitivity and reset rate. Hence the period is decreased further and the control area is decreased, giving much better control. It is apparent that the addition of derivative action decidedly improves control for values of self-regulation $0 \leq \mu \leq 1$. For processes having $\mu > 1$ derivative offers little advantage from the standpoint of load-change disturbances. However, as pointed out in reference (9) start-up of a batch process requires the use of derivative to prevent overpeaking. Hence derivative is almost always a desirable response.

ACKNOWLEDGMENT

The authors wish to acknowledge the aid of Mrs. Doreen Tessaro and Ray Johnson, both of the Engineering Research Department, for their aid in computational and graphical work.

BIBLIOGRAPHY

- 1 "Time Lag in a Control System," by A. Callender, D. R. Hartree, and A. Porter, *Philosophical Transactions of the Royal Society of London*, vol. 235, 1936, pp. 415-444.
- 2 "Optimum Settings for Automatic Controllers," by J. G. Ziegler and N. B. Nichols, *Trans. ASME*, vol. 64, 1942, pp. 759-768.
- 3 "Process Lags in Automatic-Control Circuits," by J. G. Ziegler and N. B. Nichols, *Trans. ASME*, vol. 65, 1943, pp. 433-444.
- 4 "The Dynamics of Automatic Controls," by R. C. Oldenbourg and H. Sartorius, book translated from the German by H. L. Mason and published by ASME, New York, N. Y., in 1948.
- 5 "The Optimum Adjustment of Regulators," by P. Hazebrook and B. L. van der Waerden, *Trans. ASME*, vol. 72, 1950, p. 317.
- 6 "Theoretical Considerations on the Optimum Adjustment of Regulators," by P. Hazebrook and B. L. van der Waerden, *Trans. ASME*, vol. 72, 1950, pp. 309-315.
- 7 "Controller Settings for Optimum Control," by W. A. Wolfe, *Trans. ASME*, vol. 73, 1951, pp. 413-418.
- 8 "Importance of Extending Nyquist Servomechanism Analysis to Include Transient Response," by R. L. Johnson and J. B. Rea, *Journal of the Aeronautical Sciences*, vol. 18, 1951, p. 43.
- 9 "A New Concept of Automatic Control," by R. E. Clarridge, *Instruments*, vol. 23, December, 1950, pp. 1248-1251.

Discussion

Y. TAKAHASHI.⁵ The authors are to be congratulated on presenting a paper with very clear conclusions and very useful control-region diagrams.

The authors' statements on the complexities of industrial processes and the presence of continuum are highly important, considering such complexities were occasionally ignored by some control mathematicians, leading to utopian conclusions such as infinite gain as an optimum.

Theoretically the horizontal asymptote in Fig. 3 (a) should be defined by S' of the following equation

$$\Delta F/Y = S'(1 + U'/p)(1 + T'p)$$

Putting this identical to the corresponding form of Equation [2] of the paper we get

$$S' = \frac{S}{2} (1 \pm \sqrt{1 - 4UT})$$

But, in most cases, especially near the optimum settings, the difference between S and S' is very slight; moreover, the authors' horizontal line of the height "20 log S " comes nearer to the exact attenuation curve than that of S' .

Compared with the results of other papers,⁶ the values from the authors' equation are among the higher. Generally, the conclusions depend upon the definition of "optimum," so if the transient response itself is considered instead of the fundamental mode of oscillation, they are influenced by the nature of disturbance, defined statistically or as a time function. For the latter case the writer tried an analysis. Assuming the disturbance of the form

$$\Delta D = \Delta D_0(1 - e^{-t/T_d})$$

and defining the optimum to be the minimum control area of $\int_0^\infty \theta(\sigma) d\sigma$, it was seen that the longer the T_d , the stronger

the optimum settings; for example, the optimum settings of proportional controls are

$$\begin{aligned} \mu = 0 \quad \mu = 1 \\ SRL = 0.89 \quad 0.91 \quad \text{for } T_d = 0 \\ SRL = 1.07 \quad 1.40 \quad \text{for } T_d = 2L \end{aligned}$$

Finally, the writer would like to point out Dr. Oppelt's comments⁶ on the importance of Ziegler-Nichols' ultimate sensitivity method. This enables us to take into account the self-regulation of the process, and according to Oppelt, its results approximately coincide with Hazebrook-Waerden's optimum values for proportional-plus-reset controls.

AUTHORS' CLOSURE

For the process $\mu = 0$ Fig. 21 below shows the integral $\int_0^\infty \left| \theta(\sigma) - \frac{1}{v_2 + \mu} \right| d\sigma$ as well as the offset and amplitude ratio for various values of v_2 . It is evident that the absolute area

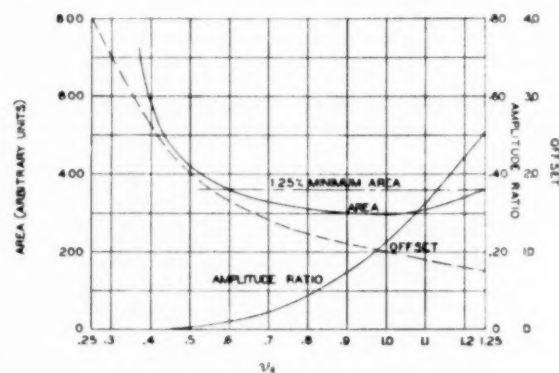


Fig. 21

defined by the integral has a very broad minimum. It appears that changing v_2 from 0.58 to 1.25 does not change the absolute area more than 25 per cent whereas the offset changes about 50 per cent. Hence, 0.25 amplitude ratio appears to give a good compromise between offset and minimum absolute area in the case of proportional control. It can also be shown that this criterion of absolute area agrees with our results for a three-term controller. The authors wish to point out that Professor Takahashi has done considerable work along these lines.⁷

Professor Takahashi's discussion brings out some interesting aspects concerning the interaction of knob settings in the cascade type of controller. As long as $U' < 1/T'$, the knob settings correctly describe the controller functions. However, when $U' > 1/T'$, the straight line approximations to the frequency response of the controller indicate that the knob labeled reset actually controls the derivative response and vice versa. Also, the sensitivity depends more strongly on the settings of the reset and derivative knobs.

It may be noted that the optimum settings given by Hazebrook and van der Waerden are based on a change in set point.

⁵ Professor, University of Tokyo, Chiba-City, Japan.

⁶ Authors' Bibliography (2, 3, 5, 6, 7), and "On the Automatic Control of Generalized Passive Systems," by Kun Li Chien, J. A. Hrones, J. B. Reswick, *Trans. ASME*, vol. 74, 1952, p. 175.

⁷ "Einige Faustformeln zur Einstellung von Regelvorgängen," by W. Oppelt, *Chemische Ingenieur Technische*, vol. 23, 1951, p. 190.

⁸ "Automatic Control," by Y. Takahashi, The Science and Technique Book Co., Kanazawa, Japan, 1949 (in Japanese.)

A Fast-Response True-Mass-Rate Flowmeter

BY YAO TZU LI¹ AND SHIH-YING LEE,² CAMBRIDGE, MASS.

A flowmeter capable of measuring directly the true rate of mass flow would have many industrial applications and would eliminate many of the shortcomings of instruments now available for flow measurements. A description and diagrams are presented of a new type of mass-rate flowmeter with a long range, a linear scale, and a very fast response.

INTRODUCTION

A FLOWMETER is an instrument that gives an output which is a function of the amount of fluid that flows through it in unit time. Since flowmeters have been used principally for measuring the flow of liquids, which are most easily measured in terms of volume, and since it is easier to design a volumetric flowmeter than a mass flowmeter, the latter has been comparatively neglected. In many applications, however, it is necessary to measure mass flow, and this measurement usually has been made by the rather clumsy expedient of applying corrections to the readings of volumetric flowmeters. If the density of the fluid stream is constant, this correction is easy to apply, but if the flow measurements must be accurate or if the density varies widely, the problem becomes more difficult.

In metering a gas, for example, the mass flow is proportional to the volumetric flow times the absolute pressure, which may vary widely, divided by the absolute temperature, which likewise may vary. Even with liquids the corrections may be appreciable; for example, a gallon of gasoline purchased on a hot summer day may contain 10 per cent less fuel than one drawn from the same pump during very cold weather. In the chemical-process industries particularly, it is becoming increasingly important to measure mass flow accurately and rapidly.

Most currently available flowmeters leave much to be desired with regard to speed of response also. A sluggish meter may read accurately on a flow that changes slowly, but may be very inaccurate on rapidly changing flows. The current emphasis on rocket and jet-engine research, hydraulic-servo development, and the measurement of strongly pulsating pipe-line flows demands that fast accurate flowmeters may be available.

This paper describes a new type of meter that measures mass-flow rate directly and accurately, with a linear input-output law and with a very short response time. It should be useful in many types of flow measurement that hitherto have been difficult or impossible.

SURVEY OF CURRENTLY AVAILABLE FLOWMETERS

Probably the simplest and most commonly used type of industrial flowmeter³ is the constant-area variable-head type, sometimes called the headmeter, of which the orifice meter, the ven-

turi meter, and the flow-nozzle meter are special forms. In general, this type of flowmeter consists of a fixed restriction in the flow passage, the pressure drop across this restriction being used to produce the flow-rate indication. For an incompressible fluid

$$W = CA \sqrt{2\rho \Delta p} \quad (1)$$

where

- W = mass-flow rate
- C = discharge coefficient
- A = area of restriction
- Δp = pressure drop across restriction
- ρ = density of fluid

Since the pressure drop from which the instrument derives its output indication is proportional to the square of the flow rate, the instrument is basically nonlinear, and in such a way that its usable range is reduced seriously. Also, the discharge coefficient C is a rather complicated function of the viscosity, density, and flow rate, and the geometrical configuration of the instrument, and is often far from a constant. For this reason it is difficult and often impossible to obtain a direct indication of either mass-flow rate or volumetric-flow rate from this instrument. In addition, if this type of flowmeter is used on compressible fluids, the compressibility still further complicates the relationship between flow and output indication.

Besides the difficulties just enumerated, the basic nonlinearity of the constant-area flowmeter makes it difficult to use for the measurement of pulsating or rapidly varying flows. Simple averaging of the output leads to large errors; if the square root of the pressure drop is averaged, the instrument becomes complicated and the square-rooting process itself often introduces errors.

The principal disadvantage of the variable-head flowmeter may be eliminated by varying the area of the restriction in such a way that the pressure drop across it remains constant at all times. The area of the orifice then becomes the primary-output quantity and can be measured easily with good accuracy. The principal nonlinearity of the previous type is thus eliminated, but the variability of the discharge coefficient remains, and in addition the calibration of the instrument is a function of the pressure, temperature, density, and viscosity of the fluid.

More elaborate flowmeters⁴ may be based on the measurement of the average flow velocity across a fixed area. Still others depend upon measuring the speed of a flow-actuated turbine or a positive-displacement motor. Flowmeters of these types measure volumetric-flow rates and if mass-flow rates are required, a density correction must be applied.

A true mass flowmeter, utilizing the Magnus principle, was proposed by Dr. W. T. D. van Dijk of the Technical University of Delft in 1941, and has since been used to some extent.⁵ Its principle of operation is shown schematically in Fig. 1. The stream of fluid to be measured passes both ways around a rotating cylinder located in an enlargement of the flow passage, and the

¹ Assistant Professor, Department of Aeronautical Engineering, Massachusetts Institute of Technology.

² Assistant Professor, Department of Mechanical Engineering, Massachusetts Institute of Technology.

³ "Fluid Meters, Their Theory and Application," ASME Research Publication, 1937.

Contributed by the Industrial Instruments and Regulators Division and the Fluid Meters Research Committee and presented at the Annual Meeting, New York, N. Y., November 30-December 5, 1952, of THE AMERICAN SOCIETY OF MECHANICAL ENGINEERS.

NOTE: Statements and opinions advanced in papers are to be understood as individual expressions of their authors and not those of the Society. Manuscript received at ASME Headquarters, November 17, 1952. Paper No. 52-A-170.

⁴ "Electromagnetic Blood Flowmeter," by J. W. Clark and J. E. Randall, *Review of Scientific Instruments*, vol. 29, 1949, p. 951.

⁵ "The Mass Flow Meter, A Method for Measuring Pulsating Flow," by D. Brand and L. A. Ginsel, *Instruments*, vol. 24, 1951, p. 331.

"A Flowmeter Designed to Measure Mass Flow by Direct Calibration," by S. M. Tennant and J. R. Turner, MS thesis in Mechanical Engineering, Massachusetts Institute of Technology, 1950.

pressure difference Δp between the mid-points of the two passages is used as an indication of the mass-flow rate.

The theory of the device depends upon the following assumptions:

1 The average circulation velocity V_c of the fluid, which is caused by the constant rotation of the cylindrical rotor, has a constant value for any fluid and for any sort of flow pattern in the two branches.

2 The actual flow velocities in the two passages are the sums of this quantity V_c and another quantity V_m , which is the flow velocity in the passage when the rotor is stationary.

3 The flow in the passages is pure potential flow, so that Bernoulli's equation applies.

If these assumptions are correct, the action of the flowmeter can be expressed in analytical form as

$$\begin{aligned}\Delta p &= p_1 - p_2 = \frac{1}{2}\rho[(V_c + V_m)^2 - (V_c - V_m)^2] \\ &= 2\rho V_c V_m \\ &= \frac{2V_c W}{A} \dots \dots \dots [2]\end{aligned}$$

where p_1 and p_2 are the pressures at the upper and lower flow passages, respectively, and A is the total cross-sectional area of the two flow passages.

Equation [2] shows that the device shown in Fig. 1 will act

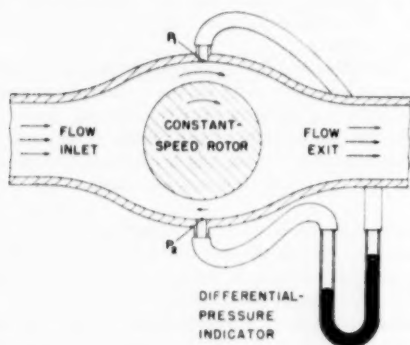


FIG. 1 MASS-RATE FLOWMETER BASED ON MAGNUS EFFECT

as a true mass flowmeter if the three assumptions are valid. Unfortunately, it appears that they are not strictly so, either in theory or in practice, with the result that meters operating according to this principle require careful calibration and complete knowledge of the properties of the fluid being metered, and therefore cannot be considered as wholly satisfactory answers to the problem of measuring mass-flow rates.

PRINCIPLE OF OPERATION OF TRUE-MASS-RATE FLOWMETER

The flowmeter to be described depends for its operation upon the measurement of the moment required to give a fluid stream a Coriolis acceleration. The operation can be described most readily by referring to the special case illustrated in Fig. 2, where the fluid is assumed to flow uniformly through a straight tube, the motion of each particle being parallel to that of the others. Assume also that the tube is rotated at a constant angular velocity ω about the axis O which intersects the axis of the tube at right angles. The Coriolis acceleration is then uniform everywhere in the fluid, and is given by the equation

$$a = 2V\omega \dots \dots \dots [3]$$

where V is the velocity of the fluid relative to the tube.

The total force acting on the tube in the direction perpendicular to its axis can be found by integration over the volume of the tube. Thus

$$\begin{aligned}F &= \int_{r_1}^{r_2} 2V\omega\rho A dr = 2V\omega\rho(r_2 - r_1)\omega \\ &= 2\omega(r_2 - r_1)W \dots \dots \dots [4]\end{aligned}$$

where W is the mass rate of flow.

Similarly, the net moment about O due to the Coriolis force is given by

$$\begin{aligned}M &= \int_{r_1}^{r_2} 2V\omega\rho A r dr = V\omega\rho(r_2^2 - r_1^2)\omega \\ &= \omega(r_2^2 - r_1^2)W \dots \dots \dots [5]\end{aligned}$$

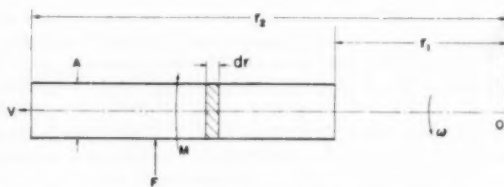


FIG. 2 FORCE AND MOMENT PRODUCED BY CORIOLIS ACCELERATION

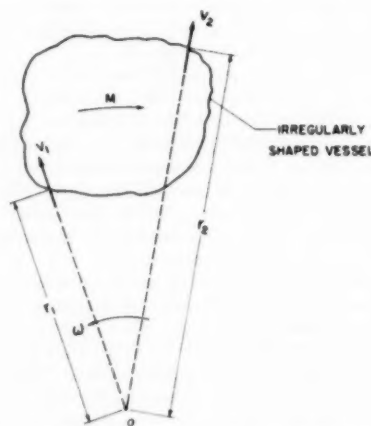


FIG. 3 GENERALIZATION OF CORIOLIS MOMENT

Thus according to Equations [4] and [5] both the force and the moment are linear functions of the mass rate of flow through the tube, which may be considered as the flow-sensing element.

The same equations can be shown to apply under much more general conditions than the simple tube of the previous case. In Fig. 3 assume a vessel of any shape whatever, with two small openings, through which fluid enters and leaves. If the vessel is held stationary, the net force exerted upon it by the fluid must pass through the point of intersection O of the fluid velocity vectors V_1 and V_2 . (It need not be assumed that the vectors are coplanar since any components that they may have parallel to the axis of rotation will be ineffective in producing a moment about that axis.) But if the net force vector passes through O it can produce no moment about O . If now the vessel is made to rotate about O with an angular velocity ω while the relative directions of the fluid velocities V_1 and V_2 with respect to the vessel remain unchanged, a net moment will be produced as a result of the Coriolis acceleration of the fluid.

The value of this moment can be found by applying the law of angular momentum, the only basic assumption being that the

influx and efflux velocity vectors remain radial as seen by an observer rotating with the vessel. If this is so, the tangential velocity of the fluid at the entrance (as seen by a stationary observer) is simply ωr_1 , and $W\omega r_1^2$ is the rate of angular momentum into the control volume which is annular volume containing this vessel. Similarly, the rate of efflux of moment of momentum is $W\omega r_2^2$, and the net moment exerted on the vessel by the fluid is the difference of the two, or

$$M = W\omega(r_2^2 - r_1^2) \dots \dots \dots [6]$$

which is identical to the previous equation. Thus it can be seen that the shape of the flow-sensing element is of no importance, nor are the properties of the fluid or the nature of the flow pattern within the vessel. The only significant requirement is that the entrance and exit velocities relative to the vessel be radial. If this condition is not fulfilled, an additional moment will be produced by the tangential components of the velocities, as in the case of a radial-flow turbine, and the simple relationship of Equation [6] will apply no longer.

One practical arrangement embodying this principle is shown in Fig. 4. The flow-sensing element in this case resembles the impeller of a centrifugal pump. It is enclosed in a housing that

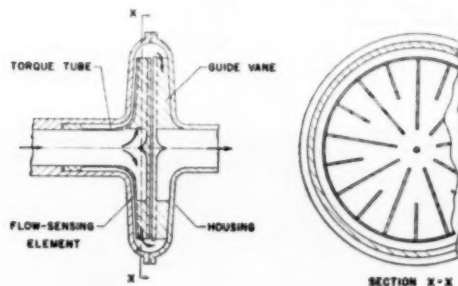


FIG. 4 IMPELLER-TYPE MASS-RATE FLOWMETER

also resembles a pump housing except that it rotates with the impeller and is mechanically connected to it by an elastic member whose distortion serves to measure the moment exerted on the impeller by the fluid, and therefore the mass-flow rate. The whole assembly is rotated at a constant rate by an external motor, and connections between the incoming and outgoing fluid lines are made through any suitable type of rotary seal.⁶ The impeller is provided with a sufficient number of radial vanes to insure that the flow is substantially radial, so that the output, taken from a device that measures torsional deflection with respect to the housing, will be an accurate measure of the mass-flow rate.

It is interesting to note that in the arrangement of Fig. 4 the torque required to drive the flow-sensing element is recovered in the guide vanes in the housing, with the result that the only torque which the driving motor must supply is that necessary to overcome bearing and seal friction and windage. It should also be noted that the signal output is independent of this frictional torque.

The device in Fig. 4, unlike some other types of flowmeters, can be used bidirectionally; if the flow reverses, the torque produced also will reverse. Similarly, the torque can be reversed by

reversing the drive motor, or the scale factor can be changed by changing the motor speed.

Another possible variant is to oscillate the housing sinusoidally instead of rotating it. With this arrangement, the Coriolis force must be separated from the force resulting from angular acceleration; hence this scheme is probably of theoretical interest only.

DESIGN CONSIDERATION FOR FLOW-SENSING ELEMENT

The basic function of the flow-sensing element is to impart a known velocity change to the flow mass in a direction normal to the flow passage. The primary consideration in the design is therefore to keep the tangential velocities of the fluid at the inlet and outlet of the flow-sensing element equal to the local velocities of the element. Other important considerations are as follows:

- 1 A small torsional moment of inertia of the flow-sensing element.
- 2 A small pressure drop associated with the flow.
- 3 Simple construction.
- 4 Compactness.

The impeller-shaped flow-sensing element just described is one possible design but is not necessarily the best because its moment

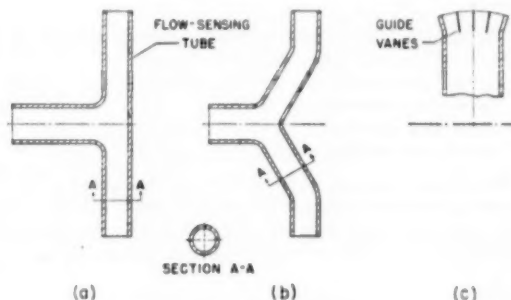


FIG. 5 FLOW-SENSING ELEMENTS
(a, T-tube; b, Y-tube; c, guide vanes.)

of inertia is considerably larger than those of some other types with the same outside diameters. A T-shaped tube, as shown in Fig. 5(a), is simple to construct and has a small moment of inertia. The Y-tube in Fig. 5(b) is a modification of the T-tube, and is somewhat to be preferred, since it reduces the pressure drop by decreasing the sharpness of the bends at the inlet and outlet.

In any type of flow-sensing element it is desirable to include guide vanes to insure radial flow. If the element is a slender tube, the wall of the tube serves sufficiently well and no additional guide vanes will be required. In some cases, however, when compressible fluids are being measured and particularly when the measuring tube is short and wide, guide vanes should be added at the outlet. A suitable arrangement is shown in Fig. 5(c); the tip of the tube is given a uniform radius and the guide vanes are arranged truly radial to the axis of rotation. This configuration, in effect, makes the tube a sector of the impeller in Fig. 4.

In theory, guide vanes also should be provided at the inlet. This is probably unnecessary in most cases because the moment of momentum of the incoming flow is small compared to the total change in moment of momentum, since r_1^2 is usually much smaller than r_2^2 .

Even in the case of the outlet it is unnecessary to use a large number of guide vanes. Since in a practical design the exit-flow speed relative to the sensing element is small compared to the tangential velocity, the error introduced by a small deviation from truly radial flow will be small, of the second order, and there-

⁶ "Mechanical Seals," by D. R. Lewis, *Machine Design*, vol. 18, 1946, p. 125.

"Sealing a Rotary Shaft Metal Bellows Construction," by R. Hammond, *Chemical Age*, London, England, vol. 55, 1946, p. 199.

"Hydraulic Seals," by F. Flick, *Machine Design*, vol. 20, 1948, p. 139.

fore inconsequential. In the design of the experimental model to be described later, a 10-deg error in the exit angle would produce only a 2 to 3 per cent error in the flow measurement.

FREQUENCY RESPONSE OF FLOW-SENSING ELEMENT

In general, increasing the frequency response of an instrument requires increasing its undamped natural frequency and providing a suitable damping ratio. The undamped natural frequency of the flow-sensing element of the flowmeter described here is given by

$$f_n = \frac{1}{2\pi} \sqrt{\frac{K}{J}} \quad [7]$$

where J is the torsional moment of inertia of the flow-sensing element and K is the torsional stiffness of its attachment to the housing.

$$\begin{aligned} K &= \frac{\text{Maximum torque produced by flow}}{\text{Maximum angular deflection}} \\ &= \frac{W_{\max} \omega r_m^2}{d_{\max}} \\ &= \frac{\rho V A \omega r_m^2}{d_{\max}} \quad [8] \end{aligned}$$

where

$$\begin{aligned} r_m &= \text{radius at which a deflection-sensing element is attached to flow-sensing element} \\ d_{\max} &= \text{maximum deflection of deflection-sensing element} \\ \rho &= \text{density of fluid} \\ V &= \text{flow velocity} \\ A &= \text{area of tubular flow-sensing element} \end{aligned}$$

The effective moment of inertia J of the flow-sensing element consists of two parts, that of the element itself and that of the fluid in the flow passage in the element. For the T-shaped configuration in Fig. 5(a) the total moment of inertia will be

$$J = \frac{2}{3} \rho A r_m^2 \left(1 + \frac{\rho_t A_t}{\rho A} \right) \quad [9]$$

where ρ_t is the density of the tube material and A_t is the cross-sectional area of the tube wall.

Substitution of Equations [8] and [9] into Equation [7] gives

$$f_n = \frac{1}{2\pi} \sqrt{\frac{3}{2} \frac{V \omega r_m}{d_{\max} r_m \left(1 + \frac{\rho_t A_t}{\rho A} \right)}} \quad [10]$$

This equation shows that for a high natural frequency of the flow-sensing element, both the rotational speed and the flow velocity should be high. The maximum deflection required to operate the deflection-sensing device depends upon its characteristics; for commonly used mechanoelectric transducers this might be 0.001 in., while if a purely mechanical indicating device is used it will be 0.1 in. or more. For this reason, as well as because of its superior frequency characteristics and other desirable properties, the electrical type usually is chosen.

As an example, in one of the experimental models to be described, the pertinent quantities were

$$\begin{aligned} d_{\max} &= 0.001 \text{ in.} \\ r_m &= \frac{1}{2} r_2 \\ V &= 160 \text{ ips} \\ \rho_t A_t / \rho A &= 0.5 \text{ (approx)} \\ \omega &= 1800 \text{ rpm} \end{aligned}$$

Substitution of these quantities in Equation [10] gives a natural frequency of approximately 600 cycles per sec (cps), which checks very well with the experimental results.

DESCRIPTION OF EXPERIMENTAL MODELS

Two experimental models of the mass flowmeter have been built and tested in order to check the theory of operation and to supply design information for further models. Both models have maximum flow ratings corresponding to 5 to 10 gpm of water, have rotor diameters of about 5 in., and operate at 1800 rpm. Figs. 6 and 7 show the first model in schematic cross section and

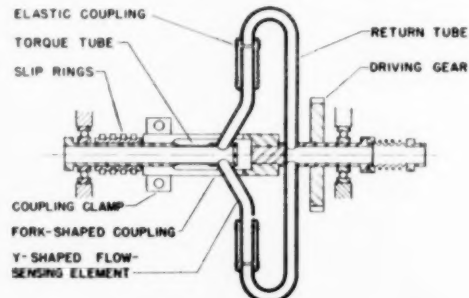


FIG. 6 SCHEMATIC SECTION OF MODEL 1 FLOWMETER

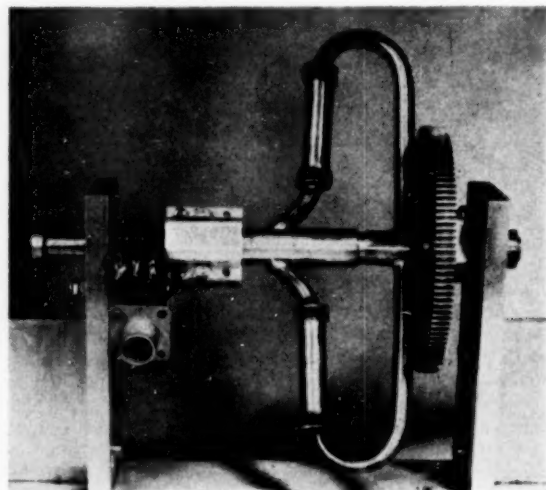


FIG. 7 MODEL 1 FLOWMETER

in a photograph. This model uses a semi-Y-shaped flow-sensing element, the flow returning to the axial outlet through two hook-shaped tubes rigidly attached to the main shaft. The gaps between the Y-tube and the return tubes are sealed by flexible bellows whose restraint to torsional motion of the Y-tube is very small. The principal restraint is that of the torque tube which forms part of the stem of the Y and to which resistance-wire strain gages are bonded to form the deflection-measuring element. The electrical connections to the strain gages are taken out through slip rings. The torque tube is an integral part of the left half of the main shaft, which also carries the slip rings, the Y-tube, and the left bearing and seal. It is coupled to the right half by a fork-shaped coupling which is cut away to provide clearance around the Y-tube. Spring-loaded face-type rotary

seals at the ends of the main shaft provide the hydraulic connections to the inlet and outlet lines.

This first model was rather crudely made since it was intended only to demonstrate the practicability of the proposed mass flowmeter. Its two-part main shaft is structurally weak and neither the bellows couplings nor the face-type fluid seals will stand high pressures. It was very satisfactory for steady-state measurements, and it showed an essentially linear calibration, unaffected by the viscosity and density of various types of fluids. These results were so encouraging that a second and considerably improved model was built.

This second flowmeter is illustrated in Figs. 8 and 9. It uses a T-tube flow-sensing element enclosed by a heavy housing; the

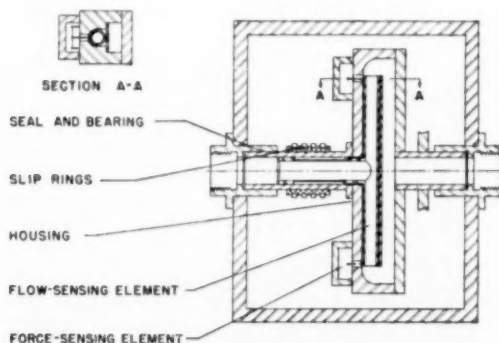


FIG. 8 SCHEMATIC SECTION OF MODEL 2 FLOWMETER

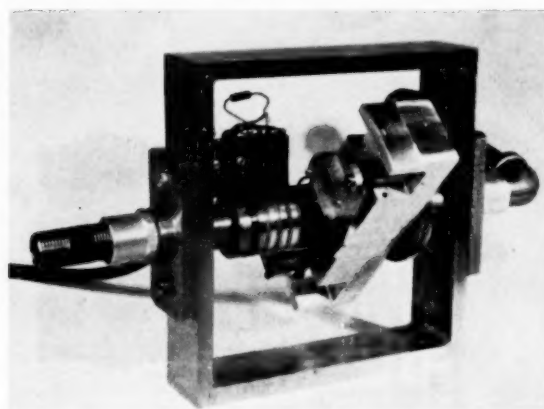


FIG. 9 MODEL 2 FLOWMETER

construction is similar to that of the impeller-type flowmeter already discussed except that the housing is rectangular instead of circular. Precision-bored cast-iron bushings mounted in the ends of the main frame served as both hydraulic seals and shaft bearings; the shaft was machined to give just enough clearance to permit free rotation and the resulting close clearance permitted very little leakage flow.

The displacement pickoffs in this model were strain gages, but of a special design to insure that the fluid being metered could not come in contact with the strain-gage wires. The construction is shown in Fig. 10; a rocker pin is supported through the center of a small flexible diaphragm, the outer end being connected to the T-tube and the inner end being provided with an insulating pin to which two sets of strain-measuring wires are attached. The free ends of the strain-gage wires are fastened to fixed pins.

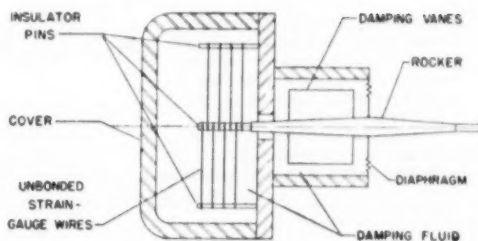


FIG. 10 FORCE-SENSING ELEMENT USED ON MODEL 2 FLOWMETER

The rocker pin also is provided with a vane and two fixed vanes are separated from it by 0.005-in. gaps; the whole strain-measuring capsule is filled with a viscous fluid which prevents external pressure from deforming the diaphragm appreciably, provides some damping to the system, and helps to protect the strain-gage wires from corrosion as well as to dissipate the heat generated by the measuring current.

Two such strain-measuring capsules are connected symmetrically to the flow-sensing element by appropriate flexible links. The symmetry of the configuration, both electrical and mechanical, the geometry of the assembly of the rocker pin, diaphragm, and strain wire, plus the liquid filling of the capsule, make negligibly small the unbalance of the bridge due to changing internal pressure. In theory, the system is completely compensated for pressure and temperature changes and is sensitive only to relative torsional motion between the T-tube and the housing; in practice, this is very nearly true and the assembly is sensitive, compact, stable, and fairly rugged.

DISCUSSION OF TEST RESULTS

The experimental work performed with these two flowmeters included the following:

- 1 Static determination of the strain-gage sensitivity in order to calculate the theoretical calibration of the flowmeter.
- 2 Experimental calibration of the flowmeter with various fluids and comparison with the results of 1.
- 3 Measurements of the transient response of the flowmeter, both undamped and damped.
- 4 Studies of accuracy of measurement of steady flow with superimposed pulsations up to 100 cps.

These four types of experiments and the results obtained are described in the following.

Theoretical Sensitivity of Flowmeter. The constant relating strain-gage output to mass-flow rate is the product of two principal factors; the first relates the flow rate to the torque generated, and the second relates the torque to the electrical output of the strain-gage bridge. This second factor can be measured directly by applying a known torque to the flow-sensing element and reading the bridge output. This possibility is a valuable feature of the flowmeter, since the first factor depends only on the geometry of the meter, which is invariable for a given instrument, and the rotational speed, which is easy to measure and which is fixed (within the frequency tolerance of the a-c system), if a synchronous motor is used as a driver. It is thus possible to calibrate the meter accurately without actually passing a known flow through it, which is usually impracticable under ordinary conditions of use.

The results of typical torque-sensitivity calibrations are plotted in Fig. 11 by the dotted lines. Multiplication of the slope of the torque versus voltage characteristic by the known flow-torque sensitivity gives the theoretical calibrations of the flowmeters which are shown by the solid lines in the same graph.

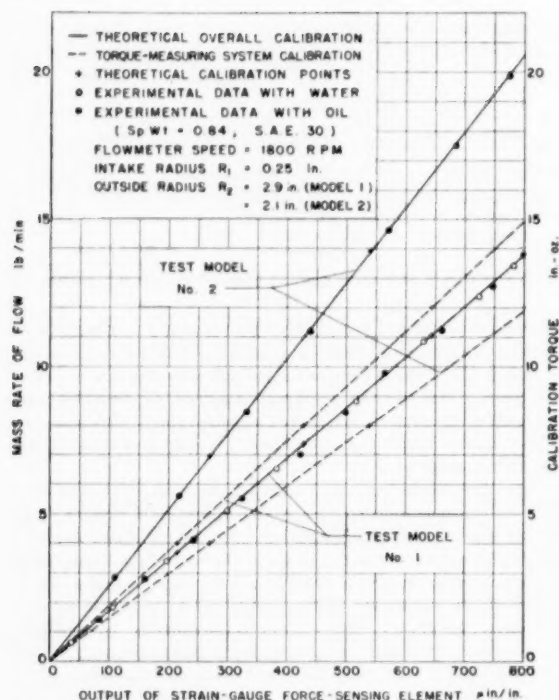


FIG. 11 FLOWMETER CALIBRATIONS FOR STEADY-FLOW CONDITIONS

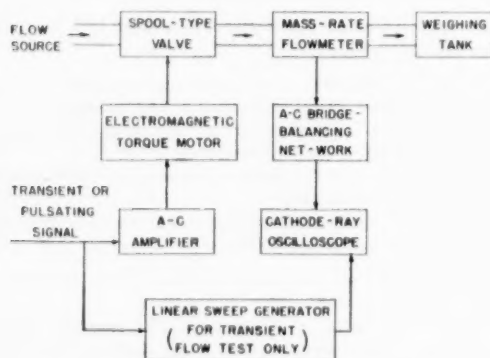


FIG. 12 FLOWMETER CALIBRATION-TEST ARRANGEMENT

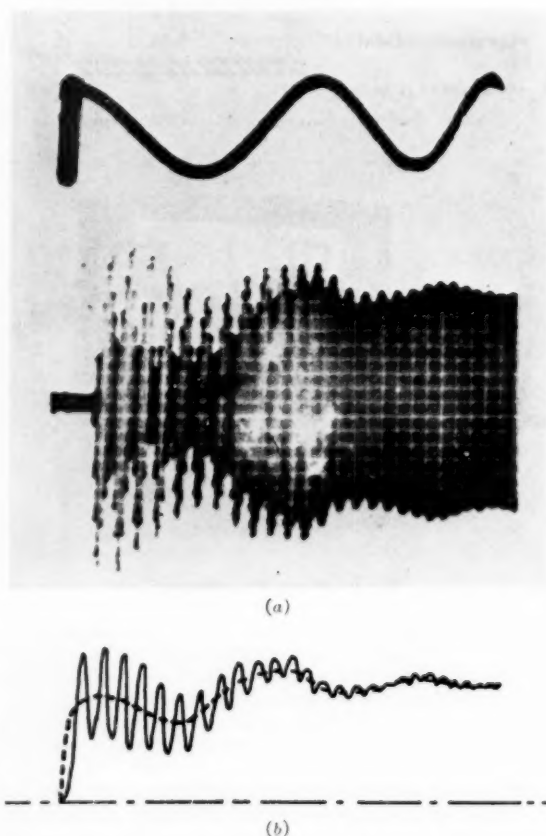
Direct Calibration for Steady Flow. The flowmeters were calibrated directly using water, petroleum-base hydraulic fluid, and nitrogen. The liquid-flow rates were determined by weighing; the resulting calibrations are plotted in Fig. 11 together with the theoretical calibrations from the previous step; the excellent agreement between the three sets of data confirms the accuracy of the theory and shows that the calibration is essentially independent of fluid density and viscosity, as predicted.

In the case of nitrogen, for which the simple weighing technique is inapplicable, a crude test was made by allowing gas to expand from a high-pressure cylinder through the flowmeter and reading the cylinder pressure before and after the run. With the experimental arrangement used, it was found difficult to obtain consistent results, primarily because the maximum attainable mass flow rate was much too small for the test flowmeter. The experi-

mental points were scattered, the maximum error being about 50 per cent. No attempt was made to improve the accuracy with gas since the particular model tested was intended for operation with liquids.

Transient Response. The dynamic performance of a device or a system is usually studied by measuring its response to one or more of three types of input signal: (a) a step input of known height; (b) a sinusoidal input of known amplitude and frequency, or (c) a known impulse. Obviously, each method requires a signal source capable of furnishing the desired signal, but such sources are difficult to construct for the case of fluid flow. It is possible, however, to generate what may be called a "random step function," which has a rise time fast enough to be considered as an ideal step but has an unknown height which varies from time to time in a random fashion. Such a function was used in the transient-response studies of the flowmeter.

The block diagram of the experimental arrangement is shown in Fig. 12. Fluid was admitted to the flowmeter through a high-speed spool-type valve controlled by an electromagnetic-torque motor which was driven by a d-c amplifier. This combination permitted very rapid and accurate control of the valve opening. The remainder of the diagram is self-explanatory; the flowmeter output was displayed on a cathode-ray tube and permanent records were made with a Polaroid camera.

FIG. 13 TRANSIENT-FLOW RECORDS FOR UNDAMPED FLOWMETER
(a, Oscillogram; b, tracing of a.)

The photographic record of one test of the undamped flowmeter is shown in Fig. 13(a). The lower record is a 60-cps timing wave

and the upper record shows the flowmeter output using a 5000-cps a-c carrier, the flowmeter response is the envelope of the carrier. This record is also shown retraced for clarity in Fig. 13(b). This shows a high-frequency oscillation at approximately 600 cps superposed upon a lower frequency oscillation. The high-frequency response is that of the flowmeter itself. The low-frequency response is due to the fluid supply system, including the connecting tubes, the accumulator, and so on. This interpretation of the figure is supported by the agreement of the observed high frequency with the calculated natural frequency, and by the fact that when the instrument was damped by filling the strain-gage capsules with a viscous fluid, the high-frequency oscillation disappeared but the low-frequency one was little affected. A photographic record of the latter case is shown in Fig. 14.

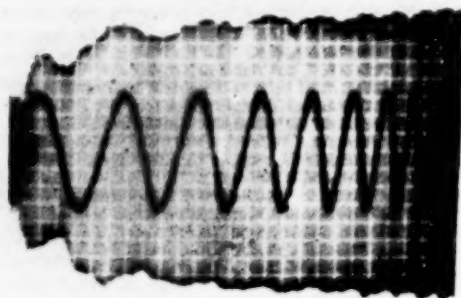


FIG. 14 TRANSIENT-FLOW RECORD FOR DAMPED FLOWMETER

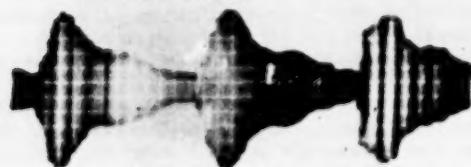


FIG. 15 PULSATING-FLOW RECORD

Measurement of Pulsating Flow. In measuring flows in which strong pulsations are superimposed upon a steady component, it is usually unimportant to measure instantaneous values; the task is normally to get a true measurement of the average flow. The essential nonlinearity and the poor dynamic characteristics of most flowmeters make this task difficult, and it is to be expected that the meter reported here would be well adapted to this application. Accordingly, in the test setup in Fig. 12, a d-c signal with an a-c signal superposed was fed into the d-c amplifier. The integrated flow was measured by weighing, as before. The flow-rate pattern was as shown in Fig. 15 and the electrical output was averaged and indicated by a vacuum-tube voltmeter. Experiments showed that the readings of voltmeter and weigh tank corresponded within 2 per cent both for steady flows and for flows with large-amplitude pulsations as high as 100 cps. Part of the remaining error may be due to the indicating system used.

No attempt was made to improve the accuracy, but it is believed that this can be done.

CONCLUSIONS

The true-mass-rate flowmeter described in this paper is based upon giving the flow a Coriolis acceleration and measuring the torque produced thereby. The equation relating torque and flow is simple and linear, and this simplicity and linearity are reflected in the design and performance of the instrument. The experimental tests on two not particularly refined models showed excellent agreement with the predicted characteristics, which agreement confirms the validity of the theory and the design assumptions.

The principal advantages of this flowmeter are the following:

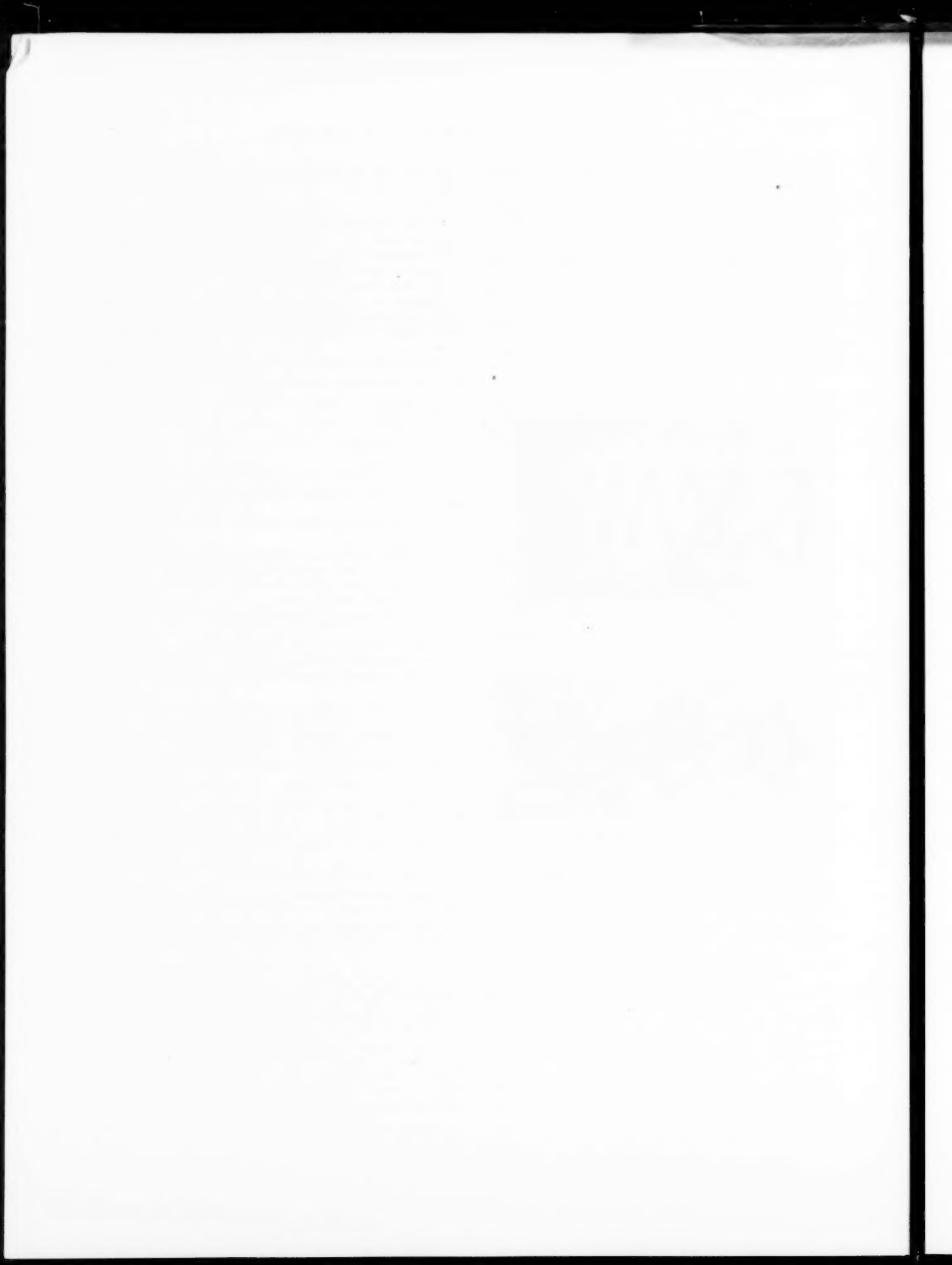
- 1 It gives the true mass-flow rate independent of
 - (a) Pressure.
 - (b) Viscosity.
 - (c) Density.
 - (d) Compressibility.
 - (e) Temperature.
 - (f) Nonhomogeneity: It will work on multiphase fluids such as mists, foams, slurries, and emulsions as well as on homogeneous fluids.
- 2 It will read flow in either direction, and the output reverses when the flow reverses.
- 3 Its speed of response is sufficiently high to permit accurate measurements on very rapidly changing flows.
- 4 It can be used to make accurate measurements of the average values of pulsating flows.
- 5 Since the output is proportional to the input, it is capable of measuring over a very wide range of flow rates.
- 6 The scale factor can be shifted easily over a fairly large range by changing the rotational speed.
- 7 It is unaffected by gravitational or other translational accelerations.
- 8 It offers very little obstruction to the flow, so that the total pressure drop through the instrument is small.
- 9 A single-point calibration, easily made in the field without using fluid flow, determines the scale factor of the instrument.
- 10 The same scale factor applies to any fluid which can be made to flow through the meter.

Although the outputs of the flowmeter models discussed in this paper were electrical, it is possible, although somewhat more awkward, to provide either an optical, a pneumatic, or a mechanical output indication. Usually, of course, the electrical output is to be preferred because of its convenience, accuracy, negligible lag, and ease of remote indication and control.

The one basic disadvantage of the meter is the necessity for rotation, which requires a constant-speed drive motor and two rotary fluid seals. It is felt, however, that provision of a drive is a small price to pay for its numerous advantages.

ACKNOWLEDGMENT

The authors are grateful to Dr. J. F. Blackburn and to Miss Constance D. Boyd for editorial assistance, and to Mr. W. S. Wu for help in the experimental work and in preparing the drawings for this paper. They also wish to thank Prof. C. S. Draper, Head of the Aeronautical Engineering Department, Prof. Walter McKay, Director of the Instrument Laboratory, Prof. J. A. Hrones, Director of the Dynamic Analysis and Control Laboratory, and other personnel of both laboratories of M.I.T. for valuable suggestions and constant encouragement.



Optimum Three-Mode Controller Settings for Automatic Start-Up

By D. W. PESSEN,¹ PHILADELPHIA, PA.

This paper presents a formula empirically derived from laboratory analog tests, which yields controller settings for a specific class of three-mode controllers. The controller settings specified by this formula will produce automatic start-up without overshooting, and, at the same time, provide close to optimum response to process load disturbances. Typical start-up and response curves obtained on an electric process analog by the use of this formula are presented. Finally, a rule of thumb is suggested, giving an indication of the maximum amount of dead time that can be tolerated in a process which must be started up automatically without overshooting.

STATEMENT OF START-UP PROBLEM

THE automatic start-up of batch or continuous processes using controllers which incorporate the reset or integral mode of control has always been a troublesome problem. Owing to the inherent nature of the reset action, appreciable overshooting of the controlled variable always tends to occur. Mathematically speaking, this can be explained by the fact that reset action is an integrating function; that is, it produces a controller output which is proportional to the time integral of the deviation. While the process is shut down, the deviation (difference between set point and controlled variable) is large, and therefore the time integral of the deviation increases rapidly until the controller output reaches an extreme limit. When the process is then started up again, the controlled variable first has to cross the set point before the time integral of the deviation can begin to diminish so that control action can take place. Overshooting is therefore unavoidable under these conditions.

Thus, on processes where overshooting must be avoided at all costs, the instrument user has been faced with two equally unsatisfactory alternatives. He can eliminate the reset response entirely, using only a proportional controller. In this case he might have to contend with appreciable offsets caused by large load or set-point changes. Or, he can use reset response, but start the process manually. This would be very time-consuming in batch processes which are started up at frequent intervals.

SOLUTION TO START-UP PROBLEM

A number of schemes have been developed in recent years attempting to solve this dilemma (1, 2, 3).² Many of these schemes are somewhat complicated and, while effective to prevent overshooting, tend to slow down the start-up operation

to such an extent that it takes the controlled variable a time longer than desirable in some cases to reach the set point. To date, the most effective method which does not suffer from these drawbacks seems to be that described by R. E. Clarridge (4). In this method the controller consists of two sections: A proportional-plus-rate or derivative-action unit, whose output is fed into a conventional proportional-plus-reset-action controller. Mechanically, these two sections may be separate, independent units, or they may be built into one integral three-mode controller. The schematic diagram (and therefore the control action) is the same in either case, and is shown in Fig. 1. While Fig. 1 shows the error-measuring element placed after the proportional-plus-rate-action unit, the error also could be measured ahead of the rate unit. For the purposes of automatic start-up, the control action would be the same.

The reference (4) mentioned explains in detail how such a controller can prevent overshooting on start-up. Very briefly, the method works as follows: As the process is started up, the controlled variable c begins to increase at a steady rate. However, the output signal $c + T \cdot dc/dt$ of the proportional-plus-rate-action unit leads the controlled variable c by a time equal to the rate-time setting T . The proportional-plus-reset-action controller thus will "think" that the controlled variable already has reached the set point, long before that is actually the case. Therefore the time integral of the deviation that had accumulated while the process was shut down can be eliminated so that by the time the controlled variable actually does reach the set point, effective control action can take place, and overshooting can be prevented.

ADJUSTMENT OF THREE-MODE CONTROLLER

The instrument user, who has installed a three-mode controller of the type described, is then faced with the problem of finding the proper combination of controller settings that will produce good start-up. The Clarridge paper (4) gives one method for finding start-up settings, but states that this method does not necessarily produce the optimum start-up performance. The paper also suggests that this whole problem be more fully investigated in order to determine what settings will give the best performance. Such an investigation, resulting in the present paper, was conducted in the hope that it would fill the existing gap, and enable the instrument user to find the proper combination of controller settings easily without having to resort to trial-and-error methods.

In order to derive a formula which will yield the proper combination of controller settings, it was decided to use an experimental approach. Start-up is a discontinuous operation involving limiting effects, so that any purely mathematical approach would have become overly complicated. Therefore it was decided to use an electric process analog, which was found to be ideally suited to this purpose. This electric process analog has been described in considerable detail in a previous paper (5). The following brief explanation of the operation of the analog should therefore suffice.

ELECTRIC PROCESS ANALOG

The heart of the analog is a bank of electrical resistors and

¹ Research Engineer, Servomechanism Laboratory, Brown Instruments Division, Minneapolis-Honeywell Regulator Company. Jun. ASME.

² Numbers in parentheses refer to the Bibliography at the end of the paper.

Contributed by the Industrial Instruments and Regulators Division and Fluid Meters Research Committee and presented at the Annual Meeting, New York, N. Y., November 30-December 5, 1952, of THE AMERICAN SOCIETY OF MECHANICAL ENGINEERS.

NOTE: Statements and opinions advanced in papers are to be understood as individual expressions of their authors and not those of the Society. Manuscript received at ASME Headquarters, August 25, 1952. Paper No. 52-A-58.

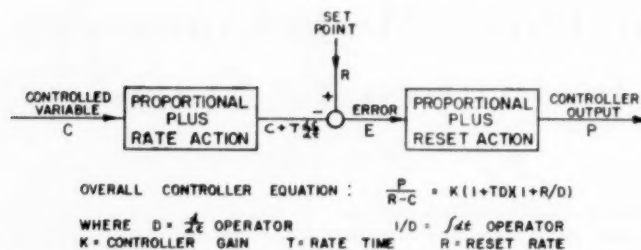


FIG. 1 BLOCK DIAGRAM OF THREE-MODE CONTROLLER USED FOR AUTOMATIC START-UP

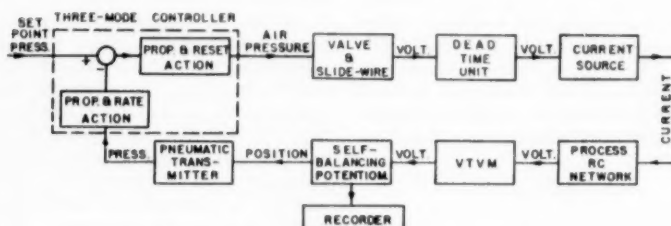


FIG. 2 BLOCK DIAGRAM OF ELECTRIC PROCESS ANALOG

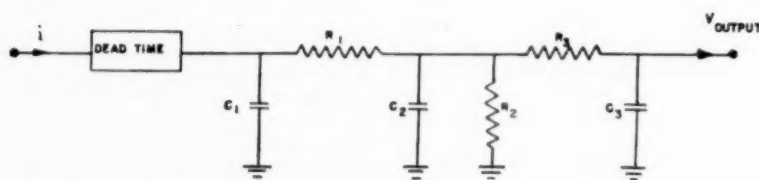


FIG. 3 OVER-ALL SCHEMATIC CONFIGURATION OF PROCESSES USED FOR ANALOG TESTS

capacitors which can be connected to simulate a wide variety of industrial processes, Fig. 2. The input signal to the "process" is produced by an electronic current source which generates a current proportional to the control-valve position. (The current flow might be analogous, for example, to the heat content of fuel flowing through the control valve into a furnace.) The output voltage of the resistance-capacitance network is analogous to the controlled variable, and is measured using a vacuum-tube-voltmeter circuit. The span and zero of this vacuum-tube voltmeter are adjustable so that the span and zero of the measuring instrument that measures the controlled variable can be simulated properly.³ The output signal is then fed into a self-balancing potentiometer recorder where it is translated into a proportional pneumatic signal having a 3-15-psi range. This pneumatic signal is transmitted to the pneumatic controller which then sends a corresponding controller output pressure to the control valve. The control-valve position is converted to a voltage by means of a slide wire. This voltage actuates the current source which thus generates a current proportional to the valve position, thereby closing the control loop. The time constants of the various components of the analog are so small as to be negligible in comparison with the time constants of the processes tested.

³ For start-up tests, the zero was slightly suppressed, so that the controlled variable always left the span on shutdown. The span was made sufficiently wide to allow control action to take place during start-up before the variable had arrived at the set point. As long as reasonable values for the zero and span of the measuring instrument are chosen, they will have no adverse effect on the start-up performance.

The analog also includes a dead-time unit which can be connected into the control loop if it is desired to simulate processes containing pure dead time. The amount of dead time introduced by this unit is continuously variable from 2 sec to 10 min.

PROCESSES TESTED

Ten different processes were tested, including two- and three-capacity processes with various amounts of dead time. The over-all process configuration is shown in Fig. 3. The respective parameter values for each process, as set up on the analog, are tabulated in Table 1.

Processes I and II were chosen as representing as fast a temperature process requiring automatic start-up as is likely to be encountered, namely, start-up time of 1 min. Process VII, in contrast, represents the slowest process (start-up time of 1 hr) which was still practical to test. The other processes tested lie somewhere between those two extremes.⁴

The process reaction curves for several of the processes (obtained by plotting the output voltage of the process after a step change in control-valve position, or current input) are shown in Fig. 4. Adding dead time to any of these processes does not

⁴ The time constant, in seconds, of any resistance-capacitance branch is equal to the product of the resistance (in megohms) and the capacitance (in microfarads). However, owing to interaction between the various resistance-capacitance branches, the effective time constants are changed. Thus, for example, process I is equivalent to three noninteracting RC branches with time constants of 65 sec, 10 sec, and 5 sec, respectively.

TABLE 1 VALUES OF PROCESS PARAMETERS SHOWN IN FIG. 3

Process	Dead time, sec	R_1			C_1	C_2	C_3	Measured—	
		megohm	megohm	megohm				P_u sec	K_u
I.....	0	0.1	0.15	0.1	100	200	100	50	16
IA.....	30	0.1	0.15	0.1	100	200	100	180	3.6
IB.....	10	0.1	0.15	0.1	100	200	100	90	4.8
IC.....	2.3	0.1	0.15	0.1	100	200	100	61	14
II.....	0	0.1	0.15	0	300	300	0	42	100
IV.....	0	0.1	0.15	0.1	300	600	300	138	20
IVA.....	30	0.1	0.15	0.1	300	600	300	290	5
IVB.....	10	0.1	0.15	0.1	300	600	300	170	15
VI.....	0	0.1	0.15	1.1	100	200	1000	156	>100
VII.....	60	0.1	0.15	3.0	100	200	1000	540	50

NOTE: P_u and K_u are period and gain, respectively, for steady cycling.

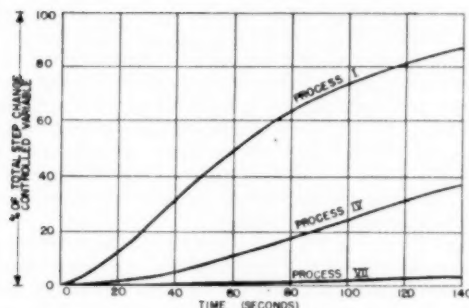


FIG. 4 PROCESS-REACTION CURVES FOR SEVERAL PROCESSES USED IN ANALOG TESTS

change the shape of the process reaction curve, but merely shifts the curve to the right along the horizontal time co-ordinate by an amount equal to the dead time.

TEST PROCEDURE

Each process was set up on the analog and placed on automatic control. After sufficient time had been allowed to let the process variable line out at the set point (around 50 per cent of full scale), the rate and reset functions were shut off, and the proportional band was narrowed progressively until it was just narrow enough to produce a steady constant-amplitude cycling of the variable. The resulting period of cycling P_u and the corresponding proportional band $(PB)_u$ necessary to produce steady cycling were noted.

The process was then shut down and started up repeatedly, using many different controller settings. Usually, four or five different reset settings, covering most of the reset range of the controller, were tried. For each reset-rate setting, four or five different proportional-band settings were tried, again covering most of the band range of the controller. Then, for each individual combination of reset rate and proportional band, the rate time was varied until a rate-time setting was found (if it could be found) which produced acceptable start-up performance. A start-up curve was considered acceptable if there was no appreciable overshoot (less than 1 per cent of full scale).

It appeared that for some processes almost any reasonable combination of reset rate and proportional band produced good start-up, provided, of course, that the proper rate-time setting was chosen. For other processes, however, notably those containing dead time, only certain combinations of reset rates and band settings provided acceptable start-up. Processes having too much dead time could not be started up acceptably at all, no matter what combinations of controller settings were tried. The effect of dead time on start-up will be discussed later.

Thus it is apparent that for many processes, a great number of different combinations of knob settings will produce equally good start-up. The problem is to find that combination of set-

tings which also results in optimum transient recovery after a process load disturbance. To this end, each combination of settings which produced acceptable start-up was tested also for transient performance. In order to make the results for different settings comparable, a standard load disturbance was applied. This consisted of switching the load resistor R_L , Fig. 3, from a value of 0.15 megohm to 0.05 megohm until the pen had dropped exactly 1 per cent of full scale. The resistor was then switched back again to 0.15 megohm and the resulting transient allowed to die out.⁶

The foregoing procedure was repeated for each process, and all combinations of settings giving acceptable start-up performance were tabulated, together with the quality of the transient performance for each of the settings. Altogether, more than 600 start-up trials were made, covering over 200 hours of recording time.

PROCESS PARAMETERS

The data obtained were tabulated, as described, and then carefully examined in order to derive a simple formula which would yield the optimum controller settings. Such a formula, if it is to be practical and applicable in the field, must be based on process parameters that are easily obtainable from the actual process. The ultimate natural process period P_u and the critical or ultimate proportional band $(PB)_u$ are two such parameters, and have been used successfully in connection with the method, described by Ziegler and Nichols (6), which gives controller settings for optimum response to load disturbances. The same two parameters also can be used to characterize the process for the purpose of finding the optimum start-up settings. The experimental determination of these two parameters from an actual installation is usually not difficult. The ultimate period P_u is found by letting the controlled variable line out at the set point, shutting off all reset and rate action, thereby placing the process on proportional control only, and then narrowing the proportional band until a small disturbance will result in steady continuous cycling of the controlled variable. The band at that point is defined as the critical or ultimate proportional band $(PB)_u$, while the period of cycling is P_u .

It also would have been possible to use the process-lag and process-reaction rate measured from the process-reaction curve (response of process to a step input change) as the two parameters. However, the lag is usually so small that it becomes impossible to measure it accurately from the chart record unless a very large step change is used to obtain the process-reaction curve. Such a large step change very often cannot be tolerated in an actual installation. In contrast, the amplitude of the steady cycling can be made very small merely by using a small enough load disturbance to induce the cycling. Accurate measurement

⁶ The length of time required for the pen to drop exactly 1 per cent of full scale is very short, and, therefore, is not a function of the controller settings, but depends only on the process parameters. Thus, for any given process, the load disturbances applied were identical for all controller settings.

of the ultimate period P_u does not suffer if the amplitude of the cycling is made small.⁶

OPTIMUM CONTROLLER SETTINGS

The formula giving the optimum controller settings that was finally derived from the tabulated data is as follows:

$$\begin{aligned}\text{Reset rate} &= 3.0/P_u \\ \text{Proportional band} &= (PB)_u \times 4 \\ \text{Rate time} &\cong P_u/2\end{aligned}$$

where P_u and the rate time are given in minutes, while the reset rate is in repeats per minute.

The last equation, which gives the rate-time adjustment, bears some explanation. The exact adjustment of the rate time is often very critical if the best possible start-up performance is desired. This is illustrated in Fig. 5. If insufficient rate action is used, then the controlled variable will overshoot the set point, as shown in Fig. 5(a). Too large a rate time will prevent overshooting, but will slow down the start-up process so that an excessive amount of time will be required for the variable to reach the set point. This is illustrated in Fig. 5(b). The optimum rate time will produce the start-up curve shown in Fig. 5(c).

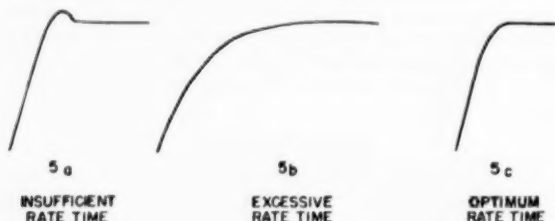


FIG. 5 EFFECT OF RATE-TIME ADJUSTMENT ON START-UP PERFORMANCE

It is difficult to specify the exact value of rate time that should be used. Usually, the settings given by the formula will be found to produce acceptable start-up performance. The formula fixes the values of reset rate and proportional band which should be used, and gives at least a first approximation as to what the rate time should be. Then, to obtain the best possible start-up curve, it usually will be necessary merely to readjust the rate-time setting slightly, as indicated in Fig. 5.

At this point it might be mentioned that quite a number of different criteria have been proposed at various times to define "optimum control response." Actually, the majority of reasonable criteria will result in controller settings that are not too drastically different from each other. For most processes there are numerous different combinations of controller settings producing good start-up, but each combination will result in a different response to load disturbances. While the use of the formula just given does not guarantee the absolute optimum response to load disturbances for every single process, it always will produce a response that comes reasonably close to satisfying the majority of the various response criteria.

TEST AND EVALUATION OF NEW FORMULA

After the formula had been derived, it was tested on the electric process analog, using many different processes, and pneu-

⁶ An approximate formula showing the relation between these two sets of parameters was given by Ziegler and Nichols (6) and is as follows:

$$\text{Process lag} = P_u/4$$

$$\text{Unit process reaction rate} = 8/(P_u)(K_u)$$

where K_u is the ultimate gain and is equal to $100/(PB)_u$.

matic controllers of three different manufacturers. (It should be stated here that the formula, of course, is applicable only to controllers having the general circuit configuration shown in Fig. 1, although it does not matter whether the error is measured after the rate unit, as shown, or ahead of it.) In all cases, the formula was found to give excellent results with respect both to start-up and transient recovery after load disturbances.

Typical chart records obtained for three different processes are reproduced in Fig. 6. For each process, the first response curve shown is the transient recovery produced when the controller was adjusted according to the Ziegler-Nichols equation, with the standard load disturbance previously described applied to the process. The second curve for each process shows the start-up performance using the controller settings given by the new formula presented here. As can be seen, the start-up performance is already fair, but some overshooting still occurs. Accordingly, the rate time was increased slightly, resulting in the third curve, which shows the optimum start-up obtainable. The standard load disturbance was then applied again to find the transient recovery to load disturbances which results when using the optimum start-up settings.

As can be seen in Fig. 6, the response to load disturbances using the new formula was in all cases, by any reasonable criterion, a significant improvement. This would seem to indicate that even for continuous processes, where automatic start-up is not required, the new formula will give better results.

The reason for this improvement is perhaps as follows: The Ziegler-Nichols equations were derived for use with a specific pneumatic controller which has the rate and reset restrictions in parallel in the follow-up circuit. Owing to the peculiarities of this circuit configuration, this type of controller becomes unstable if the product RT (product of reset rate and rate time) approaches unity. In fact, at $RT = 1$, the controller gain theoretically becomes infinite. Thus the Ziegler-Nichols equations of necessity must specify controller settings such that the product RT is kept well below unity, namely, equal to 0.25, even though a higher value otherwise might be more desirable. With the new type of controller configuration shown in Fig. 1, the need for keeping RT well below unity does not exist any more. Accordingly, the new formula makes $RT = 1.50$, resulting in improved controller response to load disturbances, in addition to automatic start-up without overshooting.

MOMENTARY VERSUS SUSTAINED LOAD CHANGES

When speaking about optimum transient recovery after a load disturbance, one really should specify whether momentary (pulse) or sustained (step) load disturbances are meant. A controller adjusted for optimum response to momentary load changes (where reset action is not required) will have a low reset rate and, if a sustained load change is then applied, the controller action will be sluggish and it will require too long a time to bring the variable back to the set point. If, however, the reset rate is increased so that the response to sustained load changes is optimum, then the reset rate will be too high for momentary load disturbances, resulting in large overshoots. This is illustrated in Fig. 7.

It would be desirable to find a formula which would provide optimum start-up settings, and, at the same time, optimum response both to momentary and sustained load changes. Obviously, this is an impossibility, and, somewhere along the line, a compromise has to be made. The new formula represents such a compromise. It will provide optimum start-up settings as well as close to optimum response to momentary load disturbances. However, the response to sustained load changes may tend to be somewhat sluggish, as shown in Fig. 7.

If, in certain applications, the response to sustained load

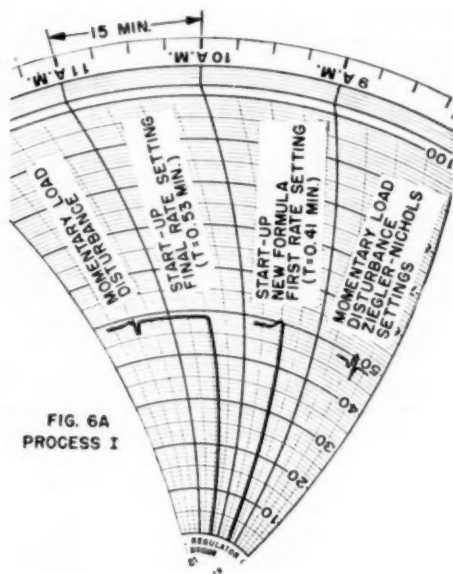
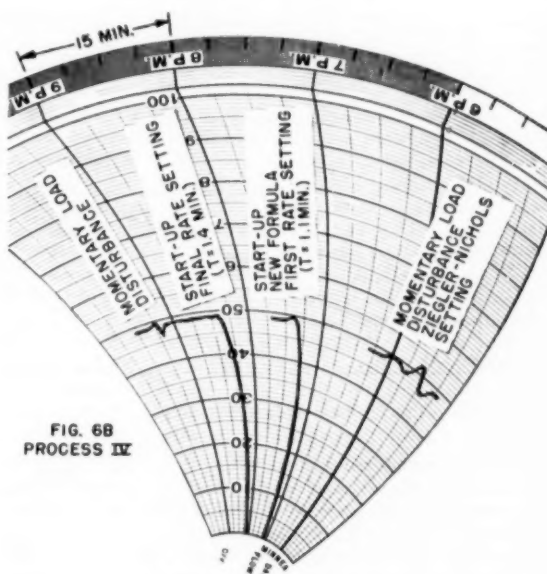
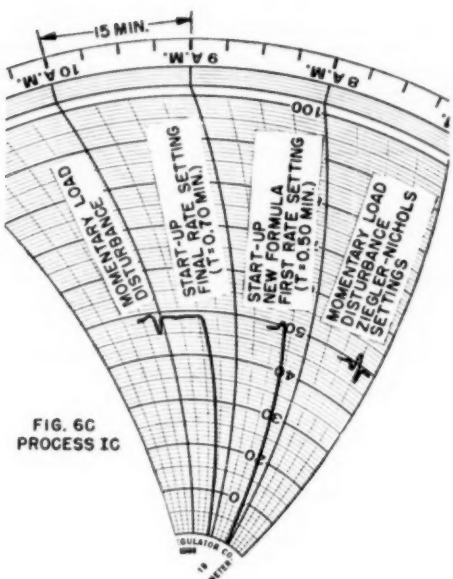

 FIG. 6A
PROCESS I

 FIG. 6B
PROCESS IV

 FIG. 6C
PROCESS IC

FIG. 6 (Left and above) TYPICAL CHART RECORDS OBTAINED IN ANALOG TESTS

automatic start-up without overshooting. To show that such a limit on dead time must exist, let us consider an extreme example: A process with dead time equal to, or greater than, the time that would be required for the controlled variable to reach the set point if the control valve were kept completely open. As this process is started up, controller action cannot go into effect until the dead time has passed. But, by that time, the variable already has reached the set point, and overshooting obviously cannot be prevented.

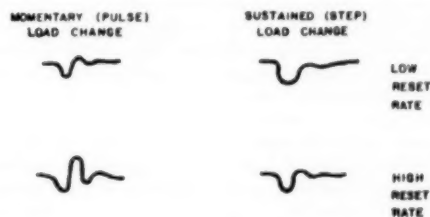


FIG. 7 EFFECT OF MOMENTARY AND SUSTAINED LOAD CHANGES

changes is more important, then the use of the following modified formula is suggested:

Reset rate = $4.0/P_u$ (instead of $3.0/P_u$)

Proportional band = $(PB)_u \times 5$ [instead of $(PB)_u \times 4$]

Rate time $\cong P_u/2$ (as before)

This modified formula will result in a faster response to sustained load changes. However, for many difficult processes the resulting start-up performance and the response to momentary load changes might suffer somewhat.

EFFECT OF DEAD TIME ON START-UP PERFORMANCE

As already mentioned, if more than a certain amount of dead time is introduced into a process, it becomes impossible to achieve

automatic start-up without overshooting. To show that such a limit on dead time must exist, let us consider an extreme example: A process with dead time equal to, or greater than, the time that would be required for the controlled variable to reach the set point if the control valve were kept completely open. As this process is started up, controller action cannot go into effect until the dead time has passed. But, by that time, the variable already has reached the set point, and overshooting obviously cannot be prevented.

"With the process on manual control, introduce a step change in valve position, and record the resulting process reaction curve, Fig. 8. Draw a tangent to the curve at the point of steepest slope. Let t_R signify the time required for this tangent to reach the final value of the controlled variable. (For a single-capacity process, this will be equal to the process time constant.) Now, if the process dead time is greater than $0.1 t_R$, then automatic start-up without overshooting will be difficult, if not impossible."

TABLE 2 EFFECT OF DEAD TIME ON START-UP PERFORMANCE

Process	I	IC	IB	IA	IV	IV B	IV A
Dead time, sec	0	2.3	10	30	0	10	30
t_R , sec	100	100	100	100	300	300	300
Dead time	0	0.02	0.1	0.3	0	0.03	0.1
t_R							
Quality of start-up	Good	Good	Poor	Impossible	Good	Good	Poor

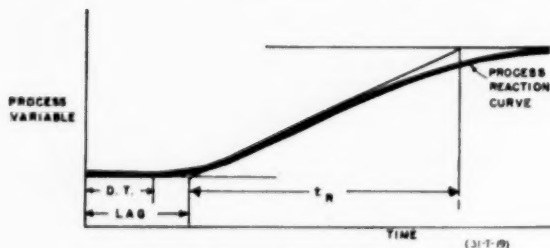


FIG. 8 PROCESS REACTION CURVE

It must be emphasized that the foregoing rule is only approximate, and has not yet been substantiated by sufficient experimental evidence. However, the purpose of this rule of thumb will have been fulfilled if it can serve as a rough guide to process designers and indicate to them whether the processes on their drawing boards stand a fair chance of being started-up automatically without producing overshoot.

Table 2 shows the correspondence between the rule given and the results obtained for several processes on the electric process analog.

SUMMARY

For some processes, a great number of different combinations of controller settings will produce acceptable automatic start-up performance without overshooting. For other processes, notably those containing a large amount of dead time, the usable combinations of controller settings may be more difficult to find. This paper presents a formula giving the proper controller settings as functions of the ultimate natural period and the ultimate proportional band of the process-control loop.

The formula fixes the values of reset rate and proportional band which should be used, and gives the approximate value of the rate time to be used as a first approximation. The controller settings specified by the formula produce not only good start-up performance, but also provide close to optimum recovery from process load disturbances. Therefore the use of the formula is recommended even in the case of continuous processes where automatic start-up is not required. In discussing optimum controller response, a distinction has been made in this paper between the response to momentary and to sustained load changes.

Finally, the paper has discussed the effect of dead time on start-up performance, and has suggested a rule of thumb giving an indication of the maximum amount of dead time tolerable on automatic start-up.

ACKNOWLEDGMENT

The author is indebted to Mr. S. P. Higgins for his valuable help and advice during the entire course of the investigation.

BIBLIOGRAPHY

- 1 "Technique for Minimizing Overshoot in Discontinuous Processes," by G. H. Toop, *Instrument Practice*, vol. 6, 1952, pp. 369-379.
- 2 "Balanced and Variable-Linked Automatic Reset," by C. H. Gest, *Instruments*, vol. 24, 1951, pp. 1292-1294.
- 3 U. S. Patent No. 2,202,218, R. L. Mallory.

4 "An Improved Pneumatic Control System," by R. E. Claridge, *Trans. ASME*, vol. 73, 1951, pp. 297-305.

5 "Electrical Analogy Method for Fundamental Investigations in Automatic Control," by D. P. Eckman and W. H. Wanamaker, *Trans. ASME*, vol. 67, 1945, pp. 81-86.

6 "Optimum Settings for Automatic Controllers," by J. G. Ziegler and N. B. Nichols, *Trans. ASME*, vol. 64, 1942, pp. 759-768.

Discussion

N. B. NICHOLS.⁷ Referring to the effect of dead time as the author's formula indicates, the optimum proportional band is approximately 4 times the ultimate proportional band or

$$(PB)_{opt} = 4(PB)_u = 4 \left(\frac{100}{2} R_1 L \right) = 200 R_1 L$$

where R_1 is the unit process reaction rate in per cent pen travel per minute per per cent valve travel, and L is the process lag in minutes. R_1 and L may be computed from the ultimate period and ultimate proportional band as indicated in the paper or from a knowledge of the process.

Assuming for the moment that the pen is considerably below the set point, we may represent the general start-up conditions in Fig. 9 of this discussion. It will be seen that the rate stage output

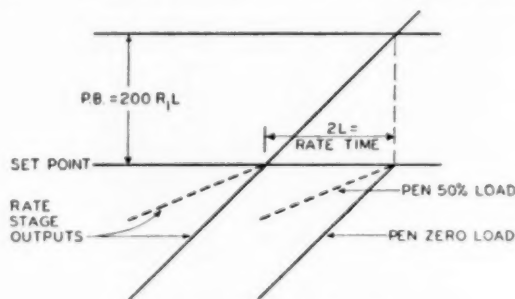


FIG. 9 START-UP UNDER ZERO LOAD

leads the pen or measured variable by the rate time which has been set at the author's optimum value of $P_u/2$ or $2L$. Depending on the process load (the controller output required to hold the measured variable constant) the pen will approach the set point at different rates. The maximum rate would be for zero load and would be equal to $100 R_1$. A 50 per cent load would reduce this to $50 R_1$. Control action will start when the rate stage output reaches the set point of the reset stage. It is then evident that the earliest possible control action will result only if the initial value of the measured variable is below the set point by at least the width of the proportional band if start-up takes place with zero load or one half the proportional band if start-up takes place at 50 per cent load.

The foregoing would indicate that satisfactory performance on start-up requires that a sufficiently wide span of the measuring element and the rate unit should be used to permit the rate unit to come into operation by at least $2L$ before the pen reaches the set

⁷ Manager, Research Division, Raytheon Manufacturing Company, Waltham, Mass. Mem. ASME.

point. The amount of span below the set point will depend on the excess capacity of the valve but the largest value required should be $200 R_s L$ or $4(PB)_u$.

The results seem to be partially proved by the author's data showing poor start-up in processes 1A, 1B, and 4A all of which have proportional bands greater than 20 per cent. Good start-up performance should be obtained on these processes with lower initial values of the measured variable.

Commenting on the location of the error-measuring element, it would, of course, be advantageous for it to precede the rate element in cases where the set point is varied by another controller in a cascade-control system.

It might be pointed out that optimum response to load changes will depend also on where the load change enters the system and that higher reset rates will give better performance when the load change enters near the valve end. The derivation of the Ziegler-Nichols relations was based on a sustained load change entering at the same place as the valve which would correspond to a voltage change in series with the dead-time element in the analog.

AUTHOR'S CLOSURE

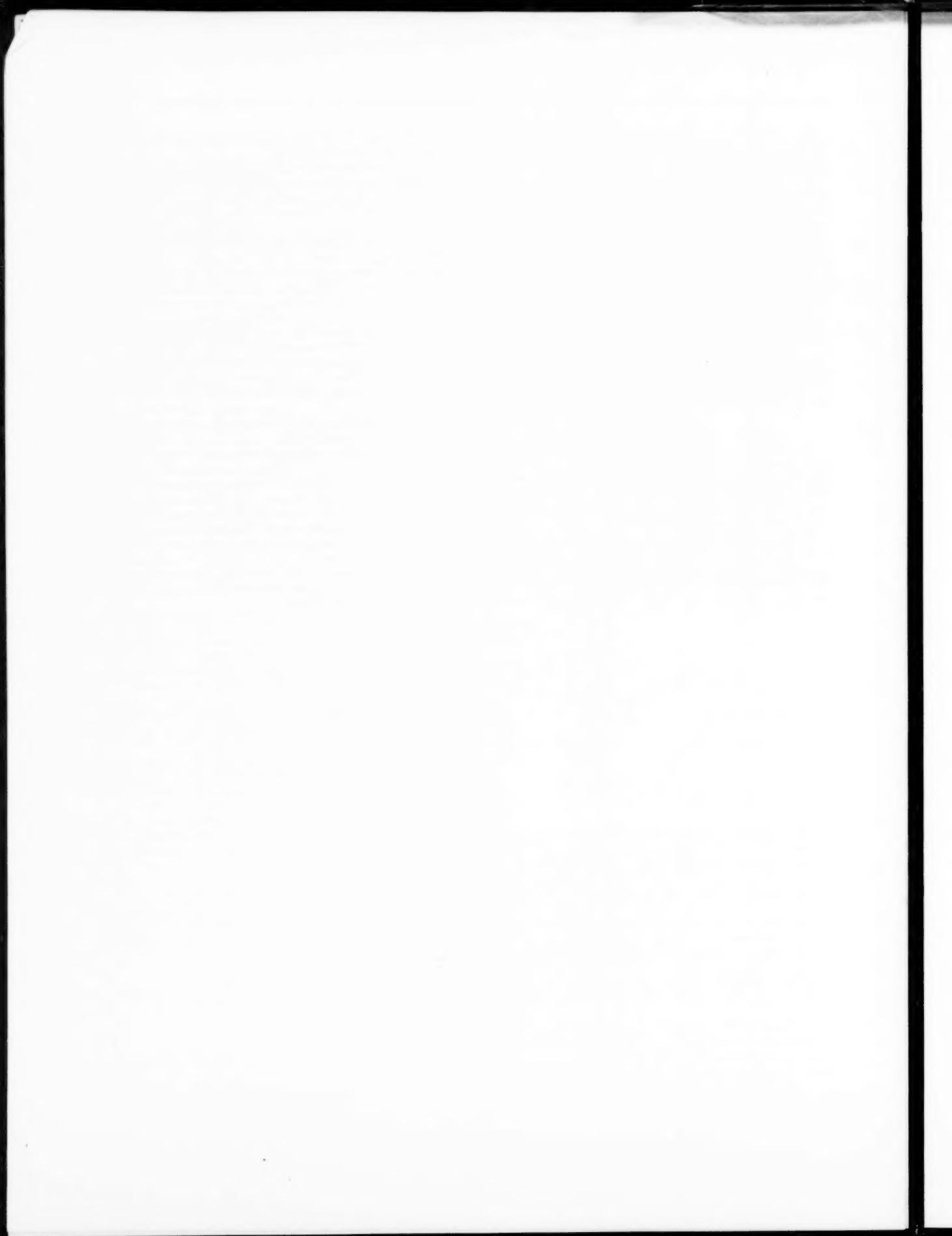
The author welcomes Mr. Nichols' comments concerning the effect of dead time on start-up performance. As was stated in the paper, the suggested rule of thumb to determine the maximum amount of dead time tolerable was not meant to be a final answer. Any analysis which helps to place this phase of the problem into a more rational light is therefore welcome.

The data presented in Table 2 were obtained with the set point at 50 per cent of full scale. If the set point is higher than this, then, as Mr. Nichols points out, overshooting can be prevented even though the dead time is larger than specified by the suggested rule of thumb. Mr. Nichols' suggested criterion seems to

be valid as long as the approximate relations given in footnote 6 of the paper can be said to apply.

Mr. Nichols' statement concerning the location of the error-measuring element is not necessarily true. A typical cascade control system might be one where the output of a temperature controller varies the set point of a flow controller. In such an application, the temperature or master controller would include rate action, but the flow or secondary controller would usually contain only the proportional and reset modes of control since rate action would not be very beneficial in the fast-responding flow-control loop. Thus, since only the master controller contains rate action, the location of the error-measuring element is immaterial. If, for some reason, the secondary controller is also a three-mode controller, then it might actually be detrimental to have the error-measuring element precede the rate-action element because this produces rate-action response to set-point changes. Since we already have rate action in the master controller, this arrangement would, in effect, cause rate action to act twice in succession on the same signal. Such control action might cause instability unless *both* rate-time settings were carefully and *individually* adjusted.

Finally, the author would like to state that the tests described in the paper did not cover exothermic processes, processes without self-regulation, multiloop systems, or systems containing saturation effects caused by poor valve sizing, improper instrument ranges, and so on. Some of these effects may make it difficult or even impossible to obtain automatic start-up without overshooting. Obviously, such cases cannot be covered by any general-purpose formula, but would have to be considered each on an individual basis. Future work along this line would seem to be called for to investigate the automatic start-up of processes subject to some of these effects.



Analogies for Hydraulic and Electric Drives in Servomechanisms

BY YAOHAN CHU¹ AND L. A. GOULD,¹ CAMBRIDGE, MASS.

The paper demonstrates the analogy between the d-c electric and hydraulic drives, commonly used in servomechanisms. This analogy is developed from their analogous basic relations, and their analogous methods of speed control are then shown. The analogous dynamic behavior of such servomechanisms is shown both in the derivation of the respective electric and hydraulic circuits and in the block diagrams. One distinguishing non-analogous character is that there is no hydraulic analogy to the mutual flux of electric machines. Nevertheless, it is shown that analogous dynamic behavior of the servomechanism resulting from an advantageous flux compounding in the electric drive can be achieved by applying certain pressure feedback in the hydraulic drive.

INTRODUCTION

THE analogy method in engineering is used to great advantage in those cases where a body of knowledge has been built up in one particular field but not in another. If one finds identical mathematical descriptions of two superficially different physical systems, it is said that the systems are analogous. Thus if one system has been studied thoroughly on the basis of its mathematical description, e.g., differential equations, the analogous system is much more readily engineered by using the accumulated knowledge already available rather than by studying the same mathematics all over again.

A more subtle use of the analogy method is from the educational point of view. By analogs, one is more easily led to perceive the basic similarities of two superficially different systems. This technique tends to introduce a degree of creative insight into the design and development of new devices based on an available body of knowledge in a field that, heretofore, is seemingly unrelated to the one under consideration.

Often analogy techniques may seem to lead to erroneous conclusions. In cases of this sort, one should not always discard the analogy, but rather investigate the reasons for assuming analogous behavior in the first place. This type of investigation often leads to a better understanding of secondary effects that may have been neglected. The net result is to provide the engineer with a means for extending his understanding of the details of a system's performance.

Direct-current generators and motors as well as positive-displacement hydraulic pumps and motors are widely used as drives in servomechanisms. Their analogous nature has long been recognized. The fact that generators are analogous to pumps and d-c motors analogous to hydraulic motors is familiar. Electrical auxiliaries such as switches, capacitors, resistors, circuit breakers, and so on, are analogous to hydraulic auxiliaries such as valves, accumulators, relief valves, and the like. However, the

¹ Massachusetts Institute of Technology.

Contributed by the Industrial Instruments and Regulators Division and the Fluid Meters Research Committee and presented at the Annual Meeting, New York, N. Y., November 30-December 5, 1952, of THE AMERICAN SOCIETY OF MECHANICAL ENGINEERS.

NOTE: Statements and opinions advanced in papers are to be understood as individual expressions of their authors and not those of the Society. Manuscript received at ASME Headquarters, September 17, 1952. Paper No. 52-A-101.

analogy is limited by the fact that d-c machines are electromechanical devices, whereas hydraulic machines are hydro-mechanical devices. Since there is no hydraulic analogy to the mutual flux of electrical machines, one cannot develop a hydraulic analogy to a machine like the amplityne. Nevertheless, the high power amplification that is characteristic of the amplityne has been paralleled by the development of hydraulic units with a similarly high power amplification.²

The knowledge of analogy between these two fields enables the designer, familiar with performance in one field, to perceive similar performance in the other field. In this paper the discussion shall be limited to those analogies related to closed-loop control systems. Nonanalogous instances will be mentioned at the appropriate places.

ANALOGIES IN BASIC RELATIONS³

If the d-c machines are idealized by ignoring saturation and armature reaction, the electromotive force and torque relations may be written as follows

$$E = K\phi N \quad [1]$$

$$T = K\phi I_0, \quad \dots, \quad \text{where } K = \frac{1}{2} \frac{d\phi}{dI_0} \quad [2]$$

where E is generated emf for a generator and counter-emf for a motor (volts); T is torque, Newton-meter; ϕ is flux, volt-sec; N is speed of armature, rad/sec; I_a is armature current, amperes; K is a dimensionless constant, depending on design of machine.

These two relations are equally valid for either a generator or a motor under the given idealized conditions. Theoretically, d-c generators may be used as motors and vice versa.

Similarly, if the positive-displacement pumps and motors are idealized by ignoring slip flow, inlet-flow loss, and various friction losses, the flow and torque relations may be written as follows

$$Q = DN, \quad [3]$$

$$T = DP_{\text{max}} \times \left(\frac{\sum_{i=1}^n \lambda_i}{\sum_{i=1}^n \lambda_i + \sum_{j=1}^m \mu_j} \right) \quad [4]$$

where Q is flow, cu m per sec; T is torque (Newton-meter); D is displacement per radian of pump or motor, cu m per radian; P is pressure difference across pump or motor, Newton-meter²; N is speed of pump or motor, rad/sec.

These relations are valid for both positive-displacement pumps or motors under idealized conditions. Theoretically, pumps and motors are interchangeable. This is true for widely used units such as the radial type, axial type, vane type, and so on.

From the foregoing four basic relations, we readily may identify the following analogous quantities:

D-C machines		Hydraulic units
E (voltage)	} is analogous, respectively, to {	Q (volumetric flow)
T (torque)		T (torque)
N (speed)		N (speed)
ϕ (flux)		D (displacement)
I_a (current)		P (pressure)

These are the fundamental analogous quantities upon which

² At the Dynamic Analysis and Control Laboratory of the Massachusetts Institute of Technology.

³ MKS units are used on account of simplicity in basic relations and using one set of units throughout the paper.

further analogies are based. On the basis of intuition, one would assume that if a current flowing through a wire is considered to be analogous to a fluid flowing through a pipe, current will be analogous to flow and voltage drop to pressure drop. In the analogies used in this paper, however, voltage is analogous to flow and current to pressure. It is important to realize that the analogies dealt with here are developed from the basic relations involved rather than from intuition.

ANALOGIES IN DRIVES

From the theory of d-c machinery, the speed of a d-c motor may be expressed as

$$N = \frac{E - I_a R_a}{K \Phi} \quad [5]$$

where I_a and R_a are armature current and resistance, respectively, E , the applied voltage, and other quantities are as indicated previously. The basic methods of speed control are, therefore, variation of the armature resistance, variation of flux, variation of applied voltage and their combinations.

The speed of a hydraulic motor may be expressed by the following relation

$$N = \frac{Q - PM}{D} \quad [6]^4$$

where P is the pressure across the motor, M the leakage coefficient, Q the supplied flow, and other quantities are as indicated previously. The basic methods of speed control are, therefore, variation of the leakage, variation of the motor displacement, variation of supplied flow, and their combinations. The Appendix demonstrates the analogies that exist between armature-resistance variation and leakage variation, field-flux variation and motor-displacement variation, and the combinations. For continuous control systems the most important methods are the applied-voltage control in the electric case (Ward-Leonard system) and supplied-flow control in the hydraulic case (hydraulic transmission). The latter two systems are shown in Fig. 1.

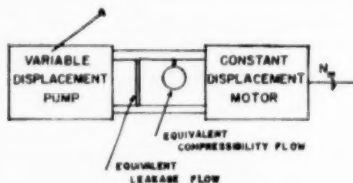


FIG. 1(a) HYDRAULIC TRANSMISSION

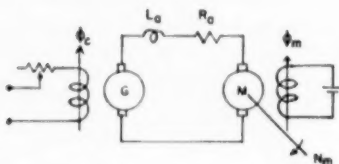


FIG. 1(b) WARD-LEONARD SYSTEM

The Ward-Leonard system is smooth and versatile in control, despite the obvious disadvantage that three full-size machines are required. Its performance is analogous to that of the hydraulic transmission. This can be shown from the derivation of the dif-

⁴ The product PM is the leakage flow. This is an approximate relationship, but it is a practical and useful one.

ferential equations of the two systems. Thus, for the Ward-Leonard system, the differential equation is derived from the armature circuit

$$\text{Voltage generated} = \text{armature inductance drop} + \text{armature resistance drop} + \text{back emf}$$

or, mathematically

$$E_g = \frac{n_a^2}{r_a} \frac{dI_a}{dt} + R_a I_a + K \Phi_m N_m \quad [7]$$

and

$$\left. \begin{aligned} K \Phi_m I_a &= T_L + T_J \\ E_g &= K_g \Phi_f \\ J \frac{dN_m}{dt} &= T_J \end{aligned} \right\} \quad [8]$$

where T_J is inertia torque, T_L load torque, and the subscript g refers to generator, m refers to motor, and a refers to armature. Note that n_a^2/r_a is equal to armature inductance L_a , where n_a is number of turns and r_a is magnetic reluctance in the armature circuit. (Note: Magnetic-circuit parameters are being used here instead of electric-circuit parameters to simplify the analysis of compounding later on.)

For the hydraulic transmission, the differential equation is derived from the flow circuit

Pump flow = compressibility flow + leakage flow + motor flow

or, mathematically

$$Q_p = \frac{V}{B} \frac{dP_m}{dt} + MP_m + D_m N_m \quad [9]$$

and

$$\left. \begin{aligned} D_m P_m &= T_L + T_J \\ Q_p &= N_p D_p \\ T_J &= J \frac{dN_m}{dt} \end{aligned} \right\} \quad [10]$$

Thus, for the analogy between the hydraulic transmission and the Ward-Leonard system, two additional parameters can be added to the list of analogous quantities as follows:

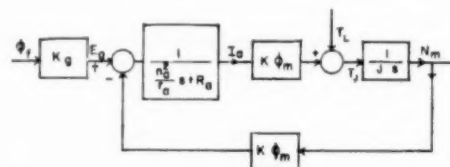


FIG. 2 BLOCK DIAGRAM FOR WARD-LEONARD SYSTEM

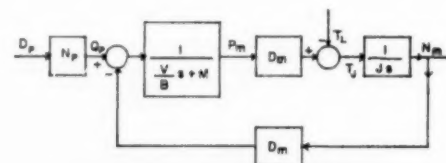


FIG. 3 BLOCK DIAGRAM FOR HYDRAULIC SYSTEM

Ward-Leonard system
 R_a (armature resistance)
 L_a (armature inductance)

Hydraulic transmission
 M (leakage coefficient)
 V/B (ratio of volume of oil under compression to bulk modulus of the oil)

For further clarification of this analogy, the block diagrams for these two systems are shown in Figs. 2 and 3.

Both these systems are quite efficient. In the steady state, they give motor speed directly proportional to control signal for no load. The maximum allowable torque load is limited only by the maximum allowable pressure across the motor in the hydraulic transmission and by the allowable dissipation associated with the armature windings of the Ward-Leonard system. However, compared to an equally rated hydraulic system, the electrical system is usually larger in size, heavier, and slower in dynamic response. The hydraulic system, however, is higher in cost at the present stage of development. Thus, as would be expected, in the final analysis the choice between the two basic types of control systems depends mainly on the application.

The effect of the source which drives the field of the electric generator or the stroke of the hydraulic pump (which varies the displacement of the pump) is an important consideration for control applications. In the electric system, the field can be driven by an electronic amplifier characterized by either high or low-output impedance. The high-impedance amplifier acts like a current source producing field current proportional to the control signal. In this case the lag between the control signal and the field current is negligible. If the amplifier has low-output impedance, it acts like a voltage source producing field voltage proportional to the control signal. In this case there is an approximate first-order lag between the field voltage and the field current.

For the hydraulic system the stroke might be driven by a spring-restrained force motor. If the spring constant of the restraining spring is high, the force motor acts like a position source. If the spring constant is low, the force motor acts like a force source. A position source is analogous to a current source, since both are characterized by negligible lag between the control signal and the output signal (field current or stroke). A force source is analogous to a voltage source, since both introduce a first-order lag between control signal and output signal.

The force motor usually is unable to drive the stroke of the pump directly because of its limited available torque, nor is a larger force motor desirable because of its larger time constant. Hence, in practice, the force motor drives a hydraulic amplifier (which acts like a position source) which in turn drives the stroke. In such a case, theoretically, there will be two lags; one due to the hydraulic amplifier and the other due to the force motor which drives the hydraulic amplifier. One finds that the lag due to the hydraulic amplifier is usually negligible compared to the lag produced by the force motor. Thus, assuming the hydraulic amplifier is ideal (no dynamic lag), one obtains the same form of

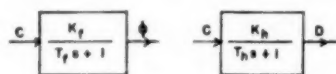


FIG. 4 ANALOGIES IN DRIVING SOURCES
 (a, Source for driving electrical system. b, Source for driving hydraulic system.)

dynamics for the hydraulic system driven by the force motor as would be obtained for the electric system driven by a low-impedance amplifier (electronic).

In practice, one usually finds that the dynamic response between control signal (input to the electronic amplifier or input to the force motor) and the field current or stroke is characterized

by a first-order lag. Thus the two systems are dynamically analogous (having similar differential equations) with respect to driving source in the practical case. Thus the block diagrams for the two cases may be drawn as shown in Fig. 4 in which the symbols are as follows:

s = Laplacian operator
 C = control signal
 K_f = static sensitivity of field flux to control signal
 K_h = static sensitivity of displacement to control signal
 T_f = time constant of lag in electrical system
 T_h = time constant of lag in hydraulic system

ANALOGIES IN COMPOUNDING OR FEEDBACK

Compounding an electrical generator involves adding one or more additional windings to the field structure of the machine so as to improve the static and dynamic regulation of the system in the presence of loads. If saturation is neglected, the flux intro-

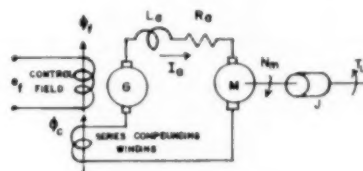


FIG. 5 COMPOUNDING OF WARD-LEONARD SYSTEM

duced by the additional field adds to the flux produced by the control winding. If the flux produced by the compounding winding is developed by the armature current (by placing the compounding winding in series with the armature circuit of the generator), the net result is armature-current feedback around the armature circuit of the machine. If this feedback is positive, by proper adjustment of the compounding-winding parameters, an improvement in both the static and dynamic performance of the system is possible. Diagrammatically, the compounded Ward-Leonard system is as shown in Fig. 5.

In terms of magnetic-circuit parameters, the following notation is used to draw the block diagram of the system:

n_f = number of turns in control field winding
 n_c = number of turns in compounding winding
 n_a = number of turns in armature winding
 r_f = reluctance of control flux path
 r_c = reluctance of compounding flux path
 r_a = reluctance of armature flux path
 R_f = control field resistance
 R_a = armature circuit resistance
 K_g = open-circuit generator voltage per unit exciting flux
 K_T = developed motor air-gap torque per unit armature current
 K_b = motor back emf per unit output speed
 J = motor and load inertia
 e_f = control field voltage
 i_f = control field current
 i_a = armature current
 ϕ_f = control field flux
 ϕ_c = compounding flux
 ϕ_a = net exciting flux
 T_L = load torque
 T_a = air-gap torque
 N_m = output speed
 s = Laplacian operator

The functional block diagrams of the compounded and uncompounded Ward-Leonard systems are shown in Figs. 6 and 7. It

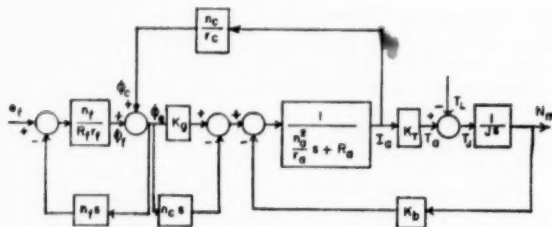


FIG. 6 BLOCK DIAGRAM FOR COMPOUNDED WARD-LEONARD SYSTEM

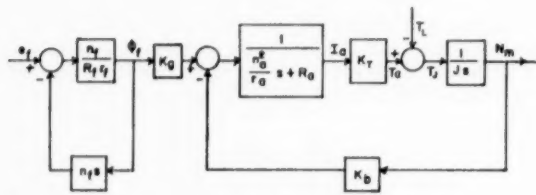


FIG. 7 BLOCK DIAGRAM FOR UNCOMPOUNDED WARD-LEONARD SYSTEM

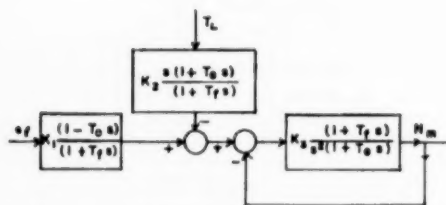


FIG. 8 SIMPLIFIED BLOCK DIAGRAM OF COMPOUNDED WARD-LEONARD SYSTEM

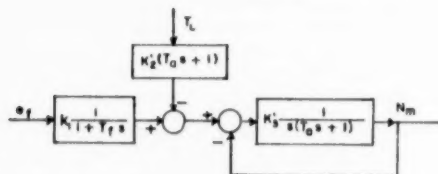


FIG. 9 SIMPLIFIED BLOCK DIAGRAM OF THE UNCOMPOUNDED WARD-LEONARD SYSTEM

is to be noted that the conversion identities between electric-circuit and magnetic-circuit parameters are

$$\phi = \frac{nI}{r}$$

$$E = n \frac{d\phi}{dt}$$

$$L = \frac{n^2}{r} \text{ (self-inductance)}$$

$$M_{12} = \frac{n_1 n_2}{r} \text{ (mutual inductance)}$$

The magnetic-circuit parameters are more convenient to use in the case of compounding, not only because flux is analogous to the displacement of the hydraulic transmission, but also because the flux may be then added or subtracted in the analysis and thus simplify the drawing of block diagrams.

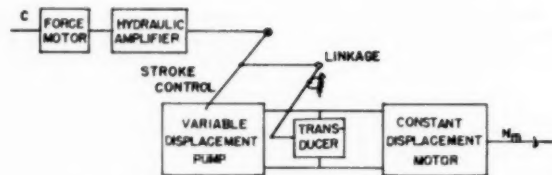


FIG. 10 COMPOUNDING OF HYDRAULIC TRANSMISSION

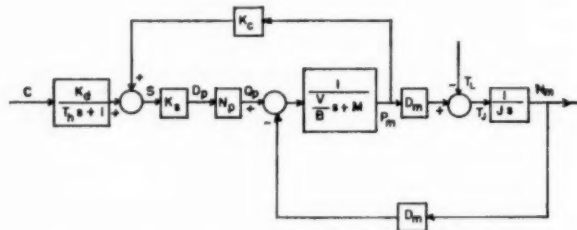


FIG. 11 BLOCK DIAGRAM OF COMPOUNDED HYDRAULIC TRANSMISSION

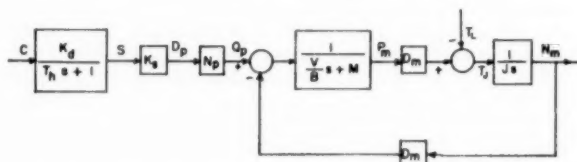


FIG. 12 BLOCK DIAGRAM OF UNCOMPOUNDED HYDRAULIC TRANSMISSION

By proper adjustment of the parameters of the compounded system, one can theoretically achieve zero regulation in the presence of steady-state loads. To achieve zero steady-state regulation, the compounding winding is chosen so that

$$\frac{K_o n_c}{R_o r_c} = 1 \quad [11]$$

Then the diagrams in Figs. 6 and 7 simplify to those of Figs. 8 and 9. In terms of the original parameters of Figs. 6 and 7, the constants of Figs. 8 and 9 are

$$\begin{aligned} K_1 &= \frac{K_g}{K_b} \frac{n_f}{r_f} & T_o &= \frac{n_c^2}{R_o r_c} \\ K_2 &= \frac{R_o}{K_b K_T} (T_f + T_o + T_a) & T_e &= \frac{T_f T_a}{T_f + T_o + T_a} \\ K_3 &= \frac{K_b K_T}{J R_o} \frac{1}{T_f + T_o + T_a} & T_f &= \frac{n_f^2}{R_f r_f} \\ K_2' &= \frac{R_o}{K_T K_b} & T_a &= \frac{n_a^2}{R_o r_a} \\ K_3' &= \frac{K_b K_T}{J R_o} \end{aligned}$$

Before examining the benefits achieved by the type of positive feedback described in the foregoing for the Ward-Leonard system, it would be logical to attempt to extend the analogy procedure by developing an analogous compounding scheme for the hydraulic transmission. In the case of the Ward-Leonard system, positive

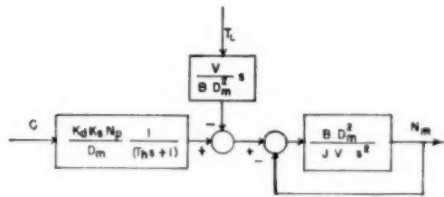


FIG. 13 SIMPLIFIED BLOCK DIAGRAM OF COMPOUNDED HYDRAULIC TRANSMISSION

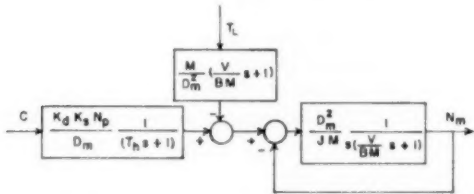


FIG. 14 SIMPLIFIED BLOCK DIAGRAM OF UNCOMPOUNDED HYDRAULIC TRANSMISSION

feedback was accomplished by feeding back a signal proportional to armature current and adding the resultant signal to the control flux. Using the analogous quantities, armature current is analogous to line pressure in the hydraulic transmission and flux is analogous to displacement. Thus, to compound the hydraulic transmission in a manner analogous to that used in the Ward-Leonard system, one would feed back a signal proportional to line pressure and add the resultant signal to the displacement. Practically, one would use a differential-pressure-to-displacement transducer linked by a lever system to the pump stroke. The scheme is shown in Fig. 10. Its block diagram is shown in Fig. 11 in which K_c is the static sensitivity between line pressure and the feedback motion, K_d is the static sensitivity between control signal and stroke, K_s is the static sensitivity between stroke and displacement, and S is the stroke. The block diagram of the uncompounded hydraulic transmission appears in Fig. 12.

If the compounding linkage is adjusted for zero steady-state regulation, then

$$\frac{K_c K_s N_p}{M} = 1 \quad [12]$$

Then the diagrams in Figs. 11 and 12 simplify to those of Figs. 13 and 14.

At this point, examination of the compounded Ward-Leonard system, Fig. 8, shows that the system is stable. This can be seen if it is noted that T_f is greater than T_a . Then the feedback loop shown in Fig. 8 is unity feedback around a double pole at the origin of the complex s -plane compensated by a phase-lead function. This type of feedback loop is stable for all values of static-loop sensitivity. On the other hand, examination of the compounded hydraulic transmission, Fig. 13, shows that the system is unstable. The feedback loop shown in Fig. 13 is unity feedback around a double pole at the origin of the complex s -plane with no compensating function. This type of feedback is unstable for all values of static-loop gain.

Thus in this case (system compounding by positive feedback), the analogy seems to fail. Further examination of Figs. 6 and 11 shows that the two systems have a basic difference, namely, that there is no analogy in the hydraulic transmission for the mutual inductance of the electric system. This does not surprise one but is rather expected. (Recall a remark at the beginning of the paper to the effect that a "hydraulic amplidyne" cannot be con-

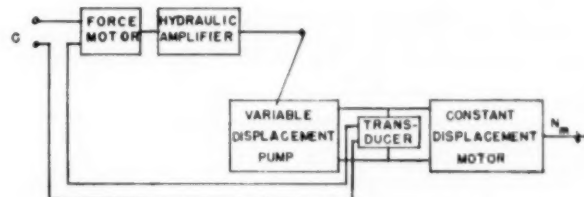


FIG. 15 MODIFIED COMPOUNDED HYDRAULIC TRANSMISSION

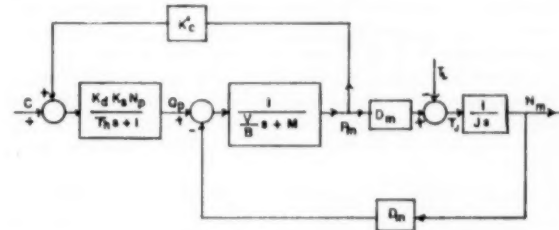


FIG. 16 BLOCK DIAGRAM OF MODIFIED COMPOUNDED HYDRAULIC TRANSMISSION

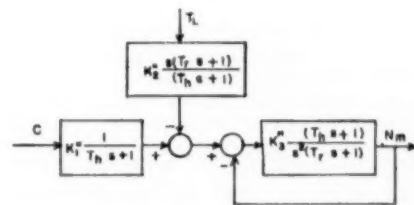


FIG. 17 SIMPLIFIED BLOCK DIAGRAM OF MODIFIED COMPOUNDED HYDRAULIC TRANSMISSION

structed.) Thus a conclusion may be drawn that whenever use is made of this mutual inductance effect in electrical systems, no complete analogy may be drawn to the equivalent hydraulic system.

A stable compounded hydraulic transmission can be achieved, however, if the compounding scheme is modified slightly so that instead of pressure feedback to the stroke, one uses pressure feedback to the control signal. The scheme is shown in Fig. 15 and its block diagram is shown in Fig. 16 where K_c' is the static sensitivity between line pressure and the feedback electrical signal.

If the compounding arrangement of the modified system is adjusted for zero steady-state regulation

$$\frac{K_c' K_d K_s N_p}{M} = 1 \quad [13]$$

Then the diagram in Fig. 16 simplifies to that in Fig. 17. In terms of the original parameters of Fig. 16 the constants of Fig. 17 are

$$\begin{aligned} K_1' &= \frac{K_d K_s N_p}{D_m} & T_p &= \frac{V}{RM} \\ K_2' &= \frac{M}{D_m^2} (T_h + T_p) & T_f &= \frac{T_h T_p}{T_h + T_p} \\ K_3' &= \frac{D_m^2}{JM (T_h + T_p)} \end{aligned}$$

Since T_h is greater than T_p , the system in Fig. 17 is stable for all values of static loop sensitivity.

If the simplified block diagrams of the two stable compounded systems, Figs. 8 and 17, are compared, it is seen that the systems are dynamically identical except for an additional numerator fac-

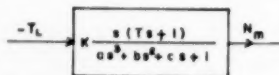


FIG. 18 BLOCK DIAGRAM OF DYNAMIC RESPONSE OF OUTPUT SPEED TO LOAD-TORQUE VARIATIONS FOR STABLE COMPOUNDED SYSTEMS

tor in the first block of the electric system, Fig. 8. The time constant T_e associated with this numerator is directly proportional to n_e and inversely proportional to K_e . In practice, the number of turns n_e in the compounding field is small, and the voltage generated per unit flux K_e is large for the compounded Ward-Leonard system. Thus the time constant T_e may be considered negligible. If this approximation is used, the dynamics of the two systems considered become identical in all respects.

The advantage of the compounding scheme used in this paper becomes evident when one examines the effect of torque disturbances on the system. To emphasize the effect of load changes, Fig. 18 shows the form of the dynamic relationship between load-torque changes and output-speed changes for both stable compounded systems.

Examining the response function in Fig. 18, it is seen that for a steady load on the system, the output speed will be unaffected; i.e., the system exhibits zero steady-state error for constant load disturbances. However, as the frequency of the load-torque variations increases, these variations will produce errors in the output speed. At a frequency determined by the parameters of the response function, a maximum output-speed error will be reached, and, above this frequency, the magnitude of the speed errors will decrease. This resonance phenomenon always appears for any system which exhibits zero regulation for constant loads. The dynamic errors that arise for varying loads can be made small if the static sensitivity K is made small. Then the output speed will be essentially insensitive to any load variations whatsoever, or, in the practical sense, the effect of load variations can be minimized over the whole frequency spectrum.

If the uncompounded systems, Figs. 9 and 14, are examined, it is seen that the advantage of zero steady-state speed error with respect to constant load does not exist. By reduction of the static sensitivity relating output speed and load torque (slope of the static torque versus speed characteristic for the system), the steady-state speed regulation may be reduced, but not to zero regulation as is possible in the compounded systems.

In actuality, both the compounded and uncompounded systems will have finite nonzero regulation due to the effects that have been neglected in the analysis. However, for a given set of equipment, the compounded system will exhibit a "flatter" torque-speed characteristic than the uncompounded system; i.e., will have smaller regulation. The compounded system, therefore, will tend to maintain a given position (for a positional servomechanism) or speed (for a speed regulator) with much smaller errors in the presence of constant load disturbances than the uncompounded system.

In conclusion, although the analogy is not exactly established in the case of compounding (owing to the fact that the mutual inductance effect does not exist in hydraulic units), yet one can still develop a hydraulic system whose dynamic characteristics are, for all practical purposes, analogous to the corresponding electric system. Since the dynamic performance is a major factor in control-system design, this sort of result is a desirable extension of knowledge gained on one class of systems to another class.

CONCLUSION

The analogy between the d-c electric and hydraulic drives commonly used in servomechanisms has been demonstrated in their basic relations, in drives, and in compounding. It is hoped that, by means of this analogy, any new development in one field would lead to a similar application in another such as the illustrated case of flux compounding.

Appendix

ANALOGIES IN VARIABLE-SPEED DRIVES*

Hydraulic

- (a) Leakage controlled (Fig. 19)
Constant-displacement pump
Constant-displacement motor

$$N_m = \frac{Q_p}{D_m} - \frac{MT_L}{D_m^2}$$

M varies

(NOTE: M is a leakage coefficient including flow through valve as well as leakage past motor and pump)

- (b) Displacement controlled (Fig. 21)
Constant-displacement pump

$$N_m = \frac{Q_p}{D_m} - \frac{MT_L}{D_m^2}$$

D_m varies

- (c) Displacement controlled (Fig. 23)

$$N_m = \frac{N_p D_p}{D_m} - \frac{MT_L}{D_m^2}$$

D_p and D_m vary

Electrical

- (a) Armature resistance controlled (Fig. 20)
Constant generator-field current
Constant motor-field current

$$N_m = \frac{E_g}{K\phi_m} - \frac{R_a T_L}{K^2 \phi_m^2}$$

R_a varies

(NOTE: R_a is total armature resistance including that of generator, motor, and control rheostat)

- (b) Flux controlled (Fig. 22)
Constant generator field current

$$N_m = \frac{E_g}{K\phi_m} - \frac{R_a T_L}{K^2 \phi_m^2}$$

ϕ_m varies

- (c) Flux controlled (Fig. 24)

$$N_m = \frac{N_g K_g \phi_g}{K_m \phi_m} - \frac{MT_L}{(K_m \phi_m)^2}$$

ϕ_g and ϕ_m vary

(NOTE: K_g , generated voltage per unit generator-field flux
 K_m , back emf per unit motor-field flux at a given motor speed)

* The hydraulic cases (a), (b), and (c) are analogous to the electrical cases (a), (b), and (c), respectively.

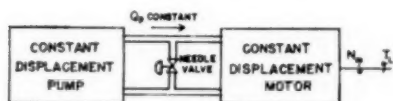


FIG. 19 LEAKAGE-CONTROLLED HYDRAULIC DRIVE
(Compare with Fig. 20.)

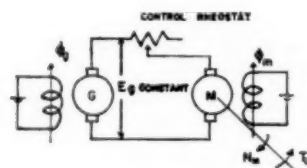


FIG. 20 ARMATURE-RESISTANCE-CONTROLLED ELECTRIC DRIVE
(Compare with Fig. 19.)

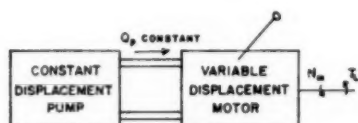


FIG. 21 DISPLACEMENT-CONTROLLED HYDRAULIC DRIVE
(Compare with Fig. 22.)

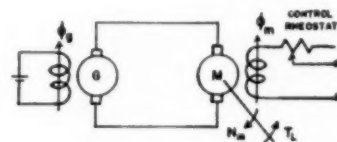


FIG. 22 FLUX-CONTROLLED ELECTRIC DRIVE
(Compare with Fig. 21.)

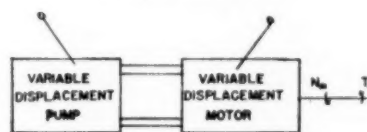


FIG. 23 DISPLACEMENT-CONTROLLED HYDRAULIC DRIVE
(Compare with Fig. 24.)

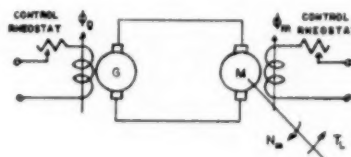


FIG. 24 FLUX-CONTROLLED ELECTRIC DRIVE
(Compare with Fig. 23.)

ACKNOWLEDGMENT

The authors wish to express their sincere thanks to Profs. Gordon S. Brown and John A. Hrones, both of the Massachusetts Institute of Technology, not only for their valuable comments and discussions but also for the opportunities of providing this material to both graduate courses of "Servomechanisms" in the Electrical Engineering Department and of "Control Problems in Mechanical Engineering" in the Mechanical Engineering Department. They also wish to express their deep appreciation for the helpful suggestions and discussions given by Mr. Paul E. Smith.

REFERENCES

- 1 "Solution of the General Voltage Regulator Problem by Electrical Analogy," by E. L. Harder, *Trans. AIEE*, vol. 66, 1947, pp. 815-825.

- 2 "Electrical Analogy Methods Applied to Servomechanisms Problems," by S. W. Herwald and G. D. McCann, *Trans. AIEE*, vol. 65, February, 1946, pp. 91-96.
- 3 "Analog Computers for Servo Problems," by D. McDonald, *Review of Scientific Instruments*, vol. 21, 1950, pp. 154-157.
- 4 "The Dynamic Characteristics of a D-C Motor With Quadrature Axis Compensation to Reduce Armature Inductance," by J. O. McDonough, SM thesis, Department of Electrical Engineering, Massachusetts Institute of Technology, 1947.
- 5 "Hydraulic Variable-Speed Transmissions as Servomotors," by G. C. Newton, Jr., *Journal of The Franklin Institute*, vol. 243, 1947, pp. 439-470.
- 6 "Laplace Transformation," by W. T. Thomson, Prentice-Hall, Inc., New York, N. Y., 1950, chapter 9.
- 7 "Designing Pneumatic and Electric Servos," by H. Ziebolz, *Machine Design*, vol. 19, September, 1947, pp. 132-138.
- 8 "Hydraulic Remote Position Controllers," by J. E. M. Coombes, *Journal of the Institute of Electrical Engineers*, vol. 94, part 2A, November 2, 1947, pp. 270-282.



Laminar-Flow Forced Convection in Rectangular Tubes

BY S. H. CLARK¹ AND W. M. KAYS,² STANFORD, CALIF.

The problem of laminar-flow heat transfer in tubes of rectangular and triangular cross section is considered. A numerical relaxation method is used to obtain minimum limiting Nusselt-number magnitudes to supplement the presently available data. Boundary conditions of both constant heat input per unit of length, and constant wall temperature are included. For the case of rectangular tubes sufficient points have been calculated so that interpolation of the limiting Nusselt numbers for any aspect ratio can be accomplished. Experimental data are presented for a square tube for both constant wall temperature and constant heat input, and for a rectangular tube, aspect ratio 2.62, for constant wall temperature. These data, together with the limiting Nusselt-number theory, provide a rational basis for estimation of entrance-length effects for rectangular tubes, and result in a correlation in the form, $N_{Nu} = \phi[N_R N_{Pr}/(l/4r_h)]$, applicable to the design of gas-flow heat exchangers.

NOMENCLATURE

The following nomenclature is used in the paper:

English Letter Symbols:

- A = total duct heat-transfer area, ft²
- A_c = duct free-flow area, ft²
- a = length of short side of rectangular-duct cross section, ft
- b = length of long side of rectangular-duct cross section, ft
- C = entrance length constant, defined by Equation [23]
- c = specific heat, Btu/lb deg F
- d = differential notation
- h = unit heat-transfer conductance averaged with respect to peripheral area (Btu/hr ft² deg F)
- h_{local} = unit heat-transfer conductance at point on periphery (Btu/hr ft² deg F)
- k = thermal conductivity of fluid $\left(\text{Btu/hr ft}^2 \frac{\text{deg F}}{\text{ft}} \right)$
- l = length of duct, or tube, ft
- P = pressure, #/ft²
- q = heat-transfer rate, Btu/hr
- r_h = tube hydraulic radius, A_c/A , ft
- t = temperature, deg F
- u = velocity of fluid in the x -direction, fps
- x = dimensional co-ordinate in direction of flow
- y, z = dimensional co-ordinates forming with x an orthogonal system, and in plane perpendicular to direction of flow

Greek Letter Symbols

- Δ = prefix denoting difference
- μ = viscosity of fluid, lb/hr ft
- ρ = density, lb/ft³
- α = thermal diffusivity ($k/\rho c$), ft²/hr
- ϕ = functional relation

Dimensionless Groupings

- N_{Nu} = Nusselt number ($4r_h h/k$), a heat-transfer modulus
- N_{Pr} = Prandtl number ($\mu c/k$), a fluid-properties modulus
- N_R = Reynolds number ($4r_h u \rho/\mu$), a flow modulus
- u^* = dimensionless velocity parameter (see Equation [11])
- t^* = dimensionless temperature parameter (see Equation [13])
- t' = dimensionless temperature parameter (see Equation [21])
- α^* = aspect ratio of rectangle, (b/a)

INTRODUCTION

Technical interest in laminar-flow forced convection in ducts of various cross sections has increased recently as a result of the trend for many gas-flow applications, toward the use of more compact heat-transfer surfaces. These surfaces, because of the high ratio of heat-transfer (and friction) area to core volume, have flow passages of small dimensions, and the Reynolds-number design range may well extend into the laminar-flow region.

Test results for 34 different compact surfaces have been presented in (1).² The data for tubular-type surfaces, such as formed by continuous fins in a plate-fin arrangement, in the *laminar-flow region* indicate that the heat-transfer conductance is strongly dependent upon flow-passage geometry, and no simple method of approximate correlation is possible, such as in the case for turbulent flow. However, laminar flow does lend itself to straightforward analytical solution, at least for certain idealized cases, and any analytical solutions are useful in reducing the test work required to complete the laminar-flow picture. Two solutions which are useful for this purpose, from the work of Graetz (2), Leveque (3), and Nusselt (4), are summarized by Norris and Streid (5). Both solutions are for *constant wall temperature*, one for circular tubes, the other for flow between infinite parallel planes (hereinafter called the "gap"). The major idealizations are constant properties and a fully developed velocity profile, but thermal boundary-layer entrance-length effects are taken into consideration.

Glaser (6) has presented additional solutions for circular tubes, gap, and square, based upon another boundary condition, *constant heat input per unit of length*, with idealizations of constant properties, and both fully developed velocity and temperature profiles. The circular tube and gap solutions also were worked out by Norris and Streid (5). The circular tube and gap have thus been analyzed fairly completely, but for the other cross-section geometries this is not the case. While a laminar-flow analysis of all possible variations of cross-section geometry encountered in plain plate-fin heat exchangers would be impractical, it is possible to approximate many by a rectangular cross section. The solutions of Glaser, described in the foregoing, represent a start

¹ Research Assistant and Graduate Student in Mechanical Engineering, Stanford University.

² Assistant Professor of Mechanical Engineering, Stanford University. Jun. ASME.

Contributed by the Heat Transfer Division of THE AMERICAN SOCIETY OF MECHANICAL ENGINEERS and presented at the Heat Transfer and Fluid Mechanics Institute, Los Angeles, Calif., June 19, 1952. (Since its presentation, this paper has been amplified in some parts.)

NOTE: Statements and opinions advanced in papers are to be understood as individual expressions of their authors and not those of the Society. Manuscript received at ASME Headquarters, November 28, 1952.

² Numbers in parentheses refer to the Bibliography at the end of the paper.

in this direction, and indicate that the Nusselt number can vary as much as 100 per cent from the square to the gap, with an apparent 10 to 20 per cent difference in Nusselt number between the constant wall temperature and constant heat-input boundary conditions.

The constant-wall-temperature solutions for the circular tube and the gap (5) indicate that in laminar flow the mean Nusselt number is a strong function of tube length. However, as tube length is increased, or Reynolds number is decreased, Nusselt number decreases and approaches a minimum, corresponding to a fully established temperature profile. The same also must be true for constant heat input, although the authors are aware of no published solutions for this boundary condition which include entrance-length effects. Examination of the complexities of the Graetz solution for such a simple geometry as the circular tube (and this solution includes only the effects of thermal entrance length, not the hydrodynamic entrance length) indicates that to obtain complete solutions for rectangles or triangles where another co-ordinate must be included, would be a very difficult, if not impracticable task. However, the "minimum" Nusselt number for any geometry, and for both constant heat input and constant wall temperature, may be obtained quite readily upon the assumption of fully established velocity and temperature profiles. Such analytically determined minimum Nusselt numbers can then form a firm base upon which complete empirical solutions, including the effects of entrance length, temperature-dependent fluid properties, natural convection, and so on, can be built with the aid of a relatively few experiments.

Because of the current need for a more adequate design basis for compact plate-fin heat exchangers in the laminar-flow region, it thus appears worth while to obtain solutions in the manner indicated for flow in rectangular passages of any aspect ratio, to obtain at least one solution for a triangular cross section, and to perform sufficient tests to support the validity of these solutions. To this end the objectives of this paper are as follows:

- 1 To present laminar-flow limiting Nusselt-number solutions for rectangular cross sections of any aspect ratio for both constant heat input per unit of length and constant wall temperature.
- 2 To present the laminar-flow limiting Nusselt-number solution for the equilateral triangle with constant heat input per unit of length.
- 3 To report on the currently available limited experimental verification of these solutions.
- 4 To present a tentative empirical correlation, based partly on analysis and partly on experiment, for the laminar-flow Nusselt number in rectangular tubes of any aspect ratio, including the effects of entrance length.

IDEALIZATIONS FOR MINIMUM NUSSULT-NUMBER ANALYSES

To obtain solutions yielding the minimum limiting Nusselt number, the idealizations are: (a) Velocity and temperature profiles are fully developed; (b) the fluid properties (ρ , c , μ , k) are constant; (c) heat conduction in the direction of flow is negligible; (d) conversion of mechanical to thermal energy due to friction is negligible relative to the heat transfer; (e) natural convection effects are negligible.

Idealizations (c), (d), and (e) are believed to introduce negligible error for the compact heat-exchanger applications under consideration. The effect of idealization (b) is the subject of a separate investigation, although some material is now available (7). Idealization (a) is perhaps not properly an idealization in that it provides the major basis for the existence of a minimum limiting Nusselt number.

The minimum Nusselt numbers for constant heat input were obtained directly for the gap and circular tube by Glaser (6). His procedure required all of the foregoing idealizations except that (a) was stated in a different form with respect to the temperature profile. Glaser specified the physically intuitive fact that $\partial t/\partial x$ is constant with respect to both flow length and cross-section position, which is fully equivalent to the specification of a fully developed temperature profile. Jakob and Rees (12) employed the same specification. Applicable to any boundary condition for fully developed temperature profile is a convenient generalized temperature distribution introduced by Seban (8), who analyzed fully developed turbulent flow in a pipe with constant wall temperature. This generalized temperature distribution, invariant in the direction of flow, is expressed in the form

$$\frac{\partial}{\partial x} \left[\frac{t_w - t}{t_w - t_m} \right] = 0 \dots \dots \dots [1]$$

It will be demonstrated that for constant heat input, Equation [1] is consistent with the constancy of $\partial t/\partial x$, while for constant wall temperature a different but useful relation is obtained for $\partial t/\partial x$, both relations being applicable to laminar as well as turbulent flow.

By carrying through the indicated differentiation of Equation [1], noting that t_w and t_m are functions of x only, the following is obtained

$$\frac{dt_w}{dx} - \frac{\partial t}{\partial x} - \frac{(t_w - t)}{(t_w - t_m)} \left(\frac{dt_w}{dx} - \frac{dt_m}{dx} \right) = 0 \dots \dots \dots [2]$$

This equation may be rearranged to

$$\frac{1}{(t_w - t_m)} \left[\frac{dt_w}{dx} - \frac{dt_m}{dx} \right] = \frac{1}{(t_w - t)} \frac{dt_w}{dx} - \frac{1}{(t_w - t)} \frac{\partial t}{\partial x} \dots [3]$$

The left-hand side of the equation is a function of x alone, whereas the two terms on the right are functions of both x and cross-section position. Since for the case of constant heat input neither of these terms is equal to zero, $\partial t/\partial x$ must equal dt_w/dx in order to cancel the dependence upon cross-section position. Thus the left side becomes equal to zero, and it can be shown directly by an energy balance that dt_m/dx is a constant. It then follows, for this boundary condition, that

$$\frac{\partial t}{\partial x} = \frac{dt_w}{dx} = \frac{dt_m}{dx} = \text{const} \dots \dots \dots [4]$$

In contrast, for the constant wall-temperature boundary condition $dt_w/dx = 0$, and Equation [2] reduces directly to

$$\frac{\partial t}{\partial x} = \frac{(t_w - t)}{(t_w - t_m)} \frac{dt_m}{dx} \dots \dots \dots [5]$$

Note that for this boundary condition dt_m/dx does vary with x , unlike the constant heat-input boundary condition.

DIFFERENTIAL EQUATIONS AND SOLUTIONS

From a consideration of the pressure and viscous forces on an element $dx \, dy \, dz$ in the direction of flow, one may deduce the hydrodynamic differential equation, consistent with the foregoing idealizations, as

$$\frac{\partial^2 u}{dy^2} + \frac{\partial^2 u}{\partial z^2} = - \frac{1}{\mu} \frac{dP}{dx} \dots \dots \dots [6]$$

Here P is assumed to be constant over the cross section and dP/dx is constant in the direction of flow for fully developed conditions.

The thermal differential equation, derived by equating an energy-balance and rate equation on the same element is

$$\frac{\partial^2 t}{\partial y^2} + \frac{\partial^2 t}{\partial z^2} = \frac{u}{\alpha} \frac{\partial t}{\partial x} \quad [7]$$

For the constant heat-input case, $\partial t/\partial x$ is constant from Equation [4], and Equation [7] becomes

$$\frac{\partial^2 t}{\partial y^2} + \frac{\partial^2 t}{\partial z^2} = \frac{u}{\alpha} \frac{\partial t}{\partial x} = \phi(u) \quad [8]$$

For the constant wall-temperature case, substituting for $\partial t/\partial x$ from Equation [5]

$$\frac{\partial^2 t}{\partial y^2} + \frac{\partial^2 t}{\partial z^2} = \frac{u}{\alpha} \frac{t_w - t}{t_w - t_m} \frac{dt_m}{dx} = \phi(u, t) \quad [9]$$

Constant Heat Input. A general solution of Equation [6] is available in the form of an infinite series, determined for the analogous differential equations for torsion in a rectangular shaft (9). Since there is no known general solution to Equations [8] and [9], a finite-difference approach, as employed by Glaser, using the relaxation technique, was adopted for these as well as Equation [6]. Then the analytical solution for Equation [6] was used to determine the accuracy of the approximate results for the velocity distribution, and to give some indication of the accuracy which may be expected from the relaxation solutions of Equations [8] and [9].

In finite-difference form, Equation [6] becomes

$$\frac{u_{m-1,n} + u_{m+1,n} - 2u_{m,n}}{(\Delta y)^2} + \frac{u_{m,n-1} + u_{m,n+1} - 2u_{m,n}}{(\Delta z)^2} = -\frac{1}{\mu} \frac{dP}{dx} \quad [10]$$

For every aspect ratio α^* considered, the net was selected so that $\Delta y = \Delta z = a/10$, where a is the length of the short side. Substituting for $(\Delta y)^2$ and $(\Delta z)^2$ and introducing a dimensionless velocity function

$$u^* = \frac{u}{a^2 dP/dx} \quad [11]$$

Equation [10] becomes

$$u_{m-1,n}^* + u_{m+1,n}^* + u_{m,n-1}^* + u_{m,n+1}^* - 4u_{m,n}^* + 0.01 = 0 \quad [12]$$

With the same net and a dimensionless temperature function defined by

$$t^* = \frac{t}{a^2 dP/dx} \quad [13]$$

Equation [8] may be written in similar form for the other working equation which must be satisfied at every interior point of the net, as follows

$$t_{m-1,n}^* + t_{m+1,n}^* + t_{m,n-1}^* + t_{m,n+1}^* - 4t_{m,n}^* + 0.01u^* = 0 \quad [14]$$

Fig. 1 shows the relaxed net for $\alpha^* = 2$ (only one quarter of the cross section is considered due to symmetry) with final values of $t^* \times 10^5$ and the remainders, in parentheses. This net is presented here to illustrate the convergence of the procedure which can be realized, in this application at least, with approximately five relaxation steps.

For the case of the square, $\alpha^* = 1$, the temperature distribution is described in Fig. 2 for later comparison with the result for constant wall temperature.

In extracting the Nusselt number, it is necessary to determine the mean velocity and mixed mean temperature (the "cup" mixing temperature is used), defined in dimensionless form by

$$u_m^* = \frac{1}{A_c} \int \int_{A_c} u^* dy dz \quad [15]$$

$$t_m^* = \frac{1}{u_m^* A_c} \int \int_{A_c} t^* u^* dy dz \quad [16]$$

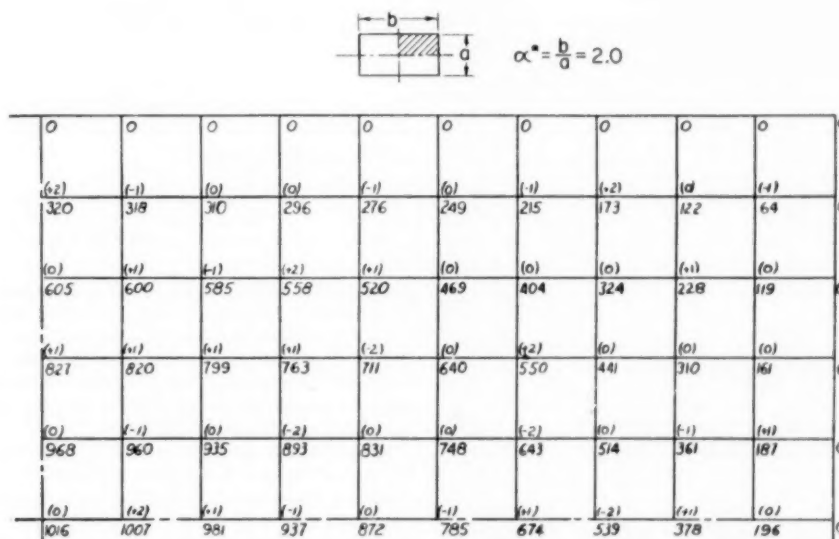


FIG. 1 RELAXATION NET EMPLOYED FOR DETERMINING TEMPERATURE DISTRIBUTION FOR $\alpha^* = 2$, CONSTANT HEAT INPUT PER UNIT OF LENGTH

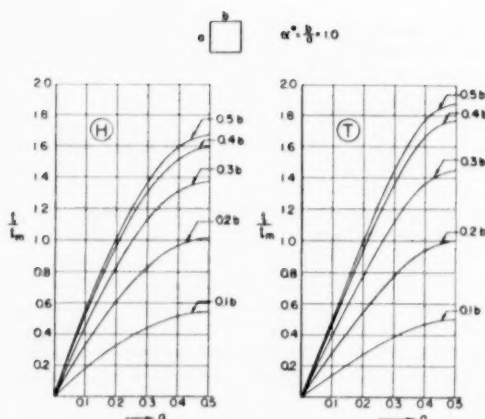


FIG. 2 TEMPERATURE PROFILES IN A SQUARE TUBE, $\alpha^* = 1$, BOTH CONSTANT HEAT INPUT AND CONSTANT WALL TEMPERATURE

The integrals were evaluated by means of a two-dimensional extension of Simpson's rule, employing the t^* and u^* results obtained in the foregoing by relaxation.

The rate equation applying to the wall area associated with a differential flow length dx , defining the mean wall-to-fluid conductance at a cross section, is

$$dq = h \Delta t_m dA = h(t_w - t_m) dA \quad [17]$$

An energy balance on a tube section of length dx yields

$$dq = \rho u_m A c \frac{\partial t}{\partial x} dx \quad [18]$$

Therefore the Nusselt number is

$$Nu_H = \frac{h(4r_h)}{k} = \frac{(4r_h)^2}{4a^2} \frac{u_m^*}{\Delta t_m^*} \quad [19]$$

Another method of evaluating the Nusselt number, which has been employed, is to evaluate the local heat-transfer conductance around the wall periphery from the temperature gradients at the wall

$$h_{\text{local}} = -\frac{k}{\Delta t_m} \left(\frac{\partial t}{\partial y} \right)_{\text{wall}}$$

Thus the temperature derivatives at the wall conveniently provide the local heat-transfer coefficient for every point on the cross-section periphery, and these may be averaged over the periphery to get the mean h entering into the Nusselt number. However, this method introduces greater error in determining Nusselt number than the procedure adopted here.

The solutions for aspect ratios of 1.0, 1.4, 2.0, 3.0, and 4.0 have been obtained. These results are presented in Table 1, and Fig. 3 shows the resulting curve of Nu_H versus $1/\alpha^*$ based upon these results.

A beginning on triangular passages also has been made, using the foregoing method, except that a triangular net is used in place of the square net for the relaxation solutions. On this basis $Nu_H = 3.00$ for the equilateral triangle.

Constant Wall Temperature. For constant properties the fully developed velocity distribution will not be influenced by the thermal boundary condition, and the solution of Equation [6] discussed in the last section will therefore also apply to the constant-wall-temperature case.

TABLE 1 LAMINAR-FLOW MINIMUM LIMITING NUSSLETT NUMBERS

	Nu_H	Nu_T
Circular tubes	4.364 (5) ^a	3.658 (5)
Equilateral triangles	3.00	
Rectangles:		
$\alpha^* = 1.00$ (square)	3.63	2.89
1.40	3.78	
2.00	4.11	3.39
3.00	4.77	
4.00	5.35	
∞ (gap)	8.235	7.60 (5)

^a Numbers in parentheses refer to the Bibliography.

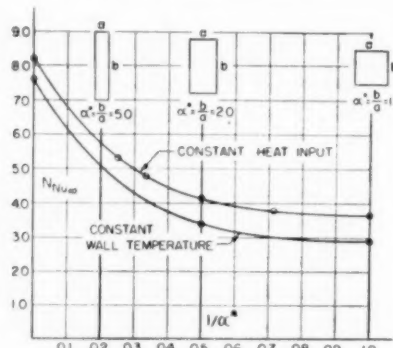


FIG. 3 MINIMUM LIMITING NUSSLETT NUMBERS FOR RECTANGULAR TUBES FOR CONSTANT HEAT INPUT AND CONSTANT WALL TEMPERATURE

Equation [9], the thermal differential equation, may be written in the finite difference form which follows, using the same net, and introducing on the right side the factor $(t_w - t)/(t_w - t_0)$

$$t_{m-1,n} + t_{m+1,n} + t_{m,n-1} + t_{m,n+1} - 4t_{m,n} = 0.01 \left[\frac{a^4}{\alpha \mu} \frac{dP}{dx} \frac{dt_m}{dx} \left(\frac{t_w - t_0}{t_w - t_m} \right) \right] u^* \left(\frac{t_w - t}{t_w - t_0} \right) \quad [20]$$

Note that the only factors on the right-hand side of Equation [20] which vary over the cross section are u^* and $(t_w - t)/(t_w - t_0)$. A dimensionless temperature t' is introduced for convenience in handling the equation

$$t' = -\frac{t}{a^4 \frac{dP}{dx} \frac{dt_m}{dx} \left(\frac{t_w - t_0}{t_w - t_m} \right)} \quad [21]$$

and Equation [20] becomes

$$t'_{m-1,n} + t'_{m+1,n} + t'_{m,n-1} + t'_{m,n+1} - 4t'_{m,n} + 0.01 u^* \left(\frac{t_w - t}{t_w - t_0} \right) = 0 \quad [22]$$

Equation [22] is in a form which may be handled by the relaxation technique. The temperature distribution for the previously obtained constant-heat-input solution was used as the first approximation, and two or three steps from this start resulted in adequate convergence. The resulting temperature distribution for the square is given in Fig. 2 for contrast with the constant-heat-input result obtained previously.

Equations [17] and [18] are independent of the boundary conditions and may be used again for this case to determine Nusselt number. This yields, in a manner similar to Equation [19], for constant wall temperature

$$Nu_T = \frac{(4r_h)^2}{4a^2} \frac{u_m^*}{\Delta t'_0} \quad [23]$$

Equations [19] and [23] differ only in the terms Δt_m^* and $\Delta t_0'$. By substituting for Δt_m^* from Equation [13] and for $\Delta t_0'$ from Equation [21], it can be shown that both Nusselt numbers vary inversely as $(t_w - t_m)$.

Evaluation of the constant-wall-temperature Nusselt number in this manner has been obtained for the square ($\alpha^* = 1$), and for a rectangular cross section ($\alpha = 2$). In addition, Nu_T for the gap is available from the Graetz solution. The difference between Nu_H and Nu_T for $\alpha^* = 1, 2$, and ∞ is constant within 15 per cent, and a graph of $(Nu_H - Nu_T)$ versus $1/\alpha^*$ provides a reasonably accurate interpolation for Nu_T for any aspect ratio. The curve of Nu_T versus $1/\alpha^*$, Fig. 3, is based upon this procedure.

Accuracy of Solutions. Comparison of the velocity distribution (on a spot-check basis) and the mean velocity from the solutions described in the foregoing with those from the infinite-series form of solutions, worked out to an accuracy of four significant figures, indicates no more than 0.5 per cent deviation from the latter in every case. There is no direct check on the results for temperature distribution and mean temperature but, on the basis of the results given, it is estimated that both are accurate to within 1 per cent. Since magnitudes of mean velocity from the infinite-series solution were used in the evaluation of Nusselt number, it depends upon the accuracy of the mean temperatures only, and hence the computed values of Nusselt number are believed to be within 1 per cent of the correct values. The method of determining the Nusselt number for any aspect ratio, on which the curves in Fig. 3 are based, certainly yields results equally as accurate.

The question of the applicability of the generalized temperature assumed by Seban (8) and used here in the constant-wall-temperature solution for the square has been considered, and was tested by using it in the determination of the lower limiting Nusselt number for the gap with constant wall temperature for which the Graetz-series solution already exists. $Nu_T = 7.60$ was evaluated, which is the same as the asymptotic value of the Graetz solution.

EXPERIMENTAL INVESTIGATION AND CORRELATIONS

An experimental investigation with air at low velocities and low heat flux was initiated in conjunction with the foregoing laminar-flow analysis with two primary objectives: (a) To verify the analysis for the minimum limiting Nusselt number for certain representative cases; and (b) to determine the influence of thermal and hydrodynamic starting length on the mean Nusselt number, for which no complete theory for rectangular tubes has been developed.

For this investigation two aspect ratios were tested; one was the square, $\alpha^* = 1.00$, tested with both constant wall temperature and constant heat input, the other a rectangle, $\alpha^* = 2.62$, tested with constant wall temperature only. Norris (5) already has indicated fairly good experimental confirmation for the constant-wall-temperature-gap ($\alpha^* = \infty$) solution.

All tests were performed in a test air duct described in (10), employing in large part the instrumentation, methods, and procedures of that reference. Both test cores were of multiple-tube construction and are shown in Figs. 4 and 5. The square tube core, Fig. 4, was built as a counterflow water-to-air heat exchanger so that either constant heat input or constant wall temperature could be approximated by varying the hot-water flow rate. Wall temperatures were measured directly by a number of thermocouples embedded in the tube walls. The rectangular tube core, Fig. 5, was built into a crossflow heat exchanger, and condensing steam provided the essentially constant wall temperature. An insulated flow mixer and converger, followed by a single shielded thermocouple, was used to determine air-outlet temperature for the square tube core. The air-outlet temperature for the rectangular tube core was established by a 27-point thermocouple traverse.

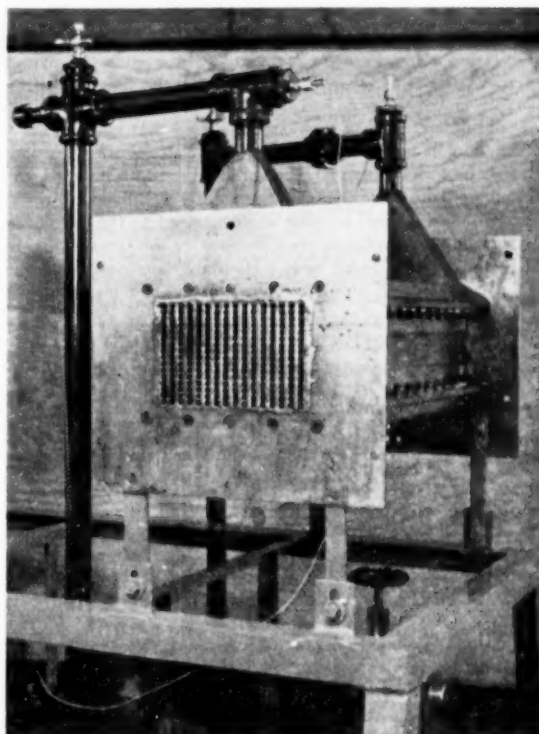


FIG. 4 SQUARE TUBE WATER-TO-AIR TEST CORE

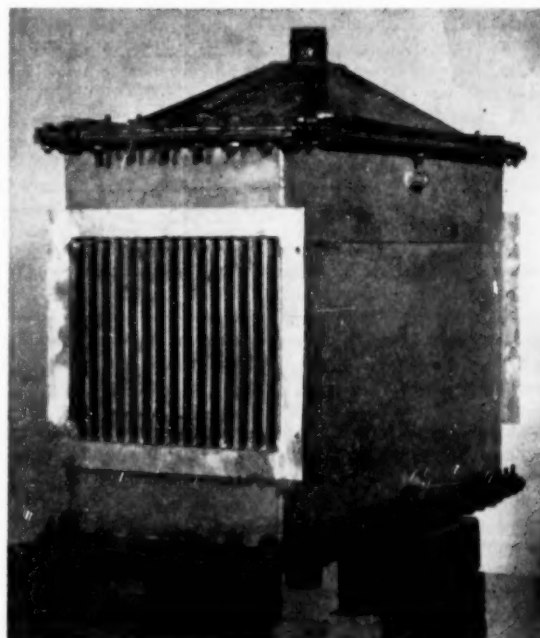


FIG. 5 STEAM-TO-AIR TEST CORE, $\alpha^* = 2.62$

Both test cores had abrupt contraction entrances. For the square tube core the ratio of tube length to hydraulic diameter ($l/4r_h$) was 100. For the rectangular tube core the over-all $l/4r_h$ was 110. However, the fins forming the flow passages of this core were made from two separate sheets so that the fins were not continuous. It has thus been assumed that $l/4r_h = 55$, although it will be shown later that the "effective" $l/4r_h$ could possibly be greater than 55, though less than 110, because while the fins were discontinuous they were fairly well lined up.

For all tests Nusselt number was evaluated on the basis of the logarithmic-mean temperature difference for the two reasons that this definition is the one most commonly employed for design, and a mean Nusselt number defined in this manner approaches

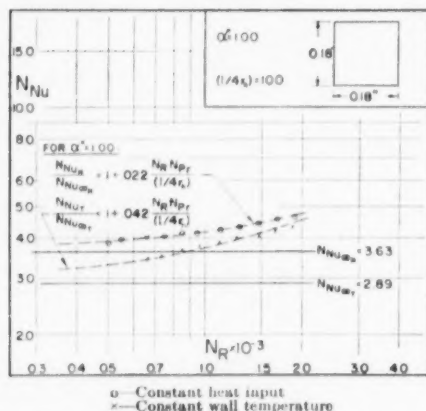


FIG. 6 TEST RESULTS, NUSSLETT NUMBER VERSUS REYNOLDS NUMBER, SQUARE TUBE CORE, $\alpha^* = 1.00$

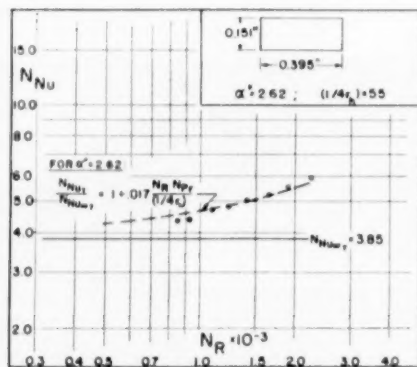


FIG. 7 TEST RESULTS, NUSSLETT NUMBER VERSUS REYNOLDS NUMBER, RECTANGULAR TUBE CORE, $\alpha^* = 2.62$, CONSTANT WALL TEMPERATURE

the local Nusselt number, i.e., the minimum limiting Nusselt number as tube length is increased or Reynolds number is decreased.

While only laminar-flow test data will be considered here, it should be added that laminar, transition, and turbulent-flow data were obtained in these tests. For both cores a very decided transition from laminar to turbulent flow took place starting at about $N_R = 2500$, so there is no uncertainty as to whether true laminar flow was obtained.

The basic test results are plotted in Figs. 6 and 7. Fig. 6 shows Nusselt number plotted as a function of Reynolds number for the

square tube core for both constant heat input (circles) and constant wall temperature (crosses). Fig. 7 is a similar plot for the rectangular tube core, $\alpha^* = 2.62$, for constant wall temperature only. Superimposed for all three series of tests are the applicable minimum limiting Nusselt numbers evaluated in the foregoing.

Verification of Limiting Nusselt-Number Analysis. From Fig. 6 it is quite apparent that the difference between constant wall temperature and constant heat input is real, and the maximum difference occurs in the limit ($N_R \rightarrow 0$). For all three tests Nusselt number decreases with Reynolds number, apparently approaching the minimum limiting Nusselt numbers, which trend is consistent with the Graetz solution for the circular tube.

For all of these data, with the exception of the two lowest Reynolds-number test points for $\alpha^* = 2.62$, the experimental uncertainty is estimated as approximately ± 5 per cent. For these two points the uncertainty may be as much as 10 per cent with the probability that the points lie low. This is due to the fact that in these cases the heat exchanger was operating at an effectiveness greater than 95 per cent, i.e., a 5 per cent approach of the exit air to the wall temperature, and the magnitude of conductance evaluated becomes sensitive to small air-outlet temperature-measurement errors.

The fact that the test points clearly approach the minimum Nusselt numbers in the limit can best be demonstrated by another type of plot, which also serves to indicate a simple empirical method of representing entrance-length effects. The more complete solutions for the circular and gap cross sections (5) indicate that the results can be represented in the form

$$N_{Nu} = \phi \left[\frac{N_R N_{Pr}}{(l/4r_h)} \right]$$

The nondimensional group on the right-hand side is the Graetz number ($16r_h^2 G c / kl$) but it is desired here to maintain the Reynolds number, Prandtl number, and tube-length ratio as separate parameters. It is when Reynolds number becomes very small, or $l/4r_h$ becomes very large, that Graetz number becomes small and Nusselt number then approaches its minimum limit. It is thus apparent that a plot of $N_{Nu}/N_{Nu_{\infty}}$ as a function of Graetz number must yield a curve that starts at the origin of the co-ordinates shown in Fig. 8.

The experimental results for the three tests are plotted in Fig. 8, employing for $N_{Nu_{\infty}}$ the data in Fig. 3. The trend of the data toward the analytically evaluated minimum Nusselt numbers is quite apparent, especially for the case of the square with constant heat input where it was possible to get to Reynolds

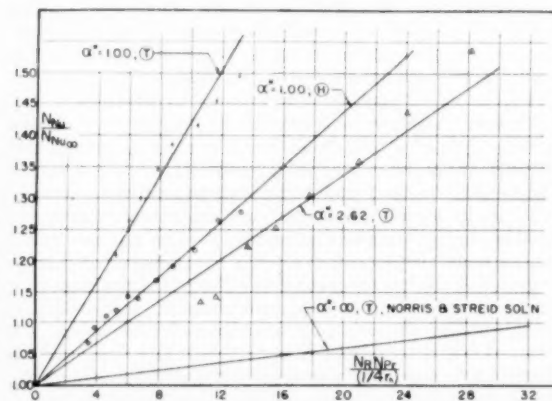


FIG. 8 RATIO OF NUSSLETT NUMBER TO MINIMUM LIMITING NUSSLETT NUMBER VERSUS $N_R N_{Pr} / (l/4r_h)$

numbers as low as 500. The results for the $\alpha^* = 2.62$ rectangle are the least convincing in this respect, but experimental uncertainty in these data due to the effect of temperature-measurement errors has been mentioned previously for the two lowest Reynolds-number test points. There also is uncertainty as to the effective $l/4r_h$ for this surface, but this will affect only the relative position of the test points, not their tendency to converge on the origin.

Correlation of Entrance-Length Effects. If the analytical solutions for the circle and gap, as presented by Norris and Streid (5), are plotted in the form of Fig. 8, it will be found that for $N_R N_{Pr} / (l/4r_h)$ less than about 60 a straight-line representation in all cases will be within 2 per cent of the given relation. Such a straight-line representation for the gap is shown in Fig. 8. The range 0–60 actually is the only portion of real interest in the design of heat exchangers using gases, for with an upper limit on the Reynolds number for laminar flow of about 2000 and with a Prandtl number of about 0.7, any $l/4r_h$ greater than 23 falls within this range. This does not apply, of course, for high Prandtl-number fluids.

In Fig. 8 straight lines have been drawn through the data points for the three series of tests. The square-tube data lie remarkably close to a straight line, and even for $\alpha^* = 2.62$ the maximum departure is only 5 per cent, and this for two test points that are somewhat suspect in terms of experimental accuracy. Close correspondence is more evident when these lines are replotted in Figs. 6 and 7 as dashed lines.

The straight-line relationship allows a simple algebraic representation of the laminar-flow characteristics of a tube

$$\frac{N_{Nu}}{N_{Nu\infty}} = 1 + C \frac{N_R N_{Pr}}{(l/4r_h)} \quad [24]$$

The constant C is the slope of the line in Fig. 8 and varies with cross-section geometry. The limited data, which at present are available on these constants for laminar flow in rectangular tubes, are plotted in Fig. 9 from the curves in Fig. 8. The dashed lines

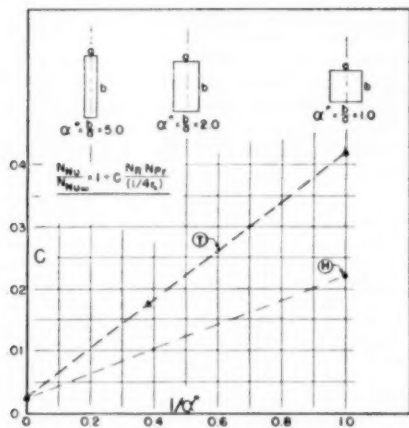


FIG. 9 SUGGESTED APPROXIMATE CORRELATION OF ENTRANCE-LENGTH EFFECTS

represent merely a tentative suggestion as to the over-all relationship. However, other considerations indicate that Fig. 9, in conjunction with Fig. 3, may be quite adequate for practical gas-flow heat-exchanger design work. Both the constant wall-temperature and constant-heat-input lines have been anchored at $1/\alpha^* = 0$ by the completely analytical constant-wall-temperature gap solution, which is inaccurate in two respects, but which, on the other hand, cannot introduce much error because the magnitude

of C is relatively so small at this end of the scale. The constant-heat-input curve should lie below the constant-wall-temperature curve. This is evident not only from the square-tube behavior, but also from some as yet unpublished circular-tube data. However, the constant C from the gap solution was obtained on the assumption of fully established parabolic velocity distribution. In the practical heat-exchanger case, where the development of the velocity profile as well as the temperature profile must be considered, and also where there is generally an abrupt contraction entrance, the entrance-length effects, and thus C , will tend to be greater. A re-examination of laminar-flow circular-tube data, presented in reference (13), indicates an excellent straight-line plot in Fig. 8, but with C about 50 per cent greater than a similar examination of the Graetz solution yields. Thus the point indicated in Fig. 9 at $1/\alpha^* = 0$ may be a little low for the constant-wall-temperature case, but is close to correct for constant heat input.

Another not completely resolved question regarding the data in Fig. 9 is the $\alpha^* = 2.62$ point ($1/\alpha^* = 0.382$), because of the aforementioned uncertainty in the effective $l/4r_h$. However, a major reason for having confidence in this datum point is that this C corresponds closely to that as determined experimentally (13) for circular tubes ($C = 0.017$ for $\alpha^* = 2.62$, $C = 0.020$ for circle). Now from the theory it is seen that the limiting Nusselt number for both this rectangular tube and the circular tube also corresponds closely ($N_{Nu} = 3.85$ for $\alpha^* = 2.62$, $N_{Nu} = 3.66$ for circular tube). This is consistent with the following reasoning: The entrance-length effects vary with different geometries because near the tube entrance the Nusselt number should become independent of geometry; thus geometries with low minimum Nusselt numbers should show larger entrance-length effects, and vice versa. This conclusion is supported by the results shown in Figs. 3 and 9. Since the circular tube C corresponds closely to the rectangular tube C , in line with this reasoning it is concluded that the $\alpha^* = 2.62$ magnitude of C in Fig. 9 is approximately correct, and that the effective $l/4r_h$ is close to 55 as used.

An additional note of caution is necessary in regard to the use of Fig. 9. While Fig. 3 applies to any fluid, the entrance-length effects indicated in Fig. 9 will vary with the Prandtl number of the fluid, being greater for low Prandtl-number fluids and less for high Prandtl-number fluids. Therefore Fig. 9 is considered to be applicable only to the Prandtl-number range of gases. It is possible that an exponent less than unity applied to the Prandtl number in Equation [23] would correlate data over a wider range of Prandtl numbers, but insufficient data are available at the present time to investigate this question further.

SUMMARY AND CONCLUSIONS

The results and conclusions of the foregoing analytical and experimental investigation may be summarized as follows:

- 1 The relaxation method of Southwell is utilized to solve the hydrodynamic and thermal differential equations for laminar flow of an incompressible fluid of constant viscosity and thermal conductivity through rectangular ducts with fully established velocity and temperature profiles. Boundary conditions of both constant heat input and constant wall temperature are considered. In addition, the equilateral-triangle duct with constant heat input is solved.

- 2 These solutions yield minimum limiting Nusselt numbers which are approached in laminar flow as tube length is increased, or as Reynolds number is decreased. The data obtained are summarized in Table 1, and in Fig. 3 the minimum Nusselt numbers for rectangular tubes are plotted as a function of aspect ratio so that an accurate interpolation is possible for any rectangular section.

- 3 Limited experimental data for air flow in a square and a

rectangular duct substantially confirm the limiting Nusselt-number analysis, and in addition provide some data on tube-entrance-length effects.

4 Until more experimental data or adequate analytical solutions are available the entrance-length effects are presented in the tentative correlation, Fig. 9, for rectangular tubes of any aspect ratio, and with both constant-heat-input and constant-wall-temperature boundary conditions.

ACKNOWLEDGMENTS

The USN Office of Naval Research, the Bureau of Ships, and the Bureau of Aeronautics are currently sponsoring a research program on compact heat-transfer surfaces at Stanford University. The authors prepared this paper as a part of this program and express their appreciation to the sponsoring organizations.

This paper was presented originally in a less complete form at the Heat Transfer and Fluid Mechanics Institute, Los Angeles, Calif., June 25-27, 1952.

BIBLIOGRAPHY

- 1 "Gas-Turbine-Plant Heat Exchangers," by W. M. Kays, A. L. London, and D. W. Johnson, ASME Research Report, April, 1951.
- 2 "Über die Wärmeleitungsfähigkeit von Flüssigkeiten," by L. Graetz, *Annalen der Physik und Chemie*, vol. 18, 1883, p. 79.
- 3 "Les Lois de la Transmission de Chaleur par Convection," by M. A. Leveque, *Annales des Mines*, vol. 13, April, 1928, p. 201.
- 4 "Der Wärmeaustausch am Berieselungskühler," by Wilhelm Nusselt, *Zeitschrift des Vereines deutscher Ingenieure*, vol. 67, 1923, p. 206.
- 5 "Laminar-Flow Heat-Transfer Coefficients for Ducts," by R. H. Norris and D. D. Streid, *Trans. ASME*, vol. 36, 1940, pp. 525-533.
- 6 "Heat Transfer and Pressure Drop in Heat Exchangers With Laminar Flow," by H. Glaser, MAP Volkenrode, Reference: MAP-VG-96-818T, March, 1947.
- 7 "Analytical Investigation of Fully Developed Laminar Flow in Tubes With Heat Transfer With Fluid Properties Variable Along the Radius," by R. G. Deissler, NACA TN 2410, July, 1951.
- 8 "Heat Transfer to a Fluid Flowing Turbulently in a Smooth Pipe With Walls at Constant Temperatures," by R. A. Seban and T. T. Shimazaki, *Trans. ASME*, vol. 73, 1951, p. 803.
- 9 "Theory of Elasticity," by S. Timoshenko and J. N. Goodier, McGraw-Hill Book Company, Inc., New York, N. Y., 1951, pp. 275, et seq.
- 10 "Heat-Transfer and Flow-Friction Characteristics of Some Compact Heat-Exchanger Surfaces, Part 1—Test System and Procedure," by W. M. Kays and A. L. London, *Trans. ASME*, vol. 72, 1950, pp. 1075-1086.
- 11 "Heat Transfer," by M. Jakob, John Wiley & Sons, Inc., New York, N. Y., vol. 1, 1949, p. 451.
- 12 "Heat Transfer to a Fluid in Laminar Flow Through an Annular Space," by M. Jakob and K. A. Rees, *Trans. American Institute of Chemical Engineers*, vol. 37, 1941, p. 619.
- 13 "Convective Heat-Transfer and Flow-Friction Behavior of Small Cylindrical Tubes—Circular and Rectangular Cross Sections," by W. M. Kays and A. L. London, *Trans. ASME*, vol. 74, 1952, pp. 1179-1189.

Effect of Stress Amplitude on Statistical Variability in Fatigue Life of 75S-T6 Aluminum Alloy¹

By G. M. SINCLAIR² AND T. J. DOLAN³

Recent studies indicate that most of the "scatter" observed in finite fatigue-life-testing of metals is an inherent characteristic of the material and does not necessarily indicate poorly adjusted machines or improper testing techniques. In the present study, groups of 17 to 57 specimens of 75S-T6 aluminum alloy were tested in rotating bending at six different stress levels. The smallest stress used was 30,000 psi and the greatest was 62,500 psi. A statistical analysis was made of fatigue-life data obtained at each of the six stresses. The distribution of the fatigue lifetimes, for each stress, was found to be approximately logarithmic-normal. The standard deviation (which is a measure of scatter in the fatigue life) was related to the stress amplitude and could be represented within the stress range investigated, by a simple exponential function. Constants of an $S-N$ relation recently proposed by W. Weibull were evaluated for a probability of failure $P = 0.50$. Results of the study are summarized in two equations and in a composite $S-N$ diagram showing lines of equal probability of failure.

INTRODUCTION

WITH the continued growth of the stock pile of experimental evidence gathered by fatigue investigators, it has become increasingly apparent that the basic problems of failure by fatigue are inherently statistical in nature. Fatigue data appear to exhibit more scatter than any other type of mechanical test data currently utilized by the design engineer. In view of this, it seems imperative that future studies in the field of fatigue be planned in such a way as to permit quantitative estimates to be made of the reliability and reproducibility of the results. In short, the adoption of statistical methods of testing and analysis appears necessary.

Recent experiments (1, 2)⁴ have demonstrated that the observed scatter is not necessarily caused by improperly adjusted testing machines or by poor testing techniques but is an inherent characteristic of the material itself. The process of failure by fatigue

involves first the nucleation of submicroscopic cracks in the metal. Subsequently, growth of these cracks continues until the effective cross-sectional area of the member is reduced to the extent that it no longer can support the applied load and sudden fracture results. The cracks appear to be nucleated in those regions which have suffered severe plastic deformation during repeated loading. Other evidence (3) indicates that the nucleation period for cracks is of relatively short duration and that the growth process is initiated very early during the fatigue test. This last point suggests that the finite fatigue life of the metal may be considerably influenced by the number of cracks which are nucleated. For example, if two specimens of the same metal are tested under identical conditions and many more cracks are nucleated in one specimen than in the other, one would expect the specimen with the larger number of cracks to have the shorter life due to the increased chance of the cracks growing together.

At the atomic and crystalline levels of association where fatigue damage is initiated, all metals are heterogeneous. The fatigue resistance of one small elemental volume will differ from the resistance of another owing to the presence of such factors as inclusions, differences in grain size, orientation, spacing of hardening particles, microresidual stresses, and so on. Thus any real metal may be considered to have a large number of weak points of varying severity distributed throughout its volume. Every fatigue specimen, therefore, contains a large number of these weak points or "nucleation" points, the number and type of which will depend upon chance. Because of this chance distribution of nucleation points, the fatigue limit and the fatigue life at a given stress will vary from specimen to specimen. It has been shown (4) that considerable scatter exists not only in the fatigue limits of metals but also in their finite fatigue lives at a given stress. This seems quite reasonable, however, when considered from the viewpoint of the foregoing discussion.

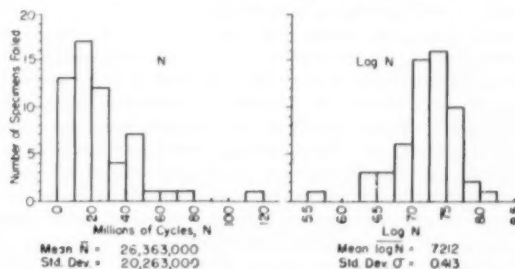


FIG. 1 FINITE FATIGUE-LIFE DISTRIBUTION AT 30,000 PSI (57 SPECIMENS)

Frequency-distribution diagrams of the number of cycles to failure N at a given stress amplitude are quite badly skewed having a long tail to the right. For example, refer to Fig. 1. When the diagram is plotted in terms of the logarithm of N , however, the tendency for right-handed skewness is apparently overcome and

¹ A research project of the Department of Theoretical and Applied Mechanics, Engineering Experiment Station, University of Illinois, Sponsored by Office of Naval Research, U. S. Navy, Contract N6-ori-71, T. O. IV; Project NR-031-005.

² Metallurgical and Ceramic Department, Westinghouse Research Laboratories, East Pittsburgh, Pa.; formerly, Research Assistant Professor of Theoretical and Applied Mechanics, University of Illinois, Urbana, Ill.

³ Research Professor of Theoretical and Applied Mechanics, University of Illinois. Jun. ASME.

⁴ Numbers in parentheses refer to the Bibliography at the end of the paper.

Contributed by the Metals Engineering, Machine Design, and Aviation Divisions and presented at the Annual Meeting, New York, N. Y., November 30-December 5, 1952, of THE AMERICAN SOCIETY OF MECHANICAL ENGINEERS.

NOTE: Statements and opinions advanced in papers are to be understood as individual expressions of their authors and not those of the Society. Manuscript received at ASME Headquarters, August 8, 1952. Paper No. 52-A-82.

the distribution assumes a more nearly normal shape. Other distribution functions for N have been suggested (5, 6); however, for the purposes of the present paper, these did not appear to offer any clear-cut advantages over the more easily handled logarithmic-normal distribution. For this reason, the present analysis is based on the assumption that the logarithm of the fatigue life N , is normally distributed at all stress levels investigated.

It was the purpose of the present study to investigate statistical variation in the fatigue life of 75S-T6 aluminum alloy and to determine, within limits, the effect of stress amplitude on this variation. The experimental program was carried out for the fatigue-stress range of greatest interest in engineering design. A total of 174 specimens were broken at six different values of cyclic stress of which 62,500 psi was the greatest and 30,000 psi, the smallest.

MATERIAL AND METHOD OF TESTING

The 75S-T6 aluminum alloy was received in $7/8$ -in.-diam bars and had average mechanical properties as shown in Table 1.

TABLE 1 MECHANICAL PROPERTIES OF 75S-T6 ALUMINUM ALLOY

Ultimate strength, psi.....	83680
Yield strength (0.2 per cent offset), psi.....	73060
Elongation (2 in.), per cent.....	16
Reduction of area, per cent.....	31.6
Charpy impact, ft.-lb.....	5.0
Rockwell B hardness.....	91.2

The bars were split longitudinally and small rotating-beam specimens were machined from each half of the bar. The specimens were in the form of cylindrical bars $1\frac{1}{4}$ in. long \times $1/4$ in. diam with the central portion gradually reduced to a minimum diameter of 0.150 in. by turning the surface contour to a radius of $3/4$ in. The specimens were given a standard finish with final scratches produced by 60 polishing paper running longitudinally. Three small rotating-cantilever-beam fatigue machines which have been described previously (9) were employed in the tests at a nominal speed of 8000 rpm. The stress in the specimen was computed from the simple beam formula $S = Mc/I$ in which S is the nominal stress amplitude at the extreme fiber of the test section. Prior to the tests, these machines were calibrated carefully by means of a sensitive weighing device which utilized SR4-type electrical-resistance strain gages as the measuring element. No apparent differences in the static calibration of these machines were found by this means. The moment M applied to the specimen could be adjusted to ± 0.01 in.-lb with the average moment setting being about 10 in.-lb. The diameter of the specimens at the critical section was determined by means of a Pratt and Whitney supermicrometer reading to 0.0001 in. Two measurements were made on the critical section 90 deg apart and the average was taken. Specimens which were out of round by more than 0.0004 in. were rejected. From these values the maximum error in applied stress was computed to be approximately 500 psi.

Fatigue-life tests were conducted for six values of stress which were 62.5, 50, 45, 40, 35, and 30 thousands of psi. From 17 to 57 specimens were tested at each of these stresses and the fatigue-life data obtained were analyzed statistically using methods of calculation which are outlined by Brownlee (7). In the interpretation of fatigue-life data all calculations were made using the logarithm of the life to failure since this quantity appeared to have an approximately normal distribution. The resultant values were transformed back to arithmetic answers for presentation in

the figures. The mean log-life, that is, $\log \bar{N}$ and the standard deviation σ , were calculated by standard procedures.⁴ Confidence limits on the mean and standard deviation⁴ were computed for the 95 per cent and 90 per cent levels, respectively (7). The 95 per cent confidence limits for the mean, for example, simply indicate that the probability is 0.95 that the mean of the total population of specimens falls between these limits determined from the sample.

RESULTS OF TESTS AND DISCUSSION

The statistics of the test data obtained at each stress are summarized in Table 2. The mean log life, $\log \bar{N}$, is given for each stress as is the standard deviation, σ , and confidence limits for these values are shown also.

For the series stressed at 30,000 psi, data are presented graphically in a frequency-distribution histogram, Fig. 1. Those charts were plotted with a cell width equal to 10,000,000 cycles in terms of N and a cell width of 0.25 in terms of $\log N$, thus covering both the distribution of N and of $\log N$. It will be observed that the distribution based on the number of cycles N is highly skew showing a long right-hand tail; however, it becomes more nearly a normal distribution when based on $\log N$. In either case, the standard deviation is quite large at this low stress.

The frequency distribution is illustrated in greater detail in Fig. 2, which gives individual fatigue-life-times obtained at the various stress amplitudes. The plotting position for the relative frequency of failure was determined by first listing the specimens in increasing order of fatigue life, such as $N_1, N_2, \dots, N_n, \dots, N_n$ where the total number in a particular group was n . The plotting position for the m th specimen then was taken as m divided by the quantity $(n + 1)$. The quantity $(n + 1)$ is used as a divisor rather than n in order to avoid obtaining an estimate of 100 per cent probability of failure at the life N_n for the n th specimen in a group of n specimens. This procedure is ordinarily used when relatively small samples are being studied.

TABLE 2 SUMMARY OF FATIGUE-LIFE DATA

Stress, psi	Number of specimens, n	Mean log life for failure, $\log \bar{N}$	95 per cent confidence limits for $\log \bar{N}$		Standard deviation of $\log N$, σ	90 per cent confidence limits for standard deviation σ	
			Lower	Upper		Lower	Upper
62500	21	4.2047	4.1884	4.2210	0.0348	0.0284	0.0484
50000	20	4.7234	4.6684	4.7784	0.1085	0.0884	0.1530
45000	20	4.7585	4.6826	4.8344	0.1273	0.1040	0.1790
40000	39	5.3331	5.2504	5.4158	0.2443	0.1956	0.2930
35000	17	6.1674	6.0507	6.2841	0.2270	0.1825	0.3316
30000	57	7.2120	7.1024	7.3216	0.4130	0.3484	0.4776

The ordinate in Fig. 2 is based on the cumulative normal distribution while the abscissa is the number of cycles to failure N , plotted to a log scale. Since the distribution of points in any group may be approximated closely by a straight line, it is appar-

$$\log \bar{N} = \frac{\sum \log N}{n}$$

$$\sigma = \left[\frac{\sum (\log N - \log \bar{N})^2}{n} \right]^{1/2}$$

where

$\log \bar{N}$ = mean log life
 σ = standard deviation
 N = fatigue life of a given specimen
 n = number of specimens in sample

⁴ For samples having less than 30 specimens, limits for variance were computed using

$$\sigma = \frac{(n-1)\sigma^2}{N^2}$$

and the roots were taken to obtain standard deviation limits.

ent that the distribution of $\log N$ is approximately normal. The solid lines which are drawn through the groups of experimental data represent the ideal logarithmic-normal curve having the same mean and the same standard deviation as calculated from the corresponding experimental data. The number of cycles to failure corresponding to $\log N$ fixes the position of the line since it must intersect the horizontal line representing 50 per cent frequency of failure at this point. The slope of the line is determined by the standard deviation and, therefore, provides a measure of the scatter in fatigue life at the various stress levels. It may be seen that the lines become more nearly vertical for the higher stresses indicating a relatively smaller amount of scatter in the number of cycles to failure.

The accurate determination of fatigue life for very small probabilities of failure by extrapolation of the straight-line portions of the diagram did not appear feasible because the lines intersect at a finite number of cycles (approximately 6×10^3). Thus, if the extrapolation is continued beyond the point of intersection, the diagram indicates that specimens stressed at a low stress have a shorter fatigue life than those stressed at a higher stress (for a given small frequency of failure). It seems probable, therefore, that curves representing the exact frequency-life relationship would deviate gradually from the straight lines shown in Fig. 2, by curving upward as very small frequencies of failure are approached. In general, agreement between the logarithmic-normal

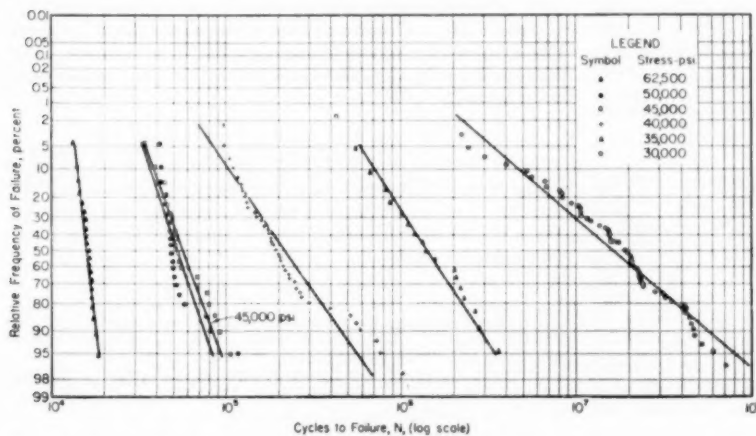


FIG. 2 LOGARITHMIC-NORMAL PROBABILITY DIAGRAM SHOWING INDIVIDUAL FATIGUE LIFETIMES OBTAINED AT DIFFERENT STRESSES

normal distribution and experimental data appeared to be reasonably close for frequencies of failure between 1 and 99 per cent. Fig. 3 presents a relationship between the flexural stress S , and the fatigue life N , for a probability of failure $P = 0.50$. The fatigue life N used here was obtained by transforming $\log N$ to arithmetic terms. The diagram was plotted in accordance with an equation recently proposed by W. Weibull (8), that is

$$(S - E) = A(N + B)^{-m} \quad [1]$$

or in logarithmic form

$$\log (S - E) = -m \log (N + B) + \log A \quad [1a]$$

which is a straight-line relationship. The terms of the equation in this form were readily evaluated graphically by adjusting the quantities E and B until a straight line was obtained in logarithmic plotting, Fig. 3. The constant m is the slope of the line and A is the intercept where $(N + B)$ equals 1. E might be interpreted as the endurance limit of the metal for $P = 0.50$ or the stress at

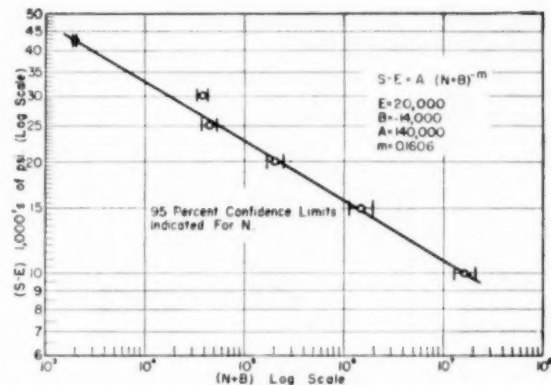


FIG. 3 RELATIONSHIP OF STRESS S AND FATIGUE LIFE N FOR A PROBABILITY OF FAILURE $P = 0.5$

which approximately 50 per cent of the specimen group will have infinite life.

Equation [1] was evaluated for the present data as

$$S - 20,000 = 140,000 (N + 14,000)^{-0.1606} \quad [1b]$$

where $30,000 < S < 62,500$.

It is sometimes assumed that the ultimate tensile strength corresponds to the stress for failure at $1/2$ or $1/4$ cycle (depending upon the range of stress involved) and that it represents a limiting value of fatigue stress. This assumption was not used for the present analysis as it appears questionable. A single loading cycle at the ultimate strength does not result in final fracture in ductile metals; therefore it does not seem that one would be justified in including this value with other data which represent a condition of fracture.

As evaluated in Equation [1b], the $S-N$ relation proposed by Weibull (8) represents the experimental values quite accurately. (In this study $30,000 < S < 62,500$ psi.) It should be noted, however, that this equation is essentially empirical, and any extrapolation should be made with caution. The relationship shown between S and N for $P = 0.50$ is

useful but it gives no information regarding the scatter in fatigue life at the various stresses. Results of an analysis of the variability in fatigue life are indicated in the next figure.

Fig. 4 presents experimental values of the standard deviation σ (which is a measure of scatter in $\log N$) for various values of flexural stress S , each plotted to a logarithmic scale. It is clear that the standard deviation became smaller when the flexural stress was increased. A relationship between σ and S is given approximately by an equation of the form

$$\sigma = \sigma_0 S^{-n} \quad [2]$$

or in logarithmic form

$$\log \sigma = -n \log S + \log \sigma_0 \quad [2a]$$

which is a straight line. The quantity n is the slope of the line and σ_0 is the intercept at $S = 1$. The equation of the straight line shown in Fig. 4 was obtained by applying the method of

least squares to the experimental points. The relation determined in this manner is as follows

$$\sigma = (8.72 \times 10^{13}) S^{-2.19} \dots \dots \dots [2b]$$

where $30,000 < S < 62,500$ psi.

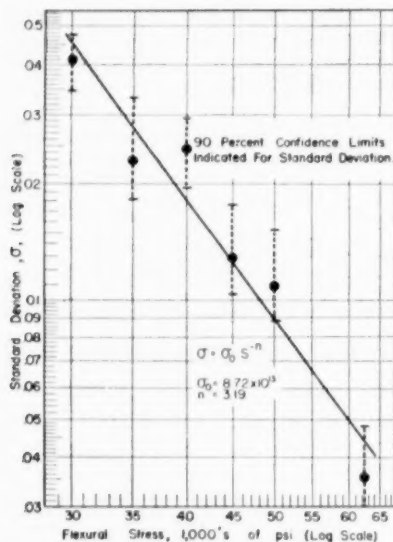


FIG. 4 RELATIONSHIP OF STANDARD DEVIATION AND FLEXURAL STRESS

Equation [1b] describes a relationship between the stress and the mean life corresponding to $\log N$. From this, an $S-N$ curve representing a probability of failure $P = 0.50$ was obtained. As Equation [2b] gives the standard deviation or relative "scatter" of $\log N$ about the mean as a function of stress, $S-N$ curves for various probabilities of failure may be determined. This is illustrated in Fig. 5, which presents $S-N$ curves for $P = 0.01, 0.10, 0.50, 0.90$, and 0.99 . It may be seen that the portion of the diagram included between $P = 0.10$ and 0.90 is a relatively narrow band. Approximately 80 per cent of a group of specimens tested to failure would be expected to fail within this region. By comparison, the region which includes 98 per cent of the specimens (enclosed by $P = 0.01$ and 0.99) is quite large, being a multiple of the first region.

It is interesting to note that the central curve, representing a probability of failure $P = 0.50$ agrees closely with an $S-N$ curve given in reference (9) for the same material. The curve presented in reference (9) was obtained by ordinary fatigue-testing methods in which no more than three specimens were tested at any given stress. It appears then that ordinary methods of testing may give a good approximation of the $S-N$ curve for $P = 0.50$ but of course no further information regarding the variability in fatigue life at the various stresses is given by the limited data.

SUMMARY AND CONCLUSIONS

A study has been made of the effect of stress on the variability in fatigue life of 75S-T6 aluminum alloy. Groups consisting of 17 to 57 specimens were tested in small cantilever-rotating-beam fatigue machines at six different values of stress. The smallest stress used was 30,000 psi and the greatest was 62,500 psi. A statistical analysis was made of fatigue-life data obtained at each of the six stresses.

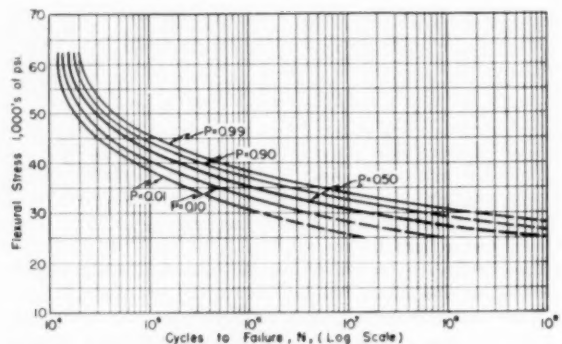


FIG. 5 COMPOSITE $S-N$ CURVES FOR VARIOUS PROBABILITIES OF FAILURE, P

As a result of this study it was concluded that the distribution of fatigue life N for a given stress is approximately logarithmic-normal, although it is believed that the logarithmic-normal relationship is increasingly in error for probabilities of failure smaller than 1 per cent.

The standard deviation (which is a measure of scatter in the fatigue life) is determined primarily by the applied stress. A relationship may be represented by a simple exponential function within the stress range investigated. In general, this variability in fatigue life decreases when the stress amplitude is increased. The extra work involved in making a statistical approach to fatigue problems appears to be justified by the additional information obtained.

ACKNOWLEDGMENT

Appreciation is expressed to the Metallurgy Branch, Office of Naval Research for continued interest in and support of this project. The assistance of Donald C. Simpson and James R. Owen in making calculations and preparing the figures is gratefully acknowledged.

BIBLIOGRAPHY

- 1 "The Statistical Nature of the Fatigue Properties of SAE 4340 Steel Forgings," by J. T. Ransom and R. F. Mehl, Preprint 87, American Society for Testing Materials, June, 1952.
- 2 "The Anisotropy of the Fatigue Properties of SAE 4340 Steel Forgings," by J. T. Ransom and R. F. Mehl, Preprint 93, American Society for Testing Materials, June, 1952.
- 3 "Use of a Recrystallization Method to Study the Nature of Damage in Fatigue of Metals," by G. M. Sinclair and T. J. Dolan, Proceedings, First U. S. National Congress of Applied Mechanics, June, 1951.
- 4 Symposium on Statistical Aspects of Fatigue, American Society for Testing Materials, Special Technical Publication No. 21, 1952.
- 5 "Fatigue Testing and Test Interpretation," by A. M. Freudenthal, Technical Report No. 26, ONR, Contract N6-ori-71, T.O. IV, Engineering Experiment Station, University of Illinois, Urbana, Ill., July, 1951.
- 6 "A Statistical Distribution Function of Wide Applicability," by W. Weibull, Trans. ASME, vol. 73, 1951, p. 293.
- 7 "Industrial Experimentation," by K. A. Brownlee, Chemical Publishing Company, Brooklyn, N. Y., 1947.
- 8 "Statistical Design of Fatigue Experiments," by W. Weibull, Trans. ASME, vol. 74, 1952, p. 109.
- 9 "The Influence of Fluctuations in Stress Amplitude on the Fatigue of Metals," by T. J. Dolan, F. E. Richart, and C. E. Work, Proceedings of the American Society for Testing Materials, vol. 49, 1949, p. 646.

Discussion

G. E. DIETER⁷ AND G. T. HORNE,⁷ The authors are to be con-

⁷ Metals Research Laboratory, Carnegie Institute of Technology, Pittsburgh, Pa.

gratulated on their contribution to the growing literature on the statistical interpretation of fatigue data. Experience in this laboratory in statistical fatigue tests on nine different materials, both ferrous and nonferrous, has shown that the scatter in fatigue life invariably decreases significantly with increase in stress level. This conclusion has been given statistical assurance by applying the F test for comparing the variabilities (standard deviations) of two sets of measurements, to these statistics at each possible combination of stress levels. The F test has been applied to the authors' data and the same conclusion verified. We feel that this type of statistical test is important and necessary to give a firmer foundation to visual "appearances" which too often can be illusory. This, we think, is the real worth of the statistical treatment of data and must precede any search for relationships between the parameters in question; we must prove, to some degree of confidence, that there is a significant change of the variables within the range in which we are working.

Since our tests have been confined to a relatively limited range of stress, it has not been possible to confirm the relationship of log σ with log stress. We do find, however, that it is not at all unusual for the dependency of σ with stress to show an anomaly, such as the authors found at 40,000 and 50,000 psi. We have attributed these simply to random variations in sampling.

The authors suggest that the parameter E in Weibull's equation for the fracture curve on an $S-N$ diagram might be interpreted as the median endurance limit; they rightly caution against extrapolation. Yet giving such a name to this parameter is, in essence, extrapolation and almost certainly in error. For one point, the equation indicates an asymptotic approach to this stress level; in materials where an endurance limit, in the accepted, defined sense, exists, the approach is a rather sharp break in the fracture curve and hardly asymptotic. We can best characterize Weibull's E and B as cutoff parameters (the equation obviously is invalid at stresses less than E and cycles less than B), but with the proviso that the range of applicability is probably less than these parameters would indicate.

R. E. PETERSON.⁹ From a design standpoint, the need for more detailed statistical information about a material depends on the consequences of failure. The usual $S-N$ curve determined from a limited number of specimens is ordinarily a rough approximation of the $P = 0.50$ curve and for many purposes this admittedly incomplete information is sufficient, particularly where weight is not a vital consideration and a generous factor of safety can be applied. In an airplane, however, all sections and parts must be reduced to a minimum, yet the consequences of failure can mean loss of many lives. Here we could well use a detailed statistical picture, not only out to $P = 0.01$, but to $P = 0.001$ and beyond. Referring to Fig. 5, the $P = 0.01, 0.1$, and 0.5 curves are about equally spaced (on the log scale), which would indicate a wide departure for, say, $P = 0.0001$ (one in ten thousand) if the extrapolation were linear. However, the authors point out in connection with Fig. 2 that extrapolation of the straight lines does not seem feasible since the lines would intersect at 6000 cycles. There are other reasons to suspect that these lines turn inward at both top and bottom where they could presumably become asymptotic to limiting values. In some of his work Professor Weibull indicates $P = 0$ curves. It would be of more than academic interest if someone would obtain a curve with 1000 points. Perhaps the authors have some comments to make with regard to the probable "shape of the tails."

F. B. STULEN.⁹ It is by means of the techniques reported in

this paper that further advancements in the laws governing fatigue failures may be made. This investigation, as well as others of this type which have been undertaken in recent years, clearly demonstrates that the variability in fatigue life and endurance limit is an important characteristic of engineering materials.

It is interesting to note that the authors of this paper were able to obtain a simple relation between the variability of fatigue life as a function of the applied stress. If the relation for the standard deviation given by Equation [2] in the paper is valid at stress values below 30,000 psi, it never will become infinite at the lower stresses. Since an infinite value of the standard deviation will occur near a true endurance limit, this material does not have a true endurance limit.

Many steels have true endurance limits and when a cumulative frequency curve is plotted for those specimens tested at a stress level in the vicinity of the endurance limit of such materials, a difficulty arises in plotting the curve. This difficulty is that some specimens will fail while others will not, regardless of the number of cycles imposed, and for this reason a discontinuity will appear in the probability curve. For example, if 5 per cent of the specimens do not fail whereas 95 per cent do fail, a discontinuity in the cumulative frequency or probability curve will occur at the 5 per cent ordinate. Under these circumstances, the standard deviation of the logarithms of failure cycles will become infinite when based on the total number of specimens tested, even though only one specimen does not fail after being tested for a sufficiently large number of cycles. For this condition the standard deviation or variance loses any significance.

The curves of equal probability shown in Fig. 5 of the paper are based on tests at constant stress. One question which arises in connection with these curves is whether the same curves of constant probability would be obtained for distributions of fatigue strength based on tests at a constant number of cycles. Such information could be obtained either by sensitivity testing or by dosage testing. It normally would seem logical to assume that the probability curves based on constant-stress testing would be identical to those based on constant-life testing. However, experimental data would be required in order to verify such an assumption.

R. T. SCHWARTZ.¹⁰ Although the scatter in fatigue undoubtedly is not due mainly to testing-machine differences, still the extent of the latter should be determined. It is believed that a static-weighting device as used does not rule out differences between machines. Factors such as bearing wear and other sources of vibration are not detected. To determine differences between machines, it is suggested that a statistical comparison be made by testing a number of specimens at one stress in each machine, and then comparing the mean values and standard deviation of each machine.

Curves for probabilities of failure below 1 per cent are desired in some design work, such as aircraft propellers. Since the log-normal distribution does not fit closely in the areas of low and high frequencies of failure (see Fig. 2 of the paper) perhaps another distribution could be found which would fit more closely. The extreme value distribution, which has been proposed, may be better.

The statements against the use of the ultimate tensile strength as a limiting value of fatigue stress are concurred in. Fatigue investigations at the Materials Laboratory have shown fatigue strength above the ultimate tensile strength in some cases even at lifetimes up to a few thousand cycles.

⁹ Manager, Mechanics Division, Westinghouse Research Laboratories, Pittsburgh, Pa.

⁹ Curtis Wright Corporation, Propeller Division, Caldwell, N. J.

¹⁰ Chief, Structural Design Data Branch, Materials Laboratory, Directorate of Research, Wright Air Development Center, Wright-Patterson Air Force Base, Ohio.

AUTHORS' CLOSURE

The authors are grateful for the interesting discussion contributed to this paper. Messrs. Dieter and Horne suggest the use of the F test for comparing variances of two sets of measurements at each possible combination of stress levels. This is, of course, a good procedure for those who may wish to test the data in greater detail than that given. It should be pointed out, however, that a similar type of statistical assurance is presented in Fig. 4 and in Table 2 where "confidence" limits for the values are indicated. In Fig. 4, for all practical purposes, a simple visual comparison is sufficient to indicate whether or not the confidence intervals for two given values of σ overlap or not. If the two confidence intervals do not overlap, then the two values being compared are different at what corresponds to the 0.05 significance level in the variance ratio or F test. It will be noted that in all cases in which the values of σ differ significantly in this way the smaller value of σ is associated with the higher stress. Use of the variance ratio test to determine whether or not the values differ significantly at the 0.001 level, for example, eliminates five out of fifteen possible combinations of values from consideration but the remaining ten combinations which do show a "difference" at this level must, of necessity, support the original conclusion.

The authors cannot wholly agree with the statements made by Mr. Dieter and Mr. Horne regarding the concept of endurance limit. The endurance limit or fatigue limit in one "accepted and defined" sense is "the limiting value of the stress below which a material can presumably endure an infinite number of stress cycles, that is, the stress at which the $S-N$ diagram becomes horizontal and appears to remain so".¹¹ It is seen that the existence of an endurance limit would not depend in any way on the manner in which the fracture curve approaches this limit, whether it be asymptotic or otherwise. The belief that only those materials which exhibit a sharp break or "knee" in the $S-N$ diagram can have an endurance limit is an unwarranted assumption which has probably arisen from the experience of early investigators working on ferrous metals which were capable of strengthening by strain aging during the test.

In evaluating the terms of Weibull's equation for $P = 0.5$ the authors indicated limits for the applicable range of stress which were taken directly from the experimental data. It is difficult to see how an appreciable error results if we remain within or close to the indicated limits. The parameter E as used here stands

¹¹ "Manual on Fatigue Testing," STP No. 91, American Society for Testing Materials, 1949, p. 4.

for the stress at which the probability of survival to infinite life is 0.5. Clearly this is a hypothetical value which could not be measured directly; nevertheless, its meaning in physical terms would be that of a specialized form of endurance limit. To consider the parameter E in this manner is no less correct than it is to speak of the "elastic limit" of a material for a particular set of conditions. In either case we simply utilize a concept which provides us with useful results.

Deciding which of the possible distribution functions will give the best agreement with actual fatigue life at small probabilities of failure is indeed an important point as both Mr. Peterson and Mr. Schwartz indicate. The present data were also plotted in accordance with the extreme value distribution as suggested by Freudenthal and with the general distribution function proposed by Weibull. The extreme value distribution gave somewhat better agreement than the log normal for the data at 30,000 psi (which also had the largest number of specimens); however, in one or two instances at the higher stresses agreement was not as good. Extrapolating the straight-line portions of the extreme value plot again resulted in an intersection at about 6000 cycles; hence the same objections against extrapolation might be raised here as were given in the text for the log normal plot. Weibull's distribution gave the best agreement with the experimental data; this is not particularly surprising in view of the added empirical parameters that it contains. For the purposes of the present paper the benefits to be derived from the use of this more complicated expression were not clear; therefore the simpler log normal distribution was used. It is felt that one of the most important steps in deciding which of the distribution functions may "best" describe actual fatigue behavior is first to obtain data under carefully controlled conditions for a relatively large sample, as Mr. Peterson proposes.

The authors agree with Mr. Schwartz in his statement that the use of static weighing devices to calibrate the machines would not rule out the possibility of differences in their dynamic characteristics. An investigation of such possible "machine effects" would be quite worth while.

Remarks made by Mr. Stulen regarding the interpretation of fatigue data are concurred in. As he states, if Equation [2] in the paper is valid at all stresses below 30,000 psi, then we should have to conclude that the material does not have a true endurance limit. Since no fundamental significance can be claimed for the form of this equation, however, the question as to whether or not this material has a true endurance limit must remain unanswered.

Grinding and Lapping Stresses in Manganese Oil-Hardening Tool Steel¹

By H. R. LETNER² AND H. J. SNYDER,³ PITTSBURGH, PA.

The biaxial stress distributions resulting from grinding and lapping annealed manganese oil-hardening tool steel were determined by sectioning the stressed surface layers and following the changes in curvature of the test specimens by optical interferometry. Two methods of sectioning, lapping, and chemical etching were tested and evaluated. Results of the study show that the plastic deformation which gives rise to the residual stress is at least partially due to mechanical forces exerted upon the surface by the abrasive grains and cannot be explained by forces of thermal origin alone. Grinding stresses were found to fluctuate rapidly close to the surface, the highest stresses being confined to a surface layer about 0.0001 in. thick. Depth of stress penetration increased with depth of cut over the range tested. Lapping stresses were found to have a nearly constant compressive value throughout the surface layer affected which, for the conditions investigated, was about 0.0002 in. thick.

NOMENCLATURE

The following nomenclature is used in the paper:

- $C_1(\)$, $C_2(\)$ = curvatures of test specimen in planes containing normal to test surface and principal stresses $\sigma_1(\)$ and $\sigma_2(\)$, respectively
 E = Young's modulus of elasticity
 w = instantaneous thickness of specimen as stressed layers are removed from test surface
 w_0 = initial thickness before any layers are removed
 z = co-ordinate parallel to thickness of specimen
 ν = Poisson's ratio
 $\sigma_1(\)$, $\sigma_2(\)$ = principal residual stresses in planes parallel to test surface

INTRODUCTION

There is increasing interest in the residual stresses caused by grinding or lapping because of the influence which they may have upon the service life of tools and parts finished by these processes. Although various opinions are found in the literature concerning the nature of these stresses and their causes, only a few investigators have published actual stress distributions resulting from these operations. Noteworthy among those who have done so are Almen (1),³ Glickman and his associates (2, 3) and Frisch and Thomsen (4). This dearth of published information is due partly to the time required to obtain reliable stress

data and partly to the overworked assumption that nominal stresses inferred from residual bending moments are a satisfactory indication of the actual stress state in the surface.

A number of investigators have observed the residual bending resulting from machining, grinding, and polishing but most of these have measured the effect of but one component of a stress system which is at least biaxial. Exceptions are the work of Henriksen (5) on machining stresses and the observations of Martindale (6) concerning the effect of abrasion upon the magnetic properties of silicon steel. Although Henriksen observed the effect of but one component of the surface stress at a time, he showed that machining stresses are biaxial and that the principal components are parallel and perpendicular to the direction of tool travel. Martindale not only observed that the components of the surface stress resulting from unidirectional abrasion of steel with emery cloth are unequal and are oriented parallel and perpendicular to the abrasion direction but also showed that they are accompanied by a corresponding magnetic anisotropy.

It is believed that the work described in subsequent paragraphs, while limited to only a few of a great variety of possible combinations of specimen materials, abrasive wheel specifications, and grinding and lapping conditions, utilizes a useful experimental approach to the problem of measuring biaxial surface stresses and points out some features of residual grinding and lapping stresses which hitherto have not been published. Many experimenters who have observed the effects of grinding stresses have employed severe grinding conditions in order to obtain measurable results. Use of the optical interference technique in the present work not only avoids the necessity for exceeding recommended grinding practice but also permits simultaneous measurement of the principal components of the biaxial surface stress.

EXPERIMENTAL PROCEDURE

Specimens. Manganese oil-hardening tool steel was selected as the specimen material because of its wide use in industry and because of its alleged sensitivity to grinding injury. Two-inch-square specimens were cut from $1/4$ -in. \times 2-in. annealed bar stock having a percentage composition of 0.92 C, 1.38 Mn, 0.019 P, 0.28 S, 0.013 Si, 0.45 Cr, 0.41 W, and the remainder Fe. These were placed on the magnetic chuck of a horizontal spindle surface grinder in groups of six and surrounded by $1/4$ -in. \times 1-in. bars of the same material, as shown in Fig. 1. Approximately 0.015 in. was gently ground from each side of the specimens and surrounding bars, using a freshly dressed 46-grit vitrified wheel of medium grade, in order to remove any decarburized material.

The specimens for the lapping test and the first grinding test were placed in a salt bath consisting of a eutectic mixture of potassium nitrate and sodium nitrite and held at 1100 F for 24 hr in an automatically controlled electric furnace. The test pieces were allowed to cool in the furnace nearly to the freezing point of the bath (295 F) and then in air to room temperature. The specimens for the second grinding test were given a similar treatment except that they were packed in sillimanite and allowed to cool all the way to room temperature before unpacking. The furnace and typical cooling curves are shown in Fig. 2. The purpose of this stress-relief anneal was to remove any machining or

¹ A contribution from the L. Leslie Byers Memorial Fellowship sustained at Mellon Institute by the Grinding Wheel Institute.

² Mellon Institute of Industrial Research.

³ Numbers in parentheses refer to the Bibliography at the end of this paper.

Contributed by the Research Committee on Cutting Fluids and Metal Cutting Data and Bibliography, and Production Engineering Division and presented at the Annual Meeting, New York, N. Y., November 30-December 5, 1952, of THE AMERICAN SOCIETY OF MECHANICAL ENGINEERS.

NOTE: Statements and opinions advanced in papers are to be understood as individual expressions of their authors and not those of the Society. Manuscript received at ASME Headquarters, August 28, 1952. Paper No. 52-A-38.

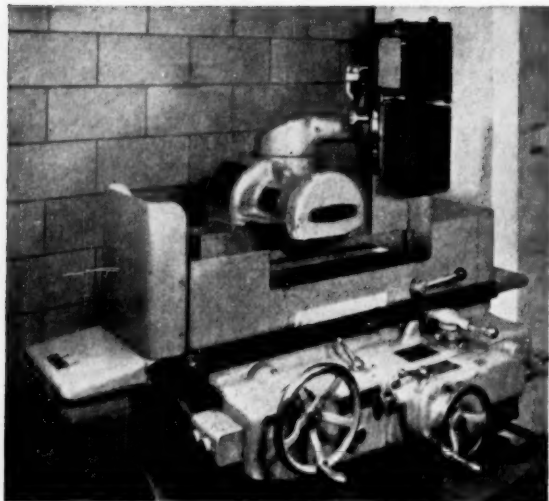


FIG. 1 SURFACE GRINDER WITH SPECIMENS IN POSITION FOR TEST

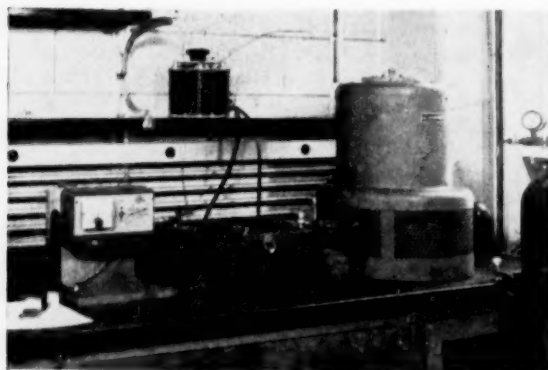


FIG. 2 HEAT-TREATING FURNACE AND TYPICAL COOLING CURVES

grinding stresses introduced during the preparation of the test pieces (7).

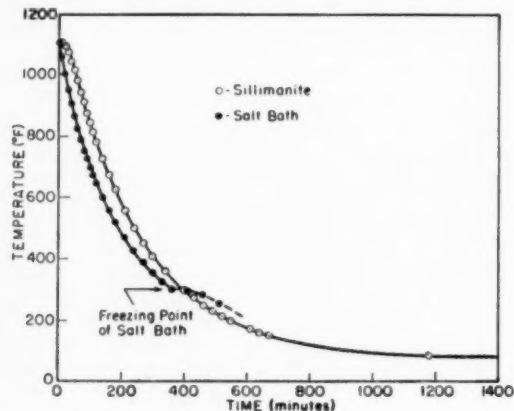
The specimens were pickled in a 10 per cent solution of sulphuric acid to remove scale and then held at 300 F for 1 hr to get rid of any hydrogen absorbed during the pickling process which might cause embrittlement. One surface of each specimen was lapped flat on the lapping machine shown in Fig. 3, employing a mixture of 800-grit aluminum-oxide abrasive in oil fed onto a rotating cast-iron plate. The lapped surfaces were rubbed lightly on 4/0 metallurgical emery paper to give them sufficient reflectivity to produce sharp interference patterns when placed in contact with a quartz optical flat and illuminated with sodium light.

Grinding Tests. Grinding tests were conducted on a 6-in. \times 18-in. horizontal spindle surface grinder with hydraulic table drive, Fig. 1, powered by a direct-current variable-speed 1.5-hp motor. Six simultaneously prepared specimens were placed on the magnetic chuck surrounded by the same 1-in. bars used when the specimens were ground to dimension as previously described. The polished surface of each specimen, reserved for curvature measurements by optical interferometry, was adjacent to the magnetic chuck and all test grinding was done on the opposite

surface. In subsequent portions of this paper these surfaces will be referred to as the reference and test surfaces, respectively. By utilizing 0.001-in.-thick paper shims and the slight inequalities in thickness caused by preparation of the reference surfaces, the specimens were arranged in a stepwise fashion so that each traverse of the table produced six different depths of cut. One complete crossfeed was removed during each test. The wheel specifications and grinding conditions, believed to lie well within the range of recommended grinding practice, were as follows:

Wheel: 8-in. \times $1\frac{1}{2}$ -in. \times $1\frac{1}{4}$ -in., J-grade, medium structure, vitrified bond, containing 48 per cent by volume of 46-grit white fused aluminum-oxide abrasive
 Wheel speed (peripheral): 6000 fpm (idling)
 Traverse speed: 50 fpm
 Crossfeed: 0.050 in. at each end of traverse
 Grinding fluid: air

The wheel was dressed with a sharp diamond prior to each test using an adaptation of the method described by Tarasov (8). Approximately 0.005 in. was removed from the face of the wheel in 0.0005-in. increments using a moderate traverse of the diamond, offset 0.5 in. from the vertical center line of the wheel and rotated 30 deg in its holder prior to each dressing so as to generate an apex angle of approximately 154 deg. Wheel speed and trav-



erse speed were measured stroboscopically. Mean wheel depths of cut were calculated from the weight losses of the specimens during grinding, the area ground, and the density of the steel. Uniformity of the cut over the entire surface of each specimen was checked by supplementary micrometer-caliper measurements near the corners before and after grinding. Dry grinding was employed to keep the number of parameters to be controlled during the tests at a minimum.

Lapping Test. The lapping test was conducted on a machine, Fig. 3, employing a rotating cast-iron lap onto which was fed a compound consisting of 1 lb of 800-grit aluminum-oxide abrasive suspended in 3 gal of light mineral oil containing about 10 per cent of lard oil. The 12-in.-diam lap rotated at a speed of 72 rpm. Three identically prepared specimens were lapped simultaneously. Each was placed in a work holder free to rotate inside the three circular wear rings in contact with the lap. Two of the specimens were lapped with only their own weights supplying the normal force against the lap; an auxiliary weight was added to the third. The resulting average pressures were 0.07 psi and 0.65 psi, respectively. All of the specimens were given four 10-min runs followed by one or two 2-hr runs. Curvature measurements and weight determinations were made at the beginning

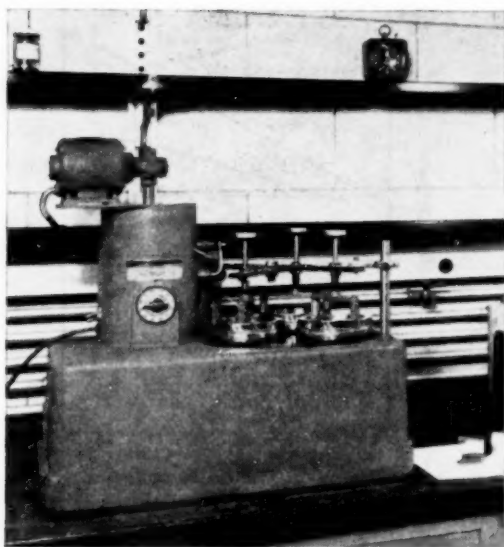


FIG. 3 LAPPING MACHINE

of the test and after each run. Removals were calculated from weight losses as in the grinding tests.

Stress Measurement. Residual-stress distributions in the ground and lapped surfaces were determined by removing thin, uniform layers from the surfaces and measuring the equilibrium curvatures of the specimens by optical interferometry (9). The principal stresses which exist in a layer at any depth w_0-w before any layers are removed are given by

$$\sigma_1(w) = \frac{E}{6(1-\nu^2)} \left\{ w^2 \left[\frac{dC_1(w)}{dw} + \nu \frac{dC_2(w)}{dw} \right] + 4w [C_1(w) + \nu C_2(w)] + 2(w_0 - 3w) [C_1(w_0) + \nu C_2(w_0)] - 2 \int_w^{w_0} [C_1(z) + \nu C_2(z)] dz \right\} \dots [1]$$

$$\sigma_2(w) = \frac{E}{6(1-\nu^2)} \left\{ w^2 \left[\frac{dC_2(w)}{dw} + \nu \frac{dC_1(w)}{dw} \right] + 4w [C_2(w) + \nu C_1(w)] + 2(w_0 - 3w) [C_2(w_0) + \nu C_1(w_0)] - 2 \int_w^{w_0} [C_2(z) + \nu C_1(z)] dz \right\} \dots [2]$$

In these equations, w_0 is the initial thickness of the specimen and w is the instantaneous thickness as successive layers are removed; C_1 and C_2 are the curvatures of the specimen in planes containing the normal to the surface and the principal stresses σ_1 and σ_2 , respectively; E is Young's modulus, ν is Poisson's ratio and z is a co-ordinate parallel to the thickness of the specimen.

If the principal stresses are equal, $C_1 = C_2$ and Equations [1] and [2] become

$$\sigma_1(w) = \sigma_2(w) = \frac{E}{6(1-\nu)} \left[w^2 \frac{dC(w)}{dw} + 4w C(w) + 2(w_0 - 3w) C(w_0) - 2 \int_w^{w_0} C(z) dz \right] \dots [3]$$

The successful application of these equations requires that the removal of surface layers should not disturb the remainder of the

specimen other than to permit elastic readjustment of the internal forces and moments to restore equilibrium; consequently, the method used to remove the layers should neither introduce nor relieve any stress in the remaining material other than that occasioned by the elastic readjustment. All of the methods customarily used are to some degree open to suspicion. Obviously, techniques such as machining and abrasion which give rise to plastic deformation of the subsurface metal cannot be used to study grinding or lapping stresses without evaluating their effects upon the stresses under investigation. Similarly, chemical methods also must be scrutinized for nonuniform removal, release of subsurface stress by intergranular penetration, and introduction of stresses of the type observed by Lihl (10).

Lapping was used to remove thin uniform layers from the ground surfaces of the specimens studied in the first grinding test. When it became evident that it would be impossible to determine the stress in layers very close to the surface by this method, the test was repeated and chemical etching was substituted as a method of removal. A 5 per cent solution of nitric acid in alcohol (nital) was used for the first 16 etches which removed between 0.002 and 0.003 in., depending upon the specimen. In order to reduce the etching time, a 5 per cent solution of nitric acid in water was used for the next 12 etches and a 10 per cent solution for the remaining removals. The specimens were immersed in the etchant and swabbed with cotton in order to improve the uniformity of the removal. Only the ground surfaces were exposed to the acid, all others having been coated with paraffin wax. Coating was accomplished by clamping a 3-in. square of plate glass against the ground surface with a C-clamp, dipping the assembly in molten wax at temperatures ranging from 120 to 160 F, and stripping off the glass plate after the assembly had cooled.

The uniformity of the etch was checked by two methods. When the surfaces were rubbed lightly on a lap known to be flat within a few wave lengths of light, almost the entire etched area contacted the lap. The total thickness of metal removed in the entire process was determined by micrometer-caliper measurements at points near each of the four corners of the specimen. The maximum deviation of a single measurement from the mean of the four on any specimen was 5 per cent. When it is considered that this particular specimen had been etched 34 times for a total removal of 0.017 in., the evenness of the etch becomes even more apparent.

The effect of the lapping and etching techniques upon three specimens of the same shape, size, composition and heat-treatment as those employed in the first grinding test and the lapping

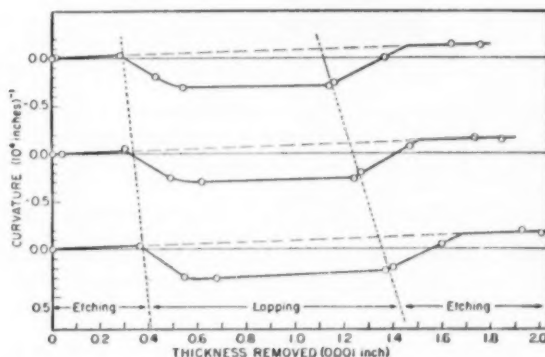


FIG. 4 CURVATURES INDUCED BY ETCHING AND LAPPING ONE SURFACE OF 2-IN. \times 2-IN. \times 1/4-IN. SPECIMENS OF STRESS-RELIEF-ANNEALED MANGANESE OIL-HARDENING TOOL STEEL

test is clearly shown in Fig. 4. The data were obtained by etching the test surfaces twice in 5 per cent nital, lapping three times on the Lapmaster at a normal pressure of 0.65 psi and again etching four times in 5 per cent nital. Snyder (11) has shown that the upward trend of the curvature values indicated by the dashed line is due to a small residual compressive stress, characteristic of the heat-treatment given the specimens. Fig. 5,

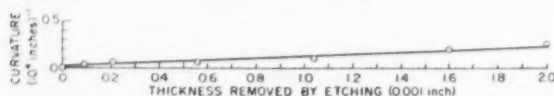


FIG. 5 CURVATURE VARIATION WITH METAL REMOVAL FROM ONE SURFACE OF 2-IN. \times 2-IN. \times 1/4-IN. SPECIMEN OF STRESS-RELIEF-ANNEALED MANGANESE OIL-HARDENING TOOL STEEL

taken from Snyder's work, shows how the curvature of a specimen of similar composition and heat-treatment varies when surface layers are removed by etching in 5 per cent nital alone. Further evidence that the increase in curvature is due to the release of a compressive stress already in the specimens and not to the introduction of a tensile stress by the etching is the fact that in Fig. 4 the straight-line portions of the curves resulting from lapping also slope upward. If compressive stresses of the type described by Lihl (10) were introduced by the etching, they obviously had no significant effect upon the curvature measurements in this work.

RESULTS

Grinding Stresses. Inspection of the interference patterns formed between the reference surfaces of the ground specimens and the optical flat revealed immediately that the stress induced in the grinding tests was at least biaxial with principal stresses oriented parallel and perpendicular to the traverse direction. The ease with which this information can be obtained by the interference method is demonstrated by the symmetrical pattern in Fig. 6. The maximum bending occurs along the minor

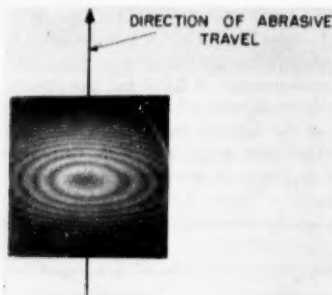


FIG. 6 INTERFERENCE PATTERN FORMED BETWEEN OPTICAL FLAT AND REFERENCE SURFACE OF GROUND SPECIMEN (Principal stresses are parallel to major and minor axes of elliptical fringes. Prior to grinding, reference surface was essentially flat.)

axis of the elliptical fringes and the minimum bending along the major axis; consequently, these are the directions of the principal stresses. In every case, the principal stresses resulting from surface grinding were parallel and perpendicular to traverse or, more fundamentally, to the trajectories of the abrasive grains along the surface.

The effect of depth of cut upon the curvatures of the specimens after the grinding tests is shown in Fig. 7. As the depth of cut increased the curvatures became algebraically greater; i.e., the specimens became more concave as viewed on the ground side.

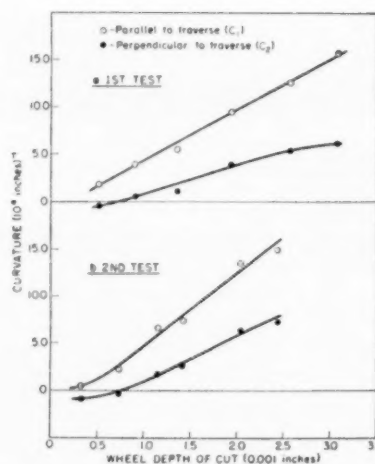


FIG. 7 DEPENDENCE OF CURVATURES OF 2-IN. \times 2-IN. \times 1/4-IN. SPECIMENS OF ANNEALED MANGANESE OIL-HARDENING TOOL STEEL UPON MEAN WHEEL DEPTH OF CUT

Fig. 7(a) reveals that at small depths of cut the transverse curvature C_2 may become negative. Fig. 7(b) further indicates that C_2 may become larger than C_1 in absolute magnitude. This is substantiated by other tests at reduced depths of cut employing similar wheels and specimens. The trend of the curvatures toward negative values as the mean depth of cut decreases implies a transition from nominal tension to nominal compression at very small depths of cut. This is in agreement with the observations of Almen (12).

The curvature parallel to traverse C_1 was always algebraically greater than that at right angles C_2 for any given specimen. Within the range investigated, the algebraic difference increased with increasing depth of cut.

Although the data for the two tests are in fair quantitative agreement, the differences in the slopes of the corresponding curves are well outside the limits of error of the curvature measurements and must be attributed to differences in the residual surface stresses. Experience has shown that the most likely source of such differences lies in the cutting condition of the wheel or in the residual thermal stresses present in the specimens before grinding. Even though precautions are taken to standardize the dressing of the wheel prior to a test, differences in the results of this operation alone are believed to be sufficient to cause the differences in Fig. 7. Furthermore, slight differences in the mean wheel depth of cut, either on the surrounding dummy bars or the specimens themselves, can cause differences in the cutting condition of the wheel. The two tests were conducted with two different wheels and, although they were specially selected for identical properties, this is another possible source of the observed differences in the two tests.

It was pointed out previously that in analyzing the residual stresses resulting from the first grinding test, sectioning of the stressed layers was accomplished by lapping. The curvature data obtained in this process are plotted in Fig. 8. Somewhat naively, a correction equal to the equilibrium curvature induced by lapping unground specimens of the same size, composition, and heat-treatment was subtracted from the measured curvatures to obtain the values in Fig. 8. Such a correction did not take into account the fact that not only was a lapping stress being introduced into the surface of the remaining metal but the grinding stress which had previously existed there also was being removed to the depth to which lapping caused plastic deformation.

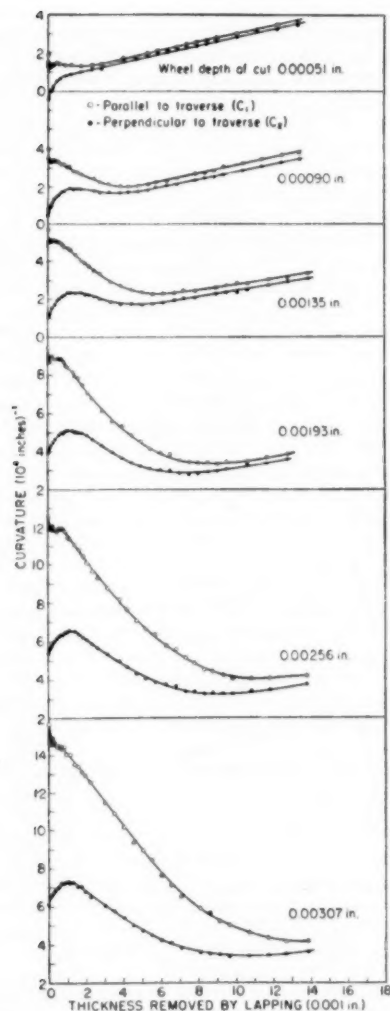


FIG. 8 CURVATURE VARIATION AS A FUNCTION OF THICKNESS OF METAL REMOVED FROM SURFACES OF 2-IN. \times 2-IN. \times 1/4-IN. SPECIMENS OF ANNEALED MANGANESE OIL-HARDENING TOOL STEEL GROUND IN FIRST TEST (Sectioned by lapping.)

As a result, the curvature changes resulting from removal of the first layer from the ground surface were much greater than would have occurred had there been no release of stress in the sub-surface metal. This caused the terms $dC_1(w)/(dw)$ and $dC_2(w)/(dw)$ in Equations [1] and [2] to be spuriously large, with the result that the calculated stresses at the surface were fantastically high. This systematic error is mentioned in passing because it is believed that other experimenters have encountered similar difficulty, either knowingly or otherwise. Almen (1), for example, mentions the use of hand-honing to measure residual stress in the ground surface of annealed spring steel at depths probably within the range of plastic deformation by the honing operation itself.

A little reflection shows that although sectioning by lapping can cause a major error in stress determinations very near the surface, the error diminishes rapidly with successive removals. The alternate lapping and etching experiment summarized in

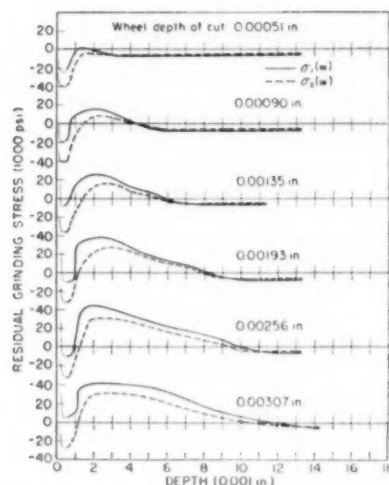


FIG. 9 RESIDUAL STRESS DISTRIBUTIONS IN ANNEALED MANGANESE OIL-HARDENING TOOL-STEEL SPECIMENS SURFACE-GROUND IN FIRST TEST

(Conditions follow: Wheel 8 in. \times 1/2 in. \times 1 1/4 in., J-grade, medium structure, vitrified bond, containing 48 per cent by volume of 46-grit white fused aluminum-oxide abrasive. Wheel speed, peripheral: 6000 fpm, idling. Traverse speed: 50 fpm. Crossfeed: 0.050 in. at each end of traverse. Grinding fluid: air.)

Fig. 4 and the results of the lapping test to be discussed later indicate that the effects of the lapping reached equilibrium during the removal of 0.0002 in. or less of the ground surface and were confined to a layer not more than 0.0003 in. thick. Assuming that all the grinding stress in this layer is removed by lapping, the data in Fig. 8 can be corrected by disregarding all experimental points up to a depth of 0.0002 in. and shifting the remainder of the points to correspond to 0.0003-in. greater depths. When this is done, the stress distributions in Fig. 9 are obtained by substituting in Equations [1] and [2] values of $C_1(w)$, $C_2(w)$, $dC_1(w)/(dw)$ and $dC_2(w)/(dw)$ derived from the corrected graphs. Dotted portions of the curves near the surface show qualitative trends indicated by the curvature versus depth data in this region. The 0.0003-in. correction is probably more than ample since 0.0003 in. is the maximum depth of stress penetration observed in any lapping test and since the grinding stresses may not be completely obliterated to the maximum depth by the plastic deformation of lapping.

Sectioning of the stressed layers of the specimens in the second grinding test by etching yielded the curvature versus depth curves in Fig. 10. Qualitatively, the curves resemble those of Fig. 8 but quantitatively they differ in two respects. (a) Most important is the fact that the slopes obtained by etching are much smaller than those obtained by lapping for depths up to 0.0002 in.; consequently, the stresses calculated from the curves in Fig. 10 are much more reasonable than those calculated from Fig. 8 in this region. (b) Comparison of the slopes of the final straight-line portions of the curves in Figs. 8 and 10 indicates that the specimens in the second test had slightly different initial thermal stresses from those in the first. This is perhaps a result of the slight difference in stress-relieving procedures mentioned previously. Stress distributions calculated by substituting values of $C_1(w)$, $C_2(w)$, $dC_1(w)/(dw)$ and $dC_2(w)/(dw)$ in Equations [1] and [2] are shown in Fig. 11. Comparison with Fig. 9 reveals the close agreement in essential features between the stress distributions obtained by the two methods of sectioning.

The distributions in Figs. 9 and 11 emphasize the unequal biaxial nature of the surface stress induced by surface-grinding

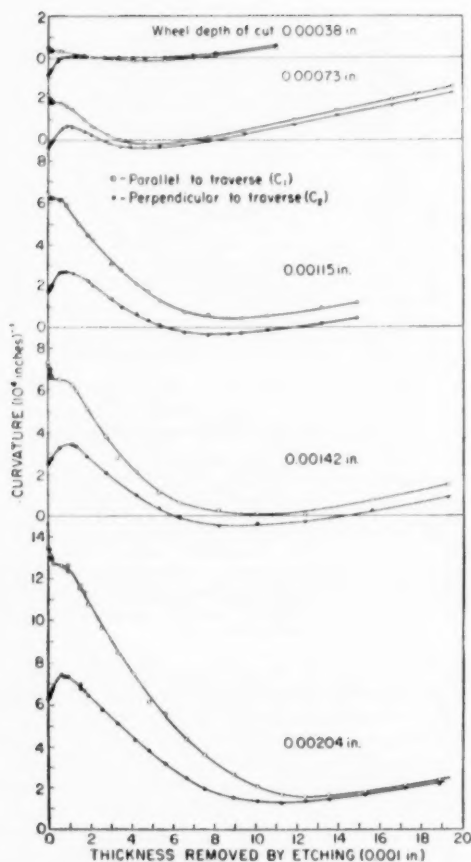


FIG. 10 CURVATURE VARIATION AS FUNCTION OF THICKNESS OF METAL REMOVED FROM SURFACES OF 2-IN. \times 2-IN. \times $\frac{1}{4}$ -IN. SPECIMENS OF ANNEALED MANGANESE OIL-HARDENING TOOL STEEL GROUND IN SECOND TEST (Sectioned by etching.)

and reveal the value of examining both principal components simultaneously. These results, together with the observations of Martindale (6), concerning manual abrasion with emery cloth, and the findings of Henriksen (5) in his machining experiments point to the conclusion that the unidirectional cutting or abrading of ferrous materials results in a residual biaxial stress distribution in which the net force parallel to the direction of the tool or grit travel is always algebraically greater than the net force at right angles to the direction of travel. There has never been a single contradiction to this conclusion in the authors' experience in surface-grinding and disk-grinding more than 200 specimens of steel, both tool and structural, and in milling and shaping a limited number of tool-steel specimens. Such a general behavior can only mean that an important part of the residual stress induced by these processes is due to anisotropic plastic deformation of the surface metal by the abrasive grits or the cutting tool.

Figs. 9 and 11 also point out the fallacy in the expression "the tensile stress caused by grinding" so frequently found in engineering literature. In all but one case, both $\sigma_1(w)$ and $\sigma_2(w)$ change sign at least twice as depth below the surface increases and, in those cases where it can be computed, Fig. 11, $\sigma_2(w)$ is compressive at the surface. The component $\sigma_1(w)$ is a maximum

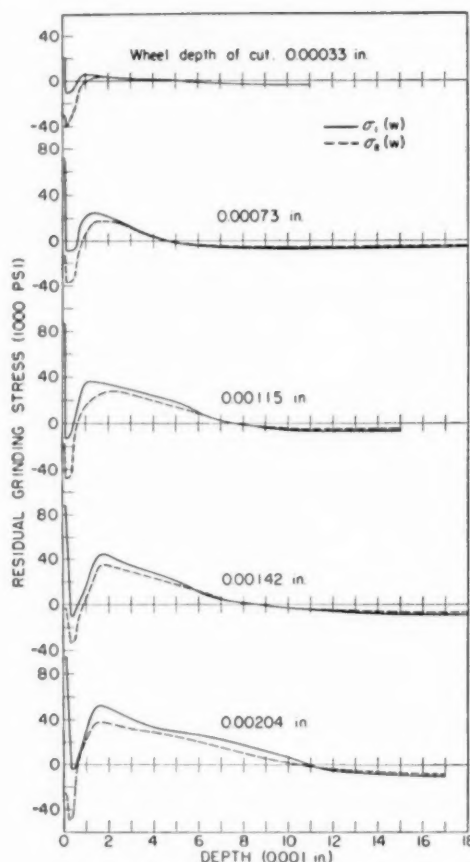


FIG. 11 RESIDUAL STRESS DISTRIBUTIONS IN ANNEALED MANGANESE OIL-HARDENING TOOL-STEEL SPECIMENS SURFACE-GROUND IN SECOND TEST

(Grinding conditions same as for Fig. 9.)

in tension at the surface, drops sharply to a minimum at a depth of about 0.0001 in., rises to another maximum in tension in the neighborhood of 0.001 or 0.002 in. and gradually decreases toward a limiting compressive value. The limiting value is believed to be due primarily to the initial thermal stress in the specimens plus a small elastic reaction to the grinding stresses nearer the surface. Glickman, Sanfirova, and Stepanov (3) found similar distributions in quenched and tempered high-chromium stainless steel but their experiments with low-carbon steel did not reveal any minimum close to the surface. Frisch and Thomsen (4) also observed no minimum in their experiments with SAE 1020 steel. It is quite possible that the magnitude of the stress fluctuation close to the surface is dependent upon the carbon and alloy contents of the steel and that the effect is either nonexistent in low-carbon steel or is too small to be detected readily. In this connection it should be pointed out that in Figs. 8 and 10 many closely spaced experimental points were required within 0.001 in. of the surface to establish the trend of the curves which gives rise to the minima in Figs. 9 and 11.

Glickman, Sanfirova, and Stepanov (3) explain the minima in their stress curves by assuming that the metal close to the surface is heated above the upper critical temperature by grinding and remains there long enough for their sorbitic structure to transform to austenite. They also assume that upon cooling,

martensite is formed in the region where minima are observed and that the volume expansion accompanying the austenite to martensite transformation is sufficient to relieve the tensile stress which would otherwise exist as a result of heating the surface to a high temperature and quickly cooling it by heat transfer to the interior of the specimen. The tensile stress at the surface is attributed to failure of a part of the austenite to transform, thereby setting up a differential volume expansion with the more completely transformed metal immediately beneath it.

A sixth specimen, ground simultaneously with the five for which data are presented in Figs. 10 and 11, was examined for evidence of the phase transformations discussed in the preceding paragraph. The average wheel depth of cut on this specimen was 0.00243 in. which is greater than on any of the other five. X-ray diffraction patterns of the ground surface showed no trace of austenite or martensite. Subsequent taper sectioning and metallographic examination completely substantiated the x-ray findings. Apparently, either the temperature of the surface did not rise above the critical during grinding or it did not remain there long enough to allow the fine spheroidized structure to transform to austenite. The lack of evidence for a phase transformation casts serious doubt upon the ability of the mechanism proposed by Glickman, Sanfirova, and Stepanov to explain the stress distributions in Figs. 9 and 11.

In view of the consistent inequality of $\sigma_1(w)$ and $\sigma_2(w)$ it seems unlikely that any explanation of the origin of residual grinding stress based solely upon thermal arguments can be complete. Plastic deformation arising either from differential thermal expansion caused by temperature gradients near the area of contact of the wheel and the work or from allotropic transformations induced by the heating and cooling of the surface metal almost certainly would result in a residual stress which is isotropic in the plane of the surface. Since this is obviously not the case, the mechanism of stress production at least must be regarded as resulting from plastic strain caused by both thermal and applied mechanical stress.

Although the exact point at which the residual stress resulting from grinding joins the initial stress resulting from the heat-treatment of the specimens is difficult to ascertain because of the gradual blending of the two, it is obvious in Figs. 9 and 11 that the depth of grinding-stress penetration increases with increasing wheel depth of cut. For the particular steel and grinding conditions employed, the depth of penetration appears to be roughly five or six times the depth of cut, within the range explored. Along with the increase in penetration there is an increase in the net positive area under the stress curves. Since this area is nearly proportional to the bending moment, it is this increase which determines the trend of the curves in Fig. 7.

The stress at the surface depends upon the depth of cut as illustrated in Fig. 12. The principal stress parallel to the abrasive trajectory, $\sigma_1(w_0)$, rises rapidly and appears to approach a limiting value with increasing depth of cut. The principal stress perpendicular to the abrasive trajectory, $\sigma_2(w_0)$, does not seem to be

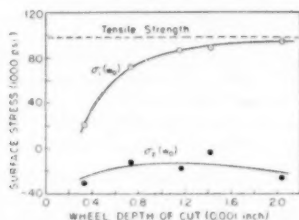


Fig. 12 BEHAVIOR OF PRINCIPAL STRESSES AT SURFACE AS FUNCTION OF DEPTH OF CUT IN GRINDING ANNEALED MANGANESE OIL-HARDENING TOOL STEEL

particularly sensitive to depth of cut in the range tested. Fig. 12 indicates that both $\sigma_1(w_0)$ and $\sigma_2(w_0)$ may have negative values which are appreciable for depths of cut of 0.0002 in. or less, other conditions being the same.

In an auxiliary experiment, tensile tests were run on three standard 0.505-in.-diameter cylindrical specimens having a 2.0-in. gage length. The tests were performed on a Southwark Tate-Emery tester. Strain was measured with an averaging extensometer and recorded automatically on a Templin-type stress-strain recorder. Results of this experiment are summarized in Table 1. These data indicate rather strongly that the limiting value approached by $\sigma_1(w_0)$ in Fig. 12 is the bulk tensile strength of the steel.

TABLE 1 MECHANICAL PROPERTIES OF ANNEALED MANGANESE OIL-HARDENING TOOL STEEL OBTAINED FROM TENSILE TESTS

Specimen no.	Yield strength at 0.2 per cent offset, psi	Tensile strength, psi
1	46000	97000
2	47000	98000
3	49000	98000

The nature of the curves in Fig. 11 indicates an interesting possibility concerning steels which give grinding-stress distributions of this type. The region of biaxial compressive stress close to the surface may have a practical value if the advantages which are claimed in the literature for compressive stresses in connection with the fatigue life of finished parts actually exist. Removal of a few ten-thousandths of an inch of metal can be accomplished in a few minutes, leaving a surface which is compressively stressed. For example, in sectioning the test specimens a 5 per cent solution of nital removed metal at a rate of about 0.00003 ipm; the action of higher concentrations and water solutions of nitric acid was more rapid. Strictly speaking, the curves in Fig. 11 represent the equilibrium stress before etching away any layers and not the stress in the new surface after removal; however, for depths in the neighborhood of 0.0002 or 0.0003 in., the difference between the two is too small to affect the reasoning.

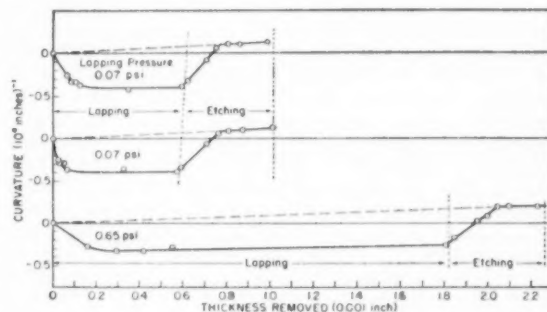


Fig. 13 CURVATURE VARIATION OF 2-IN. \times 2-IN. \times 1/4-IN. ANNEALED SPECIMENS OF MANGANESE OIL-HARDENING TOOL STEEL DURING LAPPING OF ONE SURFACE AND SUBSEQUENT SECTIONING OF LAPPED SURFACE BY ETCHING

Lapping Stresses. Curvature measurements at periodic intervals during the lapping test and during subsequent sectioning of the lapped surfaces by etching resulted in the graphs shown in Fig. 13. The plotted points are averages of the curvatures along two orthogonal directions in the plane of the specimen. Corresponding values for the two directions agreed within the estimated error of measurement, indicating that the test pieces were bent spherically. As lapping progressed, the curvature decreased to a limiting negative value which was independent of both the length

of the test and the total amount of metal removed, ignoring small effects of the initial thermal stresses. Although the higher lapping pressure removed metal at a more rapid rate, the magnitude of the final equilibrium curvature resulting from it was slightly less than for the lower pressure.

The lapping-stress distributions in Fig. 14 were calculated by substituting in Equation (3) values of $C(w)$ and $dC(w)/(dw)$ from those portions of the curves in Fig. 13 obtained by etching. The rectangularity of the distributions and the sharpness of the lower boundary of the stressed layer are somewhat idealized in the graphs; however, Fig. 13 indicates that the change in the slope $dC(w)/(dw)$ is quite abrupt at the lower boundary. As a result, the stress distributions must have slopes in this region at least approaching the vertical portions of the curves as shown in Fig. 14.

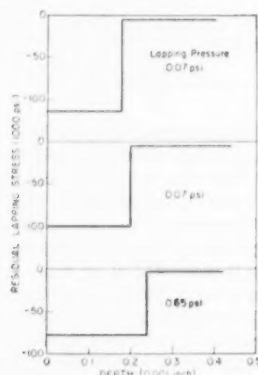


FIG. 14 RESIDUAL STRESS DISTRIBUTIONS IN ANNEALED MANGANESE OIL-HARDENING TOOL STEEL RESULTING FROM LAPPING WITH 800-GRIT ALUMINUM-OXIDE ABRASIVE IN OIL ON ROTATING CAST-IRON LAP

It is apparent from the data that the stress induced by the particular lapping procedure tested is one of uniform compression in the plane of the surface. It is nearly constant throughout a layer extending about 0.0002 in. below the surface and then decreases sharply to a negligible value. Although the stress is quite high, the bending caused by it is small because of the shallowness of the layer in which the stress acts. The lack of directionality of the stress is a consequence of the directional symmetry of the abrasive trajectories across the surface but the freedom of the abrasive to roll and the lightness of the cut also may be contributing factors. It is not clear whether the predominance of compression is due primarily to the gouging action of the loose abrasive or whether the shallowness of the cut is an important factor, as in the case of grinding with bonded abrasives. Some evidence for the latter effect is seen in Fig. 14 where the stress resulting from the higher lapping pressure, and presumably larger grain depth of cut, is less compressive than those resulting from the lower pressure between the specimen and the lap. Another effect of lapping pressure evident in Fig. 14 is the slightly greater depth of stress penetration in the specimen lapped at the higher pressure.

CONCLUSIONS

1 The stress resulting from surface grinding is biaxial. The principal stresses lie parallel to the surface and are oriented parallel and perpendicular to the abrasive trajectories. This behavior is not peculiar to grinding but seems to be true of all surfacing methods employing unidirectional cutting with fixed points or edges.

2 Residual grinding stress is a result of plastic deformation of the surface metal. Although temperature is a factor in determining resistance to deformation, grinding stress is not due solely to deformation caused by thermal stress but to deformation caused by mechanical stress as well.

3 The residual stress resulting from surface-grinding manganese oil-hardening tool steel fluctuates rapidly as a function of depth at distances very close to the surface. This may or may not be a general behavior of all steels under similar test conditions.

4 Under the conditions employed in the grinding tests, the principal stress parallel to the abrasive trajectory in a layer extending about 0.0001 in. below the surface increases with depth of cut toward a limiting value which agrees closely with the bulk tensile strength of the steel. The corresponding principal stress perpendicular to the trajectory is compressive throughout the range tested and does not vary appreciably with depth of cut. There is some indication that both stresses assume compressive values at wheel depths of cut of 0.0002 in. or less.

5 The thickness of the layer plastically deformed by surface-grinding manganese oil-hardening tool steel increases with depth of cut and is five or six times the latter in the range tested.

6 The residual stress induced by lapping with loose abrasive under conditions employed in the lapping test is one of equal biaxial compression. The stress has a high compressive value throughout the plastically deformed layer which is 0.0002 or 0.0003 in. thick, and drops sharply to a negligible value at its lower boundary.

7 The so-called nominal stress is not a reliable indication of the true stress resulting from either grinding or lapping.

ACKNOWLEDGMENT

The authors wish to acknowledge the assistance of Mr. Paul R. Dorn and Mr. Gene E. Geiger in obtaining the data upon which this paper is based.

BIBLIOGRAPHY

- 1 "Shot Blasting to Increase Fatigue Resistance," by J. O. Almen, *SAE Journal Transactions*, vol. 51, 1943, p. 256.
- 2 "Residual Stresses Caused by Grinding," by L. A. Glickman and V. A. Stepanov, *Journal of Technical Physics*, vol. 16, 1946, pp. 791-802.
- 3 "Origin of Residual Stresses in Grinding High Chromium Stainless Steels," by L. A. Glickman, T. P. Sanfirova, and V. A. Stepanov, *Journal of Technical Physics*, vol. 19, 1949, pp. 441-447.
- 4 "Residual Grinding Stresses in Mild Steel," by J. Frisch and E. G. Thomsen, *Trans. ASME*, vol. 73, 1951, pp. 337-346.
- 5 "Residual Stresses in Machined Surfaces," by E. K. Henriksen, *Trans. ASME*, vol. 73, 1951, pp. 69-76.
- 6 "Anisotropic Strains Produced by Surface Abrasion and Their Effect on the Magnetic Properties of Silicon Sheet Steel," by R. G. Martindale, *Journal of the Institute of Electrical Engineers*, vol. 95, 1948, pp. 620-626.
- 7 "Ferrous Metallurgical Design," by J. H. Hollomon and L. D. Jaffe, John Wiley & Sons, Inc., New York, N. Y., 1947, pp. 267-268.
- 8 "Grindability of Tool Steels," by L. P. Tarasov, *Transactions of the American Society of Metals*, vol. 43, 1951, pp. 1144-1174.
- 9 "Application of Optical Interference to the Study of Residual Surface Stresses," by H. R. Letner, to be published in *Proceedings of the SESA*, vol. 10, no. 2, 1953, pp. 23-36.
- 10 "Änderung des Spannungszustandes der Werkstoffoberfläche durch Ätzen," by F. Lühl, *Archiv für Metallkunde*, vol. 1, 1946, pp. 16-25.
- 11 "The Effect of Quenching and Tempering on Residual Stresses in Manganese Oil Hardening Tool Steel," by H. J. Snyder, thesis, University of Pittsburgh, 1952, p. 19; *Transactions of the American Society for Metals*, vol. 45, 1953, pp. 605-619.
- 12 "Fatigue Weakness of Surfaces," by J. O. Almen, *Product Engineering*, vol. 21, 1950, p. 131.

Discussion

E. K. HENRIKSEN.⁴ The authors have shown how a carefully executed experimental method can disclose some important details in the stress distribution. This is an excellent result and needs no further comment.

Lihl, authors' reference (10), tried to scare everybody who works with stresses, with his statement that it is impossible to remove metal by etching without producing new stresses, a very discouraging statement indeed. It is therefore very fortunate that the authors have shown in this paper that it is possible to remove layers of metal and still keep the stresses under perfect control. This eliminates one of the uncertain aspects of stress determination.

The other uncertain aspect is that of obtaining an initially stress-free test piece.

The authors' stress distributions (see Figs. 9 and 11) seem to indicate that the grinding stresses taper off into a "limiting stress" of the order of 5000-10,000 psi in compression, and they explain this limiting stress (partly at least) as an effect of the previous heat-treatment (for stress relief).

If this is correct, then it seems to be almost impossible to obtain a stress-free test piece.

The writer questions this statement.

It does not seem likely that a thermal treatment for stress relief should create compressive stresses in the interior. One should rather expect compressive stresses at the surface and tensile stresses in the interior, as found by Snyder, authors' reference (11).

In the opinion of the writer, the limiting stresses are essentially the balancing stresses that must appear in order to create an equilibrium with the grinding stresses.

The information given in the paper offers two different possibilities for checking this opinion.

In the first place, by using the curves for grinding stresses shown in Fig. 11, it is possible to calculate the complete distribution of the necessary balancing stresses, by using area and mo-

ment. The agreement is fairly satisfactory, but by taking the bending stresses from the curvature data, and using the area from the original stress curve in Fig. 11, it is possible to arrive at a new resultant balancing stress curve, as shown in the lower part of Fig. 15 and drawn with dotted lines in Fig. 16 of this discussion.

It can be argued which of the two is the more correct one. The

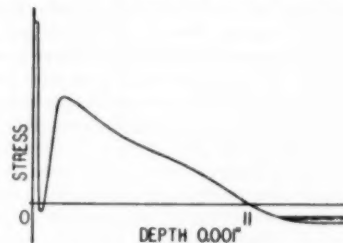


FIG. 16 GRINDING STRESSES FOR DEPTH OF CUT 0.00204 IN. WITH BALANCING STRESSES

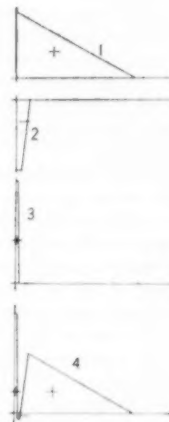


FIG. 17 RESULTING GRINDING STRESSES (4), AS COMPOSED OF CUTTING STRESSES (1), BURNISHING STRESSES (2), AND THERMAL STRESSES (3)

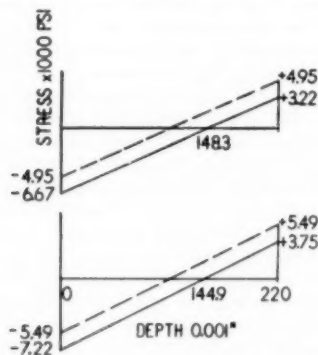


FIG. 15 BALANCING STRESSES, PRODUCED BY GRINDING STRESSES (Depth of cut 0.00204 in.)

ment. This has been done for the curve representing 0.00204-in. depth of cut, and the results are shown in the upper part of Fig. 15 of this discussion. The resulting stresses are drawn into the original stress curve (the full line in Fig. 16, herewith).

The balancing stresses contain a set of bending stresses, which should conform with the curvature data given in Fig. 10 of the paper. The bending stresses, as calculated from Fig. 11, amount to ± 4950 psi, while the curvature data give bending stresses of

difference is within 10 per cent, and either one of the two values as shown in Fig. 16, offers a reasonable approximation to the original limiting stress. The discrepancy that still exists is of the order of 1000-2000 psi only, and in all probability can be accounted for by the experimental error.

It seems therefore reasonable to assume that the authors' test pieces for "second grinding test" have been essentially stress-free.

The writer would like to suggest an explanation of the violent variations of the grinding stresses near the surface.

Referring to Fig. 17 of this discussion, curve 1 represents stresses which are due to the mechanical cutting action of the abrasive grains.

Curve 2 represents a set of compressive stresses due to the burnishing effect, and curve 3 represents a highly concentrated tensile stress due to the heating of the surface of the workpiece during grinding.

When the three curves are combined, they give curve 4, which has the same characteristic shape as the curves in Figs. 9 and 11 of the paper.

There is no "qualitative" difference between curve 1 and curve 3, and, therefore, it may be difficult to distinguish quantitatively between the mechanical and the thermal stress effect.

⁴ Professor, Department of Materials Processing, College of Engineering, Cornell University, Ithaca, N. Y.

AUTHORS' CLOSURE

The authors are grateful to Professor Henriksen for the thoroughness with which he has examined their paper and believe that those points upon which there is a difference of opinion can be satisfactorily clarified. While they appreciate his very complimentary remarks concerning the ability of their experimental technique to produce stress-free specimens, there are certain facts in the data which indicate that the particular groups of specimens employed contained uniform compressive stresses in the region of interest. They believe that these have no significant bearing on the conclusions drawn concerning grinding and lapping stresses and feel optimistic concerning the possibility of preparing specimens which are essentially stress-free. Subsequent to the work described in the paper, specimens have been prepared which exhibit only a few hundred psi throughout half their thickness. Such specimens are stress-free for all practical purposes but the small stress which they contain can easily be measured by the technique described in the paper.

The authors agree that the stress-relieving treatment results in compressive stress near the surfaces and balancing tensile stress on the interior. Snyder (11) found that a specimen of the same steel, heat-treated in a similar way, exhibits a compressive stress from the surface to a depth of about 0.025 in. All of the stress distributions in Figs. 9 and 11 lie well within this distance from the original surface of the specimens before grinding; consequently, one would expect to find compressive stresses resulting from the stress-relieving procedure immediately below the metal plastically deformed by grinding.

Using the second alternative method mentioned by Professor Henriksen and having the advantage of the original stress curves and the exact specimen thickness (0.213 in.), the authors calculated the reaction stresses at the surface of the same specimen selected by Professor Henriksen and found them to be -7200 psi parallel to traverse and -4800 psi perpendicular to traverse. The first figure agrees closely with Professor Henriksen's corresponding value in the lower part of Fig. 15. At a depth of 0.017 in. below the surface, the maximum depth at which $\sigma_1(w)$ and $\sigma_2(w)$ were measured, the corresponding values are -6300 and -4200 psi, respectively. At the same depth, the experimentally determined values of $\sigma_1(w)$ and $\sigma_2(w)$ are -10,200 and -8300 psi. This leaves -3900 psi parallel to traverse and -4100 psi perpendicular to traverse still unaccounted for.

A similar calculation for the specimen in Fig. 11 ground at a depth of cut of 0.00033 in. revealed that the reaction stresses at a depth of 0.011 in. are -100 psi parallel to traverse and +300 psi perpendicular to traverse. The corresponding values of $\sigma_1(w)$ and $\sigma_2(w)$ are -3800 and -3300 psi, leaving stresses of -3700 and -3600 psi not accounted for.

One can further convince himself that not all of the stress near the ends of the distribution curves in Figs. 9 and 11 is reaction to residual grinding stress nearer the surface by studying the curves in Figs. 8 and 10. If a specimen is completely stress-free before grinding, it will again be completely stress-free after all the metal containing grinding stresses has been removed. Its curvature will again be zero and remain so as successive layers are removed. This is obviously not the case in Figs. 8 and 10 where

the terminal slopes of the curves attest to the removal of stresses still present in the specimens.

The reasoning in the preceding paragraph suggests another method for determining the reaction stresses. Equations [1] and [2] give the principal stresses at any level w in the specimen before any layers are removed. In a specimen which is stress-free prior to grinding, these stresses will consist only of the grinding stresses and the reaction stresses. When the layer containing the grinding stresses has been completely removed, all of the stresses given by the equations are reaction stresses. Since $C_1(w)$, $C_2(w)$, $dC_1(w)/dw$ and $dC_2(w)/dw$ are then zero, the only nonzero terms remaining in Equation [1] are

$$\frac{E}{3(1-\nu^2)} \left\{ (w_0 - 3w) [C_1(w_0) + \nu C_2(w_0)] - \int_w^{w_0} [C_1(z) + \nu C_2(z)] dz \right\}$$

These, and similar terms of Equation [2], can be used to calculate the reaction stresses.

If one makes such calculations for all the specimens in Fig. 11 and compares them with the corresponding values of $\sigma_1(w)$ and $\sigma_2(w)$ at depths corresponding to the ends of the experimental curves, he finds unaccounted-for stresses ranging from -3500 to -5100 psi. Moreover, he finds that for each specimen the components of these stresses parallel and perpendicular to traverse agree with each other within 200 psi. Because of the general agreement of these stresses with that found by Snyder (11) at corresponding depths in a similarly heat-treated specimen and the very close agreement of the components in mutually perpendicular directions, it is believed that these are residual thermal stresses, resulting from the stress-relieving treatment, which still exist in the specimens.

The authors find Professor Henriksen's suggested synthesis of grinding stresses stimulating. Attempts to completely separate the contributions of thermal and mechanical stresses to the residual grinding stress are difficult because of the temperature dependence of the flow strength of steel. Auxiliary experiments show that temperatures in the transformation range of steel can be reached in the area of contact between the wheel and the work during severe grinding and it is reasonable to assume that temperatures approaching this are attained under less severe conditions. This alone produces an instantaneous compressive stress well above that required for plastic flow. An approximate calculation shows that the temperature gradient is steep and that the thermal stress sufficient to cause flow decreases rapidly with depth. Whether it is as shallow as indicated by curve 3 of Fig. 17 or extends to the depth indicated by curve 1 is not clear.

Although the stress distributions resulting from the use of different grinding conditions are qualitatively similar, extension of the work described in the paper to the study of other parameters shows that prominent features of the distribution curves are more sensitive to some parameters than to others. The authors believe that a systematic study of all the parameters involved can lead to a more satisfactory explanation of the origin of grinding stresses and to better control of them in commercial practice.

Workpiece and Surface Temperatures in Milling

By A. O. SCHMIDT,¹ MILWAUKEE, WIS.

The temperature gradient in a workpiece while being milled and the existence of very high instantaneous surface temperatures during the cut have been determined experimentally. It has been proved in many tests and often can be observed visually that tool tips frequently fail because of the very high temperatures attained near the cutting edge.

RECENT investigations have shown that metal cutting involves many unique and complex problems of heat flow, temperature distribution, friction, and behavior of metals. This paper reports mainly the state of workpieces with respect to sensible heat. The temperature gradient in workpieces while being milled and the existence of very high instantaneous surface temperatures during the cut have been determined experimentally.

Work done in a metal-cutting operation can be measured in the form of heat in the workpiece, chips, and tool. Most of the heat is in the chips, but usually from 5 to 30 per cent of the total heat goes into the workpiece with the greater percentage occurring at lower speeds. It has been proved in many tests and often can be observed visually that tool tips frequently fail because of the very high temperatures attained near the cutting edge. However, excessive temperatures in the workpiece are seldom noticed in casual or general observations, but special tests confirm that high instantaneous temperatures occur in the machined surface of a workpiece during the machining process.

In these and prior tests (1),² when measuring the surface temperature of equal-sized steel workpieces with a manually operated external "Alnor" low-range thermocouple immediately after a milling cut had been taken, it was found that a number of factors entered into what then was determined as the surface temperature. Cutting speed and feed had the main influence upon the surface temperature. Increases in either the cutting speed or the feed led to decreases in the workpiece-surface temperatures after the cut. Rake angles also had a certain effect on these temperature readings. Negative rake angles, which require more power than positive angles under otherwise identical conditions, caused higher surface temperatures and more deformation of the microstructure near the surface of the workpiece than did positive rake angles (2), Figs. 1 and 2. Average chip temperatures would also increase with a finer feed or greater negative rake angle as shown in Fig. 3. The workpiece temperature, obtained with a surface thermocouple after a cut had been completed, was influenced by the size, specific heat, and heat conductivity of the workpiece and

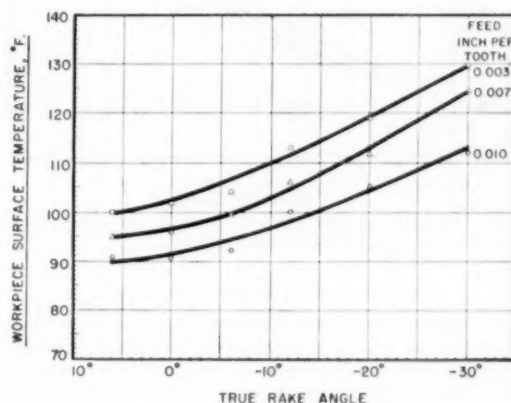


FIG. 1 SURFACE TEMPERATURE OF WORKPIECE MEASURED WITH THERMOCOUPLE IMMEDIATELY AFTER MILLING
(Cutting speed, 100 fpm; room temperature, 70 F; material cut 1-in.-diam test bars SAE 1055 normalized; depth of cut, 0.125 in.)

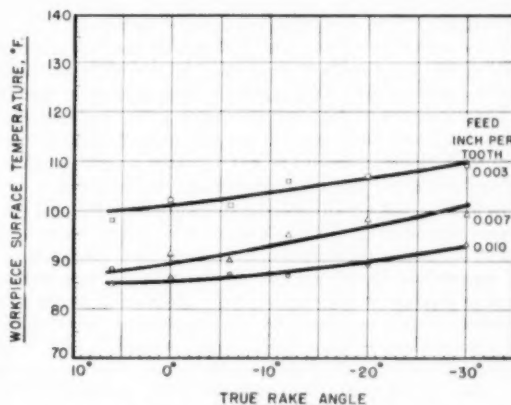


FIG. 2 SURFACE TEMPERATURE OF WORKPIECE MEASURED WITH THERMOCOUPLE IMMEDIATELY AFTER MILLING
(Cutting speed, 1185 fpm; room temperature, 70 F; material cut 1-in.-diam test bars SAE 1055 normalized; depth of cut, 0.125 in.)

holding devices. Only average workpiece-surface temperatures existing several seconds after the surface had been formed were measured previously, because of the difficulties encountered in trying to determine the magnitude of the instantaneous temperatures during the cut (3). Ordinarily, larger workpieces dissipate the heat of cutting very rapidly and no effects seem to be visible, but temper colors often appear on very thin sections of machined surfaces. However, since more heat and greater temperature increases are produced by finer chips, as has been measured in milling, drilling, and turning tests, still higher temperatures are therefore encountered in grinding and similar operations. In practice, it has been observed that buffing can draw the temper of the surface of hardened-steel workpieces.

¹ Research Engineer, Kearney & Trecker Corporation. Mem. ASME.

² Numbers in parentheses refer to the Bibliography at the end of the paper.

Contributed by the Research Committees on Cutting Fluids, and Metal Cutting Data and Bibliography, and Production Engineering Division and presented at the Annual Meeting, New York, N. Y., November 30-December 5, 1952, of THE AMERICAN SOCIETY OF MECHANICAL ENGINEERS.

NOTE: Statements and opinions advanced in papers are to be understood as individual expressions of their authors and not those of the Society. Manuscript received at ASME Headquarters, October 14, 1952. Paper No. 52-A-86.

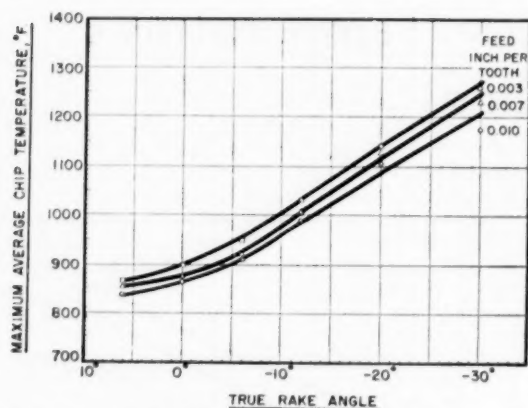


FIG. 3 AVERAGE TEMPERATURE OF CHIPS FOR CUTS IDENTICAL TO THOSE PLOTTED IN FIG. 2

TEMPERATURE GRADIENT IN WORKPIECE

The main object in the tests reported here was to determine experimentally as closely as possible the maximum temperature occurring in or near the surface of a workpiece while it was being milled. Temperature readings were taken at several different levels in the workpiece as seen in the test arrangement shown in Fig. 4. The test bar had a slot in the center where the thermocouple P indicated the temperature as the tool cut through the workpiece material. As was to be expected, the temperatures recorded were highest when the surface being cut was closest to the thermocouple. The general distribution of maximum temperatures in a workpiece during and shortly after machining is illustrated in Fig. 5. For the last cut the thickness of the remaining layer was only 0.025 in., Fig. 4, and the potentiometer used did not respond fast enough to indicate the peak temperatures which were consequently obtained with temperature-indicating crayons. When the distance S was 0.125 in. or greater, a time lag always occurred before the maximum temperature was attained.

The highest temperature reading at P during the first cut, for a distance S of 0.750 in., was obtained 8 sec after the tool had finished machining the surface of a steel test bar. As the cutting tool approached closer to P the temperature increase was obtained in a progressively shorter time. Because of better heat-conducting properties, these elevated temperatures were reached sooner in nonferrous materials than they were in steel. When steel test pieces of SAE 1030 were milled at speeds above 400 fpm, blue temper colors were visible on the underside of the 0.025-in-thick layer after the last cut. Therefore temperatures were high enough and existed for a time sufficient to produce temper colors in the thin sections of the test bar and to change the colors of temperature-indicating crayon marks. The potentiometer responded too slowly at this point to indicate a temperature anywhere near the maximum surface temperature in the workpiece, the temperature gradient being very steep in the shallow subsurface region. Only when the temperatures farther away from the surface were measured was it possible to use this thermocouple equipment with better accuracy, since it took a number of seconds before the maximum temperature was reached. This meant that an entire section of the workpiece had been heated up. Since a general temperature rise throughout a workpiece is caused by the cutting action, the tool can be considered as a heat source. This heating action of the tool can be reproduced by a heating element adjusted to obtain temperatures in the workpiece similar to those recorded during an actual metal-cutting operation.

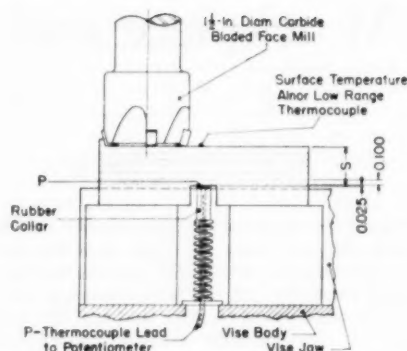


FIG. 4 TEST ARRANGEMENT FOR MEASUREMENT OF WORKPIECE TEMPERATURES

(In determination of maximum surface temperature, cutter was replaced by an oxyacetylene flame moving over workpiece at same feed rate and causing an identical temperature rise at P .)

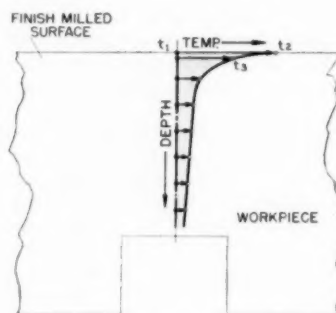


FIG. 5 AID TO INTERPRETATION OF CHARTS INDICATING MAXIMUM TEMPERATURES ATTAINED AT AND BENEATH THE SURFACE OF A MILLED WORKPIECE

In the next series of tests, an oxyacetylene flame mounted on a carrier which moved at the same feed rates as used in machining was employed to simulate the heat-producing action of a tool. The maximum temperature in Figs. 6 to 15 is the temperature, measured at the workpiece surface of an oxyacetylene flame or the gaseous layer beneath it which caused a temperature gradient in the workpiece similar to that produced by the cutting tool. The test bars, $1/2 \times 1 1/8 \times 4$ in., were made of SAE 1090 (170, 311, and 387 Bhn), gray cast iron, free-machining brass, aluminum, and magnesium. On these graphs are plotted the temperatures measured at various distances from the surface being machined. In most cases each plotted point is the average of three tests made with a sharp cutter. The three-bladed cutter used for the tests plotted in Figs. 6 to 15 had a 6-deg negative primary radial rake 0.020 in. wide at the cutting edge of the carbide blades which were placed at a 15-deg positive radial rake angle in the cutter body. The peripheral clearance angle was 6 deg, the face-relief angle 3 deg, the face-clearance angle 5 deg, and the face cutting-edge angle 1 deg.

With a test bar $1/2$ in. wide the heat flow was not influenced unduly by the cooler holding devices. Comparative cuts were taken on test specimens of various widths up to 1 in. On test bars wider than $1/4$ in. the temperatures were almost equal, while on those narrower than $1/4$ in., the temperatures were lower because the heat was conducted away at a faster rate by the relatively cold vise jaws. However, when test pieces $1/8$ in. wide were insulated from the vise jaws the temperatures measured were higher, but not as high as those for $1/4$ -in. or larger thickness.

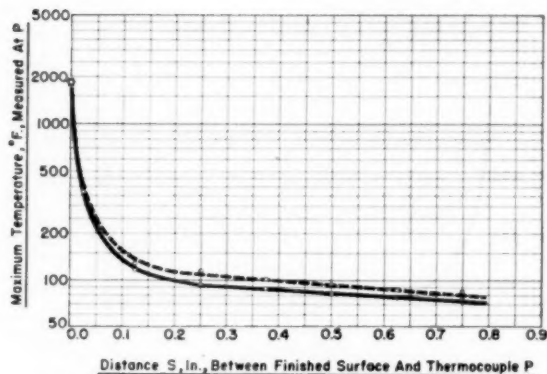


FIG. 6 INFLUENCE OF WIDTH OF WORKPIECE UPON MAXIMUM SURFACE TEMPERATURE OF SAE 1030 WORKPIECE, 180 BHN, AND TEMPERATURES AT DISTANCE S

(Cutting speed 328 fpm; feed 0.0055 in. per tooth. Solid line for workpiece $1/4$ in. thick; dotted line for $1/2$ in. thickness.)

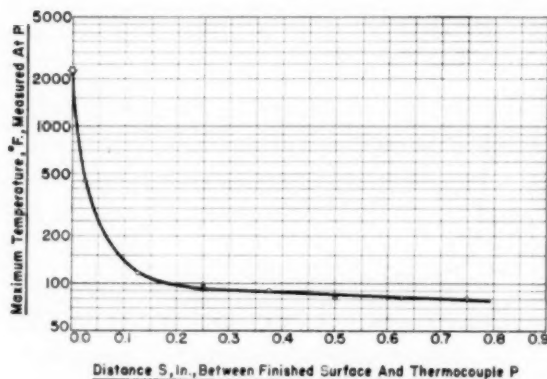


FIG. 8 MAXIMUM SURFACE TEMPERATURE OF SAE 1090 WORKPIECE, 311 BHN, AND TEMPERATURES AT DISTANCE S

(Cutting speed, 590 fpm; feed 0.0055 in. per tooth.)

Workpiece temperatures as recorded when cutting SAE 1030 test bars of 180 Bhn at a cutting speed of 328 fpm are shown in Fig. 6. The solid line indicates the temperature of a test bar $1/4$ in. wide while the dotted line represents temperatures of a test bar $1/2$ in. wide. Values for test bars of $1/2$ in., $3/4$ in., and 1 in. width fell between these curves. The graphs, Figs. 7 to 15, are for test bars $1/2$ in. wide.

Test results when milling SAE 1090 test bars of 170, 311, and 387 Bhn under identical conditions, are presented in Figs. 7, 8, and 9. Each data point plotted in Fig. 7 is the average of six tests. That the data in Fig. 8 are almost the same as those in Fig. 7 suggests the cutting action must have been very similar despite the difference in hardness. The highest temperature increases, Fig. 9, were measured when cutting the same steel at 387 Bhn. In all the tests shown in Figs. 7, 8, and 9, the cutting speed was 590 fpm, and the feed 25 ipm or 0.0055 in. per tooth.

Fig. 10 shows the temperature values obtained at a lower cutting speed of 80 fpm and a feed of 0.0055 in. per tooth, all conditions, excepting speed, being the same as for the tests plotted in Fig. 7. The temperatures obtained indicate that the workpiece heats up much more during the slow cut, because a greater quantity of heat can flow from the shear zone to the workpiece. It should be noted that the workpiece temperature closest to the surface and the indicated maximum surface temperature were,

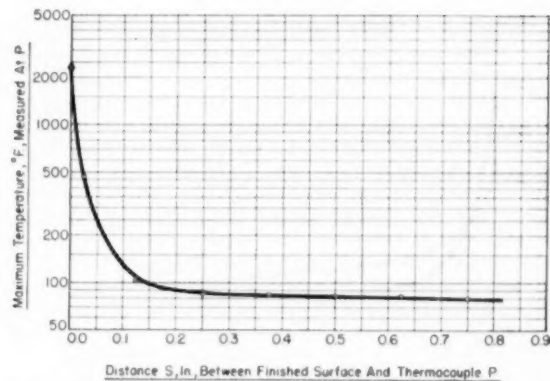


FIG. 7 MAXIMUM SURFACE TEMPERATURE OF SAE 1090 WORKPIECE, 170 BHN, AND TEMPERATURES AT DISTANCE S

(Cutting speed, 590 fpm; feed 0.0055 in. per tooth.)

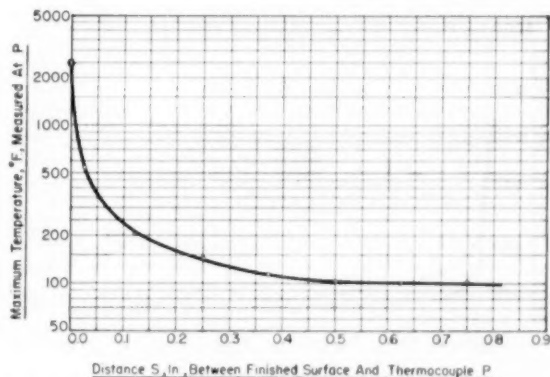


FIG. 9 MAXIMUM SURFACE TEMPERATURE OF SAE 1090 WORKPIECE, 387 BHN, AND TEMPERATURES AT DISTANCE S

(Cutting speed 590 fpm; feed 0.0055 in. per tooth.)

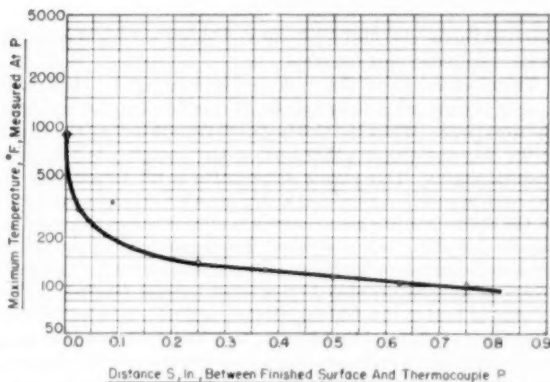


FIG. 10 MAXIMUM SURFACE TEMPERATURE OF SAE 1090 WORKPIECE, 170 BHN, AND TEMPERATURES AT DISTANCE S

(Cutting speed, 80 fpm; feed 0.0055 in. per tooth.)

however, much lower than they were at the higher speed. The slow-moving oxyacetylene flame was mounted some distance away from the workpiece to cause the same temperature rises as the cutter at 80 fpm cutting speed. In Fig. 11 are shown two tem-

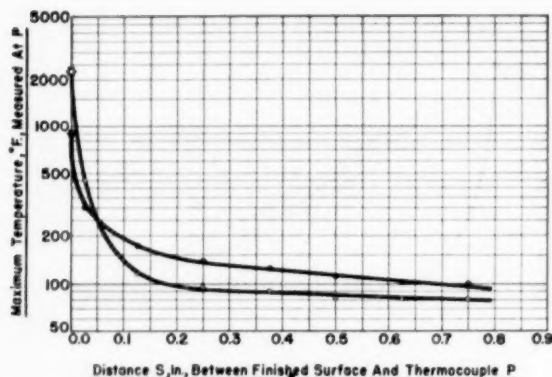


FIG. 11 MAXIMUM SURFACE TEMPERATURE OF SAE 1090 WORKPIECE, 170 BHN, AND TEMPERATURES AT DISTANCE S (Cutting speed 590 fpm [o] and, 80 fpm [—], feed 0.0055 in. per tooth.)

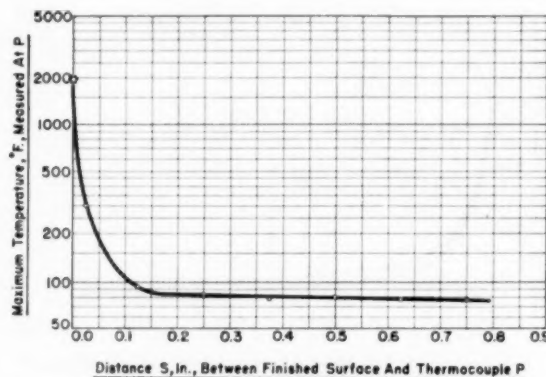


FIG. 12 MAXIMUM SURFACE TEMPERATURE OF GRAY CAST-IRON WORKPIECE AND TEMPERATURES AT DISTANCE S (Cutting speed, 590 fpm; feed 0.0055 in. per tooth.)

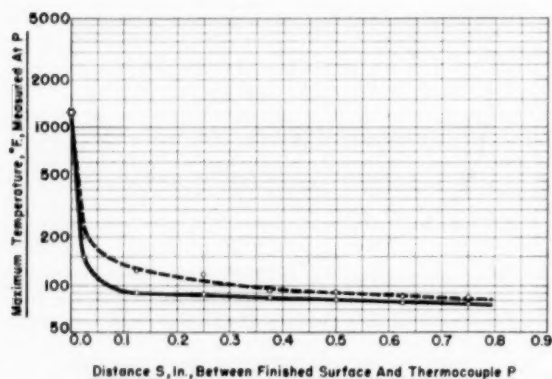


FIG. 13 MAXIMUM SURFACE TEMPERATURE OF 24S-T AL-ALLOY WORKPIECES AND TEMPERATURES AT DISTANCE S (Cutting speed, 590 fpm; feed 0.0055 in. per tooth. Solid line, sharp cutter; dashed line, dull cutter.)

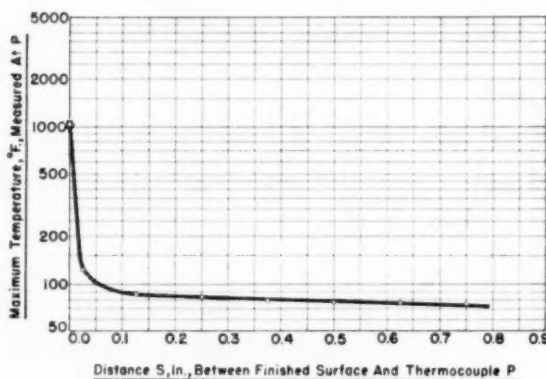


FIG. 14 MAXIMUM SURFACE TEMPERATURE OF BRASS WORKPIECE AND TEMPERATURES AT DISTANCE S (Cutting speed 590 fpm; feed 0.0055 in. per tooth.)

perature curves obtained for lower and higher cutting speeds, all other conditions being the same.

The temperature of the workpiece surface can be attributed mainly to the work done or heat evolved in forming the chip from the workpiece. When the tool begins to remove a chip, the metal in the chip and also in a thin layer in the workpiece is deformed simultaneously. This plastic deformation is the largest part of the work required in removing a chip from a workpiece and most of the work done in a metal-cutting operation occurs therefore as heat in the chip. An additional, but much smaller, source of the heat in the chip is the friction between the tool and chip which occurs as soon as the chip begins to move over the tool. The amount of heat in the chip constitutes, as a rule, between 50 and 75 per cent of the total heat in chip, tool, and workpiece together. The smaller figure of 50 per cent applies to the lower speeds; the heat in the chips increases to 75 per cent at about 200 fpm (4). At the lower speeds a measurable part of the heat from the shear zone is transferred by conduction to the workpiece since there is contact for longer periods of time. Less of this happens at higher cutting speeds.

Temperature values as obtained when milling gray cast iron are shown in Fig. 12. The effect of a worn cutter when milling 24S-T aluminum alloy is shown by the dashed line in Fig. 13 in comparison to the temperatures obtained with a sharp cutter as

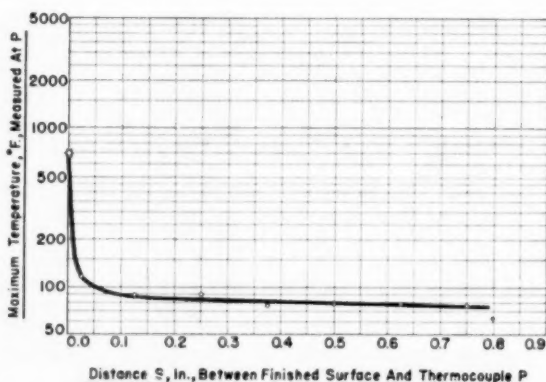


FIG. 15 MAXIMUM SURFACE TEMPERATURE OF A MG-ALLOY WORKPIECE AND TEMPERATURES AT DISTANCE S (Cutting speed, 590 fpm; feed 0.0055 in. per tooth.)

indicated by the solid line. In this case the wear could be considered minor and no difference in the cutting action had been noticed by ordinary observations. Free-machining brass, which has generally lower power requirements, also registered low tem-

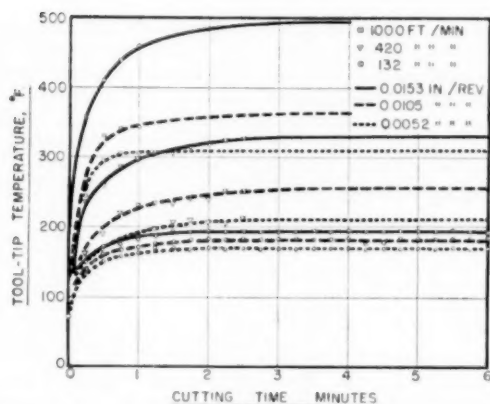


FIG. 16 TOOL-TIP TEMPERATURES AS INFLUENCED BY CHANGES IN CUTTING SPEED AND FEED WHEN TURNING MAGNESIUM

temperatures in the workpiece as can be seen in Fig. 14. Magnesium alloys are usually exceptionally easy to machine and this was confirmed by correspondingly low values of workpiece temperature measurements, Fig. 15. Although the maximum surface temperature as plotted for milling magnesium alloys is low in comparison to those for the other materials, it is much higher than the temperature measured near the tip of a lathe tool, Fig. 16, machining the same material at a comparable speed and feed (5).

COMPUTATION OF TEMPERATURES

Quantitative values of metal-cutting temperatures have been calculated by Shaw (6) based on the analysis of a moving heat source by Blok (7) and Jaeger (8). Another procedure to calculate metal-cutting temperatures as influenced by speed, feed, and physical properties of tool and workpiece materials has been proposed by Loewen (9) postulating a stationary and a moving heat source.

From a consideration of the brutish separation of the chip material from the workpiece, and the diminishing amount or degree of deformation at points successively further away from the surface, it can be concluded that a temperature gradient or differential exists across the depth of the deformed layer immediately following its formation. Although the exact manner of temperature distribution is not known, it is possible to make simple computations based on an average uniform temperature assumed to exist across this comparatively thin layer immediately after machining.

In x-ray diffraction investigations (2), the depth of penetration of plastic deformation beneath the surface of a milled workpiece was found to be several thousandths of an inch, varying with the rake angle. Under the specific test conditions—590 fpm cutting speed, 0.005 in. per tooth feed, 0.100 in. depth of cut, and 6-deg negative rake angle—the affected surface layer was 0.004 in. deep.

It has been established in correlative tests that, of the total

work expended in a metal-cutting operation under conditions similar to those existing in these tests at 600 fpm cutting speed, approximately 10 per cent of the entire energy is confined to the workpiece in the form of heat. All of this machining heat in the workpiece must be contained initially in the thin deformed surface layer for a short period of time before dispersing itself to the cooler metal beneath. Thus it is possible to compute for this layer a maximum average temperature which, although lower than the instantaneous surface temperature, at least provides an indication of the magnitude of that temperature, e.g., higher than tool-tip or surface temperatures measured during the cut. If the heat existing for a short period of time in a very small segment of the cold-worked surface layer completely insulated is considered, the results of the temperature computation will be the same.

If the surface layer is taken as a body of weight W having a mean heat capacity c_m , an initial temperature t_1 , and a maximum average temperature t_2 after introduction of a quantity of heat Q , then

$$Q = Wc_m(t_2 - t_1)$$

or

$$Q = Wc_m\Delta t$$

where

$$\Delta t = t_2 - t_1$$

Hence

$$\Delta t = \frac{Q}{Wc_m}$$

SAMPLE DATA AND COMPUTATIONS FOR SAE 1030 STEEL

For convenience, all computations are based on 1 cu. in. of steel machined:

Heat capacity at 2250 F, c_m0.165 Btu/lb deg F

Volume of surface layer in relation to 1 cu. in. of chips.....
.....(0.004 in.)(0.5 in.)(20 in.) = 0.040 cu. in.

Weight of surface volume, W
.....(0.040 cu. in.)(0.282 lb/cu in.) = 0.0113 lb

Total work....(0.96 hp/cu in./min \times 1 cu in.) = 0.96 hp min

Total equivalent heat.....
.....(0.96 hp min)(42.41 Btu/hp min) = 40.71 Btu

Heat in workpiece, Q (0.10)(40.71 Btu) = 4.07 Btu

Average maximum temperature rise in surface layer

$$\Delta t = \frac{4.07 \text{ Btu}}{(0.0113 \text{ lb})(0.165 \text{ Btu/lb deg F})} = 2183 \text{ F}$$

Average maximum temperature in surface layer

$$t_2 = t_1 + \Delta t = 70 \text{ F} + 2183 \text{ F} = 2253 \text{ F}$$

The computation of Δt involves a preliminary selection of published values for c_m until t_2 and the temperature at which c_m was determined are in reasonable agreement (see Table 1).

It will be noted that the computed temperature values listed in

TABLE 1 COMPUTED VALUES OF SURFACE-LAYER TEMPERATURES

(For cutting speed of 590 fpm, feed 0.0055 in. per tooth)

Material	Density, lb/cu in.	H at capacity, cm. Btu/lb deg F	For 1 cu in. of metal machined					Plastically Deformed Surface Layer—		
			Total energy	Heat in	Volume,	Weight,	Max avg	Max avg	Max avg	Max avg
			Hp min	workpiece, Q, Btu	cu in.	W, lb	temp rise, Δt , deg F	temp, t_2 , deg F	temp, t_1 , deg F	temp, t_2 , deg F
SAE 1030.....	0.282	0.165	0.96	40.71	4.07	0.040	0.0113	2183	2253	2253
SAE 1090, 170 Bhn.....	0.282	0.168	1.06	44.80	4.48	0.040	0.0113	2360	2430	2430
SAE 1090, 311 Bhn.....	0.282	0.170	1.17	49.60	4.96	0.040	0.0113	2582	2652	2652
SAE 1090, 387 Bhn.....	0.282	0.185	1.32	56.20	5.62	0.040	0.0113	2688	2758	2758
Cast iron.....	0.264	0.162	0.75	31.81	3.18	0.040	0.0106	1852	1922	1922
Brass.....	0.311	0.118	0.50	21.21	2.12	0.040	0.0124	1449	1519	1519
Aluminum, 24S-T.....	0.097	0.262	0.40	16.96	1.70	0.040	0.0039	1664	1734	1734
Magnesium alloy.....	0.065	0.300	0.28	11.87	1.19	0.040	0.0026	1526	1596	1596

the last column of Table 1 are higher than the flame temperatures. This is understandable, since in adjusting the flame so as to duplicate the thermocouple temperatures obtained in machining, heat was introduced into the workpiece through a much larger area of contact than was the case with the cutter and, therefore, the flame temperatures would be lower. If as a substitute for the cutting tip a smaller heat source, more closely resembling in size the heat-producing action of the cutter, could have been used, its temperature would have had to be greater in order to introduce a comparable amount of heat into the work.

The high temperatures suggested in this paper are not ordinarily noticed or measured since they are flash temperatures accompanying the generation and transfer of comparatively small quantities of heat which are generally quickly distributed throughout the large volume of the workpiece.

The temperature of the workpiece (t_1 , Fig. 5) in the last pass across a 0.025-in. thickness was determined with a fair degree of accuracy and it can be stated safely that the temperature t_2 on the surface must have been still higher. This can be verified by computing the maximum average temperature for the 0.025-in-thick remainder of the workpiece by the foregoing method of thermal balance. These computed temperatures in all cases will be greater than those determined experimentally.

Such high surface temperatures also were determined in the experiments of Bowden and Ridler (10) in which a rotating ring of mild steel was in contact with a stationary cylinder made of another metal having a melting point lower than that of steel. The maximum temperature, obtained with the thermocouple thus constituted by virtue of the dissimilar metals in contact, was the melting temperature of the metal having the lower melting point. This melting temperature could be obtained either by increasing the load on the cylinder at a definite speed or by increasing the speed while maintaining the load constant. Once the melting temperature had been reached the temperature would remain at that point whether speed or load was increased further. These tests have a definite relationship to a metal-cutting operation because two dissimilar metals, the tool and workpiece, are engaged in relative sliding movements at high speed and tremendous pressures. Fig. 17 is an illustration of the general location of heat sources in

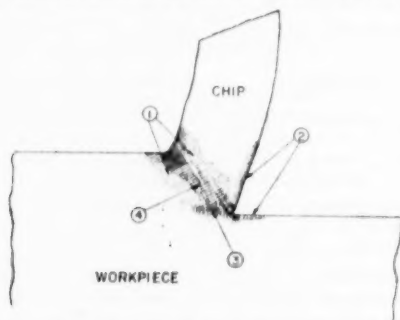


FIG. 17 HEAT SOURCES DURING CHIP FORMATION
(1, due to compression; 2, due to friction; 3, due to tear; 4 due to shear.)

chip and workpiece. The tests reported here, in which the tool material was tungsten carbide having a higher melting point than any of the workpiece materials, indicate that at the workpiece surface an instantaneous temperature exists which can be close to the melting point of the workpiece material.

The amount of heat in the workpiece has been computed by Chao and Trigger (11). Their analysis pointed out that the heat in the workpiece will decrease with increasing cutting speeds. This has been confirmed experimentally with sharp cutters. As long as the tool remains sharp the amount of heat in the work-

piece can be considered as being mainly part of that heat caused by the tool through deformation in and around the shear zone while forming a chip as illustrated in Fig. 18. However, as soon as the cutting edge begins to wear, the relief angle will be decreased and additional heat will occur in the workpiece due to friction, Fig. 19. Rate of wear at the cutting edge usually increases with harder and tougher workpiece materials and at higher cutting speeds. Generally, workpieces are large enough to

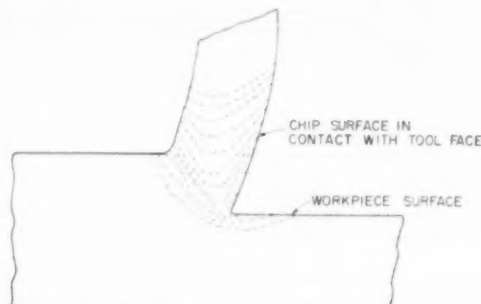


FIG. 18 THERMAL PICTURE DURING CONTINUOUS CHIP FORMATION WITH SHARP TOOL

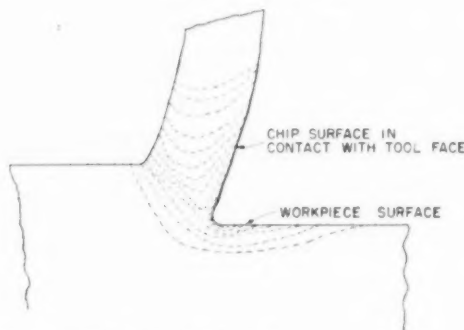


FIG. 19 THERMAL PICTURE DURING CONTINUOUS CHIP FORMATION WITH DULLED TOOL

absorb the heat of machining without detriment. Only when thin-walled sections or tough materials are machined at cutting speeds sufficiently high to entail more rapid tool wear, will the heat in the workpiece become troublesome. In such cases lower cutting speeds, more positive rake angles, and abundant application of coolants can prevent warpage and distortion.

CONCLUSIONS

Instantaneous workpiece-surface temperatures, which are much higher than measured tool-tip temperatures, can occur in a metal-cutting operation.

The surface temperatures depend upon the workpiece material being machined; those materials which require more power under otherwise identical conditions of speed, feed, depth of cut, and tool angles also will have higher temperatures at the surface and in the workpiece.

The maximum surface temperature is lower with decreased cutting speeds, but at the same time the temperatures within the workpiece are higher because a larger percentage of heat flows into the workpiece at the slower rate of separation of chips.

Extremely high cutting speeds in steel milling and in machining of other high-strength materials cause rapid deterioration at the cutting edge and therefore very high temperatures at the machined surface, which often results in warpage of the workpiece.

ACKNOWLEDGMENT

Grateful acknowledgment is made to Mr. J. R. Roubik of the author's company for his help in carrying out these tests.

BIBLIOGRAPHY

- 1 "An Investigation of Radial Rake Angles in Face Milling," by J. B. Armitage and A. O. Schmidt, *Trans. ASME*, vol. 66, 1944, pp. 633-643; *Western Metals*, vol. 3, July, 1945, pp. 11-16, August, 1945, pp. 11-16; *Mechanical Engineering*, vol. 67, 1945, pp. 403-406; pp. 453-456; pp. 507-510; *Canadian Machinery and Manufacturing News*, vol. 56, no. 9, pp. 114-116, 227; no. 10, pp. 81-84, 156; no. 11, pp. 90-93.
- 2 "X-Ray Diffraction as a Gage for Measuring Cold Work Produced in Milling," by F. Zankl, A. G. Barkow, and A. O. Schmidt, *Trans. ASME*, vol. 69, 1947, pp. 307-318; *Iron Age*, vol. 159, 1947, pp. 44-50.
- 3 "Measurements of Temperatures in Metal Cutting," by A. O. Schmidt, O. W. Boston, and W. W. Gilbert, *Trans. ASME*, vol. 68, 1946, pp. 47-49; *Tool and Die Journal*, vol. 11, 1945, pp. 115-120.
- 4 "Distribution of Heat Generated in Drilling," by A. O. Schmidt and J. R. Roubik, *Trans. ASME*, vol. 71, 1949, pp. 245-252; *The Tool Engineer*, vol. 21, 1949, pp. 20-23.
- 5 "Metal Cutting Temperatures and Tool Wear," by A. O. Schmidt, *The Tool Engineer*, vol. 29, July, 1952, pp. 33-35, and August, 1952, pp. 51-54.
- 6 "Metal Cutting Principles," by M. C. Shaw, Massachusetts Institute of Technology, 1952.
- 7 "Theoretical Study of Temperature Rise at Surfaces of Actual Contact Under Oiliness Lubricating Conditions," by H. Blok, *Proceedings of General Discussion on Lubrication*, The Institution of Mechanical Engineers, London, England, 1938, pp. 222-235.
- 8 "Moving Source of Heat and the Temperature at Sliding Contacts," by J. C. Jaeger, *Proceedings of the Royal Society, New South Wales*, vol. 76, 1942, pp. 203-224.
- 9 "Thermal Aspects of Metal Cutting," by E. G. Loewen, Dissertation, Massachusetts Institute of Technology, 1952.
- 10 "The Surface Temperature of Sliding Metals," by F. P. Bowden and K. E. W. Ridler, *Proceedings of the Royal Society, London, England*, series A, vol. 154, 1936, pp. 640-656.
- 11 "The Significance of the Thermal Number in Metal Machining," by B. T. Chao and K. J. Trigger, *ASME Paper No. 52-SA-58*; *The Engineer's Digest*, London, England, vol. 12, September, 1952, pp. 311-313.

Discussion

W. W. GILBERT.³ The author has made a noteworthy contribution to metal-cutting literature by introducing an equivalent heat source in place of the actual cutting tool. An oxyacetylene flame, moving at the same rate as the milling cutter, is adjusted to give temperature distribution in the workpiece similar to that obtained when milling. The surface temperature found by this equivalent heat method compares favorably with the computed values of temperatures except when cutting brass, aluminum, and magnesium alloy. It would be desirable to know more details on the type of oxyacetylene flame used since a relatively broad, lower-temperature flame would give considerably different surface temperatures than a concentrated flame.

Most temperature studies have been made of the temperature between the tool and the chip. It is pleasing to see the temperature on the workpiece investigated since this temperature has a direct influence upon the properties of the surface of the part being machined.

In the computations of the maximum average temperature rise, it would appear that a deformed layer on the surface of the metal having a thickness of 0.004 in. was used for the computations of heat for all of the materials listed in Table 1 of the paper. Since the chip formation is considerably different for steel, brass, and magnesium it would appear that the depth of the deformed surface would be different for these materials, and therefore the computed temperatures should vary also. It would be of interest

to know if the author's studies of depth on deformed surfaces have shown any variations between different types of materials.

In Figs. 13, 18, and 19 of the paper it has been shown that the dulling of a cutting tool affects the workpiece temperature. This would indicate that rubbing on the flank of the tool has a definite influence upon work at the point of the tool and the subsequent temperature. It would be of value to our metal-cutting science to have this type of analysis further investigated, since most of the previous work has considered only the work and temperatures of shear, and of friction between tool and work.

V. PASCHKIS.⁴ The problems of heat generation and temperature distribution in cutting operations are of great importance but difficult to solve. Change in thermal properties and change of geometric configuration are but two of the factors involved which make computation difficult. The rapid change of temperature, the steep temperature gradients, and the difficulties of surface-temperature measurements make an experimental approach difficult.

Therefore, any attempt at an analysis, such as the one presented in this paper, is most welcome. The writer would like to take exception to one concept only. The author states that the heat in the workpiece due to machining must be contained initially in the thin deformed layer.

Heat is generated at the surface continuously during the cutting operation; this heat generation results, of course, in an increase in surface temperature. Disregarding the heat loss to the surrounding air, the heat generated at the surface flows into the workpiece, heating first the thin deformed layer; but as soon as its temperature rises, heat flows to layers deeper in the workpiece. Thus at no time will the heat due to machining be contained in the deformed layer. If this concept of the author must be discarded, the corresponding correlations do not hold.

K. J. TRIGGER⁵ AND B. T. CHAO.⁶ The author has presented another interesting and thought-provoking paper on the problems of heat in metal cutting. Such a study is of definite interest because residual stresses existing in a machined surface are influenced not only by the mechanism of plastic deformation but also by the temperature gradient. The method of simulating cutting-tool heat effects by means of a torch is intriguing, and it suggests other means of studying the heat problem. This paper, like many previous publications by the author, contributes to the basic information on the heat-flow phase of metal-cutting science.

That the average chip temperature increases with finer feeds is readily confirmed by consideration of the fundamental aspects of chip formation. Limiting the case to the formation of a type-2 chip (a built-up edge introduces continually varying conditions in chip formation), a decrease in feed increases the shearing strain significantly; over 35 per cent as the feed is decreased from 0.0126 ipr to 0.0025 ipr in lathe turning. Since the temperature rise at the shear zone is proportional to the shearing strain, and since most (75 to 90 per cent) of the total heat in the chip is due to chip shear, it follows that the average chip temperature increases with a decrease in feed. Similarly, a decrease in cutting speed increases the amount of shear-zone heat because of the increase in shearing strain. Since there is more shear-zone heat, and since more time is allowed for heat transfer to the workpiece, one would expect more heat in the workpiece at lower speeds and/or feeds.

⁴ Technical Director, Heat and Mass Flow Analyzer Laboratory, Department of Mechanical Engineering, Columbia University, New York, N. Y. Mem. ASME.

⁵ Professor of Mechanical Engineering, University of Illinois, Urbana, Ill. Mem. ASME.

⁶ Assistant Professor of Mechanical Engineering, University of Illinois, Urbana, Ill.

³ Professor of Production Engineering, University of Michigan, Ann Arbor, Mich.

It is gratifying to note that the author's experimental results reveal that an extremely steep temperature gradient usually exists momentarily at the surface of the workpiece, and that increases in cutting speed and/or feed decrease the proportion of total heat which goes into the workpiece.

With reference to the calculation of surface temperatures as reported in Table 1 of the paper, there are some speculative points which need further discussion. The writers are aware that the author considers some of the assumptions to be of questionable validity and they offer the following comments as suggestions:

It was assumed that the deformed layer on the workpiece surface and the thermal layer were of the same thickness and that a uniform temperature existed across this layer immediately after machining. Thermal energy in a metal manifests itself by vibration of the atoms within the lattice and by vibration of the lattice as a whole. This vibrational response to an energy input is virtually instantaneous, of the order of 10^{-13} second. The specific heat of a metal is a measure of the number of ways by which it can absorb energy, including transformational effects as well as vibrations. It follows, then, that the temperature rise caused by plastic deformation is virtually coincident with the deformation, and that the specific heat varies continuously and instantly over the temperature range involved. This interpretation has been employed by the writers in a previous paper.⁷

As a consequence of the foregoing argument, it is reasonable to consider the deformed layer and the thermal layer to be the same, but only in so far as the heat due to workpiece deformation is concerned. Whether it is equally reasonable to assume that a uniform temperature exists across the thin layer of deformed metal, depends upon the uniformity of plastic deformation.

If the workpiece is heated entirely by deformation work expended in the surface layers, the author's assumptions are justifiable. However, he states that 10 per cent of the total work in cutting goes into the workpiece and cites previous results derived from drilling tests on magnesium alloys. To what extent this same proportion is applicable to cast iron, brass, aluminum alloys, and steels is not known accurately. Furthermore, in discussing the milling results of SAE 1090 steel bars of various hardness, the author offers the explanation, "The temperatures obtained indicate that the workpiece heats up much more during the slow cut, because a greater quantity of heat can flow from the shear zone to the workpiece." This means that the temperature rise of the workpiece material is, in part, due to the flow of heat from the source at the shear zone. Hence, in the author's interpretation, deformation work expended in the thin surface-layer material constitutes only a part of the sensible heat in the workpiece. As a consequence, calculations based on the author's assumption necessarily must be in error to an extent not answerable at present.

Huxley once said that what one could get out of the mathematical mill depended solely on what one puts into it. This appears to be the case in the computations of the surface-layer temperatures as listed in Table 1. Consider the foregoing comments regarding variability of the specific heat in the sample calculation for 1030 steel. The specific heat is taken as 0.165 Btu/lb deg F at 2250 F. This is, according to the Metals Handbook,⁸ the specific heat of gamma iron at 2192 F and does not represent the conditions existing during the heating from room temperature of

the surface layer. If one uses the varying specific heat and includes transformational effects (where the specific heat is momentarily infinite), the maximum surface temperature in the sample computation is approximately 1920 F. The effect of such considerations in the specific heat is evident in Table 1 where the reported surface temperatures in the harder steels and in the aluminum and magnesium alloys are considerably above the melting point (in some cases about 400 F) of the alloy.

Two other points are suggested for further study. More quantitative data are needed on other materials and cutting conditions in so far as the proportion of heat to the workpiece is concerned, and additional work is necessary concerning the thickness of the affected workpiece layer. It does not appear that all metals are affected to the same depth because of varying mechanical properties and chip-formation characteristics.

The writers question the significance of Fig. 16 of the paper, since it represents results obtained under conditions entirely different from those present during metal cutting. A temperature extrapolated from a measured value 0.060 in. from the source of heat under cutting conditions with an extremely steep temperature gradient is a hazardous procedure.

In summary, the writers feel that the author has contributed another important paper to metal-cutting science. The existence of "flash" temperatures is a real probability, though it might be argued that the existence of such high temperatures, even for a short time, would result in recrystallization of the distorted and work-hardened surface and therefore would remove the efforts of such plastic deformation. Metallographers have estimated that the surface layers of specimens of steel may attain temperatures of 1000 deg C (1832 F) during the polishing operation. Thus the existence of flash temperatures of a comparable magnitude in the workpiece surface during machining are not unexpected. The author has presented a number of challenging problems, the solutions of which will lead to a better understanding of metal-cutting science. The writers offer their warm congratulations.

AUTHOR'S CLOSURE

The comments in the discussion are highly appreciated since they are helpful in an understanding of the scope of this experimental investigation. While we speak generally of metal cutting, experimental data can be accepted only within definite limits and generalization can be made only within clearly stated boundaries.

Professor Gilbert correctly pointed out that the depth of deformation should be different for various materials. This was not considered in the computation for temperatures since we did not have enough values for the depth of deformation of all materials used in these milling tests. The 0.004 in. depth of deformation is for mild steel at the speeds and feeds used. These computations for maximum temperature were carried out and included in the paper only because they did come close to the oxyacetylene-flame temperatures in the "equivalent" heat source. Although these experimental and computed temperature values can be disputed, this report attempts to show heat and temperature relations in a metal-cutting operation not considered before. It is hoped that some better analysis, e.g., by Dr. Paschke on the Heat and Mass Flow Analyzer, will be carried out to ascertain more accurate numerical values of these phenomena.

Professors Trigger and Chao also made a valuable contribution to this paper by their discussion. Their statements further indicate how much more we still have to learn about the whole problem and the methods of attack.

⁷ "An Analytical Evaluation of Metal-Cutting Temperatures," K. J. Trigger and B. T. Chao, *Trans., ASME*, vol. 73, 1951, pp. 57-68.

⁸ American Society for Metals, Cleveland, Ohio.

Creep of Neoprene in Shear Under Static Conditions; Ten Years

By W. NEWLIN KEEN,¹ WILMINGTON, DEL.

This paper, representing more than a decade of research on the static creep of neoprene vulcanizates, supplements a previous paper by the author. The test procedure is given, and the effects of composition, age, and temperature on the creep characteristics of the vulcanizates are reported. The author's data indicate that neoprene vulcanizates can be designed with creep-resistant properties equal to or superior to those of natural rubber.

INTRODUCTION

IN 1945 the author presented a paper² showing the results of static creep tests conducted at room temperature extending over a period of 3 years, 9 months. That report shows how the creep in shear of neoprene vulcanizates, in the hardness range of 40 to 60 durometer (Shore Type A), is influenced by:

- 1 Degree of vulcanization.
- 2 Preconditioning in shear at elevated temperatures.
- 3 Change in composition.

These tests have been continued, and this paper presents the results obtained during a period of nearly 11 years. The effects of natural aging for this period of time on some of the mechanical properties of the vulcanizates also are included. The study has been extended for some of the vulcanizates to include the effect of changes in test temperatures.

TESTING PROCEDURE

The test method described in the original paper is briefly summarized here. Yerzley shear specimens (ASTM D945)³ were tested under a constant stress of 17.75 psi and at a controlled temperature of 82 F \pm 2 F. (In 1948 the temperature of the physical testing room was reduced to 75 F \pm 2 F.) Fig. 1 is a schematic sketch showing the details of the loading bar with its knife-edge construction and adjustable linkage which permit the bar to be leveled as creep takes place in the specimen. Creep in inches is measured by a dial gage (0.001 in.) equipped with a special jig. The data from the long-time creep test are expressed in terms of per cent relative creep, defined as follows:

Per cent relative creep

$$= \frac{\text{Total deformation} - \text{initial deformation}}{\text{Initial deformation}} \times 100$$

Initial deformation is defined as the deformation obtained 5 min after loading.

¹ Organic Chemicals Department, Rubber Chemicals Division, E. I. du Pont de Nemours & Company, Jun. ASME.

² "Creep of Neoprene in Shear Under Static Conditions," by W. N. Keen, Trans. ASME, vol. 68, 1946, pp. 237-240.

³ American Society for Testing Materials Method D945-52T, Standards on Rubber Products, prepared by ASTM Committee D-11.

Contributed by the Rubber and Plastics Division and presented at the Annual Meeting, New York, N. Y., November 30-December 5, 1952, of THE AMERICAN SOCIETY OF MECHANICAL ENGINEERS.

NOTE: Statements and opinions advanced in papers are to be understood as individual expressions of their authors and not those of the Society. Manuscript received at ASME Headquarters, December 16, 1952.

In the original paper the creep data were plotted using log-log co-ordinates. The effect of such co-ordinates in condensing the time scale makes it difficult to assess properly the value of tests in which the important variable is the length of time of the testing period. Therefore the long-time creep data are plotted as per cent relative creep versus time, using rectangular co-ordinates.

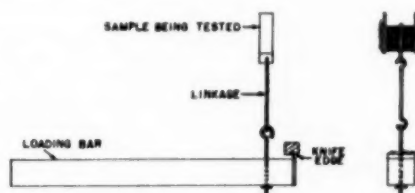


Fig. 1 TESTING APPARATUS

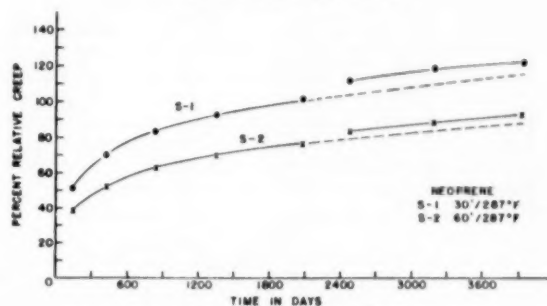


Fig. 2 INFLUENCE OF CURE ON CREEP OF NEOPRENE

FACTORS AFFECTING CREEP CHARACTERISTICS

Degree of Vulcanization. Fig. 2 shows the influence of the degree of vulcanization on the static creep characteristics of a neoprene composition. It will be noted that each of the curves shows a discontinuity between 2100 and 2400 days. In view of all data collected in this study, it is believed that this break in the curve was caused by an external disturbance to the specimen and not by the shearing stress. Therefore the original curve is continued as a broken line to indicate the probable per cent relative creep which would have been obtained had no outside disturbance occurred. As the degree or state of vulcanization is increased (S-1 versus S-2 in Fig. 2) the rate and magnitude of the per cent relative creep are decreased. This confirms the conclusions drawn in the original paper. These curves clearly indicate the importance of curing neoprene to a high state of vulcanization for applications requiring low creep.

Preconditioning to Reduce Creep. Another way to reduce the creep of some vulcanizates is by the preconditioning method. Preconditioning of the neoprene (S-3D) and the natural rubber (S-7D) specimens, shown in Fig. 3, consisted of straining them 30 per cent in shear and heating them in this condition for 24 hr at 158 F. After heating, the specimens were removed from the jig and permitted to rest for 1 week at 82 F before being mounted

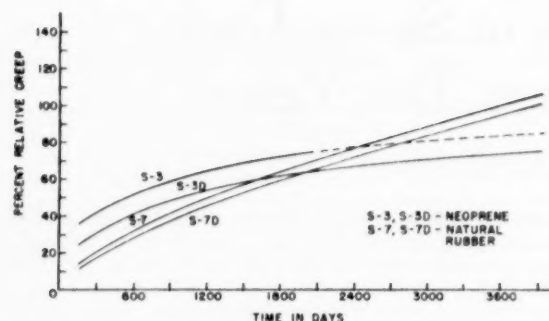


FIG. 3 EFFECT OF PRECONDITIONING ON CREEP

on the static-creep test stand. Fig. 3 indicates that this type of preconditioning reduced the magnitude of the creep for both neoprene and natural-rubber vulcanizates. For the particular vulcanizates studied, the effect of preconditioning is considerably greater for the neoprene than for the natural-rubber stock. It appears that preconditioning offers some possibilities in developing products having maximum resistance to creep.

Effect of Changing Composition. The rubber technologist has two methods of changing the composition of his products.

TABLE 1 IDENTIFICATION OF COMPOUNDS

Specimen	ASTM grade no.	Cure, min/deg F	Hardness Shore A	Per cent set, ASTM method B
S-1	SC-425	30/287	44	39
S-2	SC-525	60/287	46	25
S-3	SC-525	30/307	47	24
S-7	RN-530	15/287	46	24
S-8	SC-614	40/307	59	32
S-11	RN-540	25/287	50	19
S-12	SC-535	25/307	48	9
S-13	SC-539	25/307	51	10
S-14	SC-540	25/307	55	25
S-15	SC-425	45/307	43	16
S-16	SC-530	45/307	46	7

TABLE 2 EFFECT OF NATURAL AGING ON MECHANICAL PROPERTIES

Specimen	Resilience, per cent at 20 per cent deformation	Frequency, cycles/min	Static modulus, psi At 5 per cent deformation	Static modulus, psi At 20 per cent deformation	Stress, psi, at 20 per cent deformation	Effective dynamic modulus, psi
Shear characteristics—original						
S-1	85	167	100	106	20	116
S-2	86	169	120	107	22	119
S-3	87	176	115	105	22	129
S-7	90	161	121	125	25	131
S-8	80	202	150	145	30	206
S-11	87	150	87	80	18	94
S-12	80	169	103	92	21	118
S-13	81	175	115	103	22	128
S-14	84	175	148	132	29	156
S-15	89	163	114	106	23	110
S-16	84	159	102	100	21	102
Shear characteristics after 10-year 9-month static-creep test						
S-1	88	170	125	120	26	134
S-2	88	172	130	125	26	136
S-3	87	172	125	125	26	136
S-7	84	173	125	120	26	138
Shear characteristics after 10-year 9-month aging in unstressed condition						
S-1	90	170	140	125	26	133
S-2	89	170	140	125	25	133
S-3	90	170	125	120	26	133
S-7	85	173	125	125	27	138

One consists of using different elastomers and the other of using different compounding materials. Table 1 classifies, according to ASTM D735⁴ (SAE-10R),⁵ compositions which have been varied by both of these methods. The data plotted in Fig. 4 show the effect of some of these changes in composition on the creep char-

⁴ American Society for Testing Materials Method D735-52T, Standards on Rubber Products, prepared by ASTM Committee D-11.

⁵ "Rubber and Synthetic Rubber Compounds for Automotive and Aeronautical Applications," SAE Handbook 1952, pp. 243-249.

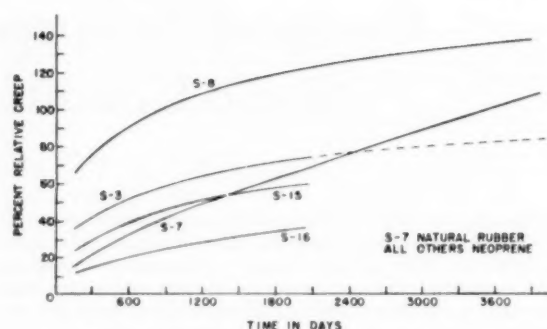


FIG. 4 INFLUENCE OF COMPOSITION ON CREEP

acteristics of the vulcanizates. The most startling variation due to composition is seen in the latter portions of the curves. Beyond approximately 1200 days, the rate of change of relative creep is much less for all neoprene stocks studied than it is for the rubber control specimen (S-7). In fact, this difference is so pronounced that the final values of the per cent relative creep of the rubber stock exceed those of specimens S-3 and S-15, although, in the earlier stages of these tests, its per cent relative creep was lower.

The numerical values for creep at the end of 10 years, 9 months are given in Table 3. The specimen S-16 represents a change in the type of neoprene used, whereas stocks S-3, S-8, and S-15 represent compounding changes with the same neoprene. (The data on specimen S-8 may be influenced by a lower state of vulcanization than exists in the other neoprene stocks.) It will be noted from Table 1 that stock S-16 has a very low compression set and this, coupled with its excellent resistance to creep, undoubtedly will make this type of composition of great interest to the design engineer.

EFFECT OF AGE ON PROPERTIES

Engineers always are interested in learning how age affects the materials with which they are working. Unfortunately, the amount of data available on long-time natural aging is limited, and, in general, both the engineers and the rubber technologists must draw their conclusions from accelerated aging tests. Since the creep tests represented in this paper extend over a period of 10 years, 9 months, they afford an excellent opportunity to ascertain the effect of this period of natural aging on the mechanical

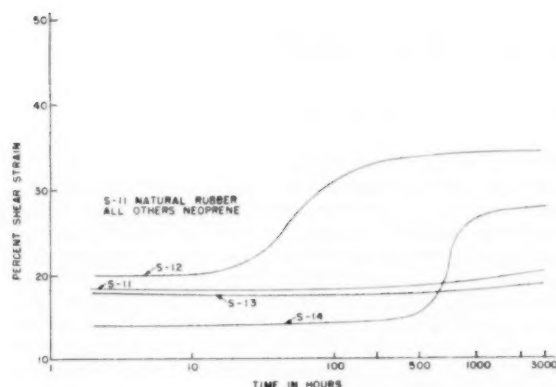


FIG. 5. NEOPRENE VERSUS RUBBER MOUNTINGS, 32 F

properties of the vulcanizates. These data are summarized in Table 2 which is similar in form to Table 2 in the earlier paper.² Table 2 of this paper shows the original mechanical properties of the shear specimens, how these properties changed while on the creep test stand, and how they changed in specimens of the same vulcanizates while stored in an unstressed condition for the same period of time. The data indicate that all vulcanizates

TABLE 3. STATIC CREEP CHARACTERISTICS IN SHEAR
(Under stress of 17.75 psi)

Specimen	Initial deformation, in. (5 min)	10 years and 9 months	
		Creep, in.	Per cent relative creep
S-1	0.0930	0.1128	121.1 (115) ^a
S-2	0.0858	0.0847	98.7 (87) ^a
S-3	0.0883	0.0840	95.2 (84) ^a
S-7	0.0707	0.0760	107.5
S-8	0.0591	0.0809	136.9
5 years and 7 months			
S-15	0.0761	0.0426	55.2
S-16	0.0853	0.0312	36.6
Specimen	Initial deformation, in. (2 hr at 32 F)	3200 hr at 32 F	
		Final deformation, in.	Shear strain, per cent
S-11	0.0925	0.0980	19.6
S-12	0.1050	0.1710	34.2
S-13	0.0840	0.0945	18.9
S-14	0.0700	0.1390	27.8
Specimen	Initial deformation, in. (2 hr at 200 F)	1416 hr at 200 F	
		Final deformation, in.	Shear strain, per cent
S-11	0.0965	0.2212	44.2
S-12	0.0820	0.1424	28.5
S-13	0.0739	0.1240	24.8
S-14	0.0619	0.1441	28.8

^a Values from curves.

tested have such excellent resistance to natural aging that changes due to this element would have little bearing on their utility. This conclusion appears to be valid for both the specimens aged under stress and those which were aged in an unstressed condition. The compression characteristics of some of these vulcanizates are given in the earlier paper.²

EFFECT OF TEST TEMPERATURE

With increasing use of elastomers in the automotive and aeronautical fields, a study of the effect of the temperature at which the product must operate has become increasingly important. Since elastomeric springs or mountings are subjected to various temperatures in service, creep tests were conducted at 32 F and 200 F under the same stress (17.75 psi) as the room-temperature tests.

The results of these tests are plotted as change in per cent

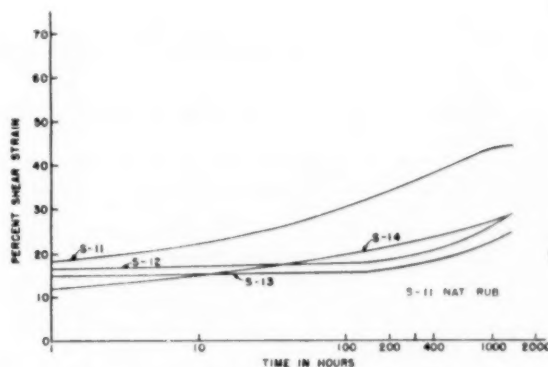


FIG. 6. NEOPRENE VERSUS RUBBER MOUNTINGS, 200 F

shear strain versus time in hours on semilog co-ordinates. These data are plotted in this manner instead of by the per cent relative-creep method because of the thermoclastic characteristics of elastomers and the relative long time (1 hr) required for the specimen to reach temperature equilibrium. From Fig. 5 it will be noted that two of the neoprene specimens (S-12 and S-14) show a delayed strain relaxation, previously reported by Morris and James.⁶ The third neoprene specimen (S-13) does not show this effect. It has not only less shear strain than the rubber control, but maintains this advantage throughout the duration of the test—3200 hrs.

The effect shown by specimens S-12 and S-14 is primarily the result of crystallization of the vulcanizates. Crystallization is a reversible process, and the vulcanizate returns to its original state when heated to a degree slightly above room temperature, either by changing the ambient temperature or by mechanical working of the vulcanizate. The specimen S-13 is based upon a type of neoprene designed to be extremely resistant to crystallization. Fig. 6 shows the creep characteristics or strain relaxation of these same compounds at 200 F. It is noted that natural rubber exhibits higher creep or greater strain relaxation at 200 F than any of the neoprene specimens. Neoprene mountings, represented by S-13 (see Figs. 5 and 6) undoubtedly will be of great interest to the design engineer because of their outstanding performance over a wide range of temperature (32 F to 200 F). The room-temperature creep characteristics of this vulcanizate will be equivalent to or better than those of specimen S-16, Fig. 4.

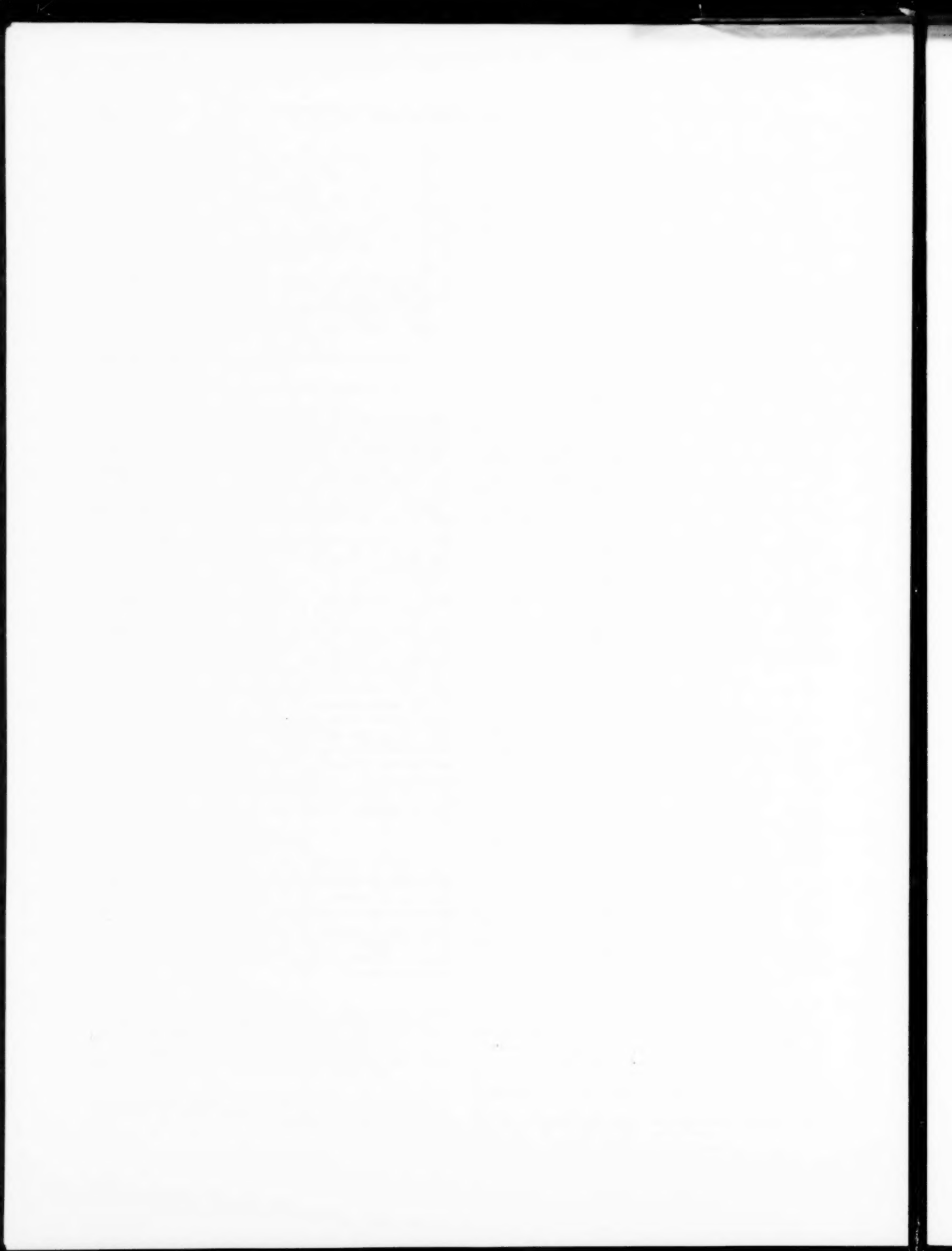
CONCLUSION

In summary, the data indicate clearly that neoprene vulcanizates can be designed to have resistance to creep equal to or better than that of natural rubber. Neoprene specimen S-13 shows outstanding performance over a range of temperatures. These facts, coupled with the well-known excellent resistance of neoprene vulcanizates to oil, heat, ozone, and natural aging, should enhance the value of this material in the eyes of the design and application engineer.

ACKNOWLEDGMENT

The author takes pleasure in acknowledging the important contributions of A. M. Neal, of the Rubber Chemicals Division, E. I. du Pont de Nemours & Company, to the progress of this work. The author is indebted also to M. A. Gass who made most of the measurements.

⁶ "Behavior of Neoprene Vibration Isolators at Various Temperatures," by R. E. Morris and R. R. James, *Rubber Age*, New York, N. Y., vol. 71, 1952, pp. 625-628.



Stress-Crazing of Plastics

By J. A. SAUER¹ AND C. C. HSIAO,² STATE COLLEGE, PA.

The effect of various factors on the inception and growth of crazing is reviewed and some of the similarities between crazing in plastics, exposure-cracking in rubber, and stress-cracking in metals are described. Various examples of stress-crazing in transparent plastics are presented and the stress-strain behavior reported for crazed, noncrazed, and oriented material. Rate of propagation of crazing also has been investigated. The test results indicate that penetration of crazing cracks in polystyrene can be represented over a limited stress range by a linear function of both time and stress magnitude. Some measures advocated for avoiding the undesirable effects of crazing include use of special coatings, annealing, and establishment of working stresses based on onset of crazing rather than on static fracture.

INTRODUCTION

THE onset of crazing in transparent plastics is an undesirable feature that greatly limits their use in engineering applications. Various factors, such as temperature, time, orientation, environment, and so on, have an influence on the initiation of crazing, but local stress intensity is probably more directly responsible for its occurrence and subsequent propagation than any other factor. The present investigation will therefore be concerned largely with this aspect although the effect of other variables will be reviewed briefly. Considerable information concerning the cause of crazing and its influence on subsequent behavior has been reported recently in the scientific literature (1, 2, 3, 4).³

Crazing in plastics has been defined as visible mechanical cracks (2) or as submicroscopic failures that result in a noticeable "blushing" of an otherwise transparent material (4). The term "crazing" also has been used to refer to a type of cracking produced randomly on the surface of unstretched rubber by light in the presence of ozone (5). This phenomenon, however, also has been referred to by other terms, such as "sun-cracking," "atmospheric-cracking," "ozone-cracking," or "exposure-cracking." Newton (6), for example, has described as exposure-cracking the fissures formed in the surface of rubber at right angles to the direction of applied stress.

In the field of metallurgy, a closely related phenomenon to crazing is the cracking of metals or alloys when stressed under certain conditions. Stress-corrosion-cracking of metals and alloys, and season-cracking of nonferrous metals, both of which have been studied intensively, are somewhat similar phenomena to crazing in that failure seems to be related to applied or induced stress. In metals, it is well known that cracks or fissures may be produced by rapid changes in temperature and these are believed to result from development of induced thermal stresses. Cracks

or local fissures also can be produced in rubber by exposure to ozone, but the phenomenon is greatly accentuated by the presence of an applied-stress system.

In all instances where crazing cracks are caused by direct action of an applied-stress system, the cracks formed are at right angles to the maximum tensile-stress direction. When stress is not applied directly, randomly directed crazing patterns can be produced and have been reported to occur in thermoplastic materials by solvent action, by x-radiation, and by ultraviolet radiation. In all these instances, stress does not seem to be directly involved. However, the possibility of the development of quite large localized internal stresses by any of these processes must not be overlooked. If such internal stresses are great enough to exceed the local failure strength of the material, crazing will result. Crazing patterns produced both by applied stress and indirectly by solvent action have been reported by Russell (2) and by Maxwell and Rahm (7).

The precise mechanism whereby solvents such as kerosene or benzene cause crazing cracks to originate and grow is not yet well established. It is generally thought that the effect depends on absorption of the solvent by the material. Absorption softens the surface and may result either in some of the material reaching a critical elongation sooner or in causing a greater share of stress to be carried by surrounding material thus tending to produce local fissures, or openings. Another possibility is that as the absorbed solvent evaporates the surface material will tend to shrink and thereby produce internal tensile stresses sufficient to cause cracks to open up. Regardless of the precise mechanism, the crazing pattern would be expected to differ from that obtained by action of an applied tensile stress in that the cracks or crazing planes no longer should form a regular parallel system, but should be directed randomly. Such, indeed, is the case as has been shown by Russell for specimens of methyl methacrylate (8).

For a given applied-stress magnitude, crazing appears to increase with duration of test (7, 9) and hence with creep elongation. Crazing also increases with increase of temperature. For polystyrene specimens, this effect has been shown by Maxwell and Rahm (7) for various temperatures from 30 to 70 C, for a stress level of 3600 psi and for various times from 5 min to 1/2 hr.

Crazing in transparent plastics also has been reported (4) to be related to orientation. On a submicroscopic scale, it is believed that crazing cracks originate as separations of adjacent regions of polymer chains as a direct result of the applied local force exceeding the secondary attractive forces. It is therefore to be expected that in a highly oriented material subjected to applied stress in the direction of orientation little or no crazing would occur since the applied forces would tend to draw the chains together rather than to separate them. This effect has been observed experimentally by Bailey (10) and by Cheatham and Dietz (11). If, however, in the same highly oriented material, the stress were applied at right angles to the direction of orientation, the chain separation should occur more easily and crazing should begin at even low stress levels.

DEPENDENCE OF CRAZING ON APPLIED STRESS

Observation of crazing in specimens subjected to applied loading reveals that the observed crazing cracks generally start on the surface and propagate in a direction perpendicular to the direction of maximum tensile stress. If a transparent plastic specimen is

¹ Professor of Engineering Mechanics, The Pennsylvania State College.

² Associate Professor of Engineering Research, The Pennsylvania State College.

³ Numbers in parentheses refer to Bibliography at end of paper. Contributed by the Rubber and Plastics Division and presented at the Annual Meeting, New York, N. Y., November 30-December 5, 1952, of THE AMERICAN SOCIETY OF MECHANICAL ENGINEERS.

NOTE: Statements and opinions advanced in papers are to be understood as individual expressions of their authors and not those of the Society. Manuscript received at ASME Headquarters, October 25, 1952. Paper No. 52-A-100.

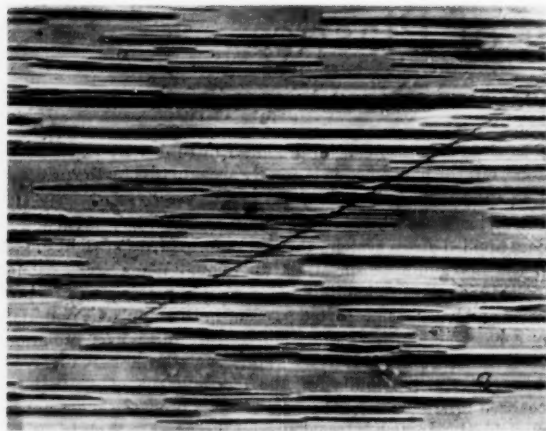


FIG. 1 CRAZING CRACKS OF LUCITE VIEWED ON MOLDED SURFACE BY TRANSMITTED LIGHT
(Diagonal mark is scratch. Applied stress, vertical; $\times 100$.)

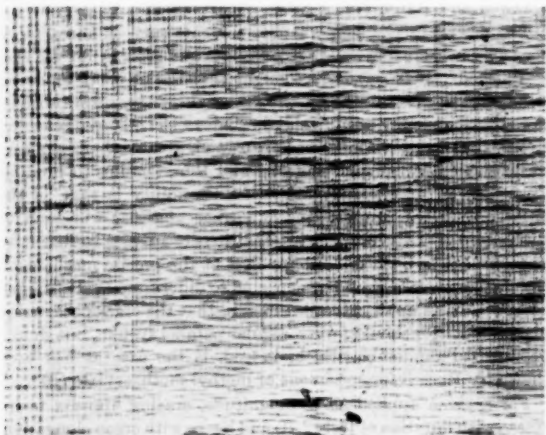


FIG. 2 CRAZING CRACKS OF LUCITE VIEWED ON MACHINED SURFACE BY TRANSMITTED LIGHT SHOWING FINE CRACKS IN HORIZONTAL DIRECTION
(Vertical lines are machine marks. Applied stress, vertical; $\times 100$.)

subjected to uniaxial tension, crazing planes will develop and grow at right angles to the direction of stressing. These crazing planes appear simply as parallel lines when viewed from their side. Micrographs indicating this behavior for polymethyl methacrylate are shown in Figs. 1 and 2.

In Fig. 1 it will be noted that many crazing cracks originate along the diagonal scratch indicating the favorable effect of stress concentration on the initiation of crazing. Also, in Fig. 2 numerous fine crazing cracks are found to commence along the machine marks. This again indicates that crazing is more easily initiated when a local discontinuity in the surface introduces a high stress-concentration factor and a resulting local stress considerably higher than the average stress in the specimen. This is what occurs at all outside edges of specimens where surface irregularities are unavoidable and hence we should expect that crazing usually will occur first on the external surfaces.

Fig. 3 shows a stress-crazing pattern for a section of a polystyrene specimen. The original specimen was $\frac{1}{2}$ in. \times $\frac{1}{2}$ in. in cross section and subjected to a constant tensile stress in its longitudinal direction. The micrograph shown is a transverse view of a

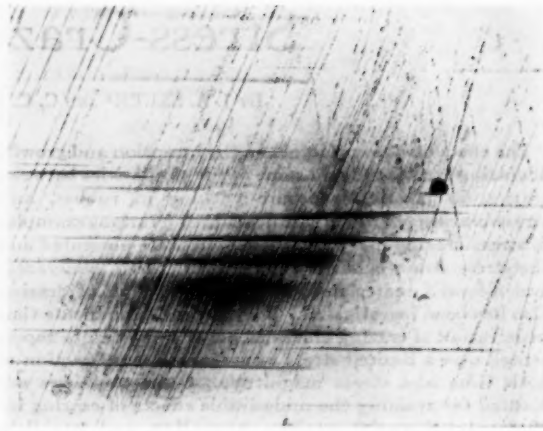


FIG. 3 CRAZING CRACKS OF POLYSTYRENE VIEWED BY TRANSMITTED LIGHT
(Direction of stress application, vertical. Inclined lines are polishing marks; $\times 100$.)

longitudinal section taken midway between the vertical surfaces. The inclined lines are polishing marks on the cut surface and the horizontal lines show the edge of the crazing planes. Some of these crazing planes have originated on the outside surface and have propagated to the interior of the specimen. However, new crazing planes not originating on the surface evidently have been formed also.

If a test specimen is subjected to a tensile load which is maintained constant until fracture occurs, then its fracture surface will show crazed regions along the external edges, and noncrazed or amorphous regions in the interior of the specimen. Fig. 4 shows such a partially crazed $\frac{1}{2}$ -in. \times $\frac{1}{2}$ -in. polymethylmethacrylate specimen. The crazing cracks are clearly visible throughout the reduced gage length of the test specimen. The relative amounts of crazed and noncrazed regions depend on the duration of test before fracture occurred.



FIG. 4 CRAZED TENSION-CREEP SPECIMEN OF POLYMETHYL-METHACRYLATE

In Fig. 5 are shown stress-crazing patterns for several polystyrene specimens with different percentages of crazed and amorphous regions. Two distinct types of crack patterns are visible in Fig. 5; one type is the fracture-crack system spreading radially outward from the more or less point source (presumably an internal impurity or flaw) located in the center of the circle on the fracture surface; the second type is the much finer crazing-crack system spreading normally inward from the surfaces of the specimen. The depth to which these crazing planes extend and the rate of penetration of these planes depend on the magnitude of the applied stress as well as on its duration, and appropriate quantitative relations for this variation are given later.

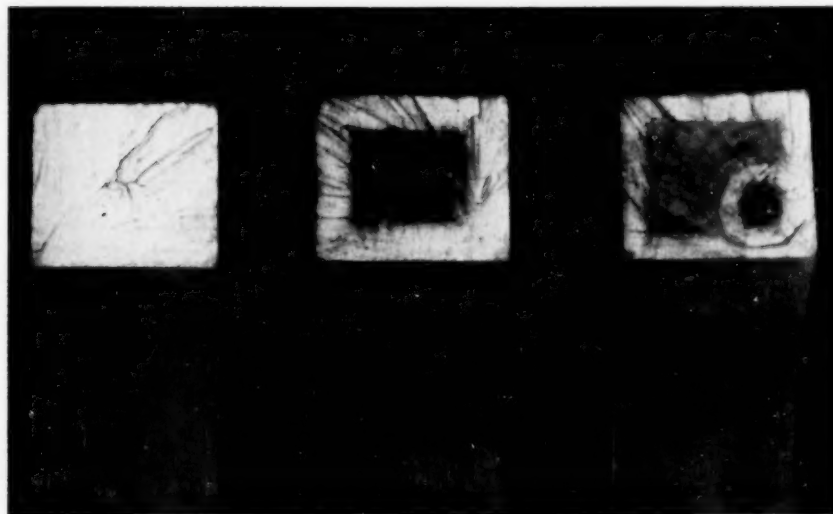


FIG. 5. FRACTURE SURFACES OF CRAZED TENSION-CREEP SPECIMENS OF POLYSTYRENE SUBJECTED TO DIFFERENT STRESSES AND DIFFERENT DURATIONS OF LOAD APPLICATION



FIG. 7. CRAZED TENSION-COMPRESSION SPECIMEN OF POLYSTYRENE

The qualitative dependence of crazing on stress magnitude and on duration of test is as follows: For comparable time periods of testing, crazing will increase with increase of applied tensile stress, and for comparable tensile stresses, crazing will increase with increase of time of testing period. Maxwell and Rahm (7) have noted that for thermal clean stress-free specimens of polystyrene no crazing at all as measured by reflected light intensity will occur until a tensile strain of 0.75 per cent is reached, but that the amount of crazing would increase rapidly as the strain was increased beyond that value. The variation of crazing with time for specimens subjected to constant load has been reported by Maxwell and Rahm (3) to be linear for times up to several hundred minutes. Sauer, Marin, and Hsiao (9) have reported that for polystyrene specimens under high tensile-stress loading, fracture occurred shortly after load was applied, with only slight or insignificant amounts of crazing around the edges of the specimen. For lower stress magnitudes, they reported that for some specimens fracture did not occur until hundreds of hours had elapsed and that crazing had by then extended over the entire cross section (as in the left diagram, Fig. 5).

It should be emphasized that crazing does not depend only on stress and time but also on the particular material under investigation. For example, for comparable stress and time as well as surface conditions, crazing cracks in polymethyl-methacrylate specimens are usually larger and less dense than those in polystyrene specimens, but at the same time do not extend as far from the surface. These characteristics may be seen by comparison of the stress-crazing patterns of Fig. 1 versus Fig. 3, and also Fig. 4 versus Fig. 5.

The effect of crazing on optical distortion can be demonstrated by the double reflection which the crazing cracks produce. This may be seen in Fig. 6 where the specimen on the left has been partly crazed as a result of being subjected to tensile stress for some time and the specimen on the right is unstressed. The double image is caused by the separate reflections arising from the crazed areas lying adjacent to the top and bottom surfaces.

A rather interesting observation reported by Sauer, Marin, and Hsiao (9) is that polystyrene specimens may be crazed completely throughout their cross section and yet continue to carry a considerable amount of load. Consider the specimen shown in Fig. 7.

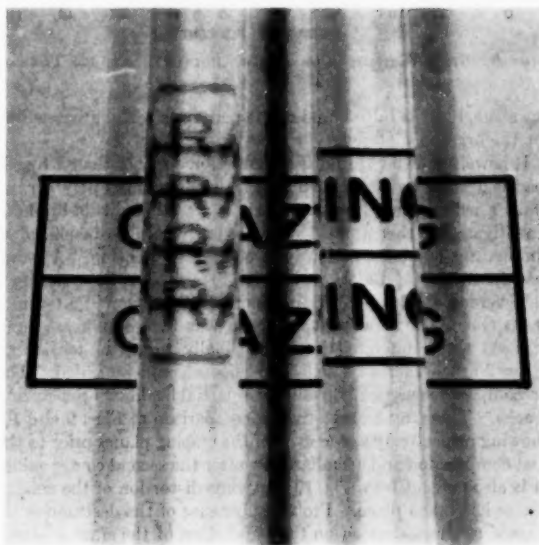


FIG. 6. VARIATION OF INDEX OF REFRACTION OF CRAZED POLYMETHYL-METHACRYLATE

This specimen was machined from a larger polystyrene specimen ($1/2$ in. \times $1/2$ in. in cross section), which had been subjected to a constant tensile stress of approximately 3000 psi for approximately 1000 hr. At the end of this time, crazing cracks extended throughout the cross-sectional area. From this larger specimen, a small round specimen was made in the shape as shown and retested in tension. Its stress-strain curve together with that of the original material is shown in Fig. 8. The data indicate the fully crazed material has approximately the same ductility and somewhat more than one half the tensile strength of the uncrazed material. There is also shown in Fig. 8 a stress-strain curve for a small specimen taken from the noncrazed portion of a larger tensile-creep specimen. It will be noted that the strength is about

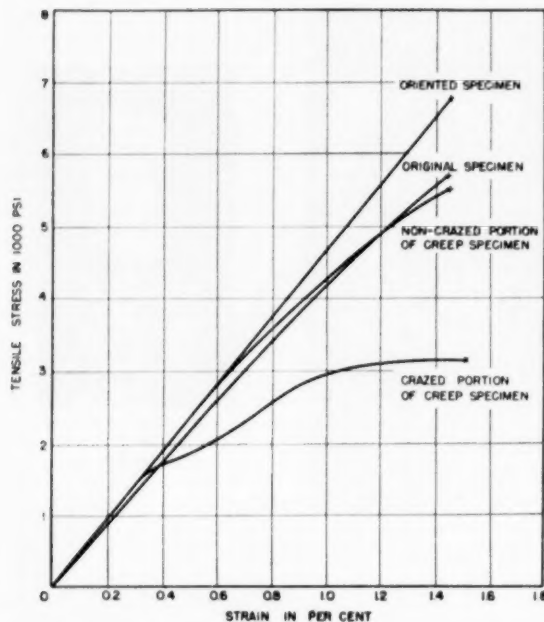


FIG. 8 STRESS-STRAIN CURVES OF POLYSTYRENE IN TENSION

the same, but the initial modulus is perhaps slightly greater than for the original material.

It is well known (4) that if a compressive rather than a tensile load is applied to a specimen of a transparent high polymer, no crazing will occur. In view of this it was thought desirable to investigate whether applied compression would be beneficial in eliminating crazing previously produced by tension. A small test specimen (of the type in Fig. 7) was cut from a larger polystyrene specimen previously completely crazed in a tension-creep test. The small test specimen was then compressed and released three different times and finally tested in tension to determine whether any beneficial effects could be noted. The precompression seemed to result in a partial healing of the crazing cracks. This may be seen from a comparison of Figs. 9 and 10, showing respectively a side view of the crazing planes prior to the first compression and a similar view after the second compression. It is also evident from Fig. 10 that some distortion of the crazing planes has taken place. Probably because of the destructive influence of the distortion on the parallelism of the crazing planes and the apparent close-up of the openings between the crazing planes, the specimen at this time was quite clear to the naked eye with little visible signs of crazing. However, when viewed under a light microscope, crazing planes could still be seen. Hence applied compression is at best only partly effective in healing crazing openings produced by tension. Also, if the precompressed samples are tested in tension, crazing cracks again open and no increase in strength is observed.

It was stated previously that orientation has an effect on crazing. It also has an effect on the stress-strain characteristics and on the ultimate breaking strength. A statistical evaluation of the fracture strength for polymers subjected to various amounts of orientation has been made by Hsiao and Sauer (4) and their predicted values check satisfactorily with the experimental data of Bailey (10) and of Cheatham and Dietz (11). One example of the effect of orientation on strength can be obtained from a comparison of the graphs in Fig. 8 marked "oriented specimen"

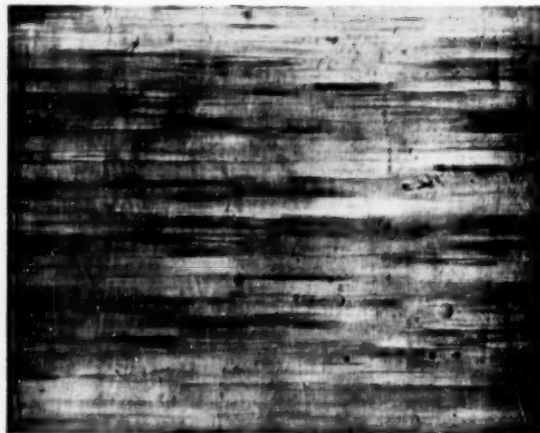
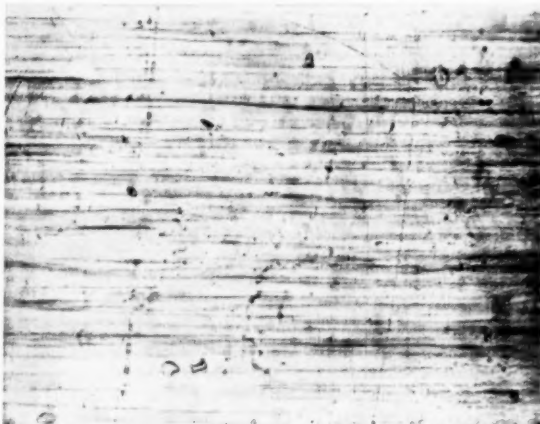
FIG. 9 CRAZING CRACKS OF POLYSTYRENE
(Direction of applied stress, vertical. Viewed by transmitted light; $\times 100$.)

FIG. 10 CRAZING CRACKS OF POLYSTYRENE VIEWED IN RADIAL DIRECTION OF ROUND SPECIMEN SHOWING DISTORTED CRAZING PLANES

(This crazed specimen has been compressed to its maximum load and ability of material to reflect light has been reduced greatly. Viewed by transmitted light. Direction of applied tensile and compressive stresses, vertical; $\times 100$.)

and "original specimen." The oriented specimen was one that had been stretch-oriented previously approximately 300 per cent in each of two biaxial directions. According to the statistical theory of Hsiao (12), its strength should be approximately 26 per cent higher than that of the unoriented sample. The graphs in Fig. 8 indicate that the experimental increase is approximately of this order of magnitude.

The particular oriented specimen, whose stress-strain behavior is shown in Fig. 8, is one that was built up of a series of laminated layers of polystyrene—each layer having been biaxially stretch-oriented to the amount mentioned. The test was conducted at a strain rate of about 190×10^{-6} in./in./sec and the loading continued until fracture occurred. The fracture surface is shown in Fig. 11. Despite the short duration of the test (1 to 5 min) some crazing occurred and this is clearly visible on the fracture surfaces.

RATE OF PROPAGATION OF CRAZING

As mentioned in the foregoing, under the action of a maintained



FIG. 11 FRACTURE SURFACE OF BIAXIALLY ORIENTED POLYSTYRENE

tensile stress, crazing cracks originate on the external surfaces of the specimen and propagate inward toward the center. To obtain information on the rate of propagation with time, it is necessary to have a continuous measure of the penetration of the crazing front. Since, however, the crazing cracks develop on all four external surfaces of the square specimens, and thus destroy visual transparency, it is not easy to measure the inward penetration of the crazing cracks until after the specimen has fractured.

Fortunately, this difficulty can be overcome by use of special coatings. As reported by previous investigators (1), crazing can be greatly retarded or even prevented from occurring by applying to the outside surfaces some synthetic-polymer coating. (For polystyrene, one such coating is a solution consisting essentially of styrene monomer.) To obtain the desired visual advance of the crazing front, one coats two opposite faces of the specimens and leaves the other two faces free. On continued application of a constant tensile load, the crazing cracks will then start as usual on the free surfaces and grow inward as time passes. The coated sides, however, will remain essentially craze-free and hence the depth of penetration of the crazing cracks can be observed easily and measured by viewing them from a direction perpendicular to the coated sides.

The type of specimen used is shown in Fig. 12. The cross section of the specimen was approximately $\frac{1}{2}$ in. \times $\frac{1}{2}$ in. and the gage length was 2 in. long. These specimens were cut from $\frac{1}{8}$ -in.-thick polystyrene sheet. On the molded surfaces (facing the observer in Fig. 12), about one half of the 2-in.-gage-length section was coated while on the other two sides the transparent coating extended to only about one quarter of the total gage length. As may be seen from the figure, the coating essentially prevented the initiation and growth of crazing from those surfaces on which it was placed, while other uncoated surfaces initiated crazing planes sufficiently intense to reflect light radiation. This method thus permitted the determination of the position of the crazing front from time to time and hence the rate of propagation of crazing could be found. The measurement of the position was made repeatedly by a micrometer at a given location and throughout the 1000 hr duration of test. The test method, though not perhaps as precise as the light-reflection method (2, 3) for determining the average amount of crazing developed throughout a given volume, is simpler and more appropriate for determining crazing penetration over long periods of time. A plot of the amount of penetration of crazing against time is given in Fig. 13 for specimens subjected to three different stress levels as indicated.

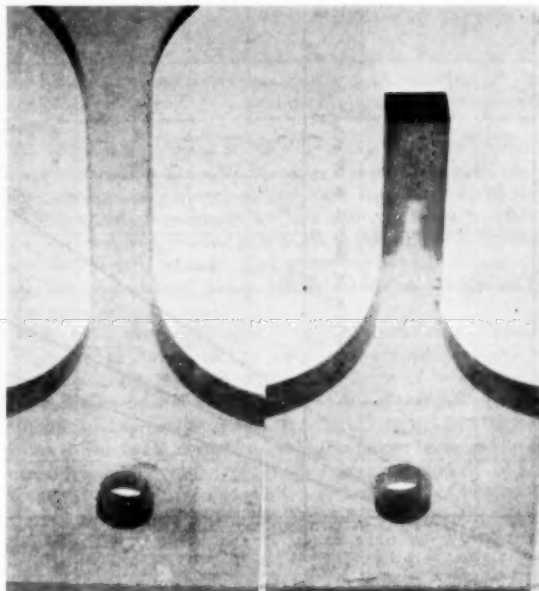


FIG. 12 COMPARISON OF SELECTIVELY COATED POLYSTYRENE SPECIMENS BEFORE AND AFTER TENSION-CREEP TEST

Owing to the fact that polystyrene is rather brittle at ordinary room temperatures, many specimens, especially those at high applied-stress levels, failed before any appreciable value of crazing could be recorded. The data indicate that the relation between penetration of crazing and time is a linear one over the stress range investigated.

It is interesting to note that these three long-time crazing curves at different stress levels show different amounts of penetration of crazing at the very start of the test. Usually, sharp crackling sounds could be heard soon after the load was applied which suggests the sudden appearance of crazing and the immediate release of a portion of energy into sound waves. If the first derivatives of these curves with respect to time are plotted against the magnitude of the corresponding stress level, it appears that the rate of displacement of the crazing front varies linearly with the stress as shown in Fig. 14. It is unfortunate that not more test points are available, but within the stress limits indicated the rate of crazing varies with the stress in the following manner

$$\dot{D} = \frac{1}{m} (\sigma - \sigma_0)$$

where

σ = stress, psi

m = slope of the straight line

\dot{D} = rate of propagation of crazing front, iph

σ_0 = constant measured in stress units

Since the velocity of crazing is thus a linear function of stress, the depth of crazing can be written by integration as

$$D - D_0 = K (\sigma - \sigma_0)(t - t_0)$$

where D_0 and t_0 are constants and $K = 1/m$. For polystyrene $D_0 = -0.015$ in., $K = 0.851 \times 10^{-3}$ in/hr/psi, $\sigma_0 = 1670$ psi, and $t_0 = -400$ hr.

Thus, within the limited range of stresses as indicated in Fig. 14, the depth of crazing may be expressed as a linear function of

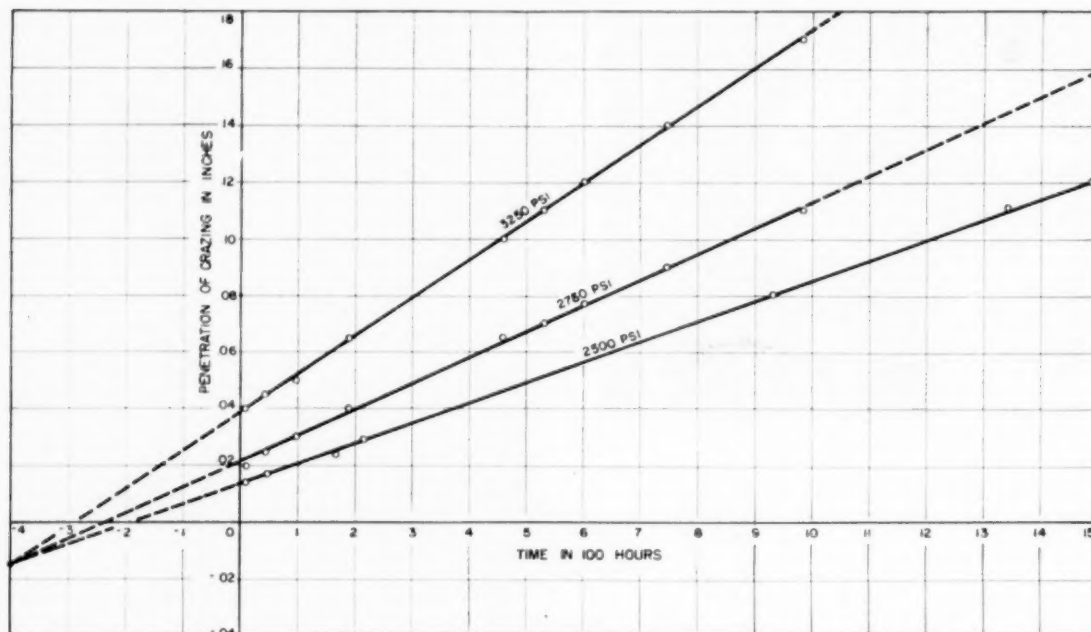


FIG. 13 LONG-TIME CRAZING CURVES OF POLYSTYRENE

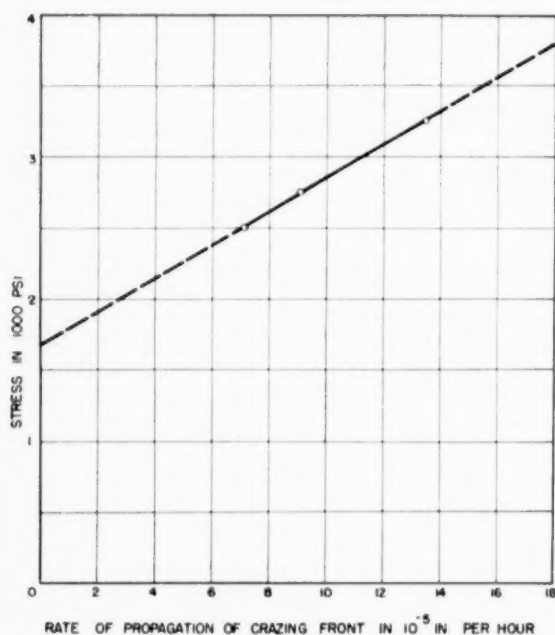


FIG. 14 EFFECT OF TENSILE STRESS ON RATE OF PROPAGATION OF CRAZING OF POLYSTYRENE

both stress magnitude and time. It is questionable whether the foregoing equations can be extended to much lower stresses but their implication that the rate of propagation of crazing goes to zero for some limiting stress value does seem to be in general agreement with experimental results (9). It is also difficult to

investigate this relation for much higher stresses than 3500 psi as the specimen tends to fracture in much shorter time periods and thus not many data on crazing can be taken. Such short-time fractures are frequently caused by obvious flaws such as that shown in Fig. 15, which result in high local stress intensities. The actual fracture cracks, as distinct from the crazing cracks, very frequently start from some point inside the specimen and then extend rapidly radially outward as Fig. 15 indicates.

DESIGN IMPLICATIONS OF CRAZING

The development of crazing in stressed transparent plastics is for the most part a highly undesirable occurrence, although beneficial use is made of this phenomenon in the use of transparent

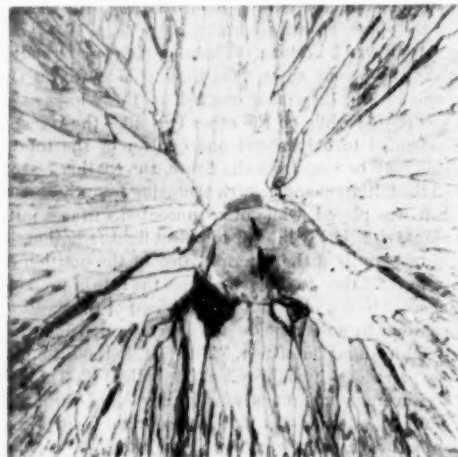


FIG. 15 FRACTURE SURFACE OF CRAZED TENSION-CREEP SPECIMEN OF POLYSTYRENE

brittle lacquers to predict the direction and approximate magnitude of surface stresses on machine and structural parts. In other applications, however, such as transparent enclosures on aircraft, transparent instrument panels, and as insulators in electronic apparatus, the initiation of crazing is cause for alarm either because of loss of transparency, loss of mechanical strength, or loss of dielectric properties as a result of moisture absorption in the crazing openings. Also, since crazing once started will continue to increase without increase of load magnitude, it is well to avoid its consequences by taking every precaution to avoid its inception.

As already noted, surface coatings are helpful and can be recommended. Also, working-stress magnitudes should be established not merely on the basis of static ultimate strength, but on strength values at which crazing is found to occur. In applications where the plastic part may be subjected to tensile stress in varying directions, full annealing of the transparent plastic sheets is highly desirable as in this way the material can be made more nearly isotropic. On the other hand, if the plastic part is to be used only under uniaxial tension, then higher working stresses can be obtained, without danger of crazing, by use of highly oriented material. Essentially, the reason is that in the oriented state all the molecular chains tend to align in the direction of orientation and crazing, which is thought to be a result of lateral separation of adjacent chains (4), cannot then occur. Of course, crazing will occur in oriented materials and at low stress values if transverse tensile rather than axial tensile stress is applied. If, therefore, the intended application is such that there is a probability of lateral as well as longitudinal tensile stresses occurring, then the isotropic annealed state is preferable to the highly oriented state.

ACKNOWLEDGMENT

The authors wish to thank Prof. D. A. Kribs of the Pennsylvania State College, for his help in making most of the crazing micrographs, and also express their appreciation to the Office of Naval Research and the department of engineering mechanics of The Pennsylvania State College for financial support.

BIBLIOGRAPHY

- 1 "Stress Pattern Crazing," by W. B. Klemperer, Theodore von Kármán Anniversary Volume, Cal. Inst. of Tech 1941, p. 328.
- 2 "Studies on Polymethyl Methacrylate, Part III, Crazing Effects," by E. W. Russell, Report Chem. 447, Royal Aircraft Establishment, Farnborough, Hants, England, August, 1948.
- 3 "Factors Affecting the Crazing of Polystyrene," by B. Maxwell and L. F. Rahm, *Plastics Laboratory Technical Report 14B*, Princeton University, Princeton, N. J., May, 1949.
- 4 "On Crazing of Linear High Polymers," by C. C. Hsiao and J. A. Sauer, *Journal of Applied Physics*, vol. 21, 1950, p. 1071.
- 5 "Sunlight and Accelerated Light Aging of Synthetic Rubbers," by R. E. Morris, R. R. James, and T. A. Werkenthin, *The Rubber Age*, vol. 51, 1942, p. 205.
- 6 "Mechanism of Exposure-Cracking of Rubbers With a Review of the Influence of Ozone," by R. G. Newton, *Rubber Chemistry and Technology*, vol. 18, 1945, p. 504.
- 7 "The Rheological Properties of Polystyrene Below 80° C.," by B. Maxwell and L. F. Rahm, *Industrial and Engineering Chemistry*, vol. 41, 1949, p. 1988.
- 8 "Crazing of Cast Polymethyl Methacrylate," by E. W. Russell, *Nature*, vol. 165, January 21, 1950, pp. 91-96.
- 9 "Creep and Damping Properties of Polystyrene," by J. A. Sauer, J. Marin, and C. C. Hsiao, *Journal of Applied Physics*, vol. 20, 1949, pp. 507-517.
- 10 "Stretch Orientation of Styrene and Its Interesting Results," by J. Bailey, *India Rubber World*, vol. 118, May, 1948, pp. 225-231.
- 11 "Effect of Orientation on the Mechanical Properties of Polystyrene," by R. G. Cheatham and A. G. H. Dietz, *Trans. ASME*, vol. 74, 1952, pp. 31-40.
- 12 "Effect of Orientation on the Ultimate Strength of Linear High Polymers," by C. C. Hsiao, *Journal of Applied Physics*, vol. 23, 1952, p. 1189.

Discussion

A. G. H. DIETZ.⁴ The authors have made interesting and valuable observations respecting crazing, a phenomenon of considerable practical and theoretical importance in the use of many plastics.

Of considerable interest is the observation that crazing starts at the surface and proceeds inward. This has been discussed informally by many observers, and some have maintained that on highly polished specimens in which even minute surface flaws have been removed, crazing may begin in the interior simultaneously with surface crazing. The writer has not had occasion to study this phenomenon closely, but would welcome comment by the authors.

When specimens are oriented by drawing, orientation appears to begin at the surface and to proceed inward as the degree of orientation increases. One of the first effects of orientation is the diminution and gradual disappearance of crazing. In partially oriented specimens, surface crazing disappears but internal crazing still occurs; the surface fracture at failure becomes fibrous whereas internal fracture remains abrupt or "brittle." When orientation proceeds far enough, fracture throughout the specimen becomes fibrous and crazing disappears altogether.

AUTHORS' CLOSURE

The authors wish to express their appreciation to Professor Dietz for the interest he has taken in this paper and for the comments he has made.

With regard to the occurrence of crazing in the interior, simultaneously with surface crazing for highly polished specimens, the authors wish to make the following comments. As it has been stated, various factors such as temperature, time, orientation, and environment have an influence on the initiation of crazing, but local stress intensity is probably more directly responsible for its occurrence and subsequent propagation than any other factor. If a simple tension specimen is highly polished so that there is no surface contamination or any stress concentration under loading, and particularly if it has no preferred molecular orientation, it appears, then, that the local stress intensities will be uniform over the cross section as well as the gage length of the specimen and it seems that there is no reason why crazing may not begin in the interior simultaneously with surface crazing. Furthermore, it could be expected that internal crazing would occur first if tensile residual stresses are present in the interior of the specimen.

The understanding of the effect of orientation on strength and crazing properties of linear high polymers has been advanced through the development of a theory which permits calculation of strength as a function of orientation in terms of strain change (12) as well as prediction of crazing. It is expected that a report on this subject will be published by the authors of this paper in the near future. In general, the statistical theory analyzes the effect of orientation of linear polymeric molecules on strength and crazing by considering their microstrength and their direction of orientation. Evidences commented on by Professor Dietz seem to support the theory fairly well. Various experimental investigations in connection with both uniaxially and biaxially oriented specimens are being carried out by the authors' group and verifications as well as modifications of the theory will be made.

The authors wish to also express their appreciation to Prof. Bryce Maxwell for his interesting remarks on the initiation of crazing, which he made orally following the presentation of the paper. Referring to reference (7) of the paper concerning his

⁴ Massachusetts Institute of Technology, Cambridge, Mass. Mem. ASME.

work he commented that under all conditions studied the criterion for the initiation of crazing is the strain in the material and by varying time or temperature this can be studied independently of stress. Then he attempted to show the agreement of the critical crazing strain obtained from both his work and that from Fig. 14 of the paper by extrapolation. A strain corresponding to a stress of approximately 1650 psi for zero rate of propagation of crazing would be 0.36 per cent which agrees quite nicely with the critical crazing strain of 0.35 per cent of reference (7).

However, the authors wish to point out the difference between the zero rate of propagation of crazing and the zero penetration of crazing, which may also be referred to as the critical crazing point. Referring to Fig. 13 of the paper and assuming that all crazing curves were straight lines and would intersect at the point as shown at the lower left corner of the figure, a stress of about 2100 psi corresponding to the zero penetration of crazing could be obtained from Fig. 14, whereas the stress for zero rate of penetration of crazing is only around 1650 psi.

Some Design Considerations for Injection-Molding Heating Chambers

By G. D. GILMORE¹ AND G. B. THAYER,² MIDLAND, MICH.

The general design of injection-molding heating chambers has become established after gradual development through several years of experience. Some of the details of design which are directly concerned with the plastic-material characteristics have been examined to a limited extent. Very little engineering-design information has been available for a careful consideration of these details. Heat-transfer and pressure losses in the heating chamber are interrelated and the geometry of the passages through which the plastic moves can be arranged for optimum heat-transfer rate with minimum pressure loss. The available theoretical, experimental, and practical information concerning the behavior of plastic materials, under high pressures, in granular and fluid conditions is considered. This information is combined into a systematic approach to the geometrical problems of the design of injection-molding heating chambers.

NOMENCLATURE

The following nomenclature is used in the paper:

- l = length of heating zone, in.
- d_1 = heater body bore diameter, in.
- d_2 = spreader diameter, in.
- a = plastic-slab thickness, in.
- α = thermal diffusivity, sq in. per sec
- T_i = heater-chamber wall temperature, deg F
- T_o = initial temperature of plastic introduced into heating chamber, deg F
- T_a = average plastic temperature at any contact time t , deg F
- t = contact time of plastic against heat source, sec
- t_c = total injection cycle, sec
- ρ = density of plastic, oz per cu in.
- R = rate of plastic throughput, lb per hr
- n = number of effective sides delivering heat to a flat slab
- w = shot weight, oz
- F_a = applied force, lb
- F_r = resisting force, lb
- μ = coefficient of friction
- L_c = length of cold granules in heating-chamber entrance before compaction, in.
- D = diameter of plunger, in.

INJECTION HEATING CHAMBER

The present-day heating chamber contains a spreader which is the essential feature of the design credited to Hans Gastrow prior to 1934. The cross section of the typical heating chamber, without construction details, is shown in Fig. 1. The thermoplastic material, and more specifically polystyrene, exists as hard

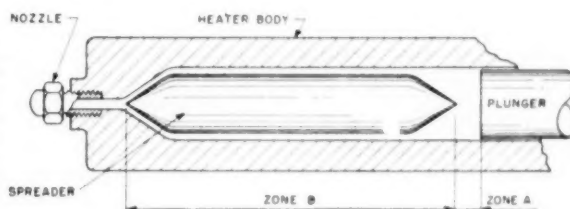


FIG. 1. DIAGRAM OF HEATING CHAMBER

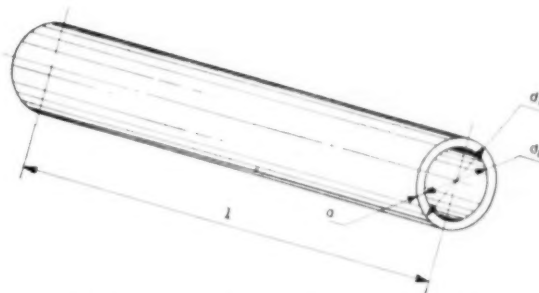


FIG. 2. "INFINITE SLAB" OF PLASTIC IN REGION B

granules where it is introduced at A. It is heated progressively and leaves the nozzle in a relatively fluid state. All conditions between these two extremes exist in the heating chamber.

HEAT-TRANSFER CONSIDERATIONS

The major absorption of heat by the plastic takes place in region B, Fig. 1. Plastic in this space has the shape of a tube as shown in Fig. 2. This tube can be considered as an infinite flat slab in its developed shape. Because of the simple geometric shape of the plastic in region B, heat-transfer equations may be applied.

The theory of heat transfer through a flat slab has been well established. The quantity of heat taken up by a unit slab of plastic depends upon three factors, as follows:

- 1 Thermal diffusivity.
- 2 Temperature difference between the heating surface and the adjacent layer of plastic.
- 3 Time of contact between plastic and heating surface.

The value of thermal diffusivity for polystyrene has been found experimentally³ to be 2.17×10^{-4} . It is reasonably constant over the operating temperature range.

It has been found convenient to express temperature differential as a ratio of actual temperature rise of the entire mass of plastic to the maximum possible temperature rise. In accordance with the terms previously listed in the nomenclature this becomes

$$\frac{T_a - T_o}{T_i - T_o} \dots \dots \dots [1]$$

¹ Technical Service Engineer, The Dow Chemical Company.
² Head of Molding Section, Plastics Technical Service, The Dow Chemical Company. Mem. ASME.
 Contributed by the Rubber and Plastics Division and presented at the Annual Meeting, New York, N. Y., November 30-December 5, 1952, of THE AMERICAN SOCIETY OF MECHANICAL ENGINEERS.
 NOTE: Statements and opinions advanced in papers are to be understood as individual expressions of their authors and not those of the Society. Manuscript received at ASME Headquarters, October 2, 1952. Paper No. 52-A-105.

³ Plastic Basic Research Laboratory, The Dow Chemical Company, Midland, Mich.

This is called the temperature-difference ratio.

It is also convenient to express contact time t in terms of the dimensions of the heating chamber and other terms commonly used in injection molding. The contact time is equal to the inventory weight, divided by the shot weight and multiplied by the total cycle. This may be expressed as follows

$$t = \frac{l \pi (d_1^2 - d_2^2) \rho t_c}{4w} \quad [2]$$

The rate of plastic throughput R in lb per hr may be introduced since it is equal to the shot weight divided by the total cycle

$$R = \frac{225w}{t_c} \quad \text{or} \quad \frac{t_c}{w} = \frac{225}{R} \quad [3]$$

Substitution of Equation [3] in Equation [2] results in the expression

$$t = \frac{225 \pi (d_1^2 - d_2^2) \rho}{4R} \quad [4]$$

The ratio of actual temperature rise to maximum possible temperature rise is a function of thermal diffusivity, slab thickness, and contact time as follows

$$\frac{T_a - T_o}{T_i - T_o} = f \left(\frac{at}{a^2} \right) \quad [5]$$

The term at/a^2 may be called the heat-flow modulus. This applies to a flat slab heated equally from two sides. If the slab is heated from only one side, the slab thickness must be considered as being twice its actual thickness, or $2a$. In this situation Equation [5] becomes

$$\frac{T_a - T_o}{T_i - T_o} = f \left[\frac{at}{(2a)^2} \right] \quad [6]$$

In the injection-molding heating chamber, heat usually is supplied through the heater body to one side of the slab. However, some heat is supplied to the other surface of the slab by the spreader. In order to apply heat-conduction Equation [5] to heating-chamber design, it is necessary to introduce a coefficient for the section thickness. This coefficient is $(5 - n^2)$, in which n is defined as the number of effective sides supplying heat to the plastic slab. Equation [5] then becomes

$$\frac{T_a - T_o}{T_i - T_o} = f \left[\frac{at}{(5 - n^2)a^2} \right] \quad [7]$$

The relationship expressed in Equation [7] is shown graphically in Fig. 3. The heat-flow modulus also is expressed in terms commonly used in injection molding. This is obtained by introducing the expression for contact time as given in Equation [4] and the elimination of d_2 since

$$d_2 = d_1 - 2a \quad [8]$$

Plastic temperature measurements have been made on several commercial heating chambers.⁴ The values of n for the various heating chambers were determined by substituting these temperature measurements, together with the heating-chamber dimensions in the heat-conduction relationship indicated in Fig. 3. The effect of spreader construction on the number of effective sides supplying heat is shown in Fig. 4. The values of n shown

⁴ "Measurement of the Heating Capacity of Injection Molding Machines," by C. E. Beyer and R. B. Dahl, *Modern Plastics*, vol. 30, September, 1952, pp. 124-126, 130, 204.

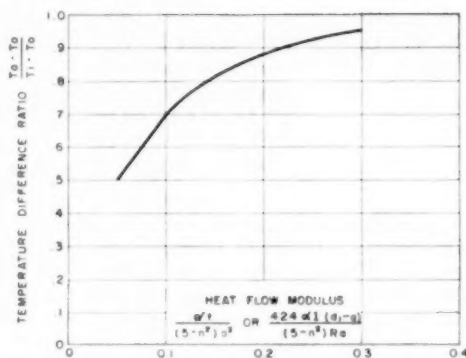


FIG. 3 TEMPERATURE-DIFFERENCE RATIO VERSUS HEAT-FLOW MODULUS FOR INFINITE SLAB

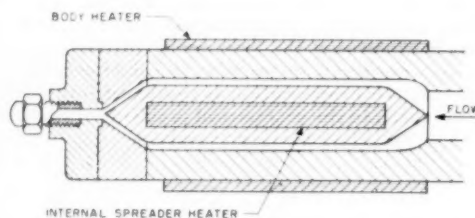


FIG. 4(a) NUMBER OF EFFECTIVE HEATING SIDES FOR VARIOUS SPREADER CONSTRUCTIONS; $n = 1.9$

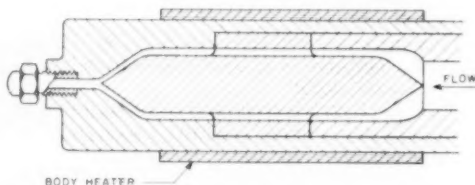


FIG. 4(b) NUMBER OF EFFECTIVE HEATING SIDES FOR VARIOUS SPREADER CONSTRUCTIONS; $n = 1.7$

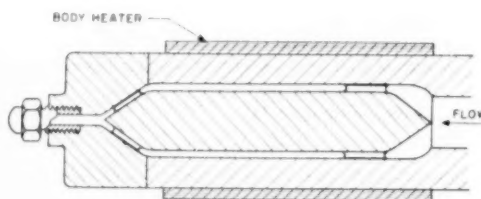


FIG. 4(c) NUMBER OF EFFECTIVE HEATING SIDES FOR VARIOUS SPREADER CONSTRUCTIONS; $n = 1.4$

are average values over the range of production rates tested. The value of n is 1.4 for a spreader which floats within the heater body. The number of effective heating sides increases to 1.7 when the spreader is located rigidly within the heater body. Incorporating an internal heater in the spreader increases the value of n to 1.9.

The effect of these three spreader designs on the output of a heating chamber may be computed by assigning dimensions to a hypothetical heating chamber similar to such chambers in regular

TABLE 1 MACHINE SPECIFICATIONS FOR HEATING CHAMBER

Shot size (maximum), oz.	14
Maximum pressure, psi	20000
Maximum speed of injection, at 20,000 psi, ipm	120
Plunger diameter, in.	3
Plunger stroke, in.	10
Heater body inside diameter, in.	4.25
Spreader diameter, in.	3.65
Heating zone length, in.	20
Output at 80 per cent heating efficiency, lb per hr.	82

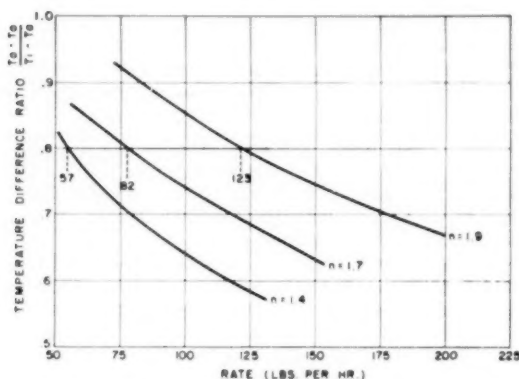


FIG. 5 EFFECT OF SPREADER CONSTRUCTION ON RATE

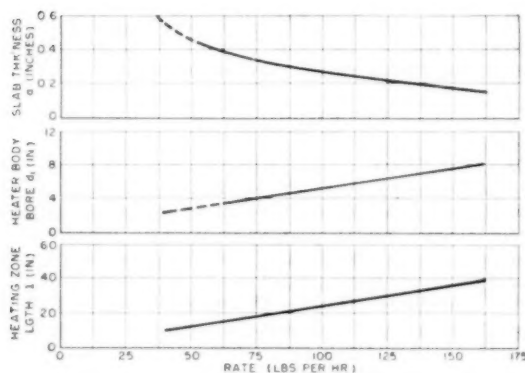


FIG. 6 HEATING-CHAMBER GEOMETRY VERSUS RATE

use in the molding industry. These dimensions are given in Table 1. The curves in Fig. 5 show the heating effects of the three designs. The curves have been drawn by substituting the dimensions assumed for the heater and the average values of n in the equation illustrated by Fig. 3.

Incorporating an internal heater in the spreader would be expected to increase the production rate from 82 to 123 lb per hr at a temperature-difference ratio of 80 per cent. Using a floating spreader in this design to provide very little contact between heater body and spreader reduces the theoretical production rate from 82 lb per hr to 57 lb per hr.

The effects of length, bore, and plastic-slab thickness on the heating rate, using a value of n of 1.70, are shown in Fig. 6.

As would be expected, any increase in the heating-zone length or heater-body bore produces a direct increase in heating rate. The effect of decreasing the section thickness of plastic by a small amount also is to increase the rate approximately in a linear fashion.

Several factors have been omitted purposely in the heat-transfer considerations presented. Their introduction, however, would complicate the situation far beyond the value which could be at-

tained at this time. Such factors as the velocity gradient in the plastic slab, frictional heating in the plastic, and heat received by conduction prior to entering the spreader section should be recognized as contributing to the heating rate of any given design.

PRESSURE-LOSS CONSIDERATIONS

Design details concerned directly with the characteristics of the plastic involve pressure requirements in addition to heat transfer. As was pointed out previously, the thermoplastic exists in the heating chamber as a hard rigid material at the entrance. The material at the nozzle end exists in a relatively fluid state although still highly viscous. At a temperature of 425 F its viscosity at zero shear is approximately 35,000 poises. Its viscosity increases rapidly to 800,000 poises at 325 F as shown in Fig. 7. It is evident this typical thermoplastic polystyrene is a highly viscous material, the viscosity of which is extremely sensitive to temperature.

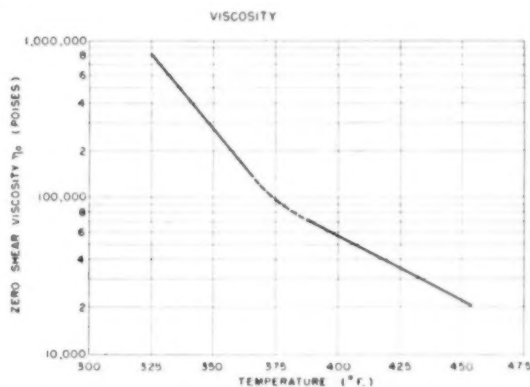


FIG. 7 VISCOSITY VERSUS TEMPERATURE; GENERAL-PURPOSE POLYSTYRENE; MOLECULAR WEIGHT, 140,000

Excellent tools are available to analyze pressure losses⁴ under ideal equilibrium conditions. These may be applied, although a wide range of conditions exist in the heating chamber as has been shown. The reliability of any pressure-loss analysis would seem questionable, but only in so far as absolute values are concerned. Using these tools in considering the heating chamber necessitates certain assumptions which may affect the numerical magnitude of the results obtained. Nevertheless, they provide a starting point and present a relative picture which, at least, points the direction in which the design should go.

Using the procedure suggested by Wiley and Pierce,⁴ the following assumptions are necessary:

- 1 The plastic in the heating chamber may be considered in two parts, the region B, occupied by the spreader, is the heating zone, while the region A, between the spreader and the plunger, is the cold zone.

- 2 In the heating zone, the plastic may vary in temperature from 100 F to 500 F. At maximum throughput, the plastic may be considered as being at an equilibrium temperature of 300 F.

- 3 Pressure loss in the cold zone can be considered independently as a friction phenomenon.

For the heating chamber with specifications as listed in Table 1, the effect on pressure loss in changing each dimension independently is plotted in Fig. 8. As might be expected, any increase

⁴ "Pressure Drop of Fluid Polystyrene in Conduits," by R. M. Wiley and J. E. Pierce, *Chemical Engineering Progress*, vol. 47, 1951, pp. 432-435.

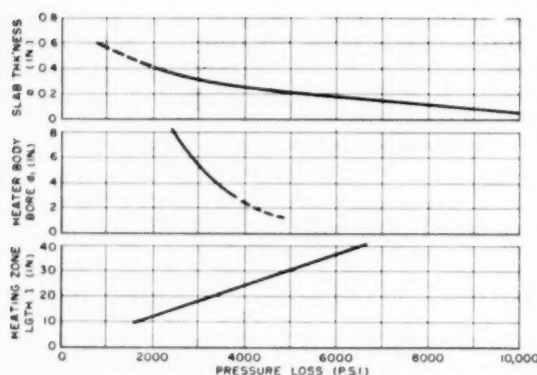


FIG. 8 HEATING-CHAMBER GEOMETRY VERSUS PRESSURE LOSS

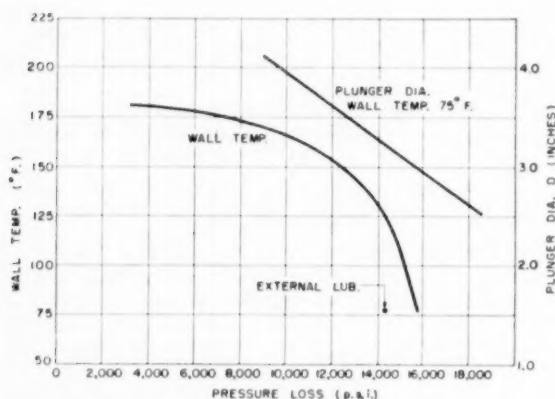


FIG. 9 PRESSURE RELATIONSHIPS IN COLD ZONE

in length results in a direct increase in pressure loss. A considerable change in heater-body bore has a negligible effect on the pressure loss. A small decrease in section thickness, on the other hand, produces a large increase in pressure loss.

Of even greater importance in analyzing the pressure losses is the cold zone. Here granules of material are compressed under very high pressure at temperatures so low they are not distorted appreciably. The result is an extremely high pressure loss.

The results of experiments in this regard have been published⁸ and for static conditions the following relationship was found

$$\frac{F_a}{F_r} = e^{4\mu L_0/D} \dots \dots \dots [9]$$

For the maximum shot size of 14 oz, taken from Table 1, the cold zone would produce pressure losses as plotted in Fig. 9. Since it is assumed that the shot size is constant the effect is plotted in terms of plunger diameter only. The effect of wall temperature results because of the change in the coefficient of friction. An increase in wall temperature of 100 F is as effective in reducing the cold-zone pressure loss as increasing the plunger diameter by a factor of 2. The effect of an external lubricant is to reduce the pressure loss, as has been experienced by many molders.

⁸ "Behavior of Granulated Polymers Under Pressure," by R. S. Spencer, G. D. Gilmore, and R. W. Wiley, *Journal of Applied Physics*, vol. 21, 1950, pp. 527-531.

SUMMARY OF RECOMMENDATIONS

It would be desirable to be able to specify an exact design incorporating a maximum heating rate and a minimum pressure loss. Since several assumptions have been made, particularly in regard to pressure losses, an exact specification cannot be drawn. There are, however, indications as to the approach to be taken. These, together with suitable experiments designed to establish the reliability of any assumed conditions, should provide sound engineering design information. Experiments of this type have been successful.⁷

Considering the specifications as listed in Table 1, the maximum heating rate with minimum pressure losses is approached in the following design changes:

- 1 Increase the heater-body bore. This actually increases the inventory and results in a smaller pressure loss.
- 2 The heating-zone length also may be increased and the section thickness decreased. These should be held to a minimum since they increase the pressure loss.
- 3 The spreader construction is very important, for by the use of an internal heater the heating rate can be increased 50 per cent.
- 4 Pressure losses may be considerably lowered by proper attention to the cold zone. A high wall temperature in the cold zone is desirable. Even a change in plunger design to accommodate its working against partially melted material should be attempted. Further decrease in pressure loss can be obtained by an increase in the plunger diameter.

These design changes, within limits, should greatly improve the heating chamber discussed. They also would apply to other specific designs patterned after the Gastrow unit.

Discussion

W. R. McLAIN.⁸ Conclusions of the paper as to the large pressure losses that are possible in the cold zone would indicate that this particular zone would be an excellent place to consider design changes. Several questions are obvious. Would it not be possible to add another controlled heating zone extending from the rear of the present heating cylinder to the point of the withdrawn end of the injection plunger? This could be insulated from the sleeve to the rear and if necessary the rear sleeve could be water-cooled. This would provide a certain amount of preheating of material which feeds in front of the piston during the time of the cycle that the injection piston is in the reversed position.

If this were possible then the pressure drop in the cold zone should be minimized as shown in Fig. 9 of the paper. Pressure loss also should be reduced in the rear of the cylinder as the viscosity would tend to drop faster in the rear ranges than in a case where no preheating is done.

This might involve certain design difficulties, but it would seem to be a possible approach to greater capacity of plasticization, as well as better preserved injection pressures.

One other question relates to several factors mentioned in the paper. Experiments possibly have been made along this line, but it still seems to present a good basis for discussion and further study. Would it be possible to alter the spreader design so that it tapered on a gentle slope for most of the length of the heater and passed through a thinner wall section at the forward end? One factor entering the functioning of the cylinder would then be a larger over-all inventory providing more contact time. If the rear slope could be plotted so that it was based on a minimum pres-

⁷ "Basic Features Influencing the Performance of Injection Moulding Machines," by E. Gaspar, a paper delivered at the British Plastics Convention, 1951.

⁸ President, Kusan, Inc., Plastics Division, Nashville, Tenn. Mem. ASME.

sure loss due to wall thickness and a progressive decrease in viscosity resulting from heat absorption, then some losses of the rear zone might be reduced.

The thicker rear-slab thickness would, of course, pick up heat more slowly, but would eliminate entry to a thin slab section of relatively low-temperature material. The front-slab thickness could possibly then be even less than at present because of the fluidity of the material by the time it reached this point. It seems that present design with almost uniform slab thickness from rear to front introduces a higher friction and lowers inventory with a resulting shorter contact time. Such design also would increase inventory of material in the heater without increasing its size.

These are questions which may have been answered, but if not satisfactorily, it would seem that work along these lines to determine precise effects would be of considerable value.

The authors indicate that each dimension is changed independently for plotting in Fig. 8. It is assumed that spreader diameter is varied with heater-body bore, so as to maintain constant slab thickness, but this is not stated clearly.

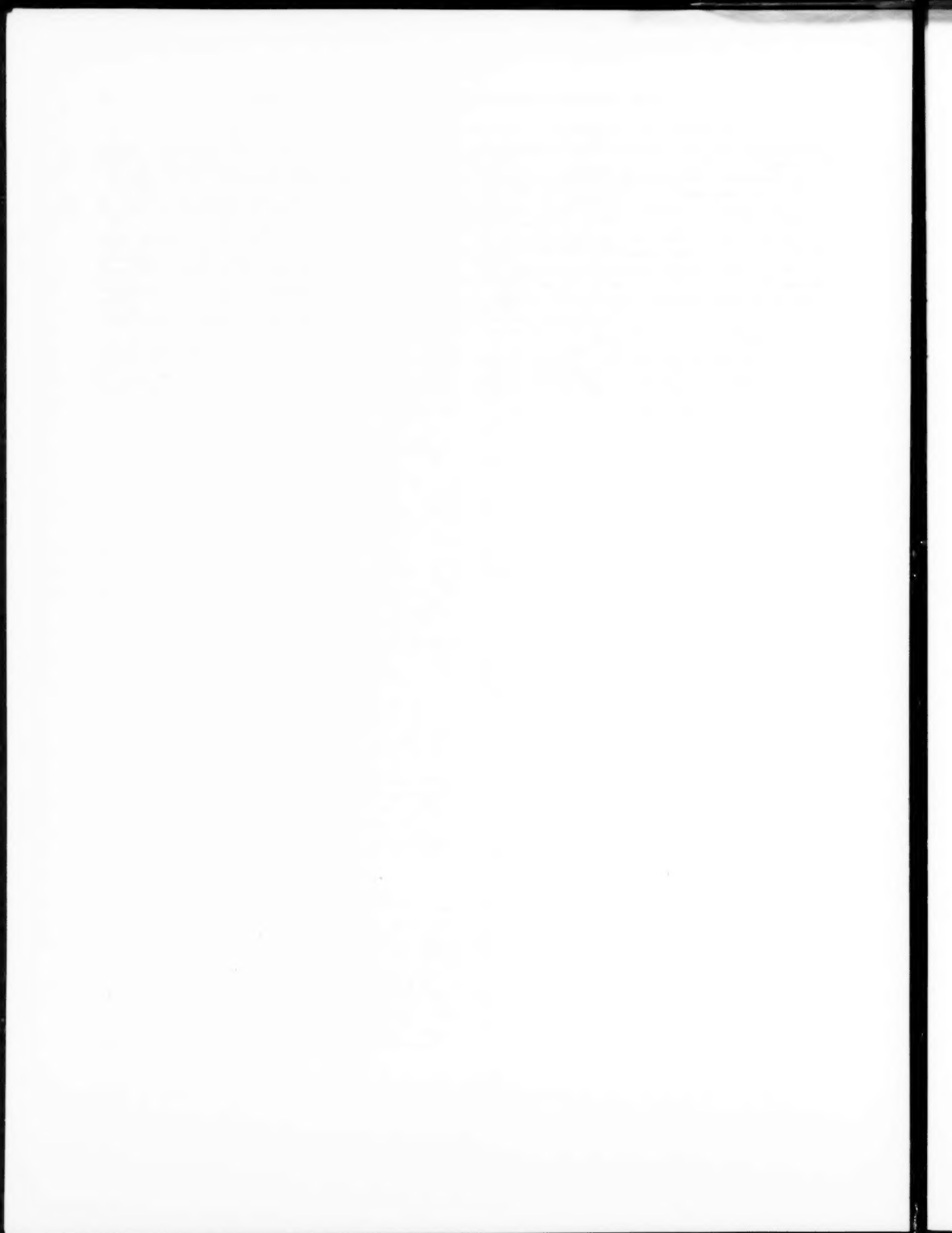
AUTHORS' CLOSURE

Mr. McLain's comments are greatly appreciated. He has raised some interesting points on which the authors can be of little assistance except to agree that further study is needed.

The addition of another controlled heating zone, wherein the plunger would operate, has excellent possibilities of increasing plasticization and decreasing pressure losses.

It would also seem that there must be an optimum design which would involve a tapered spreader. Such an analysis requires clarification of assumptions already made in this paper. Pressure losses through straight sections, where temperature variations exist, is only one to be considered. As was pointed out in the paper, the knowledge of pressure requirements is limited to equilibrium conditions.

Mr. McLain's assumption is correct, in that the spreader diameter is varied with the heater-body bore while maintaining a constant slab thickness, in plotting Fig. 8. While this was implied, the authors agree that it should have been clearly stated in the paper.



Furnace Heat Absorption in a Spreader-Stoker-Fired Steam Generator

1 Furnace Heat-Absorption Efficiency as Shown by Enthalpy of Gases Leaving the Furnace

By J. W. MYERS¹ AND R. C. COREY,² PITTSBURGH, PA.

This paper is part of the fifth of a series of reports on investigations of heat absorption and distribution of heat transfer in large steam-boiler furnaces, sponsored by the ASME Special Research Committee on Furnace Performance Factors. The furnace heat absorption was determined from the temperature and composition of the furnace exit gases in fifteen tests on a steam generator rated at 165,000 lb per hr of steam at 915 psig and 740 F at the superheater outlet, and which is fired by a spreader stoker on a front-discharge traveling grate. The effect on furnace heat-absorption efficiency is shown for variation of (a) the heat available in the furnace, (b) the excess air, (c) the percentage of combustion air admitted over the fuel bed, and (d) the condition of the furnace walls with respect to ash deposits. Detailed data on the distribution of gas temperature and of excess air in the furnace are presented. The experimental values for the furnace heat-absorption efficiency did not compare favorably with values calculated by either the Stefan-Boltzmann or the Wohlenberg equations. There is evidence, however, that the performance of a spreader-stoker-fired furnace might be predicted by the Wohlenberg equation if it were modified to allow for heat transfer resulting from a combination of suspension and fixed-bed burning.

INTRODUCTION

AN investigation was conducted to determine the furnace heat-absorption efficiency and the distribution of heat transfer on the furnace walls of boiler No. 2 at the Whiting Plant of the Carbide & Carbon Chemicals Co., Whiting, Ind. The unit is a two-drum boiler rated at 165,000 lb of steam per hr, and fired with a spreader stoker on a traveling grate. This is the fifth in a series of comprehensive investigations of heat transfer in steam-boiler furnaces by the Special Research Committee on Furnace Performance Factors of the Society. Three of the former investigations were on pulverized-coal-fired units (1),³ and one was on a natural-gas-fired furnace (2). The present investigation is the first concerned with spreader-stoker firing.

This paper presents the results of the determination of furnace heat-absorption efficiency by the Combustion Research Section of

the Bureau of Mines, as part of the research program (in co-operation with the committee) to study factors affecting furnace performance. The distribution of heat transfer on the furnace walls is the subject of the companion paper to this one (3).

Fifteen tests were made on the subject boiler to determine the effect on furnace heat absorption of variations of load, excess air, and conditions of overfire air. The available time did not permit a study of the effect of varying the speed of the feeders and the trajectory of the coal. Accordingly, normal operating procedure was followed with respect to feeder adjustments.

The furnace heat absorption has been defined as the heat transferred by convection to the furnace walls, not including the screen, and the heat transferred by radiation to the furnace walls, including the screen. The heat absorption in the furnace was obtained as the difference between the net heat available and the heat losses, the latter including the sensible heat in all the products of combustion and the radiation and convection losses. With slight modification, method b, paragraph 7, of the ASME Test Code for Stationary Steam-Generating Units was followed.

The net heat available was obtained by an over-all heat balance of the entire unit, using the temperature and composition of the gases at the air-heater outlet and the flow rate and enthalpy of the steam generated. Calculation of the sensible heat in the gases leaving the furnace necessitated measurement of the gas temperature and composition ahead of the screen at the furnace outlet. These determinations were made by techniques and equipment developed by the Bureau of Mines for furnace testing (4).

In addition to the temperature and composition of the gas at the furnace outlet similar data were obtained near the mid-elevation in the furnace for three of the tests, to study fluid-flow and heat-transfer patterns within the combustion chamber. Dust loading of the stack gases was measured for several of the tests by Western Precipitation Corporation to study the effects of operating variables upon the fly-ash concentration and to provide necessary data for material-balance calculations. The gas-temperature and composition data, and computed results, are tabulated completely in the paper.

METHODS OF TEST

Description of Furnace. Fig. 1 is a sectional side elevation of the unit, showing the arrangement of the component parts. The furnace is approximately 25½ ft high from the top of the grate to the center of the screen at the furnace outlet. The width is 18 ft 6¾ in. and the depth from front wall to rear wall 14 ft 6 in. The furnace volume is 6600 cu ft. The rear furnace wall, from the lower drum to the outlet, is nearly completely water-cooled and consists of 3½-in. tubes on 3½-in. centers. The front wall and the portion of the rear wall below the lower drum consist of 3½-in. tubes on 6-in. spacing, and the two side walls consist of 3½-in. tubes on 6-in. spacing. All walls contained a 3-in. layer of tile directly behind, and in contact with the tubes. The rear-wall

¹Chemical Engineer, Combustion Research Section, Coal Branch, Bureau of Mines.

²Chief, Bituminous Coal Utilization and Preparation Branch, Region VIII, Bureau of Mines. Mem. ASME.

³Numbers in parentheses refer to the Bibliography at the end of the paper.

Contributed by the Research Committee on Furnace Performance Factors and the Fuels Division and presented at the Annual Meeting, New York, N. Y., November 30-December 5, 1952, of THE AMERICAN SOCIETY OF MECHANICAL ENGINEERS.

NOTE: Statements and opinions advanced in papers are to be understood as individual expressions of their authors and not those of the Society. Manuscript received at ASME Headquarters, November 6, 1952. Paper No. 52-A-143.

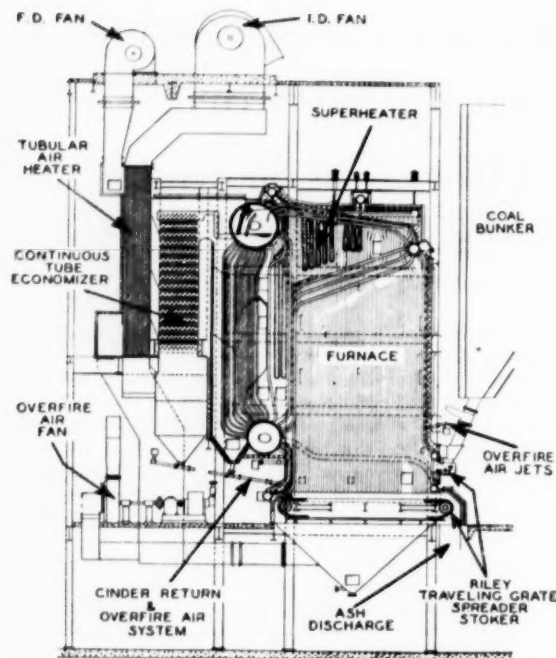


FIG. 1 SECTIONAL SIDE ELEVATION OF BOILER NO. 2, CARBIDE & CARBON CHEMICALS COMPANY, WHITING, IND.

tubes are bent forward and arranged in three rows to form the screen, with a spacing of 12 in. center to center between rows and a spacing of $10\frac{1}{4}$ in. center to center between tubes in each row. The screen tubes enter a header at the front of the unit. The distance from the rear wall to the header is 13 ft 10 in., giving a furnace-outlet area of 241 sq ft. The total projected area of water-cooled surface in the furnace is 1240 sq ft, including the area of the furnace outlet. The effective radiant heating surface, calculated by the method of Mullikin (5) is 1752 sq ft.

The furnace is fired with a spreader stoker on a continuous-front-discharge traveling grate consisting of two sections. There are six individually adjustable feeders on the front wall, each supplied by a separate duct with coal from an overhead bunker. Cinders from the dust collector and from the last pass of the boiler are reinjected to the furnace through nozzles located on the rear wall 18 in. above the grate surface. There are 10 nozzles for the dust collector and 8 for the boiler hopper spaced approximately uniformly across the wall, except that there is none close to the corners. The cinder-return system is arranged for continuous reinjection only. In addition to the air supplied with the cinders, overfire air is admitted through 15 jets evenly spaced 30 in. above the grate in the rear wall, through 11 jets 8 ft 4 in. above the grate in the front wall, and through 12 nozzles just under the coal feeders. The overfire-air system is arranged for using either cold or preheated air.

Combustion air is supplied by a forced-draft fan and preheated in a tubular-type air heater. An induced-draft fan is mounted on the roof between the air-heater outlet and the stack. A separate blower is used to supply the high-pressure overfire jets.

Location of Survey Points. The gas-temperature and composition surveys at the furnace outlet were made by means of a water-cooled high-velocity thermocouple probe inserted through observation doors and specially installed openings on each side of the furnace about 9 in. below the lower row of screen tubes. Meas-

urements were made at three positions in each of the seven doors, giving the distribution shown in Fig. 2 which is a diagram of the furnace outlet in a plane parallel to the screen tubes, as viewed from above and from the front wall. The sampling doors are designated by letters, and the arbitrary positions, chosen to represent equal area divisions, are designated by numbers. The opening could not be placed at the desired location on the right side owing to obstructions outside the furnace. Therefore measurements were made at two locations, A and B, and weighted with respect to area in obtaining average values at the furnace outlet.



FIG. 2 DISTRIBUTION OF SAMPLING POINTS AT FURNACE OUTLET

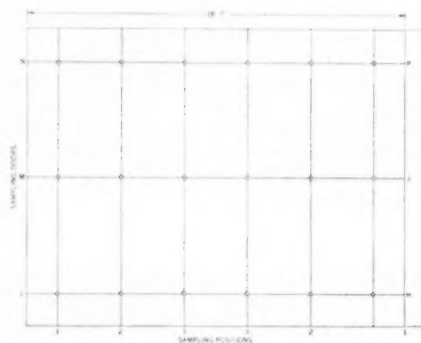


FIG. 3 DISTRIBUTION OF SAMPLING POINTS AT MID-ELEVATION IN FURNACE

In three of the tests gas-temperature and composition surveys were made at an elevation about 15 ft above the grate to study fluid-flow and heat-transfer patterns within the furnace. The distribution of sampling points was similar but not identical to that at the furnace outlet and is shown in Fig. 3, a section through the furnace normal to the walls.

Gas composition was determined at the induced-draft-fan outlet, and both temperature and composition were determined at the air-heater outlet to provide data for calculating the heat balance for the entire unit. At the air-heater outlet the determinations were made at two positions in each of six openings in the duct.

Instrumentation and Analytical Methods. The instrumentation and techniques employed for determining the gas temperature and composition were discussed in detail in recent publications (4, 6). Only such procedures as deviated from former practice will be discussed in this paper.

Since coal scales are not used at this plant, the firing rate could not be determined by the usual method of direct weighing. Therefore an accurate temperature survey was made on the flue gas at

the air-heater outlet to provide data for calculating the heat input by heat balances on the entire unit. Bare chromel-alumel thermocouples were considered satisfactory for this purpose because the gas temperatures were relatively low and the duct was well insulated, reducing to a minimum the errors resulting from radiation from the couple. The other gas and air temperatures required for a heat balance on the air heater were obtained with resistance thermometers in the appropriate ducts and connected to recording instruments on the plant control board. Steam-flow rate, steam temperature and pressure, drafts, and other pertinent data were obtained with regular plant instruments.

The humidity of the air was determined by wet and dry-bulb measurements on a stream tapped from the duct between the forced-draft fan and the air heater.

Coal samples were obtained from each of the six chutes serving the individual coal feeders. Increments representing the full depth of the chute were taken at regular intervals with a scoop, following ASTM specifications as closely as possible. The gross samples were shipped to the laboratories, where screen analyses were made. All other analyses were made by the Coal Analysis Section of the Bureau of Mines. Samples of the ash-pit refuse, the reinjected cinders, and ash from the discharge end of the grate were also obtained for analysis.

The dust concentration was determined in the stack gases for several of the tests by the Western Precipitation Corporation, following procedures recommended by the company and by the ASME Code.

General Test Procedure. The load was adjusted to the desired value several hours before each test was begun to insure equilibrium conditions in the fuel bed. The air rate also was adjusted to give approximately the desired excess-air value. The overfire-air rate, for most of the tests, was adjusted to the minimum amount required to eliminate excessive smoke and fly dust in the stack discharge. For two of the tests, however, considerably more than the required minimum of overfire air was used.

When conditions permitted, the ash pit was cleaned just before the test and again after the test, a representative sample being taken of the material discharged after the test. When this was not feasible, samples were taken at intervals at the discharge end of the grate through each of six inspection doors. In several tests ash samples were taken from both locations to evaluate the accuracy of the grate samples.

Each test was begun as soon as final adjustments to the air rate gave the desired excess-air value at the induced-draft-fan outlet. The actual test period continued for a variable time interval of up to 4 hr, depending upon the ease of making some of the determinations. In 11 of the tests gas-composition surveys were made at the air heater or at the induced-draft fan immediately before and after the furnace-outlet survey. One test was similar to these 11 except that the furnace-outlet survey was interrupted and the second air-heater survey was made just before resuming operations at the furnace outlet. The three final tests included gas-temperature and composition measurements at an elevation near the middle of the furnace. In one of these tests the air-heater surveys were made at the beginning and end of the test period, while in the other two tests an additional survey was made at the air heater between the surveys at the furnace outlet and at the lower elevation. During 12 of the tests the temperatures at the air heater were determined with the recording potentiometer simultaneously with gas-composition data, but in three of the tests these temperatures were obtained by means of a portable potentiometer simultaneously with the furnace traverses.

Coal sampling was started at the beginning of the tests and continued until the desired gross sample size was obtained. In all cases the shipping containers were filled completely to minimize changes of moisture content.

METHODS OF CALCULATION

Flue-Gas Temperature. The flue-gas temperature at the furnace outlet was taken as the arithmetic average of the individual readings at the survey positions, except that the readings for several points were weighted according to the area represented as discussed earlier.

Numerous tests were run to compare the performance of the type E and G radiation shields used in the survey with that of the MHVT shield, which has been accepted widely as a reference standard. However, these tests were inconclusive because of rapid and wide fluctuations of temperature in this furnace. Accordingly, the observed temperatures were corrected to the MHVT basis by using factors from a previous investigation (6) in a furnace with more stable temperature conditions. These factors include the calibration corrections of the individual thermocouples.

The temperature at the air heater was obtained by averaging arithmetically the observed values from the surveys corrected for the thermocouple calibration.

Gas-Composition Data. The gas composition at the furnace outlet varied considerably with the sampling location, the oxygen concentration being much too high at a number of points to be measured by the automatic oxygen recorder. Therefore it was considered that the gas composition at the air-heater outlet would be more representative of average conditions in the furnace due to mixing of the gases that occurs between the furnace and air heater. Leakage between the two locations was negligible because the air heater was of the tubular type and the boiler casing was very tight.

Early in the test series it was discovered that the gas composition at one point in the outlet from the induced-draft fan was essentially the same as the average value for the air-heater outlet. This suggested the possibility of using the composition at that one point of the fan outlet to represent the average conditions in the furnace. Some concern was felt over the possibility of leakage at the fan shaft, but a plot of the observed oxygen-concentration data showed that no error was introduced from this source. This is seen in Fig. 4 in which the average oxygen-meter reading at the air-heater outlet is plotted against the meter reading at the fan outlet. The greatest deviation occurred when the oxygen con-

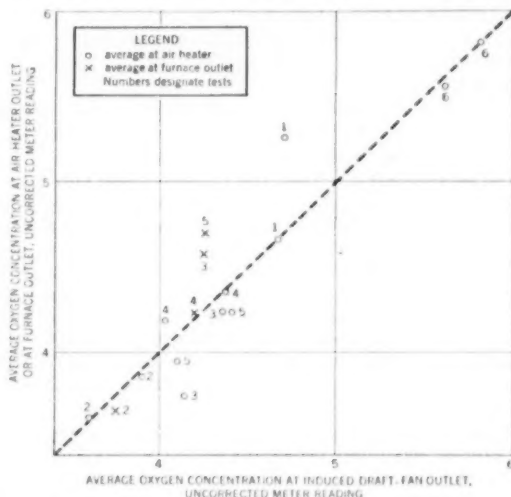


FIG. 4 COMPARISON OF OXYGEN CONCENTRATION AT INDUCED-DRAFT FAN WITH CONCENTRATION AT AIR-HEATER OUTLET AND AT FURNACE OUTLET

(Duplicate points indicate more than one survey during test.)

centration was lower at the fan than at the air heater. Therefore the discrepancies were ascribed to fluctuations in conditions rather than to leakage of air into the system.

The possibility also was considered that this good agreement may have resulted from a fortuitous selection of the sampling point in the duct leading from the induced-draft fan. Consequently, a survey was made in this duct, with the results shown in Fig. 5. The four values at one point were obtained at different times during the survey. Since the variation at this

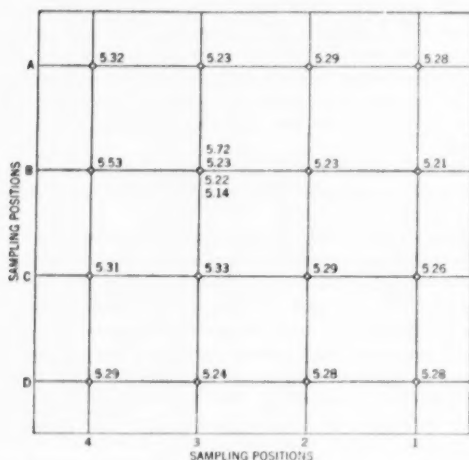


FIG. 5 DISTRIBUTION OF OXYGEN CONCENTRATION ACROSS OUTLET DUCT OF INDUCED-DRAFT FAN
(Numbers indicate uncorrected readings of oxygen meter.)

point is greater than the variation over the entire survey, it was concluded that the gas was very well mixed by the fan and that the variations in composition result from fluctuations in average conditions in the furnace. Accordingly, it was decided to use the gas composition at the fan outlet in the material and heat-balance calculations. In addition to being more representative of the average conditions at any time, the simplicity of the measurement enabled a large number of determinations to be made during a test. This provided better averages with respect to time than would one or two lengthy surveys at some other point in the system.

It is believed that the foregoing method could be applied readily to other furnaces with tubular air heaters where the casing is fairly tight and the fan shaft is sealed reasonably well.

Heat Balance on Entire Unit. Since no means were provided for direct weighing of the coal supplied to the furnace, it was necessary to make a heat balance on the entire unit. The heat input in the coal and in the combustion air and the total heat losses were obtained in terms of the quantity of coal used. The heat transferred to the steam is the difference between the heat input and the losses. The heat transferred to the steam was obtained also from the hourly rate of steam flow and from the steam properties. These two methods of determining the heat transferred from the combustion products to the steam provided the necessary information for calculating the coal-feed rate.

Furnace Heat and Material Balance. The heat absorption in the furnace was calculated as the difference between the net heat available in the furnace and heat lost from the furnace in the products of combustion and by radiation and convection from the furnace casing. The net heat available is the sum of the lower heating value of the fuel fired (corrected for unburned combustible), the sensible heat of the returned cinders, and the enthalpy

above 80 F of the air used for combustion. The enthalpy and quantity of the preheated air were obtained by a heat balance on the air heater, using the temperatures of the gas and air entering and leaving the heater and the quantities of the constituents in the flue gas. The quantity of the unheated air was obtained by difference and its enthalpy was calculated for the temperature entering the heater.

The dust concentration in the flue gas was determined for five of the tests covering a wide range in steam load and in excess air. From these data, values were interpolated for all the other tests. Since the fly dust was not analyzed, the combustible content was assumed to be equal to that of the collected cinders, which was determined for all tests. This assumption was based upon results of investigations by Holton and Engdahl (7) and Morrow, Holton, and Wagner (8). No facilities were available for determining the quantity of collected cinders returned to the furnace. On the basis of the predicted performance of the dust collector and of data given by the authors, previously cited, it was estimated that the concentration of cinders and dust at the furnace outlet was twenty times the fly-ash concentration at the stack. From these data and assumptions and from the combustible content of the asphalt refuse it was possible to calculate the distribution of ash and unburned carbon between the stack and the ashpit.

In making the heat balance it was assumed that the temperature of the ash and cinders at the furnace outlet was the same as that of the gases, and that the temperature of the reinjected cinders was the mean value between the gas temperatures at the last boiler pass and at the entrance to the dust collector. A constant temperature of 680 F was assumed for the discharge from the ashpit. A mean-specific-heat value of 0.27 Btu per lb deg F was used for all the solid products of combustion.

The enthalpy of the furnace-exit gases was calculated from the quantities of the individual gas constituents and their heat content, above 80 F, obtained from the tables of Heck (9). The heat loss from the casing of the unit was obtained from the ABMA Standard Radiation Loss Chart, shown in the ASME Power Test Code for Stationary Steam Generating Units (1946). For the furnace, the radiation loss was taken as one half that of the entire unit.

RESULTS OF TESTS

Description of Tests. Four tests, Nos. 4, 5, 11, and 15, were made at full load; six tests, Nos. 1, 2, 3, 7, 10, and 14, at three-quarter load; and five tests, Nos. 6, 8, 9, 12, and 13, at half load. The object was to determine the effect on furnace heat-absorption efficiency of load, excess air, and different conditions of overfire air. The excess air ranged from a minimum of 17 per cent at three-quarter load to a maximum of 65 per cent at low load. The range was narrower for the full load owing to limitations imposed by the capacity of the induced-draft fan. The pertinent operating data and results obtained during the fifteen tests are summarized in Table 1.⁴

The fuel burned was a high-volatile-C bituminous coal from the No. 9 Seam, Ohio County, Ky. Although the coal was strip-mined, the analysis was very uniform, including even the moisture content, during the series of tests. The characteristics of the fuel and the combustible content of the various solid residues are shown in Table 2.

Distribution of Temperature and Gas Composition. Since the distribution of temperature and gas composition, as well as overall efficiency values, are frequently significant performance characteristics, such data at the individual survey points are included in Tables 3 and 5. In three of the tests, Nos. 13, 14, and 15, the survey included measurements at the mid-elevation of the

⁴ The symbol kB used in tables and figures signifies 1000 Btu.

TABLE 1 SUMMARY OF DATA AND RESULTS. ASME FURNACE HEAT-ABSORPTION TESTS. BOILER NO 2, WHITING, IND. JUNE, 1951

Test number	1	2	3	4	5	6	7	8	9	10	11	12	13	14	15
1 Start of test, Central standard time	6-11	6-12	6-13	6-14	6-15	6-16	6-17	6-18	6-19	6-20	6-21	6-22	6-23	6-24	6-25
2 Actual duration of test, hr	3:05 PM	11:21 AM	3:21 PM	1:19 PM	12:16 PM	11:13 AM	5:15 PM	12:13 PM	1:04 PM	12:10 PM	12:22 PM	10:50 AM	2:00 PM	11:41 AM	12:46 PM
3 Corrected time of test, hr	4:00	2:66	4:05	3:00	3:50	3:00	3:00	3:00	2:55	3:00	3:00	3:00	3:00	3:00	3:00
4 Superheater outlet header pressure, psig	127	118	127	127	127	127	127	127	127	127	127	127	127	127	127
5 Superheater outlet header pressure, psia	127	118	127	127	127	127	127	127	127	127	127	127	127	127	127
6 Coal feed rate, lb per hr	736	736	736	736	736	736	736	736	736	736	736	736	736	736	736
7 Coal feed rate, lb per hr	13,554	12,331	12,616	16,953	17,011	9,226	12,871	9,293	9,607	13,250	17,269	8,672	8,766	12,608	17,389
8 Grate speed, ft per hr	10.0	9.6	11.4	11.0	11.0	7.4	7.4	7.4	7.4	7.4	7.4	7.4	7.4	7.4	7.4
9 Depth of ash at end of grate, in.	2.00	1.50	1.50	1.25	1.25	1.25	1.25	1.25	1.25	1.25	1.25	1.25	1.25	1.25	1.25
10 Depth of ash at end of grate, in.	2.00	1.50	1.50	1.25	1.25	1.25	1.25	1.25	1.25	1.25	1.25	1.25	1.25	1.25	1.25
11 Heat loss from air, lb per lb of coal	0.005	0.005	0.005	0.005	0.005	0.005	0.005	0.005	0.005	0.005	0.005	0.005	0.005	0.005	0.005
12 Total heat loss, lb per lb of coal	0.005	0.005	0.005	0.005	0.005	0.005	0.005	0.005	0.005	0.005	0.005	0.005	0.005	0.005	0.005
13 Total heat loss, lb per lb of coal	0.005	0.005	0.005	0.005	0.005	0.005	0.005	0.005	0.005	0.005	0.005	0.005	0.005	0.005	0.005
14 Clinders retracted to furnace, estimated, lb per lb of coal	0.005	0.005	0.005	0.005	0.005	0.005	0.005	0.005	0.005	0.005	0.005	0.005	0.005	0.005	0.005
15 Heat loss from air, lb per lb of coal	0.005	0.005	0.005	0.005	0.005	0.005	0.005	0.005	0.005	0.005	0.005	0.005	0.005	0.005	0.005
16 With dust collector clinder return	0.005	0.005	0.005	0.005	0.005	0.005	0.005	0.005	0.005	0.005	0.005	0.005	0.005	0.005	0.005
17 With dust collector clinder return	0.005	0.005	0.005	0.005	0.005	0.005	0.005	0.005	0.005	0.005	0.005	0.005	0.005	0.005	0.005
18 Under coal feeder	0.005	0.005	0.005	0.005	0.005	0.005	0.005	0.005	0.005	0.005	0.005	0.005	0.005	0.005	0.005
19 Over coal feeder	0.005	0.005	0.005	0.005	0.005	0.005	0.005	0.005	0.005	0.005	0.005	0.005	0.005	0.005	0.005
20 Overfire air, per cent of total air	10.4	9.3	17.5	17.5	17.5	17.5	17.5	17.5	17.5	17.5	17.5	17.5	17.5	17.5	17.5
21 Average correction of furnace, estimated, lb per lb of coal	0.005	0.005	0.005	0.005	0.005	0.005	0.005	0.005	0.005	0.005	0.005	0.005	0.005	0.005	0.005
22 Average correction of furnace, estimated, lb per lb of coal	0.005	0.005	0.005	0.005	0.005	0.005	0.005	0.005	0.005	0.005	0.005	0.005	0.005	0.005	0.005
23 Heat loss from air, lb per lb of coal	0.005	0.005	0.005	0.005	0.005	0.005	0.005	0.005	0.005	0.005	0.005	0.005	0.005	0.005	0.005
24 Heat loss from air, lb per lb of coal	0.005	0.005	0.005	0.005	0.005	0.005	0.005	0.005	0.005	0.005	0.005	0.005	0.005	0.005	0.005
25 Heat loss from air, lb per lb of coal	0.005	0.005	0.005	0.005	0.005	0.005	0.005	0.005	0.005	0.005	0.005	0.005	0.005	0.005	0.005
26 Heat loss from air, lb per lb of coal	0.005	0.005	0.005	0.005	0.005	0.005	0.005	0.005	0.005	0.005	0.005	0.005	0.005	0.005	0.005
27 Heat loss from air, lb per lb of coal	0.005	0.005	0.005	0.005	0.005	0.005	0.005	0.005	0.005	0.005	0.005	0.005	0.005	0.005	0.005
28 Heat loss from air, lb per lb of coal	0.005	0.005	0.005	0.005	0.005	0.005	0.005	0.005	0.005	0.005	0.005	0.005	0.005	0.005	0.005
29 Average temperature of gas entering air preheater, °F	12.98	15.77	13.46	14.28	14.14	10.77	11.70	13.98	11.84	11.26	12.58	12.35	12.65	12.44	12.48
30 Average temperature of gas leaving air preheater, °F	5.86	3.31	4.94	4.76	4.61	8.53	7.44	8.41	7.28	6.79	6.43	6.43	6.43	6.43	6.43
31 Average temperature of air entering air preheater, °F	81.06	81.42	81.20	81.20	81.20	81.20	81.20	81.20	81.20	81.20	81.20	81.20	81.20	81.20	81.20
32 Average temperature of air leaving air preheater, °F	12.80	10.97	12.15	11.71	11.42	15.62	15.62	15.62	15.62	15.62	15.62	15.62	15.62	15.62	15.62
33 Average temperature of air entering air preheater, °F	12.80	10.97	12.15	11.71	11.42	15.62	15.62	15.62	15.62	15.62	15.62	15.62	15.62	15.62	15.62
34 Average temperature of air leaving air preheater, °F	12.80	10.97	12.15	11.71	11.42	15.62	15.62	15.62	15.62	15.62	15.62	15.62	15.62	15.62	15.62
35 Sensible heat of total air entering furnace, Btu per lb of coal	156,600	142,600	149,400	197,300	200,000	107,700	152,900	108,700	113,200	152,900	199,800	101,500	102,900	149,700	202,000
36 Sensible heat of total air leaving furnace, Btu per lb of coal	180	53	110	370	370	140	240	43	120	250	430	4,220	4,220	6,800	10,550
37 Heat loss due to unburned carbon, Btu per lb of coal	165,400	146,200	154,400	204,400	207,700	113,300	166,300	111,100	118,300	166,300	207,700	101,500	101,500	166,300	211,900
38 Sensible heat in wet gas and fly ash leaving furnace, Btu per lb of coal	79,600	70,100	86,400	111,200	111,200	62,100	90,800	53,400	63,000	90,800	111,200	53,400	53,400	86,400	111,200
39 Heat loss by radiation from furnace, Btu per lb of coal	730	510	510	600	600	580	580	580	580	580	580	580	580	580	580
40 Total sensible heat and radiation losses, Btu per lb of coal	80,900	71,000	87,000	111,400	111,400	62,700	91,300	53,900	63,600	91,300	111,400	53,900	53,900	87,000	111,400
41 Total absorbed in furnace, Btu per lb of coal	80,900	71,000	87,000	111,400	111,400	62,700	91,300	53,900	63,600	91,300	111,400	53,900	53,900	87,000	111,400
42 Sensible heat of total air entering unit, Btu per lb of coal	149,400	142,600	149,400	197,300	200,000	107,700	152,900	108,700	113,200	152,900	199,800	101,500	102,900	149,700	202,000
43 Heat loss by radiation from unit, Btu per lb of coal	1,210	1,160	1,200	1,200	1,200	1,180	1,180	1,180	1,180	1,180	1,180	1,180	1,180	1,180	1,180
44 Sensible heat in wet gas leaving unit, Btu per lb of coal	13,700	10,100	12,000	17,000	17,000	9,760	14,200	7,270	9,760	14,200	19,000	7,510	7,510	12,000	17,000
45 Sensible heat in ash and fly ash leaving unit, Btu per lb of coal	160	160	160	160	160	160	160	160	160	160	160	160	160	160	160
46 Total heat losses from unit, Btu per lb of coal	15,000	11,460	13,360	18,360	18,360	10,080	14,520	7,430	9,920	14,360	20,160	7,670	7,670	12,160	17,160
47 Heat transferred to steam, Btu per lb of coal	242,000	239,000	242,000	270,000	270,000	146,000	207,000	130,000	160,000	207,000	242,000	130,000	130,000	207,000	242,000
48 Heat transferred to steam, Btu per lb of coal	242,000	239,000	242,000	270,000	270,000	146,000	207,000	130,000	160,000	207,000	242,000	130,000	130,000	207,000	242,000
49 Heat transferred to steam, Btu per lb of coal	242,000	239,000	242,000	270,000	270,000	146,000	207,000	130,000	160,000	207,000	242,000	130,000	130,000	207,000	242,000
50 Heat absorption in furnace, Btu per lb of coal	47.1	42.9	48.7	51.9	51.9	28.4	41.4	32.9	47.6	51.7	53.7	28.6	28.6	41.4	53.7
51 Heat absorption in furnace, Btu per lb of coal	47.1	42.9	48.7	51.9	51.9	28.4	41.4	32.9	47.6	51.7	53.7	28.6	28.6	41.4	53.7
52 Furnace heat absorption efficiency, per cent	50.5	51.4	47.3	44.5	44.5	44.0	41.4	31.5	44.0	42.3	45.0	29.2	29.2	41.4	45.0

1/ Includes only time for obtaining data; elapsed time for several tests was longer owing to interruptions.
 2/ This and subsequent figures were rounded after calculation.
 3/ All enthalpy quantities referred to base of 80 °F.
 4/ Corrected for unburned carbon.
 5/ Includes heat loss due to unburned carbon.
 6/ Based on effective radiant heating surface of 2752 sq ft.

TABLE 2 PROPERTIES OF COAL AND ASH

1	2	3	4	5	6	7	8	9	10	11	12	13	14	15
Test number	6-11	6-12	6-13	6-14	6-15	6-16	6-19	6-20	6-21	6-22	6-23	6-23	6-25	6-26
2 Date														
3 Coal, proximate analysis, per cent as fired														
4 Moisture	8.9	8.6	8.2	8.9	7.9	8.8	8.8	7.7	8.8	8.3	7.8	7.8	8.4	8.8
5 Volatile matter	39.4	38.9	39.4	38.3	39.3	40.4	39.1	39.5	39.5	39.3	40.0	40.2	39.4	38.6
6 Fixed carbon	44.5	45.2	45.1	46.1	45.9	45.8	45.3	45.7	44.4	44.6	44.8	44.6	45.6	45.6
7 Ash	7.2	7.3	7.3	6.7	6.9	6.8	6.9	7.1	7.3	7.8	7.4	7.4	6.9	7.0
8 Coal, ultimate analysis, per cent as fired														
9 Hydrogen	5.7	5.6	5.7	5.7	5.8	5.8	5.7	5.7	5.8	5.7	5.7	5.8	5.8	5.7
10 Carbon	67.0	66.9	67.2	67.1	67.6	67.3	67.8	68.0	66.6	66.6	67.3	67.3	67.1	66.9
11 Nitrogen	1.5	1.5	1.5	1.5	1.5	1.5	1.5	1.5	1.4	1.4	1.5	1.4	1.5	1.5
12 Oxygen	15.8	15.6	15.3	15.8	15.1	15.4	15.2	14.8	15.6	14.9	14.8	14.7	15.0	15.5
13 Sulfur	2.8	3.1	3.0	3.2	3.1	3.2	3.0	2.9	3.3	3.6	3.3	3.4	3.4	3.4
14 High heating value, Btu per lb as fired	12,060	12,080	12,180	12,150	12,290	12,210	12,400	12,310	12,070	12,100	12,230	12,250	12,200	12,140
15 Grindability, Hardgrove index	61	59	60	59	54	58	57	62	55	56	61	57	60	60
16 Cone fusibility of ash, F (ASTM)														
17 I.D.T.	1940	1940	1940	2000	2000	1940	2030	2130	2000	2000	1940	2000	1970	1940
18 S.T.	2130	2050	2100	2100	2180	2100	2130	2230	2150	2090	2100	2080	2170	2100
19 F.T.	2260	2180	2360	2260	2470	2310	2420	2420	2420	2360	2360	2420	2420	2260
20 Screen analysis of coal, cumulative per cent retained on screen size, in.														
21 1-1/2	0.08	0.29	0.23	0.38	0.24	0.16	0.25	0.23	0.07	0.10	0.14	0.33	0.05	0.06
22 1-5/16	1.92	2.47	1.94	2.00	1.56	1.36	1.37	0.71	1.21	0.96	1.73	1.36	1.10	0.96
23 1	16.7	15.8	16.6	15.6	15.8	14.8	13.7	13.8	12.5	11.6	15.0	13.3	11.5	10.9
24 3/4	29.5	25.3	29.9	30.5	29.6	27.4	28.0	25.7	20.3	22.4	25.8	24.1	21.4	20.6
25 1/2	51.2	45.8	50.4	52.2	53.7	53.2	50.4	51.6	43.7	47.0	47.2	46.1	45.0	42.3
26 3/8	61.6	56.3	59.7	62.1	62.3	61.9	62.4	63.2	56.1	53.2	58.1	56.8	57.0	54.4
27 1/4	72.7	72.0	72.3	75.8	74.5	74.1	71.5	77.9	73.7	72.0	74.3	73.2	74.1	71.7
28 3/16	76.0	75.3	75.6	79.1	77.9	77.1	75.0	81.0	77.9	75.9	77.8	77.0	77.9	75.9
29 1/8	83.4	85.3	82.7	86.2	84.6	84.0	81.8	85.8	85.5	83.4	85.2	84.9	85.7	84.0
30 0.055	90.9	91.7	89.0	91.7	90.7	90.6	87.4	89.7	92.5	89.7	92.3	91.5	90.9	90.3
31 Dust-collector cinders														
32 Combustible, per cent	13.5	28.0	13.3	13.2	18.3	10.0	12.4	22.1	8.2	13.8	16.8	19.4	13.0	20.3
33 Ash, per cent	86.5	72.0	86.7	86.8	81.7	90.0	87.6	77.9	91.8	86.2	83.2	80.6	87.0	79.7
34 Combustible, per cent retained on U.S. No. 20 screen	1.1	1.4	0.2	2.2	6.6	1.2	0.6	0.6	1.5	2.8	0.6	1.4	1.0	4.3
35 Combustible, per cent retained on U.S. No. 50 screen	10.5	17.8	7.6	11.0	17.4	5.6	12.9	9.8	11.7	22.4	9.8	13.1	11.1	23.4
36 Combustible, per cent retained on U.S. No. 100 screen	33.5	35.9	26.0	34.0	44.7	28.8	35.8	25.4	43.8	53.7	31.1	31.3	38.8	64.7
37 Combustible, per cent retained on U.S. No. 200 screen	69.1	69.1	66.6	69.9	75.4	46.7	71.3	68.6	77.3	79.2	69.0	68.8	75.0	88.4
38 Ash-pit refuse														
39 Combustible, per cent	41.9	58.1		7.3	6.3		10.5		3.7	5.0			2.3	4.1
40 Ash, per cent				92.7	93.7		89.5		96.3	95.0			97.7	95.9
41 Ash from discharge end of grate														
42 Combustible, per cent	2.1	4.2		2.5	1.8	2.7	2.0	1.4	3.5	1.8	2.9	1.6	1.3	
43 Ash, per cent	97.9	95.8		97.5	98.2	97.3	98.0	98.6	96.5	98.2	97.1	98.4	98.7	

TABLE 3 OBSERVED* TEMPERATURE OF GAS, DEG F, IN FURNACE

		AT FURNACE OUTLET															AT MID ELEVATION OF FURNACE				
Door	Position	Test No.															Door	Position	Test No.		
		1	2	3	4	5	6	7	8	9	10	11	12	13	14	15			13	14	15
A	1	1230	1430	1510	1920	1540	1370	1470	1470	1490	1370	1510	1470	1450	1700	1730	H	1	1760	1680	1950
	2	1340	1520	1700	1870	1580	1450	1570	1600	1770	1410	1450	1620	1610	1800	1630		2	1930	1980	1760
	3	1380	1600	1700	1760	1560	1480	1500	1620	1660	1490	1440	1660	1580	1670	1550		3	1920	1920	1630
B	1	1350	1550	1670	2110	1820	1450	1730	1550	1500	1550	1730	1550	1570	1780	2010	J	1	1600	1730	2270
	2	1430	1870	1800	2020	1720	1480	1750	1720	1820	1430	1610	1790	1740	1880	1780		2	1650	1850	2310
	3	1450	1950	1870	1830	1660	1510	1640	1750	1840	1580	1530	1760	1740	1720	1630		3	1730	2120	2140
C	1	1470	1630	1610	2230	2000	1500	1850	1560	1510	1470	1960	1520	1570	1730	2140	K	1	1340	1600	1690
	2	1770	1950	1800	2080	1940	1650	1720	1750	1760	1640	1800	1690	1760	1800	1910		2	1410	1700	1920
	3	1810	1990	1950	1970	1890	1710	1700	1780	1830	1640	1670	1690	1790	1690	1750		3	1480	1730	1870
D	1	1820	1630	1650	2040	2080	1390	1840	1460	1440	1760	2080	1430	1470	1790	2100	L	1	1700	1410	1220
	2	1990	1880	1900	2170	2180	1600	1900	1610	1630	1970	2190	1600	1610	1940	2180		2	1820	1630	1270
	3	2060	1960	1980	2120	2220	1710	1990	1700	1710	2020	2280	1690	1670	2000	2210		3	1910	1510	1480
E	1	1450	1480	1620	1320	1600	1390	1350	1560	1490	1420	1160	1370	1380	1460	1230	M	1	1610	1850	1980
	2	1470	1700	1710	1550	1720	1460	1670	1700	1660	1470	1350	1580	1540	1520	1510		2	1830	2240	2270
	3	1430	1760	1760	1630	1730	1520	1640	1670	1720	1340	1410	1620	1570	1480	1530		3	1930	2250	2160
F	1	1660	1660	1670	1590	1810	1430	1660	1630	1500	1780	1360	1480	1560	1680	1430	N	1	1430	1920	1870
	2	1720	1870	1880	1820	1970	1580	1850	1790	1710	1770	1570	1640	1760	1760	1670		2	1470	1770	1850
	3	1710	1950	1990	1800	2040	1760	1800	1840	1800	1600	1680	1690	1820	1870	1730		3	1490	1720	1980
G	1	1820	1580	1640	1990	1690	1360	1630	1510	1420	1720	1700	1460	1470	1620	1670		1	1430	1920	1870
	2	2050	1860	1790	2090	2060	1550	1880	1610	1560	1940	2200	1610	1610	1820	1870		2	1470	1770	1850
	3	2080	2010	2020	2120	2180	1740	2060	1720	1660	2030	2190	1680	1670	1960	1980		3	1490	1720	1980

* Uncorrected for shield effects.

furnace, and measurements were made at the furnace outlet for all the tests. The temperatures in Table 3 are observed values, determined with the high-velocity thermocouple. For the heat-absorption calculations the averages were converted to the MHVT basis by adding the corrections shown in Table 4. This table was prepared from data in earlier publications, mentioned previously.

TABLE 4 CORRECTIONS TO BE ADDED TO OBSERVED TEMPERATURES TO CONVERT TO RAW MHVT BASIS. ASME FURNACE HEAT-ABSORPTION TESTS. BOILER NO. 2, WHITING, IND.

Observed temp, deg F	Correction, deg F	Observed temp, deg F	Correction, deg F
1600	0	2100	39
1700	0	2200	47
1800	15	2300	55
1900	23	2400	62
2000	31	2500	70

The gas compositions in Table 4 are expressed as per cent excess air, since such values are generally more familiar than are the oxygen percentages measured by the instrument.

Distribution plots of the temperature and excess air were prepared for all the tests. Examination of these plots revealed that the patterns of both gas temperature and excess air depended essentially upon the mass flow of flue gas through the furnace and that they were independent of load and excess air, except as these quantities control the mass-flow rate. Fig. 6 shows the plots of three typical tests that are sufficient to illustrate the various types of patterns obtained in the entire series of tests. Similar plots for the other tests may be constructed readily from the data of Tables 3 and 5.

The most uniform excess-air distribution occurred at the very low mass-flow rates, test No. 13. The minimum value occurred near the center of the plan of the furnace outlet and the value increased slightly toward each side wall. Little change was noted from the front to the rear wall. As the mass flow increased to 170,000 lb per hr the distribution shifted from the pattern with

the gradient predominantly from the center to the sides to a pattern whose gradients were essentially from front to rear as in test No. 3. The gradient also is somewhat steeper than for the low mass-flow rate. The front-to-rear pattern was maintained with increased mass-flow rates, but the distribution changed much more sharply at the highest rates, test No. 11.

The effect of mixing the gases as they pass upward through the furnace is illustrated by the two excess-air plots for test No. 13. Although the general appearance of the pattern is the same at the furnace outlet as at the lower elevation, the steep gradients at the lower level were smoothed considerably by the time the gases had reached the screen. This is shown by the wider spacing of the contour lines.

The excess-air plots furnish a clue relative to the velocity distribution of the gases as they leave the furnace. It was mentioned earlier that the average excess air was obtained from an analysis of gas after being mixed by the induced-draft fan. Therefore, if this value does not agree with an average obtained from the furnace-outlet survey, it indicates that the velocity distribution at the furnace outlet is not uniform. For example, in the plot for test No. 11 it appears that a contour line of about 70 or 80 per cent excess air would represent the average value weighted for area, whereas the true average is approximately 42 per cent. This suggests that the mass velocity in the areas with excess air less than 42 per cent was considerably higher than the velocity in the remainder of the furnace outlet. For test No. 11 this area includes about one fourth of the furnace outlet near the rear wall. Similarly, for test No. 3, the mass velocity is higher in the rear third of the furnace outlet. In test No. 13 the velocity appears to be higher in the center third of the area at the lower elevation but may be fairly uniform at the outlet, since the contour at the average value bisects the area approximately.

The temperature plots show gradual displacement of the maximum value from the center of the furnace outlet to the rear wall as the mass flow of gas increases. At the low mass-flow rate

TABLE 5 EXCESS AIR,^a PER CENT, IN FURNACE
AT FURNACE OUTLET

AT FURNACE OUTLET																	AT MID ELEVATION OF FURNACE				
Door	Position	Test No.															Door	Position	Test No.		
		1	2	3	4	5	6	7	8	9	10	11	12	13	14	15			13	14	15
A	1	42.5	29.6	47.4	22.5	35.9	71.7	69.5	21.7	46.2	98.3	69.2	35.2	40.4	45.0	48.5	H	1	47.3	67.8	41.7
	2	42.3	26.9	45.7	21.1	43.6	67.1	63.4	21.2	31.1	98.3	94.8	30.4	24.2	46.0	56.0		2	32.4	45.5	105.1
	3	44.5	21.0	46.3	25.7	48.0	71.3	75.9	19.0	37.2	110.2	109.0	35.1	37.1	59.2	72.6		3	34.9	68.0	63.4
B	1	42.3	33.9	53.1	20.5	33.9	66.2	47.5	31.1	56.0	75.9	63.3	36.3	35.3	43.1	39.8	J	1	69.6	41.7	24.7
	2	46.3	24.5	48.3	25.7	52.8	70.7	60.5	21.6	38.0	87.2	104.5	31.5	33.7	42.4	69.6		2	41.6	24.2	16.8
	3	44.5	12.6	41.5	38.4	64.1	67.3	72.2	20.2	39.2	93.2	120.2	35.9	34.9	54.9	90.5		3	37.7	16.9	90.0
C	1	45.1	38.4	53.5	10.1	39.5	70.7	52.4	28.6	55.2	84.4	52.7	42.6	38.6	40.2	25.4	K	1	43.3	31.9	78.1
	2	45.4	20.0	45.4	32.3	37.2	63.6	87.7	25.7	42.1	84.6	83.8	38.3	33.8	36.7	60.3		2	44.1	20.7	46.0
	3	43.6	10.0	33.9	36.8	51.2	60.5	94.6	24.7	38.1	94.6	109.6	34.9	33.7	44.3	82.8		3	40.7	18.3	90.1
D	1	43.3	38.7	43.1	23.2	7.1	79.0	36.3	36.7	58.6	61.7	32.3	44.1	40.2	32.3	28.6	L	1	70.4	106.2	84.4
	2	42.0	17.9	25.8	16.9	3.3	62.5	33.0	31.7	47.3	37.7	18.7	43.3	36.7	26.8	30.6		2	57.8	114.6	156.2
	3	43.6	7.1	15.3	27.0	4.4	50.9	34.6	26.3	39.6	43.4	18.8	36.5	35.0	17.7	31.9		3	46.8	112.9	192.8
E	1	86.6	18.3	33.2	38.4	77.6	73.7	80.0	43.9	70.8	114.6	107.2	58.1	48.5	58.9	59.6	M	1	71.7	60.1	53.2
	2	68.8	11.6	38.7	50.8	73.2	82.8	65.2	32.1	61.6	106.2	118.2	51.4	44.4	65.1	74.8		2	44.6	21.6	21.8
	3	71.7	11.5	43.6	41.6	71.8	75.5	77.1	23.3	51.7	98.3	130.2	44.3	39.6	55.2	70.6		3	28.4	11.2	49.7
F	1	71.7	11.0	39.8	32.3	63.0	72.9	63.0	39.2	74.5	73.0	109.0	61.6	53.2	60.6	65.0	N	1	56.0	10.7	27.8
	2	63.0	7.6	31.0	32.0	48.0	69.5	50.0	26.4	55.8	68.1	99.4	46.2	35.8	53.5	62.8		2	43.9	16.0	28.4
	3	63.6	8.7	34.4	38.1	36.4	55.1	70.0	25.7	42.8	94.6	104.5	43.0	29.3	39.2	68.9		3	40.4	17.2	28.1
G	1	61.8	19.1	30.3	14.1	69.2	86.9	57.8	44.3	72.4	52.6	60.0	66.0	47.5	61.3	53.9		1			
	2	35.3	7.6	18.8	19.1	16.4	70.2	35.1	29.4	61.7	34.9	15.8	45.0	39.6	39.8	30.4		2			
	3	37.7	4.5	19.2	32.8	10.1	49.0	28.1	22.8	48.4	37.9	21.2	38.0	33.2	21.6	20.2		3			

^a Obtained from oxygen meter readings, corrected for meter calibration.

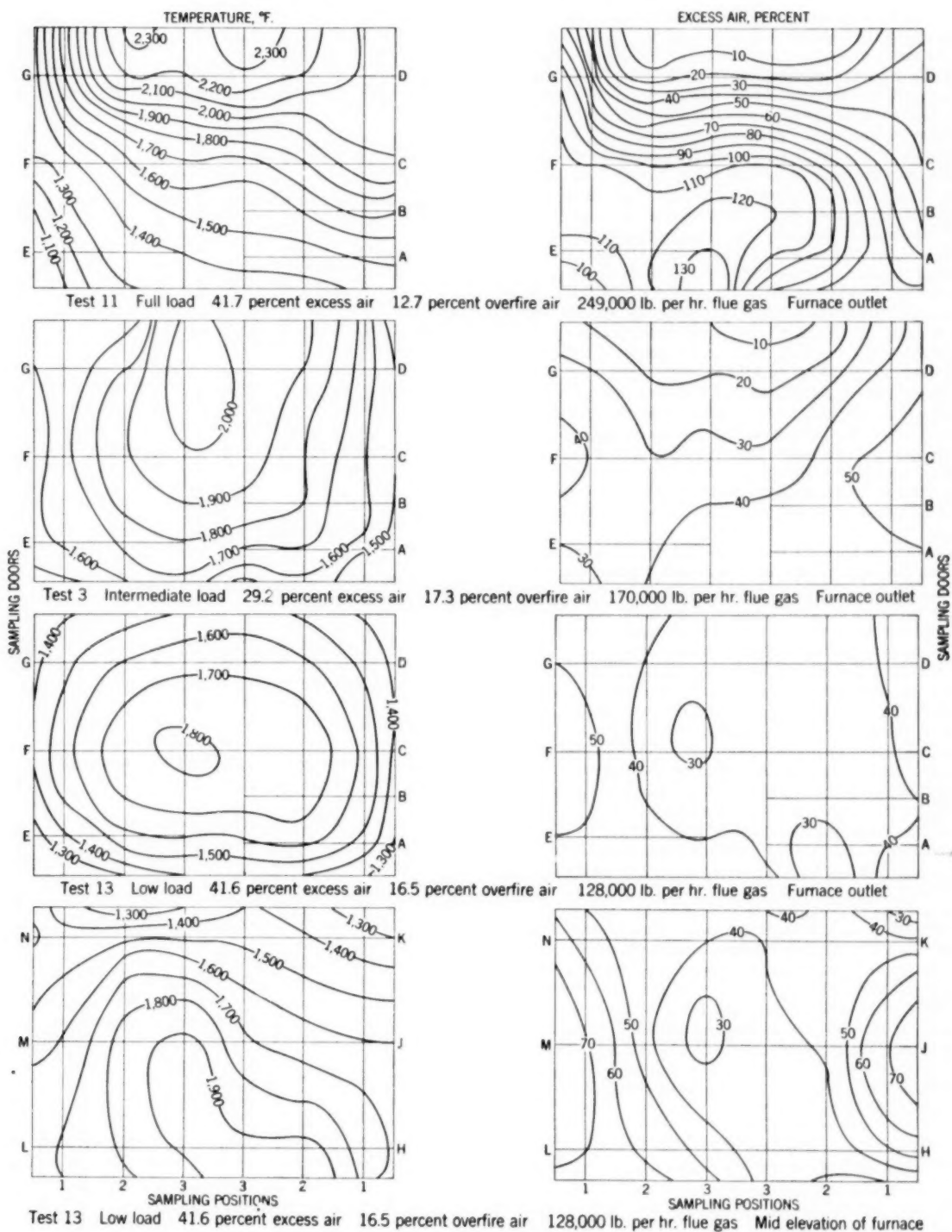


FIG. 6 DISTRIBUTION OF TEMPERATURE AND EXCESS AIR IN FURNACE AT DIFFERENT MASS-FLOW RATES OF FLUE GAS

(test No. 13) the contour lines are essentially concentric with the high spot in the center of the area. At medium flow rate (test No. 3) the maximum value extends from the center to the rear wall, with the gradient predominantly from the center to the front and side walls of the furnace. At the high gas-flow rate (test No. 11) the gradient is from front to rear and is much steeper than those at lower gas-flow rates. The high values are near the rear wall.

In general, the high temperatures are located at regions of low excess air. This may be ascribed to two causes. The theoretical flame temperature is higher with the lower excess air, and the mass velocity was apparently greater in the regions of low excess air, as discussed previously. At the higher velocities a smaller portion of sensible heat of the gases would be transferred to the surroundings, owing to the shorter residence time of the gases. At the low gas-flow rate (test No. 13) the gas composition was fairly uniform and the gas velocity apparently did not vary widely. In this case the high spot is in the center because radiation loss from the center would be less than the combined radiation and convection from the gas near the walls.

The temperature gradients were smoothed somewhat between the lower elevation and the furnace outlet, but the most significant change was shifting of the maximum temperature from near the front of the furnace to the center (test No. 13). In other tests at higher mass-flow rates, not shown in this plot, the maximum temperature moved from the center of the furnace to the rear wall in traveling upward from the mid-elevation to the furnace outlet.

There is no apparent reason for the better distribution of gas composition and velocity at lower mass-flow rates. Ordinarily it would seem that greater turbulence would result at the higher rates and give a better distribution of the gases. Variation in the distribution of overfire air among the various nozzles may be a possible reason for the behavior noted in this furnace.

The use of hot overfire air did not have any noticeable effect upon the distribution of either gas temperature or composition. Test No. 5, with the overfire air at 320 F, and test No. 11, with the overfire air at 85 F, were used for this comparison. The total gas-flow rate for these two tests was almost identical, with 245,000 lb per hr for test No. 5 and 249,000 lb per hr for test No. 11. However, the percentage of total air admitted over the grate was 8.9 and 12.7 for test Nos. 5 and 11, respectively. The temperature gradient was slightly higher near the left wall for test No. 11, but the difference was too small to signify any trend. The relative excess-air patterns for both tests were nearly identical, except that the general level was higher for test No. 11. The average for this test was 41.7 compared to 22.8 per cent for test No. 5.

Furnace Heat-Absorption Efficiency. The calculated furnace heat-absorption efficiency for the several tests is recorded in Table 1. Attempts to correlate these values with excess air and net heat available gave unsatisfactory results. It was apparent, therefore, that other factors must influence the heat-absorption efficiency. Slag and ash deposits usually have considerable effect on furnace performance, and in this particular unit there is evidence that the relative proportions of air introduced under and over the fuel bed have some influence. Both factors will be discussed in more detail.

CORRELATION OF RESULTS

As an aid to quick reference, a condensed summary of the test data and results necessary for correlation is presented in Table 6. This table includes the slag and ash effectiveness factors and the heat-absorption efficiency corrected to theoretically clean wall conditions by means of these factors.

Effect of Slag and Ash on Furnace Performance. The unsatisfactory correlation of measured heat-absorption efficiency with operating conditions, mentioned previously, was ascribed to

TABLE 6 CONDENSED SUMMARY OF OPERATING CONDITIONS AND RESULTS

1 Test number	2	3	4	5	6	7	8	9	10	11	12	13	14	15
2 Rate of steam generation, M lb per hr	127	118	121	162	167	86	123	88	91	123	161	83	84	123
3 Excess air at I D fan, per cent	37.9	16.9	29.2	27.5	22.8	65.6	52.7	27.4	51.3	58.4	41.7	45.1	41.6	41.5
4 Overfire air, per cent of total air	14.3	19.0	17.3	17.2	8.9	16.6	14.7	16.7	18.7	11.8	12.7	16.5	16.5	15.4
5 Overfire-air temperature, F	104	93	84	85	320	97	106	97	101	88	85	93	94	99
6 Net heat available in furnace, kB/(hr)(sq ft.)	93.3	89.4	88.1	116.7	118.9	64.6	91.7	63.8	67.6	91.7	119.4	60.2	61.1	89.2
7 Heat absorption in furnace, kB/(hr)(sq ft.)	47.1	42.9	41.7	51.9	48.9	28.4	38.0	32.9	31.1	38.8	51.7	29.6	30.0	39.7
8 Furnace heat-absorption efficiency, per cent	50.5	51.4	47.3	44.5	41.1	44.0	41.4	51.5	46.0	42.3	45.0	49.2	49.1	44.5
9 Slag and ash effectiveness factor	0.95	0.85	0.85	0.86	0.80	0.83	0.86	0.84	0.86	0.86	0.85	0.87	0.87	0.86
10 Heat absorption in furnace, corrected to clean wall conditions, kB/(hr)(sq ft.)	49.6	50.5	49.1	60.4	61.1	34.2	44.2	39.2	36.2	45.1	61.2	34.0	34.5	46.2
11 Furnace heat-absorption efficiency, corrected to clean wall conditions, per cent	53.2	60.5	55.7	51.7	51.4	53.0	48.1	61.3	53.5	49.2	52.9	56.6	56.4	51.7
Furnace heat-absorption efficiency calculated by the Wohlerberg equation, per cent														
12 Original $\eta_{0.311}$	40.5	49.7	43.8	41.6	42.4	33.9	36.0	49.7	39.3	34.4	36.6	42.9	44.1	40.1
13 Assumed $\eta_{0.410}$	53.0	65.2	57.5	54.3	55.4	44.3	47.1	65.2	51.4	44.9	47.7	56.3	57.8	52.5

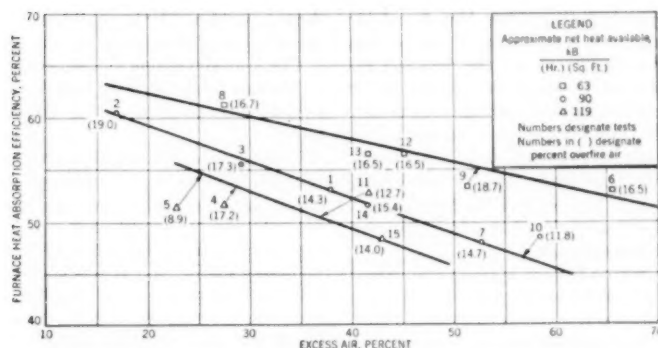


FIG. 7 FURNACE HEAT-ABSORPTION EFFICIENCY CORRECTED TO CLEAN WALL CONDITIONS AS AFFECTED BY NET HEAT AVAILABLE AND EXCESS AIR

variable slag and ash deposits on the furnace walls. Accordingly, the heat-absorption-efficiency values were corrected to clean wall conditions by means of "effectiveness factors" from Part 2 of this report by Feeley and Miller (3) and obtained by the method of Mumford and Bice (10). The magnitude of these factors, shown in Table 6, varies from 0.80 to 0.95.

The furnace heat-absorption efficiency, corrected to clean wall conditions, is shown in Fig. 7 as a function of excess air and net heat available. At the low loads, that is, low values of net heat, the correlation is good except for test No. 9. At the intermediate loads good correlation is obtained for all the tests except No. 10. The slope of the curve is less steep at the low loads, indicating that the effect of excess air is less pronounced at the low loads. This effect is consistent with the results of other investigations.

The quantity and accuracy of the data for the high-load tests were inadequate to permit accurate location of the curve. Accordingly, the curve representing this group was constructed parallel to the curve of the medium-load group, since experience with other furnaces has shown that excess air generally has about the same effect on heat-absorption efficiency at both load conditions.

The lack of correlation for test No. 11 was ascribed to inaccurate data, since the efficiency was greater than the values at intermediate load, with all other test conditions apparently similar. The difference in overfire-air temperature was thought to be responsible for the unsatisfactory agreement of test No. 5. In this test overfire air at 320 F was used, whereas the overfire-air temperature varied from 84 to 106 F for all the other tests.

Effect of Overfire Air. Except for the two tests noted previously, there appears to be some relationship between the deviations of the individual test points from the curves in Fig. 7 and the portion of total air introduced over the fuel bed. Thus test No. 9, with overfire air greater than for the other low-load tests, is located considerably below the corresponding curve. Similarly, test No. 10 had the lowest percentage of overfire air for the intermediate-load tests and is located considerably above the appropriate curve. Likewise, test No. 15, with a lower overfire-air value than test No. 4, has a higher heat-absorption efficiency than has test No. 4, relative to the mean curve at high load. This relationship leads to the conclusion that the heat-absorption efficiency may be a function of overfire air as well as of excess air and net heat available.

Fig. 8 is a plot of furnace heat-absorption efficiency, corrected to clean wall conditions, as related to excess air at various values of overfire air and of net heat available. In the construction of this figure it was assumed that, within the range of the variables in these tests, the efficiency was related linearly with excess air and

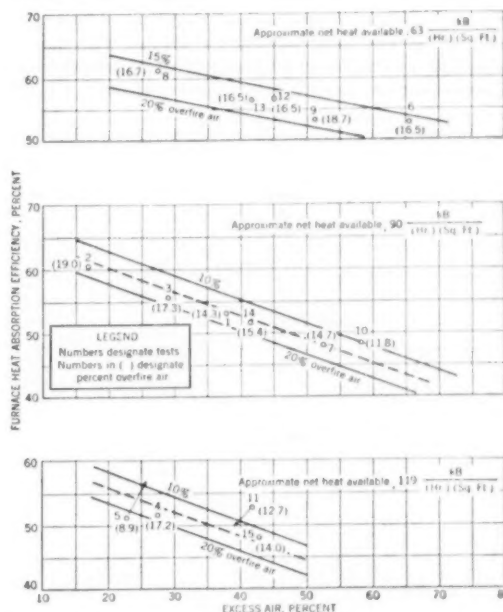


FIG. 8 FURNACE HEAT-ABSORPTION EFFICIENCY CORRECTED TO CLEAN WALL CONDITIONS AS AFFECTED BY NET HEAT AVAILABLE, EXCESS AIR, AND OVERFIRE AIR

with overfire air. The overfire-air parameters then were calculated to give the best fit with the experimental data for the low- and intermediate-load tests. For the full-load tests, however, a different procedure was followed, owing to the scarcity and uncertainty of the experimental data. In this case the slope and spacing of the lines were assumed to be the same as for the intermediate-load tests, and their relative location, as a group, was chosen to give the best fit with test Nos. 4 and 15. Test Nos. 5 and 11 were not used in the correlation for reasons mentioned previously. The figure is shown in three parts, each representing a different load value, to avoid the confusion that would result from overlapping in certain regions if all three groups of curves had been plotted on the same co-ordinates.

It is evident that including overfire air as a parameter improved the correlation considerably for test Nos. 9, 10, 4, and 15, but the agreement for test Nos. 1 and 2 is not quite as good as in Fig. 7. Thus the over-all agreement was improved at the expense of a less satisfactory correlation for two of the tests. There is no

noticeable improvement in the correlation of test Nos. 5 and 11.

Again the same general relationship between the effect of excess air and the net heat available is evident for the low- and intermediate-load tests. The increased slope of the curves at intermediate load shows that the effect of excess air is more pronounced than at low loads. On the other hand, the effect of overfire air on the heat-absorption efficiency is more pronounced at the low loads. There is no apparent reason for this effect. It may result from better penetration of the air jets at lower velocities of air through the grates, or to a different distribution of the overfire air among the various groups of jets at different loads.

At first glance the effect of overfire air may appear paradoxical, inasmuch as Fig. 8 shows higher heat-absorption efficiency at the lower values of overfire air, whereas it is conceded generally that the use of overfire air improves boiler efficiency. However, it should be pointed out that the primary advantage of overfire jets is improved combustion; consequently, the over-all efficiency of the unit will be greater. On the other hand, the furnace heat absorption calculated on the basis of the liberated heat will not be affected by the unburned carbon losses. Therefore it is possible that the overfire air may influence the heat absorption in a different manner than it does the completeness of combustion.

The relationship between the variables can be more simply represented by Fig. 9 which shows the effect of net heat available

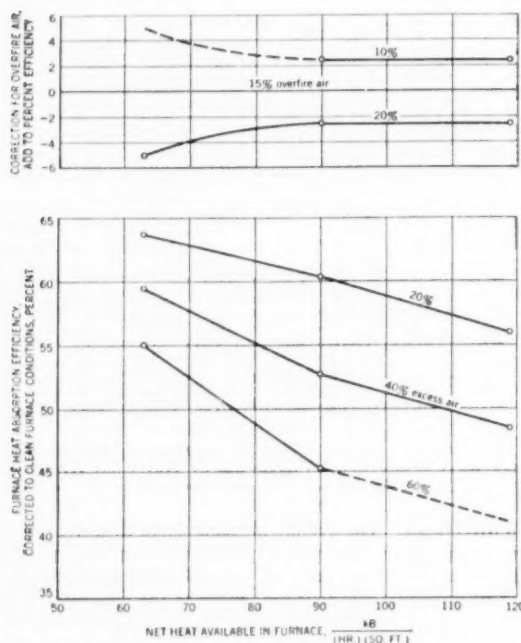


FIG. 9 EFFECT OF OPERATING CONDITIONS ON FURNACE PERFORMANCE FOR CLEAN WALL CONDITIONS

on furnace heat-absorption efficiency for different values of excess air and of overfire air. Data used in constructing the curves were obtained from Fig. 8. The lower portion of the figure shows the heat-absorption efficiency at different values of excess air for a single value (15 per cent) of the portion of combustion air introduced over the fuel bed. The upper part of the figure gives corrections to be added for operation at any value of overfire air within the limits observed in the tests.

Data were available only at the points indicated, and the

dotted portions of the curves were located approximately by linear extrapolation of the data in Fig. 8.

The heat-absorption efficiencies are for theoretically clean wall conditions, from which the actual efficiency at any condition may be found by multiplying by the appropriate ash effectiveness factor.

The curves of this figure show more clearly the effect of net heat available on the heat-absorption efficiency. At 20 per cent excess air the efficiency varies almost linearly with net heat available. At the higher values of excess air the shape of the curves signifies that the net heat available has less effect on efficiency at high load values than at low values. This effect may be due to increased convection heat transfer compensating for the lower radiation at the high mass-flow rates. However, it should be noted that the data are less reliable in this region of operation, as discussed earlier.

Correlation by Wohlenberg's Method. Application of the Stefan-Boltzmann law to the calculation of furnace heat absorption, as suggested by Mullikin (5), has been generally satisfactory for pulverized-coal firing. However, when this method was applied to the present investigation the correlation was unsatisfactory. This is probably due to different heat-transfer processes of a fixed fuel bed as compared to those of suspension burning. Mullikin recognized this and gave correction factors to be used with stoker-fired furnaces. Nevertheless, the results were not satisfactory even when these corrections were considered.

It was thought that the Wohlenberg method (11) of calculating furnace performance would be more satisfactory. It is conceded that the method is empirical, in contrast with the Stefan-Boltzmann law, but this empirical nature permits the use of a large number of parameters to express a wide variety of furnace conditions.

The Wohlenberg equation relates the fraction of the liberated energy absorbed by the furnace walls μ to the other variables in the following manner

$$\mu = FK_1K_2K_3K_4K_5K_6K_7K_8 + C$$

where F represents the μ -value for a certain base condition. Values of 0.311 and 0.452 are used for stoker firing and pulverized-fuel firing, respectively. The K terms and C are correction factors for obtaining μ when the conditions are other than those for the base problem. These factors are determined empirically from the furnace volume, effective radiant heating surface, heat-liberation rate, total furnace area, percentage of excess air, heating value of coal, and the preheat in the combustion air. The effective radiant heating surface in turn is obtained empirically from the total area and the dimensions and arrangement of water tubes. A correction factor is provided for calculating the effective radiant heating surface for walls covered with ash deposits. However, this correction was not used in the present discussion. Inasmuch as the experimental values of furnace heat absorption already have been corrected to clean conditions, all comparisons are made on that basis.

The μ -values in the Wohlenberg equation were calculated for the series of tests with the recommended value of 0.311 used for F . Fig. 10 shows the calculated furnace heat-absorption efficiency, taken as 100μ , plotted against the corresponding experimental value for each test. Although the points are displaced a considerable distance from the 45-deg line denoting equal values, it is evident that most of the data could be represented fairly well with a straight line; that is a fairly consistent relationship is observed between the actual efficiency and the calculated efficiency, although they are not identical.

The development of the Wohlenberg equation was based largely upon data in a report of the ASME Committee on Absorption of Radiant Heat in Boiler Furnaces (12). Accordingly, it was assumed that the equation factors for stoker firing applied

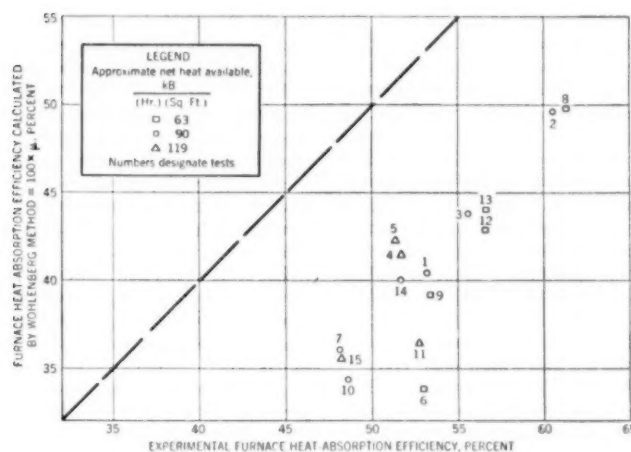


FIG. 10 COMPARISON OF FURNACE HEAT-ABSORPTION EFFICIENCY CALCULATED BY WOHLBERG METHOD TO EFFICIENCY DETERMINED EXPERIMENTALLY
(F -value in Wohlenberg equation = 0.311. Efficiency corrected to clean furnace conditions.)

specifically to the underfeed and chain-grate stokers used in that investigation. However, in spreader-stoker operation a considerable portion of the fuel is burned in suspension. Therefore it is likely that the F -value should lie between those given by Wohlenberg for stoker firing and for pulverized-coal firing.

Accordingly, a value of 0.41, obtained by trial and error, was assumed for F , and the μ -values were recalculated and plotted as shown in Fig. 11. Actually, revised values should be used for both F and K_7 , but the results would be the same for this study. Revision of the F -factor merely altered the relative position of all the points without changing the general pattern.

Some similarity is evident between Figs. 11 and 7. In Fig. 7 the low-load tests and the intermediate-load tests could be represented by straight lines except for test Nos. 9 and 10. The same situation holds true for Fig. 11 as shown by the dotted lines. However, two additional tests, Nos. 6 and 13, do not fit with the others in Fig. 11. The fact that the data in this figure can be correlated according to load suggests that the Wohlenberg method does not correct adequately for the rate of heat liberation in a spreader-stoker-fired furnace. The deviation of tests Nos. 9 and 10 is again apparent because the Wohlenberg correlation has no provision for the effects of overfire air. It will be recalled that the percentage of air admitted over the fuel bed in these two tests differed considerably from that for the other tests in the respective groups designated by net heat available. Likewise the scattering of the full-load tests shown in Fig. 7 persists in Fig. 11. As was mentioned earlier, the data for test No. 11 are believed to be in error, and the use of hot overfire air may be responsible for the deviation of test No. 5.

Although a fair correlation may be obtained by this method if suitable constants and factors are used, it appears that any analysis of heat-transfer processes in a spreader-stoker-fired furnace is complicated by the fact that both fuel bed and suspension burning occur simultaneously with this method of firing.

SUMMARY AND CONCLUSIONS

Furnace heat absorption was measured in a stoker-fired boiler furnace at Whiting, Ind., in co-operation with the ASME Furnace Performance Factors Committee. The objective was to provide basic data on furnace performance and to relate the heat-transfer rates to the temperature drop through the wall tubes, the latter being determined concurrently by other investigators. The furnace heat absorption was determined as the difference between

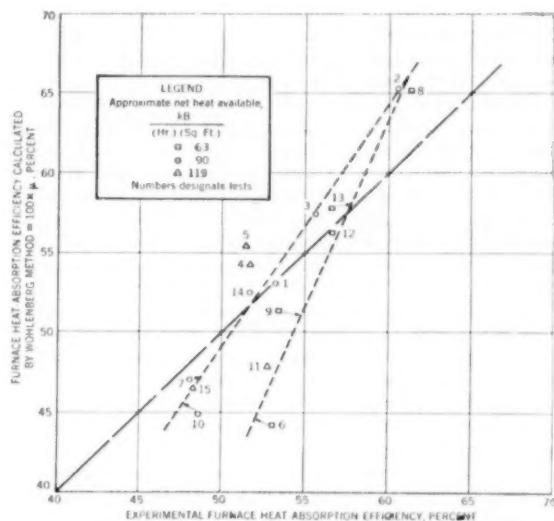


FIG. 11 COMPARISON OF FURNACE HEAT-ABSORPTION EFFICIENCY CALCULATED BY WOHLBERG METHOD TO EFFICIENCY DETERMINED EXPERIMENTALLY
(F -value in Wohlenberg equation assumed at 0.41. Efficiency corrected to clean furnace conditions.)

the net heat input and the heat losses, which comprise the sensible heat in the products of combustion and the radiation and convection losses from the furnace casing. The net heat input was determined by heat-balance calculations on the entire unit. The sensible heat in the furnace exit gases was obtained from temperature and composition measurements, employing techniques developed specifically for furnace testing.

Fifteen tests were made to determine the effect on furnace heat absorption of variations in load, excess air, the percentage of combustion air admitted over the fuel bed, overfire-air temperature, and slag and ash deposits. Only two values of excess air were used at full load owing to capacity limitations of the induced-draft fan. Limitations on the time available prevented studying the effects of variations in the adjustment of the feeders and grates. Design and construction features of the furnace necessi-

tated operation with continuous reinjection of cinders from the last pass of the boiler and from the dust-collector hopper.

A study of the data obtained at the furnace outlet showed that distribution of gas temperature and excess air depended essentially upon the mass flow of flue gas through the furnace. At low mass-flow rates the highest temperature occurred at the center of the outlet, and the gradient was nearly uniform toward all of the walls. As the gas-flow rate increased, the high-temperature zone extended gradually toward the rear wall. At the highest mass-flow rates the highest temperatures were found at the rear wall. The gradient was predominantly from front to rear and much steeper than it was at lower flow rates. The temperature spread at the furnace exit ranged from 300 F at low mass-flow rates to 1000 F at high flow rates.

The excess-air distribution at the furnace outlet was quite uniform at low mass-flow rates of the flue gas, with a slight gradient from the center toward the side walls. At higher gas-flow rates the excess air varied considerably from the front to the rear wall, the higher values occurring near the front of the furnace. The minimum spread in excess-air values was 30 to 50 per cent at the lowest mass-flow rate, while the highest spread, 15 to 130 per cent, occurred at the highest gas-flow rate. The distribution normally would be expected to be more uniform at the higher mass-flow rates, owing to greater turbulence. The opposite condition in this furnace was ascribed to less effective penetration of the overfire air and to nonuniform resistance of the fuel bed to the combustion air at the higher rates.

It was concluded that high gas temperatures generally occurred at the same locations as did low excess air, owing to higher theoretical flame temperatures and to a shorter residence time of the gas in these regions. A variation in mass velocity, and consequently residence time, was apparent from comparison of the excess-air values at the furnace outlet with the true average excess air measured at the induced-draft fan. These data showed that the mass velocity was highest in regions of low excess air.

Data from surveys near the mid-elevation of the furnace for three of the tests, at different mass-flow rates, showed that the distribution of both temperature and excess air improved as the gases traveled upward to the furnace outlet. The use of hot overfire air had no apparent effect on distribution of either temperature or excess air at the furnace outlet, as compared with the distribution when using cold overfire air.

An attempt to correlate furnace-heat absorption efficiency with net heat available and excess air was unsatisfactory. This lack of correlation was ascribed to slag and ash deposits, since such deposits generally have considerable influence on the performance of coal-fired furnaces. Accordingly, the heat-absorption efficiencies were corrected to theoretically clean wall conditions by using slag and ash effectiveness factors. These factors, based upon visual observations of the furnace walls during the tests, varied from 0.80 to 0.88 for all tests except one, for which the factor was 0.95. Although eliminating the effects of the wall deposits improved the correlation considerably, there was still poor agreement in several instances. There was evidence that the percentage of combustion air admitted over the fuel bed was responsible for the lack of agreement. Accordingly, overfire air was included as an additional parameter and improved the general correlation for the series of tests. However, one test, using hot overfire air, did not fit well with the other tests in which cold overfire air was used.

The maximum corrected furnace heat-absorption efficiency was 61.3 per cent at low load, with 27 per cent excess air, and with 16.7 per cent of the air introduced over the fuel bed. The lowest efficiency, 48.1 per cent, was obtained at intermediate load, with 53 per cent excess air, and with 14.7 per cent overfire air. Al-

though the plotted results show that the minimum efficiency would occur at full load and high excess air, these conditions were not attainable, owing to reasons cited previously.

The furnace heat-absorption efficiency decreased with increasing values of net heat available, with all other conditions held constant. At 20 per cent excess air and 15 per cent overfire air the efficiency varied almost linearly from 63.7 to 56.0 per cent at hourly net heat-input rates of 63 and 119 kB per sq ft, respectively.⁴ At higher excess-air values, up to 60 per cent, the net heat available had a greater effect on efficiency at low heat-input rates than at high rates.

The heat-absorption efficiency decreased linearly with an increase of excess air at low and intermediate values of net heat available, the rate of decrease being more pronounced at the intermediate-load value. For example, at an hourly net-heat rate of 90 kB per sq ft, the efficiency decreased from 60.4 per cent to 45.3 per cent with an increase in excess air of from 20 to 60 per cent. At a heat-input rate of 63 kB per sq ft, an increase in excess air from 20 to 60 per cent resulted in a decrease of efficiency from 63.7 per cent to 55.0. Although the data were inconclusive, there is evidence that the effect of excess air at high heat-input rates was similar to that at intermediate rates.

The amount of overfire air had a greater effect on heat-absorption efficiency at low than at intermediate loads. At low load and at 20 per cent excess air, an increase in overfire air from 15 to 20 per cent caused a decrease from 63.7 to 58.7 per cent in the efficiency. At intermediate net heat input a reduction in efficiency of 61.4 to 58.9 per cent resulted from an increase of 15 to 20 per cent in overfire air. The relationship between efficiency and overfire air appeared to be linear and to be independent of excess air at all values of net heat available. Although conclusive data are not available, the results of one test suggest that the use of hot overfire air would result in a decrease of efficiency as compared with the efficiency when using cold overfire air.

The experimental value of furnace heat-absorption efficiency was compared with values calculated by the Wohlenberg method. The experimental values were 22 to 37 per cent higher than the calculated values when using the equation factors recommended by Wohlenberg for stoker-fired furnaces. Better agreement was found by using assumed equation factors that lie between those recommended for stoker firing and for pulverized-coal firing. Nevertheless, the deviations between the calculated and experimental values could be correlated according to the net heat available. It was concluded, therefore, that the factors in the Wohlenberg equation are not adequate to correct for the rate of heat liberation in spreader-stoker-fired furnaces. Likewise, no method is provided for correcting the calculated value for the amount of overfire air, whereas it was shown that the percentage of overfire air had some influence upon the experimental heat-absorption efficiency.

Inasmuch as difficulty was experienced in correlating furnace performance with operating conditions, it was concluded that more extensive investigations would be required to evaluate fully the effect of all the possible variables on the performance of spreader-stoker-fired furnaces. These variables are greater in number than for other methods of firing and include, among the more important items, grate speed, speed and trajectory adjustments of feeders, depth of fuel bed, distribution of coal on the grate, distribution of underfire and overfire air, arrangement and dimensions of the overfire-air jet, temperature of the overfire air, and the method of reinjecting cinders.

It was concluded further that predicting the performance of a spreader-stoker-fired furnace by empirical methods is complicated by difficulties in analyzing the heat-transfer process for a combination of suspension and fixed-bed burning which is peculiar to this method of firing.

ACKNOWLEDGMENTS

The authors gratefully acknowledge, with appreciation and thanks, the contributions to this investigation made by the following:

The ASME Special Research Committee on Furnace Performance Factors, for the opportunity to participate in this project, and the individual committee members for helpful suggestions.

Dr. L. C. McCabe, Chief, Fuels and Explosives Division, Bureau of Mines, who authorized the Bureau's work on this investigation.

J. H. Garrison, J. W. Trull, and R. S. Potts of the Whiting Plant, Carbide & Carbon Chemicals Company, and their staff, for their assistance in preparing for and conducting the tests.

J. R. Brauweiler, Western Precipitation Corporation, who conducted the extensive dust-loading tests that constituted an important part of the investigation.

The service engineers and the research and design engineers, Riley Stoker Corporation, for their part in preparing for and in conducting the tests.

The engineers and assistants of the Combustion Research Section, Bureau of Mines: J. Jonakin, E. G. Graf, L. A. Spano, C. H. Schwartz, J. J. Pfeiffer, and G. R. Kollar, who capably performed the difficult test work that formed the basis of this paper.

J. H. Cramer, formerly of the Combustion Research Section, for assistance in conducting the tests.

The Bailey Meter Company, for the loan of a recording oxygen meter.

BIBLIOGRAPHY

1 "An Investigation of the Variation in Heat Absorption in a Pulverized-Coal-Fired Water-Cooled Steam-Boiler Furnace—Parts 1 to 4," by L. B. Schueler, W. T. Reid, Paul Cohen, R. C. Corey, A. R. Mumford, C. G. R. Humphreys, and G. W. Bice, *Trans. ASME*, vol. 70, 1948, pp. 553-619.

"Furnace Heat Absorption in Paddy's Run Pulverized-Coal-Fired Steam Generator, Using Turbulent Burners, Louisville, Ky.," Parts 1 to 3, by R. I. Wheeler, M. H. Howard, R. C. Corey, Paul

Cohen, and H. H. Hemenway, *Trans. ASME*, vol. 72, 1950, pp. 893-948.

"Furnace Heat Absorption in Pulverized-Coal-Fired Steam Generator, Willow Island Station," Parts 1 and 2, by J. W. Myers, R. C. Corey, F. G. Ely, and N. H. Twyman, *Trans. ASME*, vol. 73, 1951, pp. 419-459.

2 "Variation in Heat Absorption in a Natural-Gas-Fired, Water-Cooled Steam-Boiler Furnace," by A. R. Mumford and R. C. Corey, *Trans. ASME*, vol. 74, 1952, pp. 1191-1215.

3 "Furnace Heat Absorption in a Spreader-Stoker-Fired Steam Generator: Part 2—"Variation in Furnace Heat Absorption as Shown by Measurement of Temperature of Exposed Side of Furnace Tubes," by F. G. Feeley, Jr., and E. C. Miller, published in this issue of the *Transactions*, pp. 925-942.

4 "Methods and Instrumentation for Furnace Heat-Absorption Studies: Temperature and Composition of Gases at Furnace Outlet," by P. Cohen, R. C. Corey, and J. W. Myers, *Trans. ASME*, vol. 71, 1949, pp. 965-978.

5 "Evaluation of Effective Radiant Heating Surface and Application of the Stefan-Boltzmann Law to Heat Absorption in Boiler Furnaces," by H. F. Mullikin, *Trans. ASME*, vol. 57, 1935, pp. 517-529.

6 "Furnace Heat Absorption in Pulverized-Coal-Fired Steam Generator, Willow Island Station. Part I. Furnace Heat-Absorption Efficiency as Shown by Temperature and Composition of Gases Leaving the Furnace," by J. W. Myers and R. C. Corey, *Trans. ASME*, vol. 73, 1951, pp. 419-431.

7 "Methods of Reducing Dust Emission From a Spreader-Stoker-Fired Boiler Furnace," by W. C. Holton and R. B. Engdahl, *Trans. ASME*, vol. 74, 1952, pp. 207-218.

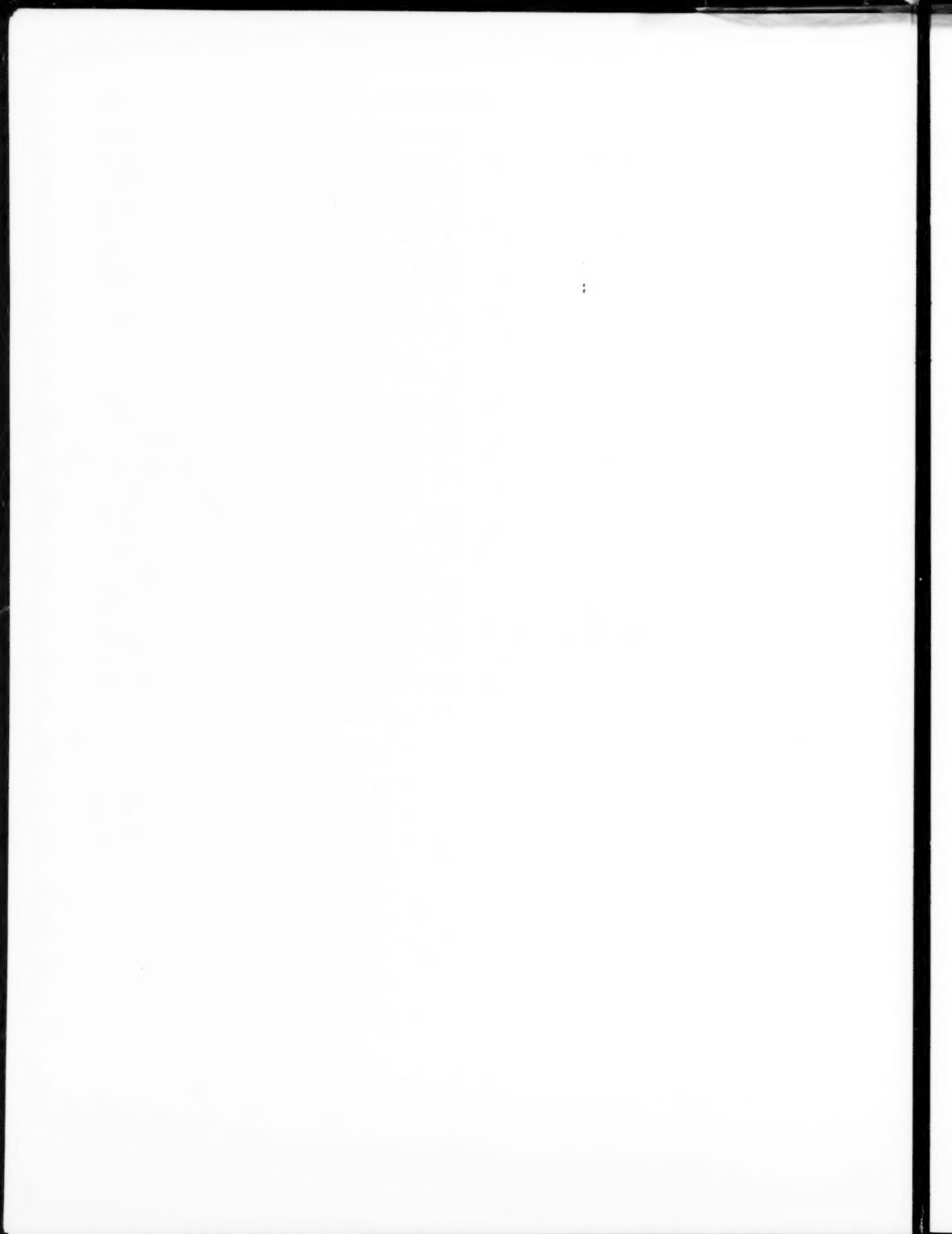
8 "An Investigation of Gravity Reinjection of Fly Ash on a Spreader-Stoker-Fired Boiler Unit," by C. H. Morrow, W. C. Holton, and H. L. Wagner, presented at the 1951 Annual Meeting of THE AMERICAN SOCIETY OF MECHANICAL ENGINEERS.

9 "The New Specific Heats," by R. C. H. Heck, *Mechanical Engineering*, vol. 62, 1940, pp. 9-12.

10 "An Investigation of the Variation in Heat Absorption in a Pulverized-Coal-Fired Water-Cooled Steam-Boiler Furnace. IV—Comparison and Correlation of the Results of Furnace Heat-Absorption Investigations," by A. R. Mumford and G. W. Bice, *Trans. ASME*, vol. 70, 1948, pp. 601-614.

11 "Review of Methods of Computing Heat Absorption in Boiler Furnaces," by W. J. Wohlenberg and H. F. Mullikin, *Trans. ASME*, vol. 57, 1935, pp. 531-540.

12 "An Experimental Investigation of Heat Absorption in Boiler Furnaces," by W. J. Wohlenberg, H. F. Mullikin, W. H. Armacost, and C. W. Gordon, *Trans. ASME*, vol. 57, 1935, pp. 541-554.



Furnace Heat Absorption in a Spreader-Stoker-Fired Steam Generator

2 Variation in Furnace Heat Absorption as Shown by Measurement of Temperature of Exposed Side of Furnace Tubes

By F. G. FEELEY, JR.,¹ AND E. C. MILLER²

This is a report of test work performed under the auspices of the ASME Special Research Committee on Furnace Performance Factors, and covers the testing of a spreader-stoker-fired furnace. Previous test work was performed on three pulverized-coal-fired furnaces and one gas-fired furnace. In so far as possible the present test work followed the technique developed on the previous tests. Furnace heat absorption was determined by furnace heat balance and also by measuring the surface temperature of the exposed side of the furnace tubes. Part 2 of this paper covers the measurement of furnace heat absorption by the latter method. The test procedure required a series of tests to determine the stack dust loading. Because of the many questions received concerning the results of this portion of the test work the data have been included.

INTRODUCTION

THE performance of furnaces and steam-generating units has long been the subject of investigation by organized research groups and independent investigators. The test work has followed two lines, one being under laboratory-controlled conditions and the other test work on furnaces of actual steam-generating units. The many variables which affect furnace performance have made the application of laboratory data to furnace design difficult. The considerable quantity of data that has been collected in the past 25 years is predominantly that relating to pulverized-coal firing. The rapid growth of spreader-stoker firing has created a need for more data for the guidance of designers and operating engineers. The ASME Special Research Committee on Furnace Performance Factors decided to meet this requirement by testing a spreader-stoker-fired steam-generating unit.

The committee announced plans to test a spreader-stoker-fired steam-generating unit and requested suggestions concerning the test work. The response to the program was favorable and the suggestions of items to be checked indicated that the exploratory work yet to be done on spreader stokers was far beyond the jurisdiction of this committee. It was impossible in the time allowed and the funds available to check but a few of the vari-

ables that were suggested, therefore the committee selected those variables which most significantly influence furnace performance.

It was decided that the test work on the spreader-stoker unit should follow, as closely as possible, the test procedures followed on the pulverized-coal-fired test units. It was agreed that the variables to be checked were rating, excess air, overfire air, and fuel size. In the course of checking these variables other data necessarily were accumulated. These supplementary data include stack-dust loading, fly-ash analyses, and carbon losses.

DESCRIPTION OF EQUIPMENT

The boiler selected for this test work is the No. 2 unit of three identical units, in the Whiting, Ind., plant of Carbide & Carbon Chemicals Company, a Division of Union Carbide and Carbon Corporation. The units were placed in service September, 1950, and the tests were run in June, 1951. Fig. 1 shows the general arrangement of this equipment. The unit is designed to deliver 165,000 lb of steam per hr continuously at 915 psig and 740 F. The furnace is 18 ft 6 $\frac{3}{4}$ in. wide, 14 ft 6 in. deep, 24 ft 6 in. high from the grate surface to the slag-screen tubes, with a furnace volume of 6600 cu ft. All tubes in the furnace envelope are 3 $\frac{1}{4}$ in. OD spaced as follows: rear wall from grate to lower drum 6 $\frac{3}{4}$ in. and from lower drum to slag screen 3 $\frac{3}{4}$ in., side walls 6 in., front wall between feeders only and extending between under-feeder and over-feeder headers 5 $\frac{1}{2}$ in., with the remainder of the front wall spaced 6 $\frac{3}{4}$ in. The three rows of slag-screen tubes have 12 in. vertical spacing and 10 $\frac{1}{8}$ in. lateral spacing. The furnace-wall refractory is tangent to the back of the tubes. The unit is fired by six spreader-stoker feeders in conjunction with an 18-ft-wide \times 18-ft-long front-discharge traveling grate. Intertube gas burners are located in the furnace side walls.

The cinder-return system continuously reinjects the fly ash from the boiler last-pass hoppers and dust-collector hoppers to the furnace. There are eight 2 $\frac{1}{2}$ -in. reinjection nozzles from the boiler hoppers and ten 2 $\frac{1}{2}$ -in. reinjection nozzles from the dust-collector hoppers. The overfire-air system consists of fifteen 1 $\frac{1}{4}$ -in. nozzles in the rear wall, eleven 1 $\frac{1}{4}$ -in. nozzles in the front wall above the feeder, and twelve $\frac{3}{4}$ -in. nozzles beneath the feeders. A single fan supplies air for the cinder-return and overfire-air systems of the three boilers. A second fan is held as a stand-by. The system uses hot air from the air preheaters but for testing one fan was arranged to supply cold air. For ease of testing, all but one test were run with cold overfire and reinjection air.

The grate ash is accumulated in an ashpit and periodically emptied onto a mechanical ash-conveyer system.

TEST EQUIPMENT

The thermocouples for measuring furnace-tube outer-surface temperatures were installed during erection of the boiler and so

¹ Mechanical Engineer, Carbide and Carbon Chemicals Company, a Division of Union Carbide and Carbon Corporation, New York, N. Y. Mem. ASME.

² Research Engineer, Riley Stoker Corporation, Worcester, Mass. Mem. ASME.

Contributed by the Research Committee on Furnace Performance Factors and the Fuels Division and presented at the Annual Meeting, New York, N. Y., November 30-December 5, 1952, of THE AMERICAN SOCIETY OF MECHANICAL ENGINEERS.

NOTE: Statements and opinions advanced in papers are to be understood as individual expressions of their authors and not those of the Society. Manuscript received at ASME Headquarters, November 24, 1952. Paper No. 52-A-142.

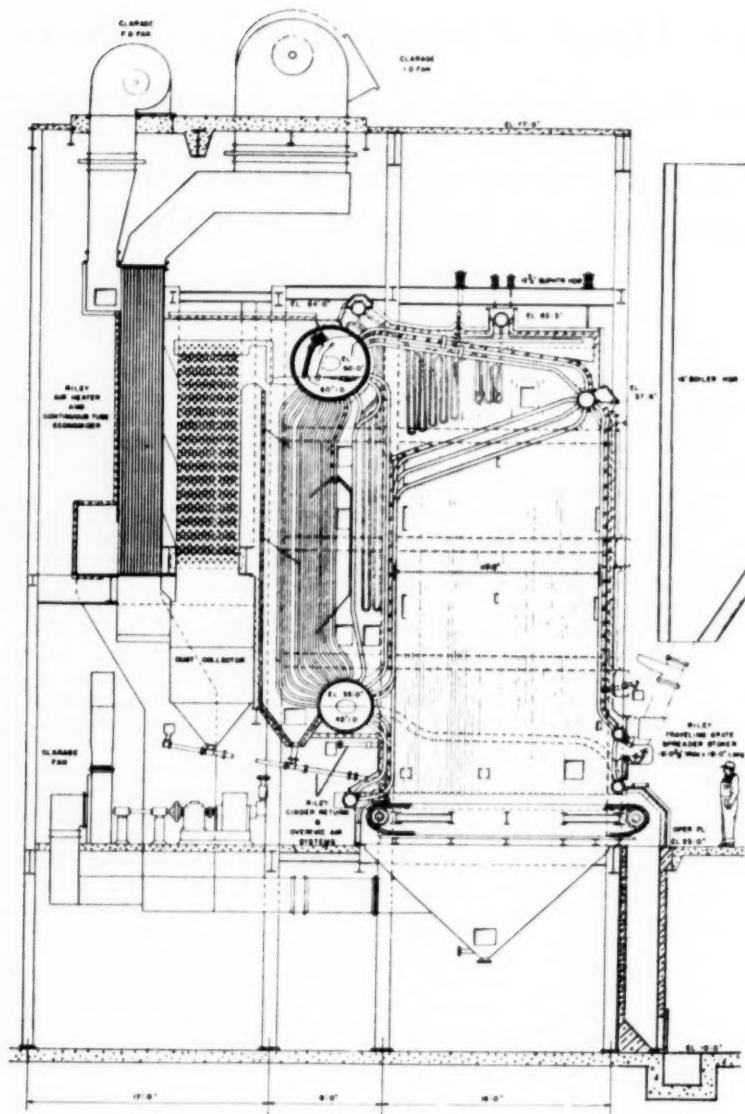


FIG. 1 GENERAL ARRANGEMENT OF TEST UNIT

were exposed to furnace gases for approximately 8 months before the tests were started. The guard-ring method of attaching the thermocouple wires to the tube surface was used. This is the method used for the Tidd and Paddy's Run tests and is illustrated in Fig. 2. The thermocouples are chromel-alumel No. 22 gage glass-insulated duplex wire. Fig. 3 shows the location and designation of the thermocouple points on the developed furnace walls. No points were installed in the slag screen owing to difficulty in carrying leads out of the hot-gas zone.

The thermocouple leads were introduced into a Speedomax recorder through soldered connections. The Speedomax is a high-speed temperature-recording unit made up of seven banks of 21 points each. For these tests, a total of only 70 temperature points was used; so each furnace wall was assigned to a separate bank. The tube-surface temperature readings corrected for

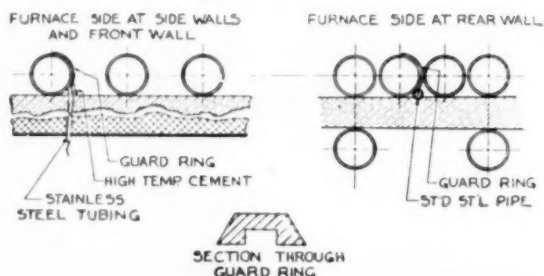


FIG. 2 DETAILS OF TUBE-SURFACE THERMOCOUPLES

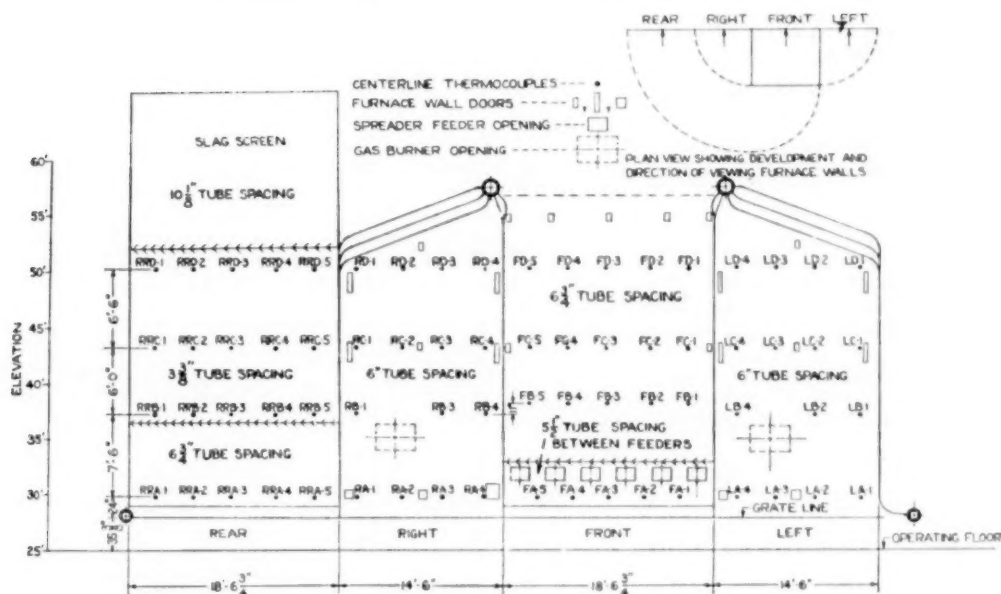


FIG. 3 THERMOCOUPLE PLAN IN DEVELOPED FURNACE WALLS

ambient temperature were recorded on a strip chart and at the same time were indicated by a pointer on a temperature scale from which they were read directly and recorded on a long sheet. The instrument produced a complete set of readings in 6 min.

TEST PROCEDURE

The test schedule was set up to obtain data at the nominal steam loads of 80,000, 120,000, and 160,000 lb per hr. Each load was to be run at 25 per cent, 40 per cent, and 60 per cent excess air, resulting in nine tests. Unfortunately, it was not possible to run a test at the 160,000 lb per hr, 60 per cent excess-air condition owing to limited induced-fan capacity. Whenever possible, two tests were run at each load condition to ascertain reproducibility of the data.

The unit was brought to the desired load and excess-air conditions and held there prior to each test. The air requirements for the cinder-return and overfire-air systems were adjusted manually to give optimum operating conditions. These auxiliary-air settings influence the furnace flame shape. The flame shape during each test period was recorded as a part of the test data.

No attempt was made to clean the furnace and boiler heat-absorbing surfaces directly before the tests as these surfaces were relatively clean.

At the close of each test period, the furnace-wall ash coating at the various elevations and sections was estimated by observation and recorded to provide data for assignment of slag-ash factors. The estimates were based on percentage of projected tube surface covered by slag.

The boiler control panel provided all necessary flow, temperature, and pressure readings. Air-flow data in the cinder-return and overfire-air ducts were obtained separately. Fuel consumption was calculated by the heat-balance method. To provide a reliable sample of coal for analysis of composition and sizing, the samples were taken across the full depth of each of the six coal chutes at 15-min intervals throughout the test period.

Owing to the rigid operating schedule the plant had to maintain, it was not always possible to empty the ashpit at the end of

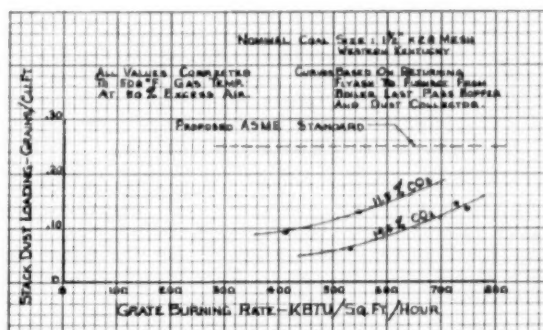


FIG. 4 STACK-DUST LOADING

each test period to obtain a grate-refuse sample. In those instances a representative sample was collected during the test from the discharge end of the grate.

Extensive stack tests were run to determine stack dust loadings and combustible content in the refuse leaving the stack. Care was exercised to assure reliable stack dust-loading measurements. Samples were obtained by traversing the stack at a level 54 ft from its base. The stack is 7 ft diam and 80 ft high. Owing to the very low stack dust loadings the weight of stack-refuse sample collected was inadequate for analysis of carbon content; for calculating stack carbon loss the carbon content of the dust-collector catch was used. A representative dust-collector catch sample was drawn from each of the ten cinder-return lines at 30-min intervals.

The dust-collector catch analyses are included in the tabulated data of Part 1³ of this paper, and the results of the stack dust

³ "Furnace Heat Absorption in a Spreader-Stoker-Fired Steam Generator—Part 1—Furnace Heat-Absorption Efficiency as Shown by Enthalpy of Gases Leaving the Furnace," by J. W. Myers and R. C. Corey, published in this issue of the Transactions, pp. 909-923.

loading are given in Fig. 4. A note of interest is the influence of excess air on stack dust loading.

METHOD OF CALCULATION

Calculation of heat absorption as shown by the measurement of the surface temperature of the exposed side of furnace tubes conformed to the methods used in previous committee tests. The basic equation is

$$Q = U A \Delta T$$

where

Q = heat absorbed, Btu per hr

U_o = over-all conductance, tube surface to boiling liquid, Btu/sq ft/hr/deg F referred to outer surface

A = effective heat-absorbing area, sq ft

ΔT = difference between tube outside-surface temperature and boiler-water saturation temperature

The equation for deriving a value for U_o is

$$U_o = \frac{U_m U_s}{U_m + U_s}$$

where

$$U_m = \frac{k}{R \log_e \frac{R}{r}}$$

U_m = conductance of tube wall, Btu/sq ft/hr/deg F

U_s = conductance at inner surface, Btu/sq ft/hr/deg F

k = conductivity of tube metal, Btu/sq ft/hr/deg F/in.

R = radius, center of tube to outer surface or thermocouple junction, in.

r = radius, center of tube to inner surface, in.

Conductance at the inner surface U_s has been assumed to equal 5000 Btu/sq ft/hr/deg F, a figure previously assumed for committee work. Interpolating from recent available data⁴ a conductivity value of tube metal k equal to 310 Btu/sq ft/hr/deg F/in. at 550 F has been used. There have been considerable discussions of this factor in the previous papers on furnace performance⁵ and values of 300 and 348 have both been used. Calculated furnace efficiency varies directly as the conductance factor.

The furnace-wall tubes are 3 1/4 in. OD with a wall thickness of 0.220 in. and inside diameter of 2.810 in. For calculating R , the thermocouple tip was assumed to be one wire diameter (0.032 in.) below the surface of the tube. Also assumed was a mill tolerance of 15 per cent on tube-wall thickness.

NET HEAT AVAILABLE

The coal feed to the steam generator was calculated by the heat-balance method, since no coal weights were available. The net heat available to the furnace was taken as the lower heating value of the coal plus the sensible heat above 80 F in the pre-

heated forced-draft air and reinjected cinders, less the loss due to unburned combustibles in the grate and stack refuse. The net available heat is shown in Table I.

EVALUATION OF HEATING SURFACE

The calculation of the waterwall heat-absorbing area takes into account the effect of tube spacing on direct radiation and re-radiation from the refractory.⁶ The Hottel curve for evaluating the effective heating surfaces of the furnace walls is shown in Fig. 5. On this basis the total waterwall heat-absorbing area of the furnace was calculated to be 1752 sq ft which includes the gross furnace-outlet area at the slag screen.

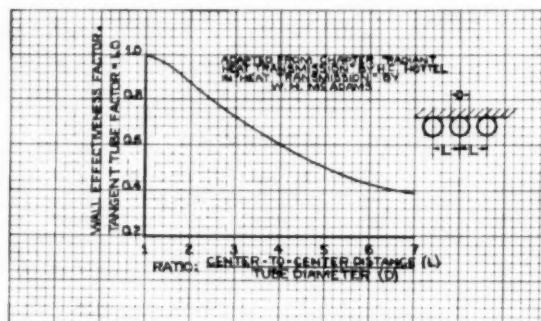


FIG. 5 WALL-EFFECTIVENESS FACTORS

The ΔT values are obtained by subtracting boiler-water saturation temperature from the test recorded values of tube-surface temperature. The ΔT values have been plotted on developed views of the furnace to give the isothermal patterns and together with the corresponding slag and ash-coverage diagrams are shown in Figs. 6 to 20, inclusive. For the purpose of obtaining wall and furnace average ΔT the isothermal areas were planimeted and weighted according to the waterwall heat-absorbing surfaces. In arriving at the level average ΔT , arithmetical averages were taken of the ΔT values at the test points on each level.

With the furnace heat absorption determined, the furnace heat-absorption efficiency then becomes

$$\text{Efficiency} = \frac{Q}{\text{Net heat available to furnace}} \times 100$$

SLAG-ASH FACTORS

The furnace heat-absorption quantities and efficiencies as derived from recorded data are on a dirty-furnace basis. In order to reduce furnace performance to a common basis of comparison one of the uncontrollable factors affecting it must be canceled out. This is the slag-ash (S-A) coverage of the water tube heat-absorbing surfaces. The estimates of tube S-A coverage have been plotted on developed views of the furnace envelope and "iso-slag-ash" lines have been drawn to show the pattern of coverage. The basis of assigning S-A multiplying factors was proposed by Mumford and Bice⁷ and corrected for tube spacing.

The back sides of the tubes were always clean except for areas

⁴ "Pipe and Tubes for Elevated Temperature Service," National Tube Company, Pittsburgh, Pa., Bulletin No. 26, p. 57.

⁵ "An Investigation of the Variation in Heat Absorption in a Pulverized-Coal-Fired Water-Cooled Steam-Boiler Furnace. Part I—Variations in Heat Absorption as Shown by Measurement of Surface Temperature of Exposed Side of Furnace Tubes," by L. B. Schueler, Trans. ASME, vol. 70, 1948, pp. 553-567.

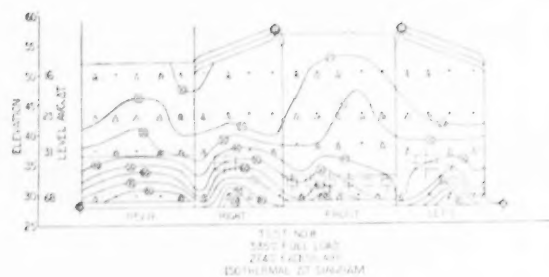
⁶ "Furnace Heat Absorption in a Pulverized-Coal-Fired Steam Generator, Willow Island Station; Part 2—Variation in Heat Absorption as Shown by Measurement of Surface Temperature of Exposed Side of Furnace Tubes," by F. G. Ely and N. H. Twyman, Trans. ASME, vol. 73, 1951, pp. 449-450.

⁶ "Radiant Heat Transmission," by H. C. Hottel, page 58 of "Heat Transmission," by W. H. McAdams, second edition, McGraw-Hill Book Company, Inc., New York, N. Y., 1942.

⁷ "An Investigation of the Variation in Heat Absorption in a Pulverized-Coal-Fired Water-Cooled Steam-Boiler Furnace. IV—Comparison and Correlation of the Results of Furnace Heat-Absorption Investigations," by A. R. Mumford and G. W. Bice, Trans. ASME, vol. 70, 1948, pp. 604-607.

TABLE 1 SUMMARY DATA AND RESULTS SHEET

TEST NUMBER	8	12	13	6	9	2	3	14	1	7	10	4	5	11	15
DATE - 1951	June 19	June 23	June 23	June 16	June 20	June 12	June 13	June 25	June 11	June 15	June 21	June 14	June 15	June 22	June 26
DURATION OF TEST	3-25	1-00	2-66	3-00	2-75	2-66	4-00	4-25	3-66	3-00	3-00	3-00	3-50	2-00	4-00
PERCENT OF FULL LOAD	53-5	50-1	51-1	52-2	55-0	71-6	72-3	71-8	76-7	74-8	74-9	98-5	101-0	97-4	99-2
PERCENT EXCESS AIR	27-4	45-1	41-6	65-6	51-3	16-8	29-2	41-5	37-9	52-7	58-4	27-5	22-8	41-7	42-9
FLAME - THOUSAND POUNDS PER HOUR															
CORRECTED FRESH-WATER FLOW	103-1	91-0	92-0	94-5	103-7	127-4	129-4	130-1	134-1	137-2	130-8	170-1	175-0	167-9	169-8
CORRECTED STEAM FLOW	88-2	82-6	84-4	86-3	90-8	118-2	120-9	123-4	126-5	123-2	123-4	162-2	166-8	160-7	163-7
BLOWDOWN	14-9	8-4	7-6	8-2	12-9	9-2	8-5	6-7	7-6	14-0	7-4	7-9	8-2	7-2	6-1
OVERALL UNIT EFFICIENCY	88-2	88-4	88-0	86-8	87-8	87-5	87-6	87-2	87-0	87-8	86-0	87-0	86-3	85-7	86-2
STEAM BURNING RATE - NETU/54, FT./HR	380	357	362	383	402	496	523	530	584	543	543	690	705	709	715
FURNACE HEAT RELEASE - NETU/CU. FT./HR	16-9	16-0	15-2	17-1	17-9	22-1	23-4	23-6	24-9	21-3	24-3	31-0	31-6	31-7	31-9
NET HEAT AVAILABLE - NETU/HR	111,800	105,500	107,000	113,100	118,400	146,100	154,400	156,200	163,400	160,700	160,700	204,400	208,400	209,200	211,900
FURNACE HEAT ABSORPTION - NETU/HR	51,500	51,800	52,600	48,000	51,500	61,300	70,500	70,000	65,500	65,000	71,400	91,500	98,700	91,500	84,000
FURNACE HEAT ABSORPTION EFF. (TEST) - %	46-1	49-1	49-2	41-5	43-4	41-9	45-6	44-7	40-1	40-5	44-4	44-6	47-4	43-7	39-6
FURNACE AVERAGE DELTA T (TEST) - OF	28-6	28-8	29-3	26-2	28-6	34-1	39-2	39-0	36-4	36-1	39-7	51-0	55-0	51-0	46-8
FURNACE AVERAGE SLAG-ASH FACTOR	.84	.87	.87	.83	.86	.85	.85	.86	.85	.86	.86	.86	.80	.85	.88
FURNACE HEAT ABSORPTION EFF. (CORRECTED) - %	54-8	56-4	56-6	50-0	50-4	49-3	53-6	52-0	42-2	47-1	51-6	52-0	59-2	51-5	45-0
FURNACE AVERAGE DELTA T (CORRECTED) - OF	34-0	33-1	33-7	31-6	33-3	40-1	46-1	45-3	38-3	42-0	45-2	59-3	68-8	60-0	53-2
STACK CARBON LOSS - %	.053	.073	.079	.074	.062	.058	.051	.079	.079	.097	.068	.188	.159	.155	.245
ASH PIT CARBON LOSS - %	.930	.253	.138	.207	.112	.966	.270	.182	.176	.152	.310	.572	.505	.444	.312
TOTAL CARBON LOSS - %	.983	.326	.217	.281	.174	1.024	.421	.261	.255	.249	.378	.760	.664	.599	.563



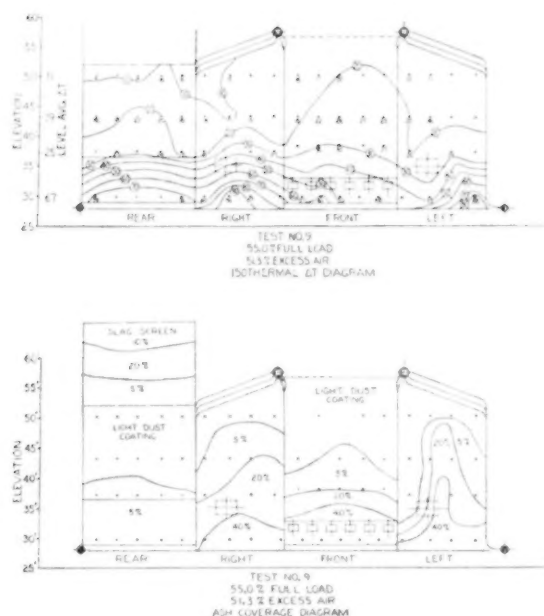


FIG. 10 ISOTHERMAL DELTA T AND ASH-COVERAGE DIAGRAM TEST No. 9

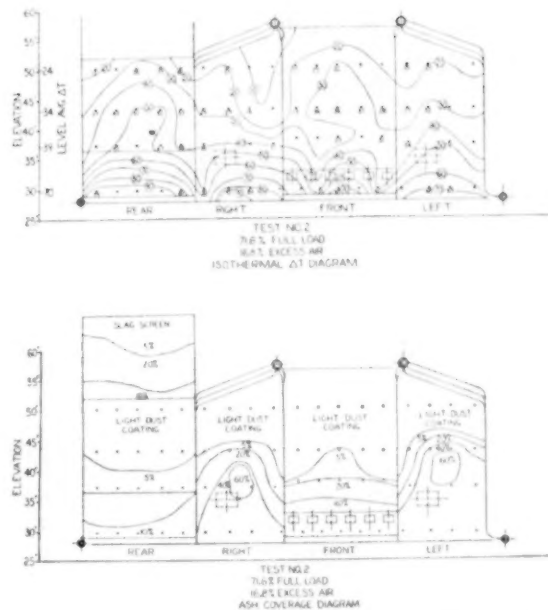


FIG. 11 ISOTHERMAL DELTA T AND ASH-COVERAGE DIAGRAM TEST No. 2

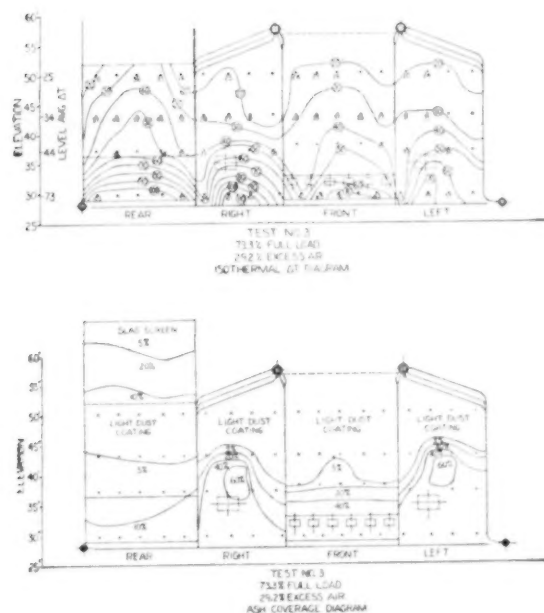


FIG. 12 ISOTHERMAL DELTA T AND ASH-COVERAGE DIAGRAM TEST No. 3

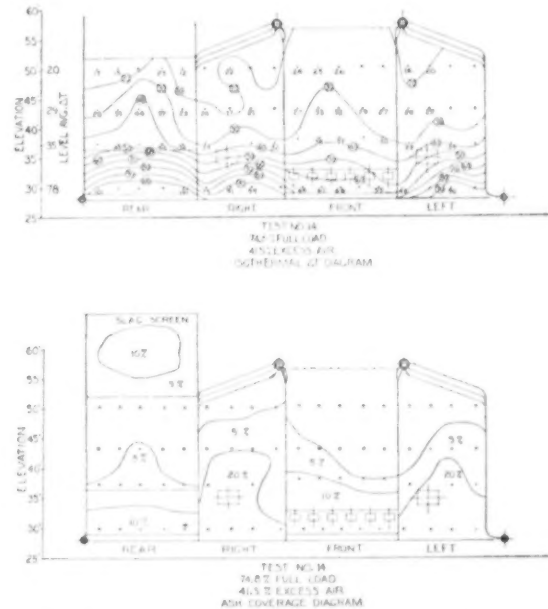


FIG. 13 ISOTHERMAL DELTA T AND ASH-COVERAGE DIAGRAM TEST No. 14

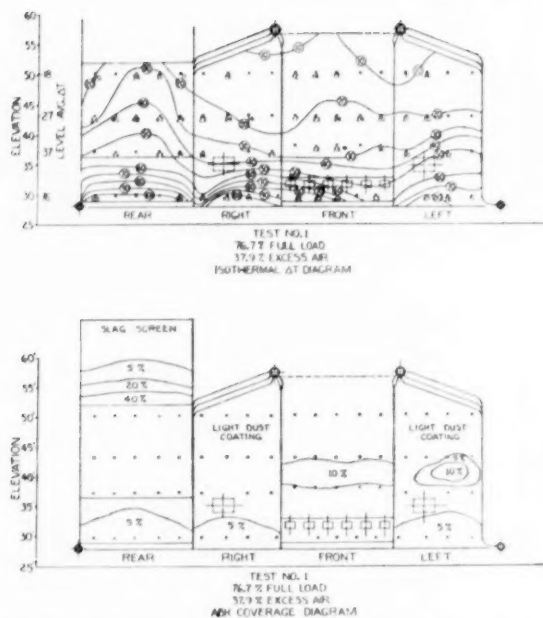


FIG. 14 ISOTHERMAL DELTA T AND ASH-COVERAGE DIAGRAM TEST No. 1

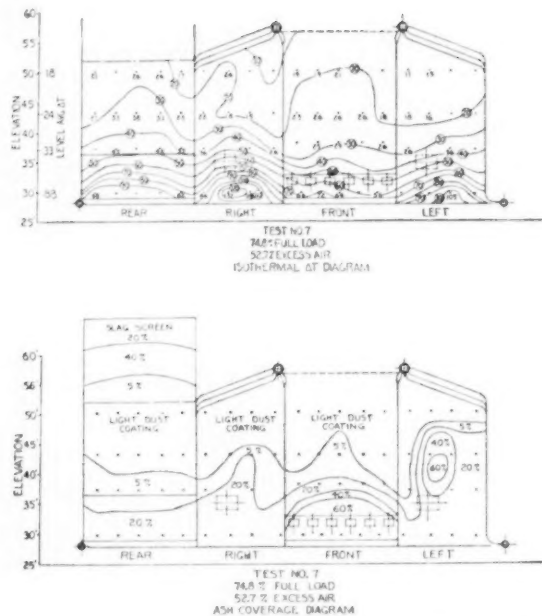


FIG. 15 ISOTHERMAL DELTA T AND ASH-COVERAGE DIAGRAM TEST No. 7

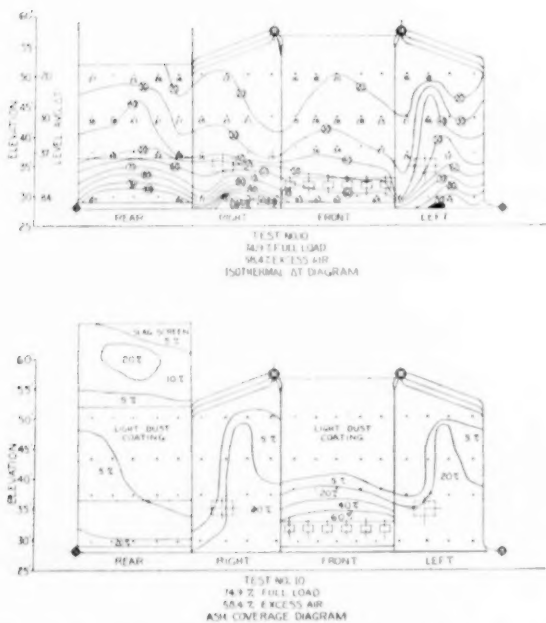


FIG. 16 ISOTHERMAL DELTA T AND ASH-COVERAGE DIAGRAM TEST No. 10

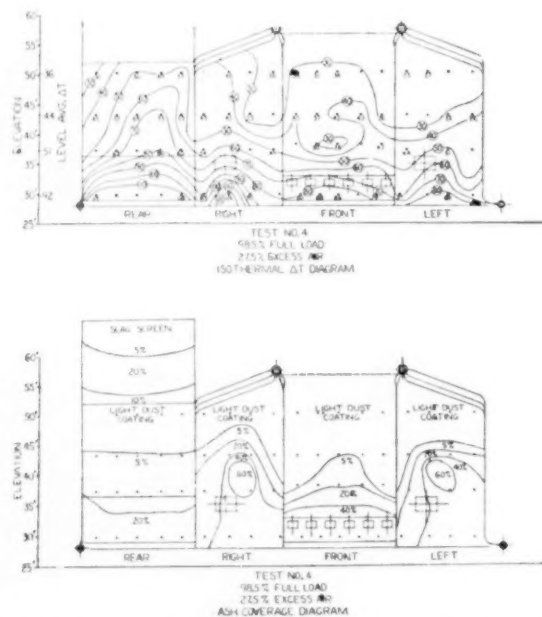
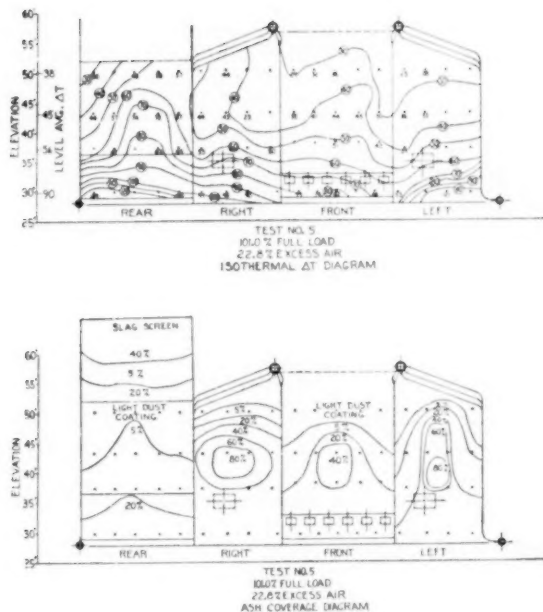
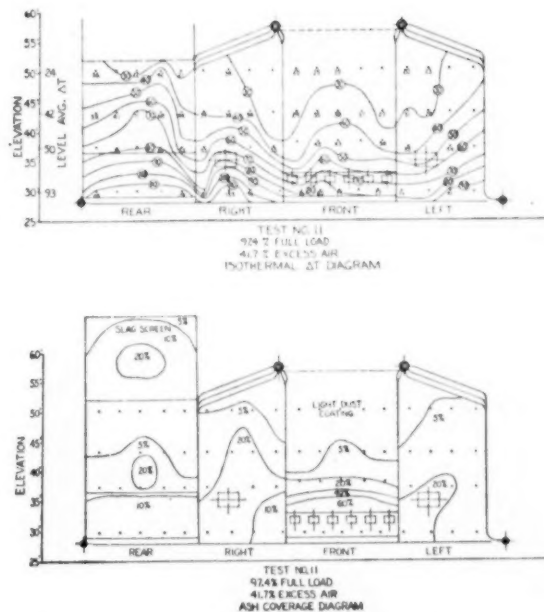
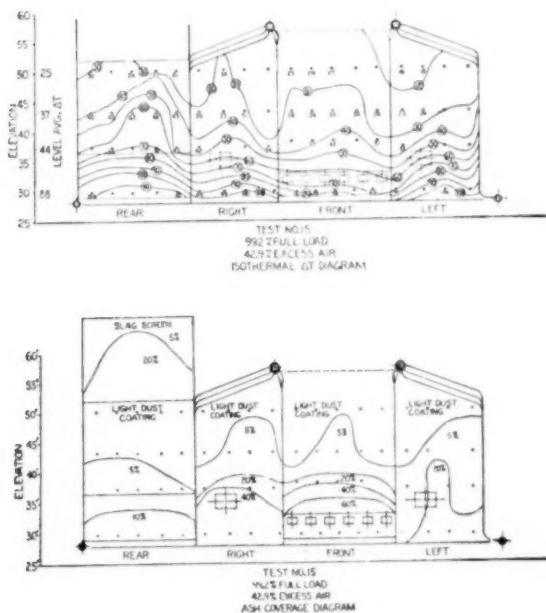


FIG. 17 ISOTHERMAL DELTA T AND ASH-COVERAGE DIAGRAM TEST No. 4

FIG. 18 ISO THERMAL ΔT AND ASH-COVERAGE DIAGRAM TEST No. 5FIG. 19 ISO THERMAL ΔT AND ASH-COVERAGE DIAGRAM TEST No. 11FIG. 20 ISO THERMAL ΔT AND ASH-COVERAGE DIAGRAM TEST No. 15

having ash coverage of 90 per cent or more. During the tests it was found that the S-A thickness was closely related to the percentages of the tube surface covered. The ash on the face of the tube does not materially affect the heat absorption of the relatively clean back side of the tubes by direct radiation from the furnace gas and reradiation from the refractory. Therefore the

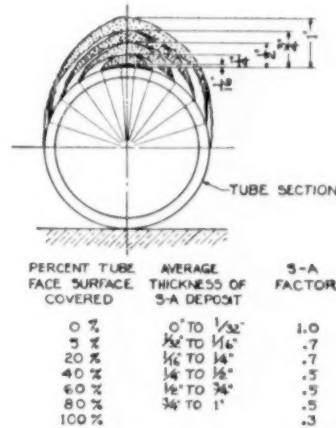


FIG. 21 ASH THICKNESS VERSUS SLAG-ASH FACTOR

estimates of S-A coverage on walls having wide tube spacing were made on a basis of percentage of projected tube surface covered, Fig. 21.

ANALYSES OF ISO THERMAL AND SLAG-ASH DIAGRAMS

A general study and comparison of all the isothermal Delta T diagrams indicates a common wall-temperature pattern at all loads and excess-air conditions even though the pattern as a whole may shift up or down. A point of similarity is the drooping of the isothermal lines at the wall joints.

The isothermals indicate that the furnace side walls, in general, have a higher Delta T value at the lower levels than either the front or rear walls. This effect is attributed to the action of the front and rear overfire-air turbulence jets which roll the flame away from their respective walls. An examination of a

Delta-T isothermal chart will show that, at the upper elevations, a given isothermal will run at a higher wall level on the rear and front walls than it will on the side walls. This is more pronounced at the low loads than at the high loads.

The deviations from the general pattern of low elevation Delta T values result from active fuel-bed placement on the grate; i.e., a heavy fire at the rear raises the rear wall low level Delta T or a well burned-out ash bed depresses the front wall low level Delta T.

The slag-ash patterns reflect the normal variations in slag and ash deposits. The walls were not cleaned prior to or during the tests.

Test Nos. 8, 12, 13, 6, and 9 were all run at approximately 50 per cent full load but grouped at nominal excess airs of 25, 40, and 60 per cent.

Test No. 8, Fig. 6, indicates smooth isothermals with no unbalanced, localized high or low-temperature areas. The right wall at the lower elevations is slightly hotter than the left wall, but the ash-coverage diagram indicates less coverage here, which accounts for the higher temperature. Good fuel distribution across the grate width is indicated by the even isothermals along the rear wall. The ash-coverage diagram indicates that the heaviest slagging occurs at the lower levels, at the high-temperature zones.

Test Nos. 12 and 13, Figs. 7 and 8, respectively, are at 40 per cent excess air. The isothermals indicate a heavier flame along the front wall of the furnace which was borne out by observation and shows up by extension of ash deposits up along the front section of the side walls.

Test Nos. 6 and 9, Figs. 9 and 10, respectively, are at 60 per cent excess air. The walls are more heavily slagged, which generally lowers the wall Delta T. Except for the areas which have localized accumulations, the temperature pattern remains unchanged.

Test Nos. 2, 3, 14, 1, 7, and 10 were all run at approximately 75 per cent full load but grouped at nominal excess airs of 25, 40, and 60 per cent.

Test Nos. 2 and 3, Figs. 11 and 12, respectively, are at 25 per cent excess air. The increase in load has raised the temperature levels at all points, although wall ash coverage is moderately heavy. The effect of flame has become more apparent as it reaches higher in the furnace.

Test Nos. 14, 1, 7, and 10, Figs. 13, 14, 15, and 16, respectively, continue the same over-all isothermal pattern except where affected by localized wall ash coverage.

Test Nos. 4, 5, 11, and 15 were all run at approximately 100 per cent full load but grouped at nominal excess air of 25 and 40 per cent.

Test Nos. 4 and 5, Figs. 17 and 18, respectively, are at 25 per cent excess air. The isothermal patterns are similar to those of the previous tests, but the Delta T level has risen as the flame reached the slag screen. Fig. 18 indicates a relatively heavy fire at the left rear corner of the grate.

Test Nos. 11 and 15, Figs. 19 and 20, respectively, are at 40 per cent excess air. There are no deviations from the normal isothermal pattern.

Influence of Rating on Level Average Delta T. The influence of rating on heat absorption at the various test elevations is shown in Fig. 22. This effect is much more pronounced at the higher elevations than at the grate. At the 2-ft level the difference between Delta T for half and full load is approximately 25 F or 27.8 per cent of the full-load Delta T while the difference of 20 F at the 22-ft level is 55 per cent of the full-load average Delta T.

Influence of Excess Air on Level Average Delta T. The influence of excess air for combustion on level average Delta T for the three test ratings is shown in Figs. 23, 24, and 25. Here again, the

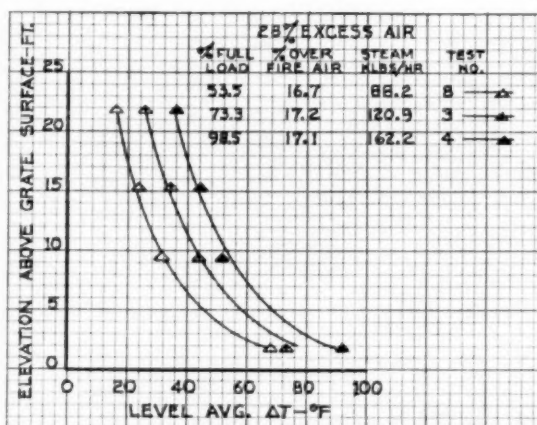


FIG. 22 RATING VERSUS LEVEL AVERAGE DELTA T

influence on average Delta T was the most pronounced in the top of the furnace but with little influence near the grate. This pattern is most pronounced at the full load rating.

Influence of Overfire Air on Level Average Delta T. The influence of overfire air on heat absorption is negligible as shown in Fig. 23. In test Nos. 4 and 5 the small difference obtained in level averages is more the result of the slight difference in excess air and load than the result of doubling the overfire air. In the over-all test pattern the correction for such variables as S-A factors removes any trace of the influence of overfire air.

CONCLUSIONS

Analyses of the isothermal diagrams and results shown in the various graphs reveal that a pattern of heat absorption has been established for the furnace envelope. The accuracy of tube-surface temperature determinations is always subject to question owing to localized ash deposits, irregularities in thermocouple application, and other less tangible factors. However, the system is sufficiently accurate to produce reliable data on the factors affecting relative heat absorption of the various furnace walls.

The basic factors influencing over-all heat absorption of the furnace tested are rating, excess air for combustion, and slag-ash coverage. Overfire air and flame shape are of secondary importance.

The rating is the most important factor in over-all heat absorption but elevations of the various surfaces above the grate have the greatest influence on relative heat absorption of the walls. The rating has less effect on heat absorption near the grate than at the top of the furnace.

At all loads heat absorption in the walls decreases rapidly as the distance from the grate increases.

Excess air for combustion affects average heat absorption at all loads but has little effect on heat absorption near the grate.

The slag-ash pattern is more stable and of less influence in spreader-stoker firing than in the pulverized-coal-fired test units.

Overfire air, when used within the limits of these tests, has negligible effect on furnace heat absorption.

The secondary data accumulated for these tests are extensive and of great value. Many of these data were required to establish the available heat in the furnace. Except where needed to show the influence on furnace heat absorption, the secondary data and analyses of these data have not been included.

ACKNOWLEDGMENTS

The authors acknowledge, with gratitude and appreciation,

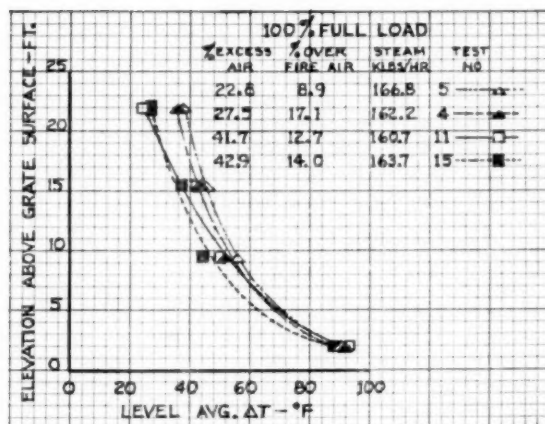


FIG. 23 EXCESS AIR VERSUS LEVEL AVERAGE DELTA T—100 PER CENT RATING

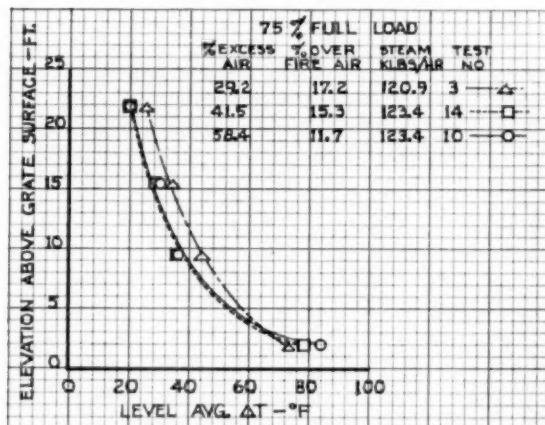


FIG. 24 EXCESS AIR VERSUS LEVEL AVERAGE DELTA T—75 PER CENT RATING

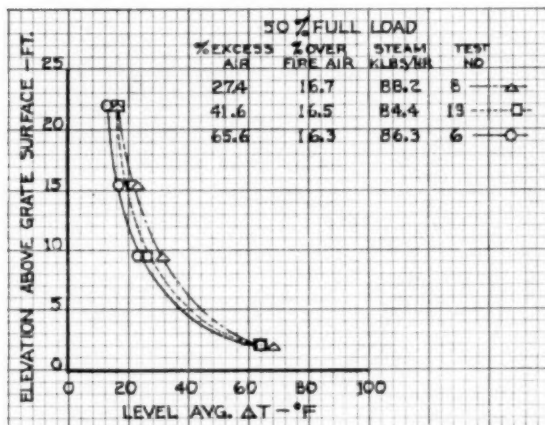


FIG. 25 EXCESS AIR VERSUS LEVEL AVERAGE DELTA T—50 PER CENT RATING

the following who, by their co-operation and contribution, made this investigation possible:

The ASME Special Research Committee on Furnace Performance Factors for their approval of this project and their assistance and guidance in planning the test program.

The officials of Carbide & Carbon Chemicals Company, a Division of Union Carbide and Carbon Corporation, who provided the test unit. Messrs. Garrison, Potts, and Trull of the Whiting Plant, for accommodating the test program and for their valued aid and suggestions.

Mr. L. E. Griffith and Mr. Ollison Craig, President and Vice-President, respectively, of Riley Stoker Corporation for their assistance and guidance.

The engineers and assistants of the Combustion Research Section of the Bureau of Mines who co-operated in the test work.

Mr. J. R. Brauweiler of the Western Precipitation Corporation for conducting the stack dust-loading tests with the Bureau of Mines.

Mr. L. B. Schueler of Diamond Power Specialty Corporation for arranging for the use of a utiliscope during the second series of tests.

The Riley Stoker service engineers, Messrs. Roy Baharian, J. K. L. Mignacca, and the engineers from the Research and Design Department, Messrs. Louis Coplan, George Hansen, and Paul Seibold for their efforts in testing and calculations.

Appendix

EFFECT OF COAL SIZE ON FURNACE HEAT ABSORPTION

A second series of tests, Nos. 16 through 24, were run to determine the effect that a smaller coal sizing (nominal $\frac{3}{4}$ in. \times 28 mesh) would have on the furnace performance. Comparison of Figs. 4 and 26 shows that the stack dust loading increased but remained well below the proposed ASME standard value. Although the diagrams are not shown here, the isothermal and slag-ash characteristics follow the same general trends as described earlier for the $1\frac{1}{2}$ in. \times 28-mesh coal. Figs. 27, 28, 29, and 30 show the level average Delta T, and their comparison with Figs. 22, 23, 24, and 25 shows that the smaller coal size has had the greatest effect at the lower levels and little, if any, effect at the upper levels.

Comparison of furnace-heat-absorption efficiencies shown in Tables 1 and 2 indicates that no noticeable over-all change has taken place because of the difference in coal sizing.

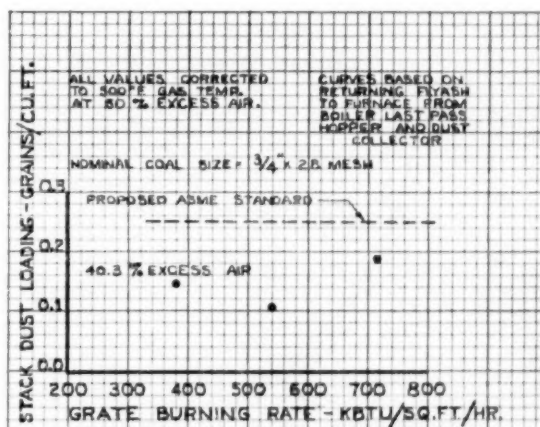


FIG. 26 STACK-DUST LOADING

TABLE 2 SUMMARY DATA AND RESULTS SHEET; EFFECTS OF COAL SIZE

TEST NUMBER	24	21	16	18	19	17	23	20	22
DATE - 1951	Oct 3	Oct 1	Sept 26	Sept 27	Sept 29	Sept 27	Oct 2	Oct 1	Oct 2
DURATION OF TEST	NBS	2.00	2.00	2.50	2.00	2.00	2.00	2.00	2.00
PERCENT OF FULL LOAD	50.4	54.0	48.8	72.0	76.0	73.0	97.6	97.4	97.2
PERCENT EXCESS AIR	26	39	62	27	43	60	27	41	44
FLOWS - THOUSAND POUNDS PER HOUR									
CORRECTED FRESHWATER FLOW	86.9	96.9	85.1	125.3	125.6	127.9	162.8	163.1	160.0
CORRECTED STEAM FLOW	93.1	89.0	80.6	118.9	125.3	120.4	161.2	160.7	160.2
BLOWDOWN	2.8	7.9	4.5	6.4	.5	2.5	1.6	2.4	1.9
GRATE BURNING RATE ---KBTU/SQ. FT./HR	358	383	358	514	538	530	685	708	700
FURNACE HEAT RELEASE---KBTU/CU. FT./HR	16.0	17.2	15.6	23.0	24.1	23.8	30.7	31.7	31.4
NET HEAT AVAILABLE-----KBTU/HR	105,300	113,000	106,000	151,700	159,000	156,800	202,400	209,200	207,500
FURNACE HEAT ABSORPTION-----KBTU/HR	47,600	50,000	43,500	79,100	72,000	66,300	76,500	75,000	78,600
FURNACE HEAT ABSORPTION EFF.(TEST)---%	45.2	44.2	41.0	46.2	45.2	42.2	37.7	35.9	38.0
FURNACE AVERAGE DELTA T (TEST)-----°F	26.6	27.8	24.1	39.0	40.0	36.9	42.5	41.7	43.7
FURNACE AVERAGE SLAG-AIR FACTOR	.81	.82	.78	.78	.77	.78	.82	.82	.82
FURNACE HEAT ABSORPTION EFF.(CORRECTED)%	55.8	54.0	52.5	59.3	58.8	54.1	46.0	43.8	46.4
FURNACE AVERAGE DELTA T (CORRECTED)---°F	32.8	33.9	30.9	50.0	52.0	47.3	51.8	50.8	53.3

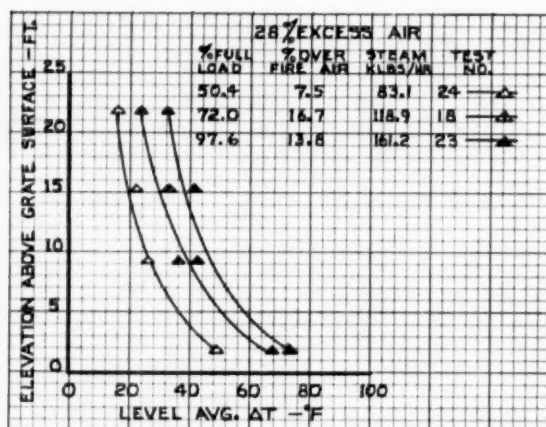


FIG. 27 RATING VERSUS LEVEL AVERAGE DELTA T

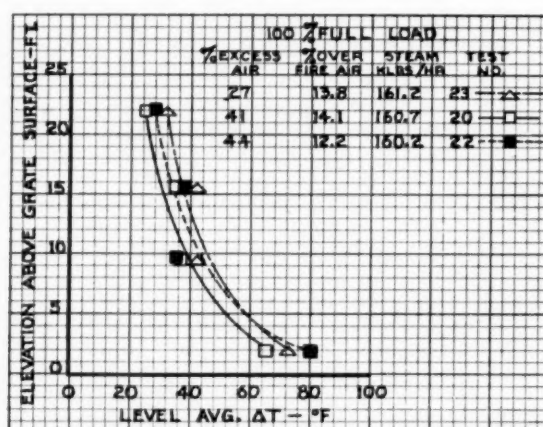


FIG. 28 EXCESS AIR VERSUS LEVEL AVERAGE DELTA T—100 PER CENT RATING

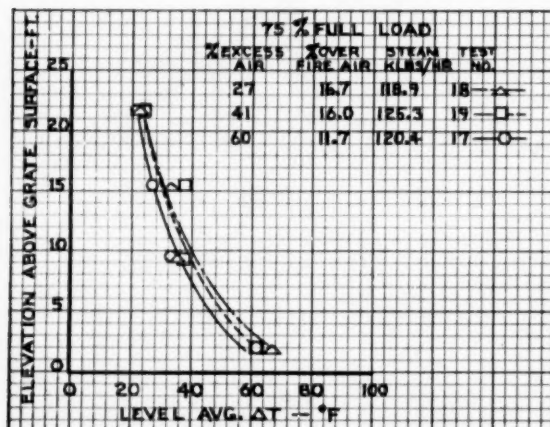


FIG. 29 EXCESS AIR VERSUS LEVEL AVERAGE DELTA T—75 PER CENT RATING

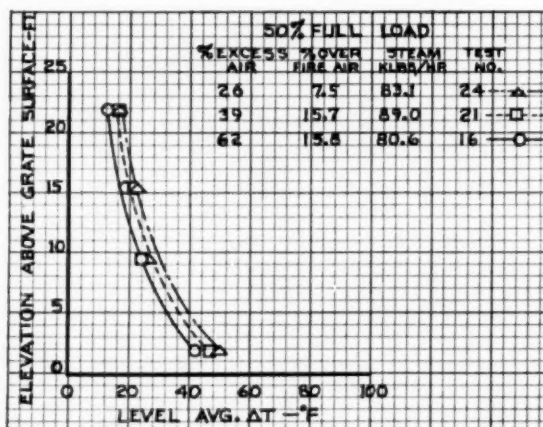


FIG. 30 EXCESS AIR VERSUS LEVEL AVERAGE DELTA T—50 PER CENT RATING

TABLE 3 COMPARATIVE TEST DATA OF DUPLICATE TESTS

LONG FURNACE FLAME						NORMAL FURNACE FLAME							
Test No.	Load x 1000	Excess Air	Furnace Efficiency	% Comb. Last D.C. Pass	Furnace Exit Flame Temp. °F	Test No.	Load x 1000	Excess Air	Furnace Efficiency	% Comb. Last D.C. Pass	Furnace Exit Flame Temp. °F		
8	88.2	27.4	54.8	23.2	22.1	1657	12	82.6	45.1	56.4	6.5	16.8	1592
2	118.2	16.8	49.3	56.6	28.0	1783	3	120.9	29.2	53.6	29.3	13.3	1797
1	126.5	37.9	42.2	36.4	13.5	1695	14	123.4	41.5	52.0	25.0	13.0	1754
5	166.8	22.8	59.2	44.9	18.3	1914	4	162.2	27.5	52.0	34.5	13.7	1928

CORRELATION OF DELTA T AND MHVT METHODS OF DETERMINING FURNACE HEAT ABSORPTION

The corrected Delta T method furnace-heat-absorption efficiencies have been plotted against the corresponding values obtained by the MHVT method and are shown in Fig. 31.

There is agreement among most of the points, but four tests, namely, Nos. 8, 2, 1, and 5 show excessive discrepancy; at the same time, their duplicate tests, Nos. 12, 3, 14, and 4 (test No. 12 is used as a duplicate of No. 8 since it is the closest to the same load conditions) fall very close to the equality curve.

With all other influencing factors held constant, the disagreement of furnace efficiencies of duplicate tests might be attributed to furnace-flame shape. Figs. 32 (a) shows the usual furnace-flame profile prevalent throughout the test series, a flame that nearly fills the furnace envelope from front to back and is completely burned out before reaching the slag screen. Test Nos. 12, 3, 14, and 4 had this type of flame shape. Fig. 32 (b) shows a furnace-flame profile that occurred on test Nos. 8, 2, 1, and 5; here the flame extends through the slag screen and partially into the superheater. Owing to the incomplete combustion of the gases before entering the slag screen, there should result a lower furnace exit-gas temperature and a higher combustible content

in the fly ash. Comparison of values given in Table 3 indicates that, except for test No. 8, the three test Nos. 2, 1, and 5 show a lower furnace exit-gas temperature than their comparative

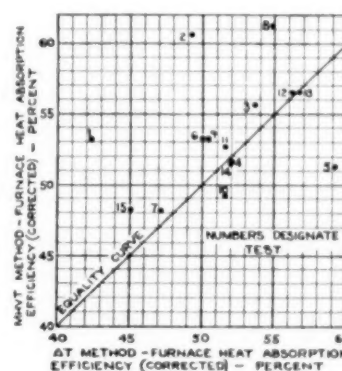


FIG. 31 COMPARISON OF FURNACE HEAT ABSORPTION BY DELTA T METHOD WITH MHVT METHOD

TABLE 4 PROPERTIES OF COAL AND ASH; NOMINAL COAL SIZE 1/4 IN. X 28 MESH

TEST NUMBER	16	17	18	19	20	21	22	23	24
DATE 1951	9-26	9-27	9-27	9-28	10-1	10-1	10-2	10-2	10-3
COAL, PROXIMATE ANALYSIS, PERCENT AS FIRED									
MOISTURE	8.5	9.3	9.0	10.9	9.7	8.6	12.4	9.0	8.4
VOLATILE MATTER	37.4	37.5	37.6	36.4	36.9	37.4	35.8	37.7	38.1
FIXED CARBON	46.9	46.2	46.1	45.4	46.2	47.0	46.7	45.9	46.1
ASH	7.2	7.0	7.3	7.3	7.2	7.0	7.1	7.4	7.4
COAL, ULTIMATE ANALYSIS, PERCENT AS FIRED									
HYDROGEN	5.6	5.8	5.6	5.7	5.7	5.6	5.9	5.6	5.6
CARBON	66.5	66.2	66.1	65.1	65.7	66.6	63.9	66.2	66.8
NITROGEN	1.3	1.4	1.5	1.4	1.4	1.5	1.4	1.5	1.5
OXYGEN	16.7	16.6	16.5	17.4	16.8	16.4	19.0	16.3	15.6
SULFUR	2.7	3.0	3.0	3.1	3.2	2.9	2.7	3.0	3.1
HIGH HEATING VALUE, BTU PER LB. AS FIRED	11,970	11,940	11,890	11,690	11,760	11,960	11,420	11,990	12,030
CONE FUSIBILITY OF ASH F (ASTM)									
I.D.T.	2,000	1,980	1,980	2,000	1,930	1,930	1,910	1,900	1,900
S.T.	2,030	2,030	2,030	2,030	2,050	2,050	2,030	2,030	2,050
F.T.	2,350	2,310	2,310	2,360	2,360	2,330	2,340	2,330	2,360
SCREEN ANALYSIS OF COAL, CUMULATIVE PER CENT RETAINED ON SCREEN SIZE, INCHES									
1/8	0.00	0.00	0.00	0.00	0.00	0.00	0.00	0.00	0.08
1/16	0.00	0.00	0.00	0.00	0.39	0.36	0.00	1.27	0.59
3/32	0.13	0.03	0.04	0.04	5.18	3.17	0.16	14.07	9.10
1/4	0.13	0.11	0.26	0.26	8.92	6.22	0.33	29.06	20.48
3/8	14.33	13.20	12.51	10.99	26.21	16.77	9.82	51.63	51.43
1/2	38.03	37.99	34.94	30.42	46.97	37.74	27.99	62.63	64.85
3/4	49.15	49.73	45.17	41.55	62.21	65.31	58.82	76.85	81.17
1	59.97	77.05	72.62	69.91	67.89	72.25	66.03	80.44	85.22
1 1/8	76.68	88.27	85.07	84.25	76.28	83.57	86.51	86.83	93.08
1 1/4	87.93	94.36	93.09	93.67	88.36	91.08	88.23	91.97	92.20
DUST COLLECTOR CINDERS									
COMBUSTIBLES, PERCENT	12.5	10.5	23.0	16.0	14.5	15.2	19.3	23.0	28.2
ASH, PERCENT	87.5	89.5	77.0	84.0	85.5	84.8	80.7	77.0	71.8
ASH PIT REFUS									
COMBUSTIBLES, PERCENT	5.7	24.8	12.0	2.0	1.4	1.2	2.4	0.9	2.0
ASH, PERCENT	94.3	75.2	88.0	98.0	98.6	98.8	97.6	99.1	98.0

TABLE 5 PROPERTIES OF COAL AND ASH; NOMINAL COAL SIZE 1 1/2 IN. X 28 MESH

TEST NUMBER	1	2	3	4	5	6	7	8	9	10	11	12	13	14	15
DATE - 1951	6-11	6-12	6-13	6-14	6-15	6-16	6-18	6-19	6-20	6-21	6-22	6-23	6-23	6-25	6-26
COAL, PROXIMATE ANALYSIS, PERCENT AS FIRED															
MOISTURE	8.9	8.6	8.2	8.9	7.9	8.8	7.4	8.8	7.7	8.8	8.3	7.8	7.8	8.4	8.8
VOLATILE MATTER	39.1	39.9	39.4	39.3	39.3	38.8	40.4	39.1	39.1	39.5	39.3	40.0	40.2	39.4	38.6
FIXED CARBON	44.5	45.2	45.1	46.1	45.9	45.3	45.3	45.3	45.7	44.4	44.6	44.8	44.6	45.3	45.6
ASH	7.2	7.3	7.3	6.7	6.9	6.8	6.9	6.8	7.1	7.3	7.6	7.4	7.4	6.9	7.0
COAL, ULTIMATE ANALYSIS, PERCENT AS FIRED															
CARBON	5.7	5.6	5.7	5.7	5.6	5.8	5.7	5.7	5.7	5.8	5.7	5.7	5.8	5.8	5.7
HYDROGEN	67.0	66.9	67.2	67.1	67.6	67.3	68.2	67.8	68.0	66.6	66.6	67.3	67.3	67.4	66.9
NITROGEN	1.5	1.5	1.5	1.5	1.5	1.5	1.5	1.5	1.5	1.4	1.4	1.5	1.5	1.5	1.5
OXYGEN	15.8	15.6	15.3	15.8	15.1	15.4	14.4	15.2	14.8	15.6	14.9	14.8	14.7	15.0	15.5
SULFUR	2.8	3.1	3.0	3.2	3.1	3.2	3.3	3.0	2.9	3.3	3.6	3.3	3.4	3.4	3.4
HIGH HEATING VALUE, BTU PER LB. AS FIRED	12,080	12,080	12,180	12,160	12,290	12,210	12,400	12,230	12,310	12,070	12,100	12,230	12,260	12,200	12,140
GRINDABILITY, HARDGROVE INDEX	61	59	60	59	54	58	57	59	62	55	56	61	57	60	60
CONE FUSIBILITY OF ASH, F. (ASTM)															
I.D.T.	1,940	1,940	1,940	2,000	2,000	2,000	2,030	2,000	2,130	2,000	2,000	1,940	2,000	1,970	1,940
S.T.	2,130	2,130	2,100	2,100	2,180	2,100	2,130	2,150	2,230	2,150	2,100	2,100	2,080	2,170	2,100
F.T.	2,260	2,180	2,360	2,260	2,470	2,310	2,420	2,420	2,420	2,420	2,360	2,360	2,420	2,420	2,260
SCREEN ANALYSIS OF COAL, CUMULATIVE PERCENT RETAINED ON SCREEN SIZE, IN.															
1-1/2	0.08	0.29	0.23	0.38	0.24	0.16	0.25	0.23	0.05	0.07	0.10	0.14	0.33	0.05	0.06
1-5/16	1.92	2.17	1.94	2.00	1.56	1.38	1.37	0.71	0.79	1.21	0.96	1.73	1.36	1.10	0.86
1	16.7	15.8	16.6	15.6	15.8	14.8	13.7	13.8	10.8	12.5	11.6	15.0	13.3	11.5	10.9
3/4	29.5	25.3	29.9	30.5	29.6	27.4	28.0	25.7	20.3	23.8	22.4	25.8	24.1	21.5	20.6
1/2	51.2	45.8	50.4	52.2	53.7	53.2	50.4	51.6	43.7	47.0	44.9	47.2	44.1	45.0	42.3
3/8	61.8	56.3	59.7	62.1	62.3	61.9	62.4	63.2	56.1	58.8	53.3	58.1	56.8	57.0	54.4
1/4	72.7	72.0	72.3	75.8	74.5	74.1	71.5	71.9	73.7	75.2	73.0	74.3	73.2	74.1	71.7
3/16	76.0	76.3	75.6	79.1	77.9	77.1	75.0	77.0	77.9	79.5	75.9	77.8	77.0	77.9	75.9
1/8	83.4	85.3	82.7	86.2	84.6	84.0	81.8	85.8	85.5	86.9	83.4	85.2	84.9	85.7	84.0
0.055	90.9	91.7	89.0	91.7	90.7	90.6	87.4	89.7	90.6	92.5	89.7	92.3	91.5	90.9	90.3
DUST-COLLECTOR CINDERS															
COMBUSTIBLE, PERCENT	13.5	28.0	13.3	13.2	18.3	10.0	12.4	22.1	10.4	8.2	13.8	16.8	18.4	13.0	20.3
ASH, CUMULATIVE PERCENT RETAINED ON U.S. NO. 20 SCREEN	86.5	72.0	86.7	86.8	81.7	90.0	87.6	77.9	89.6	91.8	86.2	83.2	80.6	87.0	79.7
SCREEN	1.1	1.4	0.2	2.2	6.6	1.2	1.2	0.6	0.2	1.5	2.8	0.6	1.4	1.0	4.3
CUMULATIVE PERCENT RETAINED ON U.S. NO. 50 SCREEN	10.5	17.8	7.6	14.0	17.4	5.6	5.6	12.9	4.9	11.7	22.4	9.8	13.1	11.1	23.4
CUMULATIVE PERCENT RETAINED ON U.S. NO. 100 SCREEN	33.5	35.9	26.0	38.0	44.7	28.8	28.8	35.8	25.4	43.8	51.7	31.1	31.3	38.8	64.7
CUMULATIVE PERCENT RETAINED ON U.S. NO. 200 SCREEN	69.1	69.1	66.6	69.9	75.4	46.7	46.7	71.3	68.6	77.3	79.2	69.0	68.8	75.0	88.4
ASH PIT REFUSE															
COMBUSTIBLE, PERCENT	41.9			7.3	6.3			10.5		3.7	5.0			2.3	4.1
ASH, PERCENT	58.1			92.7	93.7			89.5		96.3	95.0			97.7	95.9
ASH FROM DISCHARGE END OF GRATE															
COMBUSTIBLE, PERCENT	2.1		4.2	2.5	1.8	2.7	2.0		1.4	3.5	1.8	2.9	1.6	1.3	
ASH, PERCENT	97.9	95.8	95.8	97.5	98.2	97.3	98.0		98.6	96.5	98.2	97.1	98.4	98.7	

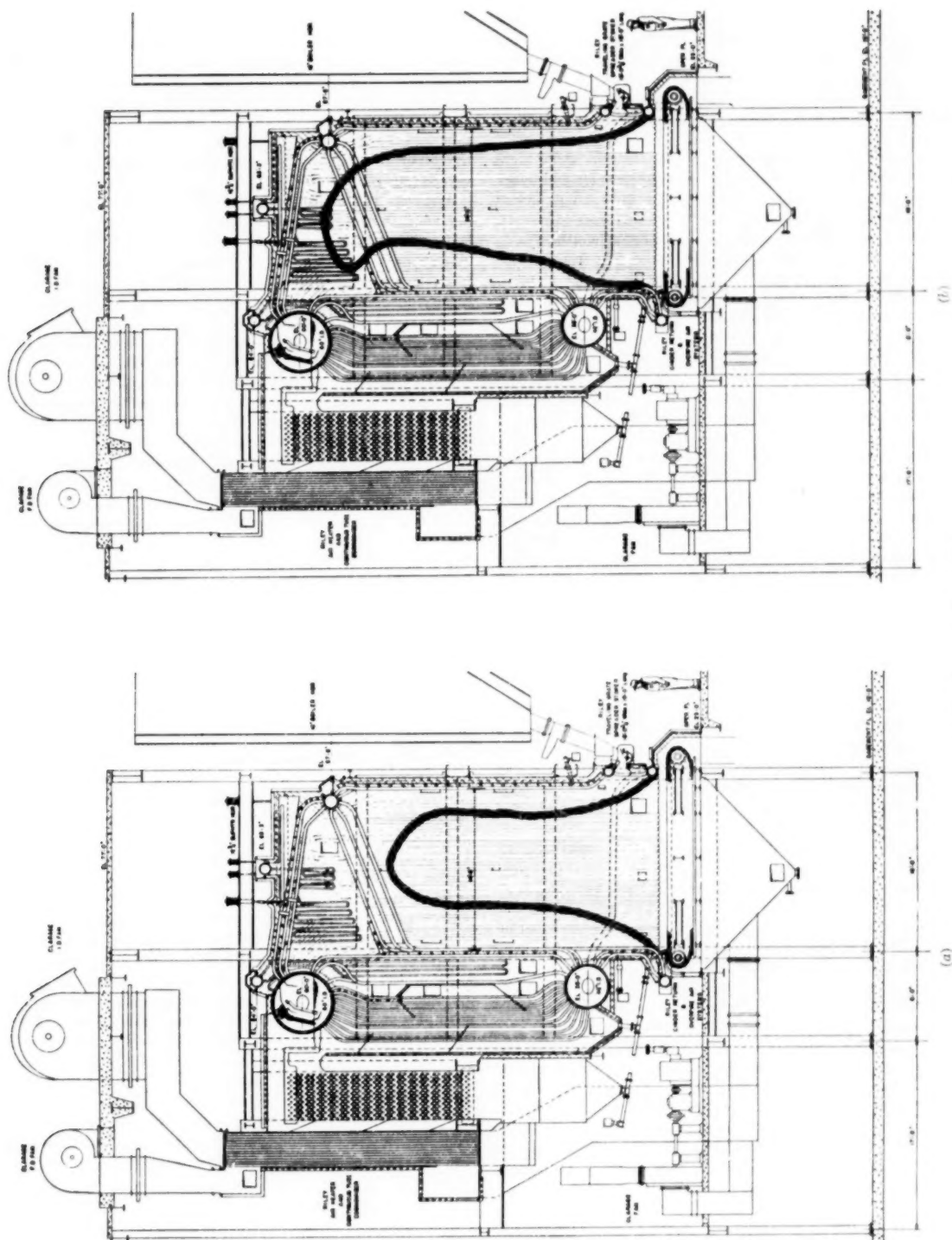


FIG. 32 FURNACE-FLAME PROFILE

test Nos. 3, 14, and 4, respectively. Without exception, the fly-ash combustible content is higher for test Nos. 8, 2, 1, and 5 than for test Nos. 12, 3, 14, and 4. However, these differences in furnace exit-gas temperature and fly-ash combustible content are not large enough to compensate fully for the difference in furnace efficiencies between the two groups of tests.

In determining the cause of unequal flame lengths under identical load conditions, comparison of fuel compositions and boiler operating conditions shows that of all the influencing factors excess air is the only inconsistent item between duplicate tests. The lower excess air would tend to increase flame length.

In the foregoing discussion, test Nos. 5 and 4 have been considered in the same category as the other three sets of tests. Actually, it is evident from Fig. 31 that by the Delta T method, test No. 5 results in a higher furnace heat-absorption efficiency than by the MHVT method, whereas the other three sets of tests show the Delta T method results in a lower efficiency than the MHVT method. Test No. 5 was the only test of the series run with hot auxiliary air (320 F) so its comparison with test No. 4 is not entirely correct except to show the exceptions to the general trend.

In view of all this, the excessive disagreement in furnace efficiencies for test Nos. 8, 2, 1, and 5 as obtained by the Delta T method and the MHVT method may be attributed to one of the following causes: The unusually long furnace flame is introducing a source of error in one of the testing methods; or the disagreement is due to the already known sources of error inherent in the testing methods, it being a coincidence that the unusually long flame shape and disagreement in efficiency happened together.

Discussion

LEROY F. DEMING.* The authors² are to be commended for the work they have done by measuring the heat absorption in a spreader-stoker-fired steam generator in service. Under the circumstances the most significant factor, load, was responsive to plant requirements and only approximated the desired test conditions. Yet it is not apparent that this condition has impaired the value of the results of the tests.

The authors indicate that the objectives of the tests were to check the variables, rating, excess air, overfire air, and fuel size. The accuracy of the authors in the check of these variables is in keeping with that of the recorded data. The information obtained should aid in more exhaustively investigating the effect of changing, not only the variables mentioned in a furnace of a given design but also the comparative performance in furnaces of different designs under similar conditions of the foregoing variables. The authors' conclusions are not questioned except as to the relative significance of the factors studied.

The shore establishments of the Navy Department operate several thousand boilers under the technical cognizance of the Bureau of Yards and Docks. Many are quite small; the largest is rated at 200,000 lb per hr. Most have had 10 years of service. Some are very old. Only a few are equipped with spreader-type stokers. However, in the areas where Navy-owned plants are located, the present and prospective costs of auxiliary power, maintenance, and fuel, and the trends in the size and composi-

tion of coal, indicate that the spreader stoker is the most economical firing equipment available today, for new installations of boilers of approximately 20,000 lb per hr capacity and larger, using solid fuel. The merits and deficiencies of the spreader stoker are being carefully studied, and developments will be followed carefully by the Navy. On behalf of an interested user and a prospective purchaser with spreader-type stokers now on order, the following observations are offered for consideration as they relate to the future:

The authors state that adjustments of cinder return and overfire air influence flame shape but conclude that, of the basic factors affecting heat absorption, overfire air and flame shape are of secondary importance. The amount of research now under way relative to the effect of different patterns of turbulence on the flame shape and on the length of flame travel indicates this conclusion is not shared universally.

Factors affecting combustion such as the use of furnace gases for cinder reinjection and turbulence, the use of more heat-recovery equipment and higher-temperature air through the grates, the length and shape of the trajectory, and the trend in size of the coal all have a relationship to the relative heat absorption in the furnace. The paper indicates that the use of coal of smaller size reduces the comparative percentage of total heat absorption that takes place close to the grate line. Further tests are necessary to determine how far this characteristic may be exploited. In the area along the east coast, where the greater percentage of United States coal is consumed, the most economical stoker coal today is single-screened bituminous size $1\frac{1}{4}$ in. \times 0 and in the near future it is anticipated the most economical size will be $\frac{3}{4}$ in. \times 0. In each case the fines constitute approximately 50 per cent of the total.

The high percentage of total furnace heat absorption that takes place in the lower part of the furnace probably constitutes a potential limitation on maximum rating. The relatively low heat absorption near the roof of the furnace obviously is an economic burden. It is true this observation seeks to relate the furnace-performance factors to economic considerations. Combustion is the primary purpose of the furnace but economic considerations have dictated that some heat-exchange surface must be provided therein. The geometry of the furnace envelope of the future, as in the past, will reflect an evaluation of performance and economic considerations in which the relative importance of each performance factor will be weighed against the economic burden it entails. Is the mechanical spreader stoker adaptable to the changes in fuel trajectory and fuel size to give optimum performance? What are the pertinent characteristics of the pneumatic spreader? The droop of the isotherms indicates heat absorption is lower in the corners than in the more exposed side walls of the furnace. This condition gives substance to the question: Why does the furnace have corners? The development of some means to prevent the unproductive recirculation of cinders, the return of fly ash to the grates and its discharge to the ash pit thus eliminating the fly-ash disposal problem are objectives which when solved will contribute to a better answer for the user's wants.

A review of current literature reveals a wide diversity of opinion regarding efficiency flexibility and performance of spreader stokers. The manufacturers' interest will be better served by a more widespread distribution of engineering reports on performance, such as the authors have compiled.

The concluding sentence of a paper presented previously by one of the authors is worthy of repetition: "Deviation from accepted practices seems desirable for there will be little progress if we assume that the popular path is the only or best way to our goal."

* Head, Power Generating Section, Department of the Navy, Bureau of Yards and Docks, Washington, D. C.

² "Furnace Heat Absorption in a Spreader-Stoker-Fired Steam Generator—Part 2 Variation in Furnace Heat Absorption as Shown by Measurement of Temperature of Exposed Side of Furnace Tubes," by F. G. Feeley, Jr., and E. C. Miller, published in this issue of the Transaction, pp. 925-940.

R. B. ENGBAHL¹⁰ AND W. C. HOLTON.¹¹ These papers^{9,12} are a result of careful and devoted work. The following request for more data and information should not detract from the fact that they make a valuable contribution to the subject.

The use of jets should be described in more detail. The mention that so many jets were located in a certain way without specification of the size, angle, or pressure, leaves out too many important variables. The omission recalls the old practice of connecting a low-pressure blower to a few large openings in a furnace wall and calling them jets. Knowing the authors as we do, we are sure that was not the case in this instance. For the record, the jet details should be specified.

An indication in Table 1 of Part 2 would be helpful for showing on which tests dust-loading measurements were made. The use of some calculated and some measured values of dust loading may help account for the variations in stack-dust loading of over 5 to 1 with only moderate variations in burning rate. Such variation seems too wide to be accepted without more supporting data.

It is unfortunate that it was not possible to determine stack emission for each test. Although the results shown in Fig. 4 of Part 2 fit a smooth curve nicely, there are not enough data to permit extrapolation. It is quite interesting to note that the curve in Fig. 4 for the dust loading at 14.5 per cent CO₂ is in good agreement with the results of previous tests at Racine, Wis., as reported by Morrow, Holton, and Wagner in 1951. The comparison is shown in Table 6 herewith.

TABLE 6 COMPARISON OF DUST LOADINGS BETWEEN WHITING AND RACINE TESTS

Racine test no.	Burning rate, K Btu per (sq ft)(hr)	CO ₂ , per cent	Stack-dust loading, gr—per cu ft, std conditions—	
			Racine	Whiting
3	595	14.8	0.087	0.085
4	619	14.4	0.069	0.092
6	591	14.5	0.080	0.082

Test Nos. 3 and 4 in Table 6 were run using a washed 2-in. X 0-in. coal from the Island Creek seam, and test No. 6 was run with washed screenings from the Illinois No. 6 seam. The agreement noted in the dust loadings is exceptionally good.

The fine performance of this modern unit is typical, and indicates that the spreader has come a long way. One defect which is still typical is the decided stratification of gases throughout the furnace. The spreader stoker will be even better when we have developed practical means to eliminate that considerable stratification.

JOINT CLOSURE BY J. W. MYERS, R. C. COREY, F. G. FEELEY, AND E. C. MILLER

The authors wish to thank the discussers for their contributions to the paper.

Mr. Deming's considerable attention to this paper is gratifying and the comments are particularly interesting. The comments concerning overfire air require some clarification. The authors did not intend to minimize the importance of this factor; on the contrary, considerable attention was given to the design and operation of this necessary adjunct of spreader stoker firing. The furnace turbulence was always maintained at sufficiently high level to assure smokeless operation and no doubt this attention to furnace turbulence influenced the low-stack dust loading.

¹⁰ Supervisor, Battelle Memorial Institute, Columbus, Ohio. Mem. ASME.

¹¹ Assistant Supervisor, Fuels Research Division, Battelle Memorial Institute, Jun. ASME.

¹² "Furnace Heat Absorption in a Spreader-Stoker-Fired Steam Generator. Part I Furnace Heat-Absorption Efficiency as Shown by Enthalpy of Gases Leaving the Furnace," by J. W. Myers and R. C. Corey, published in this issue of the Transactions, pp. 909-923.

The adaptability of the mechanical spreader stoker to changes in fuel consist is well established. This mechanical stoker handles easily fuel sizes of greater range than those commonly accepted for good spreader firing. However, the authors are not familiar with pneumatic spreader stokers except for bulky fuels such as bagasse and wood.

The droop of the isotherms in the furnace corners is to be expected because of the relative position of this surface with respect to the flame center, but corners will probably remain in furnaces because of construction problems.

The fact that the test unit does reinject all the dust collected and at the same time has a low dust emission from the stack indicates that Mr. Deming's desire for fly-ash disposal by reinjection into the furnace has been met in this case.

The comments by Mr. Deming relative to the large number of factors that influence the heat absorption of spreader-stoker-fired furnaces is in agreement with the conclusions of the authors. He also agrees that further tests are necessary to evaluate more accurately the effects of some of these variables. Unfortunately, the authors were unable to do this in the limited scope of this investigation.

Mr. Deming states that results of other investigations do not confirm the conclusions in this paper that overfire air and flame shape are of secondary importance to other factors affecting furnace performance. It was not the intention of the authors to imply that this is true in all cases, but that the conclusions applied only to this particular furnace and within the limited range of variables studied.

The comments by Messrs. Engdahl and Holton are greatly appreciated. The previous works by them on allied subjects were of great help to the test crew and to the authors. Their question on overfire air can be only briefly covered due to the limited scope of this paper.

The location of the reinjection and overfire systems listed under Description of Equipment are shown in Fig. 1 of Part 2. The eighteen reinjection nozzles enter the furnace through the rear wall approximately 18 in. above the grate. These nozzles received air from the overfire air system and the air was controlled at 12 i.w.g. for half load and 25 i.w.g. at full load. The fifteen rear-wall overfire air nozzles, shown above the reinjection nozzles, were the principal source of furnace turbulence and operated with air pressure controlled between 12 i.w.g. at half load and 25 i.w.g. at full load. The top front overfire air nozzles were used at full load only with 2 i.w.g. The 3/4 in. nozzles located beneath the feeder opening operated at 23 i.w.g.

With further reference to the comments of Messrs. Engdahl and Holton, Table 7 of this closure shows additional data on the dust loading. The burning rate, mass-flow rate of wet flue gas, and dust concentrations are included. As shown in this table, dust-concentration measurements were made for only five of the tests; the values for all the other tests were obtained by extra-

TABLE 7 DUST-LOADING DATA FOR WHITING TESTS

Test no.	Steam rate, M lb per hr	Burning rate, K Btu per (hr)(sq ft)	Wet flue gas, M lb per hr	Dust concentration, grains per cu ft ^a	
				Measured	Extrapolated
1	127	554	191		0.120
2	118	496	149		0.059
3	121	523	170	0.084	
4	162	690	218	0.196	
5	167	705	248	0.188	
6	86	383	155		0.132
7	123	543	203		0.145
8	88	380	124		0.056
9	91	402	149	0.116	
10	123	543	212	0.147	
11	161	708	249		0.217
12	83	357	129		0.090
13	84	362	128		0.080
14	123	530	187		0.124
15	164	715	254		0.230

^a Volume measured at stack conditions of temperature and pressure.

pulation of curves similar to those in Fig. 4 of Part 2. Admittedly, there is a very wide range in the dust-concentration values obtained by extrapolation. The maximum value, for test No. 15, is nearly five times as great as the minimum value for test No. 2. However, there is also a wide range, approximately 2.3 to 1, in the measured values for a smaller variation in operating conditions. The measured value for test No. 3 may have been low, since it was the result of a single determination and was not confirmed. From Fig. 4 of Part 2 values as high as 0.11 appear plausible for the dust concentration in test No. 3. However, conceding this higher value to be more accurate, the range in the extrapolated values is still nearly 4 to 1.

Although the table shows that both the measured and extrapolated dust-concentration values vary more than the burning rate, percentagewise, this does not seem to be sufficient evidence that the values are in error. It is conceivable that, at the higher mass-flow rates of flue gas, the carryover of dust may increase at a much greater rate than does the velocity of the air through the grates. It will be noted that the higher concentration occurred at high mass-flow rates.

For the purpose of the material-balance calculations in this paper, errors in the dust loading were insignificant. However, it would probably be wise to point out the serious limitations on accuracy introduced by the process of extrapolation.

The Venturi as a Meter for Gas-Solids Mixtures

By LEONARD FARBAR,¹ BERKELEY, CALIF.

This investigation was undertaken to determine the behavior of a Venturi tube when metering the solids phase in a gas-solids mixture for the condition of constant gravimetric gas-flow rate. The Venturi tubes were used in both a horizontal and vertical section of 17-mm-ID glass conduit and had throat diameters of 0.500 in. and 0.375 in., respectively. The gas-solids mixtures consisted of air and alumina-silica catalyst (an aggregate mixture containing a size range varying from 10 to 220 microns) with solids loadings as high as 10 lb of solids per lb of air. Results on four different gas-flow rates indicated a linear relationship between the Venturi pressure differential and the solids-flow rate over the range of loadings attainable with the experimental equipment. The linear relationship was observed for each Venturi size in both the horizontal and vertical location; the slope of these lines increased with increased air-flow rate and decreasing Venturi throat diameter. Pressure recovery in the diffuser section of the Venturi was observed and found to vary in nonlinear fashion with the solids rate. It appears that the Venturi may be used with satisfactory results in the metering of a solids phase in a gas-solids mixture when the gravimetric gas-flow rate is held constant. In plants and pilot plants handling powdered solids by pneumatic conveyance, the Venturi may serve as a useful tool in indicating any instantaneous changes in the solids-flow rate as well as the gas-flow rate.

INTRODUCTION

THE use of the Venturi tube for metering true or Newtonian fluids has been investigated thoroughly and standards have been adopted which allow a high degree of accuracy as shown by Jorissen (1)² in his excellent review on the Venturi tube. The use of the Venturi tube to meter a multiphase mixture appears to have received little, if any, attention in the literature. The handling of solid material in powdered form has become increasingly important in many of the chemical and process industries, where the trend toward synthesis by catalysis in relatively large-capacity plants makes the metering of a gas-solids mixture a rather important variable in plant operation.

Those industries burning powdered combustibles would find that a solids meter would serve as a useful tool in plant-performance control, inasmuch as instantaneous changes in plant operation could be observed readily.

The purpose of this paper is to present the results on metering

¹ Associate Professor of Mechanical Engineering, University of California. Mem. ASME.

² Numbers in parentheses refer to the Bibliography at the end of the paper.

Contributed by the Research Committee on Fluid Meters and presented at the Annual Meeting, New York, N. Y., November 30-December 5, 1952, of THE AMERICAN SOCIETY OF MECHANICAL ENGINEERS.

NOTE: Statements and opinions advanced in papers are to be understood as individual expressions of their authors and not those of the Society. Manuscript received at ASME Headquarters, August 28, 1952. Paper No. 52-A-31.

powdered alumina-silica catalyst (an aggregate mixture of wide size range) when flowing in combination with a gas through a Venturi tube; the gas gravimetric flow rate held constant and the solids flow varied over a relatively wide range.

EXPERIMENTAL APPARATUS AND EXPERIMENTAL PROCEDURE

The experimental system is shown diagrammatically in Fig. 1. The system consists of a flanged-connected Pyrex glass conduit, 17 mm ID; a solids feed tank and platform-scale weighing system; a multiple-effect cyclone separator forming a closed recirculating system for the handling of solids. The gaseous phase was handled on a once-through basis, the power being supplied by an industrial-type vacuum cleaner on the cyclone-separator outlet. The gaseous phase (air) was metered at inlet to the system by a calibrated ISA nozzle. The general arrangement of system details is shown in Fig. 2, while the details of the solids feed tank and weighing system are shown in Fig. 3.

The dimensional details of the two series of Venturi tubes used in this investigation are shown in Fig. 4. The tube flanges were made to match the system flanges, which were manufactured with a pressure connection to each flange face. As may be noted in Fig. 1, the Venturi tube could be placed either in the horizontal or vertical position with sufficient approach length.

Calibrated draft gages and U-tube manometers having a least count of 0.01 in. and 0.1 in. of manometer fluid, respectively, were used to measure pressures and pressure differentials.

The powdered alumina-silica catalyst (specific gravity of 2.45) used as the solids phase had an average bulk density of 36 pcf when oven-dried to 350 F, and an average size distribution as shown in Table 1.

TABLE 1 PARTICLE-SIZE DISTRIBUTION BY SCREENING

Tyler screen	Opening, microns	Weight per cent passed	Weight per cent retained
65	298	95	5
100	147	85	15
150	104	74	26
200	74	50	50
270	53	45	55
325	44	33	67
Fines	Below 44		33

These values are the average of a number of screenings made under various conditions and over varying Ro-Tap shaking periods. In view of the relatively large percentage of fines, size determinations were made using an elutriation method. Photomicrographs (250 magnification) of the various fractions obtained by elutriation are shown in Fig. 7; the resulting distribution curve obtained by elutriation is shown in Fig. 5. It is of interest to note that the particles shown in Fig. 7 appear to have the same general shape regardless of the size range into which they may fall. The results shown in Fig. 5 indicate that approximately 11.0 weight per cent of the material are particles smaller than 12 microns in size.

Screen analysis and elutriation analyses made at various times on the material being recirculated continuously indicated a small reduction in the percentage of very large particles with the main bulk of the weight shifting to the region of 40 to 80-micron par-

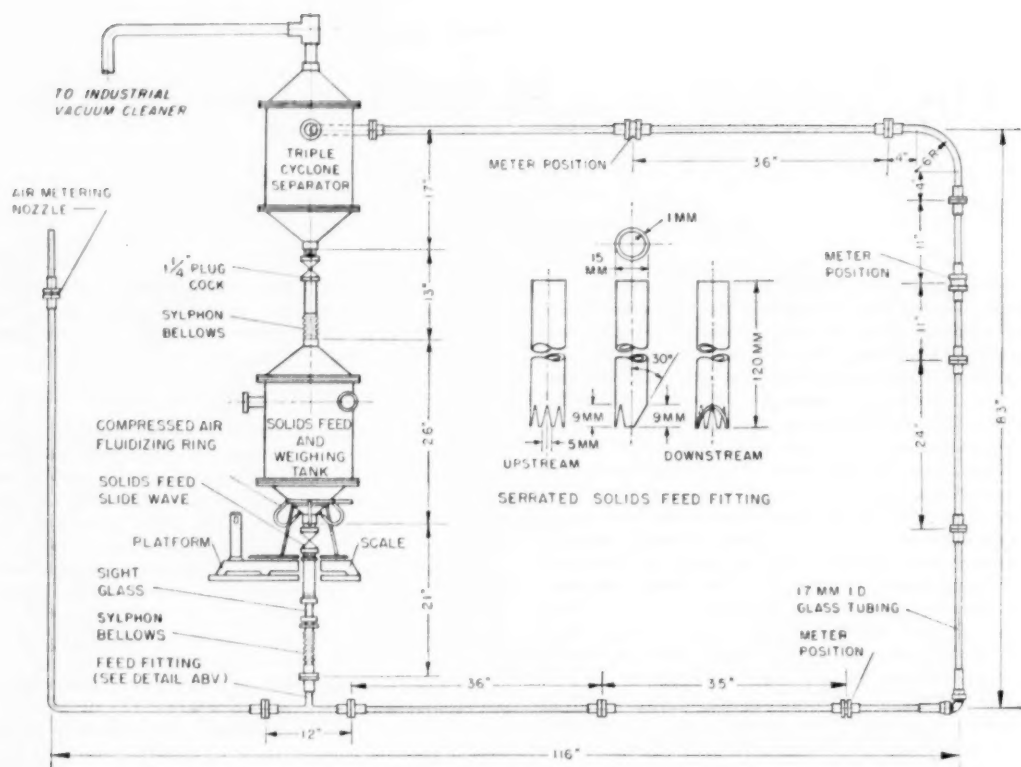


FIG. 1 FLOW DIAGRAM OF GENERAL ARRANGEMENT OF EXPERIMENTAL EQUIPMENT

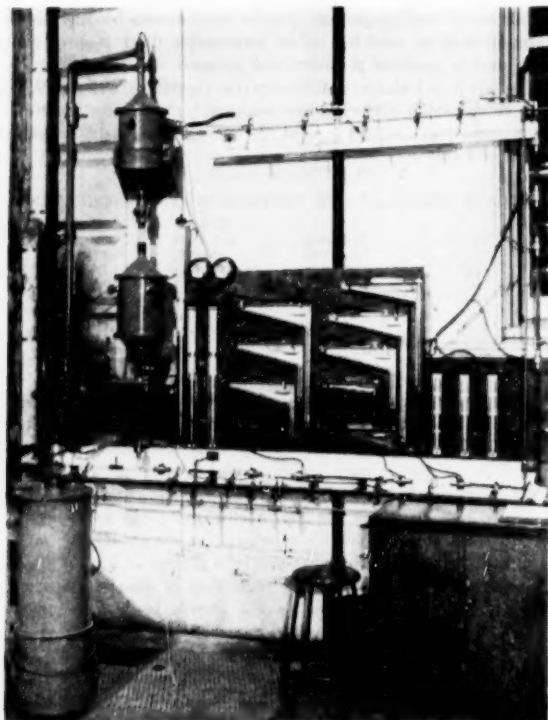


FIG. 2 EXPERIMENTAL SYSTEM

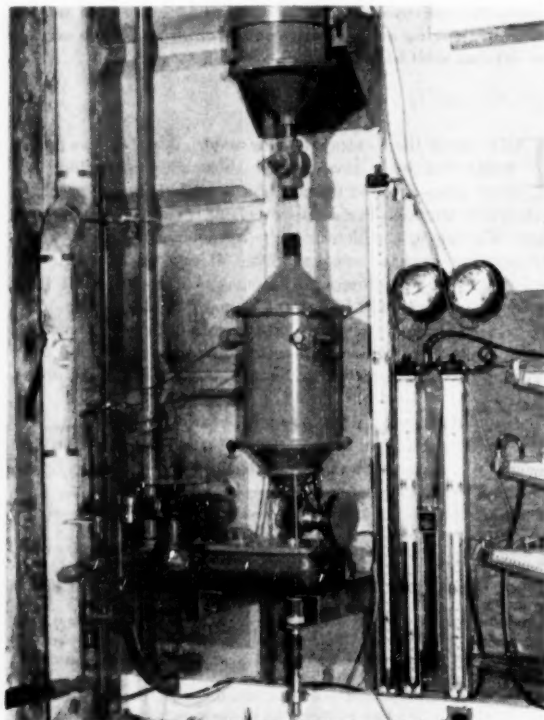


FIG. 3 SOLIDS-HANDLING SYSTEM

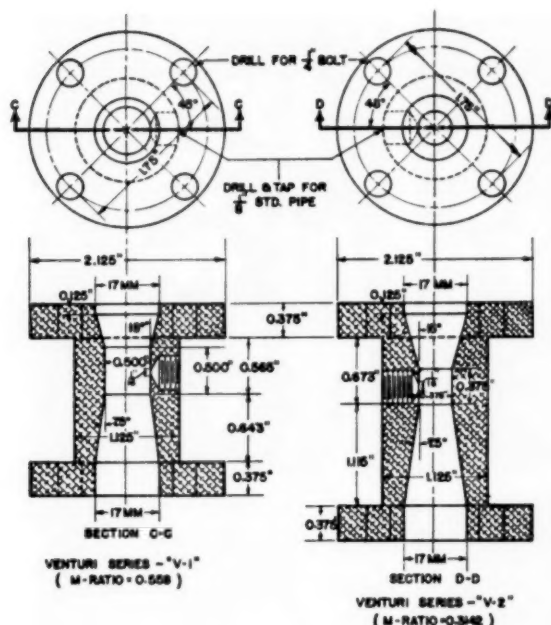


FIG. 4 METER DETAILS

ticles. These attritional effects appeared to have a negligible effect on the reproducibility of results for the system.

The Venturi tubes were calibrated in terms of the inlet-air metering nozzle prior to any tests made with solids and immediately after a series of mixture runs. The experimental procedure used was as follows:

(a) The powdered solids were prepared by fluidizing thoroughly the material in the solids feed tank.

(b) The Venturi-tube calibration checked with air flow alone.

(c) The solids slide valve adjusted to yield a uniform solids-flow rate as the air gravimetric flow rate was held constant at some predetermined value.

(d) The initial and incremental weight decrease of the solids-feed tank were recorded and plotted against elapsed time, Fig. 6, as soon as the solids-flow rate appeared stable.

(e) Pressure and pressure differentials were observed and recorded at intervals for the duration of the run.

(f) Upon completion of any run the solids-feed slide valve was closed and the flow system cleared of solids; the vacuum unit was shut off; the solids in the cyclone separator were returned to the feed tank; the weight of the feed tank observed and compared to the initial weight of the tank prior to feeding any solids into the system, thus yielding a check on any losses that may have occurred.

(g) The air rate was re-established; a different solids rate set, and the procedure as outlined in items (c) to (f) was followed for a group of fixed air rates over the range of solids-flow rates permitted by the system power.

For the range up to 3.0 in., pressures and pressure differentials were read to 0.01 in. of water; beyond the range of 3.0 in., the least count on the manometers was 0.1 in. of manometer fluid. Time and platform-scale weight was observed to within 0.2 sec and 15 grams, respectively.

The flow behavior of the system has been described previously (2); no difficulties were encountered with plugging pressure taps or system instability. The use of the serrated flow fitting

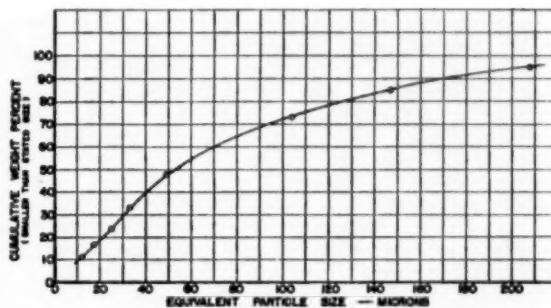


FIG. 5 PARTICLE-SIZE-DISTRIBUTION CURVE

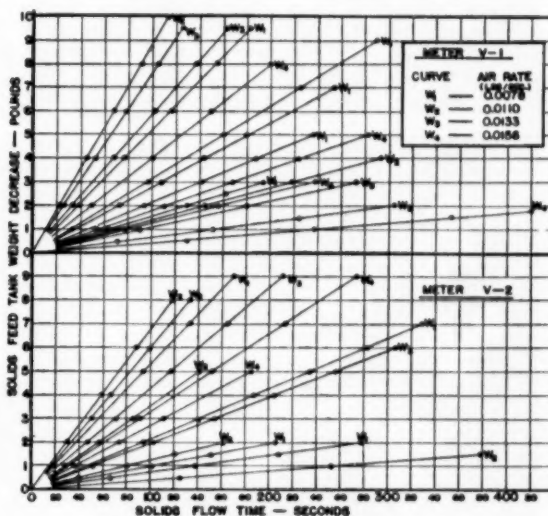


FIG. 6 SOLIDS-FEED LABORATORY CONTROL CURVES

in the solids mixing tee, shown in Fig. 1, aided materially in the control of the system stability as evidenced by Fig. 6 which indicates the ease with which the solids flowed at a constant rate.

The periodic calibrations made on the Venturi tubes served to indicate the extent of erosion that might be occurring within the tube. Within the limits of experimental accuracy, no effects on the meter performance were noted after the initially polished surface had been roughened uniformly by the sandblasting action of the solids.

EXPERIMENTAL RESULTS AND DISCUSSION

The total-energy equation as applied to the two phases (assumed incompressible) and the converging section of the Venturi for steady-state conditions and uniform distribution may be written as follows:

$$W_f \left[\frac{P_u - P_t}{\rho_f} + Z_u - Z_t + \frac{V_{fu}^2 - V_{ft}^2}{2g} - (K_f + K_s) \frac{V_{ft}^2}{2g} \right] + W_s \left[\frac{P_u - P_t}{\rho_s} + Z_u - Z_t + \frac{V_{su}^2 - V_{st}^2}{2g} \right] = 0 \quad [1]$$

where

W = substance gravimetric flow rate, lb per sec

P = pressure at section, psf



- (a) under 12 microns
- (b) 12 - 17 microns
- (c) 17 - 25 microns
- (d) 25 - 33 microns
- (e) 33 - 49 microns
- (f) 49 - 74 microns
- (g) 74 - 208 microns

FIG. 7 PHOTOMICROGRAPHS OF CATALYST PARTICLES: $\times 250$

 A = cross-sectional area, sq ft

Subscripts *f* and *s* refer to fluid (gas) and solids phase, respectively.

(c) Some average particle size flowing at the same rate W_{+} as the particles making up the aggregate mixture.

Equation [1] may be rewritten after combining terms and rearranging as

$$\frac{P_u - P_t}{\rho_f} \left[1 + \frac{W_s \rho_f}{W_f \rho_s} \right] = \frac{V_{ft}^3}{2g} \left[1 + K_f + K_s + \frac{W_s V_{st}^2}{W_f V_{ft}^3} \right] - \frac{V_{fu}^2}{2g} \left[1 + \frac{W_s V_{su}^2}{W_f V_{fu}^3} \right] + \left[1 + \frac{W_s}{W_f} \right] (Z_t - Z_u) \quad [1a]$$

Noting that the fluid density is very small relative to the solids density; applying the continuity relationship to the fluid phase and letting M equal the ratio of the Venturi-throat cross-sectional area to the inlet cross-sectional area, Equation [1a] becomes for

$$\rho_f \ll \rho_s, MA_u = A_t \text{ and } W_f = MA_u V_{ft} \rho_f$$

$$P_u - P_t = \left[\frac{W_f^3}{2g A_u^2 \rho_f M^2} (1 + K_{f+u} - M^2) + \rho_f (Z_t - Z_u) \right] + \left\{ \frac{W_f}{2g A_u^2 \rho_f} \left[\frac{V_{st}^3}{M^3 V_{ft}^3} - \frac{V_{su}^3}{V_{fu}^3} \right] + \frac{\rho_f}{W_f} (Z_t - Z_u) \right\} W_s \quad [2]$$

For a particular Venturi tube in a given position and for a constant fluid gravimetric flow rate Equation [2] indicates a linear relationship between Venturi differential and the solids flow rate W_s , with the first term on the right-hand side of the equation being the intercept and the multiplier of the solids-flow rate, W_s being the slope. The series of tests made for which the experimental results are shown in Fig. 8, appear to substantiate the relationship predicted by Equation [2]. The experimental results shown in Fig. 8 indicate the intercept to be essentially independent of the solids frictional coefficient K_s , or that the wall frictional effects experienced by the solids are negligible in comparison to the fluid frictional effects. This condition may result from the relatively high fluid velocities as was found by Wood and Bailey (3) in their investigation on the conveyance of granular material. Therefore it would appear that the assumption of a solids wall frictional loss need be made only when the fluid velocities are sufficiently low so that the solid particles strike the wall.

Inasmuch as the elevation term $(Z_t - Z_u)$ has essentially a constant value for a given Venturi and contributes only to the increase in intercept and slope for the vertical placement of the Venturi, this term will be neglected in the interest of simplifying the analysis; hence Equation [2] becomes

$$P_u - P_t = \frac{W_f^3}{2g A_u^2 M^2 \rho_f} [1 + K_{f+u} - M^2] + \frac{W_f}{2g A_u^2 \rho_f} \left[\frac{V_{st}^3}{M^3 V_{ft}^3} - \frac{V_{su}^3}{V_{fu}^3} \right] W_s \quad [3]$$

For a given Venturi, Equation [3] predicts an intercept change as being proportional to the square of the fluid gravimetric

flow rate; within the experimental accuracy this was found to be the case for the results shown in Fig. 8. Experimental results for constant fluid gravimetric flow rate show a change in the intercept that is more than proportional to $1/M^2$. In Table 2 the average value of the intercept ratio for the two meters is approximately 4.36 or about 40 per cent greater than that predicted. This increase may be accounted for by the fluid-density changes and discharge-coefficient changes that occurred in going from the larger to the smaller-diameter Venturi. Venturi calibrations yielded slightly higher discharge coefficients for the 0.500-in. tube than for the 0.375-in. tube.

The experimental results shown in Fig. 8 indicate the relationship between Venturi pressure differential and solids-flow rate to be a linear one and as predicted by Equation [2]. The results for Venturi V-2 at an intermediate gas rate show some curvature at the higher solids-flow rate which may have been caused by compressible effects within the Venturi tube. The slopes of these lines increase both with increasing gas rate and with decreasing Venturi-area ratio.

The slope as given by Equation [3] may be written as

$$\text{Slope is proportional to } W_f \left(\frac{V_{st}^2}{M^2 V_{ft}^3} \right)$$

neglecting the term $(V_{su}/V_{fu})^3$ which will not greatly influence the changes in slope, inasmuch as its maximum value will be unity for nonaccelerating particles when the Venturi is in the horizontal position and less than unity for the meter in the vertical position. When the Venturi is in the horizontal position and the solid particles have reached their steady-state velocity, the slope changes are then directly proportional to the gas-flow changes. Under actual conditions the particles are still accelerating at the Venturi throat; hence the slope change will be other than directly proportional to the gas-flow rate. When the Venturi tube is placed in the vertical position and the particles have reached a steady-state velocity, then the difference between the particle and fluid velocity will be the terminal or free-fall velocity of the particle in the stream and the changes in slope should be slightly more than proportional to the change in gas-flow rate. The effect of particles still accelerating at the throat would effect the slope change in the same direction.

The slope is further increased by a decrease in the M -ratio, and by Equation [3] this increase is proportional to $1/M^2$. The experimental evidence indicates this change in slope to be considerably greater than proportional to $1/M^2$. The ratio of intercepts and slopes are shown in Table 2 for the various gas-flow rates investigated.

Considering the relatively wide size range of particles which made up the aggregate mixture, it is rather remarkable that the experimental results so closely substantiated the general predictions obtainable from Equation [2]. Although the trends shown in Fig. 8 and Table 2 are definitely in accordance with the analysis, the author believes neither the experimental data

TABLE 2 INTERCEPT AND SLOPE RATIOS FOR VENTURI TUBES V-1 AND V-2

Air-rate ratio			Venturi tube V-1				Venturi tube V-2			
Rate	Ratio	(Ratio) ^a	Horizontal		Vertical		Horizontal		Vertical	
			Intercept	Slope	Intercept	Slope	Intercept	Slope	Intercept	Slope
W_2/W_1	1.41	1.98	2.0	1.32	1.82	1.58	1.93	1.47	2.02	1.6
W_3/W_1	1.71	2.91	3.0	1.75	2.82	1.92	2.82	1.92	2.95	2.07
W_4/W_1	2.0	4.0	4.1	1.97	3.95	2.11	3.89	2.47	4.14	2.54
W_2/W_2	1.21	1.46	1.5	1.32	1.55	1.21	1.46	1.31	1.46	1.29
W_3/W_2	1.42	2.01	2.05	1.49	2.17	1.53	2.01	1.68	2.04	1.59
W_4/W_2	1.17	1.37	1.37	1.13	1.40	1.10	1.37	1.29	1.40	1.23
Air rate, lb per sec			Intercept ratio ^a		Slope ratio ^a					
			Hor	Vert	Hor	Vert				
$W_1 = 0.0078$			4.55	4.14	5.5	4.25				
$W_2 = 0.0110$			4.4	4.6	6.14	4.3				
$W_3 = 0.0133$			4.28	4.32	6.05	4.6				
$W_4 = 0.0156$			4.31	4.32	6.95	5.14				

^a Ratio (V-2/V-1).

nor the variables contained in Equation [2] are such as to allow the prediction of Venturi-tube characteristics in metering gas-solids mixtures without calibration.

Returning to Equation [1a] and assuming the fluid density constant and negligible in comparison to the solids density, the flow to be frictionless (or a discharge coefficient of unity for the true fluid), and the solids velocity equal to the fluid velocity there results the following relationship

$$\frac{(P_u - P_t)_{\text{mixture}}}{(P_u - P_t)_{w_s=0}} = 1 + \frac{W_s}{W_f} \quad [4]$$

which is exactly the same as may be obtained from the relationship proposed by Carlson, et al. (4), for mixtures flowing in nozzles and based on an analysis in which the density change of the mixture was proportional to the solids-flow concentration in the gas.

Fig. 9 shows the plot of Equation [4] and its relationship to the results obtained in this investigation which indicates that the assumption of a density change in proportion to the flowing phases results in a predicted mixture differential which is considerably greater than that actually observed in the Venturi tubes. The ratios obtained from the experimental results on the Venturi tubes shown in Fig. 9 are quite similar to the results obtained by Gästerstadt (5) on the specific pressure drop for the pneumatic conveyance of grain, in that the pressure-differential ratio appears to be slightly lower at the higher air rates for each tube. Fig. 9 further shows the advantage to be obtained by having a large throat diameter and horizontal placement of the Venturi tubes.

Pressure measurements were taken of the diffuser end of the Venturi tube, and the recovery pressure in per cent of the meter-mixture differential has been plotted against solids-flow rate in Fig. 10. The recovery for gas flowing alone conformed, in general, to the Venturi-tube pressure-recovery data presented by Warren (6). As the solids phase was added, the percentage

recovery decreased rapidly with increasing solids rate, the rate of change of this decrease being greater for the smaller-diameter tube. For very high solids rates, the loss in the diffuser section was found to exceed the Venturi pressure differential by a considerable amount in some cases. The pressure fluctuations that were observed across the diffuser section at high loadings indicated to a certain extent the degree of turbulence that existed in this section. This excessive turbulence in the diffuser section probably was caused by the solids velocity being greater than the fluid velocity, which would result in excessive losses at high loadings.

Although this investigation was limited to rather small Venturi tubes, the results seem to indicate that the Venturi may be used to meter the solids phase in a gas-solids mixture when the gravimetric gas-flow rate is held constant. This may be accomplished by using a calibrated blower for the gas phase or by use of an orifice meter and controller in the clean-gas system. In view of the lack of sufficient data for the prediction of line slopes when metering the mixture, a calibration covering several solids-flow rates must be made. In systems where a calibration cannot be made, the Venturi tube may still serve a most useful purpose by indicating instantaneous changes in the solids-flow rate.

CONCLUSIONS

Certain conclusions may be drawn with respect to the metering of the solids phase in a gas-solids mixture flowing through a Venturi tube when the flow is essentially incompressible and the gravimetric flow rate of the gas phase is held constant.

For the range of solids loading covered in this investigation the pressure-differential versus solids-flow-rate relationship was a linear one for the Venturi tubes used in metering the gas-solids mixtures.

As predicted by theoretical conditions, the pressure differentials for vertical placement of the Venturi tubes were found to be greater than those for horizontal placement.

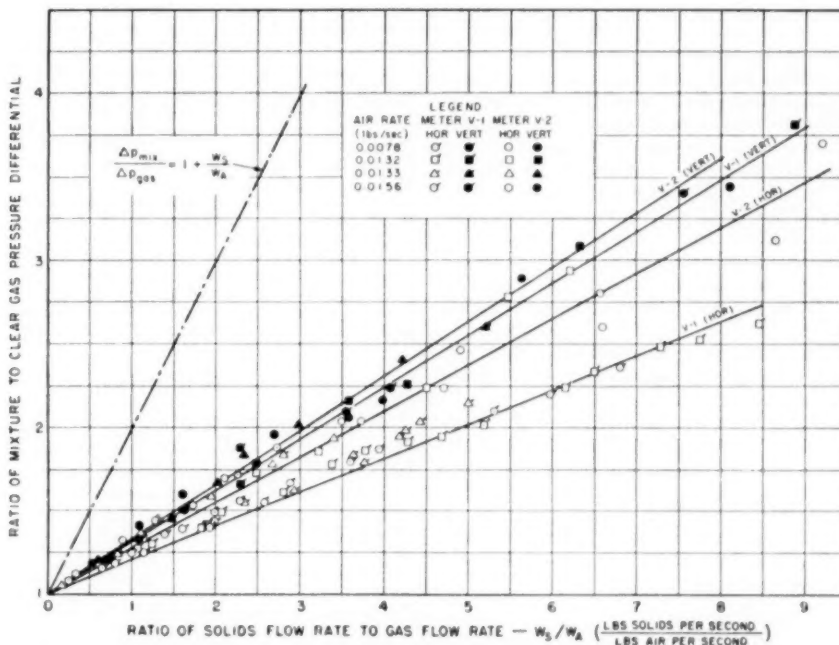


FIG. 9 PRESSURE-DIFFERENTIAL RATIO VERSUS FLOW RATIO FOR 0.500-IN. AND 0.375-IN. VENTURI

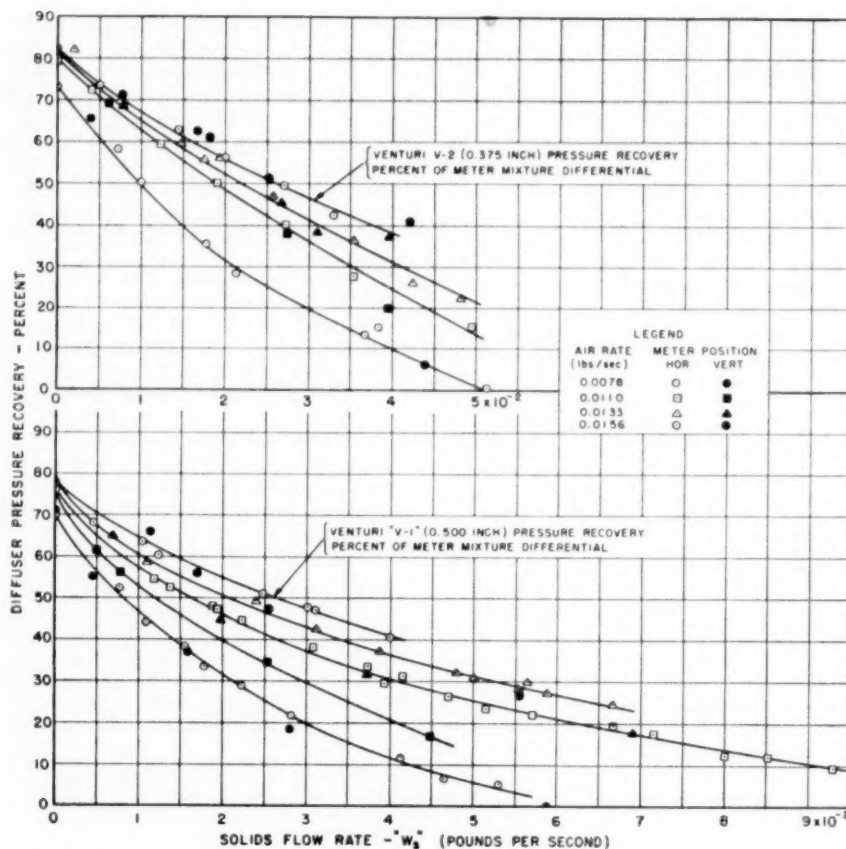


FIG. 10 VENTURI RECOVERY PRESSURE, PER CENT OF METER DIFFERENTIAL, VERSUS SOLIDS-FLOW RATE FOR VARIOUS CONSTANT AIR-FLOW RATES

The slope of the straight-line relationship appears to depend primarily on the gravimetric gas-flow rate and the Venturi-area ratio. The slope increases with increased gas rate and decreasing area ratio as predicted by application of the general energy equation. Although the line slopes cannot be determined readily from theory, the use of the Venturi is not restricted since the meter may be calibrated in place or used to indicate instantaneous changes of solids flow.

The Venturi-area ratio should be as high as possible to reduce power losses resulting from excessive pressure differentials at high loadings and to keep velocities within the range of minimum erosion for the system.

The Venturi-diffuser section is quite effective in recovering pressure at light solids loadings but drops rapidly in effectiveness as the solids loading is increased.

Further investigation of the variables involved seems necessary in order to determine whether the Venturi-tube flow constants can be predicted from the constants of the system.

ACKNOWLEDGMENT

This investigation, a part of the research program in multi-phase flow at the University of California, was supported in part through a Research Corporation grant.

BIBLIOGRAPHY

- 1 "Discharge Measurement by Means of Venturi Tubes," by A. L. Jorissen, Trans. ASME, vol. 73, 1951, p. 403.

- 2 "Flow Characteristics of Solids-Gas Mixtures in a Horizontal and Vertical Circular Conduit," by L. Farbar, *Industrial and Engineering Chemistry*, vol. 41, 1949, p. 1184.

- 3 "The Horizontal Carriage of Granular Material by an Injector-Driven Air Stream," by S. A. Wood and A. Bailey, *Journal and Proceedings of The Institution of Mechanical Engineers*, vol. 142, December, 1939, p. 157.

- 4 "Meter for Flowing Mixtures of Air and Pulverized Coal," by H. M. Carlson, P. M. Frazier, and R. B. Engdahl, Trans. ASME, vol. 70, 1948, p. 65.

- 5 "Die Experimentelle Untersuchung des Pneumatischen Fordervorganges," by H. Gästerstadt, *Vereines deutscher Ingenieure, Forschungsarbeiten*, vol. 265, 1924, pp. 3-75.

- 6 "A Study of Head Loss in Venturi-Meter Diffuser Sections," by J. Warren, Trans. ASME, vol. 73, 1951, p. 399.

Discussion

J. D. HUMMELL,³ R. B. ENGDALH,⁴ H. M. CARLSON,⁵ and P. M. FRAZIER.⁶ The experimental data and equations presented in this paper point out the factors which must be considered in the design of a Venturi to meter gas-solids mixtures. Apparent dis-

³ Research Engineer, Battelle Memorial Institute, Columbus, Ohio. Jun. ASME.

⁴ Supervisor, Battelle Memorial Institute, Columbus, Ohio. Mem. ASME.

⁵ Assistant Professor, Mechanical Engineering Department, Speed Scientific School, University of Louisville, Louisville, Ky. Jun. ASME.

⁶ Oak Ridge, Tenn. Jun. ASME.

crepancies from the results given in the author's reference (4) can be justified if the equations presented are used in their basic form.

Assuming frictionless flow and the velocity of the solids equal to the velocity of the gas in the pipe, Equation [3] of the paper can be used to develop

$$\frac{\Delta P_{mix}}{\Delta P_{clear\ gas}} = 1 + \frac{\left[\left(\frac{V_{st}}{V_{ft}} \right)^2 - M^2 \right]}{1 - M^2} \frac{W_s}{W_f}$$

When $V_{st} = V_{ft}$, this equation is that of the author's Equation [4] with a slope of 1. Otherwise, the slope of the plot of this equation is a function of M , V_{st} , and V_{ft} . With M constant, the slope will be less for the smaller values of the ratio V_{st}/V_{ft} . Therefore the slope will depend upon the acceleration of the particles in the nozzle which will be influenced by the particle size and density. The larger and denser particles will accelerate less and, therefore, will decrease the slope. The data presented here were obtained with material of 2.45 specific gravity, 50 per cent of which was larger than 200 mesh. For the work in reference (4) of the paper, the specific gravity was 1.3 and only 7 per cent was larger than 200 mesh. Qualitatively, this may explain the difference in the laboratory data of the two experiments. Further work is necessary to determine quantitatively the effect of the size and density on the velocity ratios.

When $V_{st} < V_{ft}$, the slope is a function of M and a decrease in M will result in an increase in the slope. The author's data show this trend since the slope for Venturi V-2 was greater than that for V-1 which had a larger M -ratio.

The intercept ratio from Equation [3] of the paper, for constant gravimetric flow rate is proportional to

$$\frac{1}{M^2} + \frac{K_{fsa}}{M^2} - 1$$

The author assumed that $1/M^2$ was sufficiently large to be predominating and reports the intercept ratio to be proportional to $1/M^2$. The value of K_{fsa} would be sufficiently small to be omitted. However, for the Venturi meters tested, the term (-1) should not be omitted especially when using ratios. The intercept ratio when proportional to $1/M^2$ is equal to 3.16, and when proportional to $1/M^2 - 1$ is equal to 4.13 compared with the experimental value of 4.36.

In the discussion of the slope of Equation [3], the author has assumed the value of $(V_{sa}/V_{fa})^2$ to be small enough to be omitted. If this term is equal to unity, then

$$S\alpha W_f \left[\frac{1}{M^2} \left(\frac{V_{st}}{V_{ft}} \right)^2 - 1 \right]$$

The value of unity should not be omitted for the same reasons as given in the foregoing discussion on the intercept ratio. The omission is even more serious when $V_{st} < V_{ft}$.

For constant gravimetric flow rate and with $V_{sa} = V_{fa}$, the slope ratio would be

$$\frac{S_2}{S_1} = \frac{M_1^2}{M_2^2} \frac{\left(\frac{V_{st}}{V_{ft}} \right)_2^2 - M_2^2}{\left(\frac{V_{st}}{V_{ft}} \right)_1^2 - M_1^2}$$

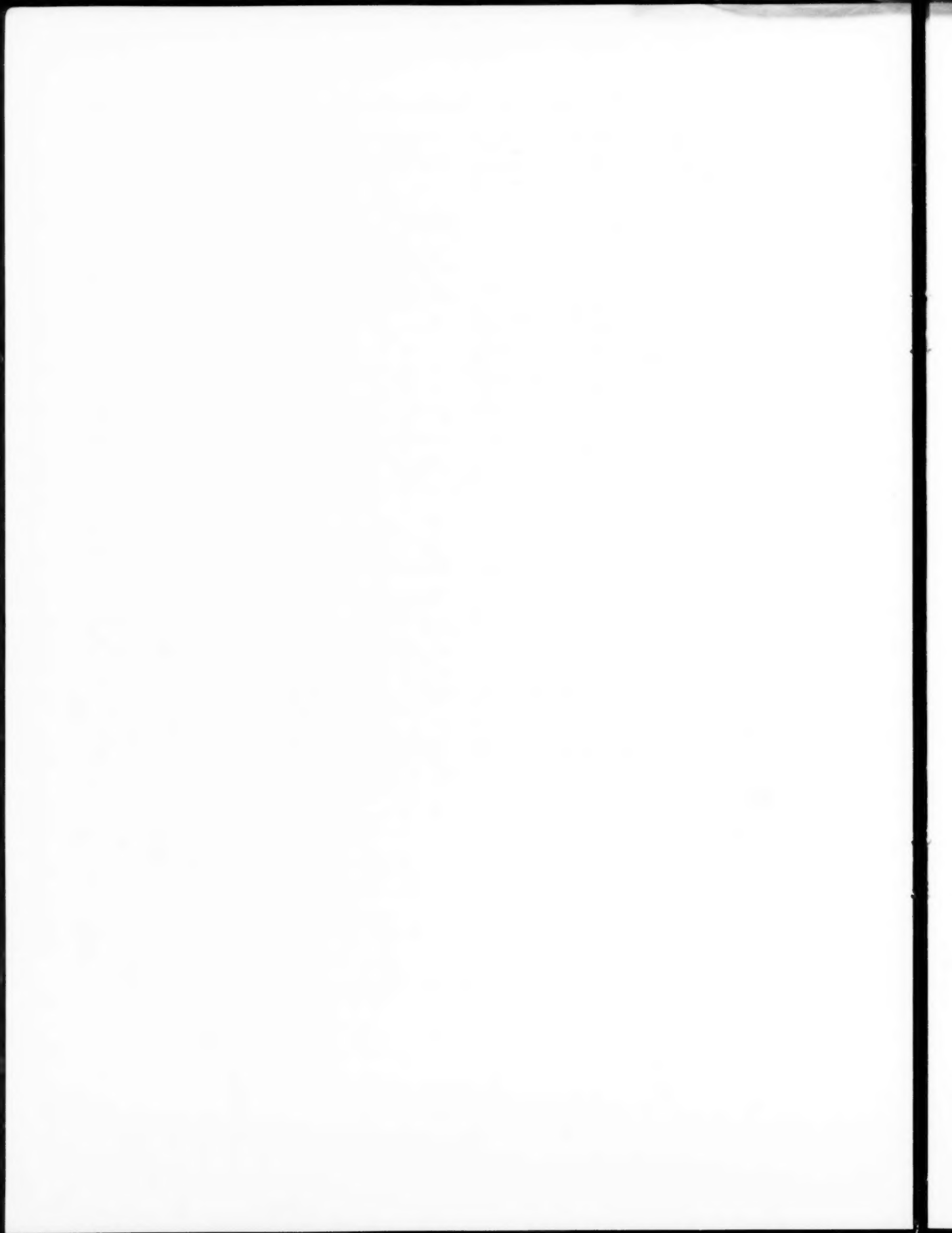
Thus the slope ratios depend not only on the M -ratio but also on the ratio of V_{st} to V_{ft} which may be equal to or less than 1. With the slope ratios from the experimental data, the velocity ratio from the foregoing equation would be about 0.8. Although this is not a precise value of the velocity ratio, it does indicate importance of evaluating the ratio for accurate analytical analysis and the need for additional study in this field.

AUTHOR'S CLOSURE

The author acknowledges with appreciation the interesting comments by Messrs. Hummel, Engdahl, Carlson, and Frazier, and thoroughly agrees that further quantitative work is necessary to determine the effect of particle size and density on the flow characteristics of gas-solids mixtures.

The author believes that any discrepancy between the results presented in this paper and the results obtained by the discussers is due not only to differences in particle size and density but also due to the influence of particles on one another under conditions of high loading. This influence exhibits itself in the manner in which the solids phase may flow in clusters of particles or in a dense and stratified layer when in a horizontal conduit.

A further complexity in the analysis is introduced when a wide-size range aggregate solids mixture is used; hence the author has avoided specifying any velocity ratios. The simplified analysis has been used to indicate the trend that theory predicts and its verification by experimental results.



Experimental Evaluation of Expansion Factors for Steam¹

By J. W. MURDOCK² AND C. J. FOLTZ,³ PHILADELPHIA, PA.

The empirical expansion factor for the orifice-metering of compressible fluids is based largely on tests of natural gas and air. This paper presents data on superheated steam for orifice ratios from 0.50 to 0.82, superheats from 29 to 255 F, and pressures of 44 to 102 psia. Expansion factors obtained were in close agreement with those of natural gas and air.

NOMENCLATURE

The following nomenclature is used in the paper:

- A = slope factor, K versus λ , dimensionless
- A_2 = area of orifice, sq in.
- C = coefficient of discharge, dimensionless
- D_1 = internal diameter of pipe at upstream tap, in.
- D_2 = diameter of orifice, in.
- E = area multiplier for thermal expansion of orifice, dimensionless
- k = ratio of specific heats, dimensionless
- K = flow coefficient (coefficient of discharge with approach factor included), dimensionless
- K_c = flow coefficient calculated from ASME equations, dimensionless
- K_e = flow coefficient for λ_e , dimensionless
- K_s = flow coefficient from steam tests, dimensionless
- K_w = flow coefficient from water tests, dimensionless
- p_1 = absolute inlet static pressure, psi
- p_2 = absolute outlet static pressure, psi
- Δp = differential pressure across primary element, psi
- R_d = Reynolds number based on orifice diameter, dimensionless
- w = gravimetric rate of flow, lb per sec
- x = ratio of pressure drop to absolute inlet pressure— $\Delta p/p_1$, dimensionless
- Y = empirical expansion factor (ratio of flow coefficient for gas to that for liquid at same value of R_d), dimensionless
- Y_e = empirical expansion factor calculated from ASME equations, dimensionless
- Y_s = empirical expansion factor from steam tests, dimensionless
- β = diameter ratio, D_2/D_1 , dimensionless
- ϵ = slope of the K_s to x/k -curve, dimensionless
- λ = reciprocal of Reynolds number, dimensionless

¹ The opinions or assertions contained in this paper are the private ones of the authors, and are not to be construed as official or reflecting the views of the Navy Department or the Naval Service at large.

² Superintendent, Instrument Division, U. S. Naval Boiler and Turbine Laboratory, Philadelphia Naval Base, Mem. ASME.

³ Engineer in Charge, Scientific Branch, Instrument Division, U. S. Naval Boiler and Turbine Laboratory, Philadelphia Naval Base, Jun. ASME.

Contributed by the Research Committee on Fluid Meters and presented at the Annual Meeting, New York, N. Y., November 30–December 5, 1952, of THE AMERICAN SOCIETY OF MECHANICAL ENGINEERS.

NOTE: Statements and opinions advanced in papers are to be understood as individual expressions of their authors and not those of the Society. Manuscript received at ASME Headquarters, September 19, 1952. Paper No. 52-A-52.

- ρ_1 = inlet density, pcf
- λ_e = reciprocal of Reynolds number when ($R_{d_e} = 10^6 D_2/15$) dimensionless
- μ_1 = absolute viscosity at inlet conditions, lb per ft sec

INTRODUCTION

The tests described in this paper were conducted at the U. S. Naval Boiler and Turbine Laboratory (1)⁴ as part of the co-operative program of the Joint AGA-ASME Committee on Orifice Research. Tests with steam and water were made to supplement those with natural gas at Rockville, Md. (2), Refugio, Texas, and others with water at the National Bureau of Standards.

Many of the data described were obtained during tests to determine interference effects of fittings placed various distances upstream from an orifice. Additional runs were made to furnish more complete evaluation of the expansion factor.

This paper presents experimental data confirming the ASME empirical expansion factor for orifice-metering of superheated steam. It is hoped that the results of the interference tests may be presented in a later paper.

ASME VALUES

Values and relationships referred to in this paper as ASME are those of reference (3). Equations for flow coefficient and expansion factor are reproduced in the Appendix.

COMPRESSIBLE FLOW

Flow measurements by differential-type meters are based on the hydraulic equation for fluids of constant density. Metering a fluid such as a gas or vapor necessitates accounting for the change in density with pressure. In devices where the minimum flow area is the throat of the primary element, such as a nozzle, the effect of density change may be computed from theoretical equations. For the sharp-edged orifice, however, the minimum flow area is at the vena contracta located downstream of the orifice rather than at its throat. The stream of compressible fluid is not restrained as it leaves the throat and it is free to expand transversely and longitudinally to the point of minimum flow area. Thus the maximum contraction of the jet will be less for a compressible fluid than for a liquid.

Dr. Edgar Buckingham (4) pointed out the difficulties of an exact mathematical solution and in (5) presented a "theoretical equation based on simplifying assumptions." In the same paper he also offered an empirical equation based on test data available in 1932. This equation was later adopted by the ASME (3), and is today the basis for all metering calculations of expansible fluids.

The ASME equation is based primarily on tests with natural gas and air. Data on superheated steam by Witte were analyzed by Dr. Buckingham (5) and seemed to agree with those of gases, but uncertainties in interpreting Witte's data and the difficulties in making accurate readings from his published figure led Dr. Buckingham to conclude that some of this agreement might be coincidental. Because of the lack of supporting data, the toler-

⁴ Numbers in parentheses refer to the Bibliography at the end of the paper.

ance for expansion factors for superheated steam has been set by the ASME (6) and (7) as twice that for gas and air.

EQUIPMENT AND PROCEDURE

Steam information supplementing that of natural gas and air was obtained with the facilities and techniques described in this section.

The orifice-meter section was fabricated in accordance with ASME standards and practices (7). Pressure differential taps were located at flange and radius (1 and 1/2) dimensions.

Orifice plates were constructed of 1/4-in. stainless steel. The hole was beveled downstream at an angle of 45 deg to a cylindrical thickness of 3/16 in. Three centering pins were drilled and tapped into the downstream side of each plate to insure concentric installation. Data were obtained on ten plates ranging from $\beta = 0.3007$ to 0.8221. Physical dimensions of these plates are given in Table 1.

TABLE 1 RÉSUMÉ OF PERTINENT INFORMATION

Orifice No.	30	11 - 12	24	10	7 - 8	18
Dimensions of the System $D_1 = 3.9852^*$						
β	0.3007	0.4949	0.6515	0.7422	0.7921	0.8221
β_2	1.1994	1.9743*	2.5990	2.9608	3.1600*	3.2794
Constants for Computing A.S.M.E. Values of Y and K						
β^4	0.0082	0.0600	0.1802	0.3034	0.3937	0.4568
$\sqrt{1 - \beta^4}$	0.9959	0.9894	0.9054	0.8366	0.7786	0.7569
$\frac{A}{A_0}$	350	626	1294	1851	2196	2407
$\frac{E}{K}$	0.433	0.431	0.473	0.516	0.548	0.570
Steam Test Reynolds Numbers and per cent Computed K Deviation from Average R_0						
R_0 Max.	450,000	1,090,000	1,490,000	2,730,000	3,070,000	3,340,000
R_0 Min.	440,000	750,000	1,090,000	1,330,000	1,510,000	1,670,000
R_0 Avg.	440,000	870,000	1,210,000	1,960,000	2,190,000	2,550,000
ΔK Dev.	0.00	0.01	0.01	0.03	0.03	0.04
$C = K \sqrt{1 - \beta^4}$ at $R_0 = 1,000,000$						
C_0 Radius	0.5977	0.6040	0.6076	0.6048	0.6123	0.6211
Flange	0.5981	0.6036	0.6058	0.6007	0.5998	0.6003
C_w Radius	0.5984	0.6064	0.6089	0.6112	0.6163	-
Flange	0.5969	0.6050	0.6054	0.6096	0.6083	-
C_s Radius	0.5942	0.6076	0.6172	0.6083	0.6142	0.6260
Flange	0.5947	0.6042	0.6132	0.6042	0.6032	0.5981
Data from Method of Least Squares						
ϵ Radius	0.2512	0.2632	0.3292	0.3408	0.4227	0.5184
Flange	0.2405	0.2561	0.3156	0.3542	0.4050	0.4516
ϵ/λ_s Radius	0.421	0.420	0.483	0.468	0.536	0.610
Flange	0.403	0.410	0.466	0.488	0.523	0.556
K_s Radius	0.5966	0.6268	0.6817	0.7289	0.7688	0.8495
Flange	0.5971	0.6253	0.6773	0.7263	0.7747	0.8117
Average $100[(K_s - Y_0)/Y_0]$						
Radius	+0.17	+0.18	+0.19	+0.40	+0.12	+0.61
Flange	+0.23	+0.37	+0.09	+0.30	+0.23	+0.18

* D_2 -Orifice 11 = 1.9746", 12 = 1.9740". Orifices 7 and 8 were identical.

The test section was a straight run of pipe, 147 diam in length, discharging into an atmospheric condenser and from there into a weighing system. Steam or water could be introduced without any change in the test section.

Inlet pressure at each set of taps was read on 0 to 300-psi-range Bourdon-tube-type test gages, smallest increment 1/2 lb. Readings were estimated to the nearest 1/10 lb. Pressure differential across each set of taps was measured with well-type differential manometers, range -4 to 56 in., smallest scale increment 1/10 in., or inverted U-tube differential manometers, range 0 to 100 in., with line pressure balanced by air pressure above the water in the manometer tubes. Readings were estimated to the nearest 1/100 in.

Two total-temperature-type thermocouple wells (8) were installed, one approximately 70 pipe diam upstream, the other 5 pipe diam downstream from the orifice. Calibrated iron-constantan thermocouple wire was used. Hot-junction tempera-

tures were read on a self-balancing potentiometer, range 0 to 40 mv, smallest increment 2/100 mv. Readings were estimated to the nearest 1/100 mv. Ice bottles were employed to provide constant cold-junction temperatures of 32 F.

Mass flow was determined by discharging into two tanks alternately and weighing. Each tank was mounted on a 0 to 4000-lb scale, smallest increment 1 lb. Data were recorded to the nearest pound. Constant level was maintained in the condenser hot well by means of a weir box.

TEST ACCURACY

The accuracy that may be obtained from a test is dependent upon the instrumentation. If a single variable is measured then it is limited by the standard used. If more than one variable is measured such as in these tests then only a probable accuracy can be estimated. The probability that each measurement will be in the same direction is small—hence, from mathematics, the overall accuracy will be the square root of the sum of the squares of the individual accuracies.

The accuracies computed in Table 2 do not refer to accidental errors in observation or improper test conditions concerning which

TABLE 2 PROBABLE TEST ACCURACY

Quantity measured	Steam tests		Water tests	
	Accuracy, per cent	Effective power	Accuracy, per cent	Effective power
Differential pressure	0.1	$\times 1/3$	0.0025	$\times 1/3$
Static pressure	0.2	$\times 1/2$	0.0100	$\times 1/2$
Temperature	0.1	$\times 1/3$	0.0025	$\times 1/3$
Density	0.3	$\times 1/2$	0.0225	$\times 1/2$
Orifice diameter	0.05	$\times 2$	0.0100	$\times 2$
Thermal expansion of primary element	0.05	$\times 1$	0.0025	$\times 1$
Weight	0.1	$\times 1$	0.0100	$\times 1$
Sum of squares	0.0600		0.0273	
Over-all accuracy, per cent	± 0.25		± 0.17	

no general predictions are possible. Each run will have its own probable accuracy. For example, 50 in. can be read on the same manometer to a greater accuracy than a differential of 10 in. Table 2 is based on the method given in reference (6)⁵ and values have been chosen for an average run.

DATA AND RESULTS

Preliminary analysis showed considerable deviation from the ASME expansion factor, as the Beta ratio decreased. The calibration of the 0.3007-ratio orifice showed such a deviation from accepted values that a thorough recheck of the system was made. It was found that minor valve leakage was present. Although this leakage was small, flow rates of the low-Beta-ratio orifices magnified its effect. Runs were made with increasing mass flow as the differential increased. This method of operation made it impossible to distinguish the effect of leakage from the expansion factor.

It was determined that this minor leakage did not affect ratios greater than 0.65, the correspondingly higher mass flow making variations negligible. Blanks and tell-tales were installed to prevent and detect leakage. Reruns of nearly constant mass flow were made on the 0.3007, 0.4949, and 0.6515 orifices. All water tests were made with the improved system.

The test data are shown in Tables 3 and 4 for steam and water, respectively, and graphically in Figs. 1 to 4, inclusive.

FLOW COEFFICIENTS

Individual steam tests can determine only the product KY of the flow coefficient and the expansion factor. The flow coefficient must be determined by calculation, water calibration, or correla-

⁵ Reference (6), p. 128.

TABLE 3 OBSERVED AND CALCULATED STEAM TEST DATA

Run No.	Time Sec.	Flow #	Temp. of	Rd x 10 ⁻⁶	Radius Tap Data			Flange Tap Data		
					P ₁	ΔP/P ₁	KY	P ₁	ΔP/P ₁	KY
Orifice 30					D ₂ = 1.1994"			β = 0.3007		
231	4680	0.456	534.5	0.44	49.4	0.2921	0.5433	49.2	0.2935	0.5442
232	3960	0.470	545.1	0.44	70.2	0.1396	0.5717	69.9	0.1403	0.5726
233	4320	0.487	552.7	0.45	99.4	0.0720	0.5829	99.2	0.0723	0.5831
Orifice 11					D ₂ = 1.9746"			β = 0.4950		
242	3600	1.286	521.5	0.75	45.3	0.3521	0.5576	45.1	0.3552	0.5576
243	3600	1.308	533.0	0.76	57.2	0.2080	0.5870	57.3	0.2087	0.5851
244	4320	1.396	544.6	0.78	99.1	0.0731	0.6113	99.2	0.0735	0.6089
245	5400	1.433	516.5	0.83	98.9	0.0750	0.6114	98.9	0.0754	0.6098
246	3600	1.350	520.6	0.79	69.2	0.1434	0.5988	69.1	0.1441	0.5981
247	5040	1.308	519.1	0.77	49.8	0.2912	0.5664	49.8	0.2922	0.5654
Orifice 12					D ₂ = 1.9740"			β = 0.4948		
255	5400	1.404	328.4	1.00	44.4	0.3547	0.5544	44.2	0.3575	0.5547
256	4680	1.483	350.4	1.03	58.3	0.2084	0.5877	58.2	0.2096	0.5870
257	3600	1.578	356.4	1.09	99.5	0.0745	0.6088	99.3	0.0749	0.6081
Orifice 24					D ₂ = 2.5990"			β = 0.6515		
269	4320	2.576	486.7	1.17	70.3	0.1403	0.6440	70.1	0.1424	0.6410
270	4320	2.431	487.9	1.11	49.0	0.2896	0.6081	48.9	0.2933	0.6056
271	3240	2.382	484.5	1.09	44.7	0.3490	0.5942	44.5	0.3537	0.5928
272	3960	2.684	489.9	1.21	99.3	0.0714	0.6648	99.1	0.0725	0.6612
273	1800	2.932	368.9	1.49	102.2	0.0690	0.6653	102.3	0.0698	0.6608
Orifice 10					D ₂ = 2.9608"			β = 0.7422		
7	5040	4.701	345.1	2.21	75.7	0.1802	0.6787	75.7	0.1830	0.6735
8	5400	3.906	344.3	1.84	75.4	0.1200	0.6936	75.3	0.1220	0.6888
9	7200	2.844	344.4	1.34	75.7	0.0606	0.7082	75.6	0.0618	0.7026
67	7200	4.760	354.7	2.19	77.5	0.1760	0.6834	77.1	0.1768	0.6854
68	5400	3.968	351.0	1.84	76.9	0.1189	0.6973	76.5	0.1193	0.6995
69	7200	2.913	345.8	1.32	75.8	0.0586	0.7123	75.8	0.0589	0.7142
70	3600	5.825	349.7	2.71	76.6	0.2945	0.6516	77.3	0.2951	0.6452
71	3600	5.048	351.0	2.35	76.2	0.2096	0.6738	76.7	0.2104	0.6681
72	3600	4.382	348.0	2.04	76.8	0.1471	0.6914	77.3	0.1477	0.6854
73	3600	3.465	346.3	1.63	76.6	0.0881	0.7077	77.0	0.0886	0.7023
74	3600	5.374	341.3	2.52	76.8	0.2342	0.6685	77.3	0.2354	0.6625
75	3600	4.761	342.8	2.23	76.0	0.1804	0.6830	76.6	0.1808	0.6769
76	3600	3.965	342.7	1.86	76.5	0.1176	0.6999	76.9	0.1185	0.6938
77	3600	2.962	340.2	1.34	75.9	0.0598	0.7132	76.4	0.0597	0.7093
Orifice 8					D ₂ = 3.1600"			β = 0.7921		
4	5400	5.579	347.7	2.43	73.5	0.1803	0.7286	73.6	0.1870	0.7145
5	5400	4.915	344.6	2.12	76.0	0.1199	0.7443	75.9	0.1244	0.7316
6	5400	3.443	345.6	1.51	75.7	0.0589	0.7635	75.6	0.0612	0.7499
64	5400	5.828	349.0	2.54	76.9	0.1806	0.7268	76.4	0.1825	0.7277
65	5400	4.809	346.8	2.09	76.3	0.1177	0.7484	75.9	0.1190	0.7482
66	6120	3.452	344.9	1.52	75.5	0.0585	0.7677	75.1	0.0593	0.7692
78	3600	7.056	352.4	3.07	76.2	0.2980	0.6921	76.9	0.3040	0.6790
79	3600	6.223	358.6	2.69	77.4	0.2079	0.7230	78.0	0.2132	0.7085
80	3600	5.261	358.6	2.27	75.1	0.1503	0.7418	75.7	0.1535	0.7283
81	4500	4.196	355.6	1.81	75.4	0.0901	0.7605	75.9	0.0921	0.7470
82	3600	6.590	354.7	2.84	77.4	0.2371	0.7146	78.0	0.2426	0.7011
83	3600	5.737	350.1	2.50	74.6	0.1815	0.7364	75.3	0.1847	0.7233
84	3600	4.855	348.8	2.11	76.2	0.1198	0.7508	76.7	0.1224	0.7379
85	5400	3.517	348.0	1.53	76.4	0.0592	0.7724	76.9	0.0606	0.7582
157	3060	5.049	497.3	1.85	75.8	0.1616	0.7393	76.4	0.1666	0.7223
158	3780	5.966	500.4	2.19	76.4	0.2402	0.7111	77.0	0.2471	0.6956
159	3600	4.155	498.0	1.52	76.8	0.1012	0.7603	77.3	0.1049	0.7415
160	2160	5.991	350.5	2.61	76.4	0.1925	0.7288	77.0	0.1974	0.7142
161	8100	5.301	478.1	1.96	75.6	0.1759	0.7379	76.2	0.1803	0.7231
Orifice 7					D ₂ = 3.1600"			β = 0.7921		
163	3600	5.848	344.4	2.57	75.4	0.1879	0.7268	76.3	0.1937	0.7074
164	5760	5.843	341.3	2.57	76.5	0.1812	0.7272	77.2	0.1885	0.7066
165	3600	4.779	338.3	2.12	76.1	0.1172	0.7426	76.7	0.1223	0.7214
166	3960	3.441	335.5	1.53	74.0	0.0603	0.7664	74.5	0.0626	0.7474
167	3600	5.886	348.0	2.56	76.9	0.1808	0.7329	77.7	0.1878	0.7109
Orifice 18					D ₂ = 3.2794"			β = 0.8221		
111	5400	8.096	364.9	3.34	77.1	0.3001	0.7304	77.9	0.3178	0.7026
112	3600	6.958	364.2	2.87	76.0	0.2063	0.7691	76.8	0.2219	0.7340
113	3600	6.014	359.8	2.48	74.9	0.1490	0.7925	75.5	0.1608	0.7568
114	3600	4.830	358.6	2.01	76.1	0.0884	0.8136	76.6	0.0950	0.7798
115	3600	7.369	358.7	3.07	76.2	0.2388	0.7517	76.9	0.2547	0.7214
116	3600	6.584	362.8	2.71	76.4	0.1771	0.7811	77.0	0.1905	0.7472
117	3600	5.494	360.3	2.27	75.8	0.1185	0.8030	76.4	0.1270	0.7696
118	3600	4.014	358.6	1.67	75.9	0.0602	0.8223	76.3	0.0650	0.7873

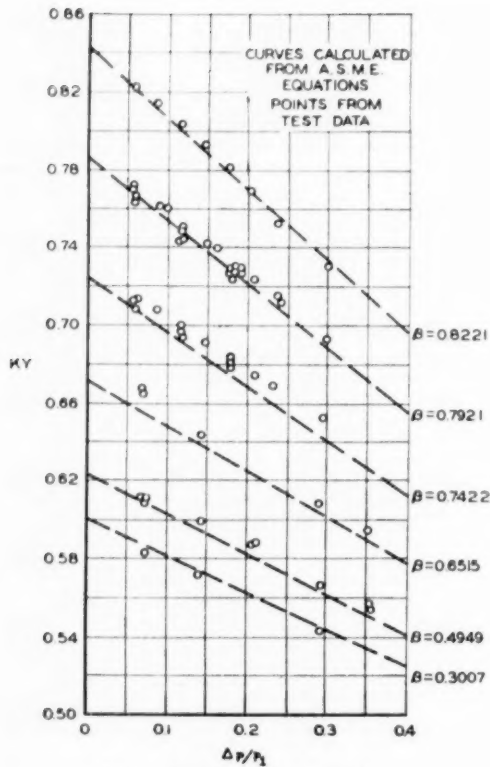


FIG. 1 STEAM DATA—RADIUS TAPS

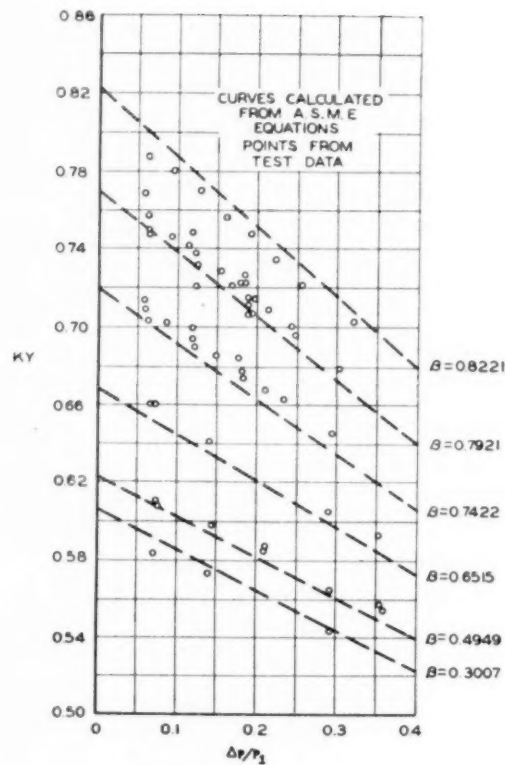


FIG. 2 STEAM DATA—FLANGE TAPS

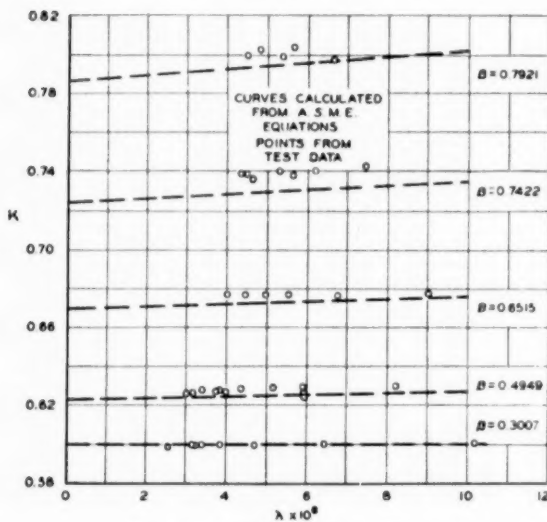


FIG. 3 WATER DATA—RADIUS TAPS

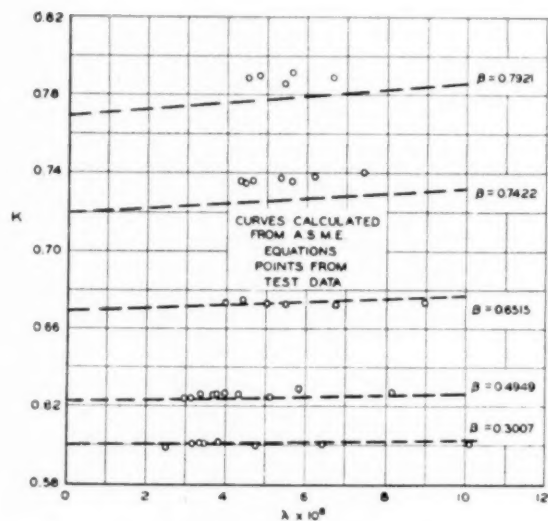


FIG. 4 WATER DATA—FLANGE TAPS

tion of several steam tests, before the expansion factor can be evaluated.

The flow coefficient K_e at $R_d = 1,000,000$ was calculated from ASME equations. The water coefficient K_w was calculated from test data. Steam test data were linear in the KY versus $\Delta p/p_1$ plots of each orifice as shown in Figs. 1 and 2. To extra-

polate these data to $\Delta p/p_1 = 0$, the mathematical method of least squares was used to prevent errors of judgment. For a K_e determined in this manner to be valid, all data for each line must be at the same Reynolds number. Although there was a considerable range of Reynolds number, the magnitude of R_d was so great that

TABLE 4 OBSERVED AND CALCULATED WATER TEST DATA

Run No.	Time Sec.	Flow w	Temp. °F	$R_d \times 10^{-6}$	$\frac{10^6}{R_d}$	Radius Tap Data		Flange Tap Data	
						Δp	K	Δp	K
Orifice 30						$D_2 = 1.1994"$		$\beta = 0.3007$	
211	3960	13,361	71	0.261	3.83	13.94	0.6002	13.92	0.6008
212	3600	15,727	72	0.312	3.20	19.37	0.5994	19.34	0.5999
213	3600	7,721	73	0.155	6.45	4.66	0.5999	4.65	0.6008
217	3240	13,399	82	0.300	3.33	14.09	0.5993	14.05	0.6002
218	3060	9,492	81	0.212	4.72	7.09	0.5984	7.06	0.5996
219	4320	4,465	80	0.098	10.20	1.558	0.6005	1.556	0.6008
240	4320	16,108	89	0.394	2.54	20.44	0.5985	20.44	0.5985
241	3960	12,551	87	0.301	3.32	12.35	0.6000	12.35	0.6000
Orifice 12						$D_2 = 1.9740"$		$\beta = 0.4948$	
258	1800	21,134	89	0.314	3.18	4.18	0.6260	4.41	0.6234
259	3240	17,728	90	0.267	3.75	3.075	0.6266	3.086	0.6255
260	3600	12,800	90	0.193	5.18	1.593	0.6246	1.611	0.6251
261	1800	20,879	95	0.335	2.99	4.28	0.6256	4.31	0.6240
262	3240	17,912	95	0.294	3.40	3.135	0.6275	3.153	0.6257
263	2520	16,316	97	0.264	3.79	2.608	0.6266	2.615	0.6257
264	2520	15,451	96	0.250	4.00	2.333	0.6274	2.340	0.6265
265	2880	14,214	96	0.230	4.35	1.972	0.6278	1.983	0.6260
266	2880	10,583	96	0.171	5.85	1.090	0.6287	1.090	0.6287
267	2880	7,541	96	0.122	8.20	0.553	0.6289	0.557	0.6267
297	2040	20,827	56	0.203	4.93	4.27	0.6240	4.28	0.6227
298	1800	21,010	57	0.205	4.88	4.29	0.6246	4.33	0.6248
Orifice 24						$D_2 = 2.5990"$		$\beta = 0.6515$	
275	1800	21,173	92	0.249	4.02	1.251	0.6774	1.266	0.6734
276	1800	18,962	92	0.223	4.48	1.006	0.6766	1.266	0.6734
277	2520	16,771	93	0.199	5.03	0.785	0.6775	0.795	0.6732
278	2880	15,066	94	0.181	5.52	0.635	0.6767	0.641	0.6735
279	2880	12,249	95	0.149	6.71	0.421	0.6758	0.425	0.6726
280	3600	8,994	96	0.111	9.01	0.227	0.6758	0.228	0.6743
Orifice 10						$D_2 = 2.9608"$		$\beta = 0.7422$	
281	2520	12,757	94	0.134	7.46	0.224	0.7433	0.226	0.7400
282	2880	14,950	96	0.161	6.21	0.311	0.7395	0.312	0.7383
283	2880	17,238	97	0.188	5.32	0.413	0.7400	0.416	0.7373
284	2880	19,658	97	0.214	4.67	0.541	0.7373	0.543	0.7359
285	1800	21,219	97	0.231	4.33	0.629	0.7381	0.632	0.7363
287	1800	20,570	97	0.224	4.46	0.593	0.7369	0.596	0.7351
288	2880	16,225	97	0.177	5.65	0.368	0.7379	0.370	0.7359
Orifice 8						$D_2 = 3.1600"$		$\beta = 0.7921$	
289	2520	15,335	93	0.150	6.67	0.217	0.7970	0.221	0.7897
290	3240	18,286	96	0.185	5.41	0.307	0.7992	0.317	0.7865
291	2520	21,379	98	0.221	4.52	0.419	0.8000	0.430	0.7897
292	2160	20,239	98	0.209	4.78	0.374	0.8016	0.384	0.7911
293	2880	17,281	98	0.178	5.62	0.271	0.8040	0.279	0.7924

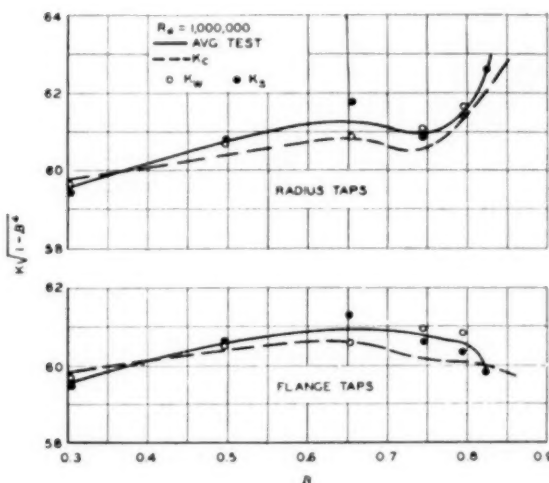


FIG. 5 COMPARISON OF FLOW COEFFICIENTS

K -variation was negligible. Table 1 shows these values, the maximum deviation of K being 0.04 per cent.

Each series of steam and water tests was conducted at different Reynolds numbers. An arbitrary value of 1,000,000 was chosen for comparison purposes. The steam and water-flow coefficients were adjusted by assuming the ASME K versus λ relationship and extrapolating to 1,000,000 paralleling the K_s versus λ curve. Fig. 5 shows the flow-coefficient relationships, the coefficient of discharge $K\sqrt{1-\beta^4}$ being used to permit a smaller grid.

By definition all of these flow coefficients are equal or

$$K = K_c = K_w = K_s$$

The ASME flow coefficient is based on the average of a series of tests on different orifice-meter sections. Equations are not valid for ratios greater than 0.75. Flow coefficients for any given orifice metering system constructed and installed in accordance with ASME requirements (7) may deviate from the average. Since no two systems can be constructed exactly alike, except by accident, minor variations in approach conditions, pipe roughness, fabrication, and location of pressure taps, and sharpness and concentricity of the orifice plates will influence the actual flow coefficient.

The flow-coefficient curve for the individual system should be similar to that of the ASME if proper test techniques are employed. Fig. 5 shows that a curve similar to that of the ASME can be drawn through the average of the steam and water points. It should be noted that the average deviation is less than 1 per cent, the scale being such that minor variations are magnified.

The steam and water-flow coefficients should be the same within the limits of test accuracy and extrapolation errors. With the exception of data obtained on the 0.6515-ratio orifice, Fig. 5 shows K_w and K_s to be in close agreement. Examination of the water data for this orifice (Figs. 3 and 4), indicated that the test points do not follow the ASME K to λ relationship; indeed these data do not show

any change in K with R_d .

From the foregoing discussion it is evident that either K_w , K_s , or their averages could be used to evaluate the expansion factor. However, because of the doubtful 0.6515-data and the lack of water data for the 0.8221-ratio orifice, K_s was used to evaluate the expansion factor.

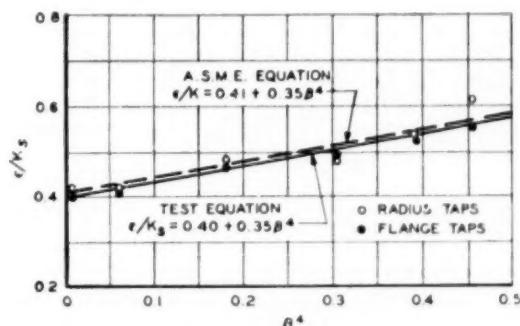


FIG. 6 EMPIRICAL EXPANSION FACTOR

EXPANSION FACTORS

The straight-line relationship of the test data for any one orifice and set of differential pressure taps permits mathematical expression in terms of the familiar $y = mx + b$ equation. Introducing the acoustic ratio x/k to permit comparison with compressible fluids of different specific-heat ratios, the data for any one orifice and tap arrangement may be expressed as follows

$$KY = K_s - \epsilon x/k \dots \dots \dots [1]$$

Since $K = K_s$, and the slope factor ϵ may be obtained in the same manner as K_s , Equation [1] can be rearranged to read as follows

$$Y_s = 1 - (\epsilon/K_s)(x/k) \dots \dots \dots [2]$$

Values of ϵ/K_s plotted as a straight line against β^2 are shown in Fig. 6. By the mathematical method of least squares, the following equation is obtained representing all the test data

$$\epsilon/K_s = 0.40 + 0.35\beta^2 \dots \dots \dots [3]$$

Substituting the value of ϵ/K_s of Equation [3] into Equation [2] the following equation for the expansion factor is obtained

$$Y_s = 1 - (0.40 + 0.35\beta^2)x/k \dots \dots \dots [4]$$

The test equation agrees closely with the ASME equation

$$Y_e = 1 - (0.41 + 0.35\beta^2)x/k \dots \dots \dots [5]$$

An alternative method of comparing the expansion factor is to compute Y_t by dividing the test KY by K_s . Fig. 7 shows the average deviations obtained by this process. The average difference for all orifices was $+0.08$ per cent.

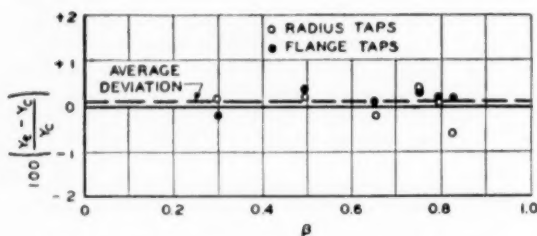


FIG. 7 AVERAGE DEVIATION OF EXPANSION FACTORS

CONCLUSIONS

From these data it is concluded that the ASME expansion factor Y is valid for superheated steam and tolerances for this vapor should be the same as that for air and gases.

ACKNOWLEDGMENTS

This work was made possible by the financial support and sponsorship of the Bureau of Ships and the Office of Naval Research. The guidance and assistance of the Joint AGA-ASME Orifice Committee was most helpful. To the personnel of the U. S. Naval Boiler and Turbine Laboratory, particularly Mr. Clarence Gregory who made the calculations and ran the water tests, the authors are grateful.

BIBLIOGRAPHY

- 1 "The Naval Boiler and Turbine Laboratory," by Capt. E. Krussfelder, USN, Transactions of the The Society of Naval Architects and Marine Engineers, vol. 53, 1927, pp. 341-358.
- 2 "Investigation of Orifice Meter Installation Requirements," Interim Research Report No. 1 of the Joint American Gas Association, The American Society of Mechanical Engineers Committee on Orifice Meters, New York, N. Y., 1951

- 3 "History of Orifice Meters and the Calibration, Construction and Operation of Orifices for Metering," Report of the Joint American Gas Association—The American Society of Mechanical Engineers Committee on Orifice Coefficients, New York, N. Y., 1935.

- 4 "Notes on Contraction Coefficients of Jets of Gas," by Edgar Buckingham, U. S. National Bureau of Standards, *Journal of Research*, vol. 6, May, 1931, pp. 765-775.

- 5 "Notes on the Orifice Meter: The Expansion Factor for Gases," by Edgar Buckingham, U. S. National Bureau of Standards, *Journal of Research*, vol. 9, July, 1932, pp. 60-69.

- 6 "Fluid Meters, Their Theory and Application," Report of The American Society of Mechanical Engineers Special Research Committee on Fluid Meters, fourth edition, New York, N. Y., 1937.

- 7 "Flow Measurement by Means of Standardized Nozzles and Orifice Plates," Power Test Code PTC 19.5; 4—1949, The American Society of Mechanical Engineers, New York, N. Y., 1949.

- 8 "Measurement of Temperatures in High-Velocity Steam," by J. W. Murdock and E. F. Fiock, *Trans. ASME*, vol. 72, 1950, pp. 1155-1161.

- 9 "Thermodynamic Properties of Steam," by J. Keenan and F. Keyes, John Wiley & Sons, Inc., New York, N. Y., 1936.

- 10 "Review of Data on Dynamic Viscosity of Water and Superheated Steam," by G. S. Hawkins, W. L. Sibbett, and H. L. Solberg, *Trans. ASME*, vol. 70, 1948, pp. 19-23.

Appendix

EQUATIONS

Y = ASME empirical expansion factor was calculated from the following equation⁶

$$Y = 1 - (0.41 + 0.35\beta^2)x/k \dots \dots \dots [5]$$

K = ASME flow coefficients were calculated from equations as given in the following:⁷

General relationships

$$K = K_s(1 + A\lambda)/(1 + A\lambda_s) \dots \dots \dots [6]$$

$$A = D_2(830 - 5000\beta + 9000\beta^2 - 4200\beta^3 + 530/\sqrt{D_1}) \dots [7]$$

$$\lambda_s = 15/10D_2 \dots \dots \dots [8]$$

K_s for radius taps

$$K_s = 0.5933 + 0.009/D_1 + (0.109 + 0.012/\sqrt{D_1})\beta^2 + 0.4(1.6 - 1/D_1)^2(0.07 + 0.5/D_1 - \beta)^{3/2} - (0.009 + 0.034/D_1)(0.5 - \beta)^{3/2} + (10/D_1^2 + 9)(\beta - 0.7)^{3/2} \dots [9]$$

K_s for flange taps

$$K_s = 0.5993 + 0.007/D_1 + (0.364 + 0.076/\sqrt{D_1})\beta^2 + 0.4(1.6 - 1/D_1)^2(0.07 + 0.5/D_1 - \beta)^{3/2} - (0.009 + 0.034/D_1)(0.5 - \beta)^{3/2} + (65/D_1^2 + 3)(\beta - 0.7)^{3/2} \dots [10]$$

Test KY : Test values of the product of the flow coefficient and the expansion factor for steam, and the flow coefficient for water ($Y = 1$), were calculated from the following equation:

$$KY = w/(0.6684_2 E \sqrt{\rho_1 \Delta P}) \dots \dots \dots [11]$$

Equation [11] was obtained by rearranging Equation [2] of reference (7).⁸

Test R_d : The Reynolds number of the orifice was calculated from the following equation⁹

$$R_d = 48w/(\pi D_2 \mu_1) \dots \dots \dots [12]$$

⁶ Equation [6], reference (3), p. 28.

⁷ Selected from Equations [10] to [18], reference (3), pp. 19-20.

⁸ Reference (7), p. 8.

⁹ Ibid., Equation [6], p. 9.

PHYSICAL VALUES

E , Values for the area multiplier for thermal expansion were taken from reference (7)¹⁰ for 18 Cr and 8 Ni material.

k , The ratio of specific heats was chosen as a constant of 1.31, being the average value shown reference (9)¹¹ for test conditions.

p_i , Values of inlet density were obtained from steam tables (9) using an energy-balance method described in reference (8) to convert total temperature-well data to inlet conditions.

μ_i , Values of viscosity of steam and water were taken from reference (10).

Discussion

K. J. BERRIAN.¹² The paper under discussion compares recent experimental work on steam-expansion factors with values given in the ASME Fluid Meters Report, Part I, 1937. The ASME values also are empirical.

It is of interest to compare these results with those obtained from a purely theoretical analysis. There is a solution of the

Eulerian equation for plane irrotational motion of an ideal compressible fluid. The relationship between the expansion factor and the pressure ratio across the orifice is represented by a slightly curved line. It checks with the ASME values at the critical-pressure ratio of 0.54, but is 0.5 per cent high at a pressure ratio of 0.80.

The ASME values are admittedly the best straight line that could be put through the available data. The actual experimental values fall on a curved line, but whether or not they coincide with the theoretical curve will require further checking.

The theoretical solution was first obtained by Chaplygin.¹³ The mathematics and the complete numerical calculations and discussions are in the writer's master's thesis presented at the Stevens Institute of Technology in 1939.

AUTHORS' CLOSURE

Mr. Berrian's comments are appreciated, and it is hoped that sufficient data may some day be available to affirm the theoretical equations he mentioned. In the meantime, it is felt that the use of the ASME empirical equation will be satisfactory for commercial flow measurement.

¹⁰ Reference (7), Fig. 3, p. 13.

¹¹ Reference (9), Fig. 8.

¹² The Jet-Vue Corporation, Waltham, Mass. Jun. ASME.

¹³ "Gas Jets," by S. Chaplygin, U. S. Advisory Committee for Aeronautics, NACA Technical Memo No. 1063, August, 1944.

Measurement of Pulsating Flow With Propeller and Turbine-Type Meters

By R. B. DOWDELL¹ AND A. H. LIDDLE, JR.,² PROVIDENCE, R. I.

Tests have been made on four different fluid meters under various conditions of unsteady flow. Results are presented, showing that in some cases accurate measurement of pulsating flow is possible.

INTRODUCTION

IT has been proved conclusively, both by theory and experiment, that it is impossible to measure pulsating flow accurately with a differential-type flowmeter when pulsations are excessive.^{3,4,5} The suppression of pulsations in a pipe line, either by filters or surge tanks, is often unsatisfactory and may prove to be a large expense; thus a meter which will measure pulsating flow accurately has long been desired. The data presented in this paper show that with the magnitude and frequency of pulsations tested, a propeller-type flowmeter will totalize accurately the flow of an incompressible fluid. The Shuntflo meter, a device which combines some of the features of a differential-type meter and some of those of a propeller-type meter, though performing accurately under some conditions, may produce readings with considerable error when measuring a compressible pulsating flow.

Test Equipment and Procedure. Two different testing setups, one utilizing water as the working medium and the other using steam, were used. Fig. 1 is a schematic diagram of the hydraulic test arrangement while Fig. 2 shows the arrangement using steam.

Hydraulic Test Equipment. All hydraulic tests were made at the hydraulics laboratory of the authors' company. Fig. 1 shows that the flow from a fixed-head tank passed through a control gate valve before entering the straight run of pipe preceding the meter. This valve was wide open at all times during testing; thus all results

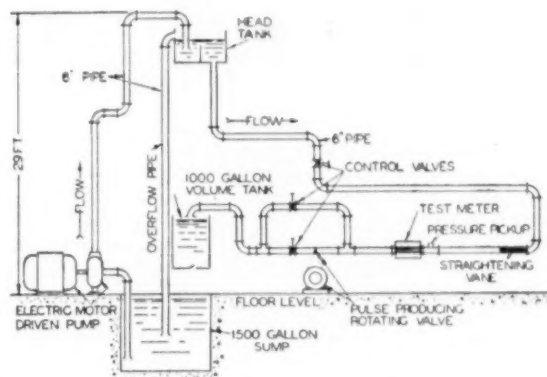


Fig. 1 ARRANGEMENT OF TEST EQUIPMENT FOR HYDRAULIC TESTING

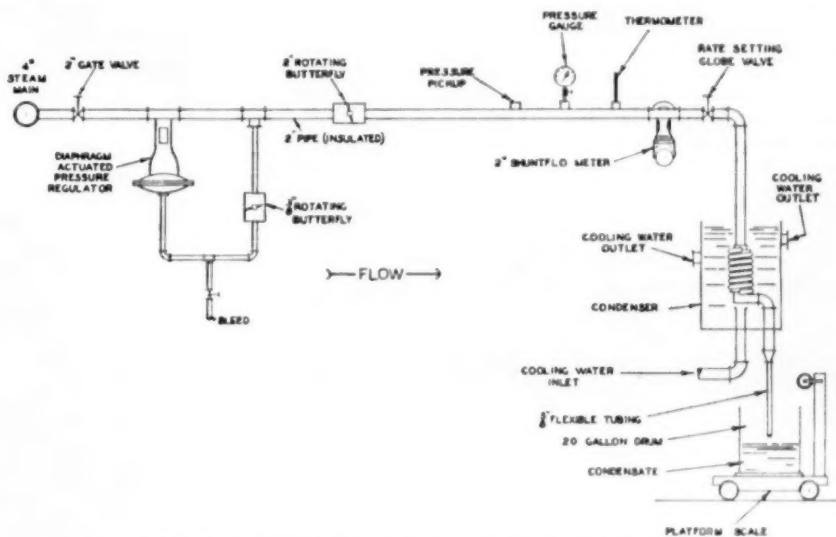


Fig. 2 ARRANGEMENT OF TEST EQUIPMENT FOR STEAM TESTING

are for a meter operating under a constant total head. The

6-in. test meters were preceded by a straight run of 52 in. of 6-in. pipe which, in turn, was preceded by a straight run of 53 in. of 8-in. pipe. These two sections of pipe were joined by an 11-in.-long, 8-in. \times 6-in. reducer. The 8-in. meter was preceded by a straight run of 94 in. of 8-in. pipe. Two sets of straightening vanes were installed in the upstream end of the 8-in. pipe to eliminate the possibility of a swirl following the elbow. The 6-in. meters were followed by a 32-in. length of straight 6-in. pipe, while 12 in. of 8-in. straight pipe and 20 in. of 6-in. pipe followed the 8-in. meter. In both cases, this entered directly into the pulsation-producing loop. This loop consisted of (1) a straight-through section of 6-in. pipe which contained a continuously rotating 6-in. butterfly valve followed by a control

¹ Research Engineer, Builders-Providence, Inc. Jun. ASME.

² Research Engineer, Builders-Providence, Inc.

³ "Basic Difficulties in Pulsating-Flow Metering," by A. R. Deschere, Trans. ASME, vol. 74, 1952, pp. 919-923.

⁴ "Pulsations in Gas-Compressor Systems," by E. G. Chilton and L. R. Handley, Trans. ASME, vol. 74, 1952, pp. 931-943.

⁵ "Pulsation and Its Effect on Flowmeters," by E. J. Ljndahl, Trans. ASME, vol. 68, 1946, p. 883.

Contributed by the Research Committee on Fluid Meters and presented at the Annual Meeting, New York, N. Y., November 30-December 5, 1952, of THE AMERICAN SOCIETY OF MECHANICAL ENGINEERS.

NOTE: Statements and opinions advanced in papers are to be understood as individual expressions of their authors and not those of the Society. Manuscript received at ASME Headquarters, August 28, 1952. Paper No. 52-A-32.

gate valve, and (2) a by-pass line containing a 6-in. gate valve. Pulsations were produced at a constant frequency by driving this rotating valve at a constant speed. The drive consisted of a chain and sprocket driven through a 48:1 reducing gear by a 2-hp 1735-rpm induction motor. Following the loop, the flow passed to the discharge spout which could be rotated so that it emptied into the sump or into the volume-measuring tank. During a run, the flow was collected in this previously calibrated, 1000-gal tank, which was equipped with a vertical gage glass reading in tenths of an inch. Readings to the nearest 0.02 in. could be made by interpolation. One tenth of an inch on the gage glass was equivalent to 1.77 gal. A minimum of 350 gal per test run was established.

The revolutions of the test-meter output spindle were measured on a combination dial and totalizing indicator. The smallest division on the dial was 0.01 revolution, permitting readings to the nearest 0.005 revolution. This revolution counter was coupled to the meter spindle by suitable gearing which incorporated a magnetic clutch, actuated by a mercury switch attached to the discharge spout. Thus the counter started and stopped automatically as the discharge spout was rotated.

The flow time was measured by an electric timer which also was actuated by a mercury switch mounted on the discharge pipe. The smallest division on the dial of the clock was 0.1 sec, permitting readings to the nearest 0.05 sec.

Immediately preceding the 6-in. test meter was a 12-in. length of straight pipe which contained an engine-indicator pressure pickup mounted on the top and a diaphragm-actuated carbon-pile pressure pickup mounted on the bottom. These pickups were used to obtain the amplitude and wave shape of the pressure variations. When testing the 8-in. meter, this pipe section was installed downstream of the meter in the 6-in. pipe section.

The meters used in the hydraulic test are shown in Figs. 3, 4, and 5. Fig. 3 is a 6-in. Propelloflo meter manufactured by the

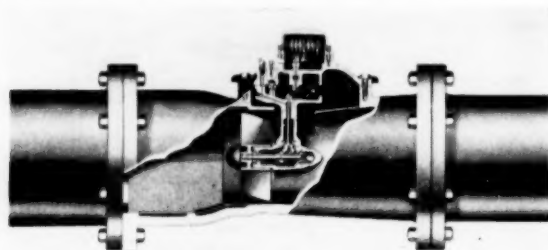


FIG. 3 - 6-IN. PROPELOFLO METER

authors' company, having a flow range from 85 to 900 gpm. Fig. 4 shows an 8-in. commercial propeller meter with a range from 100 to 1200 gpm. This latter meter will be designated as meter A.

Both of these are axial-type meters consisting of a hard-rubber helical-type propeller mounted on a shaft coincident with the pipe axis. The motion of the propeller is reduced through a suitable gear train to the output spindle. The principal difference between these two meters is the converging diverging shape of the Propelloflo meter in contrast to the straight pipe section and larger propeller of meter A.

The third meter tested and shown in Fig. 5 is a 6-in. commercial turbine-type meter, having a range from 80 to 1600 gpm. Hereafter this meter will be designated as meter B. It consists of two hard-rubber propellers, one having a right-hand and the other a left-hand helix, mounted on a vertical spindle. The incoming water is divided into two streams, one passing through

the upper propeller and the second stream passing through the lower propeller. The motion of the shaft is reduced through gears to the output spindle which normally drives a calibrated revolution counter registering in gallons. During these tests the meter counter was replaced by the same magnetic-clutch revolution counter, as used on the other meters.

Hydraulic Test Procedure. For each meter, after calibration, tests were run at three different pulse amplitudes and two different pulse frequencies. The frequency was set by the gear ratio between the motor and the pulse valve, while the amplitude was maintained by adjusting the control valves. For each amplitude and frequency, readings were taken over the entire rate of flow range obtainable. This flow range was limited by the piping arrangement and head available.

At a given amplitude and frequency, a run was first taken at the minimum flow rate by closing both control valves, and then

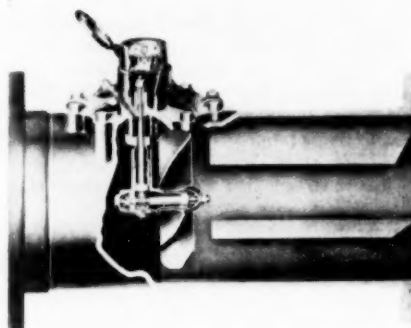


FIG. 4 - METER A, 8-IN. PROPELLER METER

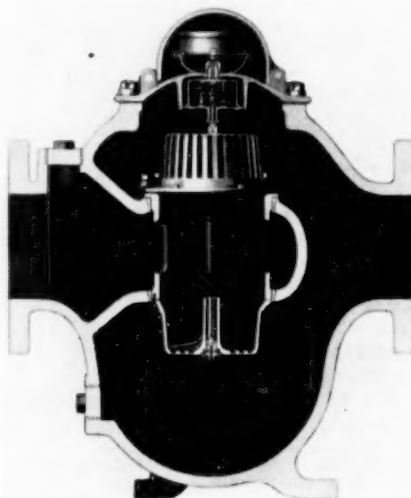


FIG. 5 - METER B, 6-IN. COMMERCIAL TURBINE-TYPE METER

slowly opening the one in the line of the pulse valve until the desired pulse amplitude was obtained on the indicator ahead of the test meter. After equilibrium was obtained, the control lever was pulled, which, through a pulley arrangement, turned the discharge pipe so that it discharged into the volume tank, and at the same instant, actuated the timer and revolution counter by

making contact in the mercury switches. At the end of a run, a second lever was pulled, which returned the discharge pipe to its initial position of discharging into the sump, breaking contact in the mercury switches and stopping the timer and revolution counter.

A point at a higher flow rate was then set by opening both valves simultaneously and then finally adjusting the control valve in the by-pass line until the correct amplitude was read on the indicator ahead of the meter.

The maximum flow rate was obtained when the control valve in the line of the pulse valve was wide open and the by-pass control valve was open just enough to give the desired pulse amplitude. A greater range of flow rate could be obtained at the lower pulse amplitude than at the higher. At least two sets of readings were taken at each valve setting.

Indicator cards were made on a continuously rotating drum at each valve setting, and pictures of the wave shape were taken at the extremes of the flow range.

Individual calibration runs were made using the same piping arrangement as that used for the pulsation tests, but with the butterfly valve stationary.

STEAM TEST EQUIPMENT

Fig. 2 is a schematic sketch of the apparatus used for the steam tests. Steam flowed from the main line, through a 2-in. gate valve, into a straight run of 2-in. pipe. A diaphragm-actuated pressure regulator was located 10 in. downstream from the gate valve. A butterfly valve (free to rotate 360 deg) was installed in the $\frac{3}{4}$ -in. supply line to the diaphragm, and a bleed valve, opening to the atmosphere, was placed between the butterfly valve and the diaphragm. The butterfly valve was rotated by a chain and sprocket driven through a variable-speed transmission by a $\frac{1}{4}$ -hp capacitor motor. For one particular run, another butterfly valve was placed in the 2-in. line, 7 in. downstream from the junction of the regulator supply line and the 2-in. pipe, and was rotated by a chain and sprocket driven directly by a $\frac{1}{4}$ -hp capacitor motor. Twenty-seven inches farther downstream, a mounting was provided for the steam-engine indicator and the diaphragm-actuated carbon-pile pickup.

A bourdon-tube pressure gage, previously calibrated on a dead-weight tester, was located 8 in. downstream from this mounting and was followed directly by a mercury-in-glass thermometer. The smallest division on the thermometer scale (0–300 F) was 2 deg F which allowed readings to the nearest 0.5 deg F, while the pressure-gage dial was divided into 1-psi intervals permitting readings to 0.1 psi.

A straight run of unobstructed 2-in. pipe, equivalent to 13 diam, was provided between the thermometer and the Shuntflo meter, and a straight run of 10 diam followed the meter.

All steam piping was well insulated with at least 1 in. of asbestos insulation.

The rate of flow of steam was controlled by a 2-in. globe valve located between the meter and the condenser.

The condensate was collected in a 20-gal barrel mounted on a 1000-lb-capacity platform scale. The smallest division on the beam of the scale was $\frac{1}{4}$ lb, and readings could be made to the nearest $\frac{1}{16}$ lb. The scale was calibrated by using test weights, and it was found to be sensitive to $\frac{1}{16}$ lb.

A test run could be started and stopped within 0.005 revolution of the large dial hand of the meter, the smallest division on this dial being 0.01 revolution. The smallest division on the stop watch used was 0.1 sec, but it could be read to 0.05 sec.

When operating under steady-flow conditions, the flow of steam to be metered passes through the body of the meter as shown in Fig. 6. The differential pressure created by the orifice causes a portion of the flow to pass upward through the nozzles

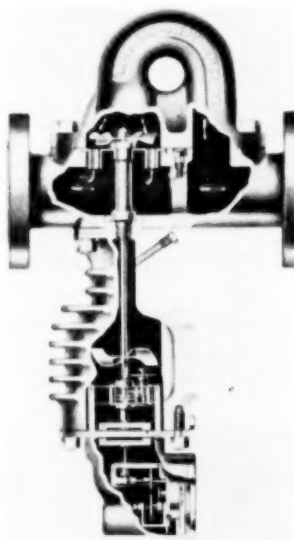


FIG. 6 2-IN. SHUNTFLO METER

and impinge on the driving fan. This portion continues through the shunt passage and rejoins the main flow before the meter outlet. The rotation of the fan shaft is controlled to a speed proportional to the rate of flow by the action of the damping fan which rotates in water in the damping chamber. The portion of the flow which is shunted through the driving fan is proportional to the total flow at all rates within the normal range of the meter; thus the speed of the fan shaft is a measure of the total flow. The speed of the fan shaft is reduced by suitable gearing in the damping liquid chamber, and final drive to the exterior counter is through a magnetic coupling.

The Shuntflo meter tested had been shop-calibrated for specific steam conditions (dry saturated steam at 12 psig) and, therefore, readings had to be corrected for variations from these conditions. Correction factors, ratios of the square roots of the specific volume of steam at calibrated conditions to the specific volume of steam at operating conditions, were obtained by using the "correction calculator," a slide rule supplied by the manufacturer.

The meter counter had been geared so that one revolution of the large dial hand was equivalent to 6.17 lb per hr of dry saturated steam at 12 psig passing through the meter. The rated maximum capacity of the meter was 296 lb per hr.

Steam Test Procedure. Steam in the 4-in. main was at 100 psig and was approximately 2 per cent moist. The 2-in. gate valve was maintained wide open during the test runs, and the various rates of flow were set by adjusting the 2-in. globe valve downstream of the meter. Before each test run the pressure regulator was adjusted to maintain an "average" pressure of approximately 12 psig as measured at the pressure gage and as explained below. By throttling in this manner, superheated steam at the same average pressure was obtained in the test line at all times.

Pulsating flow was obtained by rotating the butterfly valve in the $\frac{3}{4}$ -in. supply line to the diaphragm of the pressure regulator. When the rotating butterfly was in the closed position, the steam supply to the diaphragm was cut off. The regulator valve then opened since the pressure of the steam acting on the diaphragm was relieved through the bleed. Accordingly, when the butterfly reassumed its open position, the steam pressure increased, closing the regulator valve. This opening and closing of

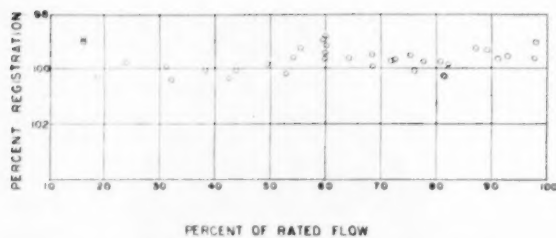


FIG. 7 CALIBRATION OF 6-IN. PROPELOFLO METER

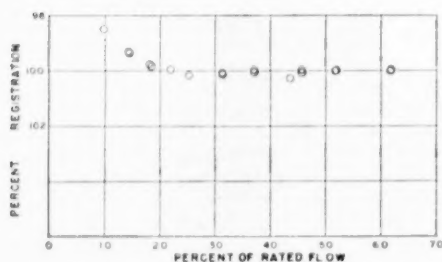


FIG. 8 CALIBRATION OF METER A

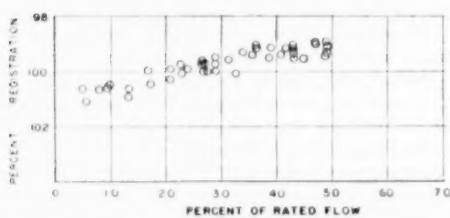


FIG. 9 CALIBRATION OF METER B

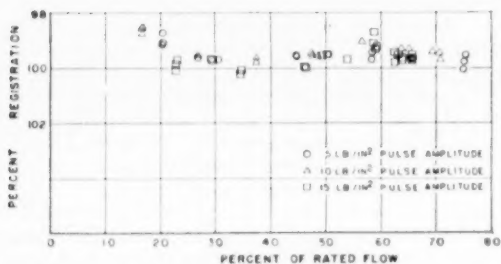


FIG. 10 PULSATION TESTS—6-IN. PROPELOFLO METER, 132.5 CPM

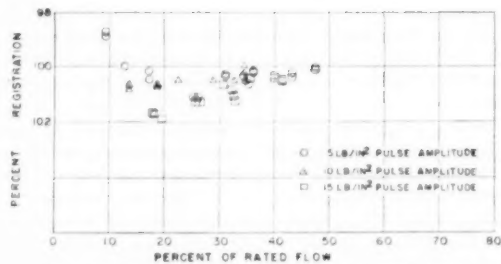


FIG. 11 PULSATION TESTS—METER A, 132.5 CPM

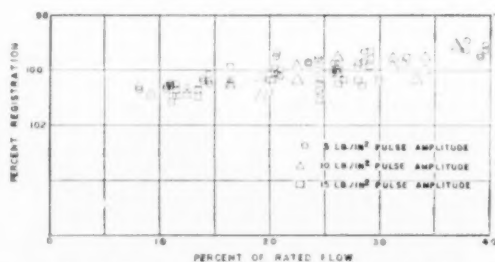


FIG. 12 PULSATION TESTS—METER B, 132.5 CPM

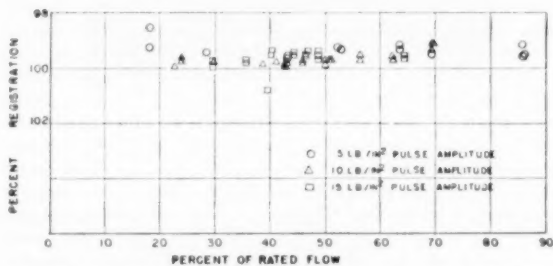


FIG. 13 PULSATION TESTS—6-IN. PROPELOFLO METER, 39.5 CPM

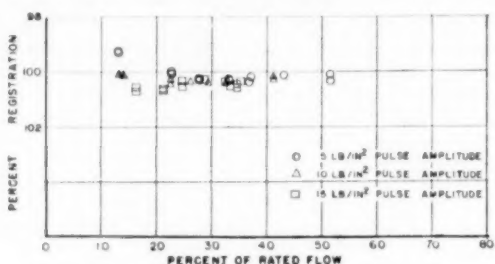


FIG. 14 PULSATION TESTS—METER A, 39.5 CPM

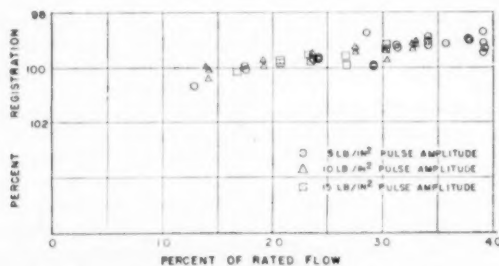


FIG. 15 PULSATION TESTS—METER B, 39.5 CPM

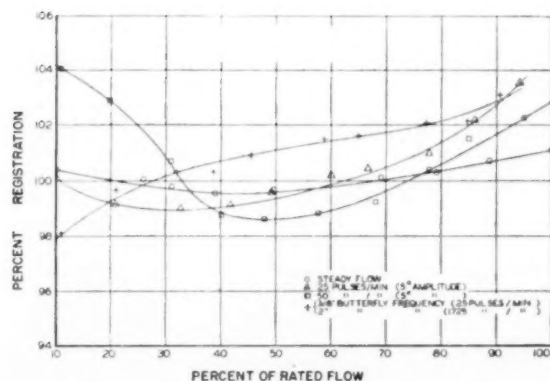


FIG. 16 PULSATION TESTS—2-IN. SHUNTFLO METER

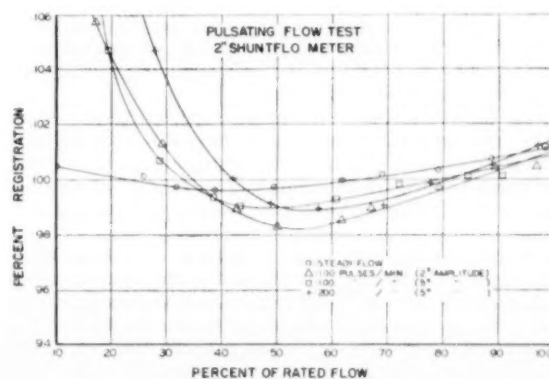


FIG. 17 PULSATION TESTS—2-IN. SHUNTFLO METER



FIG. 18 METER A, 5-PSI PULSE AMPLITUDE, 132.5 CPM, MINIMUM FLOW RATE



FIG. 19 PROPELLOFLO, 15-PSI PULSE AMPLITUDE, 132.5 CPM, MAXIMUM FLOW RATE

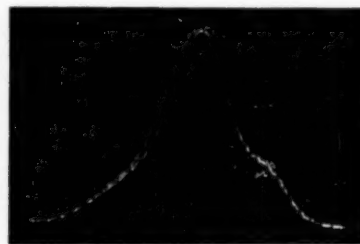


FIG. 20 METER A, 15-PSI PULSE AMPLITUDE, 132.5 CPM, MINIMUM FLOW RATE



FIG. 21 SHUNTFLO METER, 5-PSI PULSE AMPLITUDE, 200 CPM, 100 PER CENT FLOW RATE

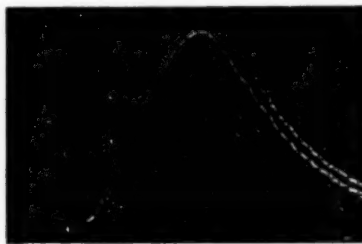


FIG. 22 SHUNTFLO METER, 5-PSI PULSE AMPLITUDE, 200 CPM, 10 PER CENT FLOW RATE

the pressure-regulator valve set up pulses in the steam flow, the frequency and amplitude of which could be controlled easily. The frequency of the pulses was set by adjusting the variable speed transmission. The amplitude of the pulses was set by adjusting the bleed valve, using the steam-engine indicator to measure the magnitude.

The second rotating butterfly valve (2 in.) was used during one of the runs to see what effect simultaneous pulsations of extremely different frequencies would have on the meter accuracy.

A test run consisted of 10 revolutions of the large dial hand of the Shuntflo meter counter. After the rate, amplitude, and frequency were set, an equalizing period of 10 min duration was permitted. A run was started by swinging the flexible tubing (about 2 in. movement of end of tubing was required) over the weighing barrel, thereby directing the flow of condensate into the barrel. This was done when the position of the large dial hand coincided with the zero graduation on the counter dial. To end the run, the foregoing procedure was reversed. The stop watch

was started and stopped simultaneously with the actions described.

The weighing barrel was filled initially with 50 or 60 lb of cold water and the weight recorded. During the test run the end of the flexible tubing hung about 1/2 in. above the bottom of the barrel so that the end was always well submerged in water. Losses due to evaporation were checked and found to be negligible. At the end of the run the gross weight was recorded.

During the run the pressure, temperature, and amplitude were checked continuously and average values recorded as data.

It might be well to state that for the pulsating-flow runs, the average pressure was determined by noting the extreme positions of the fluctuations of the pressure-gage hand caused by the pulsations and taking the mid-point as the average value.

The per cent error was calculated by subtracting algebraically the net weight (pounds) of the collected condensate from the corrected meter registration (pounds) and expressing this value as a percentage of the net weight of the collected condensate. The per cent error was added algebraically to 100 per cent to obtain per cent registration.

TEST RESULTS

The results of the hydraulic tests are shown in Figs. 7 to 15, inclusive, and the results of the steam tests are shown in Figs. 16 and 17. Figs. 7, 8, and 9 are the calibration runs of the hydraulic tests, while Figs. 16 and 17 show the calibration of the Shuntflo meter.

Hydraulic Test Results. Meter constants of 44.13 gal per

revolution of the meter-output spindle for the Propelloflo, 70.7 gal per revolution for meter A, and 326.6 gal per revolution for meter B were determined from their calibration curve and used to calculate the per cent registration.

Figs. 10, 11, and 12 give the results of 5, 10, and 15 psi, respectively, pressure pulses at a frequency of 132.5 cycles per min (cpm). Each point lies within 2 per cent of the true flow through the meter, and the spread of points is similar to that obtained with no pulse. This same statement holds for the tests at a lower frequency of 39.5 cpm, as shown in Figs. 13, 14, and 15. Figs. 18 to 22, inclusive, show typical wave shapes obtained from photographs of the oscilloscope for these tests. The only conclusion that can be drawn from these plots is that in the range of flow tested, the propeller meter will totalize accurately the flow of a pulsating incompressible fluid when the pulsations are similar in amplitude, frequency, and form to those produced for this test.

It is quite possible that under certain frequencies of pulsations, resonance may occur and may lead to large errors in flow readings. Factors influencing the motion of the propeller are (1) the combined moment of inertia of the propeller and its gears, (2) the frequency and shape of the forced pulsations, (3) the frictional resistance of the propeller and gears, and (4) the instantaneous torque applied to the propeller by the fluid. This last factor depends upon the form of the flow variation, the speed of the propeller, and the average flow rate. Thus the propeller speed and the totalizing accuracy will depend on these variables. A complete test program would require a large number of tests covering a wide band of frequencies and pulsation amplitudes under various wave forms and with various propellers. An analytical investigation of this problem is under way, but no solution has been found at this time. However, the results show some of the amplitudes, frequencies, and wave forms of pulsations under which it is possible to obtain accurate measurements of pulsating flow.⁸

Steam Test Results. Results for the tests of the Shuntflo meter given in Figs. 16 and 17, show that large errors are encountered at both the lower and the upper extremities of the flow range. The reason for the inability of the Shuntflo meter to totalize accurately the pulsating flow may lie in the fact that the quantity of flow shunted through the propeller depends roughly upon the differential across the orifice. For steady flow, in order that the meter may read accurately, the quantity of flow through the propeller must be directly proportional to the flow through the main body of the meter. Since this shunted flow depends upon the pressure drop across the orifice, in unsteady flow it is not likely to be proportional to the flow through the orifice. Rather, it will depend upon the unsteady-flow terms in the basic energy equation and the distortion of the pressure variations as they pass through the orifice.⁹

ACKNOWLEDGMENTS

The authors are indebted to Builders-Providence, Inc., for permission to present the results of the testing that was done in its laboratories. Also, they are indebted to the many individuals who co-operated in any way to facilitate the writing of this paper.

Mr. I. O. Miner,⁷ especially, gave many valuable suggestions and assistance. Mr. C. C. Cost and Mr. S. O. Clavatta rendered great assistance both in the preparation and in the running of the test.

⁷ It is interesting to note that the results of all the hydraulic tests under conditions of pulsating flow were within the manufacturer's accuracy commitments for steady flow.

⁸ Vice-President and Chief Engineer of Builders-Providence, Inc., who originally proposed the experiments.

Discussion

E. G. CHILTON.⁸ The authors' approach to the measurement of pulsating flow indicates that at least a certain portion of pulsating-flow instances can be measured with good accuracy by properly designed turbine-type-meter installations. They do not claim applicability of their results beyond the scope of their investigation, and, in fact, indicate some of the possible limitations of the turbine-type meter. It is this writer's sincere hope that this valuable work be continued to determine the range of applicability of these meters to pulsating flow and their limitations.

While the inertia of a well-designed rotor can be kept low, it has a finite value which will limit its frequency response, and it would be of interest to know what these limits are for typical commercial meters.

Assuming that the pulsating flow to be measured has only frequency components below this limit, and the meter requires negligible torque, its rotational speed will always be proportional to the volume flow rate at the meter, V . It would appear that any damping or friction introduced into the meter would reduce its accuracy and this seems borne out by the results of test on the Shuntflo meter (see Figs. 6, 16, and 17 of the paper) although these figures also include the effects of gas flow.

In pulsating gas flow the effect of density variations with pressure may become important, which was well pointed out by Hall,⁹ and in that case even the ideal meter will indicate only the local volume flow rate V , while the actual meter will respond in varying degrees not only to changes in V but also to dynamic pressure ρV^2 , and thus gives results whose error depends on the absolute value of V as well as the amplitude of the pressure pulses.

Unfortunately, cases that require measurement of pulsating gas flow are much more frequent than those of liquid flow, at least in the petroleum and natural-gas industries, and, unless these pulsation amplitudes are reduced to certain allowable maxima, erroneous flow readings are likely to result with turbine-type meters as well as the usual inferential flowmeters.

A. R. DESCHERE.¹⁰ The authors appear to have done a thorough and ingenious job of testing their equipment. The results of their work seem to be in at least qualitative agreement with the basic theory underlying the metering of pulsating flow.

Time rate of change of velocity and of density are the two factors which influence the metering of pulsating fluids by methods designed primarily for steady flow. For incompressible fluids, the density variation will be negligible, leaving only the velocity variations with time to influence the meter. Since these velocity variations will be accompanied by pressure surges proportional to the accelerations and decelerations, these influences should essentially cancel in a fluctuating flow, thus permitting a turbine-type instrument to give a satisfactory cumulative reading.

For compressible flow, the variations of velocity and density act in a nonlinear manner so that neither the instantaneous nor cumulative response could be expected to be correct for units of this type in the general case of violent fluctuations. Although some of this error in the Shuntflo instrument may arise from the influence of the orifice in the main line, the writer questions whether the propeller meter totalizes correctly the pulsating flow passing directly through it under conditions of severe pulsations.

V. P. HEAD.¹¹ The rotating butterfly valve may prove a useful

⁸ Shell Development Company, Emeryville, Calif. Jun. ASME.

⁹ "Orifice and Flow Coefficients in Pulsating Flow," by Newman A. Hall, Trans. ASME, vol. 74, 1952, p. 925.

¹⁰ Chief, Rocket Development Section, Robin and Haas Company, Huntsville, Ala. Mem. ASME.

¹¹ Director of Hydraulic Research, Fischer & Porter Company, Hatboro, Pa. Jun. ASME.

device for many who wish to study pulsation in the laboratory. However, in further work anticipated by the authors, it should be borne in mind that line "pressure" fluctuations are not a measure of "flow pulsation." Considerable doubt exists as to whether those tests conducted with water really did have "excessive" flow pulsation from the viewpoint of flow-measurement accuracy with any type of flowmeter. When wave lengths are much greater than the entire lengths of pipe involved, it is reasonable to suppose that a fully damped inferential meter of the variable-head or variable-area type will indicate the rms flow value, and that the difference between rms flow and average flow will be the "error" due to pulsating flow.

Arbitrary guesswork after a glance at the test setup, Fig. 1 of the paper, suggests that some 700 lb of water may be contained between the head tank and the pressure pickup, and if peak-to-peak pressure fluctuations of 15 psi at 132.5 cpm were caused entirely by the oscillation of the mass of water, the flow amplitude would not exceed plus and minus 60 gpm. Since some of the pressure variation would be associated with variable drop across the upstream control valve, the actual flow variation would be somewhat less. Had the pressure pickup been located closer to the head tank, even though the same flow amplitude existed throughout the pipe, the pressure fluctuations would have been reduced correspondingly. Now consider the tests on "meter A," where some effects are discernible at low flow. At 20 per cent and 40 per cent of the rated flow of this meter, or 240 or 480 gpm, a superimposed flow pulsation of plus and minus 60 gpm would produce differences between rms and average flow of 1.5 per cent and 0.4 per cent, respectively, which are almost precisely the errors shown between Fig. 8 and Fig. 11 of the paper.

At the higher rates covered by most of these tests, the flow pulsations would have quite negligible effects on any type of flowmeter. The further complexity of the manner in which pressure fluctuations must depend upon frequency and valve settings accentuates the need for flow pulsation evaluation. A hot-wire anemometer or electromagnetic flowmeter would be helpful. Even a mechanical pulsometer connected differentially across a valve, with peak readings compared with steady readings at the same average flow and valve setting might be helpful. The fallacy of using line-pressure fluctuations has been brought home repeatedly to the writer, who has observed that some methods of decreasing flow pulsations and successfully eliminating inferential meter errors in liquid flow may be accompanied by increase in line-pressure fluctuations at the meter location.

AUTHORS' CLOSURE

The authors wish to thank Messrs. Chilton, Deschere, and Head for their generous comments and will attempt to discuss some of the points mentioned by them. However, in the following closure more questions are asked than are answered.

Hope is expressed by the authors, along with Dr. Chilton, that this work be continued until definite limits are established within which the accurate measurement of unsteady flow with a propeller-type meter is possible. However, it is their opinion that the reduction of the problem to one of determining the upper limit of frequency response is an oversimplification. It is the average of the rotor velocity over a complete cycle which will indicate the flow and it is therefore quite possible, even with a poor frequency response, that this average of the rotor will give a good indication of the mean flow.

The question of the effect of damping further complicates the problem. Of course, some damping was present in all tests which were made. It is quite likely that a small amount of damping can be considered to have a linear effect, while any appreciable damping would act in a nonlinear manner, and thus increase the error.

At present, a solution to the problem of measuring a compressible pulsating flow may be more urgent than that of the incompressible problem, not only in the petroleum and natural-gas industries, but innumerable other industries also. However, a solution to the problem in the incompressible case is often the first step in the solution of the compressible case. As Mr. Deschere mentioned, the compressible case will have nonlinear effects entering due to the variations of density along with the velocity. However, if the damping also acts in a nonlinear manner, it is too much for man's poor mind to foresee the result without a solution to the proper dynamical equations. It is quite likely that there are combinations of the various variables such as pulse amplitude, frequency, wave shape, propeller inertia, and damping which will give accurate results for a pulsating compressible fluid. The problem at hand is to determine these combinations.

Mr. Head's suggestion that the flow variations should be measured rather than the pressure variations, received a great deal of thought before the test program was undertaken. The authors could find no satisfactory method to measure these flow variations. If a practical method were available, the complete test program would have been unnecessary. The hot-wire anemometer and the electromagnetic flowmeter mentioned by Mr. Head have serious drawbacks for this type of application.

The flow pulsation and the pressure pulsation are adequately related by the application of the unsteady continuity and energy equations found in many standard texts and given also in reference (3). In most cases this relation cannot be solved explicitly, but yet it is known to exist. It is not too difficult, under field conditions, to obtain the pressure variation. If the magnitude of the

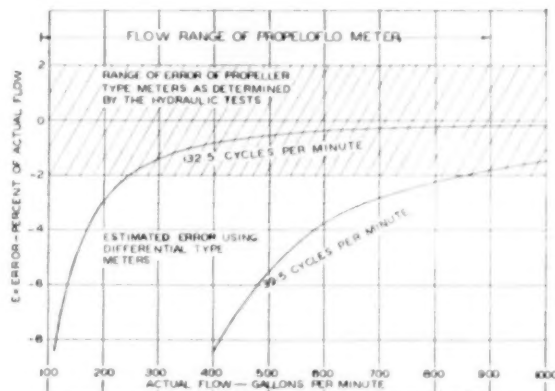


FIG. 23 ESTIMATED ERROR USING A DIFFERENTIAL-TYPE METER COMPARED TO ERROR FOUND IN PROPELLER-TYPE METERS BY THE HYDRAULIC TESTS WITH A 15-PSI PULSE AMPLITUDE

error when measuring a pulsating flow can be related to the pressure variation rather than the flow variation, then a more usable solution to the problem will have been found.

The authors must commend Mr. Head on his arbitrary guesswork. This guesswork prompted an attempt by the authors to calculate the magnitude of the error which would have been obtained had a differential producer been used under the same flow conditions as existed during these tests.

The application of the unsteady continuity, and Bernoulli's equations to the system used for the propeller tests with a length of uniform pipe between the meter and the head tank lead to the following two equations

$$E = 1 - \left[\frac{1}{2} \left(\frac{W_0}{W_1} \right)^2 + 1 \right]^{1/2}$$

$$W_0 = \frac{A_2 g \Delta P}{2\omega L}$$

when a flow variation of the form $W = W_1 + W_0 \sin \omega t$ is assumed.

- E = error in differential producing device
- W_0 = amplitude of flow variation
- W_1 = mean or average flow
- A_2 = cross section area of pipe
- g = local acceleration of gravity
- ΔP = amplitude of the pressure pulse
- ω = circular frequency of the pulsation
- L = length of upstream piping taken as 50 ft.

t = time

Fig. 23 shows the magnitude of error which would have been present in a differential producer when operating under the same conditions as existed when testing the propeller meters with 15-psi pulse amplitude. As can be seen, some of the tests were made in regions where a damped differential producer would have given a satisfactory indication of the flow; however, throughout a considerable part of the range a differential producer would have given a large error in the flow indication.

Again, the authors wish to thank those who have shown an interest in this work, and express the hope that it will be carried to a successful conclusion.

The Pitot-Venturi Flow Element Water Service Report

By H. W. STOLL,¹ ROCHESTER, N. Y.

The first paper by the author² presented in detail the design characteristics of the pitot-venturi flow element and how they are influenced by air flow. Tests clearly show that liquid-flow performance cannot be predicted from air-flow runs and, instead, actual liquid-flow conditions are required to establish a dependable relationship between velocity and differential produced. The test setup and the instrumentation needs are described. Four-inch and six-inch pipe were used and the performance curves for these are discussed. Flow equations are included and a brief analysis of them is given.

IN an earlier paper² on the pitot-venturi flow element, information was presented which described this type of primary element and showed the influence of design features on performance. Flow equations and installation information also were included. In determining these characteristics air flowing at 14.7 psia at 75 F was used. The over-all metering loss associated with this type of flow element is relatively small and, consequently, the extension of its application in the field of liquid-flow measurement in closed channels appeared to be of value. Accordingly, a fellowship was established at the University of Rochester to investigate this type of measurement. This resulted in a thesis³ which treated the entire problem in a very detailed fashion. This report indicated that it would be worthwhile to pursue the project at greater length. The purpose of this second paper is to report performance information using water as the flowing material. Also included is a further analysis on the velocity-differential equations associated with this element. Fig. 1 shows the element and Fig. 2 is a cross-sectional drawing of it.

TEST FACILITIES

All tests were run using the facilities of the hydraulics laboratory of the University of Rochester. The general features of the setup are shown in Fig. 3. As shown, the motor-driven centrifugal pump delivered water to the metering section through a hand-operated flow-control valve located immediately downstream from the pump. A vertical loop located at the discharge point was provided to insure that the metering section was always filled with water. A swivel-type connection also was included so that out-flow water could be diverted to and from the weigh tank. The initial testing was done using 4-in. pipe throughout. Later, when the 6-in. pipe runs were made, a section of 4-in. pipe was replaced by a 20-diam length of 6-in. pipe.

¹ Application Engineering Department, Taylor Instrument Companies. Mem. ASME.

² "Pitot-Venturi Flow Element," by H. W. Stoll, *Journal of Applied Mechanics*, Trans. ASME, vol. 73, 1951, p. 963.

³ Master's thesis by Edward H. Carmen, University of Rochester Hydraulic Laboratory, Rochester, N. Y., 1952.

Contributed by the Research Committee on Fluid Meters and presented at the Annual Meeting, New York, N. Y., November 30-December 5, 1952, of THE AMERICAN SOCIETY OF MECHANICAL ENGINEERS.

NOTE: Statements and opinions advanced in papers are to be understood as individual expressions of their authors, and not those of the Society. Manuscript received at ASME Headquarters, January 5, 1953.

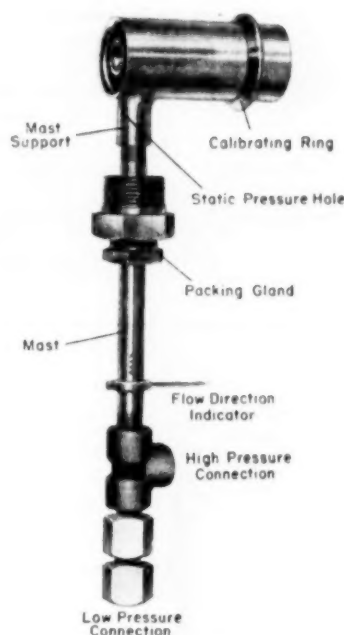


FIG. 1 PITOT-VENTURI FLOW ELEMENT

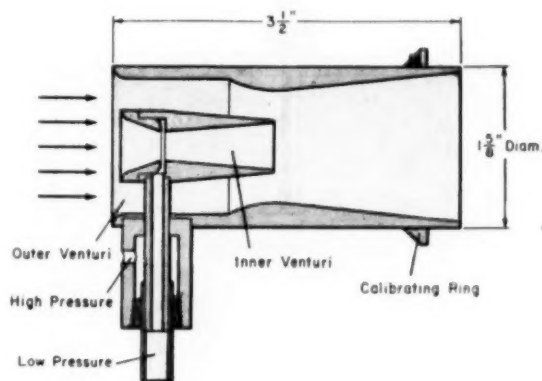


FIG. 2 CROSS SECTION OF PITOT-VENTURI FLOW ELEMENT

In both runs, the pitot-venturi flow element was supported by the pipe wall, as shown in Fig. 4. Care was exercised to minimize as much as possible any source of local disturbance and for this reason no surface discontinuity was permitted at the opening in the pipe through which the pitot-venturi element was inserted. The metering run also was equipped with pressure taps immediately upstream and downstream from the element so that the pressure drop at various velocities as a result of the presence of

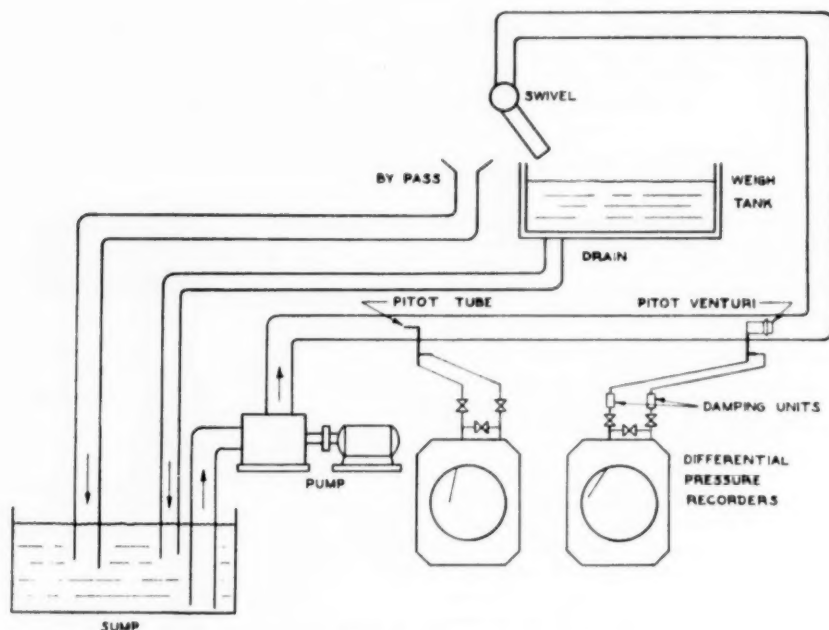


FIG. 3 WATER TEST EQUIPMENT FOR PITOT-VENTURI

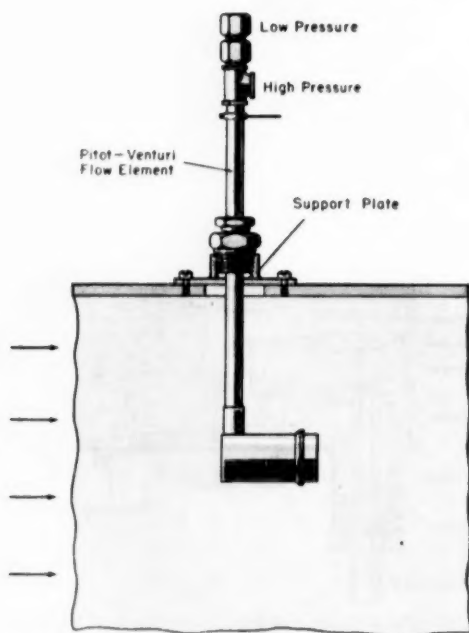


FIG. 4 PITOT-VENTURI MOUNTED THROUGH SIDE WALL OF PIPE

the element could be measured. A pitot tube was installed in the 4-in. pipe run at a point 20 diam upstream from the pitot-venturi element to determine the differential pressure-gain relationship as a function of velocity.

Bellows-type differential-pressure-measuring instruments were used throughout, because of their relatively high-speed response. The cubic-inch volume exchange per per cent of pen travel was

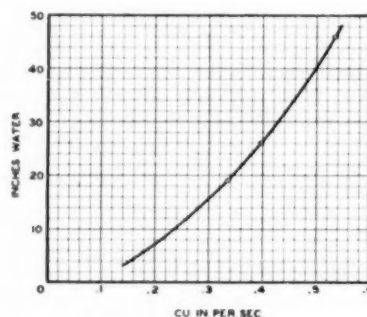


FIG. 5 PRESSURE DROP VERSUS FLOW RATE THROUGH INNER THROAT OF PITOT-VENTURI

0.01, and the time constant of the instrument under water-filled conditions was 0.78 sec (for clarity, time constant is defined as the number of seconds required for 63.2 per cent of the change to take place). The entrance into the low-pressure piezometer chamber of the inner venturi consisted of a narrow annular slit approximately 0.037-in. wide. The high-pressure tap consisted of a 0.25-in.-diam hole drilled into the upstream face of the mast. Any tendency, therefore, to reduce the response rate of the measuring system results from the resistance to flow through the low-pressure line. Fig. 5 graphically illustrates flow from the high-pressure side into the low-pressure side for various differentials developed by the pitot-venturi in water service. The maximum flow-rate of water to the manometer because of its bellows motion is 0.93 cu in. per sec. From Fig. 5 it is seen that this rate would cause a very large pressure drop in the measuring circuit. Therefore it appears that the chart records obtained using this type of manometer reflect quite closely the differential pressure developed across the pressure taps of the pitot-venturi element.

It is noted from an analysis of the rate of differential-pressure

change obtained using a high-speed chart drive, that the instantaneous flow rate of fluid between the manometer and the pitot-venturi element equals 0.92 cu in. per sec. This means that the fluid "noise" possessed both frequency and amplitude which utilized the full speed-of-response characteristic of the manometer.

UNDAMPED FLOW RECORDS

Undamped flow records in 6-in. and 4-in. pipes are shown in Figs. 6(a through d). The manometer range is 50 in. of water. It is clear that the fluid noise in the 6-in. pipe, even under lower-velocity conditions, appeared appreciably more pronounced than in the 4-in. line, and this is attributed to the reduced damping influence which resulted as the pipe size was increased. The

maximum chart travel was an acceptable amplitude of the desired record, it was found that the pressure wave required an amplitude reduction to $1/2$ of its former value, which meant that the time constant of the system had to be increased by a factor of 7. Accordingly, flow resistances in the form of multiple-orifice units, Fig. 8, were added to provide a time constant which was 7 times the initial value. A typical flow record with damping units located in both lines to the manometer is shown in Fig. 9. The "come-up" curve for a step change in flow rate, before and after making the time-constant change through the addition of damping units, is shown in Fig. 10.

For performance similar to that shown, the time constant of the measuring circuit should be 21 sec. The addition of a trans-

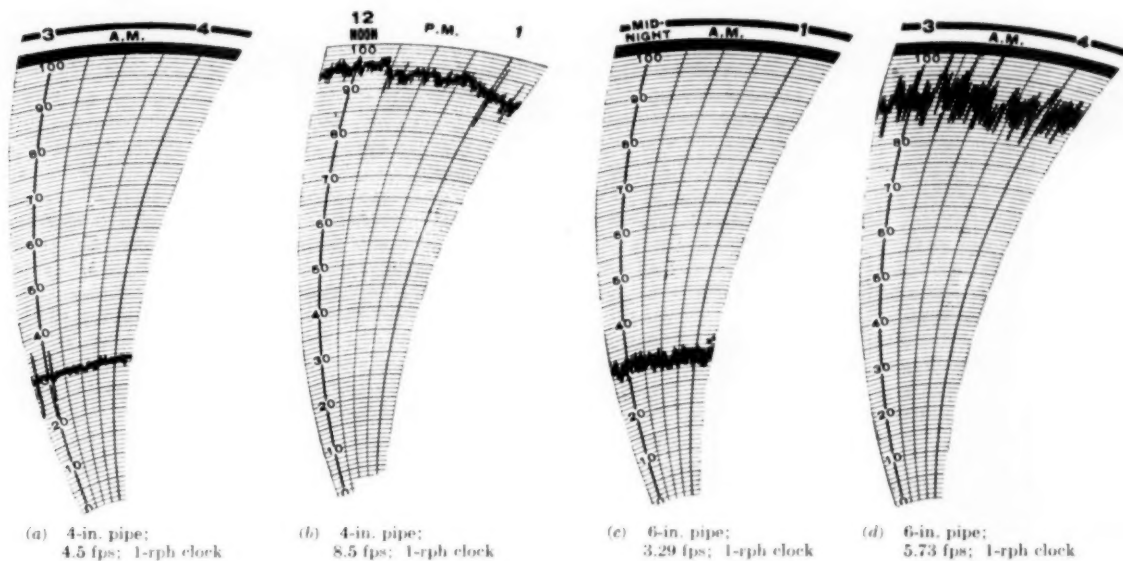


FIG. 6 UNDAMPED FLOW RECORDS

author has observed performance in 20-in. pipe, and the "band width" exceeded that shown in the 6-in. pipe under equal-velocity conditions. The actual pen motion possesses no symmetry whatsoever, and to illustrate this, 1 revolution per hr chart clocks were replaced with 4 revolution per hr clocks, and 6-in. pipe flow records, as shown in Figs. 7(a and b), were obtained.

From an industrial as well as from a calibrating viewpoint, it is desirable to have a legible record using a circular chart whose rotation is 1 revolution per day, or a strip chart having a speed of 1 in. per hr. One way of achieving this is to increase the time constant of the measuring circuit by the addition of correctly designed resistances. The term "correctly designed" is used because it is of utmost importance that these resistances exhibit similar time constants regardless of direction of flow through them. Any tendency toward shifting as a function of direction will prevent the record from being a representative average of the imposed pressure wave.

It is the author's belief that the test conditions encountered are representative of field conditions. Therefore a detailed analysis of the chart record, such as Fig. 7(a), is justified in determining the magnitude of a fluid-flow resistance (or pulsation-damping device as it is commonly called) to be located in the differential-pressure-measuring circuit. The first step was to superimpose a smooth curve which could be considered as an instantaneous average of the chart record. Assuming that a 0.5 per cent of

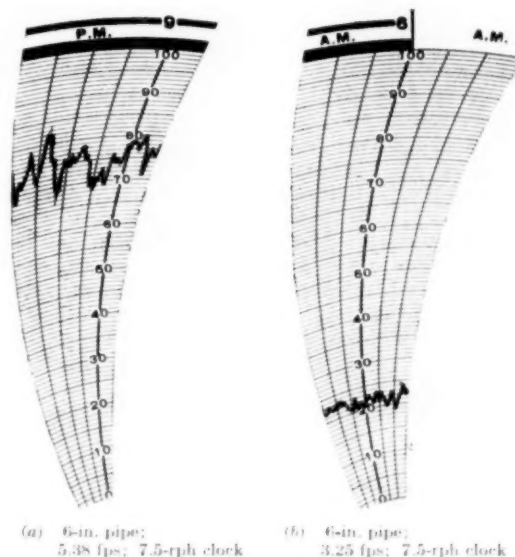


FIG. 7 CHART-RECORD ANALYSIS

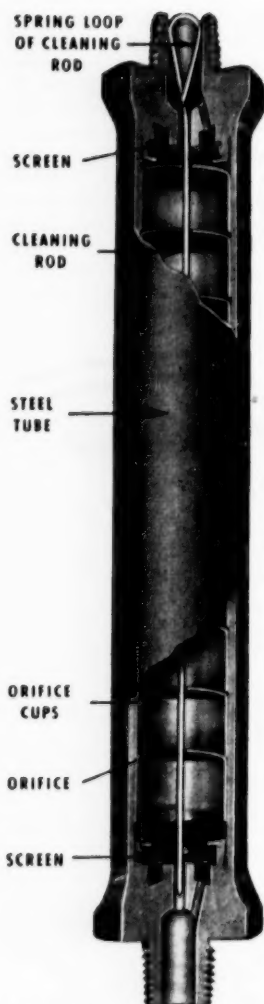


FIG. 8 MULTIPLE-ORIFICE-TYPE DAMPING UNIT

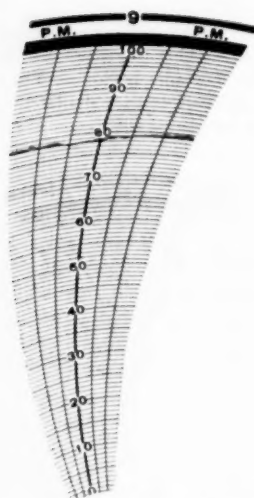


FIG. 9 TYPICAL FLOW RECORD WITH DAMPING UNITS (6-in. pipe; 5.38 fps; 7.5-rph clock)

mission length between the pitot-venturi and the manometer, as well as using a manometer with an adjustable response rate (for example, a mercury manometer with its damping valve) lengthens the time constant of the measuring circuit and reduces the importance of the added flow resistors.

In finding the relationship between velocity and differential pressure produced for the pitot-venturi flow element, the manual flow-control valve was adjusted to provide various readings on the recording manometer, and the transfer rates were determined using the weigh tank and stop watch. At the same time, pitot-tube readings also were recorded with the 4-in. pipe runs only. It is important to mention that all of the 4-in. pipe performance data were obtained under close-coupled conditions with no adjustment of the time constant to reduce the noise amplitude. On the other hand, all of the 6-in. pipe observations were made under "damped" conditions. In both the 4-in. and 6-in. pipe runs, the pitot-venturi was located so that its center line coincided with the pipe center line. Tests revealed that the differential pressure increased as the unit was deflected more than 5 deg from the longitudinal axis of the pipe. However, an angular motion of less than 5 deg each side of center was ineffective in so far as the differential pressure was concerned.

The calibrating ring provided a means for varying the differential pressure produced for a given velocity throughput. Fig. 11 shows velocity versus differential pressure for various calibrating-ring positions in 4-in. and 6-in. pipe. Note that by plotting the results on log-log paper, a close approximation to a straight line results. In the previous paper,² this particular phase on graphic presentation and flow-equation derivation was treated in some detail and, therefore, will not be repeated here. Suffice it to say that the liquid equation taken from the earlier paper and repeated herewith continues to apply

$$v_1 = K_{pv} \left(\frac{5.362h}{g_f} \right)^n, \text{ fps}$$

$$Q_1 (\text{gpm at 60 F}) = \frac{2.448D^2}{g_t} K_{pv} (g_f)^{1-n} (5.362h)^n$$

where

- v = velocity at flowing conditions, fps
- K_{pv} = pitot-venturi flow coefficient (adapted form)
- h = pitot-venturi differential pressure, in. of water
- n = differential-pressure exponent (established by tests)
- g_t = specific gravity of liquid at base 60 F, water = 1
- g_f = specific gravity of liquid at flowing conditions, water = 1
- D = inside pipe diameter, in.

The slope of the curve on log-log paper is equal to the exponent n . Examination of Fig. 11 reveals a change in slope with a change in pipe size even though no change in the element has been made. Consequently, it is concluded that n to some extent is a function of pipe size. Reflecting again on a single experience in a 20-in. line, very close agreement was obtained with 6-in.-line performance, revealing that the pipe-line influence diminishes quickly from a 6-in. size on upward. The variation of n with ring position is shown in Figs. 12 and 13 for the two pipe sizes involved.

INTERPRETATION OF TEST DATA

It should be mentioned again that the basic information collected was "in. of water" differential versus lb per sec of flowing water. As an aid in comparing performance in various sizes of pipe, the mass rate of transfer first was converted to equivalent volume rate of transfer. Then, by combining pipe cross-sectional area with this latter figure, velocity was obtained. This velocity is an average value taken over the entire pipe cross-sectional area. It is not the average velocity across a plane which

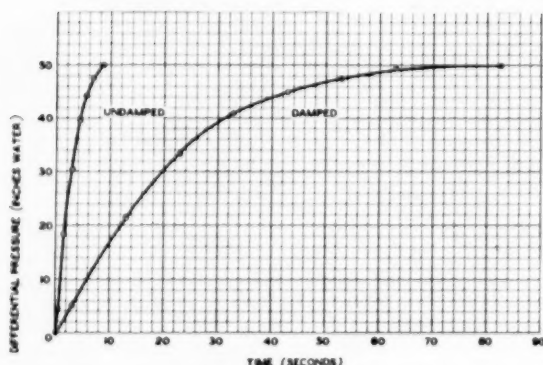


FIG. 10 SPEED OF RESPONSE FOR DAMPED AND UNDAMPED DIFFERENTIAL-PRESSURE-MEASURING CIRCUIT

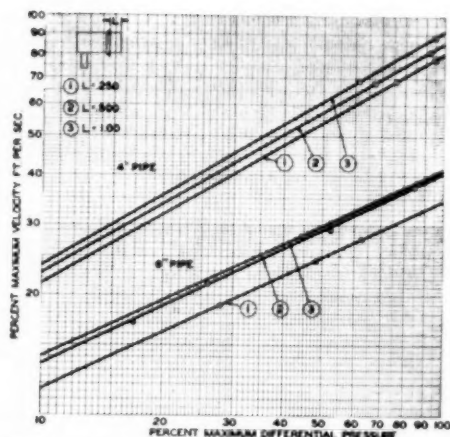


FIG. 11 DIFFERENTIAL PRESSURE-VELOCITY CURVES FOR VARIOUS RING POSITIONS

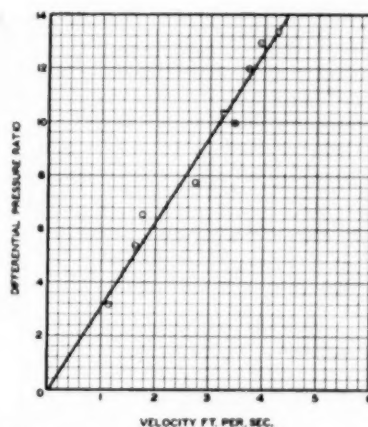


FIG. 14 RATIO OF PITOT-VENTURI DIFFERENTIAL TO PITOT-TUBE DIFFERENTIAL VERSUS VELOCITY IN 4-IN. PIPE

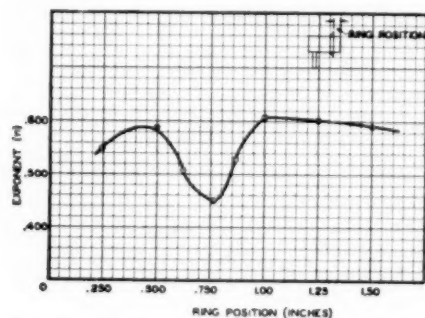


FIG. 12 EXPONENTIAL VERSUS RING POSITION ON PITOT-VENTURI IN 4-IN. PIPE

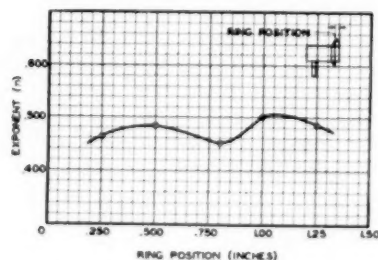


FIG. 13 EXPONENTIAL VERSUS RING POSITION ON PITOT-VENTURI IN 6-IN. PIPE

includes the pitot-venturi. For this reason, similar velocities appear to produce greater differential pressures as pipe size decreases when actually this is due to the greater-percentage area which the pitot-venturi occupies as the pipe size is reduced. The estimated cross-sectional area of the element is 2.63 sq in. This amounts to 20.7 per cent of 4-in-pipe area and 9.2 per cent of 6-in-pipe area.

Were the pitot-venturi functioning in ideal fashion, the value of n would be 0.500. Instead, its value is close to 0.430. By definition, n is equal to the difference in logarithm of upstream average velocity divided by the difference in logarithm of the corresponding differential pressures. As the velocity of fluid is increased, its willingness to flow around the pitot-venturi instead

of through it decreases, which means that the differential pressure thus developed is larger than that corresponding to the average velocity change. This tendency explains why n is less than the ideal 0.500, for the denominator of the foregoing defining ratio increases faster percentage-wise than does the numerator. The calibrating ring offers resistance to the outside flow and hence its position also influences n .

In determining the position of the calibrating ring, tests are first run in a wind tunnel and the ring is set to provide a differential pressure of 16 in. of water with air flowing at a velocity of 5000 fpm at 14.7 psia and 70 F. The pitot-venturi element then is inserted in a 6-in. water line and its performance observed. A calibration curve is issued relating average upstream velocity or flow rate versus differential produced. Because of dimensional and surface variations, each element must be calibrated individually. Furthermore, since the differential exponent differs from 0.500, the square-root chart as well as the square-root integrator and planimeter will be in error unless modified in design. If the flows vary by no more than plus or minus

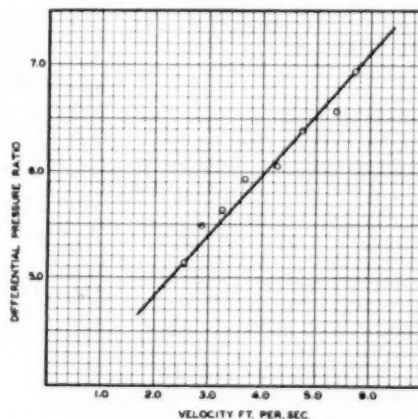


FIG. 15 RATIO OF PITOT-VENTURI DIFFERENTIAL TO PITOT-TUBE DIFFERENTIAL VERSUS VELOCITY IN 6-IN. PIPE

10 per cent of maximum, a manometer range can be selected which in turn will position the normal flow so that it will agree with the printed values on a square-root chart or scale. The difference between the differential exponent and the square-root exponent of 0.500 will determine the error in readings as the flow deviates from the normal value.

There apparently is no correlation between performance characteristics of the pitot-venturi when air data are compared with water data. Table 1 lists air and water performance data.

TABLE 1 COMPARISON OF PITOT-VENTURI PERFORMANCE DATA

Air		Water	
K_{pv}	n	K_{pv}	n
0.382	0.483	0.404	0.442
0.409	0.477	0.375	0.452
0.382	0.483	0.515	0.407
0.428	0.473	0.377	0.451
0.535	0.453	0.389	0.440

Though not of too much significance, it is interesting to observe the variation of gain which the pitot-venturi exhibits relative to a pitot tube as a function of velocity. This is shown in Figs. 14 and 15 for the 4-in. and 6-in. pipe used.

CONCLUSION

1 The differential pressure as developed by the pitot-venturi flow element is subject to continual variation when used in liquid-filled lines in which there is a centrifugal pump or equivalent, even though the flow is considered steady and, therefore, the time constant of the measuring system is very important. An over-all value of 21 sec is recommended.

2 Bellows-type or force-balance type of differential-pressure instruments are suggested because of response rate and low volume change per per cent differential-change characteristics.

3 Based on performance data using 4-in., 6-in., and 20-in. pipe, it is fairly well established that 6-in. line tests are representative.

4 Liquid-flow characteristics are such that average pipe velocity plotted against pitot-venturi differential on log-log paper gives a straight-line relationship.

5 Each pitot-venturi flow element must be calibrated individually.

6 Data obtained do not treat velocity of fluid through the inner venturi throat, but instead give an average value taken over the entire pipe cross section.

7 No standardizing procedure in water service has been determined whereby the ring position can be established. Instead, a wind-tunnel test is made and the ring is set to produce specific air-flow performance.

ACKNOWLEDGMENT

The author is deeply grateful for the extensive assistance rendered by Ray Owen and Douglas Decker of the Application Engineering Department of the Taylor Instrument Companies in obtaining all of the performance data.

ADDENDUM

The velocity versus differential-pressure equations includes two variables n and K_{pv} which are determined from tests. Whenever n differs from .500, K_{pv} is not a dimensionless number. Instead, it becomes dependent on velocity, differential and density to the extent that it is a function of the difference between n and 0.500.

In order to predict the performance of the pitot-venturi under conditions which are apart from test conditions, it becomes necessary to set $n = .500$ and observe the variation of K_{pv} as a function of the Reynolds Number. Keeping in mind that the primary source of differential pressure is the fluid flow through the inner venturi, it appears correct to use the Reynolds Number for the

throat as an index. Tests have shown that the entrance velocity at the inner venturi is only about 70 per cent of the upstream velocity. Also, it has not been completely established how this percentage varies with pipe size and velocity, so it is our present practice to simply solve for the throat Reynolds Number under application conditions, using the average pipeline velocity instead of the throat velocity. Test conditions are then specified to duplicate as close as possible the expected field conditions and a calibrating run is made.

The calibration curve furnished with the element is a solution of the flow equations given in the main body of the paper with $n = .500$. K_{pv} , however, is not a constant until the throat Reynolds Number exceeds 16,000.

Discussion

E. J. LINDAHL.⁴ Under conditions of pulsating flow, restrictions placed in gage lines to "smooth out" the operation of the secondary element can cause erroneous indications on the secondary element. Partially closed needle valves in gage lines between the primary and secondary elements of a flowmeter may give a smooth record on the secondary element, but also may give a reading which indicates that the flow is several times as great as the actual flow.

The writer has the feeling that the damping devices placed in the gage lines also may cause erroneous readings and would like to know if the author has taken this possibility of error into account. If truly pulsating flow exists, it would seem that under no consideration should a damping device of any kind be used in the gage lines.

AUTHOR'S CLOSURE

The flow of water in our test equipment was not of a pulsating nature. Instead, the undamped wave form showed no symmetry whatsoever.

In order to establish the validity of the records obtained using damping units, a by-pass utilizing a gate valve was installed across both damping units. When both of these external loops were wide open, it was clearly observed that the recorded record had widths which were reported in the paper and when the gate valves were closed, the resulting record was observed to be an arithmetical average.

⁴ Professor and Head of Mechanical Engineering Department, University of Wyoming, Laramie, Wyo. Mem. ASME.

AN ASME PAPER

Its Preparation, Submission and Publication, and Presentation

To a large degree the papers prepared and presented under the ASME sponsorship are evidence by which its professional standing and leadership are judged. It follows, therefore, that to qualify for ASME sponsorship, a paper must not only present suitable subject matter, but it must be well written and conform to recognized standards of good English and literary style.

The pamphlet on "AN ASME PAPER" is designed to aid authors in meeting these requirements and to acquaint them with rules of the Society relating to the preparation and submission of manuscripts and accompanying illustrations. It also includes suggestions for the presentation of papers before Society meetings.

CONTENTS

PREPARATION OF A PAPER—

General Information—Style, Preferred Spelling, Length Limitation, Approvals and Clearances.

Contents of the Paper—Title, Author's Name, Abstract, Body of Paper, Appendixes, Acknowledgments, Bibliographies, Tables, Captions, Photographs, Other Illustrations.

Writing the Paper—Outline Tabulations, Tables, Graphs, Charts for Computation, Drawings, Mathematics, Accuracy, Headings and Numbering, Lantern Slides, Motion Pictures, Typing, Number of Copies.

SUBMISSION AND PUBLICATION OF A PAPER—

Intention to Submit Paper Required in Advance, Meeting Dates, Due Dates for Manuscript, Discussers, Review and Acceptance, Proofs, Advance Copies and Reprints, Discussion and Closure, Publication by Others.

PRESENTATION OF A PAPER—

Time Limit, Addressing Your Audience, Public Address Systems, Use of Slides.

REFERENCES—

References on Writing and Speaking, Engineering Standards.

Price 40¢. No discount allowed. A remittance must accompany all orders for \$5.00 or less. U. S. Postage Stamps are acceptable.

THE AMERICAN SOCIETY OF MECHANICAL ENGINEERS
29 West 39th Street, New York 18, N. Y.

6 NEW ASME BOOKS

For Mechanical Engineers

1952 ASME TRANSACTIONS

2600 PAGES—CLOTH BOUND
\$15 (\$7.50 TO ASME MEMBERS)

Here is a truly valuable book for those engaged in heat transfer work. Within its pages over 150 eminent engineers of twelve countries review developments in the mechanism of heat transfer and in the design of apparatus relating thereto which have been made in the past ten years . . . consider the numerous engineering applications of heat transfer . . . appraise new fundamental discoveries in the field . . . and discuss modern methods of approach to heat transfer problems.

Coverage includes heat transfer with change of state; heat transfer between fluids and surfaces; conduction in solids and fluids; radiation, instrumentation, measurement techniques and analogies; and special problems such as heat transfer in turbine blade cooling, in liquid metals, in gas turbines, and in piston engines.

The 93 papers and discussions which make up this volume were presented at the IME-ASME Conference held in London, 1951.

PROCEEDINGS of The First U. S. National Congress of Applied Mechanics

1000 PAGES—CLOTH BOUND
\$20 (\$16 TO ASME MEMBERS)

Nowhere else will you find in a single volume so much tested and adaptable information on major trends and developments throughout the mechanical engineering field. Containing 228 papers and discussions, this massive reference places at your fingertips the experience of 350 experts, each a specialist in his field, with problems associated with fuels, gas turbine power, heat transfer, hydraulics, fluid meters and measurement, industrial instruments, lubrication, machine design, metal cutting, petroleum mechanical engineering, plastics, properties of metals, steam power generation, and applied mechanics.

Additionally, there are carefully prepared bibliographies keyed to many of the articles giving sources for further information; numerous illustrations to help you visualize new developments; and hundreds of tables, graphs, and charts which supplement and clarify the text.

One hundred and fifty nationally recognized authorities have pooled their knowledge and experience to make possible this record of advances in modern applied mechanics. The coverage embraces many of the significant problems encountered in the following branches of the field: dynamics, vibrations, impact, elasticity, photoelasticity, plate theory, plasticity, behavior of materials, fluid flow, aerodynamics, and heat.

There are 130 papers in the collection and in them research workers and engineers concerned with design and development will find an unequalled amount of reference material for constant consultation.

Held at a practical level for the information of designers, tool engineers, and production executives, this new Second Edition gives the kind of help that cuts costs, steps up production, and standardizes practice. Fabrication methods, chip control, tool chatter and surface quality of work are treated in detail; composition, types, and functions of cutting fluids and the handling of cutting oils are thoroughly discussed; feeds and speeds for machining various metals are given; forces, power, and cutting speeds for specific cutting conditions when turning a variety of metals are recommended; and consideration is given to cost of cutting operations. In addition, there are 330 tables giving data on feeds, speeds, and depths of cut to be used when turning commonly used steels and cast irons.

AUTOBIOGRAPHIES OF Dexter S. Kimball and W. F. Durand

\$4 each (\$3.20 TO ASME MEMBERS)

REMEMBER, the Autobiography of Dexter S. Kimball, is the vital story of a dynamic era and the equally engrossing story of an intrepid leader in industry, engineering, and education. What Dean Kimball remembers ranges from the San Francisco of the eighties to the college campus of today, and from engineering education to engineering practice. Also reflected is his outstanding work with the War Production Board in Washington, presidency of the ASME, and his guiding role in the expansion of Cornell and its establishment as a great engineering school.

In ADVENTURES in the Navy, in Education, Science, Engineering, and in War, Dr. Durand has recorded what he considers to be the most interesting and important events of his life. They include his part, as a young cadet engineer, in the design of power plants for the first steel ships of the U. S. Navy, his researches at Cornell on the performance of ship propellers, the aeronautical engineering problems encountered at the NACA where he served as its first president and in other capacities for nearly thirty years, and his activities after retirement from Stanford University as consultant on the Hoover Dam and other similar projects, and as a participant in the encyclopedic summary of Aerodynamic Theory.

General Discussion ON HEAT TRANSFER

500 PAGES—CLOTH BOUND
\$10 TO MEMBERS AND NONMEMBERS

MANUAL ON THE CUTTING OF METALS

222 PAGES—CLOTH BOUND
\$10 (\$8 TO ASME MEMBERS)

Published by

THE AMERICAN SOCIETY OF MECHANICAL ENGINEERS

29 West 39th Street New York 18, New York